CHARACTERISATION OF OCEAN ISLAND BASALT SOURCES: ST. HELENA

David John Chaffey

Submitted in fulfilment of the requirements for the degree of Doctor of Philosophy

Department of Earth Sciences

The University of Leeds

August, 1988

UNIVERSITY LIBRARY LEED

By reflecting on any scientific problem, one was bound to make some progress, for every scientific proposition, without exception, is incorrect. This comes of the inadequacy of human thought and the impossibility of comprehending nature, so that any logical formulation is bound not to fit somewhere.

- Albert Einstein.

View SSE to Sandy Bay from High Peak (065318) showing the deeply dissected effusive centre of the SW volcano, St.Helena.

ABSTRACT

The extrusive and intrusive members of the St.Helena rock suite *(SHRS)* are formed in an *intra-oceanic plate tectonic setting* as part of two *shield volcanoes.* The SHRS vary from *picrobasalts to phonolites.* The former represent *mantle derived melts,* whereas the remainder of the suite have undergone differing degrees of *crystal fractionation.* A stratigraphic framework is developed to illustrate temporal geochemical variations over 2 Ma of subaerial activity. This is accomplished in conjunction with a detailed field study of the SHRS by *Baker(1968)* which is shown to be largely accurate. It is demonstrated that ascending magma batches are substantially modified by *crystal fractionation* and subsequent *alteration processes. Petrogenetic modelling* shows that the genesis of the SHRS is consistent with *small degree (1-10%) melting of an olivine - clinopyroxene - orthopyroxene - garnet source* containing a *residual K-rich phase.* Combined Sr-Nd-Pb isotope and fractionation corrected trace element data for fresh rocks enable consideration of changing thermal and chemical fluxes impinging on and interacting with the base of the lithosphere over a period of at least 2 Ma. The existence of *two geochemically distinct components* in the source region is indicated. *A HIMU (high $^{238}U/^{204}Pb$) component has extremely radiogenic Pb isotopes ($^{206}Pb/^{204}Pb$ >20.8) with $^{143}Nd/^{144}Nd$ and $^{87}Sr/^{86}Sr$ displaced below the mantle array. The complementary depleted component has less radiogenic Pb and Sr isotopic compositions and more radiogenic Nd compositions.* The limited variation of geochemical compositions in the SHRS (caused by mixing of these components) is attributed to the dissimilarity of the components in terms of their trace element abundance and their similarity in terms of ratios of highly incompatible elements. *Coupled trace element and isotope variations* are evident during the *activity of each volcano. During shield development an increase in incompatible trace element enrichment occurs. This is coupled to a decrease in $^{143}Nd/^{144}Nd$, whilst Sr and Pb become progressively more radiogenic.* The time dependent variations are thought to be consistent with *mixing and melting processes occurring at the base of, or within the lithosphere.* A decrease in the signature of the depleted component at the end of activity of the NE volcano and SW volcano is the inferred result of a *decreasing*

thermal flux acting on the base of the lithosphere. With lower heat input less fusion of the depleted component (from the asthenosphere or lithosphere) occurs resulting in an increased HIMU signature in the erupted products through time. Previous explanations for the development of the dominant HIMU component are critically reviewed by considering shared isotope and trace element characteristics for HIMU OIB. U-Th-Pb systematics suggest the HIMU component has remained *discrete from other mantle components for approximately 2 Ga . The fractionation event producing the HIMU component is shown to cause an increase in U/Pb and a decrease in Rb/Sr and Th/U.* This is thought to be consistent with a model suggested by *Hofmann and White(1980,1982) in which HIMU represents ancient recycled altered oceanic crust.* It is demonstrated that other models are less tenable. It is thought that the HIMU characteristics necessitate *modification of oceanic crust in subduction zones* in addition to the geochemical changes caused by *hydrothermal alteration of oceanic crust.*

CONTENTS.

ABSTRACT..... i

CONTENTS. iii

LIST OF FIGURES..... xi

LIST OF TABLES..... xvi

ABBREVIATIONS. xvii

ACKNOWLEDGEMENTS..... xviii

CHAPTER 1: INTRODUCTION.

1.1; Characterising a magma source: statement of problem..... 1
1.2; Characterisation of the St.Helena magma source..... 2
1.3; Approach 4

CHAPTER 2: TECTONIC SETTING : INTRAPLATE MAGMATISM.

2.1; Introduction..... 6
2.2; Vertical structure of
the oceanic crust and lithosphere 7
2.2.1; What is the lithosphere exactly? 7
2.2.2; What is the thickness of the lithosphere? 8
2.2.3; The detailed structure of the lithosphere..... 10
2.3; The effect of thermal anomalies on
oceanic lithospheric structure 13
2.4; Summary 20
2.5; Tectonic setting of St.Helena..... 21

CHAPTER 3 : GEOLOGICAL RELATIONS : THE BASIS OF A CHEMOSTRATIGRAPHY.

3.1; Introduction 26

3.2; Physiography 26

3.3; Previous research 30

3.3.1; Previous volcanological research 30

3.3.2; Previous geochemical research 36

3.4; A revised stratigraphy 37

3.4.1; The North-Eastern volcano 37

3.4.1.1; Basal breccia dyke complex 38

3.4.1.2; The Main shield 39

3.4.1.3; Late pyroclastics 41

3.4.1.4; Summary of the NEMS 41

3.4.2; South Western volcano 42

3.4.2.1; South Western Lower shield 42

3.4.2.2; South Western Main shield 44

3.4.2.3; South Western Upper shield 44

3.4.2.4; Eastern Flank flows 45

3.4.3; Relationship between lavas and intrusives 45

3.4.3.1; Minor intrusives 45

3.4.3.2; Major intrusives 45

3.5; Sampling strategy 47

3.6; Representation of the stratigraphy 50

3.7; K - Ar geochronology 52

CHAPTER 4 : PETROGRAPHY, MINERAL CHEMISTRY AND AN INTRODUCTION TO GEOCHEMISTRY.

4.1; Introduction 56
4.2; Compositional range of the St.Helena rock suite 57
4.3; Textural relationships 60
4.4; Mineral chemistry 66
4.4.1; Olivine 69
4.4.2; Pyroxene 69
4.4.3; Plagioclase 72
4.4.4; Alkali- Feldspar 72
4.4.5; Accessory minerals 72
4.5; An introduction to geochemistry 75
4.5.1; Introduction 75
4.5.2; Classification 76
4.5.3; Introduction to crystal fractionation process 81
4.5.4; Representation of crystal fractionation processes 83
4.5.5; Temporal variations in major element chemistry 99

CHAPTER 5 : EVIDENCE FOR POST ERUPTIVE ALTERATION.

5.1; Introduction 103
5.2; Minimising the effects of alteration 105
5.2.1; Field studies 105
5.2.2; Sample preparation 105
5.2.3; Thin section studies 106
5.2.4; Loss on Ignition (LOI) 106
5.3; Geochemical identification of altered samples 106

CHAPTER 6 : TRACE ELEMENT SOURCE CHARACTERISTICS OF THE SHRS : REMOVING THE EFFECTS OF CRYSTAL FRACTIONATION AND PARTIAL MELTING.

6.1; Introduction 117
6.2; Correction of major element compositions to primitive compositions by least squares modelling 120
6.2.1; Method 120
6.2.2; An appraisal of the validity of input parameters to the model 123
6.2.2.1; Process 123
6.2.2.2; Parent composition 125
6.2.2.3; Daughter composition 129
6.2.2.4; Mineral extract compositions 129
6.2.3; Results of least squares modelling 132
6.3; Correction of trace elements for crystal fractionation 135
6.4 Calculation of trace element characteristics of source 147
6.4.1; Possible mantle mineral assemblages 147
6.4.2; A method of evaluating the source mineral assemblage 149
6.4.2.1; Choice of source 149
6.4.2.2; Calculation of Kd 151
6.4.3; Nature and proportion of the K-rich mantle phase 159
6.4.4; Calculating the source assemblage by inversion - the method of Hofmann and Feigenson(1983) 163
6.4.5; Calculating source characteristics by inversion - method of Budahn and Schmitt(1985) 167
6.4.5.1; Constraining input parameters - C_l - Chondrite normalised abundances of observed melts 170
6.4.5.2; Constraining input parameters - P - the primary melt norm 171
6.4.5.3 Partition coefficients 171
6.4.5.4; Results of the method of Budahn and Schmitt 172
6.5; Summary of the modelling exercises 174

6.6; Implications of models suggesting small degrees of fusion of source. 174

CHAPTER 7 : TRACE ELEMENT AND ISOTOPE CONSTRAINTS ON SOURCE REGION CHARACTERISTICS.

7.1; Introduction 180
7.2; Incompatible trace element variations 180
7.3; Isotope results 190
7.3.1; Sr and Nd isotopes 190
7.3.2; Pb isotopes 197
7.4; Coupled isotope and trace element variations 206
7.5; Interactions between mantle components beneath St.Helena 212
7.5.1; Identification of mantle components 212
7.5.2; When did mixing of the components occur? 215
7.5.3; The geometric framework of magma production 217
7.5.4; Mechanism for mixing of components 219
7.5.5; Relative contribution of components in the geometric framework of magma generation 222
7.6; Summary 229

CHAPTER 8 : THE ORIGIN OF THE HIMU MANTLE COMPONENT.

8.1; Introduction 233
8.2; Isotopic characteristics of HIMU 234
8.3; Trace element characteristics of the HIMU source 244
8.3.1; Comparison of trace element geochemistry of S. Atlantic OIB .. 244
8.3.2; Trace element characteristics of other HIMU OIB sources 250
8.3.3; Formation of the trace element characteristics of the HIMU OIB 258
8.4; Mechanisms for production of HIMU characteristics 267
8.4.1; Methods of U/Pb fractionation 267

8.4.2; Continuous core growth through Earth history..... 269
8.4.3; Recycling of altered oceanic crust
via subduction zones - seawater alteration processes 269
8.4.4; Recycling of altered oceanic
crust via subduction zones - Subduction processing 274
8.4.5; Continental lithosphere processes..... 280
8.5; Storage and transport mechanisms for HIMU 282
8.5.1; Storage of the HIMU component 283
8.5.2; Transport of the HIMU component..... 285
8.6; Summary 288

CHAPTER 9 : SUMMARY.

9.1; Introduction..... 290
9.2; High level modifications of magmas and volcanics 290
9.3; Source characteristics of the SHRS 292
9.4; Aquisition of the HIMU isotopic characteristics..... 296

REFERENCES..... xix

APPENDIX A: SAMPLE LOCATIONS.

Table A1; List of sample characteristics..... xxxix

APPENDIX B: SAMPLE PREPARATION AND ANALYTICAL TECHNIQUES.

B1; Sample preparation..... xlvii
B2; XRF analysis..... xlvii

B2.1; Major element analysis xlvii
B2.2; Trace element analysis xlviii
B2.3; Machine operating conditions xlviii
B3; Inductively Coupled Plasma determinations of REE xlviii
B4; INAA determinations of REE, Th ,Hf, Ta and U l
B5; Electron microprobe analysis of minerals l
B6; Isotope analytical techniques l
B6.1; Sr isotopic analysis l
B6.2; Sr concentration determinations by isotope dilution li
B6.3; Nd isotopic analysis li
B6.4; Pb isotopic analysis lii

APPENDIX C: ANALYTICAL RESULTS.

C1.1; Microprobe data for phases liii
C1.2; Whole rock analyses lx

APPENDIX D: ISOTOPE SYSTEMATICS.

D1; Sr-Nd isotope systematics lxx
D2; U-Th-Pb systematics lxxi

APPENDIX E: THEORETICAL BASIS OF LEAST SQUARES MODELLING.

E1; An introduction to least squares modelling lxxi

APPENDIX F: THEORETICAL BASIS OF TRACE ELEMENT PARTITIONING.

F1; Partition coefficients and element definitions lxxiii

F2; Representation of trace element variations lxxiv

F3; Simple melting model equations lxxv

LIST OF FIGURES.

1.1; Characterisation of a magma source: the oceanic setting..... 3

2.1a; Lateral lithospheric structure variations (long term)..... 9
2.1b; Comparison of definitions of the elastic lithosphere 9
2.2a; Geoid anomaly, Oahu..... 15
2.2b; Free air gravity anomaly 15
2.2c; Hawaiian crustal structure 15
2.3; Cape Verde's thermal plume structure 19
2.4; Free-air gravity anomaly map, environs of St.Helena 22
2.5; Calculated hotspot tracks for S.Atlantic islands..... 24

3.1; Location map of St.Helena 27
3.2; Physical features : St.Helena 28
3.3a; Photograph - Shark's Valley 31
3.3b; Photograph - Flagstaff Hill..... 31
3.4; Simplified geological sketch map : St.Helena..... 34
3.5; Stratigraphic divisions: St.Helena volcanics 35
3.6a; Photograph - dyke relationships in the NEMS..... 40
3.6b; Photograph - typical shield sequence in the NEMS 40
3.7a; Photograph - Shield section in the SWMS 43
3.7b; Photograph - N flank of the SWMS 43
3.8; Photograph - Lot and the dissected SWLS 46
3.9; Comparison of K-Ar data of Baker et al.(1967) and that of this study 53

4.1; Total alkalis versus silica classification for SHRS 58
4.2; Modal proportions of phenocrysts and matrix in SHRS..... 61
4.3a; Photomicrograph, ankaramite SC 173 62
4.3b; Photomicrograph, alkali basalt SC 125 62
4.4a; Photomicrograph, alkali basalt SC 26 63
4.4b; Photomicrograph, hawaiite SC 141 63

4.5a; Photomicrograph, hawaiite SC 168 64
4.5b; Photomicrograph, trachyte SC 93 64
4.6a; Photomicrograph, phonolite SC 149 67
4.6b; Photomicrograph, xenolith within phonolite SC 154 67
4.7a; Variation in Forsterite content of olivine phenocrysts in SHRS 70
4.7b; Variation in Mg number of pyroxene phenocrysts in SHRS 70
4.7c; Variation in Anorthite content of feldspar phenocrysts in SHRS 70
4.8; Compositional variation of olivine and pyroxene in SHRS 71
4.9; Compositional variation of feldspar in SHRS 73
4.10; Compositional variation in Fe-Ti oxide minerals for SHRS 74
4.11a; Na_2O vs K_2O classification for S.Atlantic OIB with 10% MgO 77
4.11b; MnO, P_2O_5, TiO_2 classification for S.Atlantic OIB 78
4.12; Spidergrams for primitive SHRS basalts in relation to other S.Atlantic OIB 79
4.13a; 2*Nb, Zr/4, Y discrimination diagram 80
4.13b; Th, Ta, Hf/3 triangular discrimination diagram for S.Atlantic OIB .. 80
4.14; Spidergrams of primitive to evolved rocks in the SHRS 82
4.15; Major element variation in the SHRS 85
4.15a; MgO vs SiO_2 in the entire SHRS 86
4.15b; MgO vs CaO, Al_2O_3 in the entire SHRS 87
4.15c; MgO vs FeO, TiO_2, MnO in the entire SHRS 88
4.15d; MgO vs Na_2O, K_2O, P_2O_5 in the entire SHRS 89
4.16; Compatible element behaviour : SHRS 92
4.16a; CaO/Al_2O_3vs Sc in the NE volcano 93
4.16b; Ni vs V in the NE volcano 93
4.16c; MgO vs Ba in the entire SHRS 93
4.17; Mineral extract polygons for the SHRS 96
4.17a; CaO vs SiO_2 extract polygons 97
4.17b; Al_2O_3 vs MgO extract polygon 97
4.14c; SiO_2 vs MgO extract polygon 98
4.14d; Na_2O vs Al_2O_3 extract polygon 98
4.18; Temporal variations of SiO_2, K_2O, MgO and Cr in the SHRS 100

5.1; Rb vs K in the SHRS 107
5.2; Behaviour of some mobile elements in the SHRS..... 110
5.2a; Nb vs Rb/Nb 111
5.2b; Nb vs K/Nb 111
5.2c; Nb vs Sr/Nb 111
5.3; Nb vs Ba/Nb 112
5.4; REE patterns comparing altered and unaltered rocks..... 112
5.5; Ba/Nb vs Y/Nb, Ba/Nb vs Rb/Nb 113

6.1; Variation in distribution coefficients for REE in mantle peridotites 118
6.2; Sequential modelling of crystal fractionation in the SHRS 124
6.3; Variation of Ni with MgO for the SHRS..... 127
6.4; Major element oxide - magnesia variation diagrams for the SHRS (corrected and uncorrected for crystal fractionation)..... 133
6.5; REE patterns for the SHRS (corrected and uncorrected for crystal fractionation 137
6.6; Variation of distribution coefficients for REE in acidic rocks..... 140
6.7; Variation in the degree of LREE enrichment as a function of MgO for the SHRS 142
6.7a; MgO vs La/Yb..... 143
6.7b; MgO vs La/Sm..... 143
6.7c; MgO vs Nd/Sm 143
6.8; REE profiles for evolved rocks in the SHRS..... 145
6.9; Calculations of MORB source composition 152
6.10; Theoretical partition coefficients necessary to form SC 68 from MORB source 154
6.11; Theoretical partition coefficients necessary to form SC 68 from N-MORB 157
6.12; Discriminant diagram of Ba vs Ba/Sr for the SHRS(corrected and uncorrected) 165
6.13; Theoretical source composition for the SHRS -

method of Budahn and Schmitt(1985)..... 169
6.14; Cartoon illustrating the different melting regimes operative beneath an ocean island erupting OIB 179

7.1a; La/Yb versus stratigraphic height in the SHRS 182
7.1b; La/Sm versus stratigraphic height in the SHRS 182
7.2; Spidergrams of primitive S.Atlantic basalts normalised to N-MORB 186
7.3; Variation in select isotope/trace elements ratios with height in the SHRS..... 188
7.3a; K/Nb 189
7.3b; La/Yb 189
7.3c; $^{207}Pb/^{204}Pb$..... 189
7.4; $^{87}Sr/^{86}Sr$ vs $^{143}Nd/^{144}Nd$ isotope diagram for the SHRS in relation to other OIB and MORB..... 191
7.5; $^{87}Sr/^{86}Sr$ vs $^{143}Nd/^{144}Nd$ in fresh samples for the SHRS..... 195
7.6; Variation of isotopic ratios with height in the SHRS 198
7.6a; $^{87}Sr/^{86}Sr$ 199
7.6b; $^{143}Nd/^{144}Nd$ 199
7.7; Pb isotopic ratios in the SHRS relative to other MORB and OIB... 200
7.7a; $^{206}Pb/^{204}Pb$ vs $^{208}Pb/^{204}Pb$ 201
7.7b; $^{206}Pb/^{204}Pb$ vs $^{207}Pb/^{204}Pb$ 201
7.8; Pb isotope correlations in the SHRS 202
7.8a; $^{206}Pb/^{204}Pb$ vs $^{208}Pb/^{204}Pb$ 203
7.8b; $^{206}Pb/^{204}Pb$ vs $^{207}Pb/^{204}Pb$ 203
7.9; Temporal variations in Pb isotopes in the SHRS..... 204
7.9a; $^{208}Pb/^{204}Pb$..... 205
7.9b; $^{207}Pb/^{204}Pb$..... 205
7.9c; $^{206}Pb/^{204}Pb$..... 205
7.10; Diagram summarising the temporal variations in geochemistry in the SHRS 207
7.10a; $^{87}Sr/^{86}Sr$ 207
7.10b; $^{143}Nd/^{144}Nd$ 207

7.10c; $^{206}Pb/^{204}Pb$ 207
7.10d; $La_{(N)}/Yb_{(N)}$ 207
7.11a; Sm/Nd versus $^{143}Nd/^{144}Nd$ in the SHRS (corrected and uncorrected) 209
7.11b; Rb/Sr versus $^{87}Sr/^{86}Sr$ in the SHRS (corrected and uncorrected) 211
7.12a; $^{206}Pb/^{204}Pb$ vs $^{87}Sr/^{86}Sr$ in oceanic basin basalts 213
7.12b; $^{206}Pb/^{204}Pb$ vs $^{143}Nd/^{144}Nd$ in oceanic basin basalts 213
7.13; Variation in the proportion of HIMU in source with varying HIMU : DMM element concentration ratios 224
7.14; Modelling of different contributions of plume and envelope melts in the SHRS 226
7.15; General model of genesis of SHRS 230

8.1; Location map of HIMU OIB 236
8.2; Modelling of the U-Th-Pb systematics of the HIMU component over the past 3.2 Ga 238
8.3; Modelling of the evolution of radiogenic $^{208}Pb^*/^{206}Pb^*$ with time 241
8.4; Spidergrams of S.Atlantic OIB normalised to Bouvet OIB 246
8.5a; K/Th vs Rb/Th in the S.Atlantic OIB 248
8.5b; La/Nb vs Ba/Nb in the S.Atlantic OIB 248
8.6; Spidergrams of HIMU OIB normalised to chondrite 251
8.7; Spidergrams of HIMU OIB normalised to St.Helena 253
8.8; Spidergrams of HIMU OIB normalised to Bouvet island basalt 256
8.9; Modelling of effect of repeated batch melting events on incompatible trace elements 259
8.10; Comparison of mineral/melt partition coefficients for phlogopite and amphibole in volcanics 262
8.11; Spidergrams of PP and PKP xenoliths from Kimberley pipes 264
8.12; Spidergrams of an average arc tholeiite compared to HIMU OIB and MORB 276
9.1; Evolutionary stages of a typical Hawaiian volcano 294
A1; Sample location map: St.Helena xxli

LIST OF TABLES :

2.1; Seismic structure of the oceanic crust..... 13

3.1; Comparison of K-Ar dates of intrusions..... 55

4.1; Distribution of phenocryst and groundmass
phases in the rocks of the SHRS..... 68
4.2; Partition coefficients of some elements compatible in
olivine and clinopyroxene 91
4.3; Summary of evidence for crystal fractionation in the SHRS..... 102

6.1; Examples of least squares modelling of crystal fractionation..... 121
6.2; Five stage incremental model for derivation of
phonolite SC 149 from ankaramite SC 113..... 131
6.3; Kd data of Le Marchand et al.(1987)..... 135
6.4; Calculated melt norm for an olivine and clinopyroxene source
containing a K-rich phase 160
6.5; Estimate of maximum degree of melting
in a source containing amphibole..... 161
6.6; Estimate of proportion of phases in a source containing amphibole ... 163
6.7; Partition coefficient data for REE used in modelling..... 172
6.8; Volume estimates for St.Helena source region volume..... 175

7.1; Results of leaching experiments conducted on 5 phonolites..... 194
7.2; Mantle mixing scenarios..... 215

8.1; Comparison of trace element ratios in oceanic basalts..... 250
8.2; Main element fractionations necessary to
produce the HIMU component..... 267
8.3; Summary of U, Th, Pb modelling conducted by Chen et al.(1987) 272

ABBREVIATIONS:

Stratigraphic units:

NEBB : NE volcano - Basal Breccias.
NEMS : NE volcano - Main shield.
SWLS : SW volcano - Lower Shield.
SWMS : SW volcano - Main Shield
SWUS : SW volcano - Upper shield.
SWEF : SW volcano - Eastern Flank flows.
SWLI : SW volcano - Late Intrusives.
Bracketed terms above denote a dyke intruded into the unit (highest level reached by dyke).

DMM:	Depleted MORB mantle component.
E-MORB:	Enriched MORB.
EPR:	East Pacific Rise.
Ga:	10^9 years.
HFS:	High Field strength (elements).
HIMU:	High time integrated $^{238}U/^{204}Pb$ mantle component.
HREE:	Heavy Rare Earth Element(s).
IAT:	Island Arc Tholeiite.
LIL:	Large Ion Lithophile (element(s)).
LOI:	Loss on Ignition.
LREE:	Light Rare Earth element(s).
LVZ:	Low velocity Zone.
Ma:	10^6 years.
MAR:	Mid Atlantic Ridge.
MORB:	Mid Ocean Ridge Basalt.
MREE:	Middle Rare Earth Element(s).
N-MORB:	Normal MORB.
OIB:	Ocean Island Basalt.
PKP:	Phlogopite K-ricterite peridotite.
REE:	Rare Earth Element(s).
SAP:	Hydrothermal seawater alteration processes.
SZP:	Subduction zone processing.
SB:	St.Helena sample number (Baker(19868)).
SC:	St.Helena sample number (this study).
SHRS:	*St.Helena Rock Suite.*
TAS:	Total alkalis silica diagram.
VAB:	Volcanic arc basalt.

ACKNOWLEDGEMENTS :

Firstly, I would like to thank the Governor and people of St.Helena for enabling me to undertake my work in such a friendly atmosphere. I would particularly like to thank the Yons of Jamestown and Cyril and Joy Allwood for making my stay comfortable and ensuring that I didn't disappear. The help of John Rogers of the Fisheries Dept in arranging seaborne transport and transporting my samples to the wharf was invaluable.

Back in Leeds, I would like to thank my supervisors, Drs Bob Cliff and Marge Wilson for being readily available for giving advice, discussion and criticism. On the technical side I would like to thank the following:

-Mr Dave Rex for undertaking K-Ar analyses.

-Mr Frank Buckley for valuable help in preparation of samples for ICP analysis.

-Mr Alan Grey for instruction on undertaking XRF analyses, data analysis and general computing advice.

-Mr Rod Green for much useful discussion on refining techniques and keeping things running smoothly in the isotope lab.

-Mr Phil Guise for reparing "la machine infernale" after I had used it.

-Dr Eric Condliffe for instruction in using the microprobe.

-The staff of the sectioning workshop for preparation of thin and polished sections.

-Tom Oddy and Dennis Pickles for putting me straight on sample preparation.

-Dr R.C. Boud for cartographic work for conferences.

-The cohabitants of 9.10d for advice on computing niceities namely, Adrian Lee, Claire Lupton, Andy Sims and Alistair Welbon.

-The use of Laser-writer from the African Gravity Project is gratefully acknowledged, as is the help of Basem El-Haddedah for producing 2.4.

I am very grateful to Graham Pearson for reading the later chapters and for numerous discussions. General discussions with Gareth Davies, Dave Gerlach, Andy Spriggs, Steve Reddy and Peter Bishop were also of value.

I would also like to thank various friends inside and outside the department for trying to make me smile. I would especially like to thank the wallflowers; Keith Rawnsley, Dave Slater, Simon Walsh and Simon Tempest for many enjoyable sessions in tights (climbing).

The continual support and encouragement of Sal Brockbank and my family are beyond thanks.

I would like to thank the following for the use of facilities outside Leeds;

Dr N.Walsh for the use of the ICP facility at Royal Holloway and Bedford New College and

Dr N.Rogers for undertaking INAA analyses at the Open University.

Finally, the financial support of NERC through a research studentship is acknowledged. The isotope facilities at Leeds are also funded by NERC.

CHAPTER 1

INTRODUCTION :

1.1; Characterising a magma source : statement of problem ;

Elucidation of the physical and chemical characteristics of oceanic magma sources is of vital importance in improving our knowledge of mantle dynamics. This is a tantalising problem because interpretation of the geochemical data obtained from volcanics is necessary in order to establish which processes have modified primary mantle melts subsequent to their segregation in the source region many kilometres below. Once the effect and nature of such processes are understood, it may be possible to remove their effects to calculate the primary magma composition. The physical and geochemical characteristics of the source region may then be considered in the context of models of mantle geodynamics. This is possible by using "geochemical fingerprinting" to identify which mantle components are present in the source region and how their proportions vary temporally and regionally. "Geochemical fingerprinting" involves an integrated isotope and trace element approach to identify mantle components. On the basis of Sr-Nd-Pb isotopes White(1985) identified five principal mantle components. The St.Helena magma source is of global significance because its isotopic composition approaches an end member composition. This led White(1985) to coin the term "St.Helena mantle component" for one of the five end members defined in Sr-Nd-Pb isotopic space. Certain incompatible element ratios which are believed to be virtually unaffected by partial melting and crystallisation events may also be used to characterise magma sources (e.g. Kay(1984)). An intrinsic part of these studies involves attempting to establish how the different components were formed.

The problem of inverting data obtained from volcanic rocks which have been modified in a variety of ways during the transit of magmas from depth is awkward. A good analogy is that of attempting to determine the origin of commuters debouching from a train at its destination (Prof. Mike O'Hara, pers.comm.). Decades of work on the modification of a magma batch from its origin in the mantle source region during its journey to the surface enable simple

formulation of the problem.

The oceanic tectonic setting provides the best opportunity for studying magma source variations because of the absence of direct contamination of ascending magmas by continental crust. Geophysical studies together with deep sea drilling projects and studies of ophiolite complexes provide good constraints on the structure of the oceanic lithosphere, through which each magma batch passes: The types of interaction that are envisaged in the oceanic tectonic setting between the time a magma batch leaves its source region and that when the resulting volcanic rock is collected are shown in Fig.1.1. This diagram summarises the processes that must be considered when elucidating source characteristics. The basic tenets of this model are discussed in chapter 2, in which definitions of the principal components of the model, namely crust, lithosphere and asthenosphere are discussed.

1.2; Characterisation of the St.Helena magma source;

The island of St.Helena provides an excellent opportunity to study variations in ocean island basalt (OIB) source geochemistry. St.Helena is eminently suitable for this purpose for three principal reasons:

(1) The intrusive and extrusive rocks of St.Helena (which throughout this study are referred to as the St.Helena rock suite (SHRS)) possess unusual isotopic characteristics (extreme radiogenic Pb compositions (Sun,1980) and Sr and Nd isotopes plotting below the "mantle array" (White and Hofmann(1982)). This should enable any interaction between this dominant component and other components to be easily discerned.

(2) Subaerial activity persisted on St.Helena for a period of more than 6 Ma (Baker et al.(1967)). Temporal variations may provide useful constraints on interactions between the components.

(3) St.Helena can be compared in a regional context with the other S.Atlantic islands which show large scale regional trace element and isotopic heterogeneity. The spatial relationships between St.Helena and other S.Atlantic

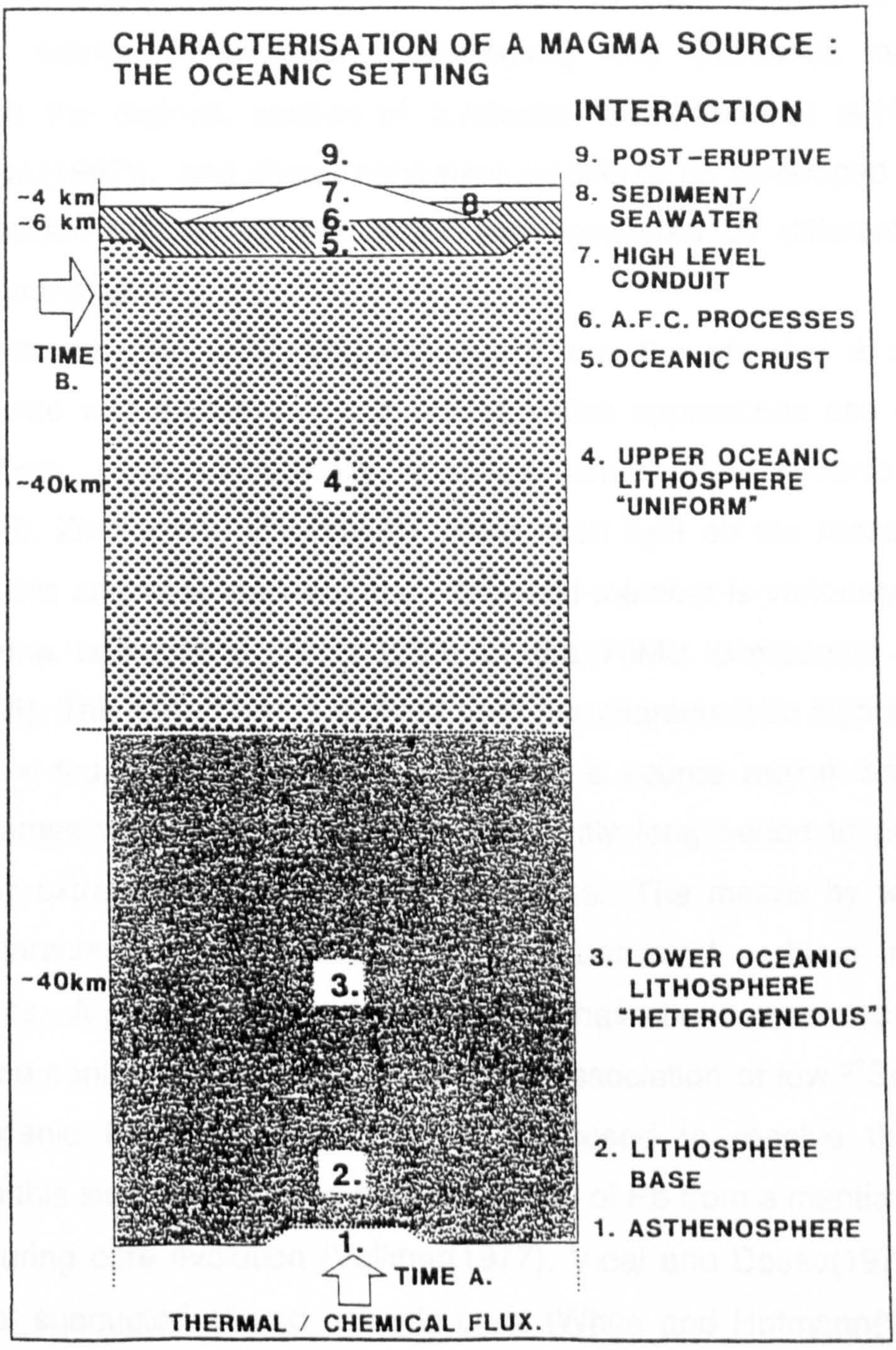

Fig.1.1. Diagram summarising the possible geochemical interactions occurring between the time a magma batch leaves the source region and collection of a sample at the surface in the oceanic intraplate tectonic setting. Arrow A denotes the possible temporal variations in thermal and chemical flux. Arrow B indicates the time effect produced by the relative motion between the lithosphere as it spreads away from the MOR and an approximately stationary plume. AFC processes are combined assimilation and fractional crystallisation processes operating in a magma chamber (De Paolo(1981)).

OIB and MORB are important as these place constraints on different scale lengths of mantle heterogeneity. Increasing the St.Helena data base supplements the regional studies of S.Atlantic OIB (Wood et al.(1981) and Weaver et al.(1987)). and allows consistent models to be developed to explain the juxtaposition of OIB sources which are dominated by different principal mantle components.

The project was also conceived because it was thought that a study of a magma source with a dominant component, which approaches one of the five end members which isotopically describe virtually all oceanic magmas (White(1985), Zindler and Hart(1986)) would shed light on the reasons for the creation of this enigmatic end member. This end member is variously known as the St.Helena component (White,1985) or the HIMU component (Hart and Zindler,1986). The latter term is derived from the characteristic high U/Pb ratios ($^{238}U/^{204}Pb$ = mu) which must be sustained in a source region discrete from mantle volumes with a lower mu for a sufficiently long period to produce the present day extreme radiogenic Pb compositions. The means by which these isotopic characteristics are produced is a fundamental problem in chemical geodynamics. A great diversity of explanations have been proposed to account for this. The controversy revolves around the association of low $^{87}Sr/^{86}Sr$ ratios with radiogenic Pb compositions. Ideas proposed to resolve this problem previous to this study have varied from extraction of Pb from a mantle segment to the core during core evolution (Vollmer(1977), Vidal and Dosso(1978)) through recycling of subducted altered oceanic crust (White and Hofmann(1980,2) and Chase(1981) to metasomatic processes occurring in the subcontinental lithosphere (Hart et al.1986).

1.3; Approach;

In order to image the temporal variations in source region characteristics a sampling program was undertaken in order to collect representative samples from the entire subaerial record of volcanic activity on St.Helena. A three month field season was undertaken in 1986 to achieve this aim. The work of Baker(1968), who mapped the island in detail and established a stratigraphy for the volcanics, proved to be of immense value in accomplishing this. A bias to

primitive compositions relatively unaffected by high level crystal fractionation processes from well constrained positions within the lava pile was made to discern isotopic and trace element variation within the source region over time.

The tectonic framework for oceanic intraplate magmatism is introduced in chapter 2. The basis for the stratigraphic framework into which the samples are placed is described in chapter 3. This is achieved by a general description of the geology of the island to act as a background to the discussion of sampling strategy and problems of sample collection, together with a critical review of previous volcanological research. The geochemical investigation of the St.Helena rock suite (SHRS) is approached by an introductory section (chapter 4) in which the petrography, mineral chemistry and geochemistry are described. This provides a basis for identifying processes which modify the primary magma composition after its egress from the mantle source region. Two principal modifying effects need to be considered : post-eruptive alteration (chapter 5) and crystal fractionation processes (chapter 6). Modelling necessary to quantify the effects of varying degrees of crystal fractionation and partial melting is described in chapter 6. It is then possible to discuss the relative roles of mixing of different source components, the degree of partial melting and oceanic lithospheric interactions in governing the bulk geochemical variations of St.Helena magmas. This is discussed in chapter 7 using trace element and isotope data. The processes by which the distinctive chemical characteristics of the St.Helena magma source were acquired is discussed in chapter 8. This involves a consideration of the new data for St.Helena in a regional context compared to other S.Atlantic islands. Chapter 9 integrates the conclusions of the previous chapters to summarise the new contribution of this study.

CHAPTER 2

TECTONIC SETTING : INTRAPLATE OCEANIC MAGMATISM :

2.1; Introduction;

Plate tectonic theory states that a number of rigid plates, thin relative to the diameter of the Earth, move around its surface. Interactions at both constructive and destructive plate margins produce a largely linear global distribution of geological phenomena such as earthquakes and volcanicity. Intraplate magmatism occurs away from the linear belts of active volcanoes and intense earthquake activity. As such, it is not fundamental to the plate tectonic model. In this model crust is generated at the Mid Ocean Ridges (MOR) (constructive plate margins) and the plate as a whole moves away from the ridge to be eventually subducted or underthrust beneath another plate (destructive plate margins). Intraplate magmatism is superimposed on the passive plates and is apparently unrelated to the major zones of activity at their margins. It will be shown, however, that intraplate magmatism has a very real, yet indirect link with the constructive and destructive plate margins. This is apparent from modern chemical geodynamics (Allegre(1982), Zindler and Hart(1986)) which involves the tenet that the mantle reservoirs feeding present day igneous activity have components derived from the recycling of material generated at either type of plate margin (via subduction zones). Thus intraplate magmatic products which become incorporated into the oceanic crust and lithosphere may be subducted to become part of the overall system. Following the cycle further through its course, it is apparent that material with a plate margin component which is injected into the convecting mantle could be erupted later in an intraplate magmatic setting. Good evidence for recycling, in recent geological times (at least) is that the oldest rocks of the ocean basin are less than 200 Ma in age. Older oceanic floor rocks have been subducted at destructive plate margins and presumably recycled.

In this chapter the physical background of the magmatism in an oceanic intraplate tectonic setting such as St.Helena is considered using various geophysical data. This is necessary to provide limits on the conditions in which a

magma is likely to be generated and the nature of the material with which it is likely to interact on its ascent. Additionally, the criteria by which the three important zones of Fig.1.1, that is crust, lithosphere and asthenosphere are defined, are considered. Physical definitions derived from geophysical modelling and definitions used by igneous petrologists for practical purposes exist. The basis of these definitions and their usefulness in relation to our understanding of intraplate oceanic magmatism is discussed. By this means a general description of the tectonic setting of intraplate oceanic magmatism is achieved. A synthesis of the vertical structure of normal oceanic lithosphere away from MOR is followed by the discussion of lithospheric structure in areas of a thermal anomaly. The data base considering the effect of a thermal anomaly on oceanic lithosphere is heavily dependent on the example of the Hawaiian chain. This example is considered in some detail before being related to the St.Helena example for which more limited data exist.

2.2 Vertical structure of the oceanic crust and lithosphere;

2.2.1; What is the lithosphere exactly?

The oceanic lithosphere is defined according to its thermorheological behaviour. In general terms it is defined as the oceanic crust together with that part of the oceanic mantle which moves as a coherent unit as the plate spreads away from the ridge. More strictly the lithosphere is defined as the oceanic crust and that part of the mantle which deforms elastically when placed under a load (e.g. Watts(1978). The asthenosphere underlies the lithosphere and behaves in an inelastic or plastic manner under similar circumstances. In the oceanic setting, lithosphere is synonymous with the rigid elastic plates, which are often termed lithospheric plates. The rheological properties of the components of this model are best described in terms of the effect of vertical crustal loading. If, for example a volcanic pile builds up on oceanic crust, the lithosphere will deform in an elastic fashion, whereas the underlying asthenosphere behaves in an inelastic or plastic manner. The asthenosphere effectively "flows" by creep processes to permit isostatic compensation of the excess mass at the surface (Bott(1982). In elastic deformation, on a crystal lattice scale, the crystal lattice will revert to its original state after a load is removed. Conversely, with plastic behaviour return

to the original state does not occur. Adjustment of the structure occurs through various creep processes. It is important to remember that the terms elastic and inelastic are dependent on the duration of the applied force. Although the asthenosphere behaves in a plastic fashion to long term crustal loading processes, it can act as an elastic solid to the short term passage of seismic waves.

In detail, the rheological definition of lithosphere and asthenosphere is not simple. In old oceanic lithosphere 3 layers are likely to exist, with a gradation between lithosphere and asthenosphere. The upper, brittle layer is 20-40km thick and elastic deformation dominates. The layer below may show some plastic behaviour (Nicolas and Poirier (1976)). In the gradational layer between lithosphere and asthenosphere power law creep deformation mechanisms operate. The gradational nature of this boundary is evident from the fact that the boundary layer operates as an elastic solid for short term deformation (up to a few thousand years), but exhibits plastic behaviour during loading periods longer than this.

2.2.2; What is the thickness of the lithosphere?

The elastic thickness of the lithosphere may be calculated where the oceanic lithosphere has been loaded by volcanic edifices. In such circumstances the excess mass of the island or seamount is supported by the elastic flexure of the lithospheric plates and large positive geoid anomalies of up to 10m amplitude and 100 - 500km wavelength are produced (Watts(1978). The geoid anomalies result from the balance between the excess topography which produces a positive geoid anomaly and the flexure of the plate which produces a negative geoid anomaly. The elastic thickness of the lithosphere may be calculated from modelling the flexural response of the lithosphere based on the equilibrium theory of deformation of a thin elastic layer overlying a weaker fluid medium (Watts(1978). By comparison of observations of actual geoid height with those predicted from the model it is possible to estimate the elastic thickness. From such models lateral variations in lithospheric thickness may be demonstrated away from a mid oceanic ridge. A recent compilation by Calmant and Cazenave(1987) is shown in Fig.2.1a. It was shown from such studies that the

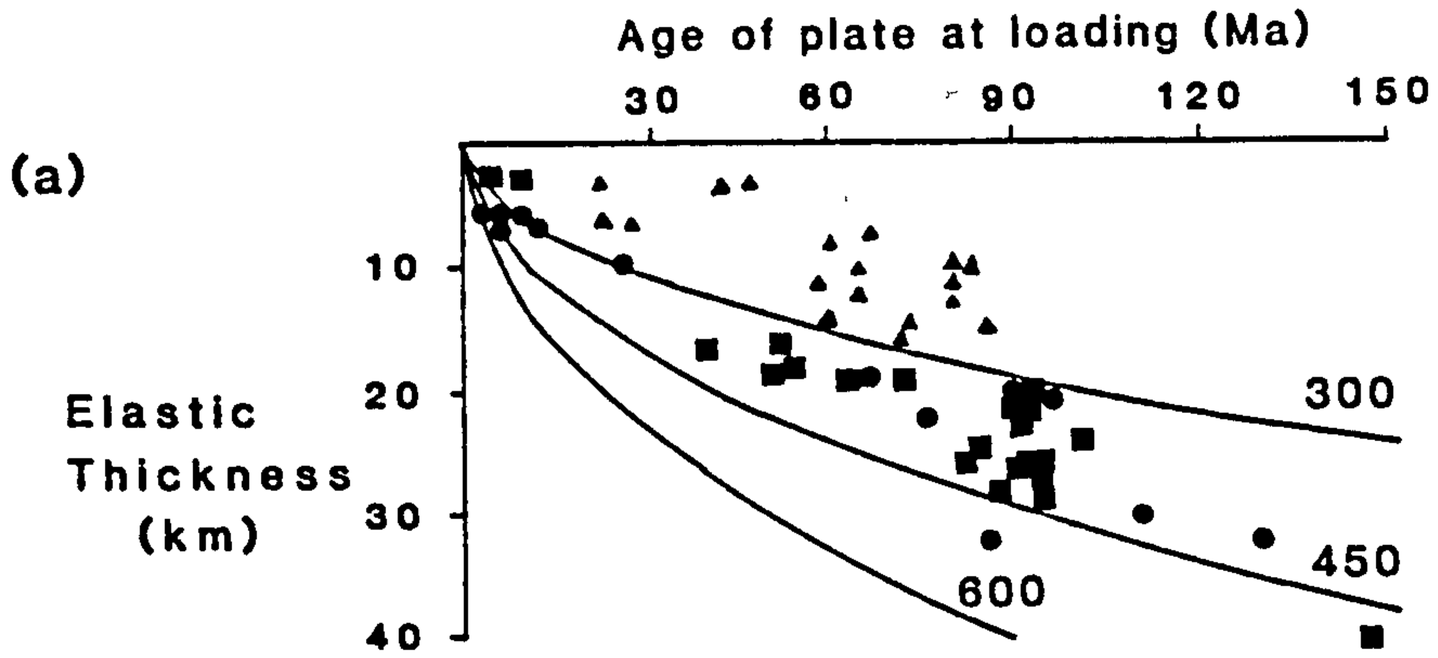

Fig.2.1a. Variation in the long term elastic thickness of the oceanic lithosphere with distance away from a MOR (expressed as age of plate at time of loading). Flexural loading models were applied to 60 oceanic volcanoes by Calmant and Cazenave(1987) to calculate these thicknesses. Squares are Indian Ocean volcanoes, circles are Atlantic Ocean and triangles are Pacific Ocean. Solid curves represent the isotherms (°C) of the cooling half space model of Forsyth(1977). The Atlantic islands scatter around the 400°C isotherm.

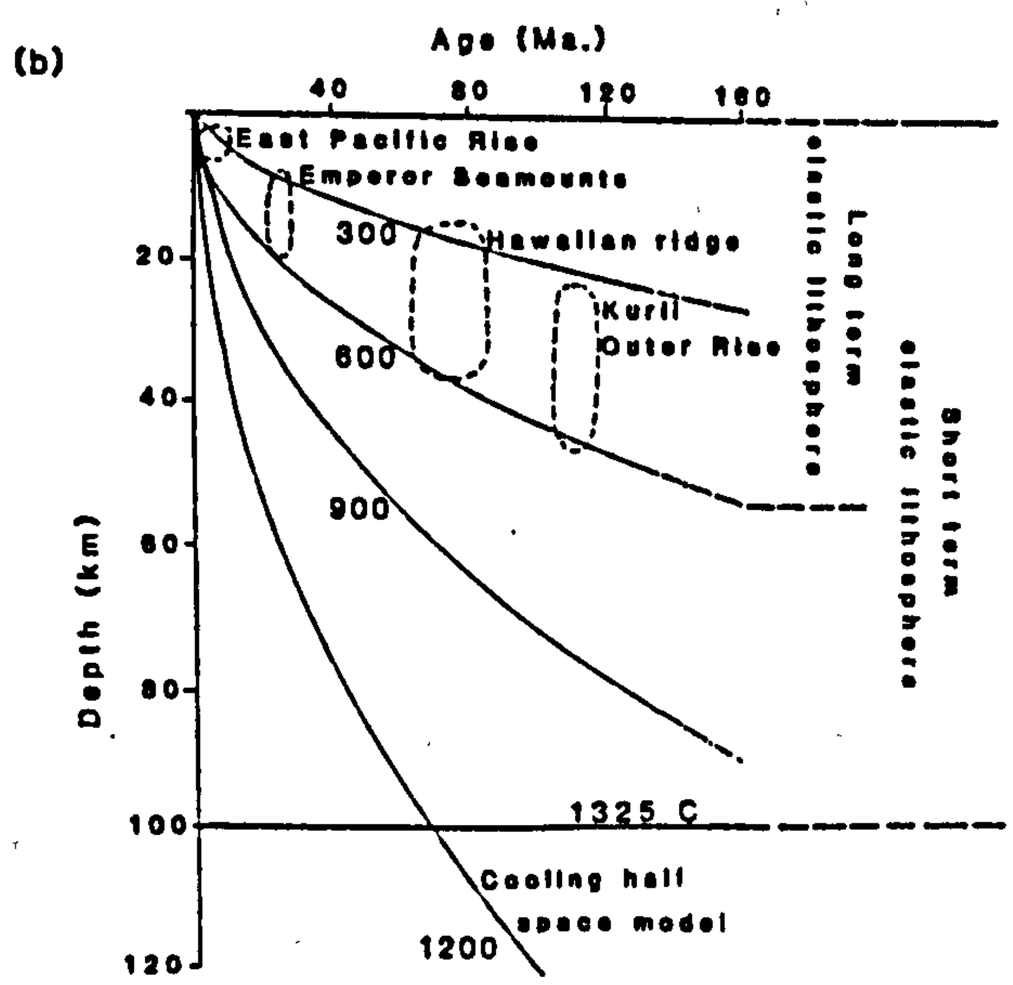

Fig.2.1b. Comparison of the long term elastic thickness of the lithosphere calculated by flexural loading models for the islands shown (Watts(1978)) and the short term thickness based on a cooling half space thermal model (Forsyth(1977)). The solid curves are isotherms (°C) of the thermal model. 1325 °C is the initial temperature. *The 1200 °C isotherm is consistent with the surface wave dispersion data for crust of 0 - 40 Ma (Forsyth(1977)).*

long term elastic thickness of the lithosphere increases approximately linearly with the square root of the plate age at the time of loading (Watts,1978). A maximum long term elastic lithosphere thickness of 40km is attained in old oceanic basins. Such compilations are in good agreement with estimates based on surface (Rayleigh) wave dispersion in the ocean basins. Modelling by Forsyth(1977) showed that surface wave velocities increase systematically with the increasing age of the ocean floor. Forsyth demonstrated that these velocities were consistent with the growth and cooling of the oceanic lithosphere as it moved away from the ocean ridges. Estimates gave the thickness of the lithosphere as 25km for crust of 5 Ma to 70km at 30 Ma. A maximum thickness of approximately 90km is achieved in old ocean basins. The differences between these two methods of calculating elastic lithospheric thickness are illustrated in Fig.2.1b. It is apparent that the long term elastic thickness of the lithosphere calculated by flexural loading models is much thinner than the short term thickness calculated by surface wave dispersion. Both thicknesses do, however, increase in a similar fashion away from the ridge axis.

2.2.3; The detailed structure of the lithosphere;

It is now necessary to consider which of these geophysical models of lithospheric structure is of most value to the igneous geochemist, who is primarily interested in the zone in which magmas are generated and the interactions that occur as melts ascend. A lithospheric thickness of 80-100 km is used by most geochemists when producing models of melt migration through old (older than 90 Ma) lithosphere. This depth range is used because melts are known to segregate at this depth from evidence that is independent of the definition of the lithosphere. This evidence is based on the identification of partial melting by the attenuation of shear waves in the low velocity zone (LVZ). These depths are also consistent with experimental petrology as partial melting of mantle rocks (anhydrous garnet lherzolite,section 2.2.3) is predicted to occur in this depth range in regions with a normal geothermal gradient. Such experiments are reviewed by Wyllie(1984). The LVZ is located at a depth of 60-250km and is characterised by a drop of S-wave velocity of between 3-6% (Bott(1982)). The LVZ is defined seismically and is not therefore directly related to the rheologically

defined asthenosphere. The definition of the asthenosphere is fundamentally different as discussed above. Although a small degree of partial melting is liable to decrease the strength of the mantle it is not necessary to produce the rheological characteristics of the asthenosphere which can be produced by diffusion controlled creep processes, even if the mantle temperature is below the solidus (Bott(1982). Thermal models are also consistent with the use of the short term elastic lithosphere as a convenient measure of lithospheric thickness. In these models, heat flow and elevation decrease away from the ridge, whilst lithospheric thickness increases roughly with the square root of temperature. The models are known as the half space plate thickening models (Forsyth(1977). The results for these (Fig.2.1b) are consistent with the choice of the short term elastic definition of the lithosphere in petrological models since the geotherms predicted at this depth intersect the melting envelope for anhydrous mantle rocks (e.g. Forsyth(1977), Wyllie(1984)).

As a result of the constraints discussed above the thickness of the lithosphere is placed at 80km in the working model of intraplate oceanic magmatism in an area of old (>90 Ma) oceanic crust (Fig.1.1). It will also be noted that the lithosphere is divided into two. The divisions of 40km are arbitrary, but the overall division is justified in order to convey the gradational, inhomogeneous nature of the lithosphere. It was stated above, that in terms of elastic properties, the brittle, upper 20-40km of the lithosphere is distinct from the material below which shows some plastic properties. Hence this is the geophysical basis of this division. This is also effectively the difference between the short term elastic lithosphere and the long term elastic lithosphere. As argued above, a similar division of the lithosphere is also justified by a consideration of the convective properties of the mantle. Some geochemists also prefer a two-way division of the lithosphere e.g. Duncan et al.(1986). A lower lithosphere that is more heterogeneous than the uniform, upper lithosphere is preferred by these authors. This model arises because they believe that as the lithosphere cools and thickens as it moves away from the MOR it will inherit the heterogeneous nature of the underlying asthenosphere. In addition, the division is also compatible with the observations of Batiza(1982) which draw attention to the volumetric importance of OIB magmatism in stable oceanic basins. The

widespread occurrence of OIB magmatism in intraplate areas is a basis for the models of Zindler et al.(1984) in which the upper mantle comprises blobs of OIB material in a convecting MORB matrix. If these models are correct it is plausible that for each batch of OIB melt that does reach the surface a greater number will fail to reach the surface. The mechanisms by which ascending magma batches become "frozen into" the lithosphere are reviewed by Spera(1984). He graphically describes this process as "magma heat death". He notes that small batches of OIB melt with a high surface to volume ratio will be particularly susceptible to this. Hence the lower part of the lithosphere is more likely to contain failed OIB melts than the upper part of the lithosphere. The upper lithosphere is likely to represent more uniform, depleted harzburgitic residuum resulting from MORB generation (Ringwood(1975)).

Further constraints are placed on the structure and composition of the mantle part of the lithosphere by the study of xenoliths erupted in basalts from the intra-oceanic setting. The only comprehensive data set for mafic and ultramafic xenoliths is that from Hawaiian volcanoes (Sen,1983,1987). Anhydrous spinel lherzolite xenoliths are most abundant with volumetrically less important plagioclase lherzolite and pyroxenite suites also occurring. The latter may contain amphibole, phlogopite and garnet. The spinel lherzolites are interpreted as fragments of oceanic lithosphere because they possess $^{3}He/^{4}He$ ratios similar to MORB (Kaneoka and Takaoka(1980)). Geothermometry estimates indicate these equilibrated at temperatures of 900 to 1100 °C (Sen(1983)). The presence of garnet peridotites are important because phase equilibria studies (Ringwood,1975) suggest that at, or below depths of 45-70km garnet lherzolite should be a stable phase. Thus magmas containing garnet bearing xenoliths must be generated at a depth of at least 45Km. Clague(1987) coupled this information to the observation that the deepest earthquakes beneath Hawaii occur at depths of 65-70km (Klein(1982)) to suggest that the main shield lavas were generated at this depth. Models of the mineralogical structure of the oceanic lithosphere derived from xenolith studies (Sen(1983), in common with phase equilibria results (Ringwood(1975) contain three divisions. Between 15-30km plagioclase lherzolite is found, spinel lherzolite is stable between depths of 30-45km and garnet lherzolite stable below this. The exact nature of

each layer is dependent on the preferred degree of depletion. For example Ringwood(1975) prefers a harzburgitic composition for the spinel lherzolite layer which is produced by depletion during MORB genesis.

It is possible to define the crustal part of the lithosphere relatively easily from seismic refraction studies such as those by Ewing(1965). The transition from crust to mantle is indicated by a marked increase in seismic velocity over a short vertical interval. This occurs at a depth of 5-8km and P-wave velocity increases to more than 7.7km/sec below the Mohorovicic discontinuity. Detailed seismic refraction work enables oceanic crustal structure to be discerned. Three main layers are formally identified, Table 2.1;

Table 2.1; Seismic structure of the oceanic crust.

Layer	Thickness	P-wave velocity	Description
1	0.4 km	1.6-2.5 km/sec	Oceanic sediments
2	1.5 km	4.0-6.0 km/sec	Oceanic volcanics
3	5.0 km	6.4-7.0 km/sec	Oceanic crust
4	-	> 7.7 km/sec	Mantle

Source Bott(1982)

In most stable oceanic basins the structure is uniform. Layer 1 corresponds to unconsolidated sediments. Layer 2 is basaltic and thought to be the source of the linear magnetic anomalies of the ocean floor. Layer 3 is more uniform in velocity and is thought to be metamorphosed basaltic crust. This structure is broadly consistent with ophiolite suites which are thought to represent obducted proto-oceanic crust, although in these, individual layers tend to be thinner and seismic velocities lower. Oceanic drilling programmes have mainly yielded information about Layers 1 and 2. Layer 3 has not been penetrated.

2.3; The effect of thermal anomalies on oceanic lithospheric structure;

In order to investigate the lithospheric structure in anomalous areas of heat flow it is necessary to use detailed studies that have been conducted at other sites of intraplate volcanicity. Attention is focussed on the Hawaiian example here because this is the most intensively studied example of a thermal anomaly

affecting a passive plate away from plate margins.

Hawaii is part of one of a number of chains of volcanic islands and seamounts that occur in the Central - NW Pacific. The Hawaiian-Emperor chain is not linear because a sharp kink occurs at Abott seamount. To the N the chain runs approximately N-S, whereas to the S it runs WNW to ESE. In the Hawaiian-Emperor example the oldest volcanoes occur in the NW and most are submerged. Progressively younger and more recently active volcanoes occur to the SE. The linear age progression along the chain may most simply be explained by a general North westerly movement of the Pacific plate over a static point source of heat (Wilson,1963). The kink in the volcanic chain at Abbot seamount is explained by a dramatic switch in direction of plate motion at 40 Ma. Alternative explanations which do not require an excess of heat but rather, magmatism develops as a lithospheric crack is propagated by crustal tension have been proposed (Green,1971), but the existence of a thermal anomaly in the Hawaiian area is indicated by several lines of evidence.

Where intraplate magmatism occurs, its effects on geophysical parameters discussed below are likely to be governed by the balance between the input of heat from below and the build-up of the volcanic pile on the crust, together with the possible underplating of the lithosphere. In the area of Hawaii a bathymetric swell occurs over a long wavelength (greater than 300km) (Ten Brink and Brocher(1988)), (Fig.2.2a). On a shorter wavelength the elastic response of the plate to the load is indicated by the localised trench (moat) immediately surrounding Hawaii. The averaged gravity profile shows a similar pattern to that of geoid anomaly (Fig.2.2b). The overall positive anomaly is produced by the excess mass of the volcanic pile. This factor exerts a greater influence on the profile than the presence of hot, less dense mantle material beneath the island, which would produce a negative anomaly.

Although the above evidence is consistent with the existence of a volume of hot, relatively low density rocks beneath Hawaii, it is important to address the problem of whether the thermal anomaly results from a continuous upwelling of hot material which has been termed a thermal plume (Morgan(1971)) or whether a pre-existing thermal anomaly is actually required. J.T. Wilson first suggested a thermal convection model to account for Hawaiian magmatism in 1963.

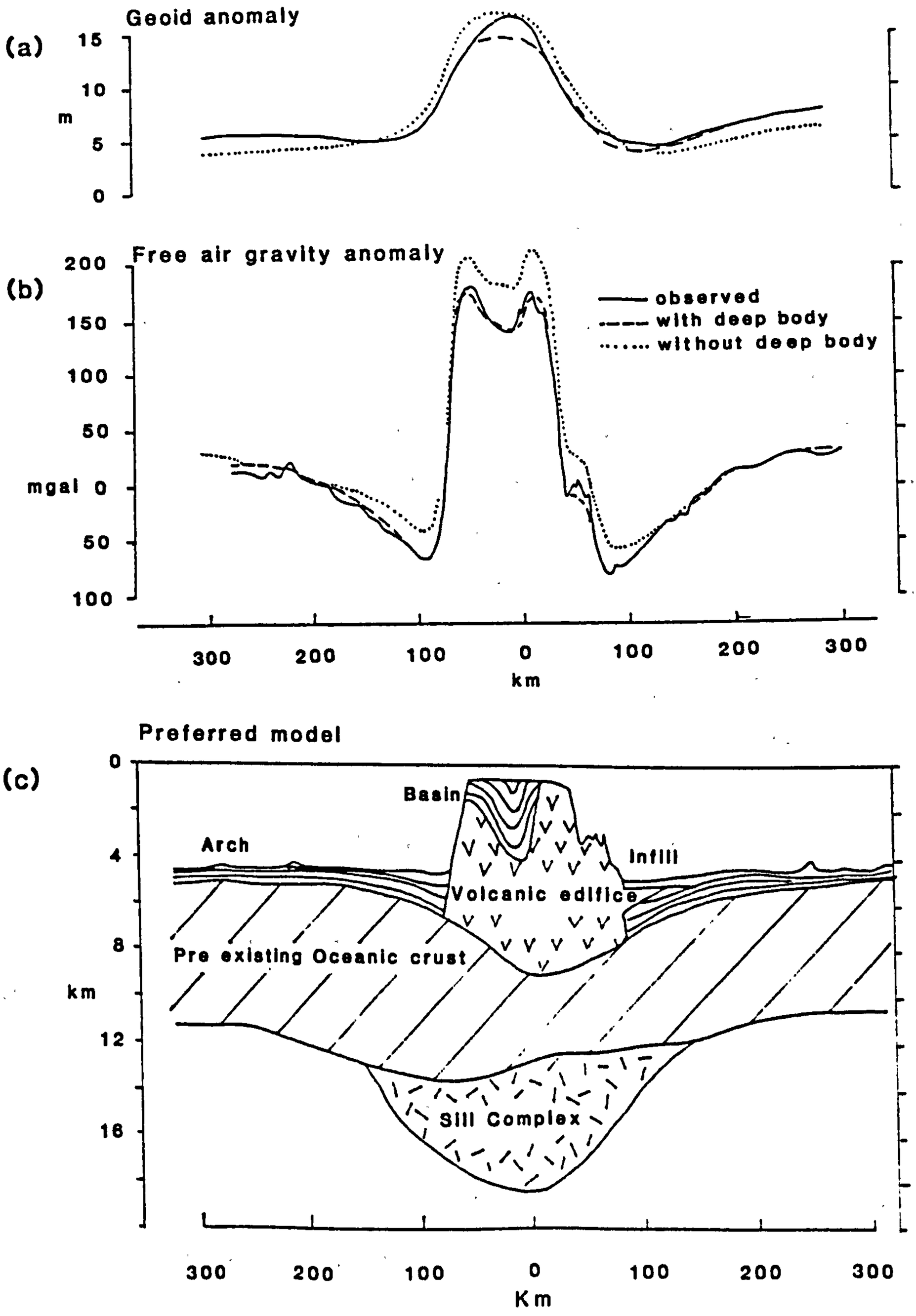

Fig.2.2. A transect across the Hawaiian archipelago to illustrate the geophysical features and their structural interpretation (Ten Brink and Brocher(1988)).

(a) Geoid anomalies

(b) Free air gravity anomaly. Models based on the presence or absence of a deep seated body (sub crustal sill complex) are depicted.

(c) Crustal structure inferred from the geophysical data.

Morgan(1971) considered plumes to be narrow (150km diameter), static thermal zones of relatively low viscosity which convect upwards at rates of approximately 2m/year. These are thought to originate deep in the mantle, possibly at the core-mantle interface. More recent work by Molnar and Stock(1987) has shown that relative to Hawaii (that is assumed to be fixed) other plumes are not static, but have average relative motions of 10-20mm/yr. The relative motion of lithospheric plates relative to a plume must still be sufficient, however, to account for hotspot tracks such as the Hawaiian - Emperor chain. A major problem with the plume hypothesis is that it is difficult to test. The only conclusive test for detection of a plume is to analyse seismic rays that pass directly beneath an island. Such tests have been conducted for Hawaii, but unfortunately have yielded ambiguous results. Some results (Kanasewich and Gutawaski(1975)) have indicated abnormally low velocities above the core mantle boundary beneath Hawaii which were thought to be consistent with Morgan's plume hypothesis. No velocity anomalies were recorded above this in the mantle, however. The interpretation of the results for the core/mantle boundary have also been questioned (Wright,1975). Hence this evidence is inconclusive and indicates, either that the plume is of a very narrow diameter, or it does not manifest itself by large velocity differences in comparison to the surrounding rocks.

Other models exist to account for intraplate volcanism, but these are also difficult to test. For example, Jackson and Shaw (1975) suggested that shear heating at the lithosphere/asthenosphere boundary could produce the melts required. However, it is difficult to envisage why this process should start and why it should be localised. The idea that the island developed along a SE developing fracture has also been proposed; this is again difficult to substantiate. However, the Hawaiian swell is most easily accounted for by thermal resetting and thinning of the ageing and thickening lithosphere by a point source of heat. Detrick and Crough(1978) noted that long-term rates of subsidence of the volcanic islands and seamounts are higher than can be accounted for by the subsidence which accompanies normal ageing and cooling of the lithosphere. Moore(1987) catalogues subsidence rates from the Hawaiian Ridge that are constrained by tide-gauge measurements, submerged carbonate reef and deep drilling together with the geophysical techniques described above. It is shown

that the Hawaiian ridge has undergone rapid and dramatic subsidence. Most volcanoes have subsided 2-4km since reaching the surface, whilst their bases have subsided 5-8km. Between one half and one third of the upbuilding of volcanoes is offset by subsidence. It is suggested that these characteristics result from the thermal resetting of a thickening plate as it passes over a "hotspot". The "hotspot" is thought to cause lithospheric thinning and a rise in seafloor elevation and the temperature is reset to that which is more typical of younger oceanic crust. The rapid subsidence that then follows occurs due to a return to normal depths expected for oceanic crust of a given age and distance from a mid oceanic ridge. Independent evidence for lithospheric thinning is provided by McNutt(1984). McNutt calculated that for lithosphere of a similar age the elastic thickness is greater for lithosphere that is being flexed in a subduction zone than for Hawaiian lithosphere. Thus, it is suggested that the lithosphere is thinned by the effect of the plume. A general problem with these models that was noted by Detrick and Crough(1978) is that it is not possible to transfer heat to the lithosphere rapidly enough to produce thinning and uplift since more than forty times the observed heat flow is required. More recent modelling, however, has suggested that small-scale convective instabilities in a plume can develop, which enable more efficient lithospheric thinning and heat transfer (e.g. Yuen and Fleitout(1985)). McNutt(1984) has suggested that the heat transfer could be accomplished by delamination of lithospheric slices caused by the influence of a plume on the base of the lithosphere.

A detailed study of the Cape Verde rise by Courtney and White(1986) gives useful constraints on the nature of a thermal plume impinging on the lithosphere. Anomalous heat flow, geoid and bathymetric values were used to constrain a variety of possible hotspot mechanisms. These authors found that models merely invoking thermal resetting of the lithosphere to within 35-40km of the surface may only explain the observed geophysical characteristics if a thermal event occurred in the last 3-12 Ma. Models involving sustained or transient thinning of the lithosphere require heat flow values that are twice those that are observed. Thus evidence of sustained uplift and volcanism over the last 20-50 Ma make simple thermal resetting unlikely. As in the Hawaiian example it is necessary to invoke methods of heat transfer other than conduction. Modelling

of the plume based on bathymetry, gravity and heat flow values place constraints on its geometry. The model produced by Courtney and White(1986) (Fig.2.3) is that of a narrow jet with a hammerhead geometry. Such a model has important implications for the locus of melt generation.

The greatest success in elucidation of Hawaiian lithospheric structure has been that in delineating high level lithospheric and crustal structure. The depths of magma generation are known from the occurrence of garnet bearing xenoliths which correspond well with the maximum recorded earthquake depths (Section 2.2.3), (Klein,1982). Possible magma storage zones between the source region and the surface have recently been reviewed by Clague(1987). No geophysical evidence exists for magma chambers at the base of the lithosphere, indeed models based on fluid dynamic solutions to melt segregation and migration problems suggest that once melts are segregated at depth, they ascend rapidly upwards because of density and viscosity contrasts between melt and matrix (Ahern and Turcotte(1979), Stolper et al.(1981), and McKenzie(1984)), section 6.6). Spera(1984) reviews evidence for the ascent rates of alkali basalts. The occurrence of metastable garnet megacrysts and and xenolith size populations have been used to estimate ascent rates which are in the order of cm/s to m/s (Spera(1984).

There is general agreement on the existence of large subcrustal magma chambers forming sill complexes beneath the Hawaiian volcanoes at 15-20km depth. This is indicated by combined gravity and seismic studies of the islands such as that by Ten Brink and Brocher(1988) which is described below. In addition CO_2 inclusions in olivines in dunites (Roeder,1965) were thought by Sen(1983) to suggest a 15km deep origin for these xenoliths. Ryan(1987) reviews evidence for the the existence of high level magma chambers beneath Kilauea and Mauna Loa volcanoes, Hawaii. An aseismic region between 4-7km is thought to provide good evidence of a high level magma chamber. Ryan(1987) points out that the magma reservoirs represent a zone of neutral buoyancy where ascending magmas become stable because of the crossover of densities between the magmas and the host rock. This stability is produced by what Ryan terms "the contractancy" variation with depth. Contractancy is simply the elimination of fractures and vesicle porosity through increasing confining

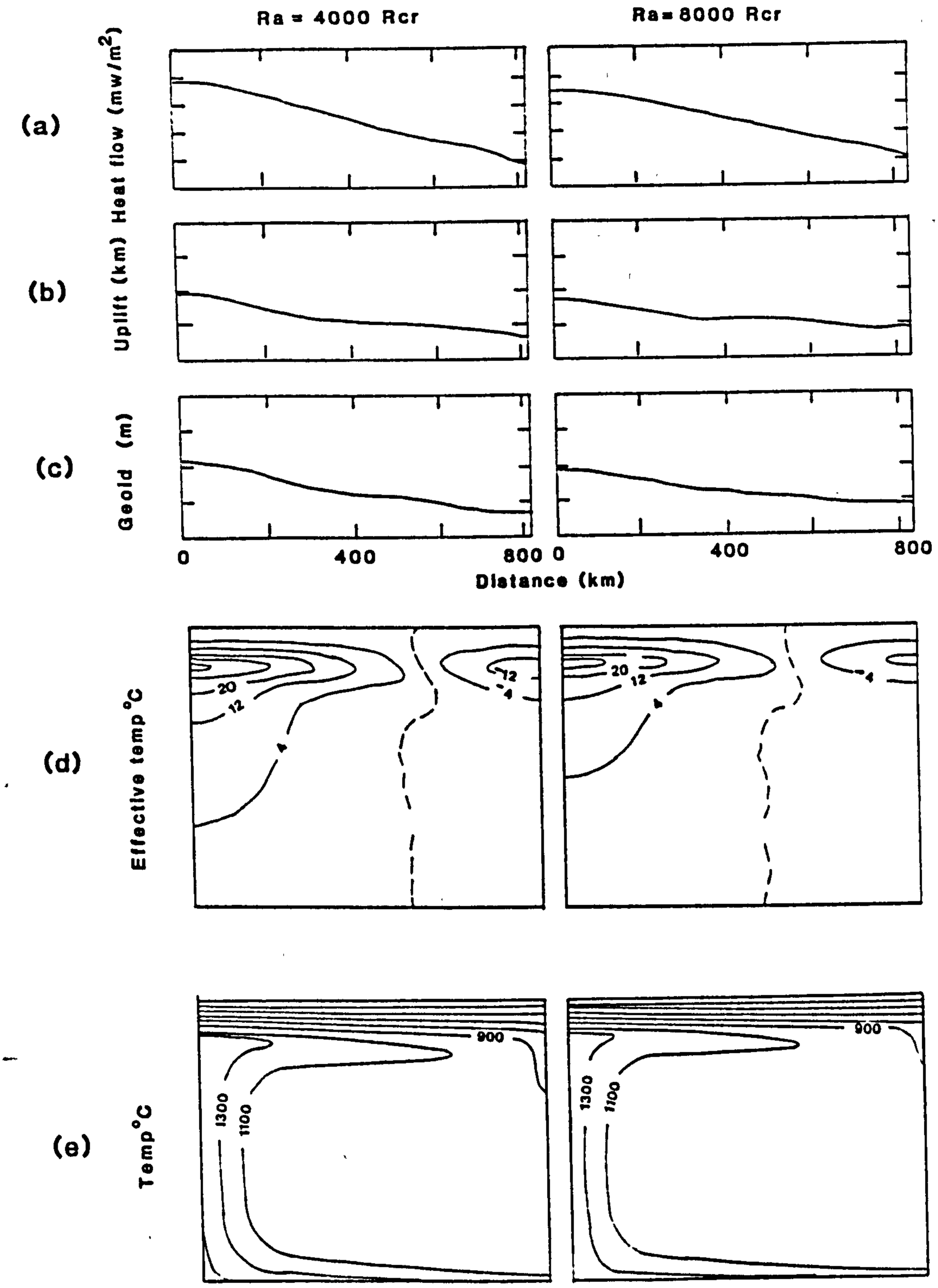

Fig.2.3. Results of modelling by Courtney and White(1986) showing the predicted form of a thermal plume (d) and (e) produced under different convective systems. It is evident that the Rayleigh value (Ra) is not critical as similar models are produced, although a decrease in plume width does occur with increasing Ra. Rcr is the critical Rayleigh number at which convection begins (c.1500). (a) - (c) show the geophysical expression of such a plume. A close fit with observed and calculated values is obtained.

pressure. This simple observation provides an explanation for why high level magma chambers can be stable systems. Ryan describes how the zone of neutral buoyancy will ascend as the volcanic system evolves from the seamount to emergent volcano stage. The result of this process will be to produce a mafic core in the volcano structure that represents cumulates that have formed at various stages in the volcanos development. Crustal structure has been imaged by coincident seismic reflection and refraction seaborne surveys. The pertinent results of an example of this type of survey by Ten Brink and Brocher(1988) are illustrated in Fig.2.2. It is evident that:

(1) Flexure of the crust with a corresponding concentric "moat/arch" pattern occurs due to loading by the volcanic edifice.
(2) Infilling of the moat by recent sediments occurs.
(3) A sill complex may be evident beneath the island.

2.4; Summary;

The principal features of the structure of old (older than 90 Ma) oceanic lithosphere when associated with the build-up of a volcanic edifice are illustrated in Fig. 1.1. The salient points are:

(1) Lithosphere approximately 80km thick.
(2) Oceanic crust approximately 5-8km thick
(3) Mantle part of lithosphere has a gradational nature.

In areas where a volcanic edifice and topographic swell occur the following features are apparent :

(1) The crust is flexed by the excess mass of the volcanic pile.
(2) A sediment filled trench occurs around volcano.
(3) Lithospheric thinning occurs.
(4) Difficult to prove the link between the formation of an island chain and the presence of a thermal plume.

2.5; Tectonic setting of St.Helena;

St.Helena is located approximately 800km E of the Mid Atlantic Ridge. The volcanic pile lies on oceanic crust of magnetic anomaly 10 (approximately 30 Ma in age (La Brecque et al.(1971)). In considering the effect that the presence of the St.Helena volcanoes has on lithospheric structure it is necessary to consider the period over which they were active. The lithosphere thickness beneath St.Helena would have been less than at present because the volcanoes ceased to be active approximately 7.0 Ma ago (section 3.7) By reference to Fig.2.1 it can be seen that the short term thickness of the elastic lithosphere calculated by Calmant and Cazenave(1987) is approximately 12km. This corresponds to a long term elastic thickness calculated from surface wave dispersion or by a cooling half space model of approximately 70km (Forsyth,1977). The latter depth is consistent with magma genesis below the lithosphere occurring in the garnet stability field (section 2.2).

The age of cessation of activity is also of importance in considering the present bathymetry and gravity anomalies in the vicinity of St.Helena. If the excess heat source which has manifested itself as volcanism is no longer present the gravity and bathymetric anomalies will have diminished as is noted in the Hawaii-Emperor chain. As a consequence the present cone of St.Helena may be less significant than the original due to subsidence (isostatic readjustments). Erosion will also have exerted an effect in reducing the height of the cone. Despite this effect the gravity data available for the area around St.Helena (Fig.2.4) indicate that a positive free-air gravity anomaly is retained, which is expected as the excess mass of the emergent volcanic pile on the crust still exists. Fig.2.4. shows that a moat configuration is still retained around St.Helena (c.f. Hawaii).

Fig.2.4 is of value in relating the St.Helena volcano to both past and present areas of plume activity in the area. The St.Helena cone appears to lie on a continuation of the Cameroon line, although the relationship is obscured by the E-W trending fracture zones that bisect the MAR. This relationship is consistent with the plate reconstructions of Morgan(1983) which suggest that the St.Helena plume may have previously existed beneath the volcanoes of the Cameroon line as shown in Fig.2.5.[3.1] Some supportive evidence for this is that it is thought that

Fig.2.4. Free-air gravity anomaly map offshore of Cameroon, Congo and Angola at a scale of 1: 8,000,000. The colour interval is in 5 mgal units ranging from ;

High (red-mauve): 70 mgal.

Low (blue) : 40 mgal.

Specific values cannot be attributed because of the confidential data of the onshore areas.

The points marked on the map represent subaerial volcanoes (V) or seamounts (marked by depth in metres). The volcanic island of St.Helena lies at approximately 16°S, 6°W.

°W 10 8 6 4 2 0 2 °E 4 6 8 10 12 14

°N 4 2 0 2 4 6 8 °S 10 12 14 16 18 20

Chain Fracture Zone

Ascension Fracture Zone

St. Helena Fracture Zone

Bioko V.

Mt. Cameroon V.

Principe V.

Soa Tome V.

Pagalu V.

AFRICA

ANGOLA ABYSSAL PLAIN

2380 m

2000 m

160 m

ST. HELENA

0 KM 200

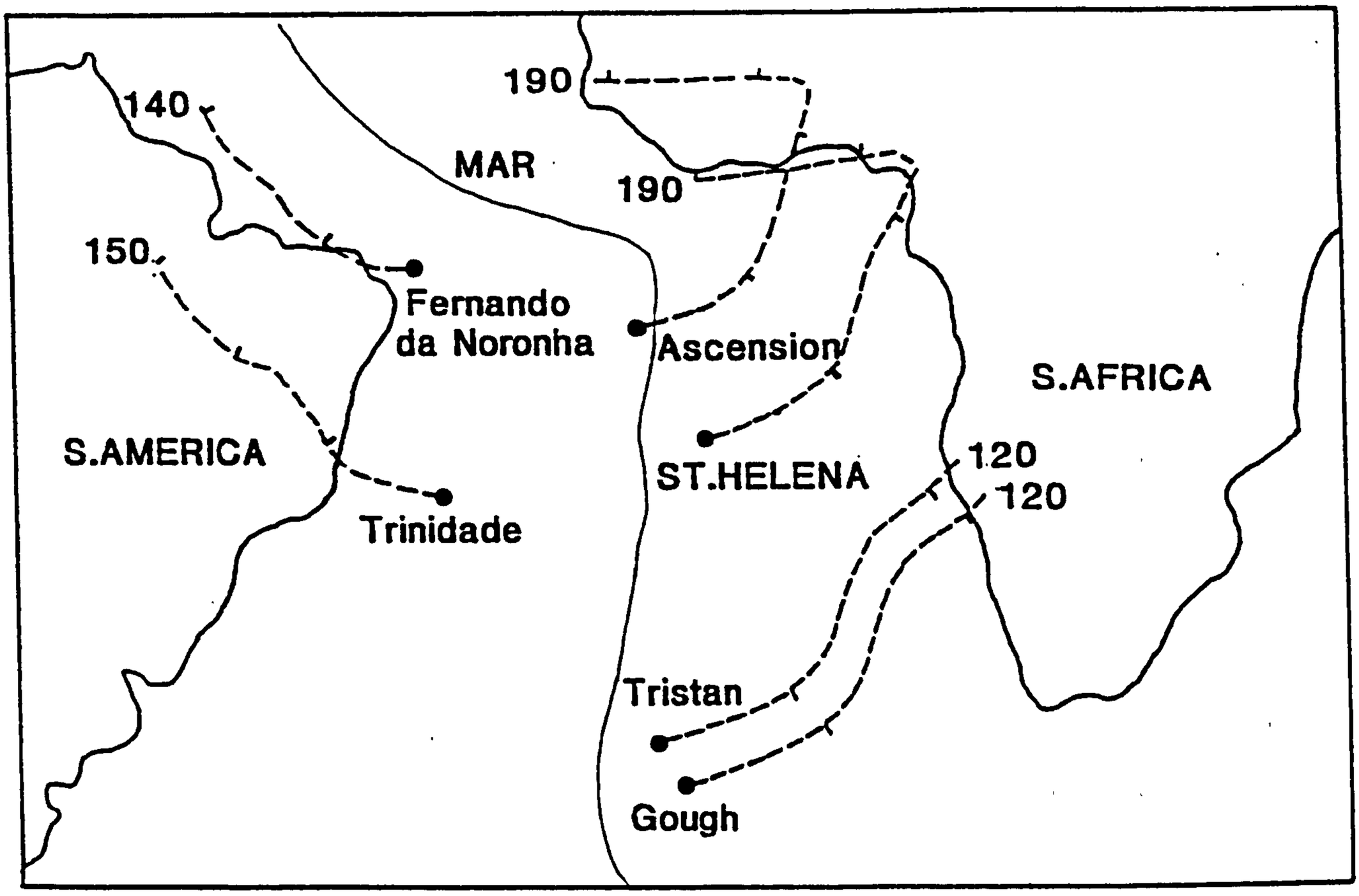

Fig.2.5. Predicted track for the St.Helena hotspot from the plate reconstructions of Morgan (1983). Other inferred hotspot tracks are shown for reference. Non-continuation after 100 Ma is due to transfer of track to other side of Atlantic. Tick marks are at 50 Ma intervals. Figure after Morgan(1983).

the lithosphere in the vicinity of Mt.Cameroon may possess similar geochemical characteristics to the SHRS (Halliday et al.(1988), section 7.5.3. This is consistent with the existence of the St.Helena plume in the Mt.Cameroon area 130 Ma ago (Halliday et al.(1986)). The two seamounts occurring to the W of St.Helena (Fig.2.4) indicate that the plume may have continued to be active subsequent to the cessation of subaerial activity on St.Helena. This suggests that the W to E movement of oceanic crust and lithosphere relative to a virtually fixed plume may have influenced the loci of volcanism on St.Helena. This is relevant as it may explain why volcanic activity on St.Helena transferred from a NE centre to a SW centre during subaerial activity (chapter 3). The implications for this occurrence on the geochemical variations observed in the SHRS are discussed in chapter 7. It should be noted that this interpretation is inconsistent with a hotspot track with a simple age progression (c.f. Hawaii) because some of the Cameroon line volcanoes are active at present (Halliday et al.(1986)). This may be because a line of weakness caused by the passage of the St.Helena plume has been recently reactivated.

In summary it may be stated that the limited geophysical data available for the environs of St.Helena are consistent with a long lived hotspot that caused the magmatism of the Cameroon line and St.Helena before forming the seamounts to the W of St.Helena. This is symptomatic of a virtually static plume coupled with significant relative movement of the lithospheric plates caused by the opening of the Atlantic.

CHAPTER 3

GEOLOGICAL RELATIONS : THE BASIS OF A CHEMOSTRATIGRAPHY :

3.1; Introduction;

In this section the geographical situation and physiography of St.Helena are described to provide a background to the problems of erection of a stratigraphy and sample collection. Previous research is outlined as a general introduction to the geology of St.Helena and to detail those modifications required by this new study. This is effected by the systematic description of the groupings of dykes and lava flows used in sampling the entire visible range of volcanics. It is necessary to justify the parameters used in the definition of the time framework, because elucidation of time related geochemical variations forms the basis of this study. These parameters are:

(1) Relative vertical position ("height") in the lava pile.

(2) Standard age relations such as the presence of unconformities and varying dyke frequencies within the volcanic structure.

(3) K-Ar geochronology :- The data of Baker et al.(1967) augmented by the data of this study.

3.2; Physiography;

The island of St.Helena is located in the South Atlantic Ocean between the latitudes of 15'54" and 16'01" S. It is approximately 800km E of the Mid Atlantic Ridge at longitude 5'37"-5'47"W. Africa lies 1800km to the E and S.America 3000km to the W (Fig.3.1). The island is remote, Daly(1927) noted that "with the exception of the still smaller Ascension island, St.Helena forms the only dry land in an area of 15,000,000km^2 or 3% of the Earth's surface". Ascension lies 1200km to the NW and Tristan da Cunha 2150km to the S (Fig.3.1). Bathymetric data (Emery and Uchupi(1984)) suggest that together with Bonaparte seamount it forms part of a linear volcanic chain normal to the Mid Atlantic ridge. This is also suggested by the gravity data discussed in section 2.5.

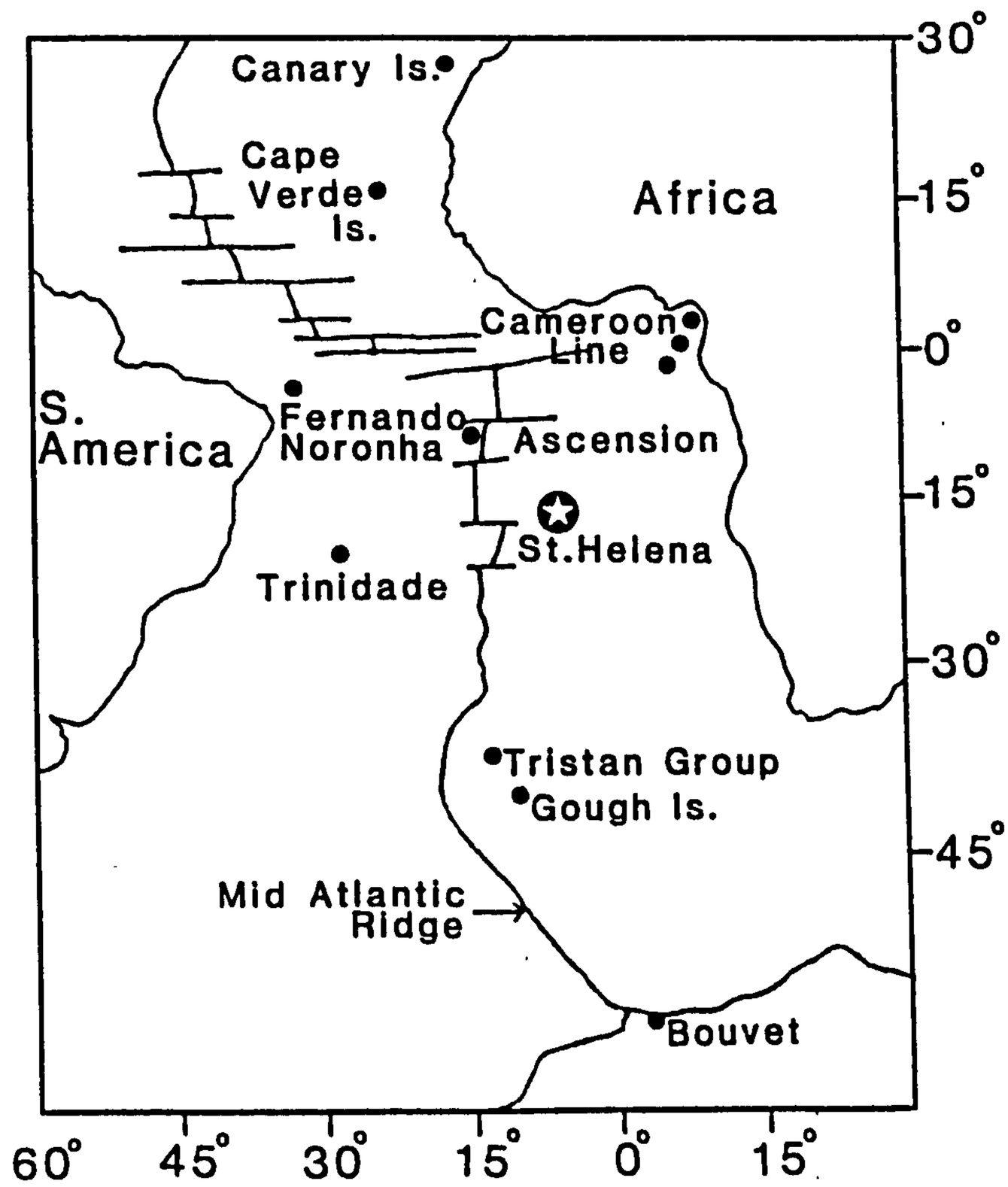

Fig.3.1. Location of St.Helena in relation to other S.Atlantic islands and the MAR.

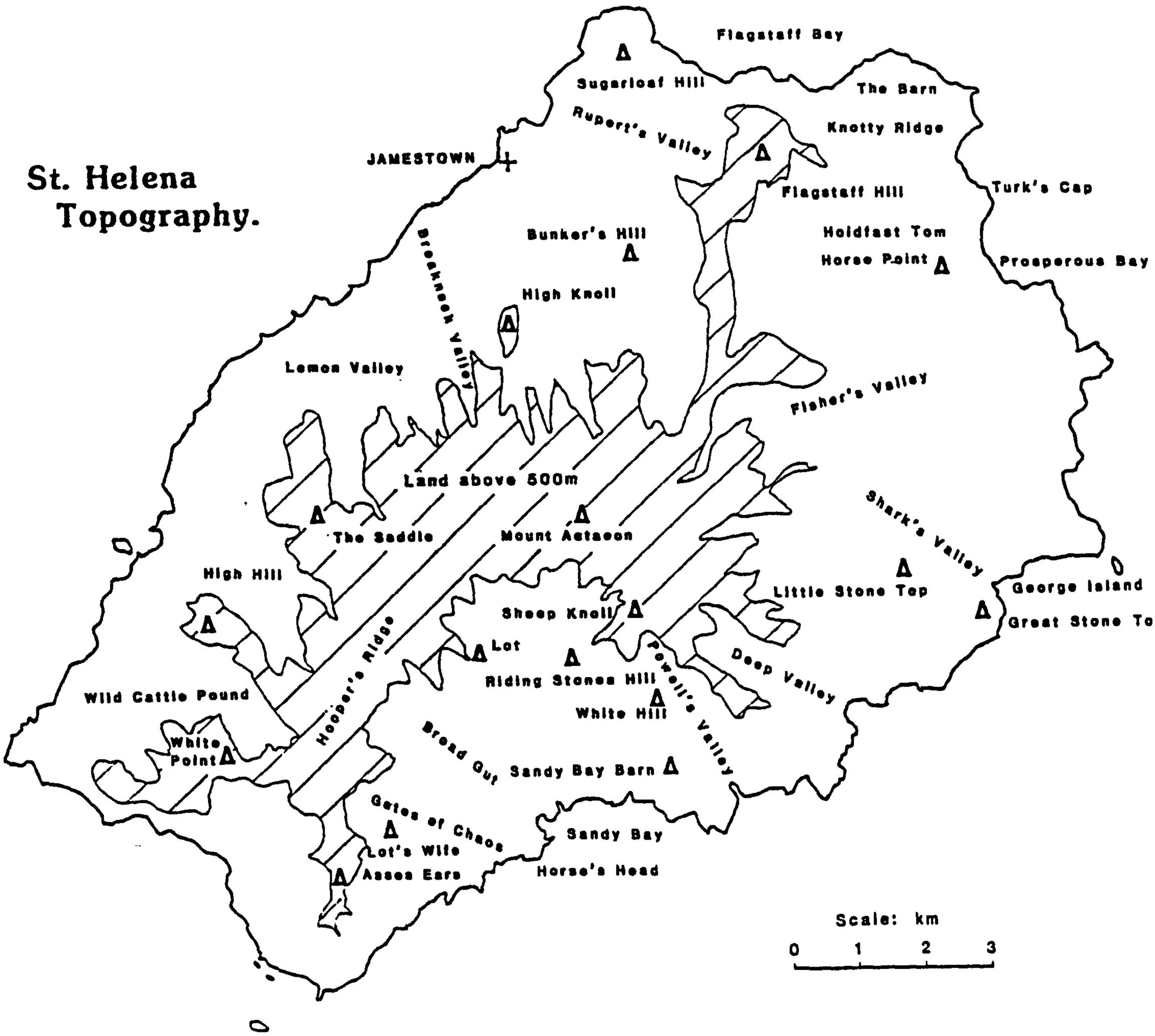

Fig.3.2. Sketch map of St.Helena showing principal place names used in text. An indication of the topography is given by the hachured region showing land over 500m. Hill tops are marked by triangles.

PAGE NUMBERING AS ORIGINAL

A topographic map of St.Helena is provided in Fig.3.2 with the place names referred to in the text for reference. This map is based on the 1:25,00 Directorate of overseas survey map DOS 360, G891. Within an area of 118km^2 there exists a great diversity of physical features. Precipitous cliffs girdle the coast of the island. Deeply incised, radiating stream valleys (Fig.3.3a) drain the central highland ridge, which runs approximately NE-SW (Fig.3.2). The suitability of a particular area for sample collection is largely governed by vegetation cover. This in turn is principally controlled by climate which is dependent on the distance from the coast and the height above sea level. Mean annual rainfall varies from 152mm in coastal regions (Jamestown) and from 762mm to 1016mm in the central hills (source : 1984 St.Helena Visitors' guide). The temperature in Jamestown varies from 14-32 °C in summer and 14-26 °C in winter, whilst it averages 5-6 °C lower in the hills. An equable climate occurs because of the island's position in the path of the SE trade winds. Owing to the dense cover of New Zealand flax (Phormium Tenax) above 600m sample collection was mainly restricted to the barren coastal zone, often colonised only by cacti. The deeply incised valleys and the erosional amphitheatres such as Sandy Bay permit sampling from various levels in the volcanic shield. Exposure is excellent in the peripheral zone although problems are posed by steep unstable cliffs (Fig.3.3a,b).

3.3; Previous research;

3.3.1; Previous volcanological research;

A succinct summary of early research is given by Mitchell-Thome(1971). One of the earliest descriptions of the geology of St.Helena was an anonymous publication of 1805. An early description was also provided by Darwin(1873,1876). This followed four days on the island during the homeward voyage of the Beagle in 1836. Darwin created a simple four fold division of basal submarine lavas, basaltic series (lavas and pyroclastics), feldspathic lava series and late phonolitic intrusives. He thought the erosional amphitheatre of Sandy Bay represented a caldera.

Fig.3.3a. The deeply incised 400m deep Shark's Valley which dissects lavas of the SWMS, SWUS and SWEF. View from Stone Tops Ridge (143320). The ease of collection from type sections is illustrated in this photograph.

Fig.3.3b. Unconformity between lavas of the NEMS in the upper part of Flagstaff Hill (low dyke frequency) and the underlying NEBB (high dyke frequency). Looking E from The Barn (139391) across the N-S striking dyke swarm to Flagstaff Hill).

An account of the geology was also provided by Oliver(1869) whilst he was serving as an artillery captain on St.Helena. This account is important as it includes the assertion that the dyke complex of The Barn and King and Queens Rocks are the oldest rocks on the island and formed part of a separate volcano. Younger feldspathic lavas of the east coast plateau and much of the high ground inland were thought to be from a different centre to the lower basalt flows. The Sandy Bay amphitheatre was again thought to be "a confused crater". Oliver described one major alkaline dyke from this area. The next geological account was given by Melliss (1875) as part of a general description of the island's topography, fauna and flora. Although a new map was produced, his interpretation of the geology followed that of Darwin and Oliver.

The first detailed work on the geology of St.Helena was undertaken by Daly during a five week stay in 1922. Daly(1927) promulgated the existence of two principal volcanoes; the older north eastern massif and the main massif centred in Sandy Bay. He further recognised the existence of the Knotty Ridge and Sandy Bay dyke complexes, but implied they were of the same age. Significantly, Daly believed that these areas showed that St.Helena *"appeared to be a composite volcano of the central type, but that the centre of eruptivity was of a considerable area, tensioned, cracked and periodically filled by lava moving up the cracks, and not the simple pipe of the text book."* He thought that the absence of a widespread superficial deposit around Sandy Bay mitigated against its origin as a crater. He used the fact that in detail the amphitheatre shape does not conform to the expected concave configuration to support this. The predicted shape of the volcanic cone is consistent with this because the occurrence of phonolites at 500m O.D. would indicate an unrealistic cone shape (the height of the caldera margin is also 500m) (Daly,1927). He also calculated by extrapolation that the cone giving rise to the main massif reached a height of over 1200m. Daly added to the detailed description of the volcano by demonstrating the existence of parasitic cones at High Knoll and the Saddle. The trachyte flow domes of The Stone Tops Ridge and Bencoolen were recognised as late, localised features.

The systematic mapping of the entire island was accomplished by Ian Baker in a nine month period in 1964/5. This work provided the basis for the present

study and has been found to be largely accurate. Baker extended Daly's findings and established a detailed stratigraphy which has required only limited modification by this author. Fig.3.4 shows a geological sketch map of St.Helena based on Baker's mapping. Fig.3.5 shows the stratigraphic divisions adopted in this study. *The abbreviations for each stratigraphic unit which are used throughout this study are given in Fig.3.5.* For ease of reference, they are also provided in the the list of abbreviations.

The conclusions of Baker(1968) are given here as a summary of previous conclusions on volcanic structure. The constraints placed on volcanic history by K-Ar age determinations are discussed further in section 3.7.

(1) Two subaerial volcanoes are identified. The oldest and smallest occurs in the NE, whereas in the SW a more large, complex shield is found. The approximate positions of the effusive centres may be recognised from Baker's determinations of the dips of lava flows (Fig.3.4).

(2) Both shields comprise predominantly basaltic lavas and scoria which are extruded from central fissure zones.

(3) The oldest rocks occurring in the base of the NE volcano are 400m of altered basaltic breccias intruded by contemporaneous and later dykes. The breccias are thought to be of submarine origin. These rocks are separated by an erosional unconformity from the earliest subaerial shield forming rocks, which are 800m in thickness. Parasitic activity is markedly subordinate . The most important cones are in the Bunkers Hill area where trachybasalt flows were extruded.

(4) The volcanics of the younger SW shield are divided into 3 main stratigraphic groups termed the Lower, Main and Upper shields;

(i) Lower shield

Baker created 4 stratigraphic subdivisions each of which comprised a quiet, effusive phase, followed by a period of explosive volcanism. The 4 main lava flow groups originated from vents in the Lot's Wife area. 17 possible scoria cones

Fig.3.4. Simplified geological sketch map of St.Helena. Geological boundaries after Baker(1988). The abbreviations used for the units in the text are given in Fig.3.5.

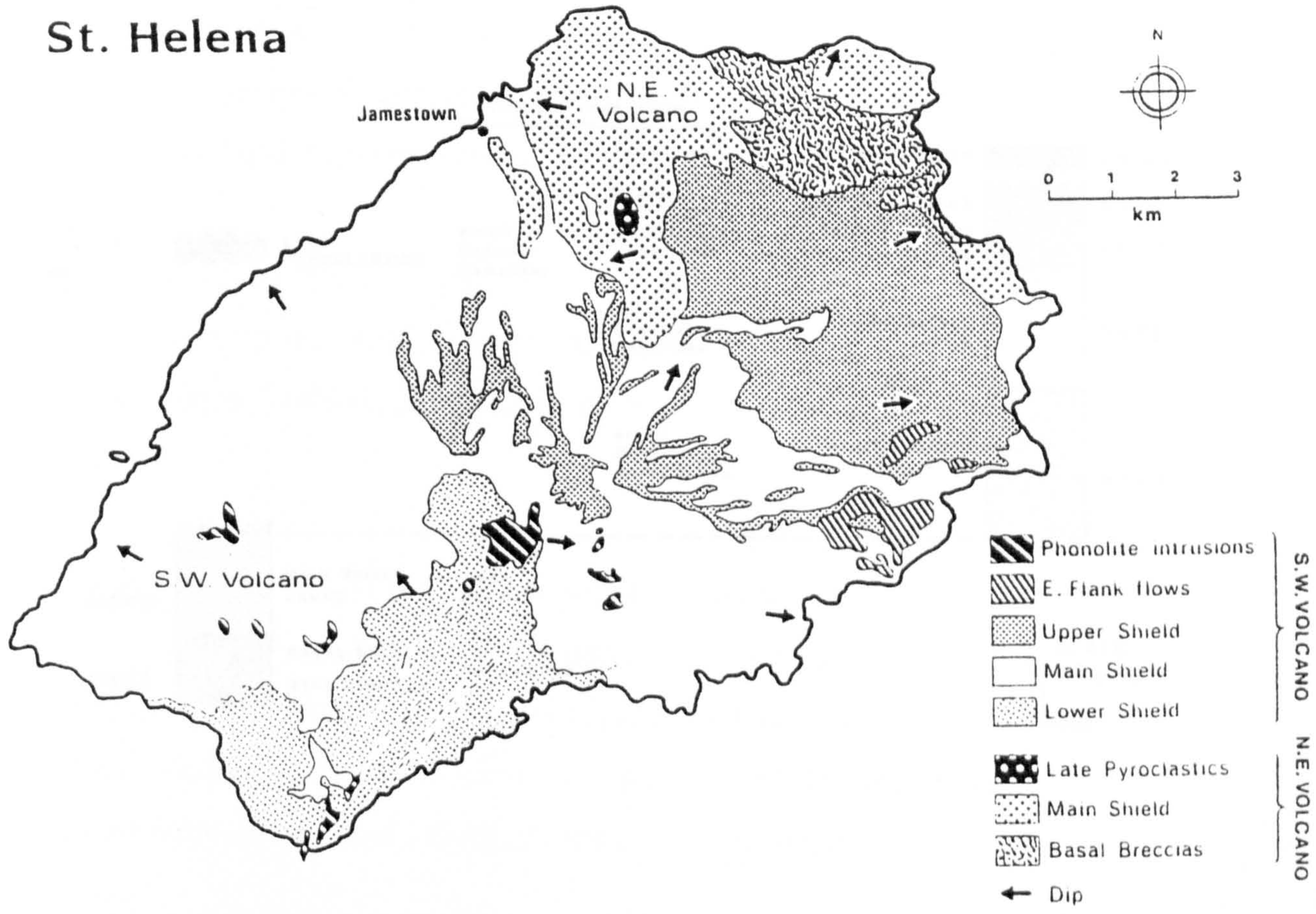

Fig.3.5. Stratigraphic divisions of the St.Helena volcanics. (after Baker,1968).

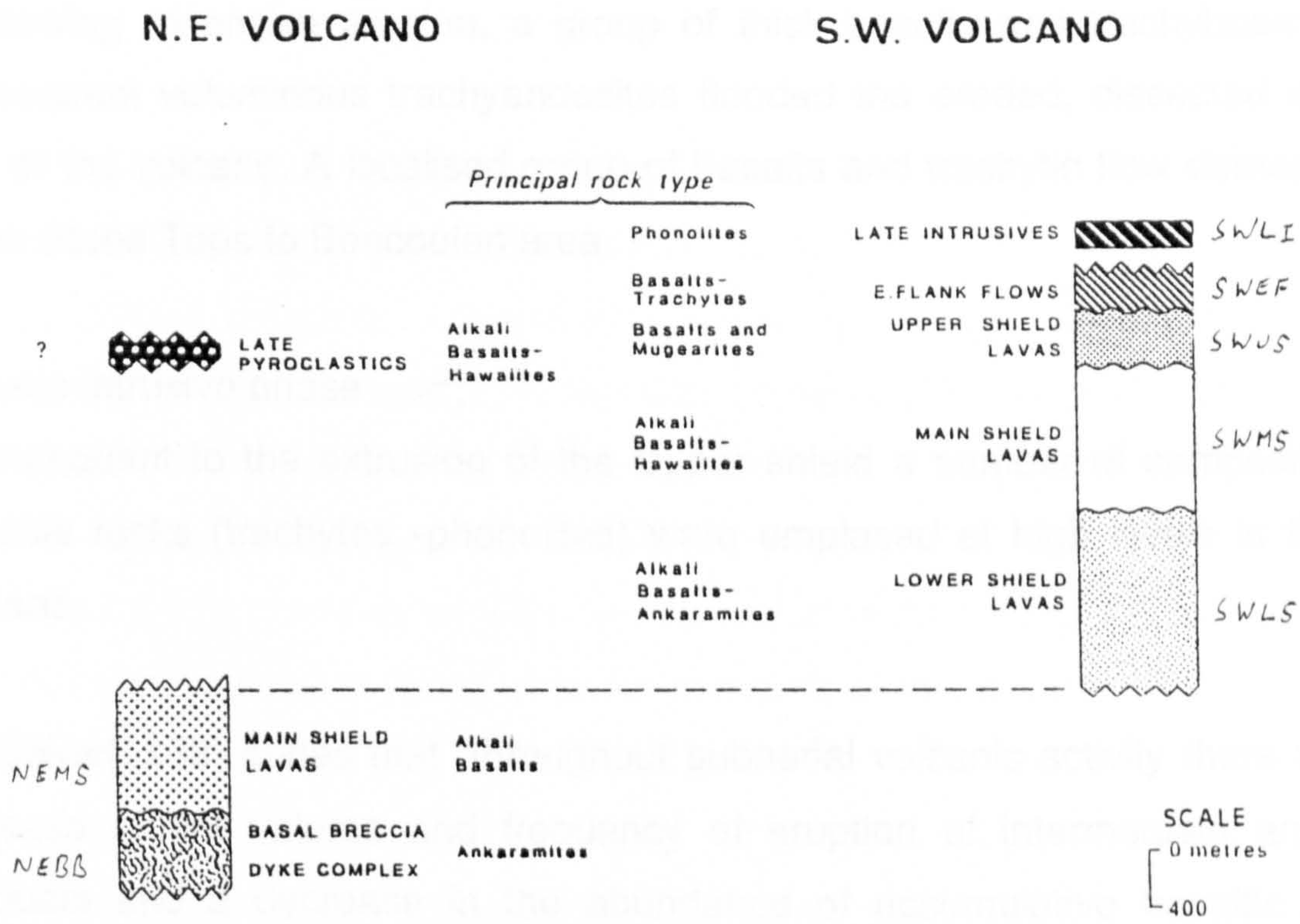

forming the explosive part of the cycle were recognised.

(ii) Main shield

The Main Shield comprises approximately 800m of lava and scoria deposits extruded from a dominant fissure system in Sandy Bay. A number of complex parasitic centres e.g. White Point, High Hill occur.

(iii) Upper shield

Following extensive erosion, a group of thick basalts and trachybasalts and subsequent voluminous trachyandesites flooded the eroded, dissected eastern part of the volcano. A localised group of basalts and trachytic flow domes occur in the Stone Tops to Bencoolen area.

(5) Late intrusive phase

Subsequent to the extrusion of the Upper shield a number of compositionally variable rocks (trachytes -phonolites) were emplaced at high levels in the SW volcano.

(6) Baker(1968) states that "throughout subaerial volcanic activity there was an increase in the volume and frequency of eruption of intermediate and salic products and a decrease in the abundance of accumulative basaltic rocks". *Overall abundances are estimated to be 70-80% basalts, 15-20% trachybasalts, 4% trachyandesites and 1% trachytes and phonolites.*

3.3.2; Previous geochemical research;

Previous geochemical research on St.Helena can be divided into major element studies specific to the island and more recent studies using trace element and isotopic data to place St.Helena in a regional context. The results of the first category of geochemical research are given here to to provide a background to the present study. Regional studies are discussed when considering the ramifications for St.Helena source characteristics (chapter 8).

The initial studies of the St.Helena volcanic suite described in the previous section were largely concerned with volcanic structure. Darwin(1876) did, however, note the existence of basaltic and feldspar phyric lava types. The first analyses of fresh specimens were performed by Daly(1927). Analyses of six

basalts showed them to be *mildly nepheline normative olivine basalts.* Five trachytes and phonolites were also analysed.

The first comprehensive geochemical work based on a large sample set was conducted by Baker(1968). He made the following observations from major element analyses and petrographic study of eighty rocks. These serve as a summary of what was previously known of the geochemistry of St.Helena volcanics.

(1) The volcanics formed a gradational suite of *basalt-trachybasalt-trachyandesite-trachyte-phonolite* (terms of Le Maitre(1962)).

(2) St.Helena volcanics are *mildly alkaline* - analyses lie above the line separating Hawaiian alkalic from tholeiitic rocks(MacDonald and Katsura,1964) and below the line separating mildly alkaline from strongly alkaline, ne bearing rocks of Tanganiyka (Saggerson and Williams,1964).

(3) The parental basalt is an *alkaline olivine basalt containing 4% normative ne.* Parental composition in terms of major elements is thought to be constant over 6.5 Ma.

(4) Variation diagrams of element abundance versus Thornton-Tuttle Differentiation index (DI) Baker(1968), Figs.33-42, p.297-306) and AFM diagrams (Fig.32, p.296) show clearly defined fractionation trends. Trace element data are insufficient to give a full description of all fractionating phases. Plots of DI versus time for rocks of known stratigraphic position (Fig.43,p313) show a slight overall increase in the degree of differentiation throughout the succession for the NE volcano. Variations are more complex for the SW volcano.

(5) The most undersaturated rocks are trachytes to phonolites of the SW volcano which are thought to have been formed by diffusion related processes in a high level magma chamber.

3.4 A revised stratigraphy;

3.4.1; The North Eastern volcano

The NE volcano was divided into a basal breccia and an overlying main shield by Baker(1968). A nebulous transition zone is also identified. Baker analysed only 3 samples from the NE volcano. As the lavas of the NE main

UNIVERSITY LIBRARY LEEDS

shield are of a similar thickness to the SWMS (Fig.3.5) this volcano merits more detailed study. Owing to major disagreements with each of Baker's units and the geochemical significance of these units, this volcano is discussed in some detail.

3.4.1.1; Basal breccia dyke complex *(NEBB);*

The oldest rocks exposed on St.Helena are found in a limited area between Flagstaff Hill and The Barn (Fig.3.2). The main fabric element in the landscape is the striking array of linear dykes striking approximately N-S (Fig.3.3b).

Owing to the high proportion of dykes (Fig.3.3b) together with the susceptibility of the breccias to alteration and erosion, only a limited number of samples could be collected. Fresh samples were only collected at Turks Cap Bay (G.R.1824 3831). The breccias, where exposed have an unstratified, poorly sorted nature. The clasts are subangular and vary in size from 30cm diameter to over 2m in diameter. The rock fragments vary from ankaramites to aphyric basalts. The samples collected in Turks Caps Bay were classified by Baker as part of the main shield. This is disputed on the following field evidence;

(1) The rocks in the Turks Cap Bay exposure are stratigraphically lower than any pyroclastics of the NEMS by more than 100m. Hence it would be necessary to infer the presence of a paleo valley for which there is no independent evidence.
(2) Stratification is not evident in the Turks Cap Bay breccias, whereas the basal NEMS pyroclastics are frequently sorted.
(3) Large diameter composite blocks of breccia > 1m diameter are not seen in the NEMS series.
(4) Dyke frequency is too high for these rocks to be part of the NEMS : many thick ankaramite dykes are truncated at the major unconformity of the NE volcano (Fig.3.3b) (Some of which cut across the Turks Cap Bay exposure).

Dykes of the basal breccia dyke complex *(NE(BB));*

The main orientation of these dykes is N-S (Baker(1968) Fig.5a,5b,p.30). During the emplacement of this dyke suite a large amount of extension has clearly occurred. In two traverses Baker measured no country rocks although exposure was better than 50%. This is partly the result of the way in which the

breccias are preferentially eroded to leave talus. Such extension is consistent with this area being the feeder zone to fissure volcanism. Baker recognises two principal dyke types: *"...regular and comparable to dykes seen elsewhere on the island or thin irregular, sinuous, highly altered with thin glassy margins" (Fig.3.6a).* Whilst broadly agreeing with Baker's two fold division of dykes significant, additional points must be made:

(1) It is suggested that a more useful subdivision of these dykes is one based on the nature of the contact i.e. glassy or non glassy. This is because the glassy margined dykes are not exclusively narrow and sinuous.

(2) Glassy margined types are slightly more susceptible to alteration. It will be demonstrated in chapter 7 that these dykes are also geochemically distinct from NEMS lavas which corroborates the field evidence.

(3) Ankaramite dykes are commonly truncated at the unconformity at the base of the NEMS, whereas many of the glassy margined dykes continue into the basal NEMS. This suggests that the two dyke varieties may have been emplaced during different time intervals.

3.4.1.2; The Main shield *(NEMS);*

The basal 400m of the NEMS were termed the transition zone by Baker. This is thought to be a misnomer because there is a clear discontinuity at the base of the NEMS for the reasons given in section 3.4.1.1 (Fig.3.3b). The lower 400m of the NEMS is, however, different in character from the remainder in that pyroclastics dominate at lower levels in the shield. In addition, glassy margined dykes (section 3.4.1.1) decrease in frequency upwards through this 400m section and were not found above this point. This suggests the presence of an unconformity between the lower parts of the shield in which pyroclastics dominate and the upper part where the situation is reversed. Because these sections were exposed in 300m high cliff sections, it was not possible to readily identify a single major unconformity similar to that separating the NEBB from the NEMS. A number of minor temporal discontinuities are indicated by the truncation of the glassy margined dykes at various levels.

Fig.3.6a. Typical dyke relationships in the NEBB. 50cm thick ankaramite dyke (note 1cm diameter cpx phenocrysts) is crosscut by a sinuous, narrow (10cm) dyke with a glassy margin. Locality; nameless valley below Knotty Ridge (128375).

Fig.3.6b. Typical shield sequence of NEMS. Thin (less than 1m) aphyric basaltic lava flows interleaved with basaltic scoria flows. A discontinuous layer of red coloured pyroclastic tuff is also evident. Locality; coastal section between Rupert's Valley and Bank's Valley Bay (093392).

The remainder of the shield possesses a predominance of lava flows over pyroclastics. Fig.3.6b is a typical shield section. Owing to the limited area of the NEMS cross correlation between the various collection areas i.e. Rupert's Valley and Flagstaff Hill to the Sugarloaf was possible. Approximately 800m of volcanics are exposed. Sampling is biased towards the lava flows because of the altered, heterogeneous nature of the pyroclastics.

3.4.1.3; Late pyroclastics (NELP);

In Upper Rupert's Valley relict basaltic lava flows intercalated with dominant pyroclastics occur. These rest unconformably on an erosion surface cut into the NEMS which is inclined at an angle of up to 45 degrees. Baker considered these rocks as part of the NE volcano because of their areal distribution. He stated, however, that "the material is obviously very much later than the shield-forming series...". Further, he stated that "the eroded surfaces on which these basaltic, highly vesicular extrusives were deposited show that Rupert's Valley was already deeply incised.... The existence of this early Rupert's Valley (a sub-radial valley to the SW volcano) suggests that the South Western shield was largely completed before the extrusion of the late north-eastern scoriaceous flows". The present author concurs with these straightforward conclusions. Owing to the difficulty in placing these volcanics in relation to other stratigraphic units great emphasis is not placed on these samples. K-Ar determinations were not possible due to the ubiquitous alteration in these volcanics. However, it is demonstrated in chapters 7 and 8 that these samples possess a close affinity with the SWUS. Thus, these samples are grouped with the SWUS. This is consistent with the interpretations of Baker that the radial relationship of Rupert's Valley to the centre of effusive activity for the SWMS indicate the NELP are erupted after the SWMS.

3.4.1.4; Summary - Temporal groups of the NEMS;

Field study of age relations in the NE volcano dictated that sampling was directed at the following groups in the NEMS:

(1) Basal breccias (NEBB).

(2) Dykes cutting NEBB, but not upper parts of NEMS. (NE(BB)).

a; Non-glassy margined ankaramites cutting NEBB only.

b; Glassy margined types cutting NEBB and lower 400m of NEMS.

(3) Fragments from pyroclastics of bottom 400 m of NEMS.

(4) Flows of main shield (NEMS).

(5) Late dykes cutting high levels in the NEMS (NE(MS)).

3.4.2; South Western volcano;

The logical subdivisions of the SW volcano into Lower, Main and Upper shields by Baker(1968) is retained. This classification is based on the occurrence of unconformities of high topographic irregularity. In addition many dykes are truncated beneath the SWMS. A significant shift of effusive centre is also indicated for the SWUS by different foci of the radially distributed dip directions (Baker,1968).

3.4.2.1; South West Lower Shield *(SWLS);*

In marked contrast to the the NEMS, the greater number of clearly defined unconformities in the SWLS enables detailed subdivision of the lava flows which were erupted over a period of 1 Ma (Baker et al.(1967)). Baker mapped four groups of lava flows alternating with four groups dominated by pyroclastics. The units are described in detail by Baker (1968), p51-66. Whilst these are useful mappable units they are unsuitable for placing samples in a time framework. This problem arises because of the large number of scoria cones (Baker suggests over 30) which have given rise to large but variable thicknesses of tuffs and agglomerates. These pyroclastics obscure relations between flows, and thus localised flows may be unrecognisable (e.g. Fig.3.7a). The use of some of Baker's units is therefore inappropriate for this purpose. This is particularly true for the Sandy Bay Series which although containing local pyroclastic flow units must correlate with the Man O'War to Lower White Rocks Series (Baker(1968). The approach taken to overcome this problem was to collect samples at a regular vertical interval from a well exposed section typical of a particular area. By this means a good representation of variations within a certain part of the SWLS, spanning several of Baker's groups is possible. Cross correlation is not valid because of the unknown extent and overlap of local flows. Areas were

Fig.3.7a. Shield section illustrating the problem of cross correlation between lava flows. A red pyroclastic (tuff) unit of variable thickness occurs in the centre of the picture. Photo taken off Egg island (030332).

Fig.3.7b; The view E from The Saddle (058347) towards Flagstaff Hill (far distance) shows the typical dip angle of the lava flows of the shield volcanoes. The uniform dip of the SWMS flows is disrupted by the parasitic cone of High Knoll (middle distance).

chosen in which pyroclastics were of limited importance. In addition to these pyroclastic flows being mostly local, pyroclastics are heterogeneous in age and composition and often highly altered.

The following type sections were established (Fig.3.2):

(1) Horses Head to Sandy Bay Barn area.

(2) Lot's Wife ridge area.

(3) Upper Broad Gut.

(4) Gates of Chaos - White Ridge- Horse Ridge.

3.4.2.2; South Western Main Shield *(SWMS);*

Baker et al.(1967) showed that the 800m of the SWMS were erupted in a similar period (1Ma) to the SWLS, yet Baker(1968,1969) did not attempt a subdivision of the SWMS. Subdivision is difficult because the SWMS covers a larger area than that occupying the SWLS, and is not so deeply dissected. The upper flows of the SWMS that have not been eroded define a typical low angle shield volcano profile, with parasitic cones occurring on the flanks (Fig.3.7b). Flows from parasitic centres again cause problems in correlation (Fig.3.7a). The method of collection for the SWMS is accordingly similar to the SWLS. Type sections were established in the following areas and samples collected about every 50m ((Fig.3.2)). These were:

(1) Powell's Valley(lower to middle SWMS)

(2) Lemon Valley to Breakneck Valley area (middle to upper flows)

(3) Local flows of White Hill.

3.4.2.3; South Western Upper Shield *(SWUS);*

Collection proved relatively easy in this group because of the limited number of flows which are clearly separated. A maximum number of eight underlying basalts to trachybasalts and four thicker overlying trachyandesites are seen in the Fishers Valley to Turks Cap section. For ease of description these units are formally named the Fisher Basalt Formation and the Tom Trachyandesite Formation.

3.4.2.4; Eastern Flank flows *(SWEF);*

These units also proved easy to sample due to their overlying unconformably the SWUS flows. These comprise the trachytic flow domes of the Great Stone Tops and Bencoolen and a localised group of basalt flows. The 80m thick group of basalt flows occurring SE of Bencoolen does not relate to flows elsewhere on the island as they are the only basalts extruded above the SWUS. These are termed the George Island Formation.

3.4.3; Relationship between lavas and intrusives;

3.4.3.1; Minor Intrusives;

The importance of dykes in the lower parts of the NE volcano have already been discussed (section 3.4.1.). The non glassy margined dykes appear to act as fissure feeders to flows that have been subsequently removed by erosion. Hence the dykes are the only means by which the early phase of activity can be sampled. In terms of petrography both early and late phase dykes were seen to be homogeneous and ten samples of each were taken to characterise them. All dykes in the NE volcano strike approximately N-S in contrast with the SW-NE strike of dykes from the SW volcano. The two dyke sets are also thought to be unrelated because the dykes of the NE volcano do not bisect the flows of the SW volcano (i.e. restricted to NE volcano), hence the the N-S striking dykes must be older(Baker(1968)).

The dyke complex of Sandy Bay was not extensively sampled because the dykes are geochemically equivalent to the lava flows of the SWLS and SWMS which they clearly feed. Conversely, the dykes intruding the NE(BB) are seen not to feed flows (these have been eroded).

3.4.3.2; Major intrusives;

A group of arcuate to pipe like late alkaline intrusives are included in this division. The discontinuous sets of NE-SW trending dykes (Fig.3.4, 3.8) are clearly related to these and they are considered together. The youngest rocks into which major bodies penetrate are at medium to high levels in the SWMS (Sheep Knoll intrusion G.R.1052 3102). Radiometric data were thought, however, to indicate that the "majority of these intrusions are later than all other

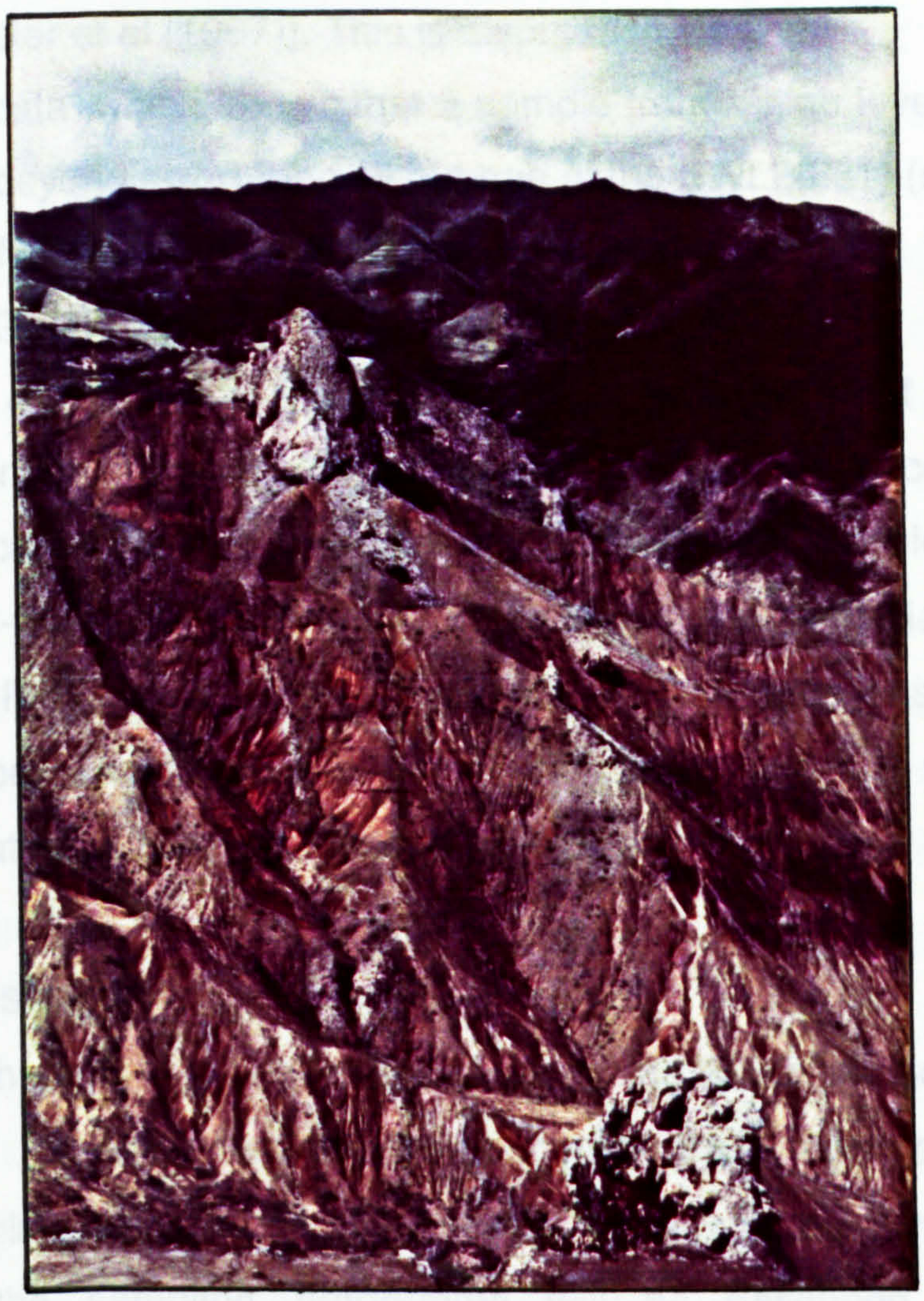

Fig.3.8. The chaotic terrain of the deeply dissected SWLS. The phonolite monolith of Lot is one of many discontinuous dykes intruded into the SWLS. View from 082302 (nameless ridge between Broad Gut and Sandy Bay valley) towards Mt. Actaeon. Lot is approximately 60m high.

major volcanic activity and may be separated from the late lavas by a marked time interval" (Baker et al.(1967)). This is disputed in view of:

(1) Radiometric data which shows that a sample from a high level in the SWMS (78) is younger (beyond error) than all but one of the SWLI (281) (section 3.7).

(2) Truncation of certain highly alkaline dykes by the overlying SWMS (e.g. in Powell's Valley, G.R.1159 3009).

(3) Continuation of dykes in a NE direction might be expected if the SWLI were significantly younger than the SWMS flows; this does not occur. These age relations are discussed further in considering the K-Ar geochronology.

Earlier pipe-like basic intrusions are also found. These are largely restricted to the Hoopers Ridge to Blue Point area (Fig.3.2). A large basic body is also found in the upper Broad Gut area. These intrusions are found within SWLS to SWMS rocks, but no age determinations have been made.

3.5; Sampling strategy;

Details of the 240 samples collected during the 1986 field season are given in Appendix A. Fig.A1 shows the distribution of these samples. The factors governing sampling will be considered from two respects. Firstly, the overall objectives of the sampling programme will be described. Secondly the extraneous factors which restricted sampling to a certain area or rock type will be considered. In accordance with the aim of the project, sampling was principally directed to primitive rocks. These samples were identified on a field basis because they are rich in olivine and pyroxene phenocrysts, whilst plagioclase is restricted to the groundmass. These rocks are clearly least affected by crystal fractionation processes and hence may represent the primary magma composition most closely. The limits used to define the most primitive rocks and the reasons for their use in describing source characteristics are discussed at greater length in chapters 5, 6 and 7. The primitive samples were collected to be fully representative of the entire duration of subaerial activity on St.Helena. This was achieved by using the stratigraphic groups established by Baker(1968) to divide the lava pile. Reassessment of the validity of this subdivision was conducted prior to this and has been discussed earlier in section 3.2. The sampling frequency was governed by the duration of activity of any particular

group as revealed by the K-Ar age determinations of Baker et al.(1967). Hence ideally the lavas of the NEMS which were erupted over a period of 3 Ma should produce a larger sample set than the volcanics of the SWLS which were erupted over a period of approximately 1Ma. Other factors, however, affected this sampling strategy. It was found for example that the SWLS contained a greater number of primitive flows than the NEMS, hence it is was more useful for showing source variations and with a higher resolution than the NEMS. The following extraneous factors were found to adversely affect the stated aim:

(a) Exposure;

This did not present a major problem as exposure was high in the non - vegetated perimeter of the island (Fig.3.3a,b) in which, with care samples representative of each group could be obtained. It is apparent from Fig.A1 that the majority of samples were collected from the peripheral zones.

(b) Access;

Cliff faces up to 400m high and unstable scree slopes presented problems in most areas, but these only proved insurmountable in the lower parts of the NEMS, which was largely restricted to pyroclastics (Fig.3.3b).

(c) Post-eruptive alteration;

Surficial alteration was a major problem owing to the climatic conditions which are conducive to intensive weathering. Normally the use of a 5 Kg sledgehammer removed the surficial weathering veneer. Pervasive alteration of rocks occurred in some some areas. This manifested itself as closely spaced fractures filled with alteration products together with zeolitisation. This problem was more difficult to overcome because a high proportion of the volcanics contained a small percentage of zeolites (usually < 3%). In these areas, lavas containing the smallest percentage of zeolites, together with the least mineralogical signs of alteration, were collected. Olivine was found to be the most useful field index for alteration as this was the most susceptible ferromagnesian mineral. A crude field terminology based on these factors was used to enable consideration of this problem on return from the field. This

classification which is applied to the samples is listed in Appendix A.

F - Fresh

Both olivine and pyroxene fresh, zeolites<<1%.

MF - Moderately fresh

Olivine showing signs of alteration (Not vitreous), pyroxenes fresh, zeolites approximately 1%.

MA - Moderately altered

Olivine completely altered to iddingsite and serpentine, pyroxene slightly altered (still vitreous), Zeolites>1%.

A - Altered

Olivine and pyroxene altered, Zeolites>>1%.

Owing to the number of rocks that were slightly affected by alteration processes, but by necessity had to be collected to represent a certain stratigraphic division, this problem is discussed in detail in chapter 5. It is shown that field criteria are a poor discriminant of samples with anomalous chemistry. The chemical variations induced by alteration and methods for filtering out such variations are considered. A number of altered samples were collected to show the maximum variation caused by this process.

(d) **Crystal fractionation processes;**

In certain stratigraphic units, particularly towards the top of the NEMS, SWMS and SWUS it was found that evolved compositions such as trachytes predominated. In these instances it was necessary to collect evolved rocks which could be corrected for crystal fractionation processes to give parental compositions prior to this process. Such samples were still valid for isotopic determinations. Sampling was, however, biased to units which contained a higher proportion of primitive compositions.

A large number of evolved rocks were collected from the Late Intrusives of the SW volcano. These rocks had been shown by Baker(1968) to be related by crystal fractionation processes and were thought to be a suitable case study for modelling fractionation processes. Anomalous $^{87}Sr/^{86}Sr$ ratios had also been

reported for these rocks by Grant et al.(1976) and this warranted further investigation to determine whether this was caused by high level processes.

3.6; Representation of the stratigraphy;

In the above sections it has been shown that it is relatively easy to create a time framework in which to place the St.Helena volcanics. In this section the methods used to portray the geochemical variations within the lava pile are described. The fundamental problems of placing a particular sample at a particular height in the succession are discussed as a guide to the accuracy of this method in portraying variations effectively.

The method of portraying geochemical variations with time is to place the samples relative to one another in a number of stacked sections (e.g. Fig.4.18). The individual type sections are those described above in section 3.4, which are defined according to major erosional unconformities. Within each section samples were placed at a particular height by measurement of their relative positions within the group. K-Ar age determinations are given for specific positions within the lava pile to indicate the time span of activity, but linear interpolations are not given as these will not be valid. Stratigraphic heights are not directly proportional to age because of the episodic nature of volcanicity.

It is immediately apparent that in trying to produce quantitative stratigraphic divisions major problems are presented by the nature and products of a volcano. The heterogeneous nature of activity, with many minor parasitic centres, produces variable thicknesses of volcanics (Fig.3.6a). Pyroclastics are particularly important in this respect. As mentioned above (section 3.4.1), the approach taken to overcome this problem was to establish a number of type sections such as the 400m + type section in Powell's Valley. These type sections are then placed in the appropriate position within a particular stratigraphic group, which is represented by its maximum thickness on the island , as calculated by Baker during his detailed mapping. Problems of cross-correlation between type sections were overcome by choosing type sections which abutted on the upper and lower boundaries of a particular stratigraphic group.

Construction of sections;

The thicknesses of sections were calculated by collection of samples from heights established by an altimeter in conjunction with 1:10,000 scale maps. Average regional dip values and standard trigonometrical constructions were then used to calculate strata thickness.

Two different classes of problem in constructing sections from this information may be identified. Firstly, there are the physical problems of the measurement of the height of a sample and relating it to other samples. Secondly, there are the problems of attempting to represent laterally heterogeneous thicknesses by a single section which have been discussed above. The height of each sample above sea level is likely to be accurate to within ±10m by the use of a barometric altimeter in conjunction with the relationships between contours and physiographic features on a 1974 compilation 1:10000 map (DOS 260). The altimeter was reset to a known height each morning and pressure variations were limited throughout the day because of the climatic situation. Thus the height from which samples are collected is one of the better constrained parameters. The main problems arise from the calculation of vertical stratigraphic interval between samples. This is dependent on the dip and strike of the lava flows which are difficult to measure because of the low angle of dip and very irregular dip surfaces. These problems were minimised by averaging the localised variations in lava flow geometry by using the regional dip values of Baker(1968). The error in dip angle is of a larger magnitude and of greater significance in producing errors than that of measuring the height of a sample but cannot be quantified. The overall error is, however, minimal in comparison with the scale on which the variations are portrayed (e.g. Fig.4.18.) and the vertical differences between samples (50m on average).

Despite these problems and the fundamental geological problem of establishing one section to represent a number of laterally different sections, it may be stated that the important feature of this method is that the relative positions of samples is assured and a good representation of the overall thickness of one unit in relation to another is given.

3.7; K-Ar geochronology;

Radiometric age data obtained using the Potassium Argon method by Baker et al.(1967) provided an initial time framework for the stratigraphic divisions described above. Baker et al.(1967) analysed 23 samples from all the main shield units of the volcanoes and the SWLI and produced adequate constraints on the duration of subaerial volcanic activity on St.Helena. These data are summarised in Fig.3.9 with respect to the principal divisions of shield activity. In order to provide more detailed constraints on the stratigraphy, additional K-Ar determinations were undertaken at Leeds University by D.C. Rex. The method is described in Briden et al.(1979). The first new determinations were initially undertaken to provide information on intermediate shield positions to those of Baker et al.(1967). It was found that these ages were not consistent with Baker's results (Fig3.9). Consequently, because of the importance of K-Ar dates in producing age corrections for radiogenic isotopes, a more detailed study was initiated.

The new data are broadly consistent with the old data regarding the cessation of activity. SB 281 (6.8±0.4 Ma) is in good agreement with SC 149 (7.0±0.28 Ma) and SC 103 (7.26±0.29 Ma). A larger discrepancy occurs regarding the initiation of subaerial activity. The oldest age determination by Baker et al.(1967) yielded 14.5± 1.0 Ma, 14.0±1.0 Ma (two separate determinations on SB 679 from the base of the NEMS). The sample with the lowest estimated stratigraphic position measured in the present study gave 8.7±0.3 Ma (SC 68). This sample, was, however obtained from a dyke in the NE(BB), which is truncated by the overlying NEMS (Fig.3.3b), so it would be expected to give an older date than SB 679. This could be explained by SC 68 undergoing argon loss in a subsequent dyke intrusion event to give an apparently younger age. Evidence for this is that SC 28, a lava flow at a higher level (in the NEMS) has a similar age (8.81±0.35 Ma) to SC 68. It seems likely, therefore, that SC 68 has suffered thermal resetting in the event that produced the late dykes of the NEMS and cannot be used to infer the age of the NE(BB).

No samples considered fresh enough for K-Ar determinations were collected between samples SC 28 and SC 68 because of alteration and poor

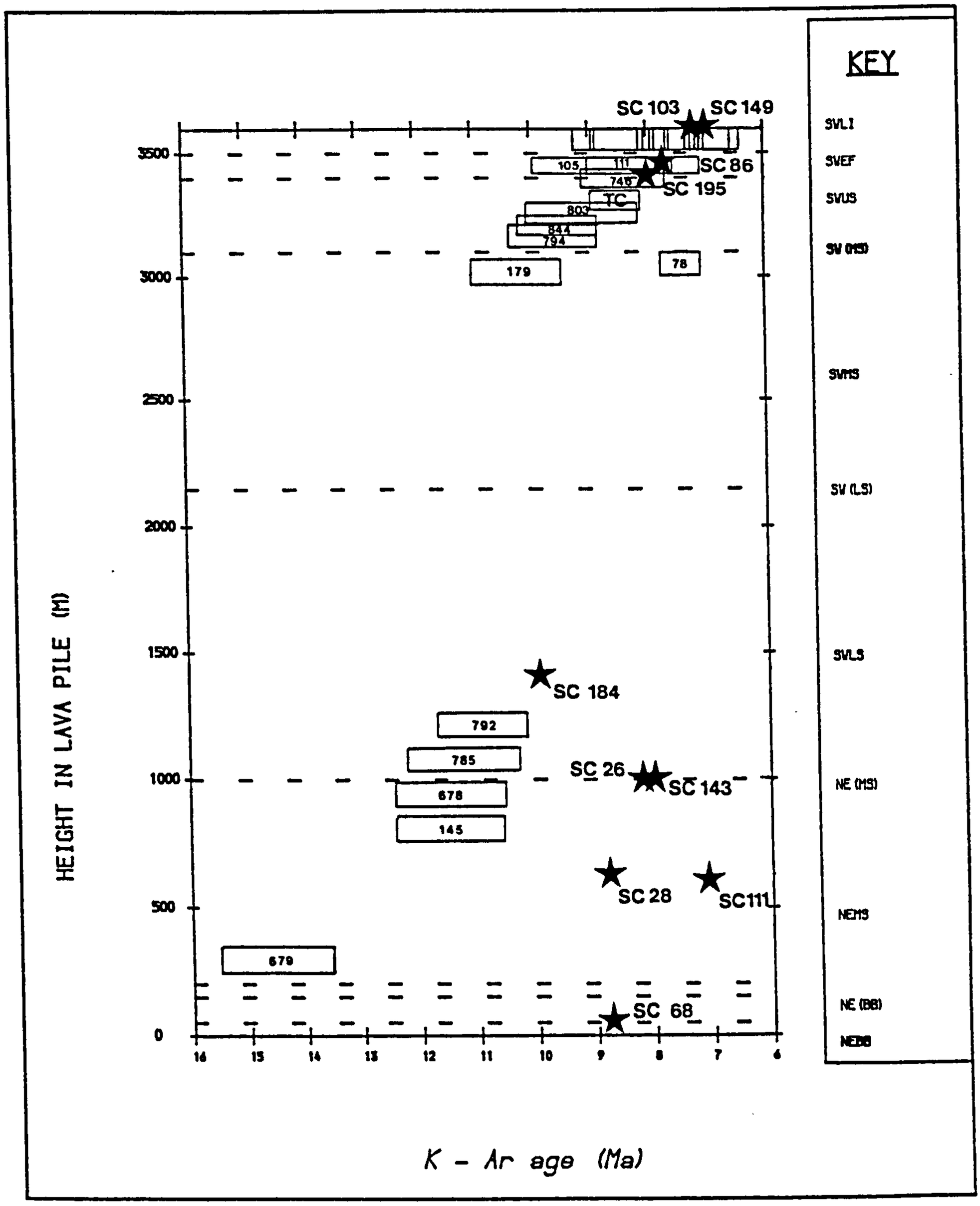

Fig.3.9. Comparison of the K-Ar data of Baker et al.(1967) and the data of this study. The data of Bakers study is denoted by rectangles with an x- dimension given by the error bar of the age (Ma). The vertical side of the box indicates that the exact position of Baker's sample in the age framework of the present study is not known. Sample numbers within the boxes are Baker's. Determinations given by asterisks are from this study. These are accurate to 3-4% D.Rex pers.comm.

exposure (unstable cliffs). The locality at which Baker collected SB 679 was visited, but only sand was evident in this area. It is noted that SB 679 sample appears anomalous in the original K-Ar age compilation of Baker et al.(1967), because it implies a much lower extrusion rate for the 800m of the NEMS than the shield of the SW volcano. There is no field evidence to suggest that the style of shield activity was different at this time. It is also thought that the age indicated by SB 679 is unreliable because comparison with other data from the NEMS (Fig.3.9) show that the the samples analysed by Baker et al.(1967) yield consistently lower ages than those from this study (see below).

The age indicated by SC 184 (Fig.3.9) suggests, if correct that the activity of the SWLS is contemporaneous with the NEBB and NEMS. The age of SC 184, is not thought to be valid, however, because it is inconsistent with the clear age progression in the NE to SW shield transition indicated by the data of Baker et al.(1967). The sample may have derived its age by acquiring excess argon , which is possible because it contains approximately 5% zeolites and is not fresh. Unfortunately no completely fresh samples could be found within the SWLS. The age of SC 184, must therefore be treated with extreme suspicion.

If the samples analysed in the present study which appear to have undergone Ar loss (SC 68, SC 111) or have excess Ar(SC 184) are excluded a clear pattern emerges with Baker's samples producing ages that are progressively discordant with increasing age from the present study (Fig.3.9). The best method of comparison of the two data sets is by comparison of specific intrusions and flank related flows which are known to be contemporaneous from field relationships. The examples in which correlation is possible are given in Table 3.1. It is seen that there is a progressive difference in age. The Leeds data are used in this study because of the technically advanced features of the present method of analysis compared to those available to Baker et al. (1967) (D.C. Rex pers.comm.)

Table 3.1; A comparison of the K-Ar data of Baker et al.(1967) and that for this study for intrusives of the SHRS.

Sample number	Intrusion	Age (Baker et al.)	Age (this study)
SC 149	Asses Ear phonolite		7.00±0.28
SB 290	" "	6.8±0.4	
SB 313	" "	7.7±1.2	
SC 103	Powell's Valley trachyte		7.26±0.29
	" "	7.5±0.4	
SC 86	SWEF basalt flows		7.64±0.31
SB 111	" "	8.1±1.0	
SB 105	" "	8.7±1.0	
SC 195	High Knoll mugearite		7.90±0.32
SB 746	" "	8.4±0.4	
SC 143	Bunkers Hill mugearite		8.08±0.33
SB 785	" "	11.4±1.0	

In summary, it can be stated that whilst the age of the youngest rocks are well constrained by K-Ar data it is not possible to determine the date of initiation of subaerial activity. The NEBB may not be dated because of the pervasive nature of alteration in these rocks. They are, however, clearly significantly older than the NEMS because of the presence of a major erosional unconformity between the two groups. Unfortunately, K-Ar data are also not able to resolve the question of whether the NE and SW centres were active concurrently during the transition of the centre of activity because no samples with few zeolites were collected from the SWLS. This problem is important in terms of the interactions that occur between ascending magma batches and surrounding rock that are discussed in chapter 7.

Owing to the uncertainties involved with K-Ar determinations, it is thought that the temporal variations within the volcanics are best represented in terms of the stratigraphic height. Interpolation of ages is misleading because of the errors involved in K-Ar determinations and the episodic nature of volcanic activity. A linear interpolation is used to correct the Sr isotopes by necessity. Typical dates are given as a general indication of the time framework (e.g Fig.4.18).

CHAPTER 4

PETROGRAPHY, MINERAL CHEMISTRY AND AN INTRODUCTION TO GEOCHEMISTRY :

4.1; Introduction;

Previous work on the petrography and mineral chemistry of the SHRS has been summarised in section 3.3.2. It is, however, necessary to reiterate in more detail the petrography and mineral chemistry of the SHRS to provide a background to the new geochemical data and modelling. As a result some overlap with the work of Baker(1968) is inevitable in this chapter. The principal differences are the description of a larger sample set and more detailed discussion of the mineral chemistry which is made possible by the use of an energy dispersive electron microprobe. The petrography and mineral chemistry of the samples are described in some detail for the following reasons:

- Thin section study enables the degree of alteration of a sample to be evaluated and hence whether it is suitable for inclusion in the geochemical study.

- Determination of mineral compositions is vital in assessing the degree to which crystal fractionation has progressed and in modelling this process.

- Textural relationships are important in indicating crystallisation histories and the relative importance of phases which have crystallised and separated.

The petrographic description is approached by firstly describing the range of whole rock compositions encountered according to the IUGS classification. This provides a framework for describing the mineral chemistry. A brief summary of the important textural relationships in relation to the IUGS defined groups is given to ensure that the mineral groups can be considered in the context of their mode of occurrence. The compositional variations within the four principal rock forming mineral groups encountered in these rocks, namely olivine, pyroxene, plagioclase feldspar and K feldspar are then described. The major and trace element geochemical characteristics of the SHRS is introduced in the final section.

4.2; Compositional range of the St.Helena rock suite;

The members of the SHRS are classified in this study according to the widely used classification proposed by the IUGS subcommission on the systematics of igneous rocks (Le Bas et al.(1986)). This is a non-genetic classification based on the total alkalis - silica (TAS) diagram which is consistent with the CIPW norm based classification proposed by Streckheisen(1976). According to the classification based on the TAS diagram (Fig.(4.1)) the SHRS varies from basalt - hawaiite - mugearite - benmoreite - trachyte - phonolite compositions. Some samples also extend to more alkalic equivalents. Thus, tephrite basanite, phono-tephrite and tephri-phonolite compositions are also encountered. The SHRS trend on the TAS diagram is, in fact, coincident with the line dividing the alkalic types such as tephri phonolite from the predominant less alkalic compositions such as basaltic trachyandesite. To simplify the description of different members of the SHRS in this study the terms that refer to the less alkalic compositions will be used throughout. The names trachybasalt, basaltic trachyandesite and trachyandesite used in Baker's study are replaced in this study by the names denoting the sodic variety of these rocks namely hawaiite, mugearite and benmoreite respectively. These are defined by $(Na_2O-2)>K_2O$ (Le Bas et al.(1986)). This enables comparison with recent work on OIB magmatism. As would be expected in rocks of an alkalic affinity the SHRS lie above the dividing line on the TAS diagram proposed by MacDonald and Katsura(1964). Similarly, in terms of CIPW normative composition, these rocks are exclusively nepheline normative and are, therefore alkalic. The group of volcanics containing less than 45% SiO_2 are termed ankaramites rather than picrobasalts in this study to indicate their pyroxene-olivine phyric nature and to enable consistency with Baker's description. The bias to primitive compositions evident in Fig.4.1 is a sampling bias resulting from the sampling strategy which is discussed in section 3.7. A "silica gap": the term coined by Chayes(1963) to account for the absence of samples of intermediate compositions within such suites does not exist. The small proportion of samples containing between 54 and 58% SiO_2 reflects the sampling objective of only collecting the most primitive samples available from a particular section of the stratigraphy. The presence of a large number of phonolites from the SWLI tends to support the idea of a silica

Fig.4.1. Position of the SHRS in the Total Alkalis Silica classification (TAS) as defined by the IUGS subcommission on the classification of igneous rocks (Le Bas et al.(1986)). Abbreviations to rock units according to Fig.3.4.

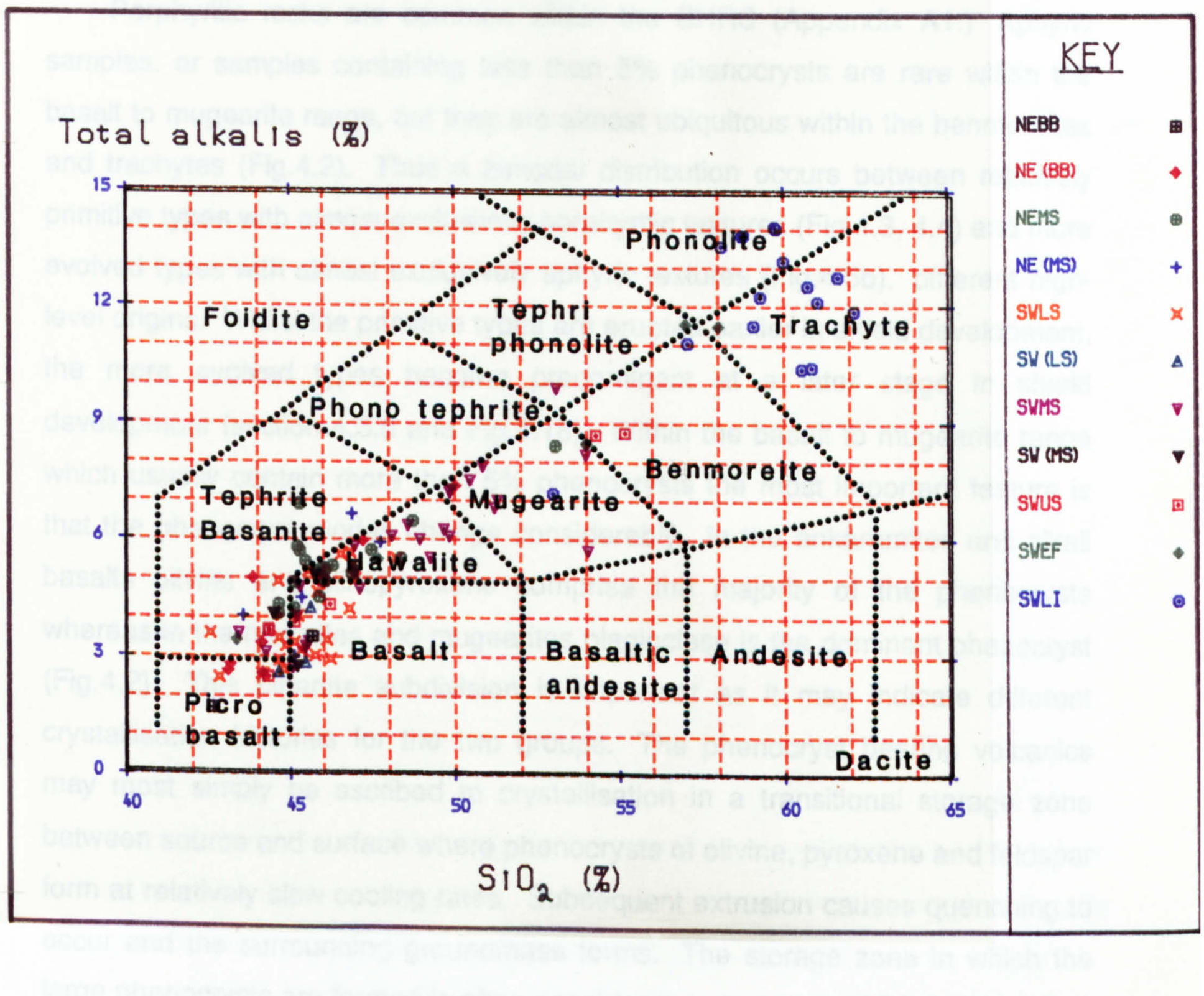
Total alkalis (%)
15
12
9
6
3
0
40
45
50
55
60
65
Foidite
Tephri phonolite
Phonolite
Trachyte
Phono tephrite
Benmoreite
Tephrite Basanite
Mugearite
Hawaiite
Basalt
Basaltic andesite
Andesite
Picro basalt
Dacite
SiO2 (%)
KEY
NEBB
NE (BB)
NEMS
NE (MS)
SWLS
SW (LS)
SWMS
SW (MS)
SWUS
SWEF
SWLI

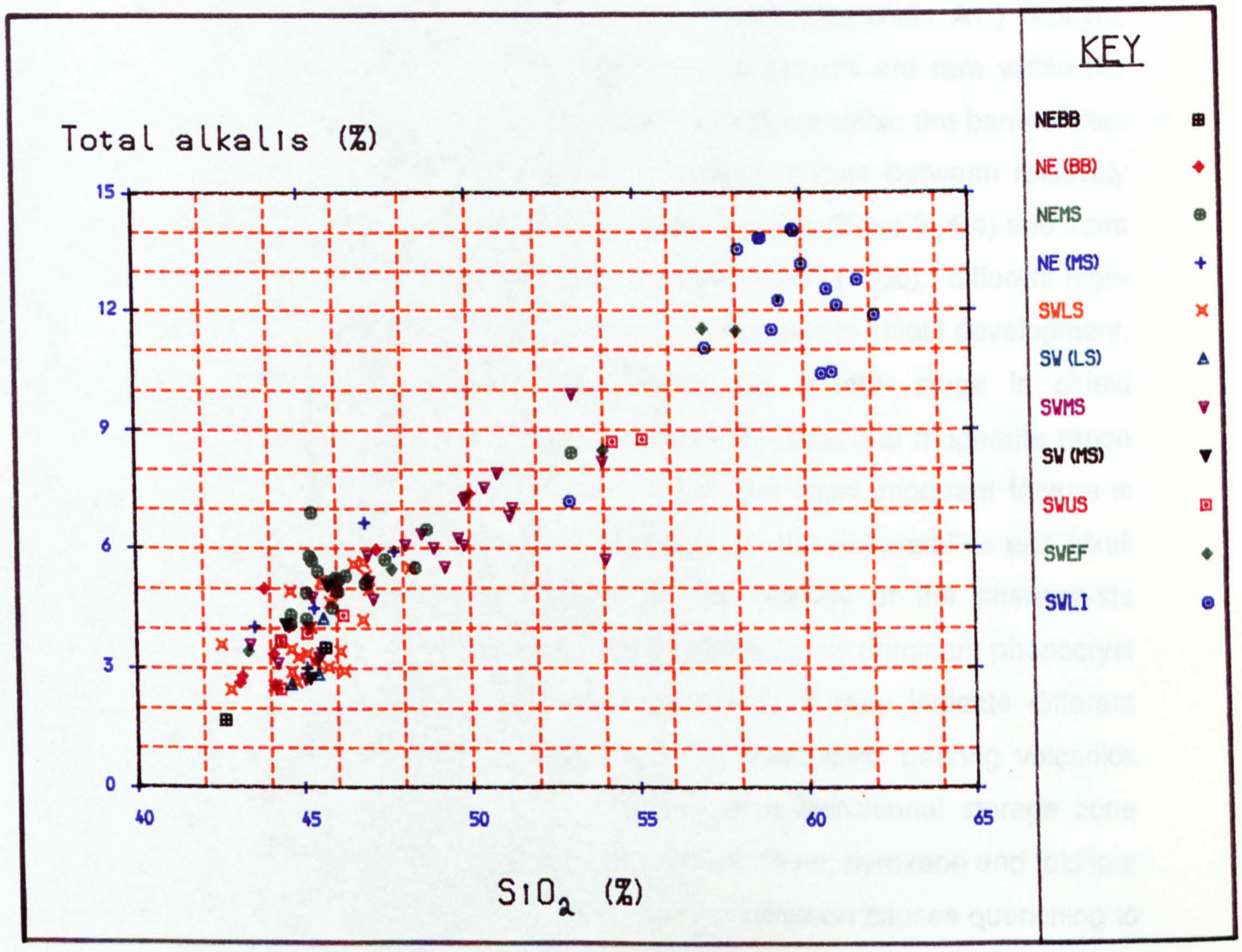
Total alkalis (%)
15
12
9
6
3
0
40
45
50
55
60
65
SiO2 (%)
KEY
NEBB
NE (BB)
NEMS
NE (MS)
SWLS
SV (LS)
SWMS
SV (MS)
SWUS
SWEF
SVLI

gap. They were, however, collected for their value in understanding this particular part of the fractionation process, and they are of minor volumetric importance (section 3.3.1 (6)), (Baker(1968)). The major element classification described above for the St.Helena rock suite provides a sufficient background to the discussion of petrography and mineral chemistry. Genetic classifications based on major elements and trace elements are discussed in the introduction to geochemistry (section 4.5).

4.3; Textural relationships;

Porphyritic rocks are common within the SHRS (Appendix A1.) Aphyric samples, or samples containing less than 5% phenocrysts are rare within the basalt to mugearite range, but they are almost ubiquitous within the benmoreites and trachytes (Fig.4.2). Thus a bimodal distribution occurs between relatively primitive types with almost exclusively porphyritic textures (Fig.4.3, 4.4) and more evolved types with almost exclusively aphyric textures (Fig.4.5b). different high-level origins. Whilst the primitive types are erupted earlier in shield development, the more evolved types become predominant at a later stage in shield development (section 4.5.5 and Fig.4.18). Within the basalt to mugearite range which usually contain more than 5% phenocrysts the most important feature is that the phenocryst modes change considerably. In the ankaramites and alkali basalts olivine and clinopyroxene comprise the majority of the phenocrysts whereas in the hawaiites and mugearites plagioclase is the dominant phenocryst (Fig.4.2). This bipartite subdivision is important as it may indicate different crystallisation histories for the two groups. The phenocryst bearing volcanics may most simply be ascribed to crystallisation in a transitional storage zone between source and surface where phenocrysts of olivine, pyroxene and feldspar form at relatively slow cooling rates. Subsequent extrusion causes quenching to occur and the surrounding groundmass forms. The storage zone in which the large phenocrysts are formed is often considered to be a large high-level magma chamber. Ryan(1987) reviews the evidence for the existence of such structures. This simple explanation has been suggested by many authors such as Cox et al.(1979) to explain what is a very common feature of volcanic rocks. During the crystallisation of more evolved magma types it appears that either a process

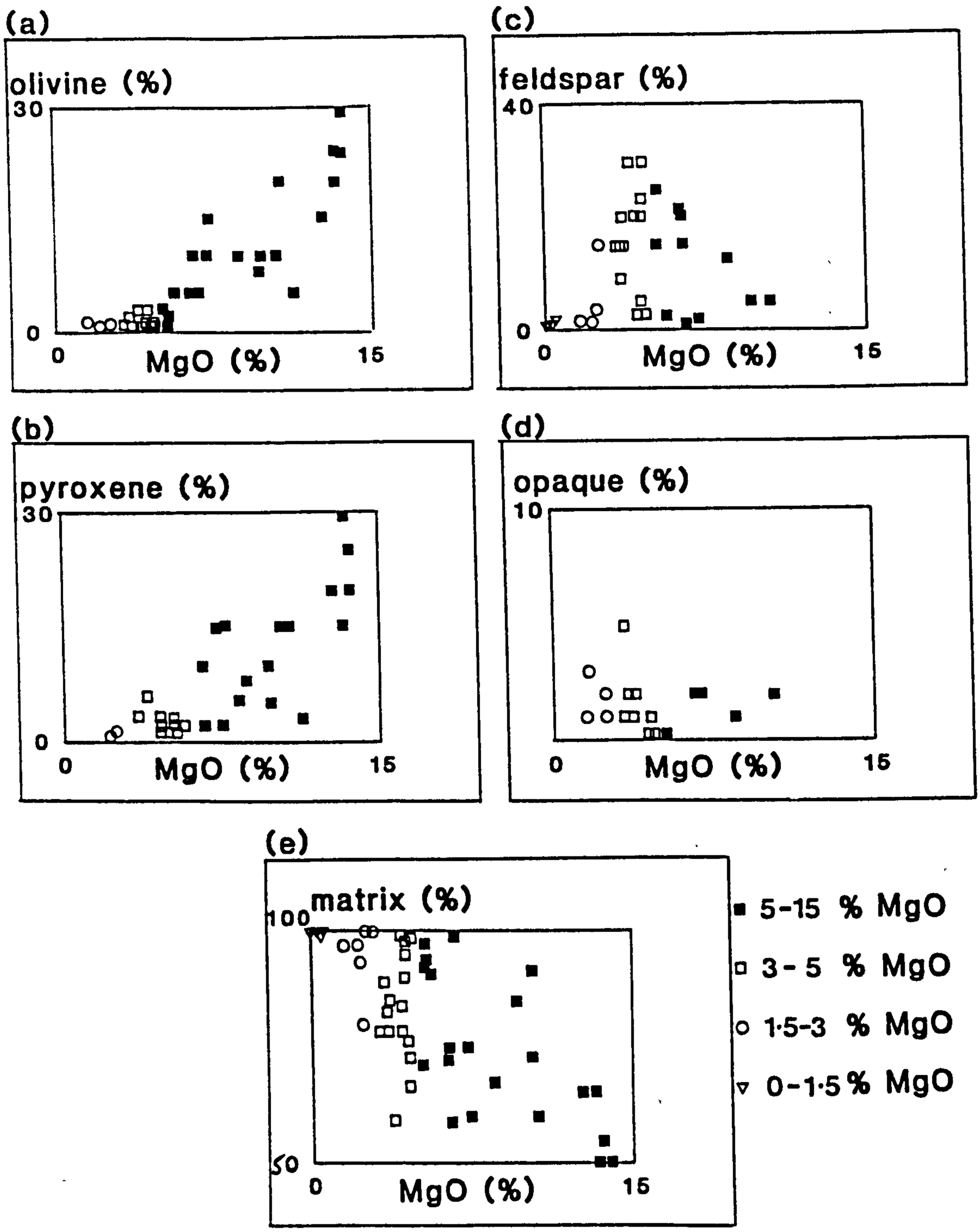

Fig.4.2. Variation in petrographic mode for phenocrysts and matrix in the SHRS as a function of the MgO content of the host rock. Estimated modes are for (a) olivine, (b) clinopyroxene, (c) feldspar, (d) opaques and (e) matrix.

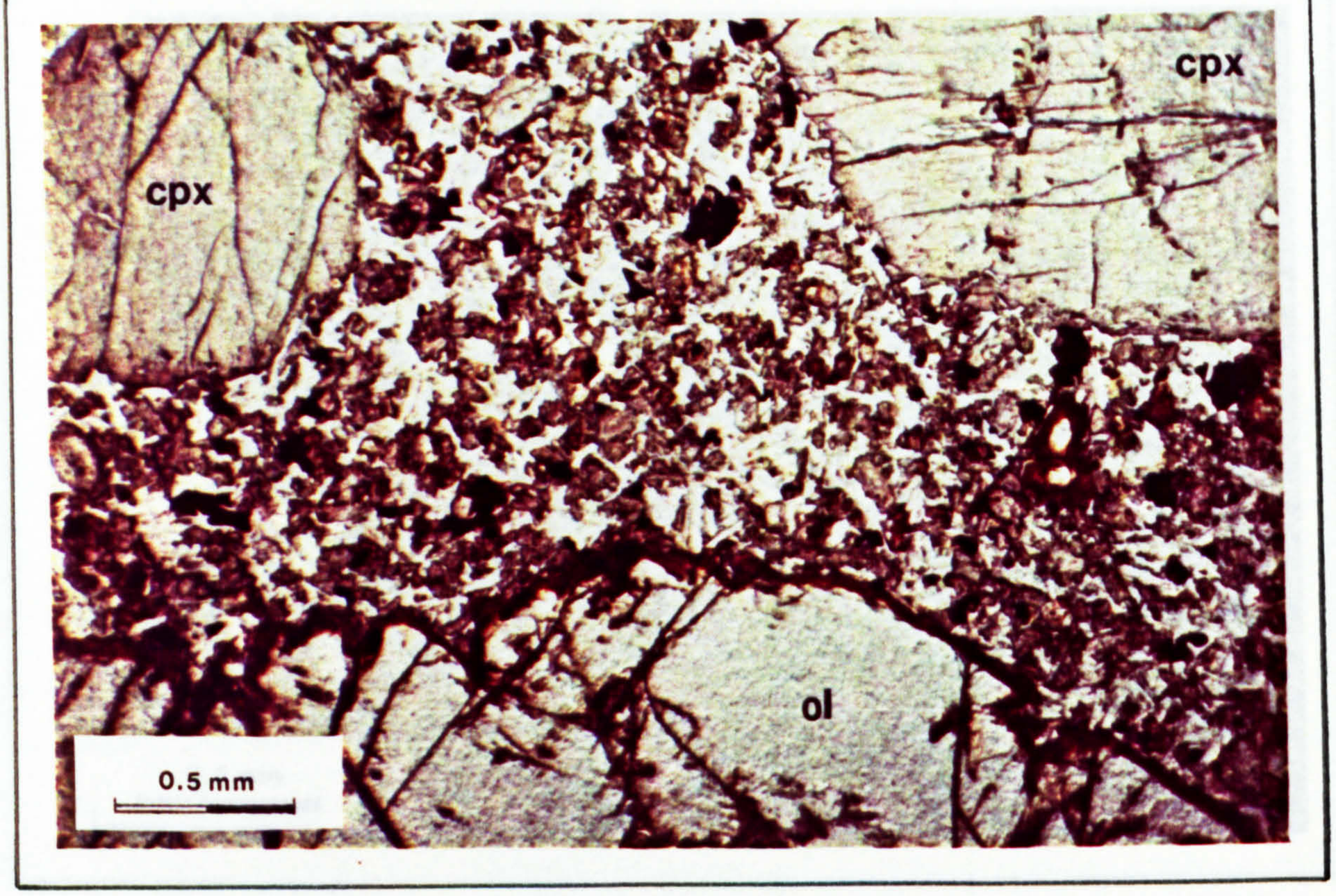

Fig.4.3a. Typical porphyritic texture of an ankaramite (SC 173, 13.2% MgO). Note euhedral iddingsitised olivine(ol) and clinopyroxene(cpx). Groundmass of olivine, clinopyroxene, plagioclase and titanomagnetite.

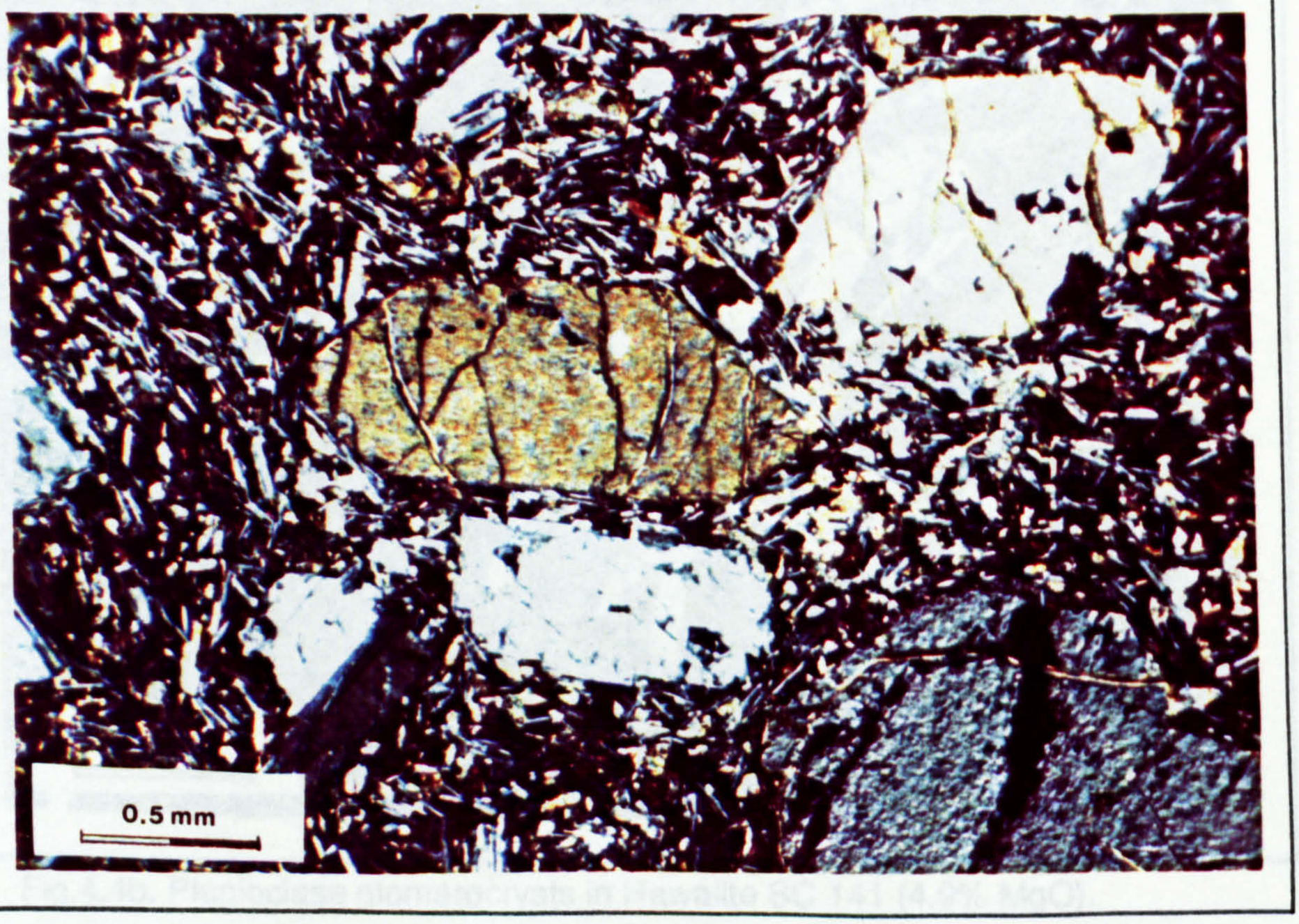

Fig.4.3b. Primitive alkali basalt SC 125 (10.8% MgO) possessing an olivine - clinopyroxene - plagioclase phenocryst and groundmass assemblage. Note euhedral ol crystals.

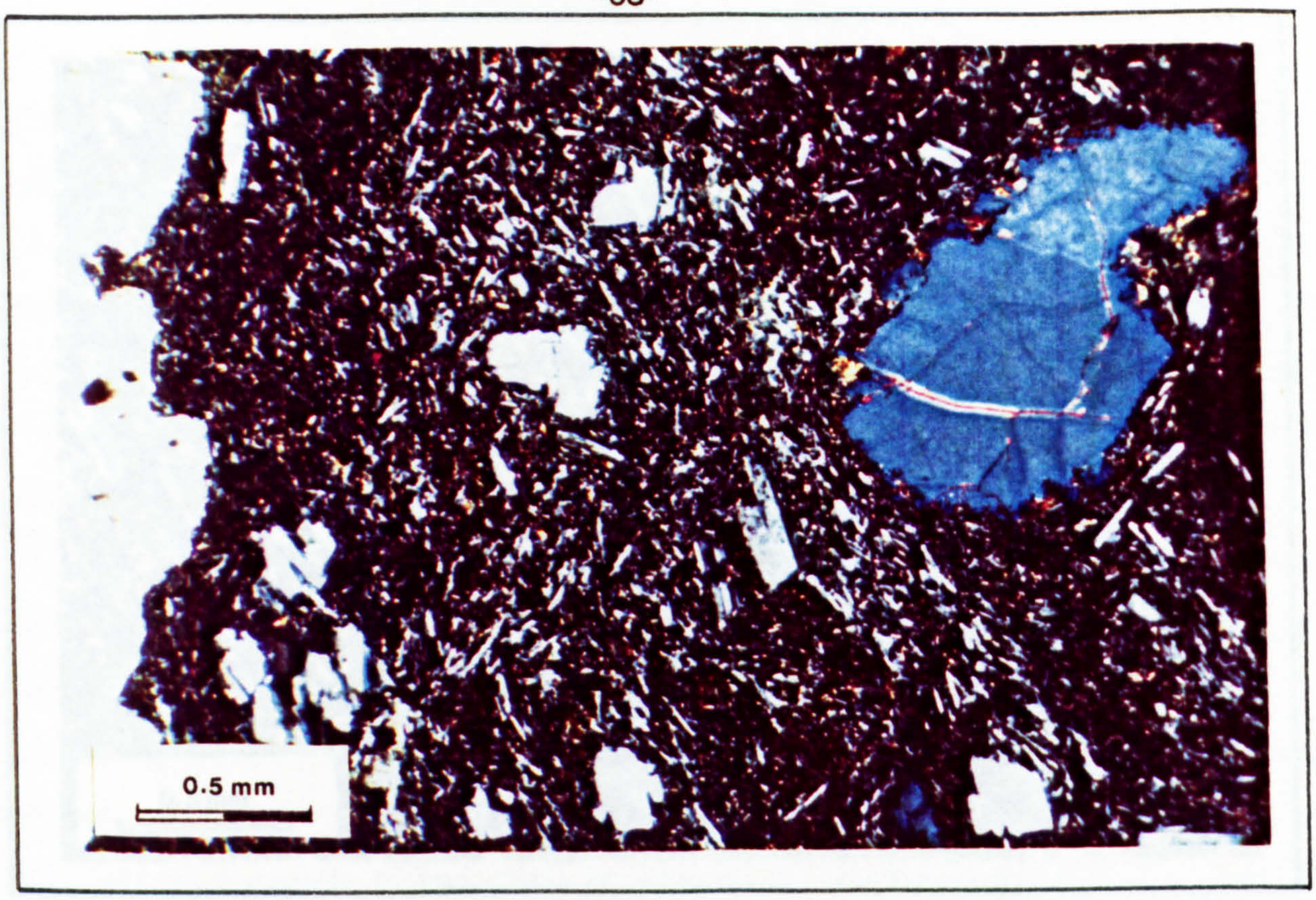

Fig.4.4a. Alkali basalt SC 26 (6.6% MgO) with plagioclase (light areas) the predominant phenocryst.

Fig.4.4b. Plagioclase glomerocrysts in Hawaiite SC 141 (4.9% MgO).

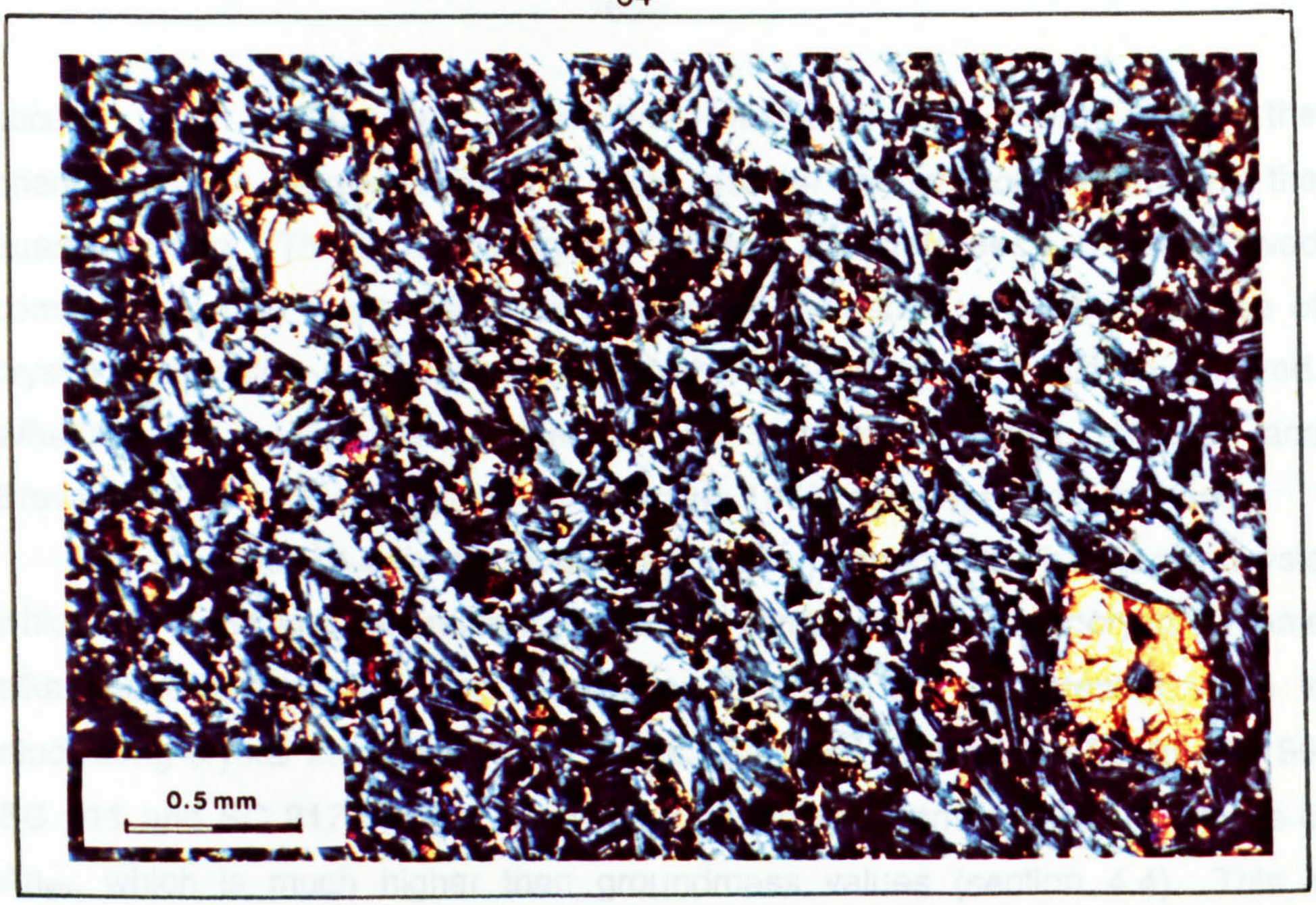

Fig.4.5a. Hawaiite SC 168 (4.5% MgO) exhibiting a typical medium to fine grained groundmass texture with a small proportion of phenocrysts. Note high proportion of opaques (titanomagnetite) in groundmass (cf SC 173, Fig.4.3a).

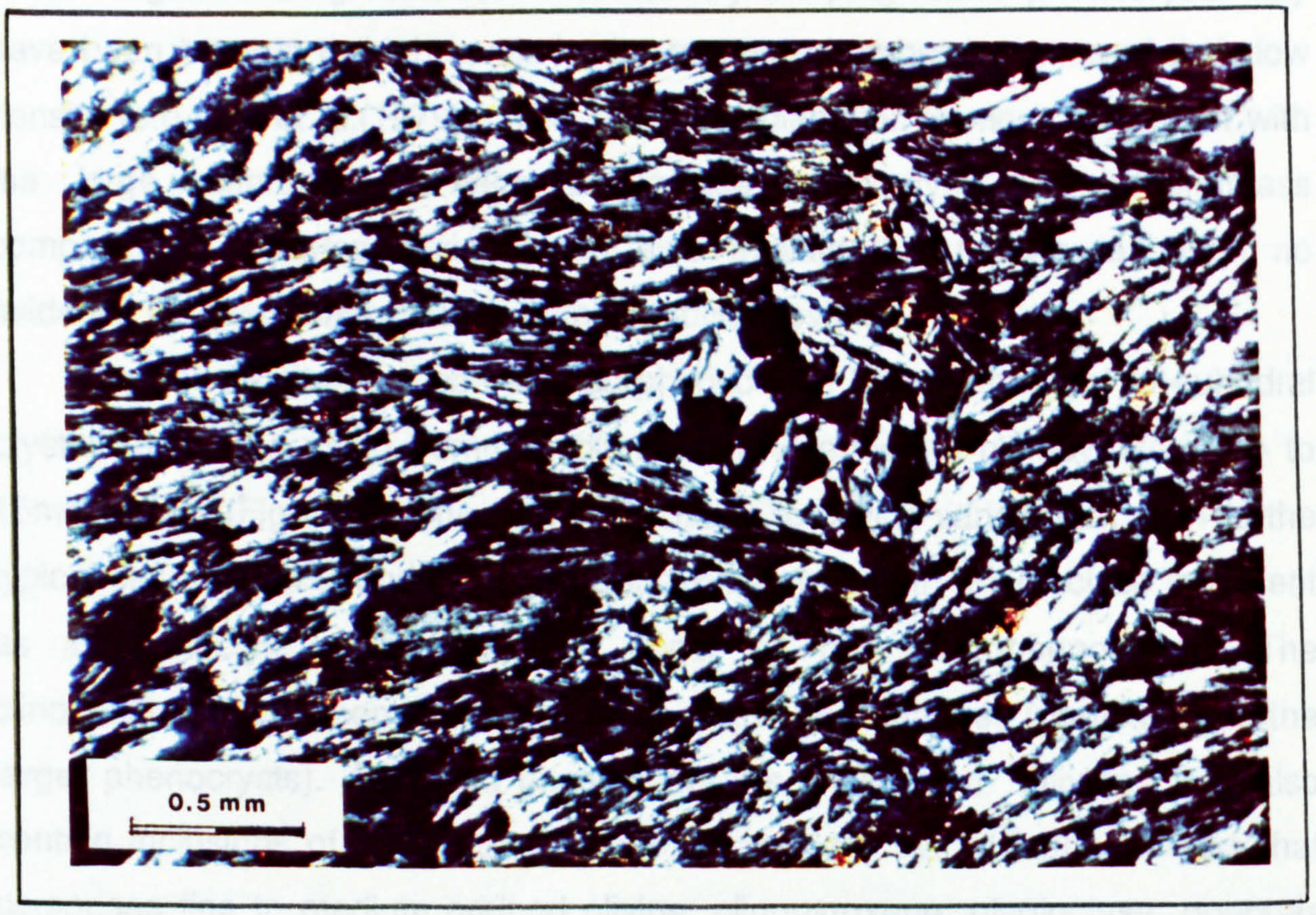

Fig.4.5b. Trachyte SC 93 (0.4% MgO) possessing a trachytoidal flow alignment of feldspar.

occurs which suppresses phenocryst nucleation, or, alternatively, the phenocrysts are separated from the liquid and the residual liquid then forms the quench texture. The latter explanation is more plausible because the evolved compositions may most readily be ascribed to formation as a consequence of crystal fractionation processes during which the phenocrysts would be removed. Whether the crystals are separated by gravitative settling (Wager and Brown(1968) or sidewall crystallisation (Irvine,1978) does not effect this issue.

The presence of large corroded plagioclase phenocrysts and glomerocrysts which are found with subordinate olivine and clinopyroxene phenocrysts in some alkali basalts, hawaiites and mugearites (Fig.4.4) are of potential value in elucidating crystal fractionation processes. Samples such as SC 26, 35, SC 96, SC 111 and SC 217 contain plagioclase phenocryst compositions in excess of An_{80}, which is much higher than groundmass values (section 4.4). This is consistent with these magmas being derived from levels of the magma chamber from which the olivine and pyroxene have been preferentially removed because of their higher settling velocities. Alternatively the plagioclase phenocrysts may have been brought to high levels in the magma chamber because of their low density (e.g Cox et al.(1979)). The second explanation is more consistent with the large difference between plagioclase phenocryst and groundmass compositions. Magma mixing could also explain this feature, although no evidence of other phases from a primitive rock is evident.

The ankaramites are coarsely porphyritic with large subhedral to euhedral crystals of olivine up to 10mm in diameter and euhedral clinopyroxene up to 15mm across (Fig.4.3a). The ratio of pyroxene to olivine varies from 1.5:1 to the typical case where abundances are approximately equal. Plagioclase is absent as a phenocryst phase but may occur as rare microphenocrysts. The clinopyroxenes may contain inclusions of olivine and opaques (particularly in the larger phenocrysts). Corroded phenocrysts are uncommon. Olivines may also contain inclusions of opaques. The phenocrysts are set in a groundmass that comprises fine to medium grained olivine, clinopyroxene, plagioclase, opaques and rare alkali feldspar.

The alkali olivine basalts (Fig.4.3b and 4.4) vary from olivine-pyroxene phyric basalts through olivine-plagioclase phyric to plagioclase phyric types.

Olivine is always equal to or of greater abundance than pyroxene. The matrix consists of intergranular plagioclase, clinopyroxene, olivine, opaques and alkali feldspar. Feldspars are often aligned in a flow texture.

The hawaiites, mugearites and benmoreites tend to be progressively more sparsely porphyritic as MgO content declines (Fig.4.2e). Olivine and/or plagioclase may occur as a phenocryst phase, although the latter is usually most abundant (Fig.4.5a). Opaque oxide pseudomorphs after amphibole may also occur as a phenocryst phase. The groundmass phases are similar to those in the alkali-olivine basalts, although biotite may also be present. A fluidal groundmass texture is common.

Trachytes are commonly aphyric although small (less than 3mm diameter) phenocrysts of plagioclase, olivine, opaque or amphibole pseudomorphs may occur (Fig.4.5b).

Phonolites (Fig.4.6), which occur exclusively as hypabyssal rocks (section 3.4.3.2) are fine to medium grained in terms of their groundmass. They may contain large (10mm long) alkali feldspar laths and euhedral nepheline crystals (5 mm diameter). Feldspar glomerocrysts are present in some samples. Aegirine augite occurs as a groundmass phase. The plutonic inclusions reported from the phonolites by Baker were found to be exceedingly rare by this author. Two small (less than 5 cm diameter) xenoliths comprising feldspar and amphibole were found. The amphibole composition is described in the following section.

The texture of rocks forming dykes (Fig.4.3b, 4.4b) is similar to the volcanics in terms of phenocryst mode. The primitive types tend to be porphyritic and the more evolved types aphyric. Typical hypabyssal, aphyric textures are rare. The phonolite and trachyte plugs and arcuate intrusions form coarser grained, equigranular types.

4.4; Mineral Chemistry;

The distribution of mineral phases within the SHRS is shown in Table.4.1. Analytical data are given in Appendix C1.

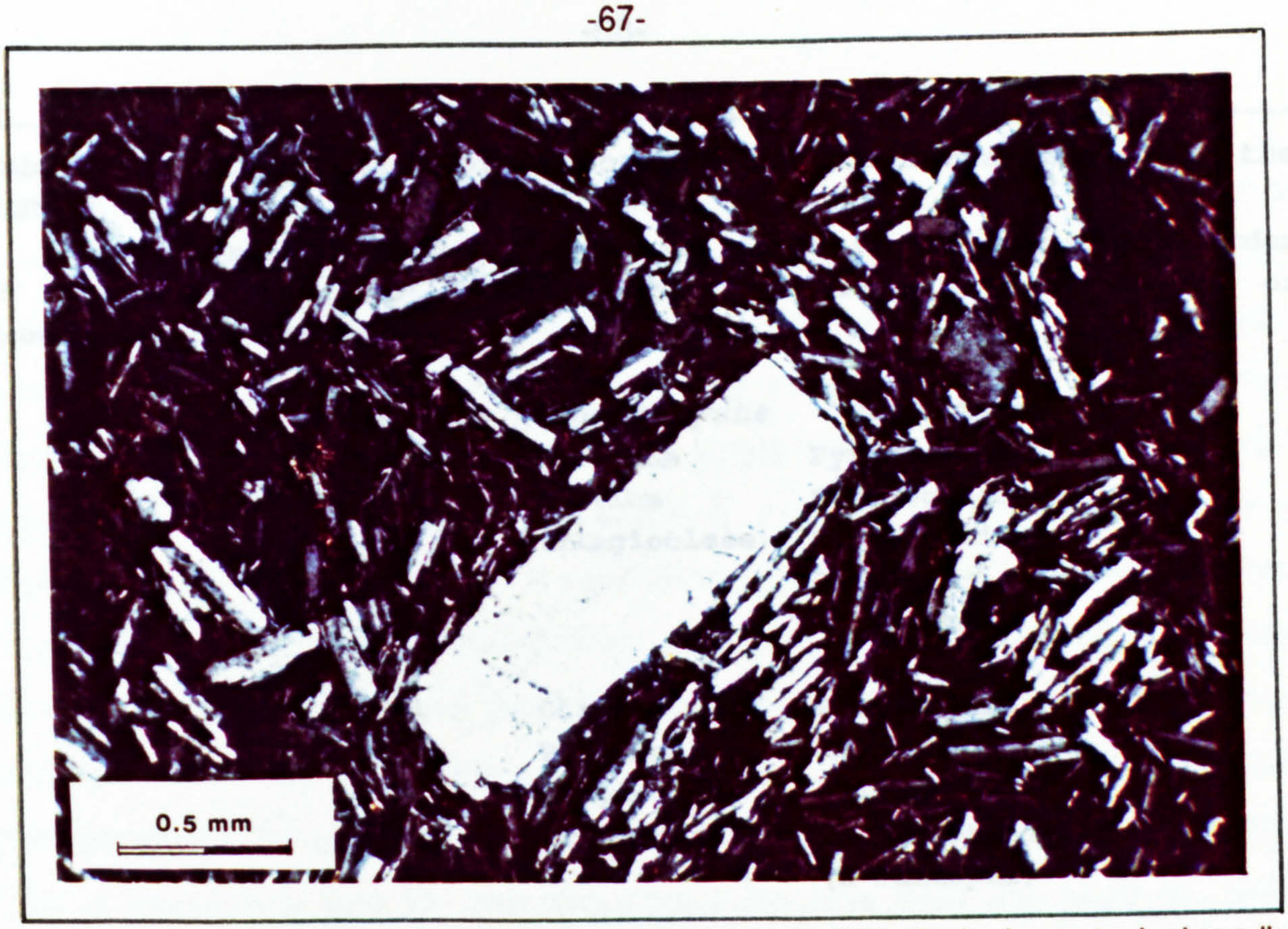

Fig.4.6a. Phonolite SC 149 MgO (approximately 0%) displaying a typical medium texture of hypabyssal origin (cf quenched groundmass texture in SC 141, Fig.4.4b). The large phenocryst is an albitic plagioclase. Clinopyroxene, feldspar and amphibole are the main groundmass phases.

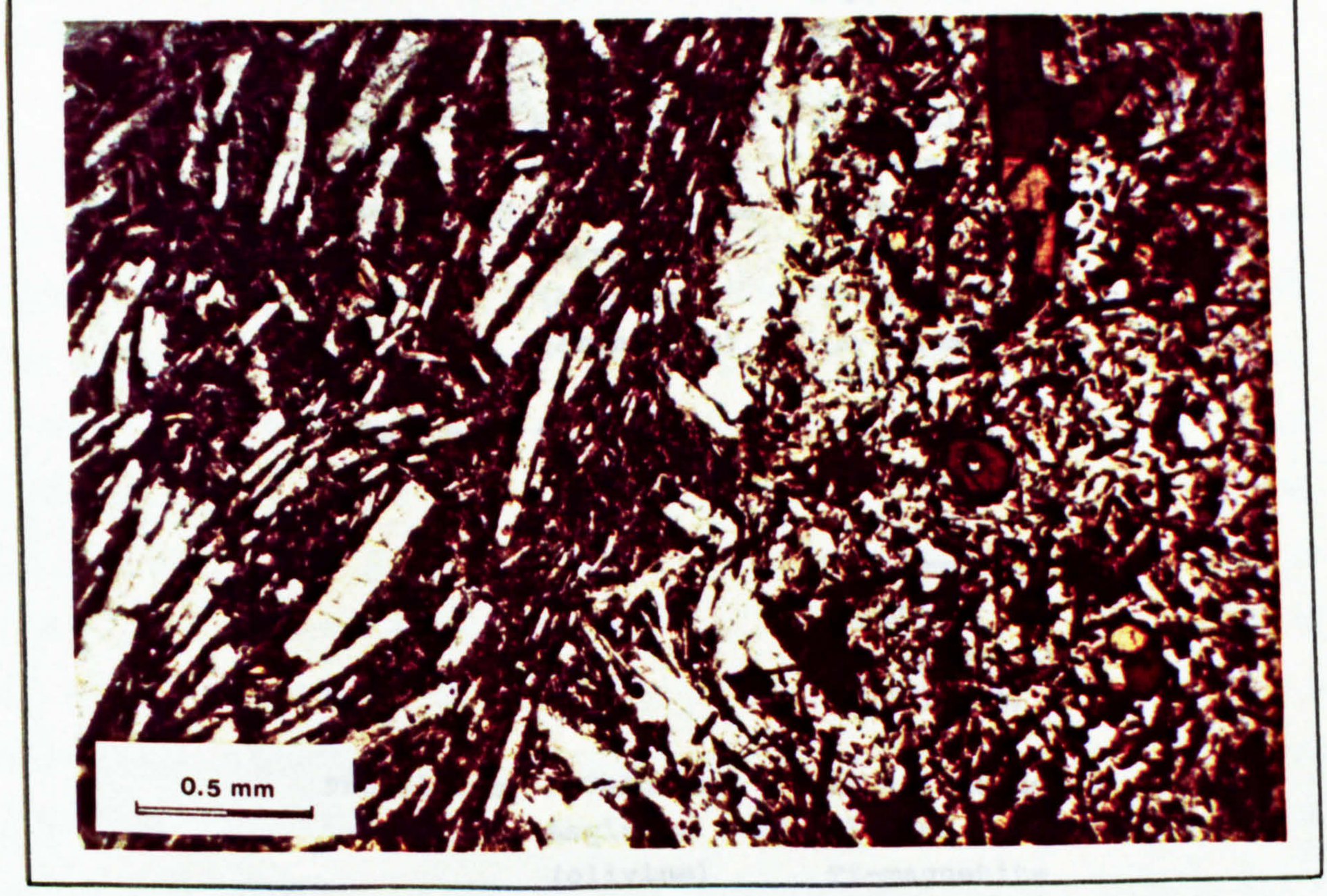

Fig.4.6b. Xenolith within phonolite SC 154. The brown acicular and tabular phase is kaersutitic amphibole that is restricted to the xenolith (right hand side).

Table 4.1; Distribution of phenocryst and groundmass phases in the SHRS.

For each rock grouping, phases are listed in the approximate order of abundance observed. Phases that are rare as phenocrysts or groundmass are bracketed.

Rock type	*Phenocrysts*	*Groundmass*
Ankaramite	Pyroxene	Pyroxene
	Olivine	Plagioclase
	(Plagioclase)	Ti-magnetite
		Olivine
		(K-Feldspar)
Alkali Basalts	Olivine	Plagioclase
	Pyroxene	Pyroxene
	Plagioclase	Olivine
	(Ti-magnetite)	Ti-magnetite
		(K-Feldspar)
Hawaiites	Olivine	Plagioclase
	Plagioclase	Pyroxene
	Ti-magnetite	Ti-magnetite
	(Pyroxene)	Olivine
		(K-Feldpar)
		(Apatite)
		(Ti-magnetite)
Mugearites + Benmoreites	Plagioclase	Plagioclase
	Olivine	Pyroxene
	Ti-magnetite	Ti-magnetite
	(Pyroxene)	(Apatite)
	(Apatite)	(Ti-magnetite)
	(Amphibole)	(K-Feldspar)
Trachytes	Olivine	K-Feldspar
	Ti-magnetite	Plagioclase
		Aegirine
		Titanomagnetite
		(Apatite)
		(Ti-magnetite)
		(Amphibole)
Phonolites	K-Feldspar	Alkali Feldspar
	Aegirine	Olivine
	(olivine)	Ti-magnetite
	(amphibole)	Nepheline
		(Aenigmatite)

4.4.1; Olivine;

Olivine occurs as an abundant phenocryst phase in the primitive rocks of St.Helena (14-5% MgO) (Fig.4.2). It is found as a groundmass phase in a wider range of compositions. The variation in forsterite content of phenocrysts as a function of MgO content in the host rock is shown in Fig.4.7a. The limited variations within olivine phenocrysts in a single sample are also evident from Fig.4.7a. The total range of compositions including groundmass olivine is illustrated in Fig.4.8. Phenocrysts vary from Fo_{85} to Fo_{60} and groundmass from Fo_{60} to Fo_{30}. This range is not entirely representative because olivine is more susceptible to post eruptive alteration processes than other ferromagnesian minerals such as pyroxene. Many olivines only remain as iddingsite pseudomorphs for which accurate analyses cannot be obtained for modelling. This is particularly true for samples containing less than 3% MgO for which olivine determinations did not produce good totals. The range in olivine compositions is consistent with magma chamber compositions evolving by crystal fractionation as originally documented by Wager and Brown(1968).

4.4.2; Pyroxene;

Clinopyroxene occurrence is coincident with that of olivine in the SHRS. It is, however, more common as a groundmass phase in evolved rocks such as phonolites and trachytes. Clinopyroxene compositions are titaniferous calcic augites approaching salites in some primitive samples such as SC 38 and SC 140. The range of compositions in terms of the Ca-Mg-Fe pyroxene quadrilateral is shown in Fig 4.8. The range of compositions is similar to the Low P crystal fractionation trends for other S.Atlantic OIB suites that are shown for comparison. TiO_2 (<4.5%), Al_2O_3 (<8.50%) and Na_2O (<0.5%) abundances in pyroxenes are high in rocks containing more than 4% MgO. This indicates the alkalic nature of the suite which was also demonstrated for Tristan and Gough islands by Le Roex(1983). Although oscillatory zoning and sector zoning are evident, overall population differences in Mg number are small (Fig.4.7b) within a particular sample and thought to be insignificant in the modelling process (chapter 6). A much larger range in Mg number in some samples is accounted for by an outer rim usually of less than 50 microns thickness which corresponds to the

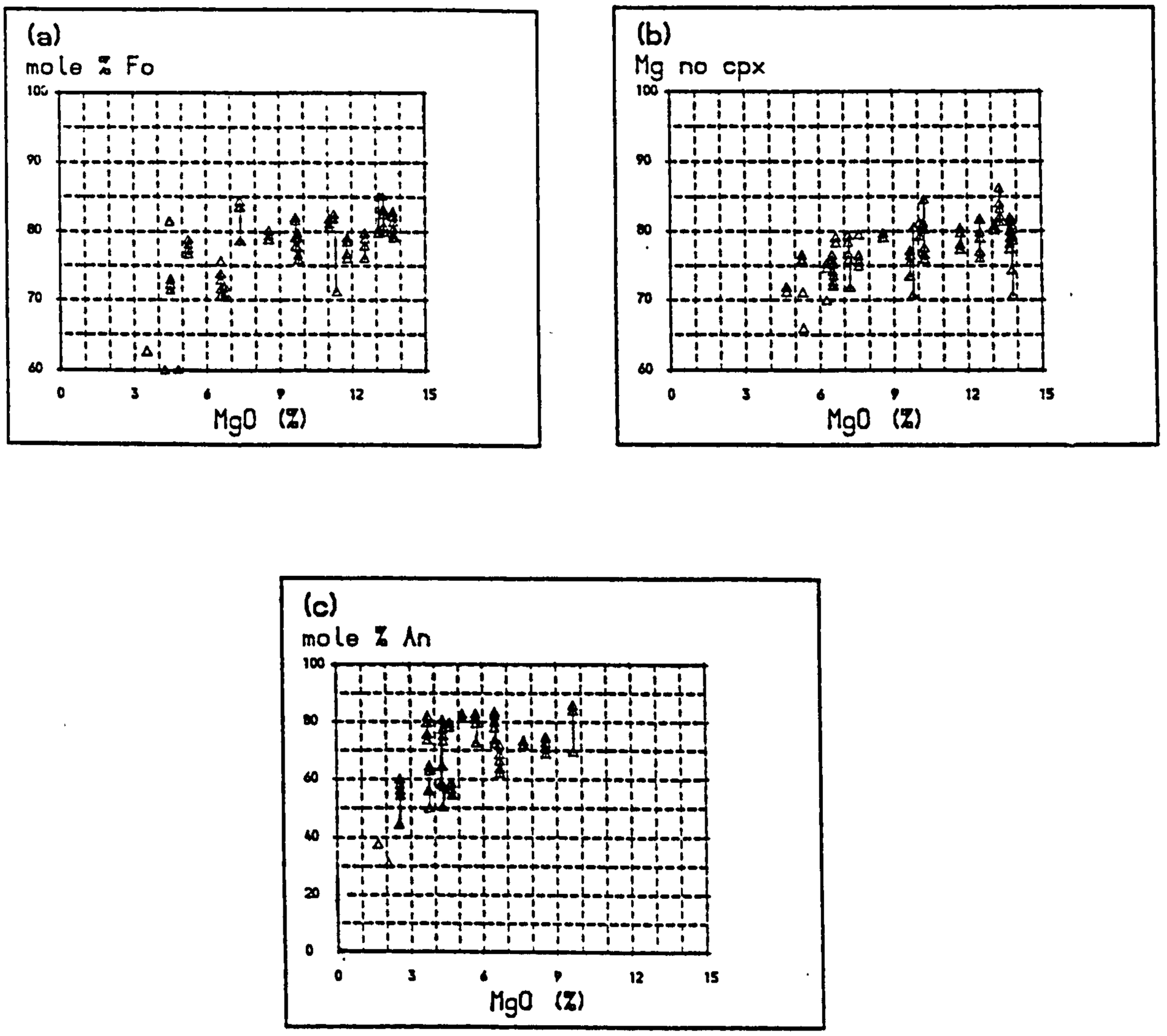

Fig.4.7. Variation in phenocryst composition as a function of MgO in host for the SHRS.

(a) Mole % Forsterite of olivine phenocrysts.

(b) Mg number of clinopyroxene phenocrysts.

(c) Mole % Anorthite of feldspar phenocrysts.

Each triangle corresponds to one analysis. Phenocrysts from the same sample are linked by vertical bars. The range in composition registered is strongly dependent on the presence or absence of a phenocryst rim corresponding to a groundmass composition and the percentage of phenocrysts. Isolated points normally indicate a virtually aphyric rock.

Fig.4.8. Compositional variation of phenocryst and groundmass clinopyroxene in the SHRS in the Diopside - Hedenbergite - Ferrosillite - Enstatite quadrilateral. Olivine variations are shown on the base of the quadrilateral between forsterite and fayalite. Symbols as for Fig.4.2. Data for pyroxenes from S.Atlantic OIB are those of Harris(1983) (Ascension), Le Roex(1984) (Tristan da Cunha and Gough Is) and Le Roex(1982) (Bouvet).

groundmass composition and formed subsequent to the core.

4.4.3; Plagioclase;

Plagioclase does not occur as a phenocryst in the most primitive rock types (Fig.4.2). It appears at approximately 10% MgO. It is ubiquitous, however, as a groundmass phase. The range of compositions encountered between primitive and evolved rocks is shown in Fig.4.9. Within plagioclase crystals a greater degree of chemical heterogeneity occurs than for olivine and clinopyroxene (Fig.4.7c). Compositional zoning of normal, oscillatory and reverse types occurs. No relationship between type of zoning and rock type is apparent. Because of the variation within and between plagioclase crystals a maximum and minimum representative value is given in Appendix C1.

4.4.4; Alkali-Feldspar;

Alkali Feldspar is found within the most evolved rocks as a phenocryst phase and occurs as a groundmass constituent in all compositions. The range of compositions from sanidine to anorthoclase is shown in Fig.4.9.

4.4.5; Accessory minerals ;

Opaque minerals may assume a high volumetric importance in some St.Helena rock types and are, therefore, of importance in modelling the effects of crystal fractionation. Opaques are found as a groundmass phase in the gamut of rock types and are exclusively titanomagnetites. Phenocrysts may occur in the more evolved rocks (Fig.4.2d). In primitive compositions Cr becomes an important constituent (up to 20 wt.%) in opaques forming chrome spinels. The range of compositions in terms of major elements is shown in Fig.4.10. Compositions vary from $Magnetite_{20}$ - $Ulvospinel_{80}$ to $Magnetite_{95}$ $Ulvospinel_{5}$. The range of compositions reflects the behaviour of Ti in the magmas as either an incompatible or compatible element. In the picrite to mugearite rock types the Ti content in the magnetite solid solution series increases as the rocks become more evolved (Ti incompatible). In the most evolved rocks (containing less than 3% MgO) in which a large amount of the available Ti has been removed by fractionation of Ti magnetite, Ti contents drop dramatically (Fig.4.10). In altered

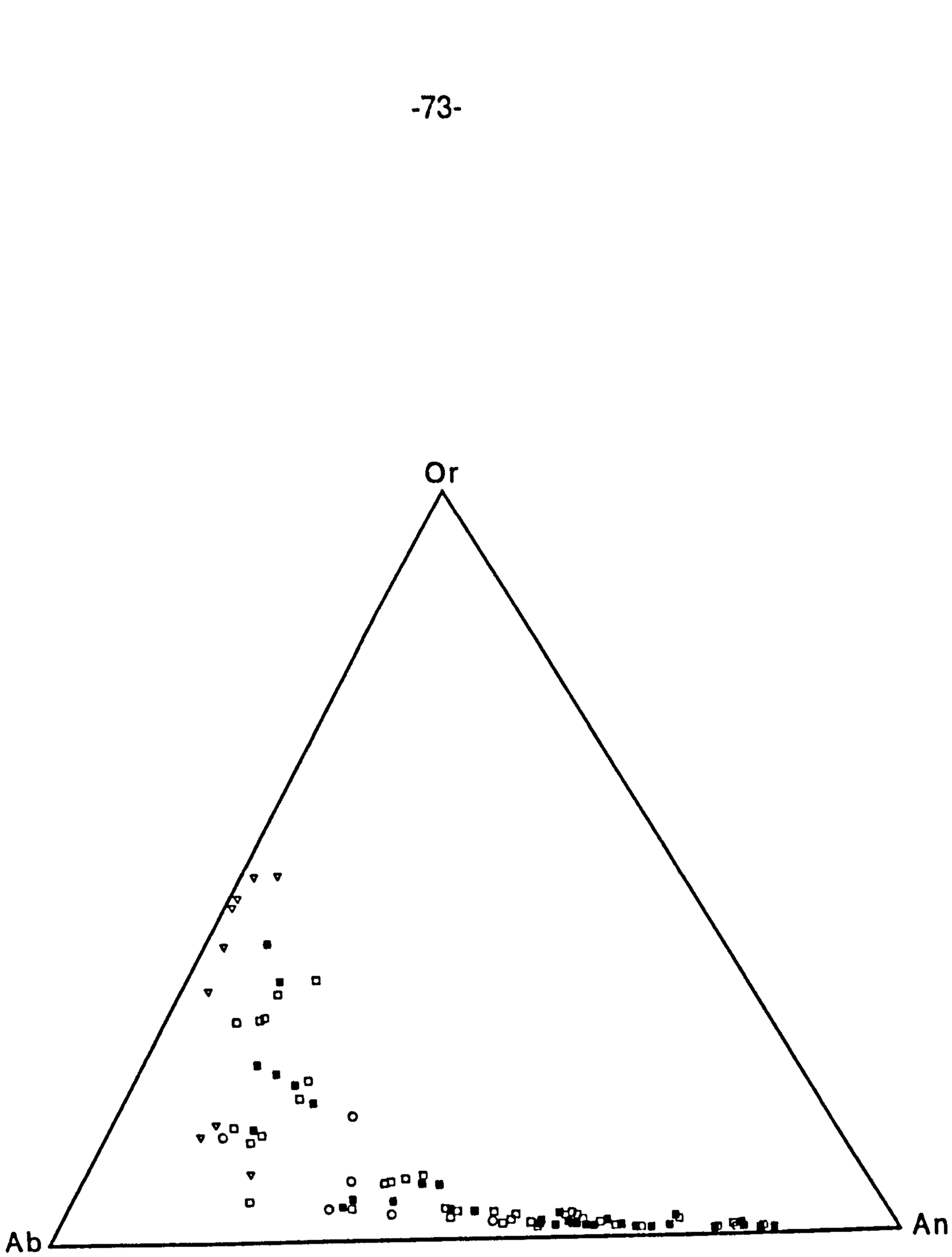

Fig.4.9. Feldspar compositional variation in the SHRS. Symbols as in Fig.4.2.

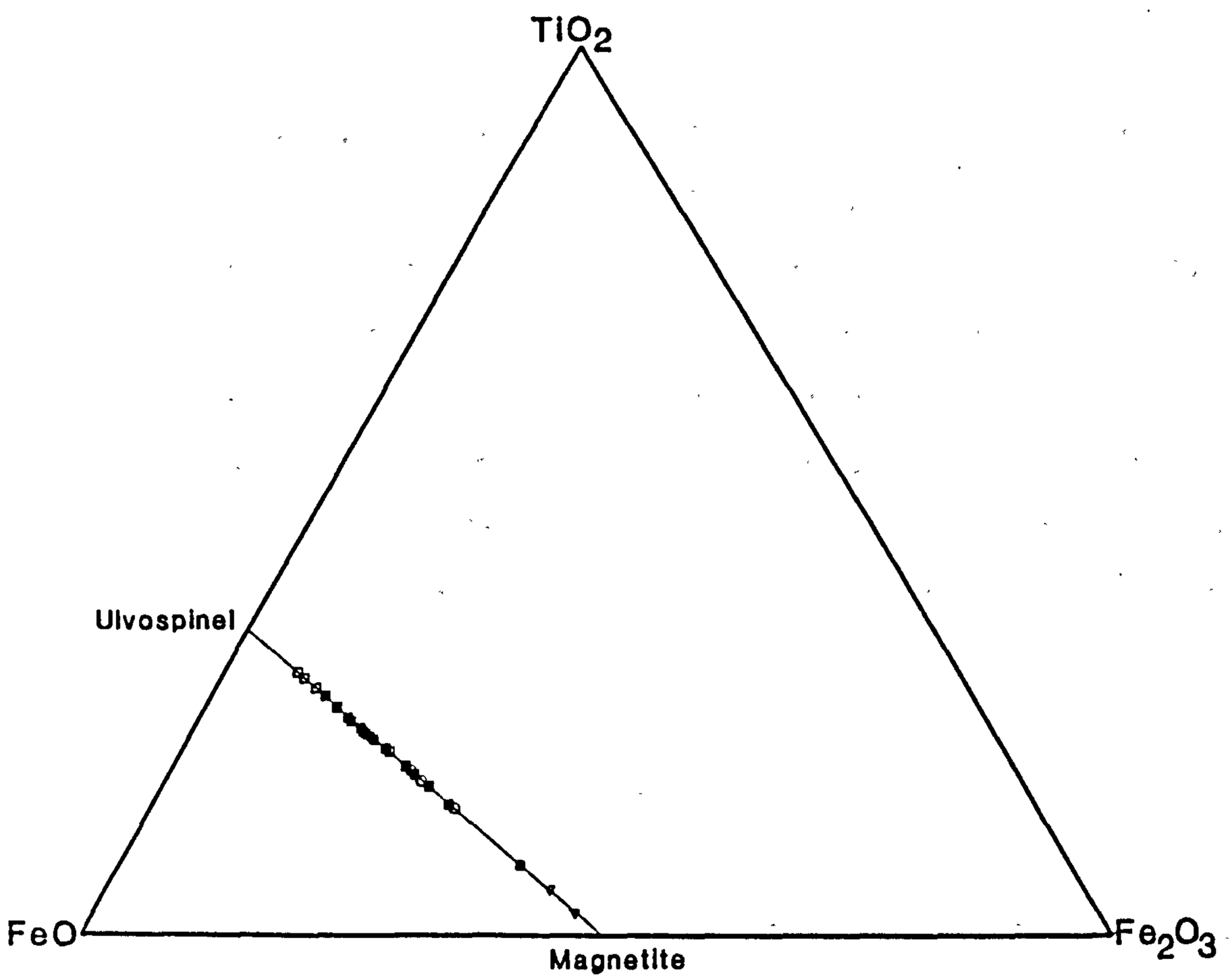

Fig.4.10. Fe-Ti oxide variations in the SHRS. Symbols as in Fig.4.2.

samples in which extensive iddingsite has developed through deuteric alteration of the olivine, altered opaques are also found in which non stoichometric Ti-maghemites occur.

Apatite occurs as fine needle-like crystals in benmoreites, trachytes and phonolites.

Nepheline may occur in the phonolites as euhedral hexagonal platelets of up to 2mm diameter.

In the most evolved rocks (< 1% MgO) such as SC 149 kaersutitic calcic amphibole is found (Fig.4.6a) (Leake(1978) classification). Amphibole is also found in rare xenoliths found within phonolites (Fig.4.6b). Aenigmatite occurs as a rare phase that accompanies amphibole. The amphibole is confined to the phonolites in the SHRS, hence it is thought that it forms as a late stage interstitial phase in the SHRS. If amphibole had formed earlier in the fractionation sequence resorbed amphibole phenocrysts would be expected in volcanics containing phenocrysts of olivine and clinopyroxene as in arc volcanics (e.g Thompson et al.(1984)).

4.5; An introduction to geochemistry;

4.5.1;Introduction;

The geochemistry of the SHRS is discussed firstly in terms of a unified major and trace element description. The major and trace elements are used to characterise the rocks in relation to other volcanic suites. The variations within the suite are then considered to illustrate the importance of crystal fractionation processes. The phases that fractionate at a particular stage of the evolution of the suite are identified by considering both major and trace element data to enable an integrated approach. In unison these descriptions act as a background to removing the effects of crystal fractionation (chapter 6). The descriptions are also necessary at this stage to act as a background to chapter 5 which discusses the effects of post-eruptive alteration.

4.5.2; Classification;

The position of the SHRS in genetic classifications based on both major and trace elements is discussed in this section. According to the modified classification of Irvine and Barager(1971) produced by Maaloe (1986), which considers primitive rocks containing 10% MgO, the SHRS belong to the sodic association (Fig.4.11a). The SHRS composition possesses relatively low K_2O contents which are intermediate between the sodic and nephelinic and tholeiitic associations in terms of K_2O and possesses a relatively low Na_2O content.

A tectonic classification for basaltic rocks based on their major elements has been developed by Mullen(1983).It is shown in Fig.4.11b. This TiO_2- 10xMnO-10xP_2O_5 classification shows that the St.Helena volcanics are typical OIB of alkalic affinity. This diagram utilises the major elements that act as incompatible elements in basic rocks and as such it is similar to the trace element based discrimination diagrams that are discussed below.

The incompatible trace element abundance of the SHRS is best illustrated on mantle normalised trace element variation diagrams or spidergrams. The basis of these diagrams and the use of the terms trace, compatible and incompatible element are described in Appendix G. Some primitive St.Helena volcanics are compared to other S.Atlantic OIB in Fig.4.12. The spidergram for St.Helena basalts is typical for intraplate volcanic products (OIB). In the SHRS the normalised abundance of elements increases progressively with increasing incompatibility from Yb to Nb. Elements more incompatible than Nb have lower abundances relative to Nb. These trace element characteristics produce relatively high ratios of highly incompatible to moderately incompatible elements which are again typical of intraplate basalts. The high degree of incompatible trace element enrichment in OIB is used extensively in classification schemes to separate intraplate magmas from those formed at plate margins. This is achieved by the use of discrimination diagrams. The earliest classifications based on HFSE elements such as Zr, Y and Nb were developed by Pearce and Cann(1973). A modified version of these classifications used by Meschede(1986) is shown in Fig.4.13a. The SHRS is seen to lie within the field of OIB. A classification utilising highly incompatible elements Th and Ta that was developed by Wood et al.(1979) is shown in Fig.4.13b. Again, St.Helena is seen

(a)

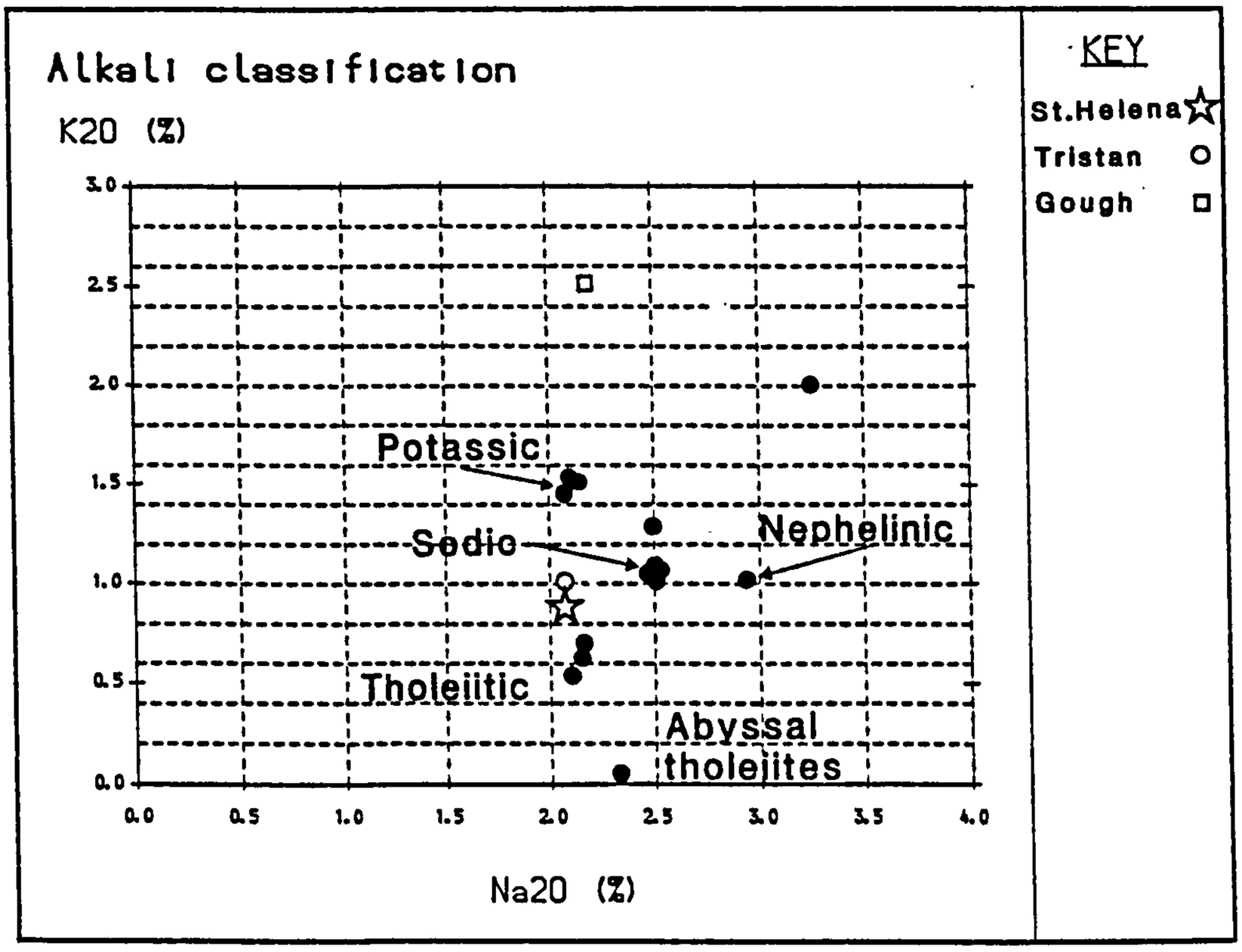

Fig.4.11a. The position of St.Helena and other S.Atlantic islands in the alkali classification scheme of Maaloe(1986). To minimise crystal fractionation effects all samples contain 10% MgO. Filled circles represent the oceanic basin basalts shown in the original classification of Irvine and Barager(1971).

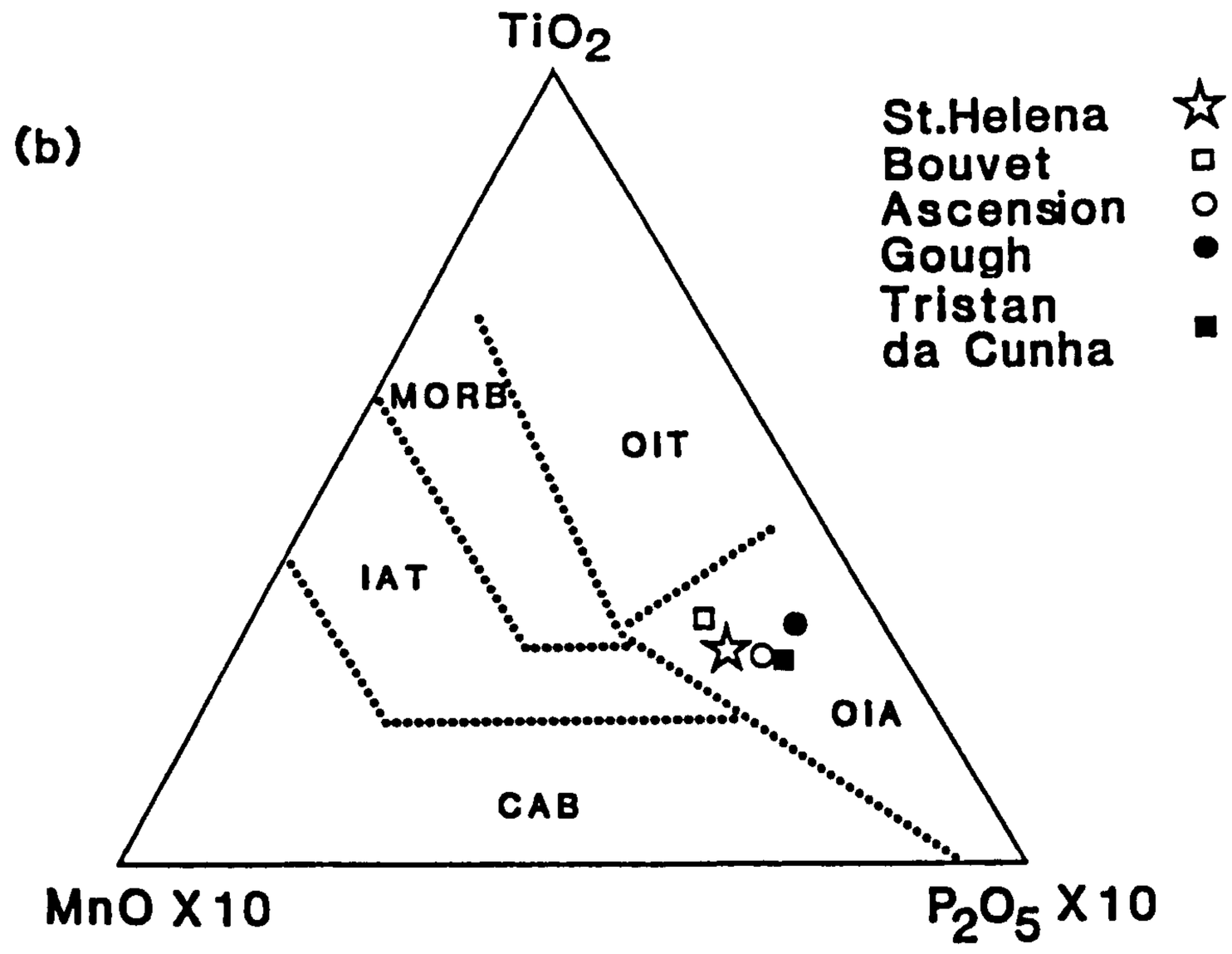

Fig.4.11b. Tectonic setting classification based on TiO_2, MnO *10 and P_2O_5 * 10. Fields defined by Mullen(1983).

MORB - Mid Oceanic Ridge Basalt.

OIA - Oceanic Island Alkali Basalt.

OIT - Oceanic Island Tholeiite.

IAT - Island Arc Tholeiite.

The position of some S.Atlantic OIB analysed by Weaver et al.(1987) are shown for comparison.

Fig.4.12. Spidergram of primitive S.Atlantic OIB. Data of Weaver et al.(1987). The samples are:

St.Helena, 26 : 1965-P5 58.

Bouvet, 2 : 1965-0 148.

Ascension, 8 : 1927-1246 17.

Tristan da Cunha, 12-1927, 1252 66.

Normalising values of Thompson (1982).

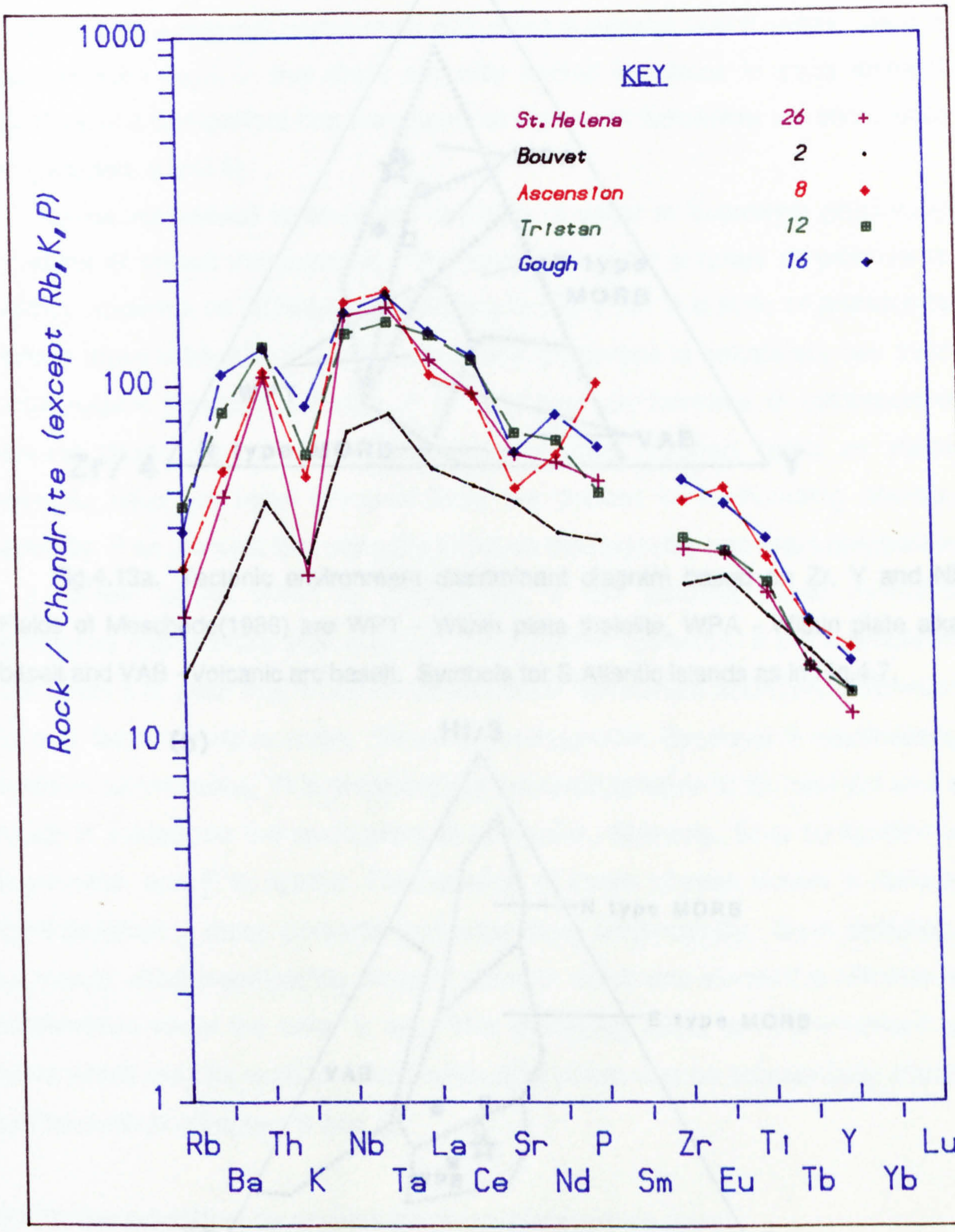
1000
100
10
1
Rock / Chondrite (except Rb, K, P)
KEY
St. Helena 26 +
Bouvet 2 •
Ascension 8 ◆
Tristan 12 ■
Gough 16 ◆
Rb Th Nb La Sr P Zr Ti Y Lu
Ba K Ta Ce Nd Sm Eu Tb Yb

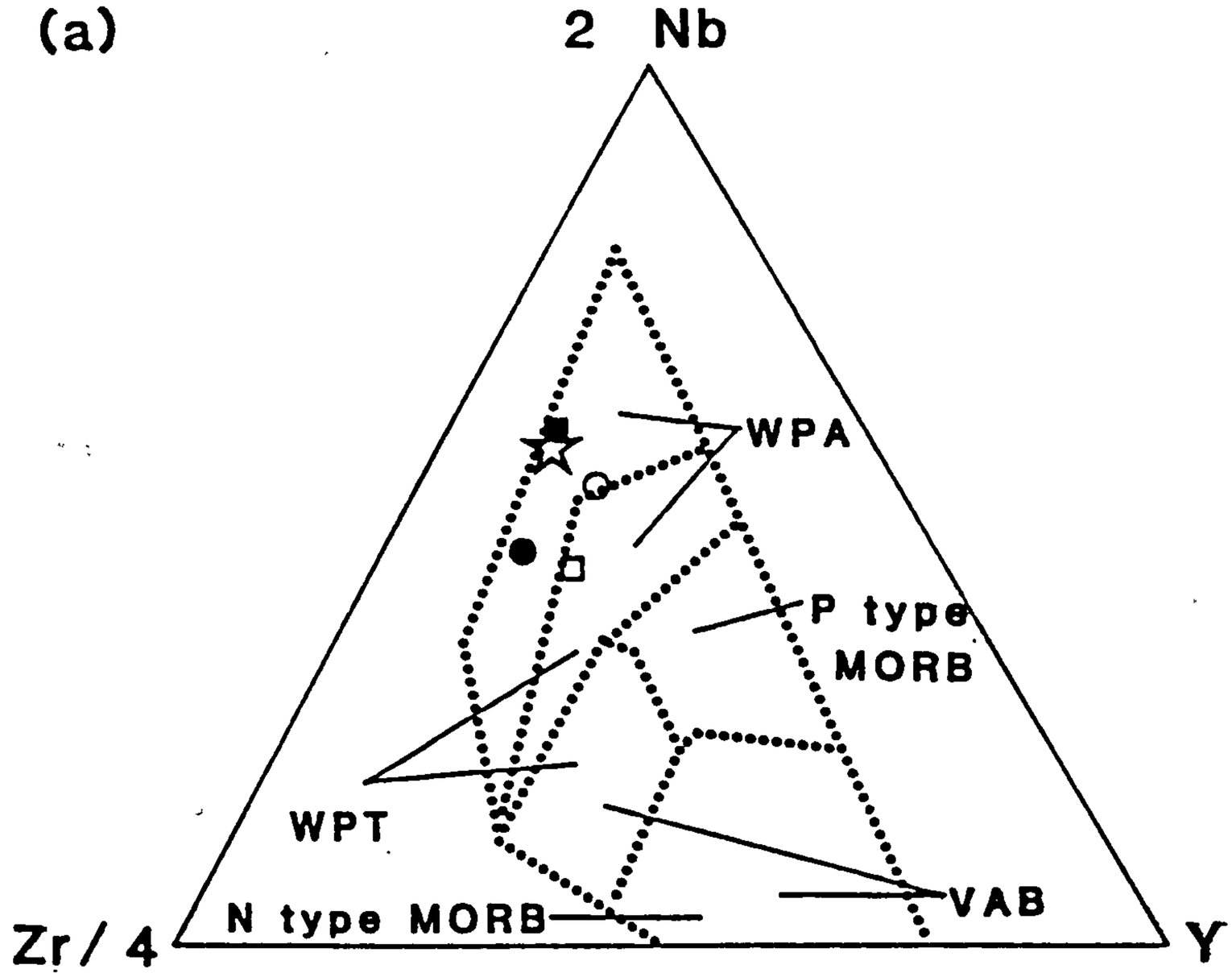

Fig.4.13a. Tectonic environment discriminant diagram based on Zr, Y and Nb. Fields of Meschede(1986) are WPT - Within plate tholeiite, WPA - Within plate alkali basalt and VAB - Volcanic arc basalt. Symbols for S.Atlantic islands as in Fig.4.7.

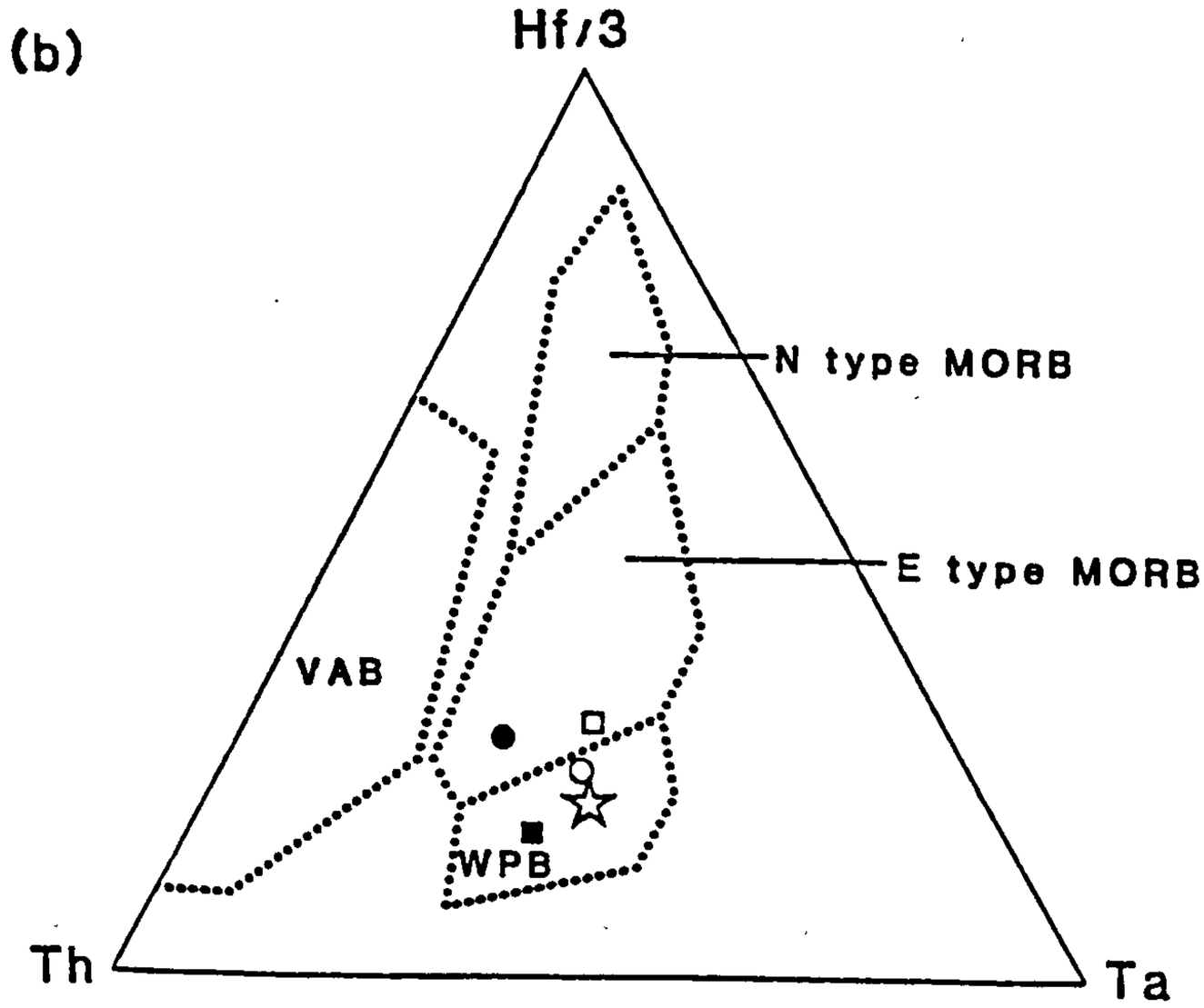

Fig.4.13b. Hf, Th, Ta discriminant diagram of Wood et al.(1979). Field abbreviations and symbols as for 4.9a. with the exception of WPB - Within Plate Basalt.

to lie within the field for OIB magmas of alkali basalt type. The significance of the trace element patterns described briefly above are discussed more fully in section 8.3 by a regional comparison with other S.Atlantic island suites. As it is apparent from Fig.4.12 that there are only limited variations in trace element abundances it is important that the effects of high level processes are considered first (chapters 5 and 6).

Mantle normalised spidergrams are also of value in illustrating graphically the effect of crystal fractionation. The spidergrams for a range of primitive to evolved volcanics on St.Helena are shown in Fig.4.14. If a suite of primitive to evolved rocks related by crystal fractionation processes is compared, two main points require discussion. Firstly, it is seen that an increase in incompatible element abundance occurs in progressively more evolved rocks as these elements have not been removed from the system in fractionating phases. Secondly, if an element that normally behaves incompatibly becomes compatible in a certain phase which is crystallising, it will possess lower chondrite normalised abundances than adjacent incompatible elements. If the example of Ti is taken it is seen that it has an intermediate normalised abundance between Eu and Gd in primitive rocks. When titanomagnetite becomes a fractionating phase in benmoreites, Ti is preferentially removed relative to Eu and Gd and a trough is evident on the spidergram at this point. Similarly, Sr is compatible in plagioclase, and P in apatite. Fractionation of these phases leaves a residual liquid depleted in those elements that enter them preferentially. Such depletions will clearly affect incompatible element ratios in which one element is affected by fractionation whilst the other is not. This modifying effect is very important as ratios which may be used to infer source differences can be substantially altered by this method (chapters 6 and 7).

4.5.3; Introduction to crystal fractionation processes;

It is apparent from Fig.4.1 that the St.Helena volcanics are silica undersaturated and display a range of variation in SiO_2 from 42 to 62 %. From the range of rock types encountered on St.Helena and their variation in mineral chemistry it seems likely that a common process is occurring to produce coherent trends such as those in Fig.4.1. The absence of continental crust in

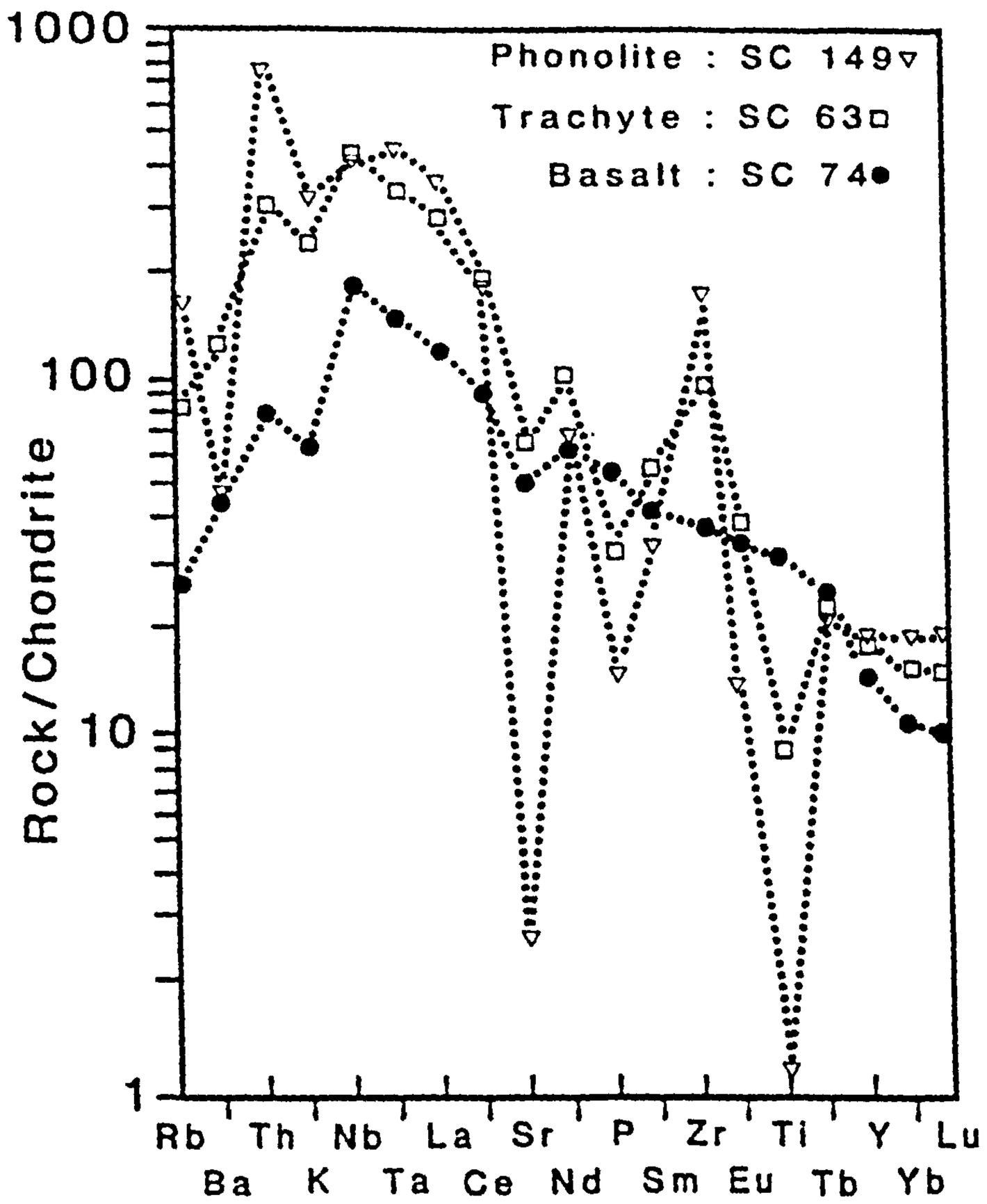

Fig.4.14. Spidergrams of some primitive to evolved rocks of the SW volcano. Normalsing values of Thompson(1982).

mature ocean basins allows the possibility of contamination of primitive magmas by more silicic continental crust to produce the trachytes and phonolites to be excluded. It appears likely that high level crystal fractionation processes causing the physical separation of certain mineral phases from the magma are consistent with the range of rock types and mineral compositions in the SHRS. Given this basic tenet it is most profitable to examine the major and trace element budgets of the St.Helena volcanics in order to assess whether crystallisation of certain phases is capable of producing the coherent chemical variations such as those seen in Fig.4.1. This is a unified approach and is more appropriate than considering the major elements and trace elements in isolation.

4.5.4; Representation of crystal fractionation processes;

The determination of which phases fractionate from a primitive magma batch to produce the geochemical characteristics of the more evolved rocks is most simply approached by considering the order in which phases would crystallise *if there were a single magma batch evolving in a closed system.* It must be remembered that a natural system is likely to be an open system (O'Hara and Matthews(1981)) and samples will come from systems developed at different times. However, the resulting chemical patterns should be similar and equate to a single liquid line of descent if the parental composition *remains approximately constant and if the crystal fractionation process remains similar* (Cox et al.(1979)). Isotopic studies are necessary to ensure that the members of a rock suite are related to the same parent. Indeed, studies by Baker and McBirney(1985) of the liquid lines of descent of the eruptive products of various zoned magma chambers and differentiated suites erupted over a long time interval show that the geochemical trends are coherent. Using this reasoning it is easiest to describe phases as crystallising early or late within a single, hypothetical evolutionary series.

In studying these crystal fractionation processes it is necessary to compare the abundance of certain elements against an index of fractionation. SiO_2 (which is widely used in Harker diagrams) is not usefully employed in this instance because it does not give a good representation of the degree of fractionation at low SiO_2 abundances. This is apparent from a plot of MgO versus SiO_2

(Fig.4.15a). It is apparent that at values of less than 45% SiO_2 a much more marked variation in MgO occurs. This characteristic has been found in many basaltic suites e.g. Wright and Fiske(1971). Thus at an early stage of crystal fractionation MgO is the most sensitive index although SiO_2 is suitable for the more evolved rocks. MgO operates as a good index in the primitive rocks for the well known reason that the early crystallising phases, that is olivine and clinopyroxene, contain a greater proportion of MgO than the residual liquid (Cox et al.(1979). Because olivine and pyroxene occur in the more evolved rocks also MgO can be used as an index across the entire range of compositions. For these reasons it is felt that MgO is the most suitable differentiation index for these samples. More complex "universal" fractionation indices such as the Thornton-Tuttle Differentiation Index are thought not to be necessary in this instance. A better "feel" for the data is enabled by use of the simplest parameters which are entirely adequate for understanding crystal fractionation processes.

The variations exhibited within the SHRS in terms of the MgO reference frame are shown in Fig.4.15. Prior to interpreting these diagrams it is necessary to outline the principles and problems involved with this method of representation.

(1) If a crystallising phase contains a higher proportion of an element than the residual liquid, then its abundance in the liquid will decrease with continued fractionation of that phase.

(2) Conversely, the element abundance in the residual liquid will increase if there is a higher concentration of an element in the liquid than in the phase that is removed.

(3) A marked slope inflection in these diagrams is of crucial importance as it indicates the onset of crystallisation of a phase which has a dominant effect on a particular element because the phase contains this element as a major structural constituent.

(4) It is important to remember that an intrinsic problem with this method of presentation is that the major elements are summed to 100%. Thus if one phase is removed it may effect the slope of the curve of an element which is not present in that phase, because its relative abundance will be changed (e.g. Cox et

(a)

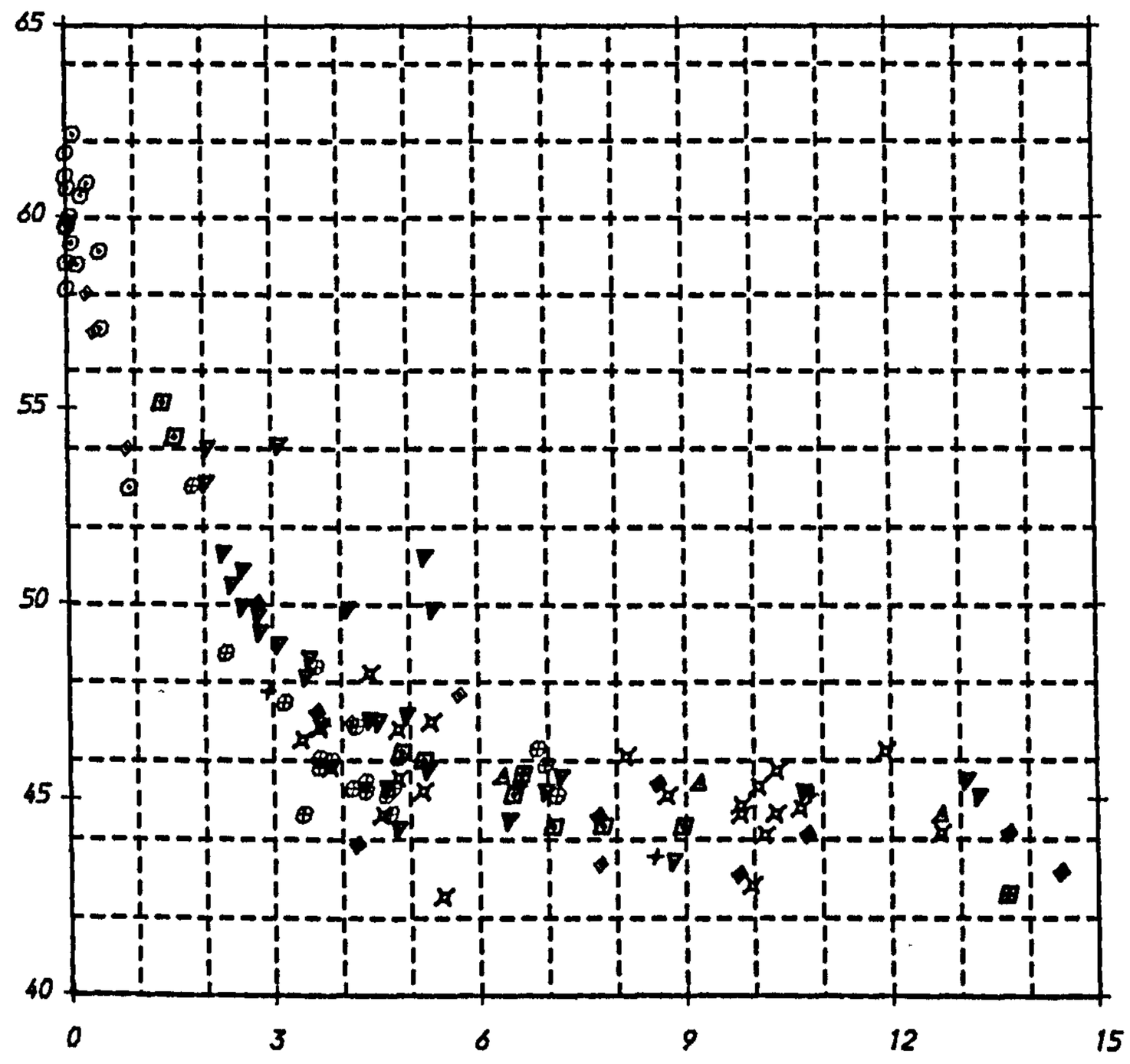
SiO2 (%)
65
60
55
50
45
40
0
3
6
9
12
15
MgO (%)
KEY
NEBB
NE (BB)
NEMS
NE (MS)
SWLS
SW (LS)
SWMS
SW (MS)
SWUS
SWEF
SWLI

(a)

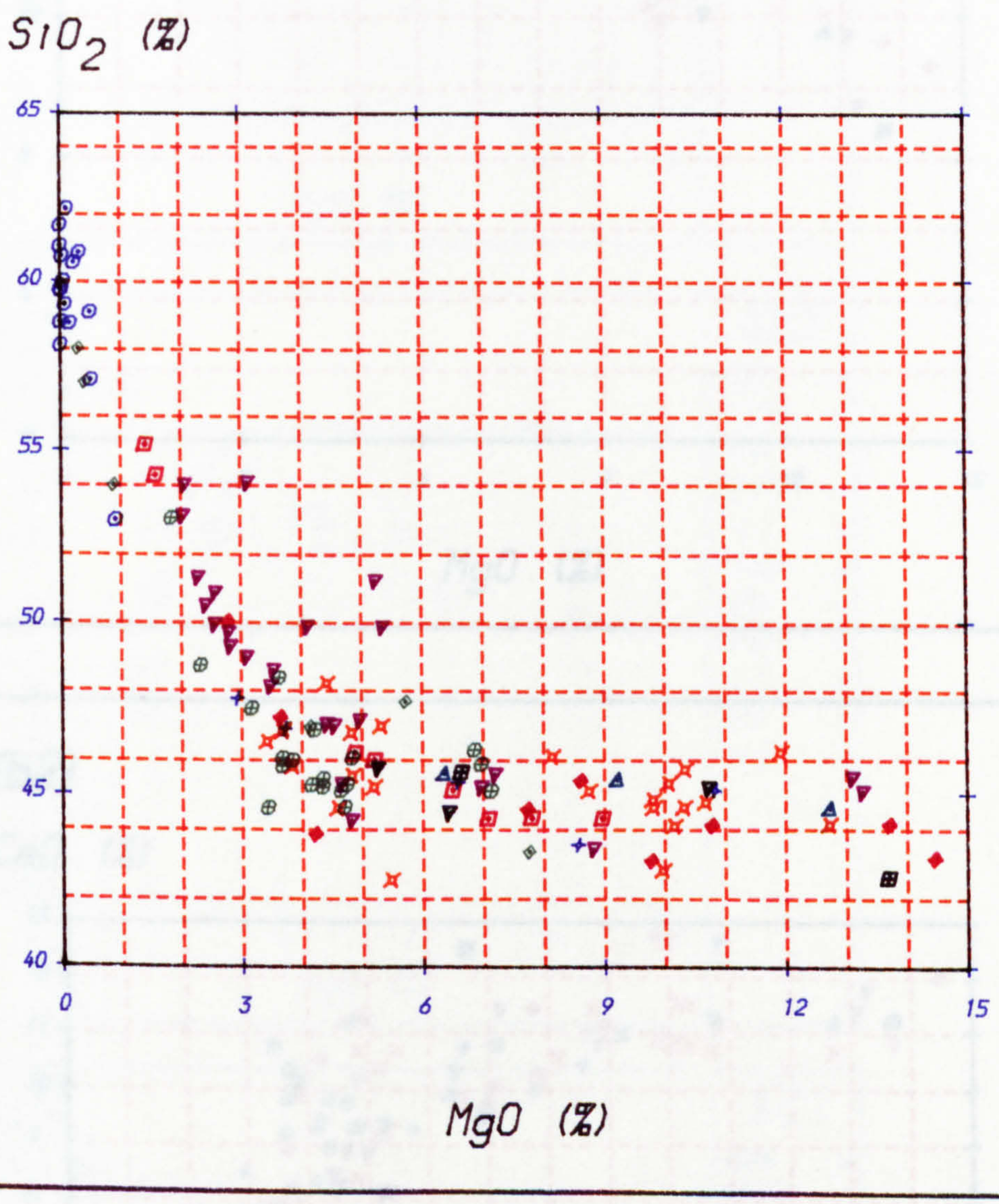
SiO2 (%)
65
60
55
50
45
40
0
3
6
9
12
15
MgO (%)
KEY
NEBB
NE (BB)
NEMS
NE (MS)
SWLS
SW (LS)
SWMS
SW (MS)
SWUS
SWEF
SWLI

(b1)

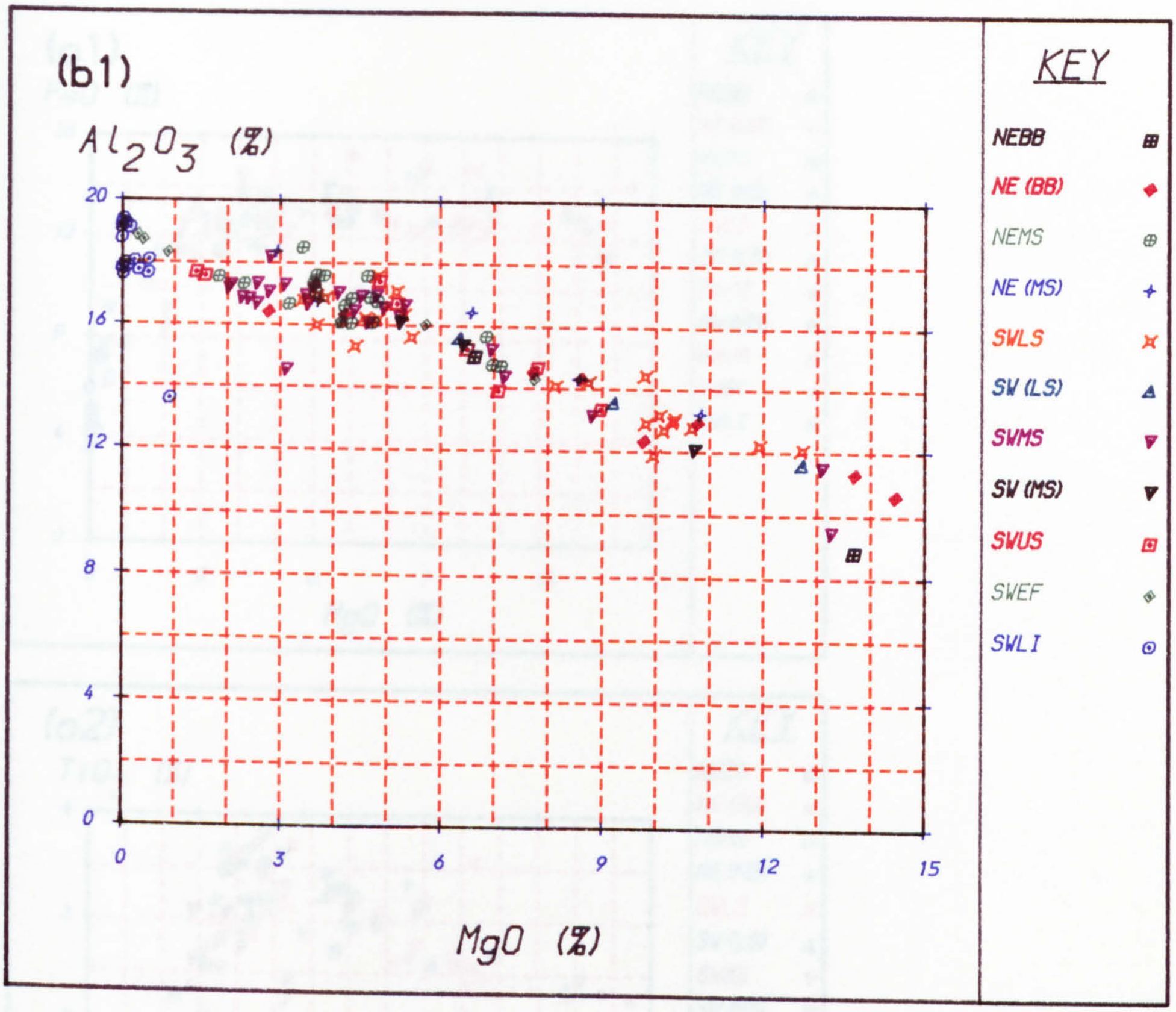
Al2O3 (%)
20
16
12
8
4
0
0
3
6
9
12
15
MgO (%)
KEY
NEBB
NE (BB)
NEMS
NE (MS)
SWLS
SW (LS)
SWMS
SW (MS)
SWUS
SWEF
SWLI

(b2)

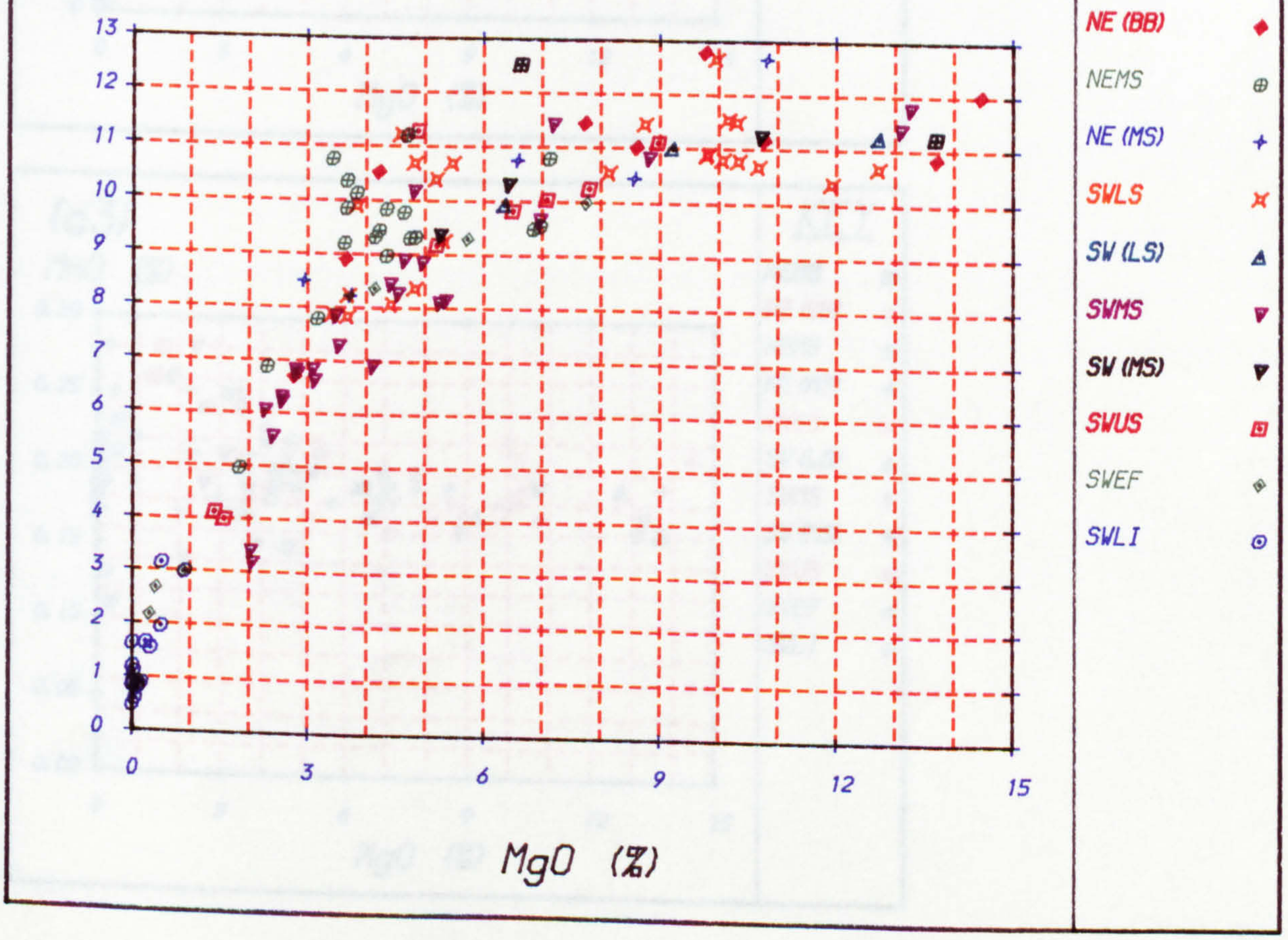
CaO (%)
13
12
11
10
9
8
7
6
5
4
3
2
1
0
0
3
6
9
12
15
MgO (%)
KEY
NEBB
NE (BB)
NEMS
NE (MS)
SWLS
SW (LS)
SWMS
SW (MS)
SWUS
SWEF
SWLI

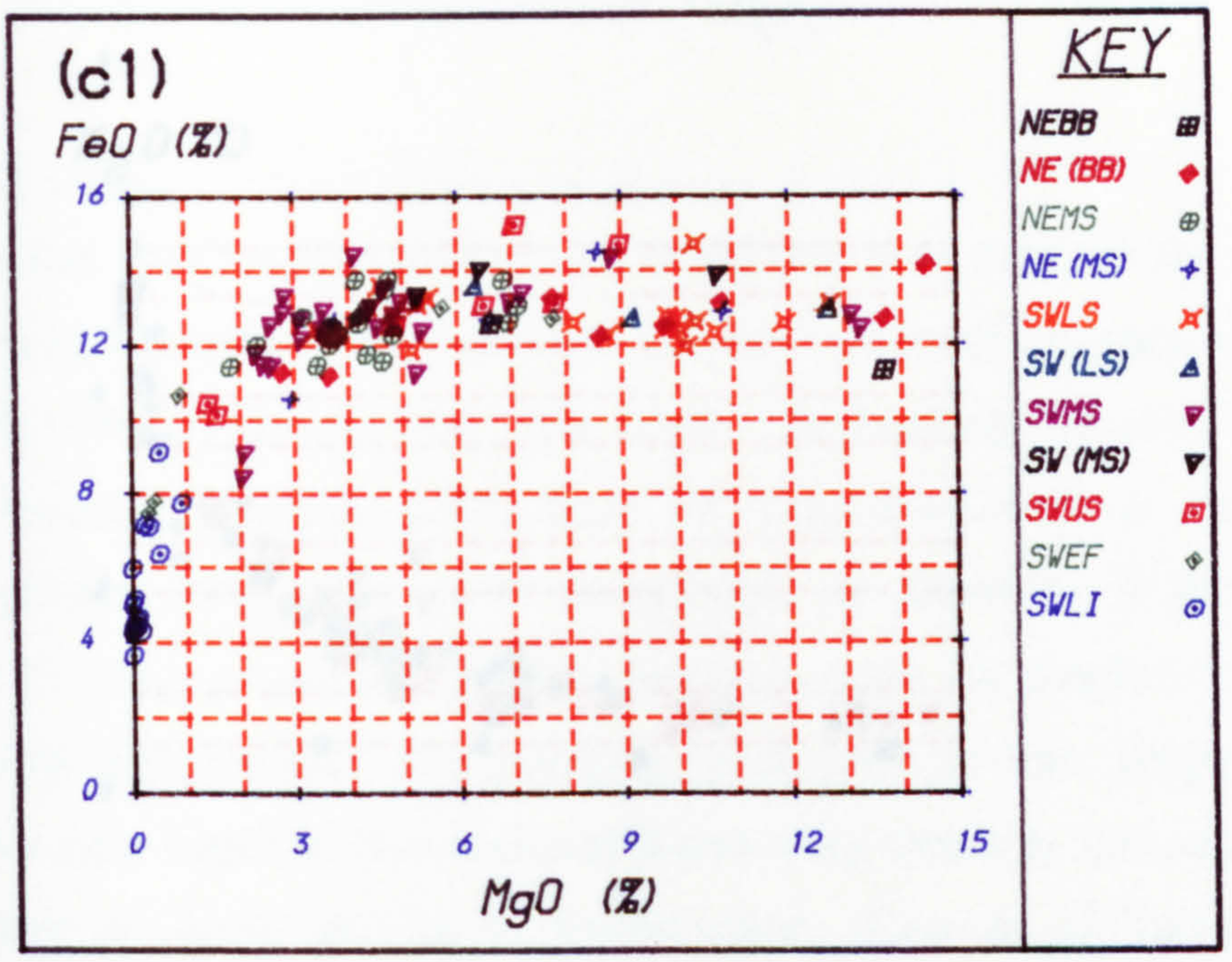
(c1)
FeO (%)
16
12
8
4
0
0
3
6
9
12
15
MgO (%)
KEY
NEBB
NE (BB)
NEMS
NE (MS)
SWLS
SW (LS)
SWMS
SW (MS)
SWUS
SWEF
SWLI

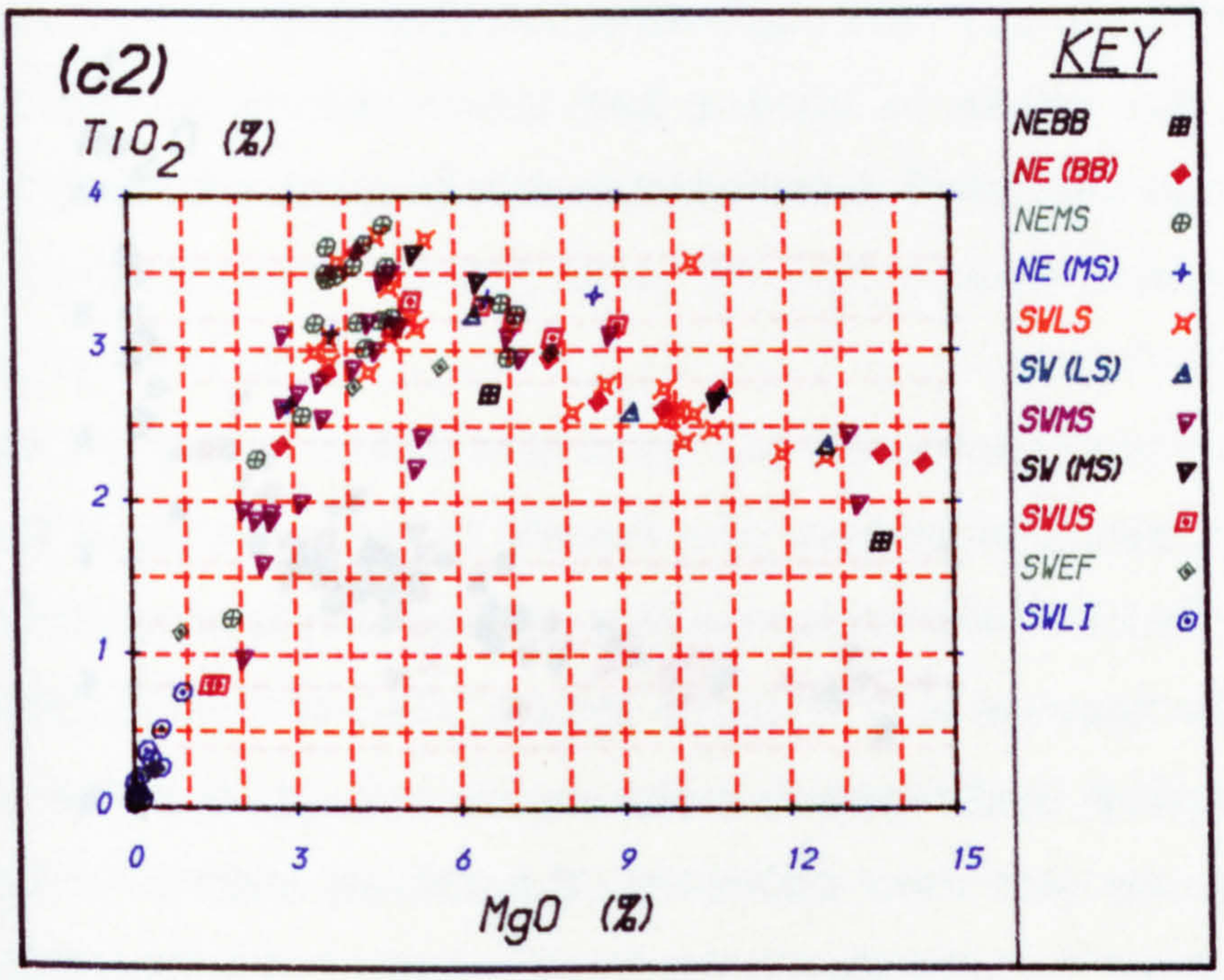
(c2)
TiO2 (%)
4
3
2
1
0
0
3
6
9
12
15
MgO (%)
KEY
NEBB
NE (BB)
NEMS
NE (MS)
SWLS
SW (LS)
SWMS
SW (MS)
SWUS
SWEF
SWLI

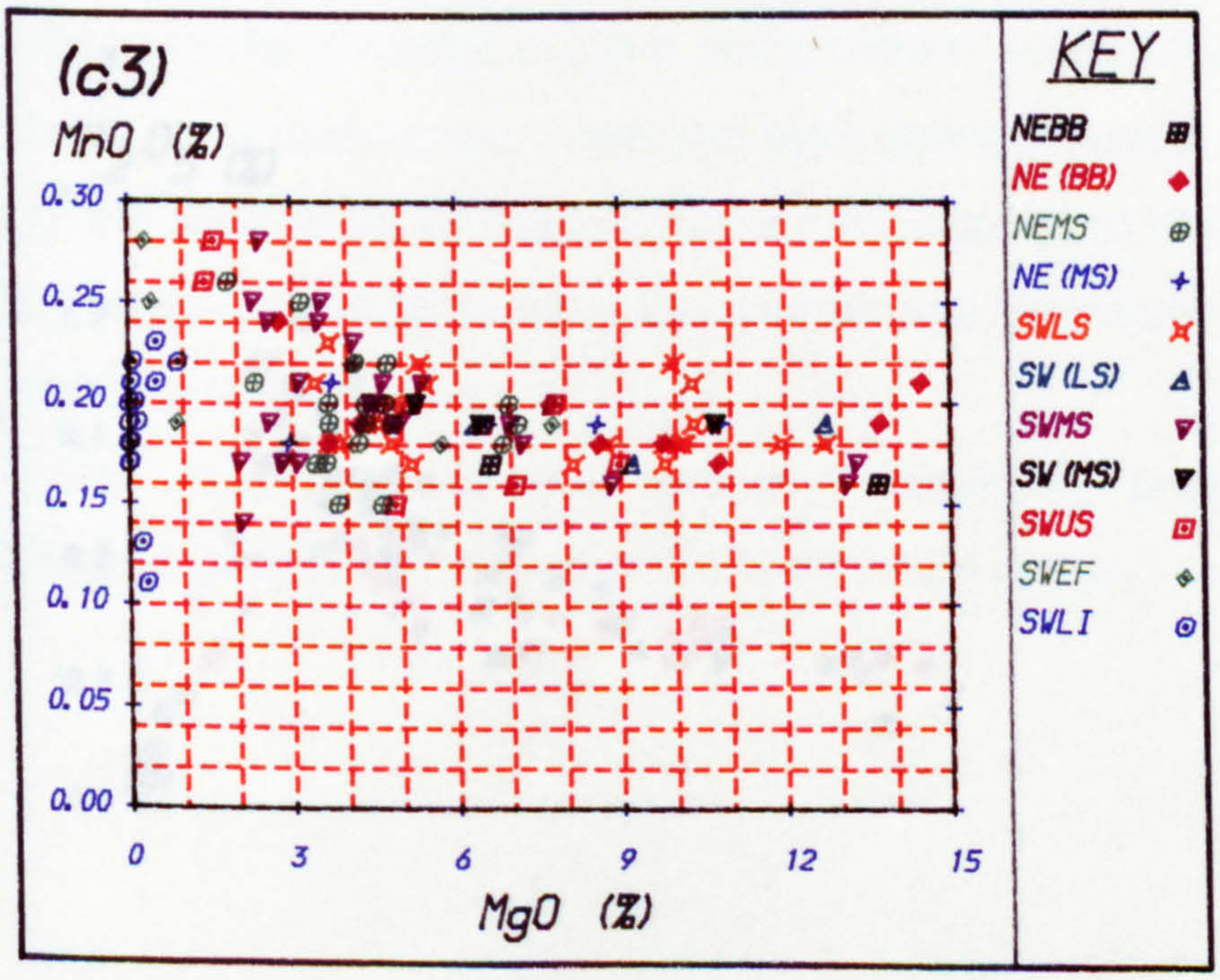
(c3)
MnO (%)
0.30
0.25
0.20
0.15
0.10
0.05
0.00
0
3
6
9
12
15
MgO (%)
KEY
NEBB
NE (BB)
NEMS
NE (MS)
SWLS
SW (LS)
SWMS
SW (MS)
SWUS
SWEF
SWLI

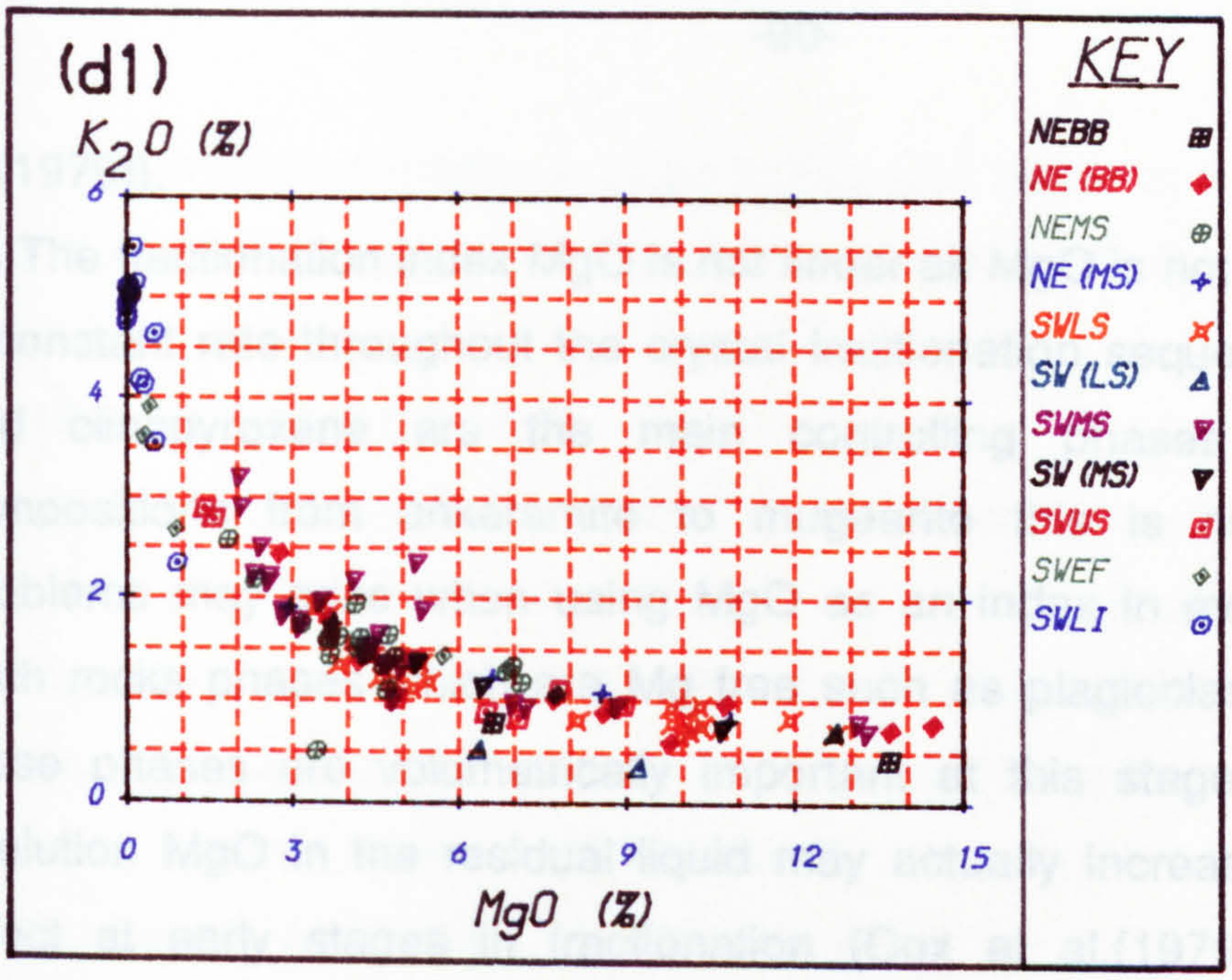
(d1)
K2O (%)
6
4
2
0
0
3
6
9
12
15
MgO (%)
KEY
NEBB
NE (BB)
NEMS
NE (MS)
SWLS
SW (LS)
SWMS
SW (MS)
SWUS
SWEF
SWLI

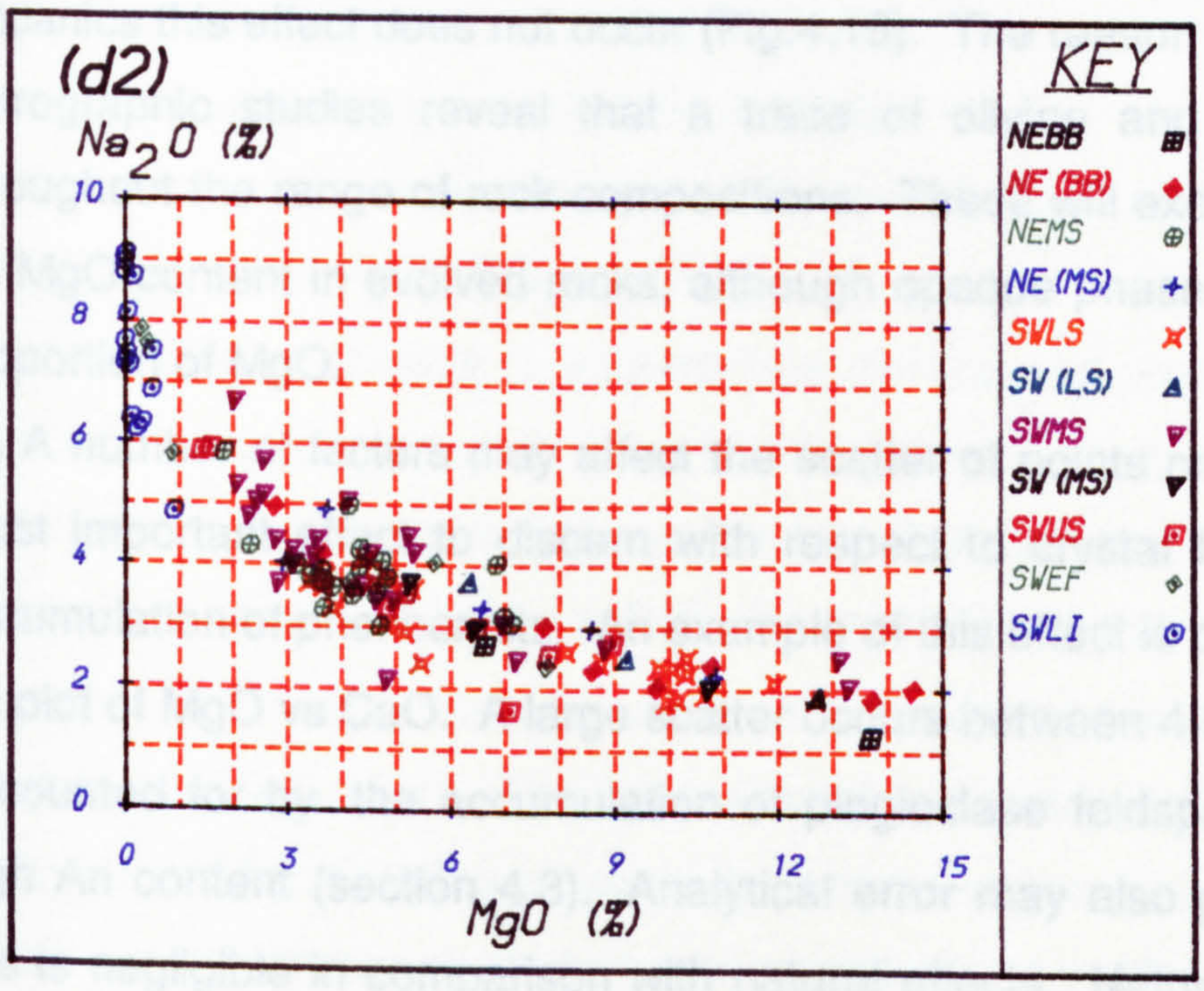
(d2)
Na2O (%)
10
8
6
4
2
0
0
3
6
9
12
15
MgO (%)
KEY
NEBB
NE (BB)
NEMS
NE (MS)
SWLS
SW (LS)
SWMS
SW (MS)
SWUS
SWEF
SWLI

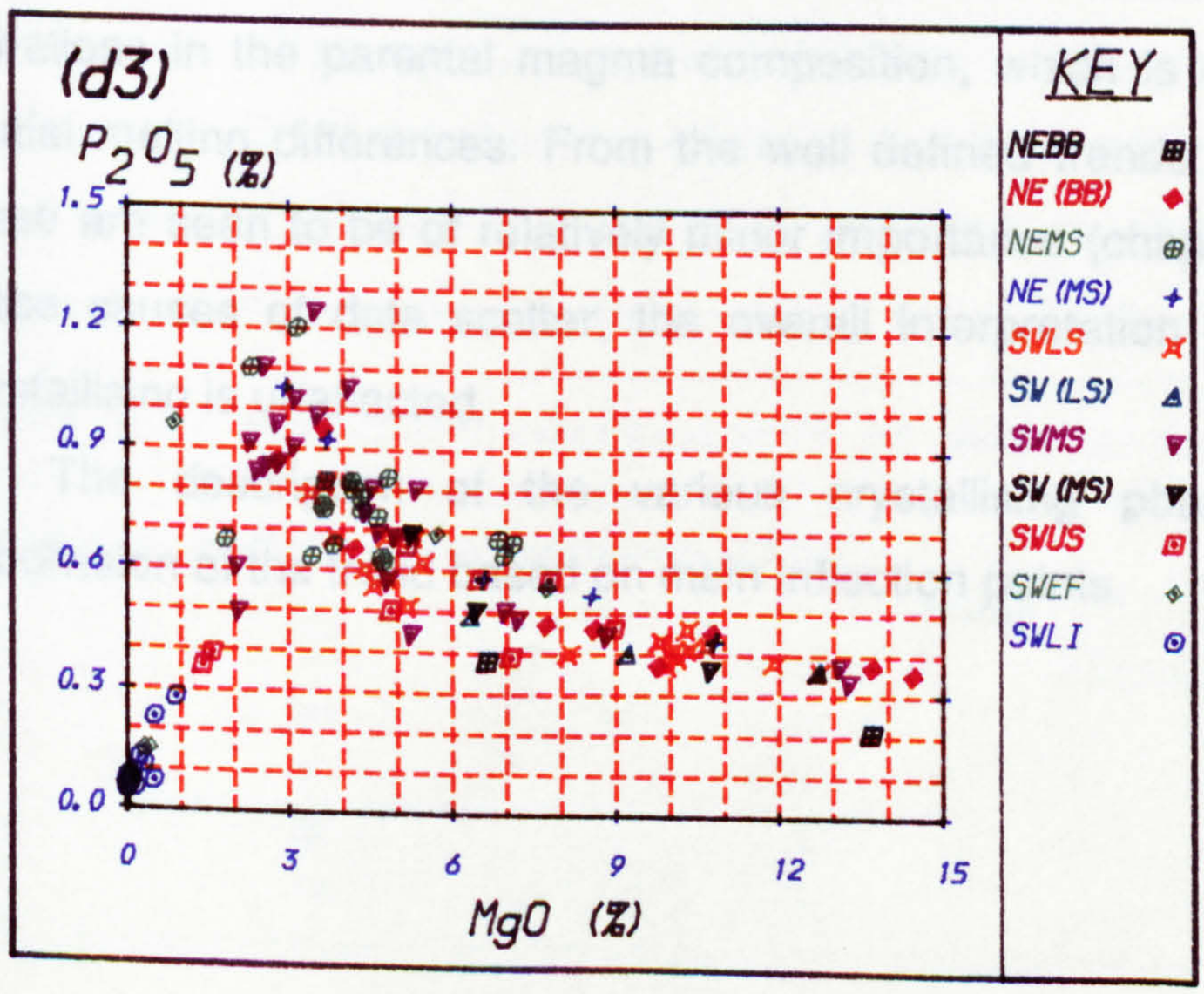
(d3)
P2O5 (%)
1.5
1.2
0.9
0.6
0.3
0.0
0
3
6
9
12
15
MgO (%)
KEY
NEBB
NE (BB)
NEMS
NE (MS)
SWLS
SW (LS)
SWMS
SW (MS)
SWUS
SWEF
SWLI

al.(1979)).

(5) The fractionation index MgO is not linear as MgO is not removed in phases at a constant rate throughout the crystal fractionation sequence. Because olivine and clinopyroxene are the main controlling phases in the majority of compositions from ankaramite to mugearite this is not a major problem. Problems may arise when using MgO as an index in more evolved rocks. In such rocks phases which are Mg free such as plagioclase may fractionate. If these phases are volumetrically important at this stage of magma chamber evolution MgO in the residual liquid may actually increase, thus reversing the effect at early stages in fractionation (Cox et al.(1979)). In the St.Helena volcanics this effect does not occur (Fig.4.15). The reason for this is that detailed petrographic studies reveal that a trace of olivine and pyroxene is present throughout the range of rock compositions. These will exert the principal control on MgO content in evolved rocks, although opaque phases also contain a small proportion of MgO.

(6) A number of factors may affect the scatter of points on such diagrams. The most important effect to discern with respect to crystal fractionation is that of accumulation of phenocrysts. An example of this effect is provided by Fig.4.15b1 - a plot of MgO vs CaO. A large scatter occurs between 4-5% MgO. This can be accounted for by the accumulation of plagioclase feldspar phenocrysts with a high An content (section 4.3). Analytical error may also produce an effect, but this is negligible in comparison with natural effects. Natural effects also include variations in the parental magma composition, which is effected by source or partial melting differences. From the well defined trends of Figs.4.1. and 4.15 these are seen to be of relatively minor importance (chapter 6 and 7). Despite these causes of data scatter, the overall interpretation of which phases are crystallising is unaffected.

The description of the various crystallising phases is achieved by subdivision of the trend based on main inflection points.

The important breaks in slope in Fig.4.15 occur at 5% MgO for CaO, FeO and K_2O. A marked kink also occurs at 3% MgO for P_2O_5. The important subdivisions are :

(1) 14% MgO to 4.5% MgO.

The marked decrease in MgO abundances occurs through fractionation of Mg rich phases which are thought to be olivine and clinopyroxene from petrographic studies (Fig.4.2). Uncommon plagioclase microphenocrysts first appear at 9% MgO, thus fractionation of these three phases is responsible for the following features between 14-4.5% MgO:

(i) Decrease in MgO (Fig.4.15a-d).

(ii) FeO approximately constant(Fig.4.15c1).

(iii) CaO approximately constant(Fig.4.15b2).

(iv) Increase in elements incompatible in the structure of these three phases i.e. K_2O, Na_2O, MnO, P_2O_5, TiO_2 and Al_2O_3.

It is now necessary to enquire how the varying proportions of the phases produce these variations. In many basaltic suites it is olivine which produces the dominant control at early stages. In the St.Helena volcanics all phases are involved. A graph of MgO vs CaO illustrates this point well (Fig.4.15b2). It is seen that CaO is approximately constant between 14 and 9% MgO whereas CaO decreases to 4% MgO. The approximately constant CaO is an indication that olivine is not fractionating alone as the concentration effect in the residual liquid would tend to increase CaO if this were the case. Thus, there is a balance between this effect and CaO being lost from the system in clinopyroxene and plagioclase. Good corroborative evidence for the fractionation of clinopyroxene at all stages is provided by a plot of Sc vs CaO/Al_2O_3 (Fig.4.16a). Sc is a trace element that is compatible in clinopyroxene, but not olivine (Table 4.2).

Table 4.2; Partition coefficients of some elements compatible in olivine and clinopyroxene. (Average values for basaltic and andesitic liquids from Henderson(1982)).

	Phase	
	olivine	clinopyroxene
Ni	14.0	2.6
V	0.03	1.3
Sc	0.17	2.7
Cr	2.1	8.4

Fig.4.16. The behaviour of some compatible elements in the SHRS:

Fig.4.16a. CaO/Al_2O_3 vs Sc in the NE volcano.

Fig.4.16b. Ni vs V

Fig.4.16c. MgO vs Ba in the entire SHRS.

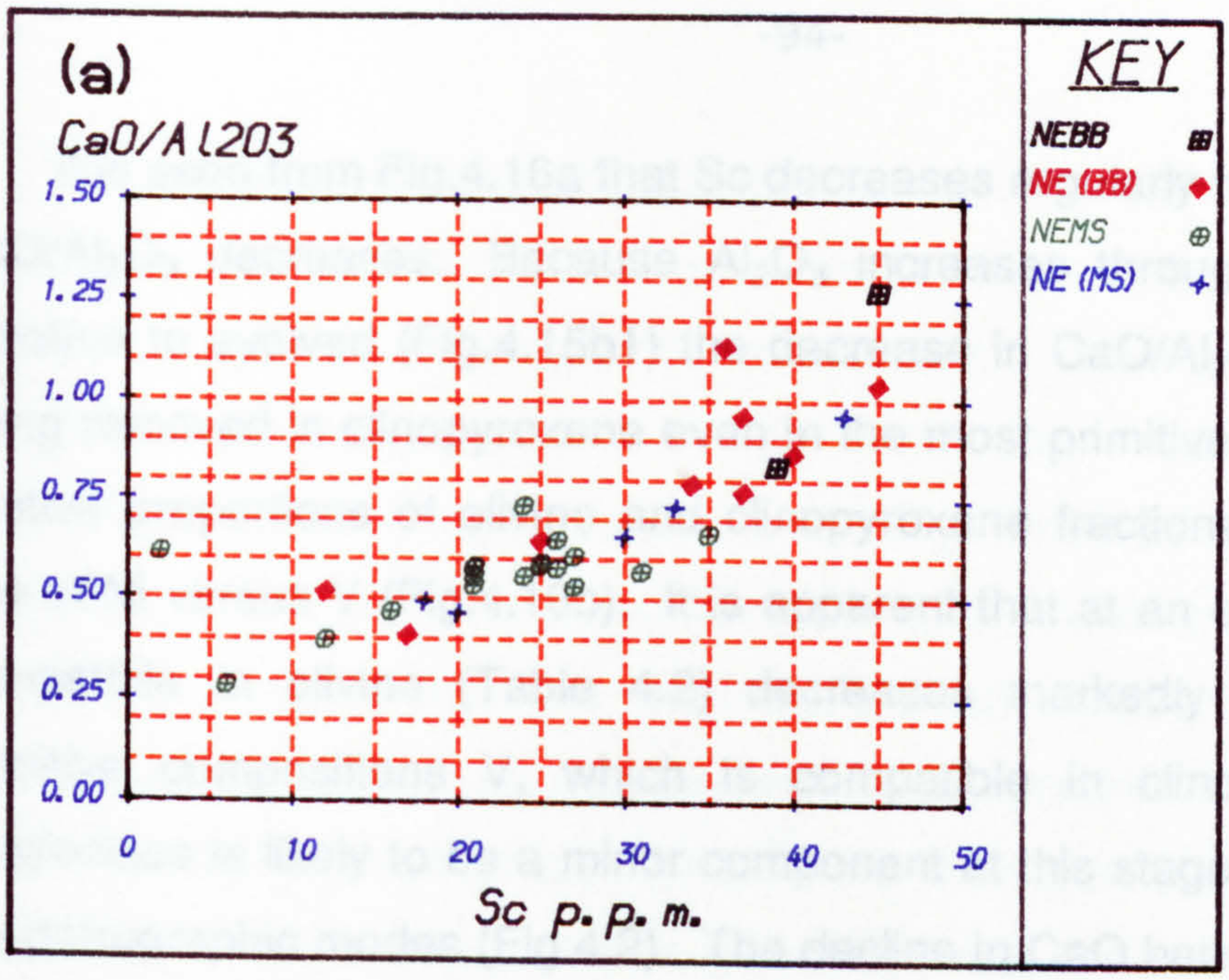
(a)
CaO/Al2O3
1.50
1.25
1.00
0.75
0.50
0.25
0.00
0
10
20
30
40
50
Sc p.p.m.
KEY
NEBB
NE (BB)
NEMS
NE (MS)

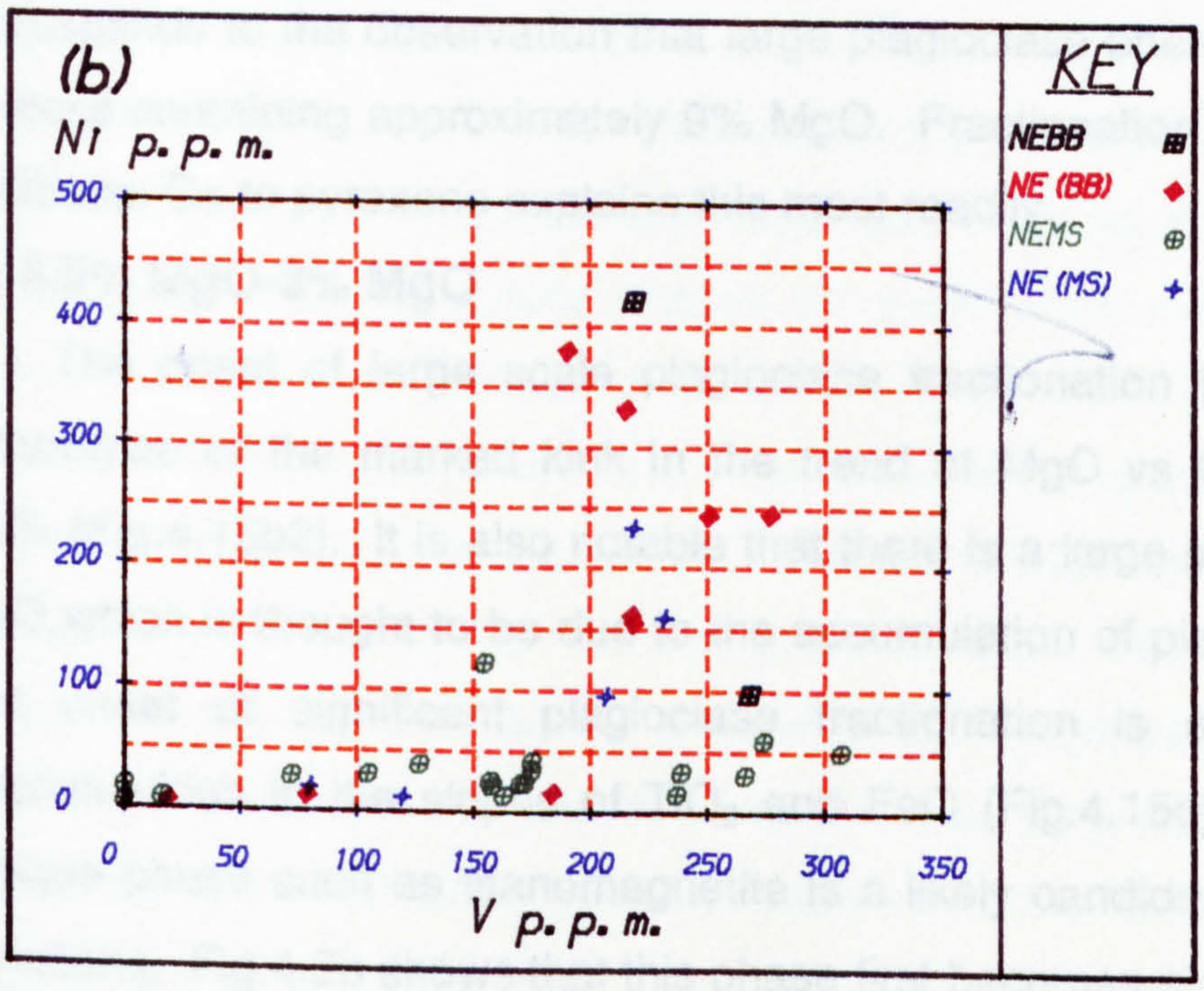
(b)
Ni p.p.m.
500
400
300
200
100
0
0
50
100
150
200
250
300
350
V p.p.m.
KEY
NEBB
NE (BB)
NEMS
NE (MS)

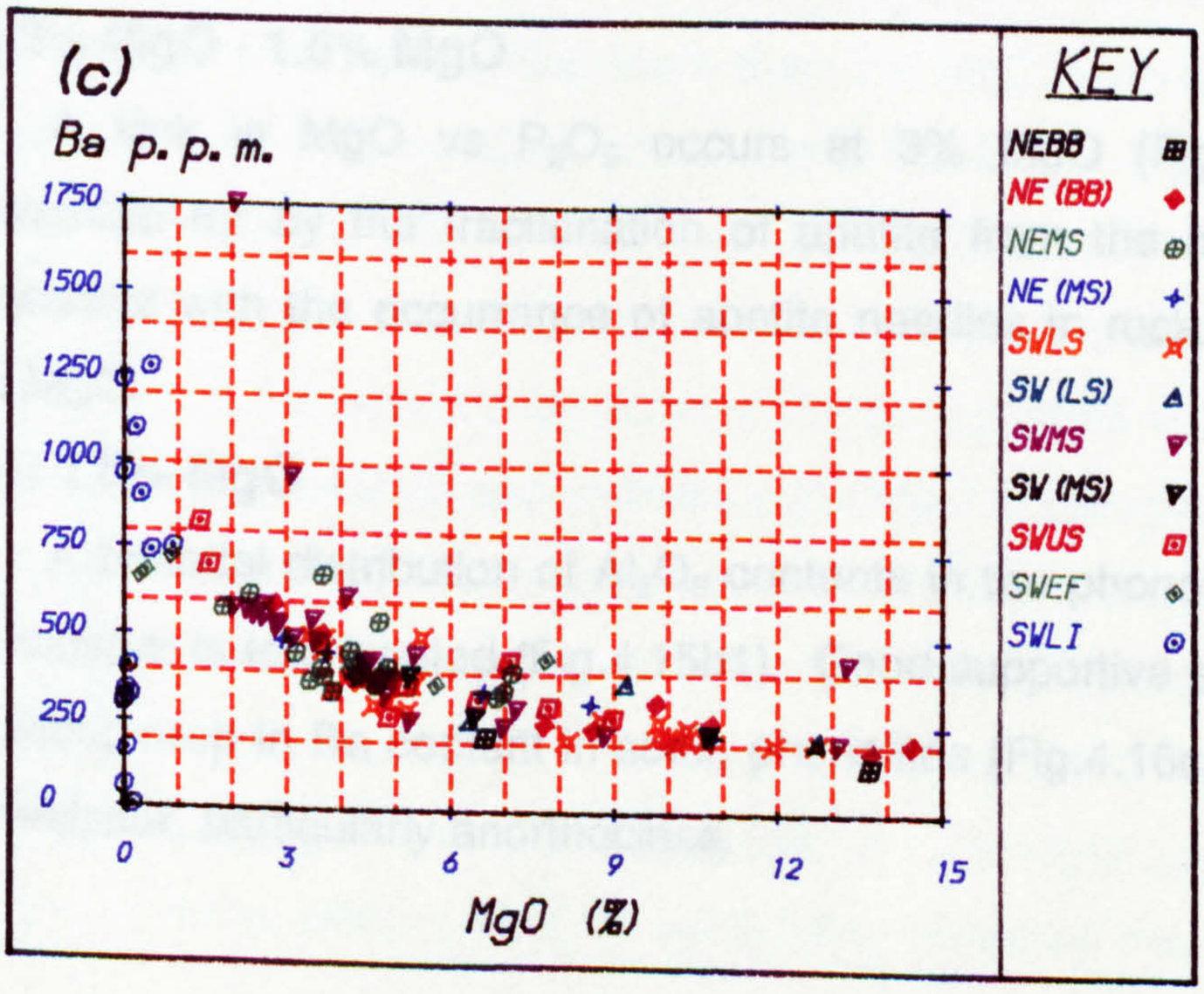
(c)
Ba p.p.m.
1750
1500
1250
1000
750
500
250
0
0
3
6
9
12
15
MgO (%)
KEY
NEBB
NE (BB)
NEMS
NE (MS)
SWLS
SW (LS)
SWMS
SW (MS)
SWUS
SWEF
SWLI

It is seen from Fig.4.16a that Sc decreases regularly from 50 to 30 p.p.m. as CaO/Al_2O_3 decreases. Because Al_2O_3 increases throughout the SHRS from primitive to evolved (Fig.4.15b1) the decrease in CaO/Al_2O_3 shows that CaO is being removed in clinopyroxene even in the most primitive rocks. An idea of the relative proportions of olivine and clinopyroxene fractionating is provided by a plot of Ni versus V (Fig.4.16b). It is apparent that at an early stage Ni which is compatible in olivine (Table 4.2) decreases markedly whereas in the less primitive compositions V, which is compatible in clinopyroxene decreases. Plagioclase is likely to be a minor component at this stage which is evident from the petrographic modes (Fig.4.2). The decline in CaO between 9 and 4.5% MgO corresponds to the observation that large plagioclase phenocrysts are first found in rocks containing approximately 9% MgO. Fractionation of a phase containing additional Ca to pyroxene explains this most readily.

(2) 4.5% MgO-3% MgO

The onset of large scale plagioclase fractionation is responsible for the occurrence of the marked kink in the trend of MgO vs CaO at approximately 4.5% (Fig.4.15b2). It is also notable that there is a large scatter in CaO at 4-5% MgO which is thought to be due to the accumulation of plagioclase phenocrysts. The onset of significant plagioclase fractionation is also accompanied by discontinuities in the slopes of TiO_2 and FeO (Fig.4.15c). Fractionation of an opaque phase such as titanomagnetite is a likely candidate for producing these variations. Fig.4.2b shows that this phase first becomes abundant in hawaiites.

(3) 3% MgO - 1.5% MgO

A kink in MgO vs P_2O_5 occurs at 3% MgO (Fig.4.15d) this may be accounted for by the fractionation of apatite from the magma body. This is consistent with the occurrence of apatite needles in rocks containing less than 3% MgO.

(4) < 1.5% MgO

A bimodal distribution of Al_2O_3 contents in the phonolites may indicate that K-Feldspar is fractionated (Fig.4.15b1). Good supportive evidence for this is the dramatic drop in Ba content in some phonolites (Fig.4.16c). Ba is compatible in K-Feldspar, particularly anorthoclase.

To act as a summary of which phases are inferred to be crystallising during the evolution of the SHRS from primitive to evolved, the pertinent two element variation diagrams showing both rock and the most primitive mineral extract compositions are presented in Fig.4.17. Fig. 4.17a. exhibits a linear fractionation vector in terms of CaO and SiO_2. The back projection of this vector intersects a triangle constructed from the most primitive observed compositions of olivine, clinopyroxene and plagioclase phenocrysts. Considered in isolation this feature could suggest that the overall composition of the mineral extract is influenced by all three phases in all rocks from primitive to evolved. However, the fact that some compositions plot inside this extract polygon suggests that plagioclase fractionation is not involved at all stages in the evolution of the chemical trends of the SHRS. The fact that two samples plot to the left of the three phase polygon suggests that these rocks may have been formed by crystal fractionation involving mineral phases compositionally more extreme than those shown. Alternatively a phase such as Cr spinel which has low CaO and MgO contents could produce this effect. If olivine and clinopyroxene are accumulative this could also produce this effect. Section 6.2.2.2 discusses whether these phases are likely to be accumulative in basic members of the SHRS. Examination of Figs.4.17b and c confirm that plagioclase is not an important fractionating phase in the primitive rocks. These diagrams possess two different vectors with the transition between them occurring at approximately 5% MgO when plagioclase fractionation becomes important. The direction of the vector in Fig.4.17c for rocks containing more than 5% MgO is uncertain, but is clearly not coincident with that for rocks containing 3-5% MgO. The back projection of the trends in rocks containing more than 5% MgO cuts the tie line between olivine and clinopyroxene extract compositions in Fig.4.17b and c. Application of the Lever Rule is not possible because of the poorly constrained nature of the trend. The abrupt transition at approximately 5% MgO is thought to be due to the onset of large scale plagioclase fractionation because the vector changes in response to the effect of a phase containing a higher proportion of Al_2O_3 and Na_2O than olivine or clinopyroxene. CaO is lower in plagioclase than clinopyroxene. A plot of Na_2O vs Al_2O_3 (Fig.4.17d) shows that at <5% MgO plagioclase becomes one of the principal phases that is crystallising because the back projection of the

Fig.4.17. Extract polygons for the SHRS. Coloured symbols represent the MgO % in the host rock which is given in the key. The mineral compositions are the most primitive observed SEM determinations .

Fig.4.17a. SiO_2 vs CaO.

Fig.4.17b. MgO vs CaO.

Fig.4.17c. Al_2O_3 vs SiO_2.

Fig.4.17d. Al_2O_3 vs Na_2O.

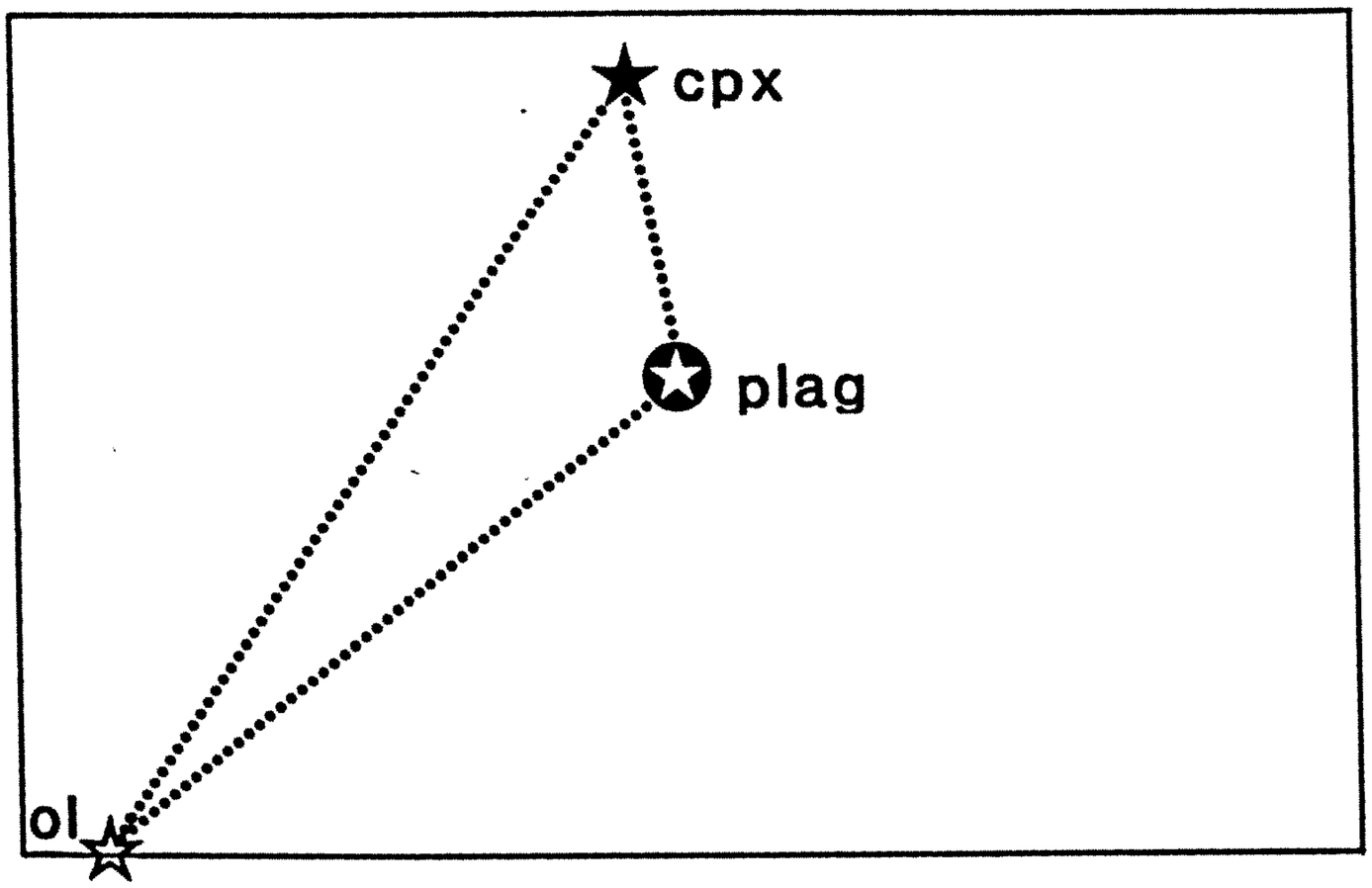
cpx
plag
ol

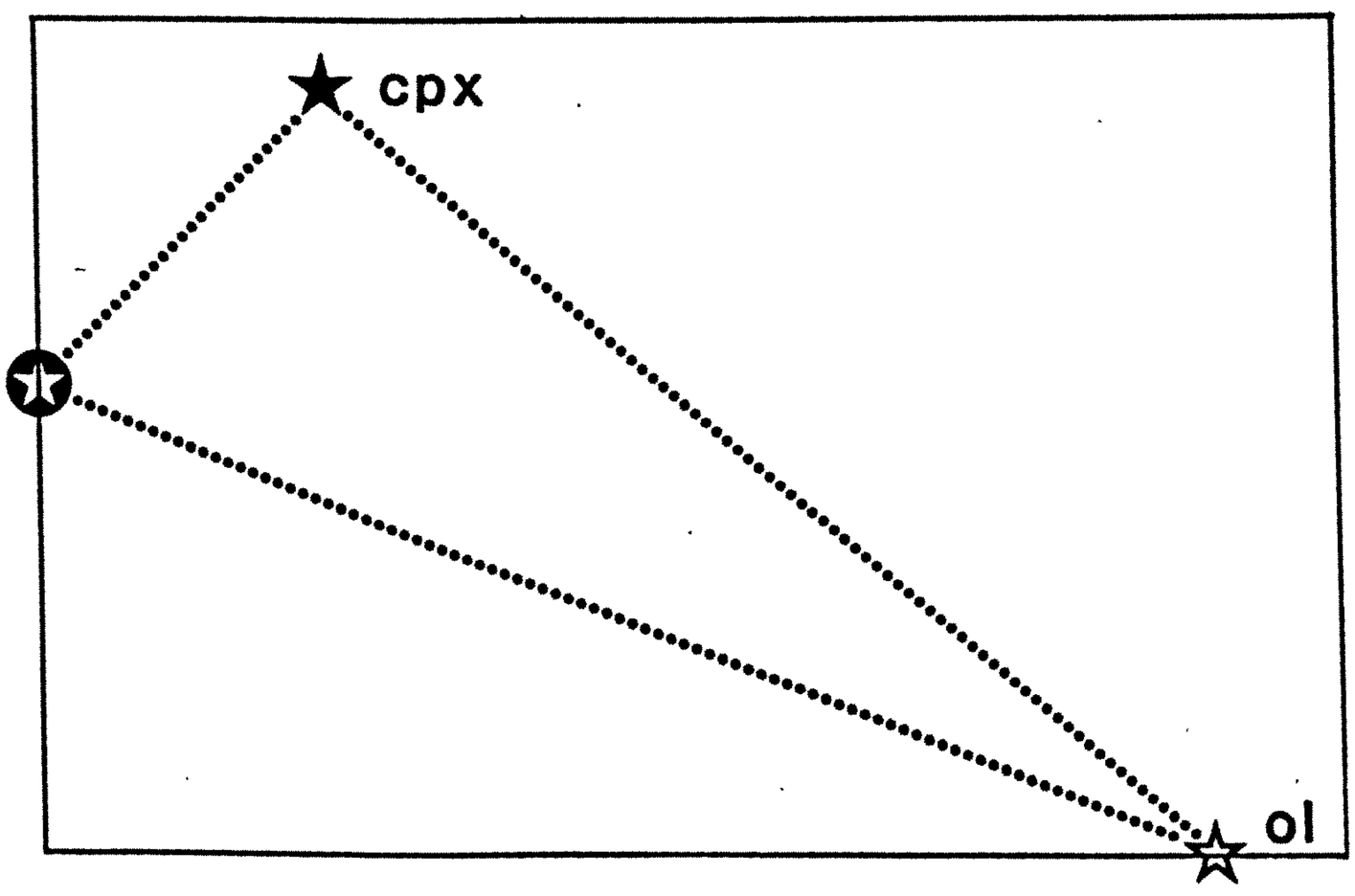
cpx
ol

(a)

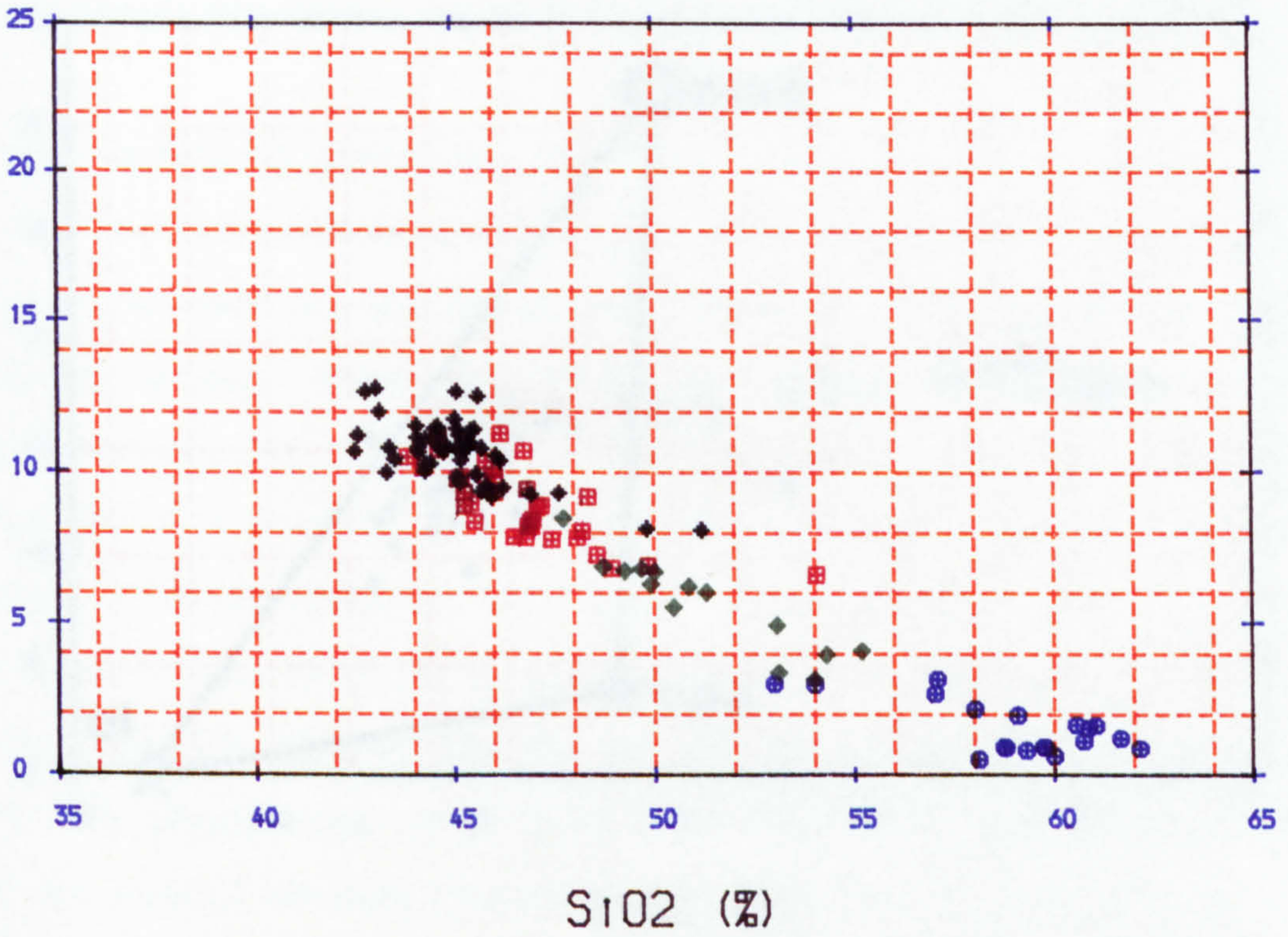
CaO (%)
25
20
15
10
5
0
35
40
45
50
55
60
65
SiO2 (%)
KEY
5-15%
3-5%
1-3%
<1%

(b)

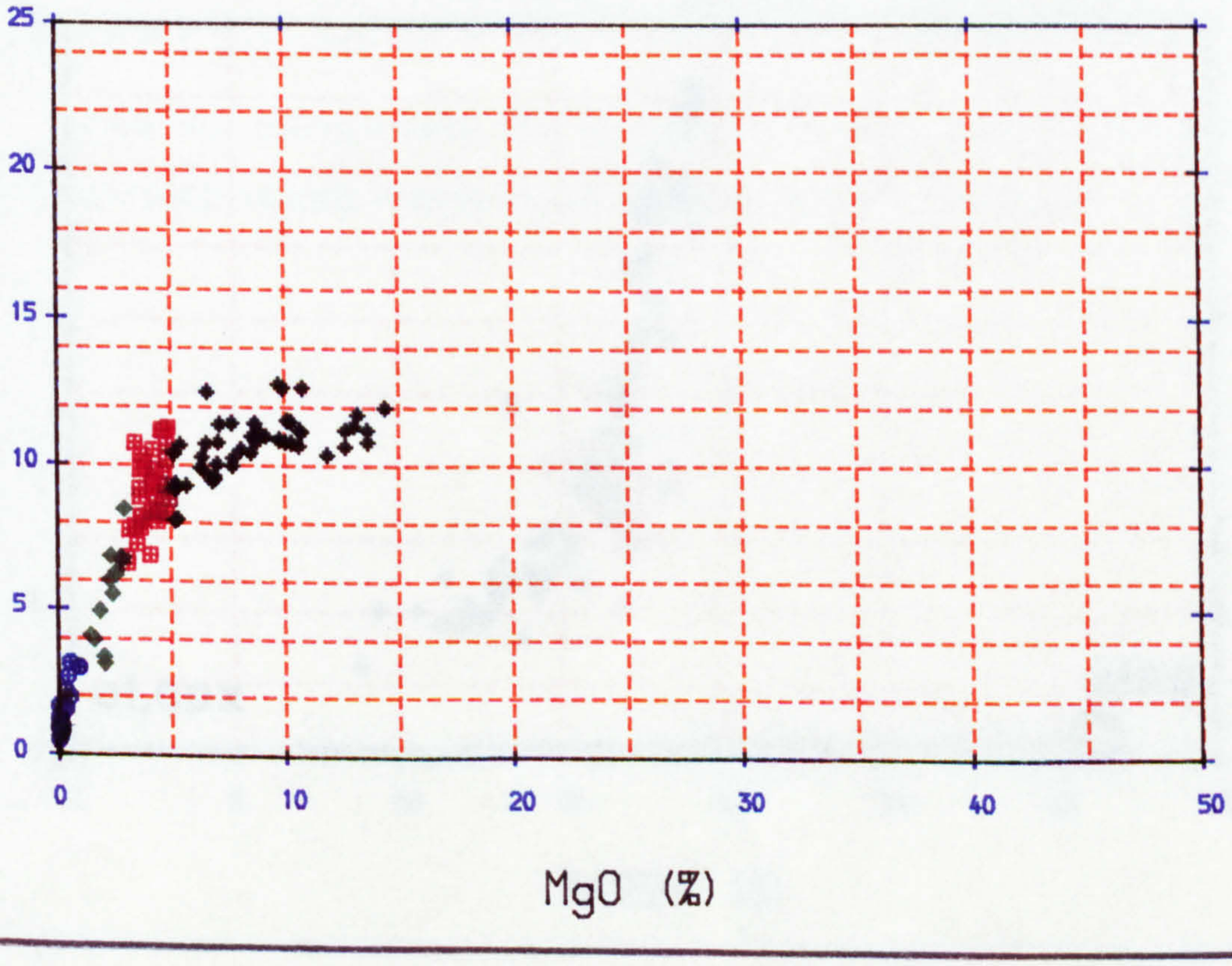
CaO (%)
25
20
15
10
5
0
0
10
20
30
40
50
MgO (%)
KEY
5-15%
3-5%
1-3%
<1%

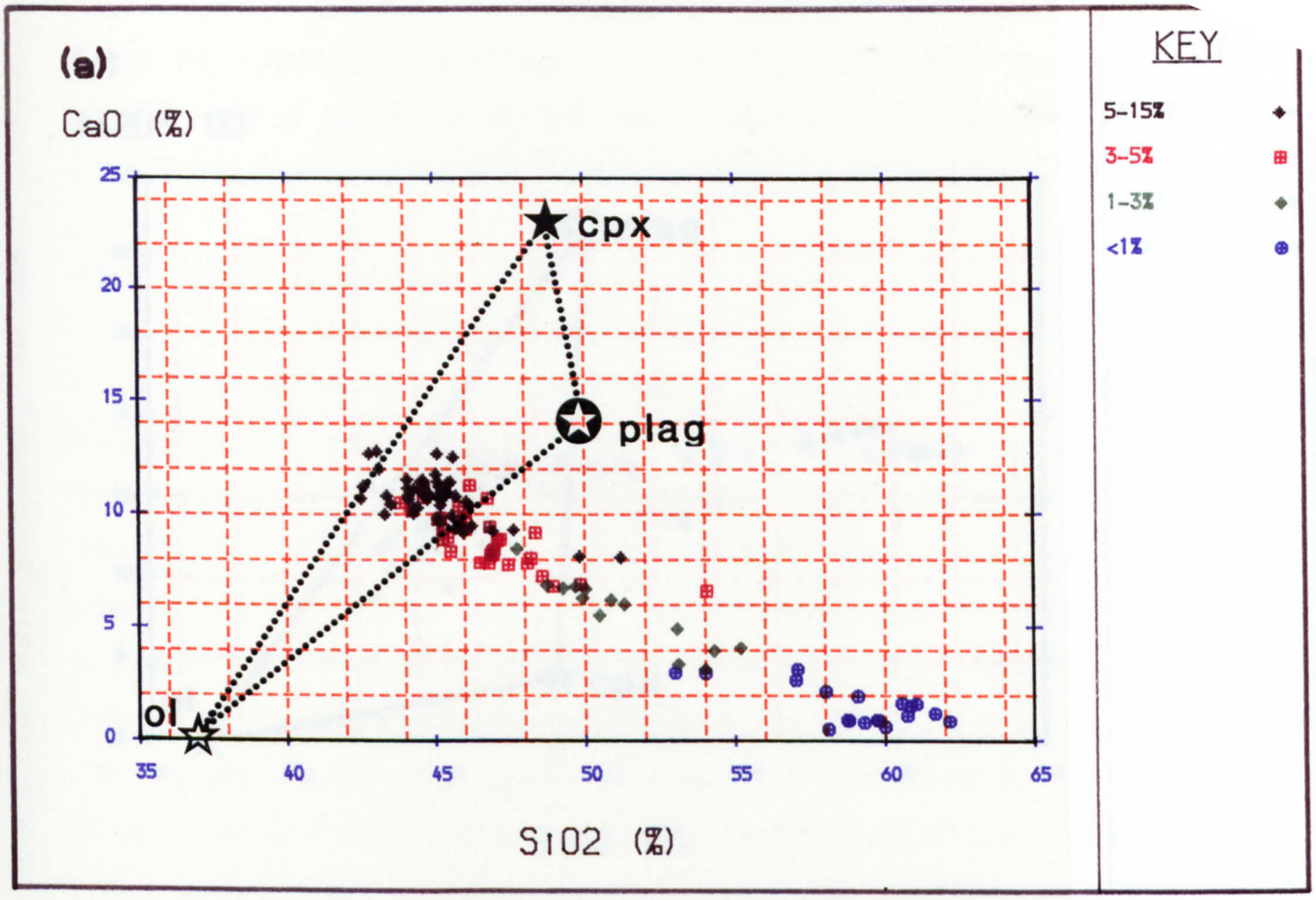
(a)
CaO (%)
cpx
plag
ol
SiO2 (%)
KEY
5-15%
3-5%
1-3%
<1%

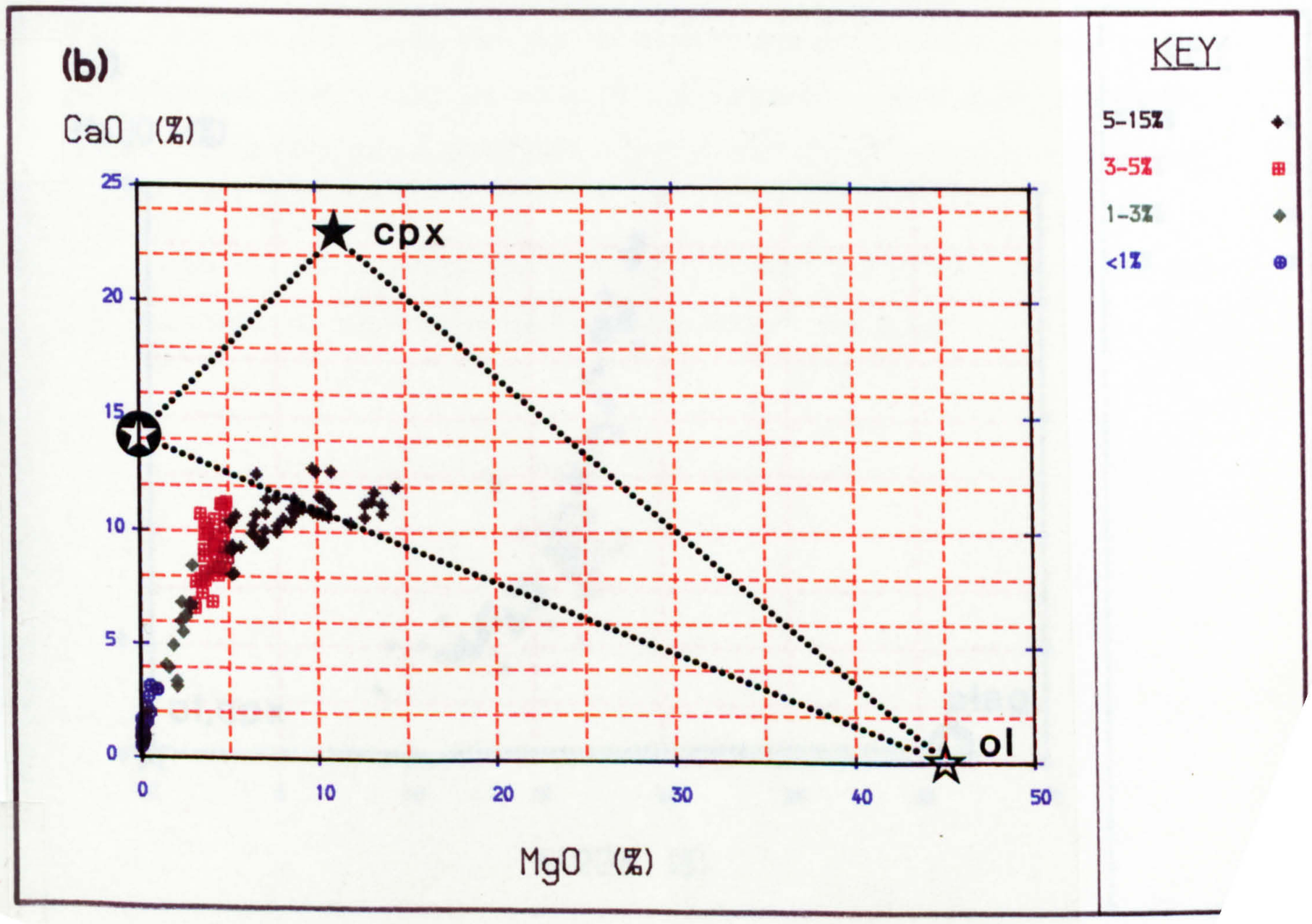
(b)
CaO (%)
cpx
plag
ol
MgO (%)
KEY
5-15%
3-5%
1-3%
<1%

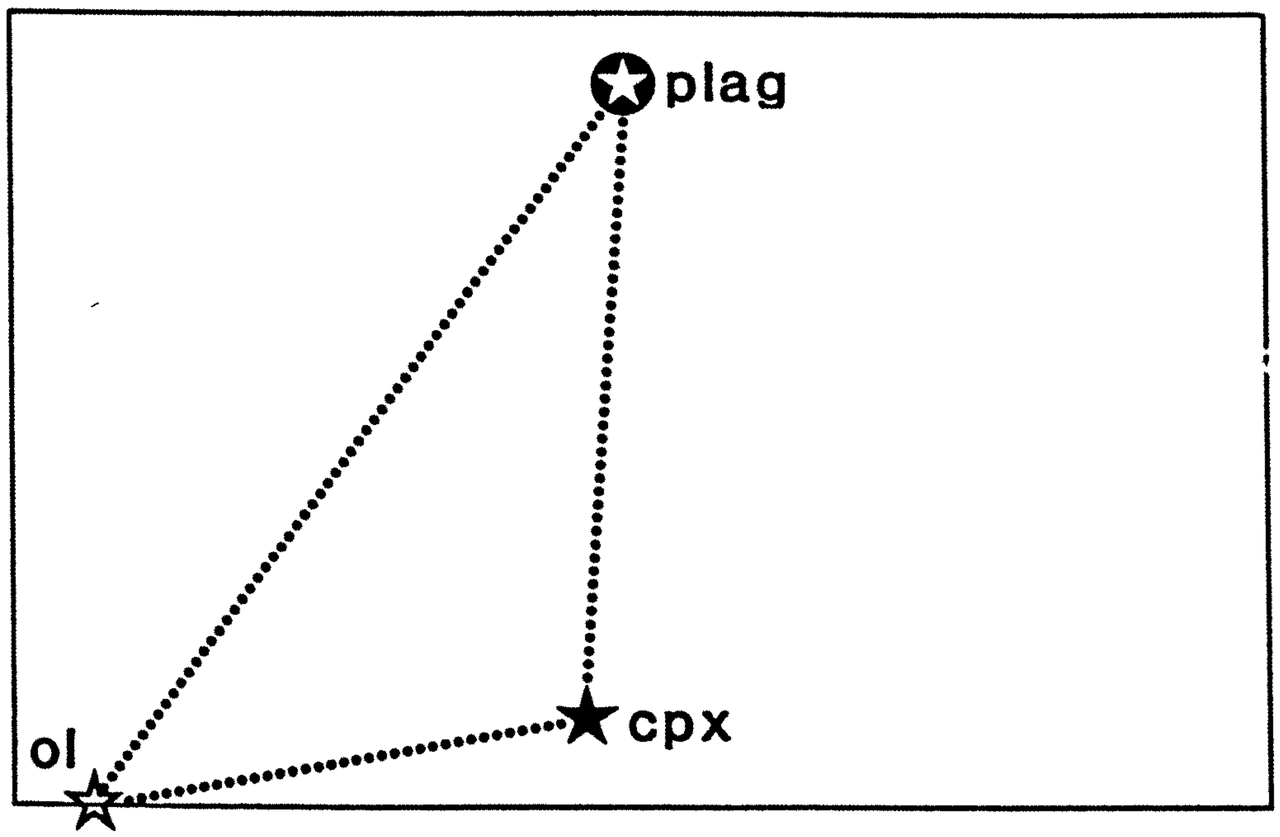
plag
ol
cpx

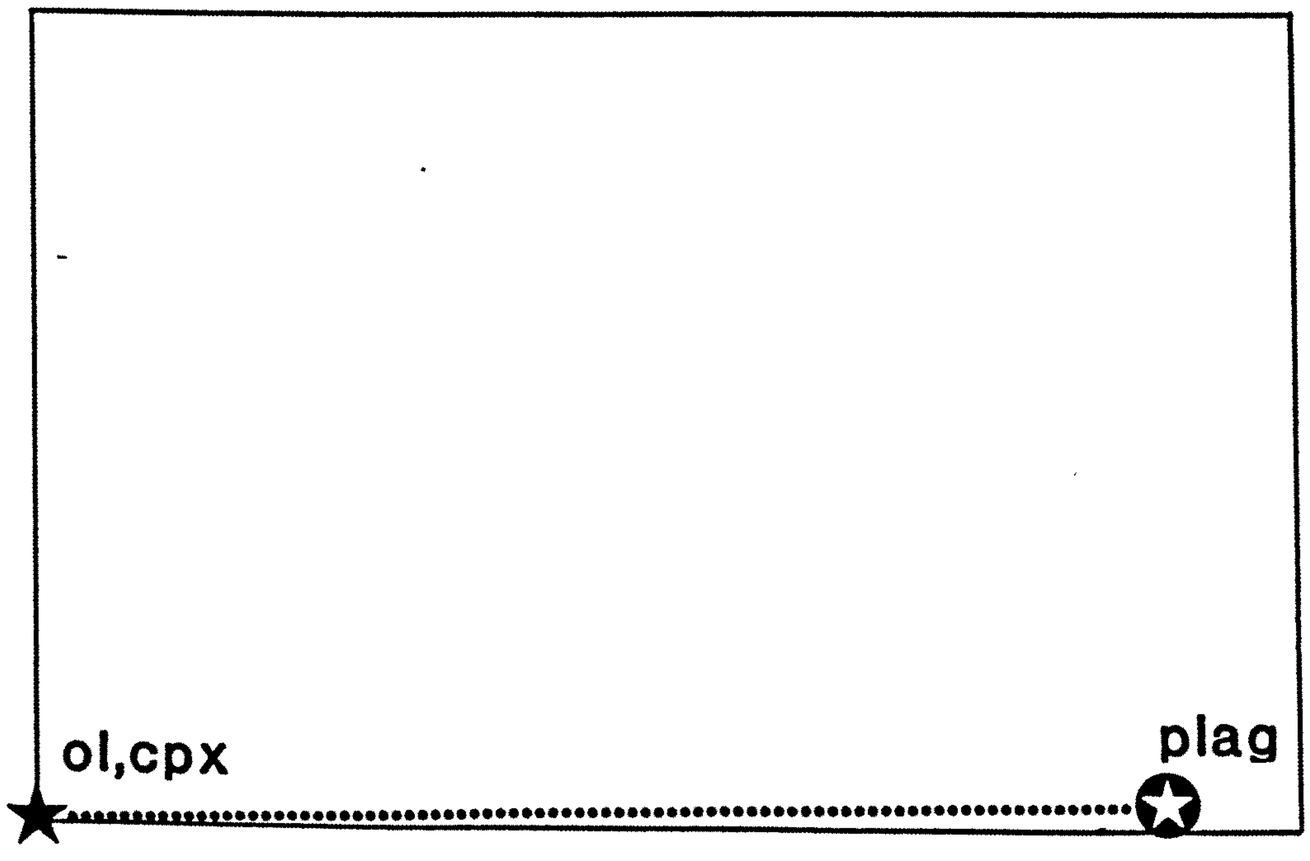
ol,cpx
plag

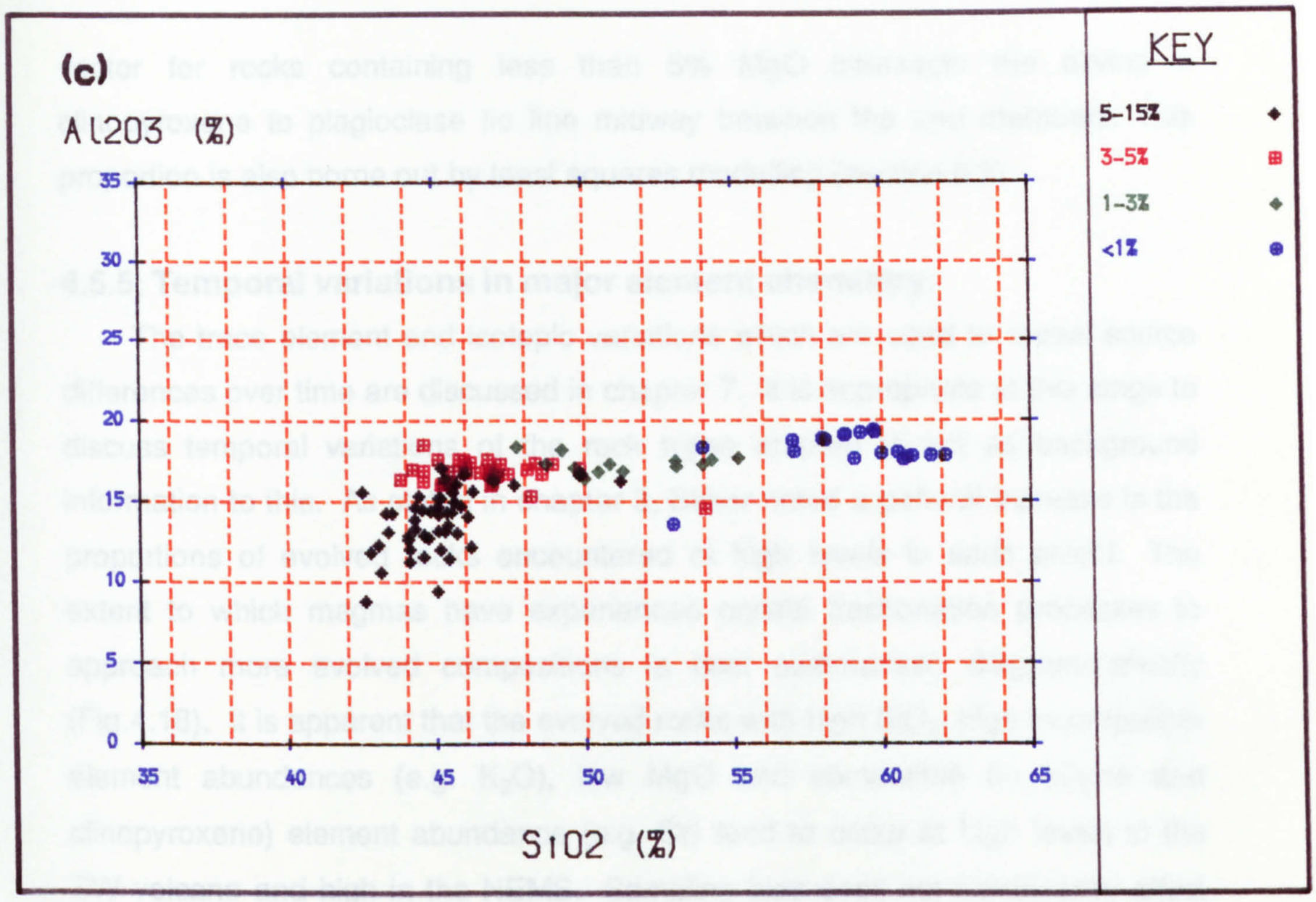
(c)
Al2O3 (%)
35
30
25
20
15
10
5
0
35
40
45
50
55
60
65
SiO2 (%)
KEY
5-15%
3-5%
1-3%
<1%

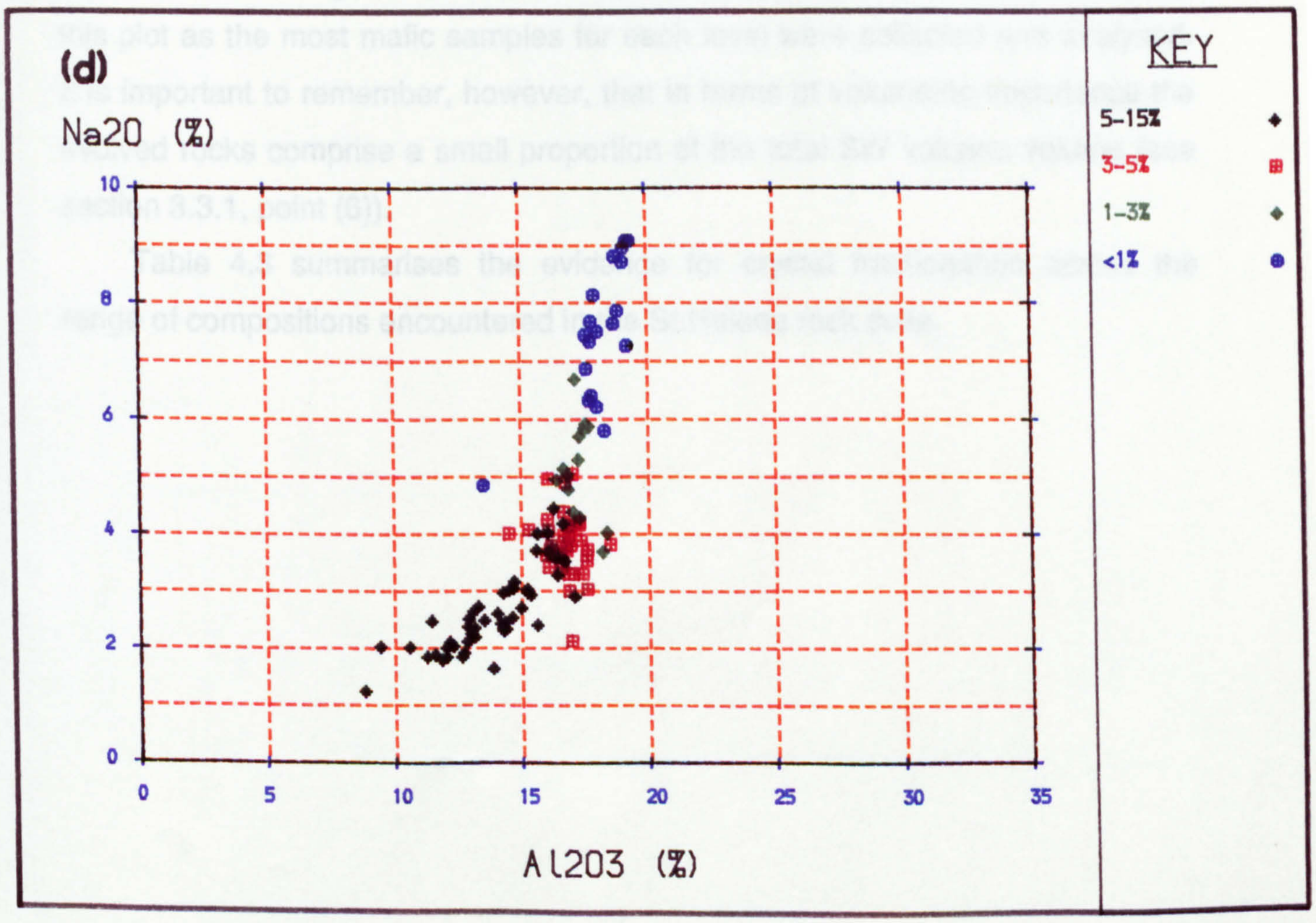
(d)
Na2O (%)
10
8
6
4
2
0
0
5
10
15
20
25
30
35
Al2O3 (%)
KEY
5-15%
3-5%
1-3%
<1%

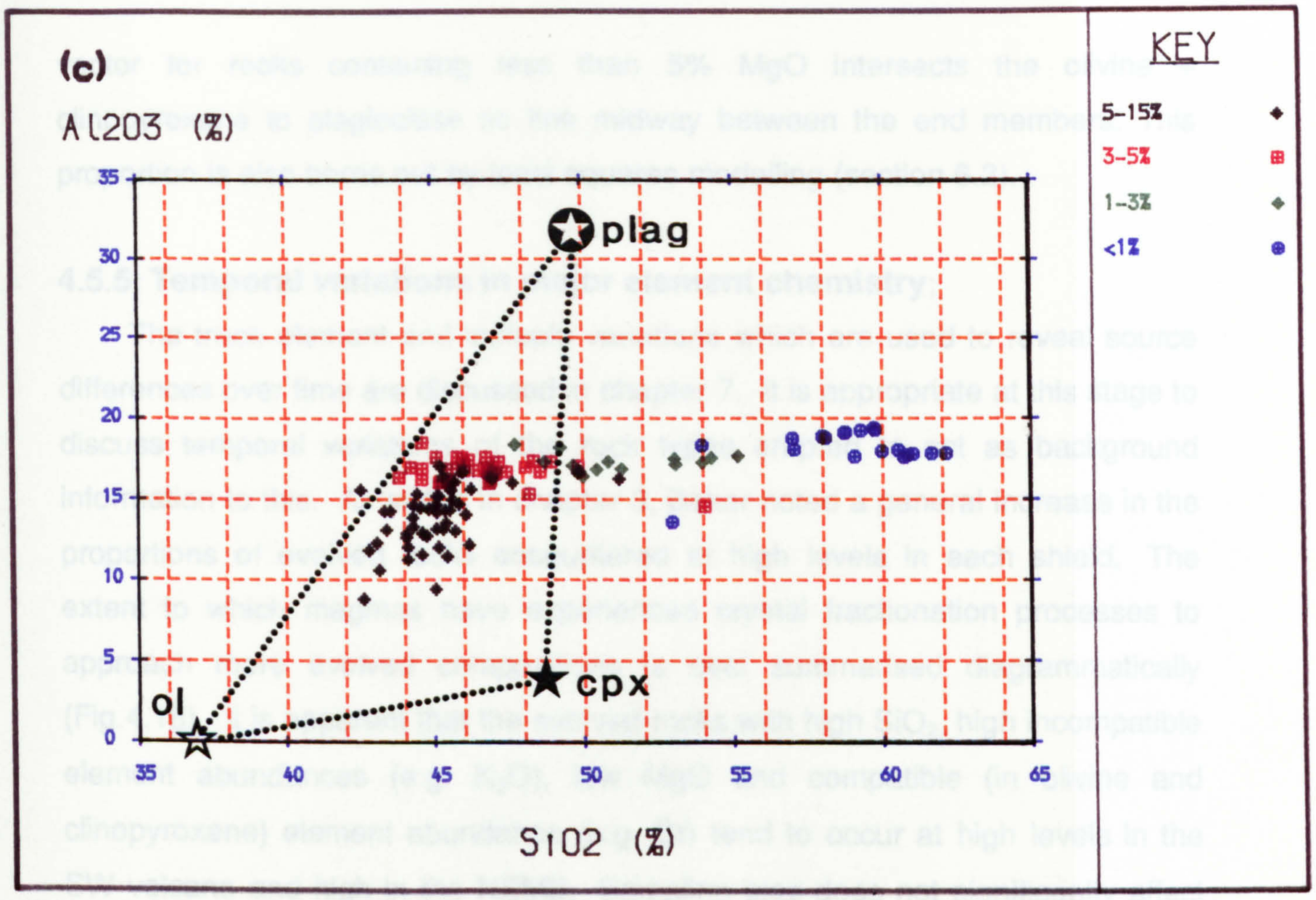
(c)
Al203 (%)
plag
ol
cpx
Si02 (%)
KEY
5-15%
3-5%
1-3%
<1%

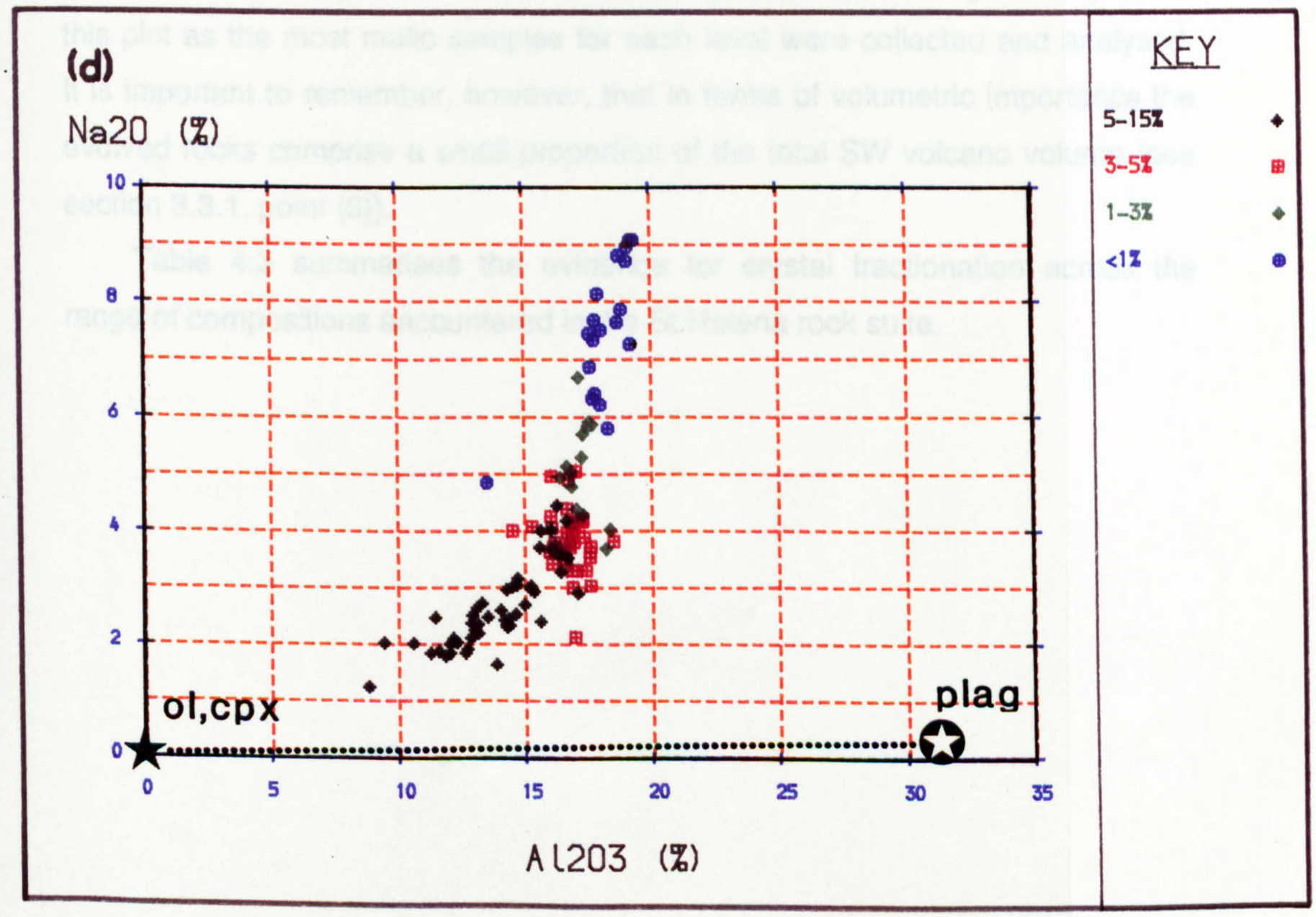
(d)
Na20 (%)
ol,cpx
plag
Al203 (%)
KEY
5-15%
3-5%
1-3%
<1%

vector for rocks containing less than 5% MgO intersects the olivine + clinopyroxene to plagioclase tie line midway between the end members. This proportion is also borne out by least squares modelling (section 6.2).

4.5.5; Temporal variations in major element chemistry;

The trace element and isotopic variations which are used to reveal source differences over time are discussed in chapter 7. It is appropriate at this stage to discuss temporal variations of the rock types erupted to act as background information to this. As stated in chapter 3, Baker noted a general increase in the proportions of evolved rocks encountered at high levels in each shield. The extent to which magmas have experienced crystal fractionation processes to approach more evolved compositions is best summarised diagrammatically (Fig.4.18). It is apparent that the evolved rocks with high SiO_2, high incompatible element abundances (e.g. K_2O), low MgO and compatible (in olivine and clinopyroxene) element abundance (e.g. Cr) tend to occur at high levels in the SW volcano and high in the NEMS. Sampling bias does not significantly affect this plot as the most mafic samples for each level were collected and analysed. It is important to remember, however, that in terms of volumetric importance the evolved rocks comprise a small proportion of the total SW volcano volume (see section 3.3.1, point (6)).

Table 4.3 summarises the evidence for crystal fractionation across the range of compositions encountered in the St.Helena rock suite.

Fig.4.18. Temporal variations of major elements and Cr in the SHRS:

(a) SiO_2 vs stratigraphic height in the SHRS.

(b) K_2O " "

(c) MgO " "

(d) Cr " "

The basis for this cross section through the lava pile is given in chapter 3. The validity of the K-Ar data are discussed in section 3.7.

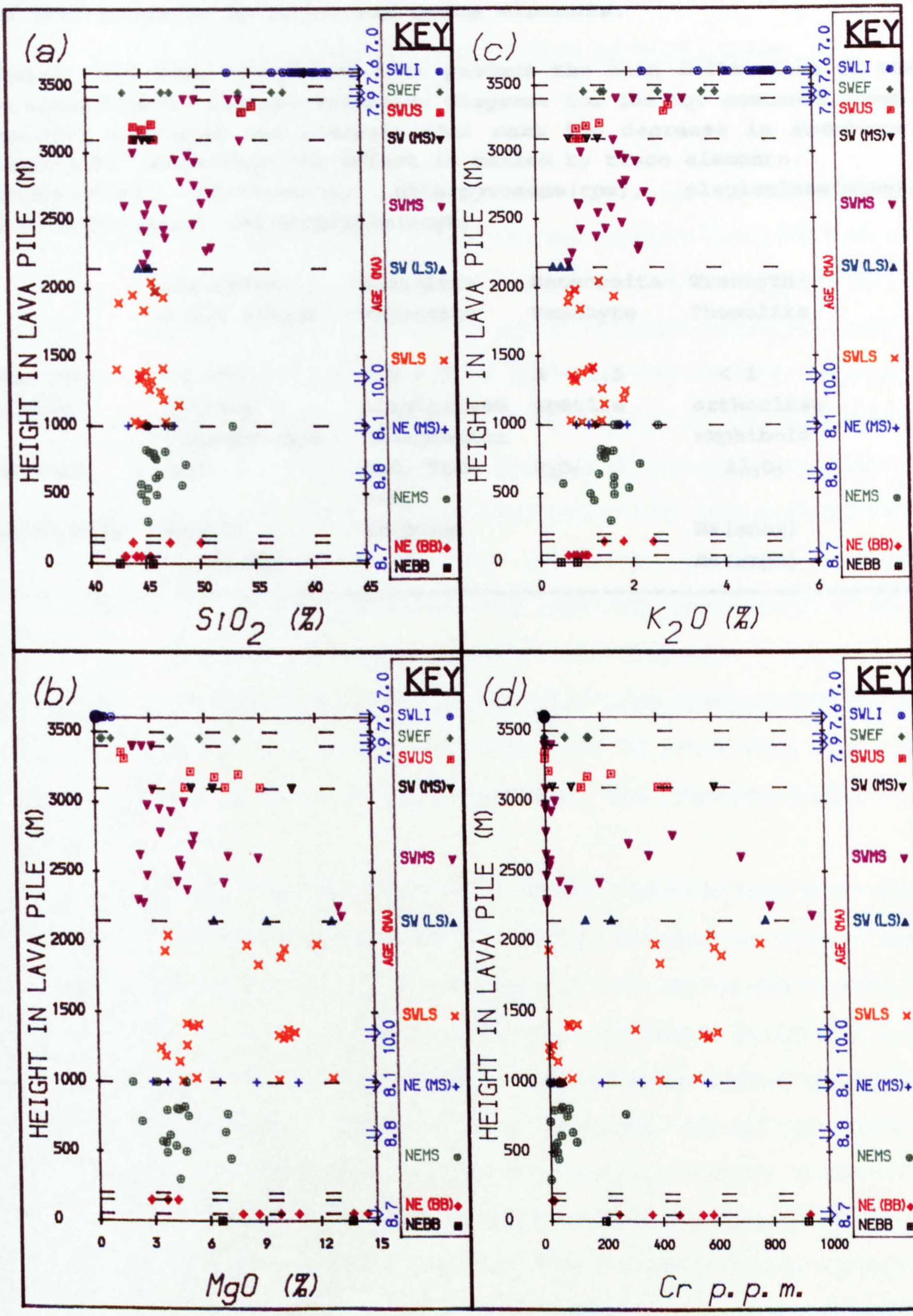
(a)
(b)
(c)
(d)
KEY
SWLI
SWEF
SWUS
SW (MS)
SVMS
SV (LS)
SVLS
NE (MS)
NEMS
NE (BB)
NEBB
AGE (MA)
7.9
7.6
7.0
8.1
10.0
8.8
8.7
HEIGHT IN LAVA PILE (M)
3500
3000
2500
2000
1500
1000
500
0
40
45
50
55
60
65
SiO2 (%)
0
2
4
6
K2O (%)
0
3
6
9
12
15
MgO (%)
0
200
400
600
800
1000
Cr p.p.m.

Table 4.3; Summary of the evidence for crystal fractionation; in the SHRS provided by major and trace elements.

"Phases" indicates the phases that produce the main inflections on the two element major element variation diagrams for the MgO contents shown. "Decline" indicates the elements that mark the decrease in abundance. "Compatible" shows when the effect is marked by trace elements.
Abbreviations: olivine(ol), clinopyroxene(cpx), plagioclase(plag), anorthoclase(anor) and amphibole(amph).

	Ankaramite-Alkali Basalt	Hawaiite-Mugearite	Benmoreite-Trachyte	Trachyte-Phonolite
MgO (%)	14 -4.5	4.5 - 3	3 - 1.5	< 1
Phases	olivine clinoyroxene	plagioclase timagnetite	apatite	orthoclase amphibole
Decline	MgO	CaO, FeO TiO_2	P_2O_5	Al_2O_3
Compatible	Ni(ol), Sc,V(cpx)	Sr(plag)		Ba(anor) Ba(amph)

CHAPTER 5

EVIDENCE FOR POST ERUPTIVE ALTERATION :

5.1; Introduction;

In attempting to determine source characteristics alteration is one of the fundamental high-level geochemical modifiers which must be taken into account. Alteration is considered here as any process which changes the physical and or chemical characteristics of an igneous rock after it has been intruded or erupted. Thus, hydrothermal circulation within the lava pile and surficial weathering processes are both included. In filtering out the effect of alteration in order to determine source characteristics we are primarily interested in the effect of alteration rather than its cause and the emphasis will be placed on detecting differences caused by alteration rather than explaining them. It will be shown that for the SHRS volcanics, alteration does affect the geochemistry of some samples, but is often manifested in different ways. Alteration is found not to correspond simply to field indices of alteration. It is further demonstrated that the effects of alteration can only be adequately removed when there is a large sample set, with relatively minor source differences. Both these prerequisites are met in this instance.

A large number of studies pertinent to alteration of lavas have been made with the realisation that interpreting source variations is futile if the effect of these processes is not recognised. The conclusions of such studies are reviewed in some detail here as they provide important background data to the present study. Studies relevant to the alteration of volcanic rocks may be usefully divided into three different categories. Firstly, there are the studies into settings similar to St.Helena where lava flows which are part of a volcanic shield are considered in relation to hydrothermal systems e.g. Morrison et al.(1978). Secondly there are the numerous studies investigating the weathering of seafloor basalts e.g Ludden and Thompson (1979). This is an important problem due to the number of dredge samples analysed to infer source characteristics for MORB and the implications for the recycling of oceanic crust in geodynamic models. Thirdly, studies of element mobility in low grade burial metamorphism are important (e.g.

Hellman et al.(1979)) as the amygdule phases found in these situations are similar to those found in unmetamorphosed, altered basalts. More recently the problem of how rocks become altered has been approached from a different direction; that of looking at the elemental budget of hydrothermal fluids in relation to where they originate and the rocks they pass through e.g. Michard et al.(1987).

Many of the studies described above concentrate on the mobilisation of REE. This is because the small differences in the physio-chemical properties of these elements make them ideal for showing how alteration processes affect a coherent group of elements. In addition the REE are often used for petrogenetic modelling or discriminant analysis of the type of eruptive environment. It is therefore important to establish that these elements are not mobilised during such alteration otherwise erroneous conclusions may be drawn regarding source region geochemistry.

These studies have shown, above all else that no general conclusions may be drawn about which elements are mobilised in a particular environment. Whilst the alkalis Rb and K are particularly susceptible to mobilisation (e.g. Chen and Frey(1985)), it is difficult to predict from normal petrographic criteria such as the volumetric proportion of amygdule phases or the loss on ignition (LOI) which samples are likely to be affected. Similarly with REE the effect of alteration on relative abundances is difficult to predict. Some studies have reported LREE enrichment (Wood et al. (1976), Humphris et al.(1978)), or variations in absolute abundance (Sun and Nesbitt (1978)) while others have shown that in other situations the REE are virtually unaffected by alteration (Humpris(1984)). When REE mobility does occur it has been explained by the crystallisation history of the lavas which governs the amount of glass and its REE content (Humphris et al.(1978)) or post crystallisation factors such as the formation of secondary phases, hydrothermal leaching and phase dilution (Hellman et al.(1979)).

5.2; Minimising the effects of alteration;

5.2.1; Field studies;

In this study, the problem of alteration affecting primary compositions was recognised at an early stage. This enabled the magnitude of the problem to be reduced by taking preventative measures during field collection. Such precautions were part of the sampling strategy and were discussed in section 3.6, but are worth reiterating here.

The effect of surficial weathering was diminished by the use of a 5kg sledgehammer to remove the weathering rinds. Samples were collected, where possible which had the lowest proportion of zeolites for a particular stratigraphic grouping. By necessity some altered samples had to be collected to be representative of a certain highly altered section of the lava pile. A field terminology was erected to classify the samples that were collected (chapter 3 and Table A1). This was based on the proportion of zeolites and the degree to which olivine, the most susceptible of the ferromagnesian minerals was altered to secondary phases. Such samples that were classified as altered or moderately altered were not used for geochemical determinations unless it was subsequently found that their stratigraphic position was of importance.

5.2.2; Sample preparation;

The details of sample preparation are given in Appendix B1. In addition to these routine methods, extra precautions were taken with slightly altered samples that were analysed as part of the study. In some samples pervasive sets of oxidised fractures occurred. If the fractures were spaced at greater than 2cm these could be removed when using the hydraulic splitter, otherwise fracture surfaces were removed by hand picking during crushing using the jaw crusher. With samples that contained large (>5mm) zeolite amygdules it was possible to remove the majority of these at the crushing stage also.

5.2.3; Thin section studies;

Thin section studies also proved only to give a general guide; some samples with a large proportion of secondary phases were found to possess a geochemical alteration signature, while others with similar proportions were found to be unaltered in terms of geochemistry. It is later shown that the proportion of secondary phases is not consistent with the degree of geochemical alteration.

5.2.4; Loss on Ignition (LOI);

Loss on ignition of a sample placed in a furnace at 1000 °C for an hour gives a crude guide to how altered a sample is because the hydrous phases such as zeolites which have formed in the rock subsequent to crystallisation will lose their structural water at this temperature. Inspection of Appendix C2 shows that in the majority of samples LOI is much less than 2%. If altered samples are to be removed from the study using this criteria an arbitrary discriminant must be introduced. It is shown later using geochemical criteria that there is not a simple relationship between LOI and chemical change. Hence LOI was not used in a definitive diagnostic manner, merely as a method by which geochemically altered samples could be preliminarily recognised.

5.3; Geochemical identification of altered samples;

Despite the precautions described above it was found that geochemical methods were required to filter out highly altered samples. This was necessary because the degree of apparent alteration in hand specimen did not correspond simply with the geochemical signature of alteration.

The first steps to identify which samples were altered involved considering elements which, from their chemical characteristics and previous studies, were known to be commonly mobilised in alteration. Rb and K are frequently seen to behave in an anomalous fashion during studies of OIB suites (e.g. Chen and Frey(1985)). If these elements are plotted against one another (Fig.5.1). it is seen that whilst the majority of samples scatter about a clearly defined trend, some samples lie off this line. The closeness of fit to the line of crystal fractionation for the majority of samples suggests that these variations are too

Fig.5.1. K_2O vs Rb in the SHRS.

The vector shown is for crystal fractionation. Samples which have experienced different degrees of Rb and K loss or gain through leaching and mobilisation plot off this trend.

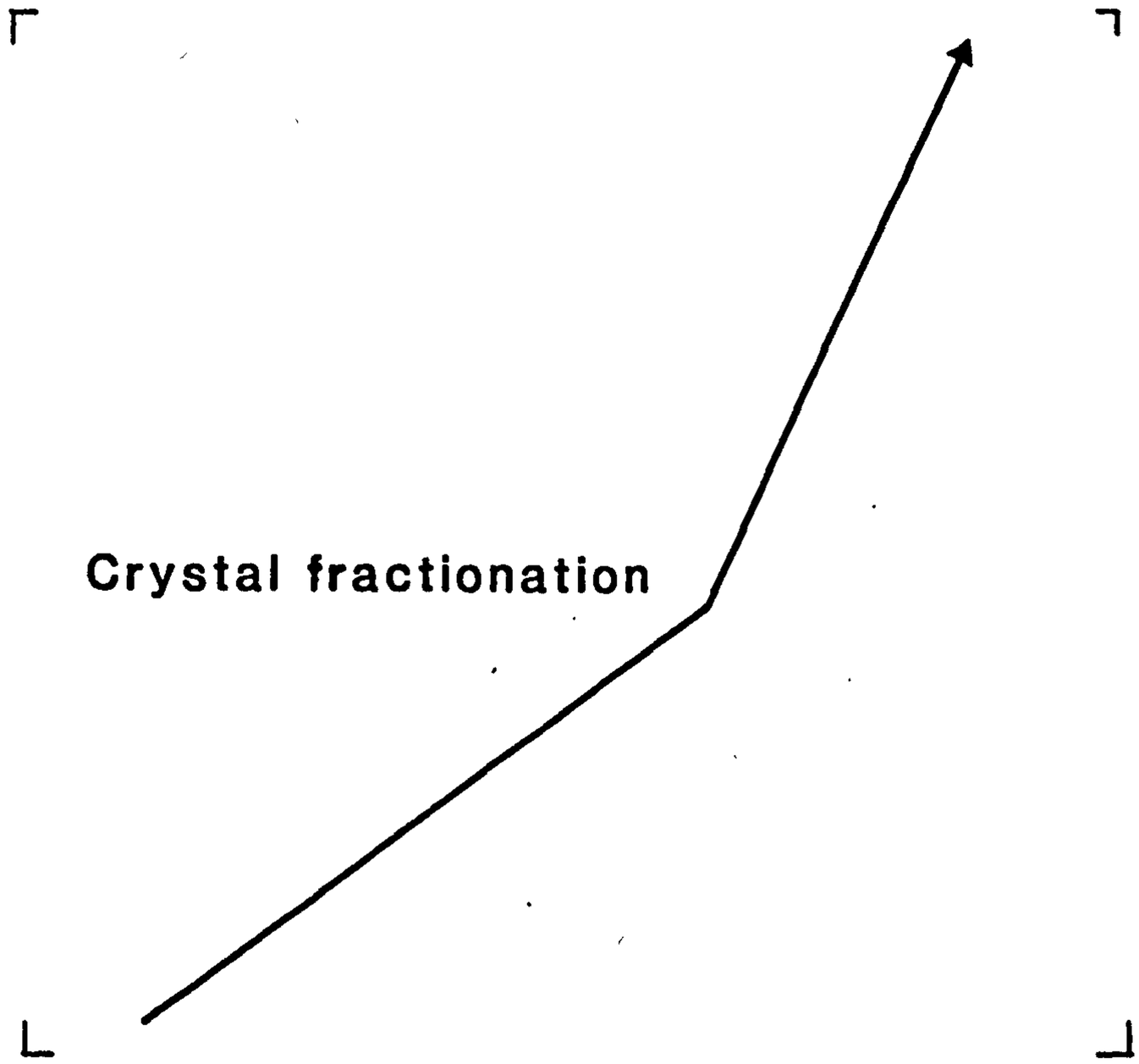
Crystal fractionation

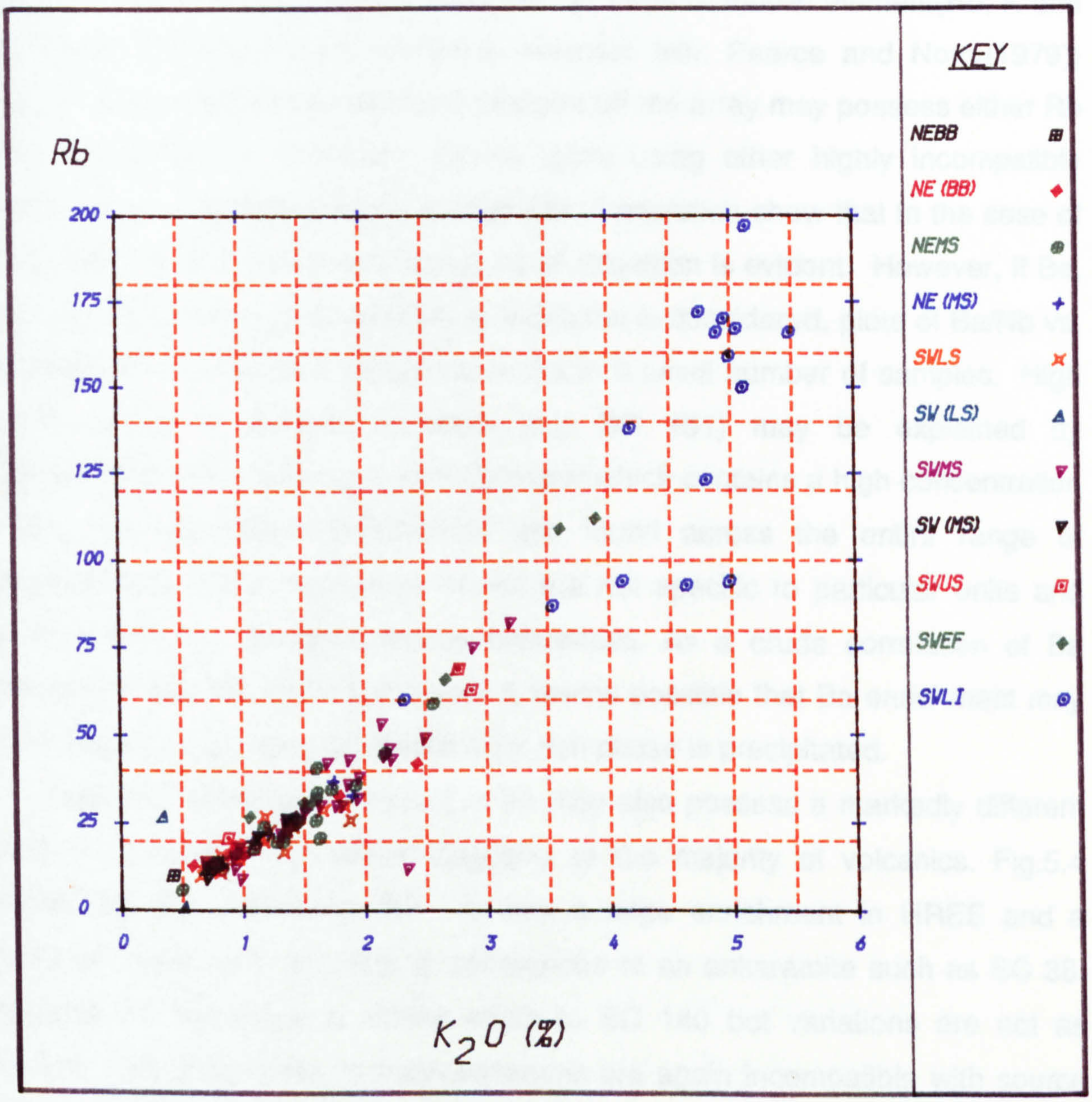
Rb
200
175
150
125
100
75
50
25
0
0
1
2
3
4
5
6
K_2O (%)
KEY
NEBB
NE (BB)
NEMS
NE (MS)
SWLS
SW (LS)
SWMS
SW (MS)
SWUS
SWEF
SWLI

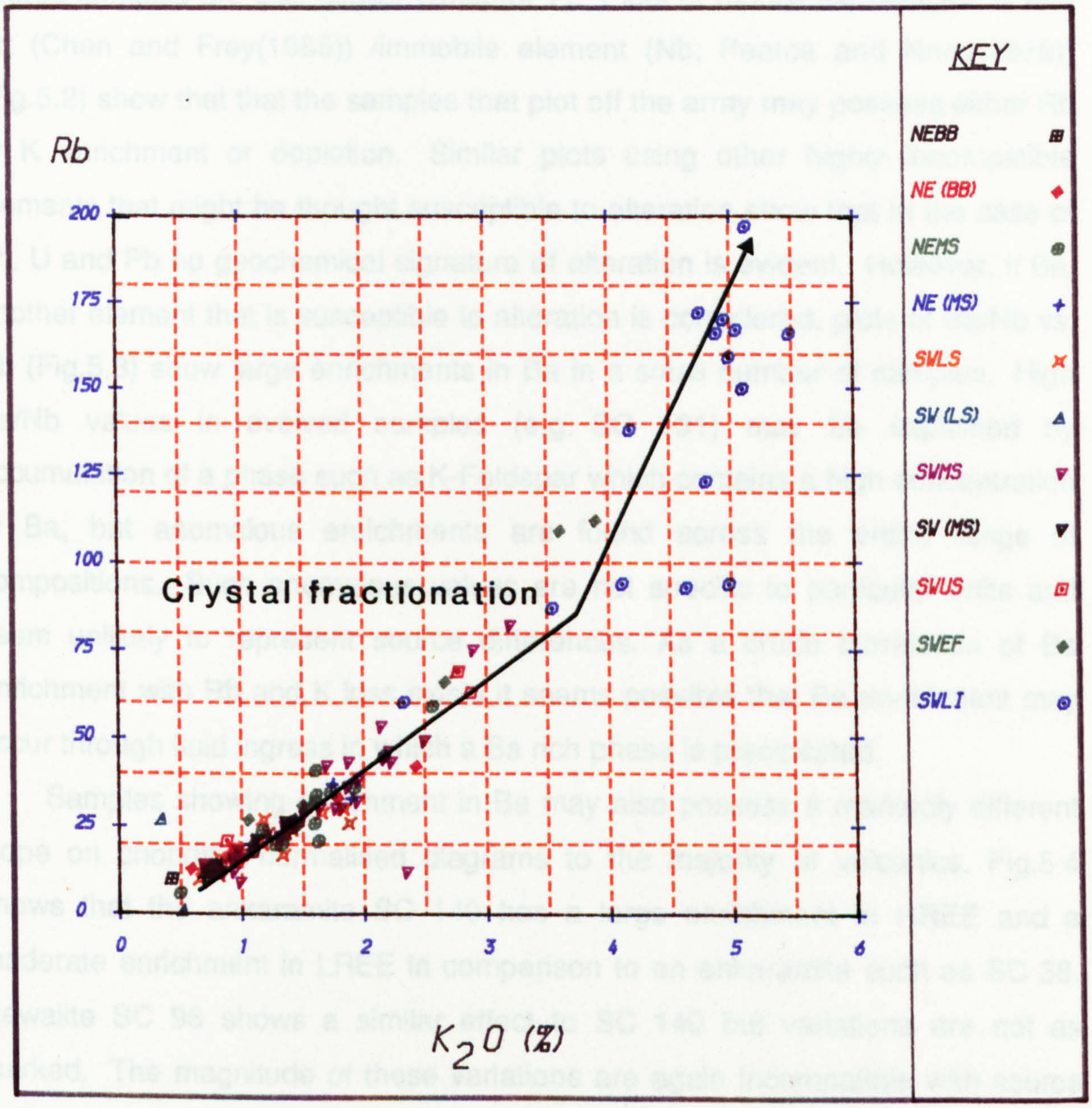
Rb
200
175
150
125
100
75
50
25
0
0
1
2
3
4
5
6
Crystal fractionation
K2O (%)
KEY
NEBB
NE (BB)
NEMS
NE (MS)
SWLS
SW (LS)
SWMS
SW (MS)
SWUS
SWEF
SWLI

large to be source variations. This is also suggested because the anomalous samples have similar ratios of immobile incompatible elements to samples that lie on the trend (e.g. Zr/Nb., Pearce and Norry (1979)). Isotopic values in slightly altered samples are also similar (Chapter 7). Plots of mobile element(Rb, K and Sr; (Chen and Frey(1985)) /immobile element (Nb; Pearce and Norry(1979)) (Fig.5.2) show that that the samples that plot off the array may possess either Rb or K enrichment or depletion. Similar plots using other highly incompatible elements that might be thought susceptible to alteration show that in the case of Th, U and Pb no geochemical signature of alteration is evident. However, if Ba, another element that is susceptible to alteration is considered, plots of Ba/Nb vs. Nb (Fig.5.3) show large enrichments in Ba in a small number of samples. High Ba/Nb values in evolved samples (e.g. SC 131) may be explained by accumulation of a phase such as K-Feldspar which contains a high concentration of Ba, but anomalous enrichments are found across the entire range of compositions. Such anomalous values are not specific to particular units and seem unlikely to represent source differences. As a crude correlation of Ba enrichment with Rb and K loss exists it seems possible that Ba enrichment may occur through fluid ingress in which a Ba rich phase is precipitated.

Samples showing enrichment in Ba may also possess a markedly different slope on chondrite normalised diagrams to the majority of volcanics. Fig.5.4 shows that the ankaramite SC 140 has a large enrichment in HREE and a moderate enrichment in LREE in comparison to an ankaramite such as SC 38. Hawaiite SC 96 shows a similar effect to SC 140 but variations are not as marked. The magnitude of these variations are again incompatible with source differences for the SHRS (no crossing REE patterns observed for other members of the SHRS (Fig.6.5)). In addition SC 96 has a high Ba/Nb ratio (Fig.5.3). It is noted that studies by Michard et al.(1987) indicate large HREE enrichments in carbonate rich hydrothermal fluids. It is thought that because such patterns are not associated with other types of hydrothermal fluids, complexing of HREE with CO_3 anions may be important in producing the REE patterns of samples such as SC 140. If the anomalous enrichment patterns are considered together (Fig.5.5) it is apparent that different styles of enrichment occur. For example while both SC 140 and SC 96 possess large Ba enrichments (Fig.5.3), the degree of

Fig.5.2. Variation of the relatively mobile elements Rb, K and Sr relative to an immobile element (Nb) in the SHRS:

(a) Nb vs Rb/Nb.

(b) Nb vs K/Nb.

(c) Nb vs Sr/Nb.

Crystal fractionation vectors are superposed. Significant variations from the crystal fractionation vectors are the result of element mobilisation during alteration.

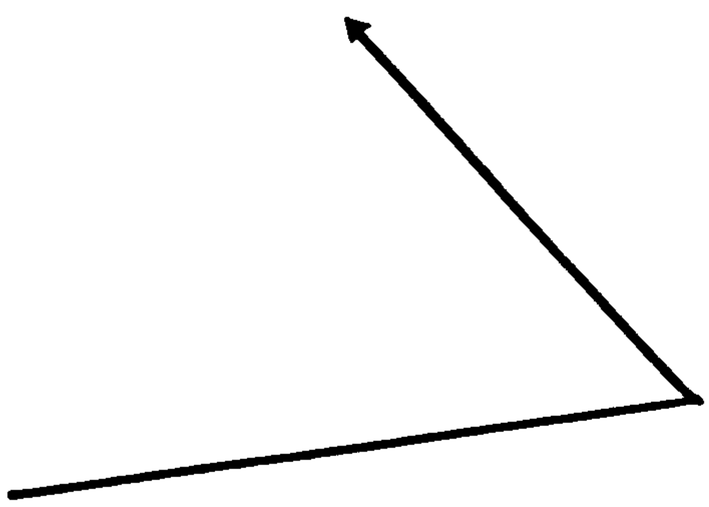

Crystal fractionation

Crystal Fractionation

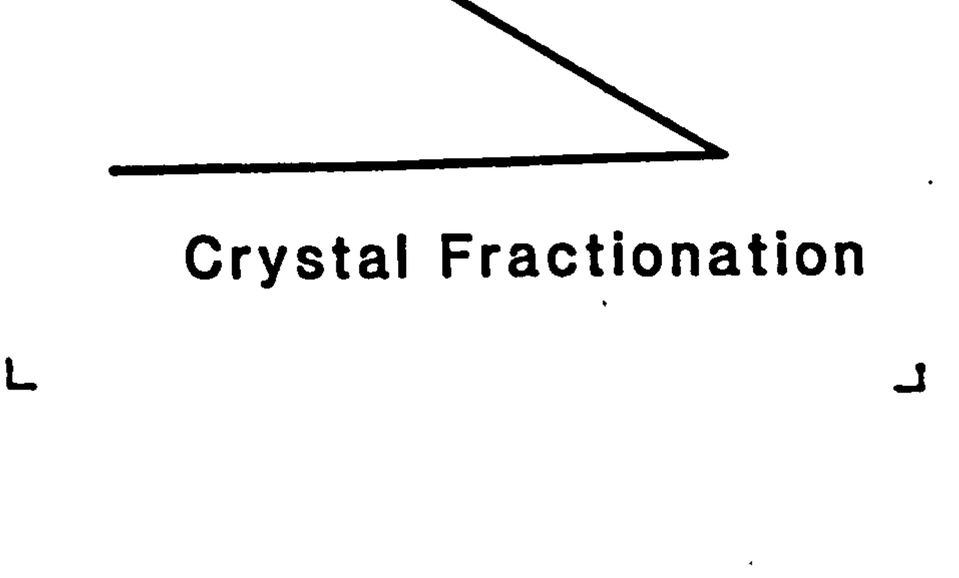

Crystal fractionation

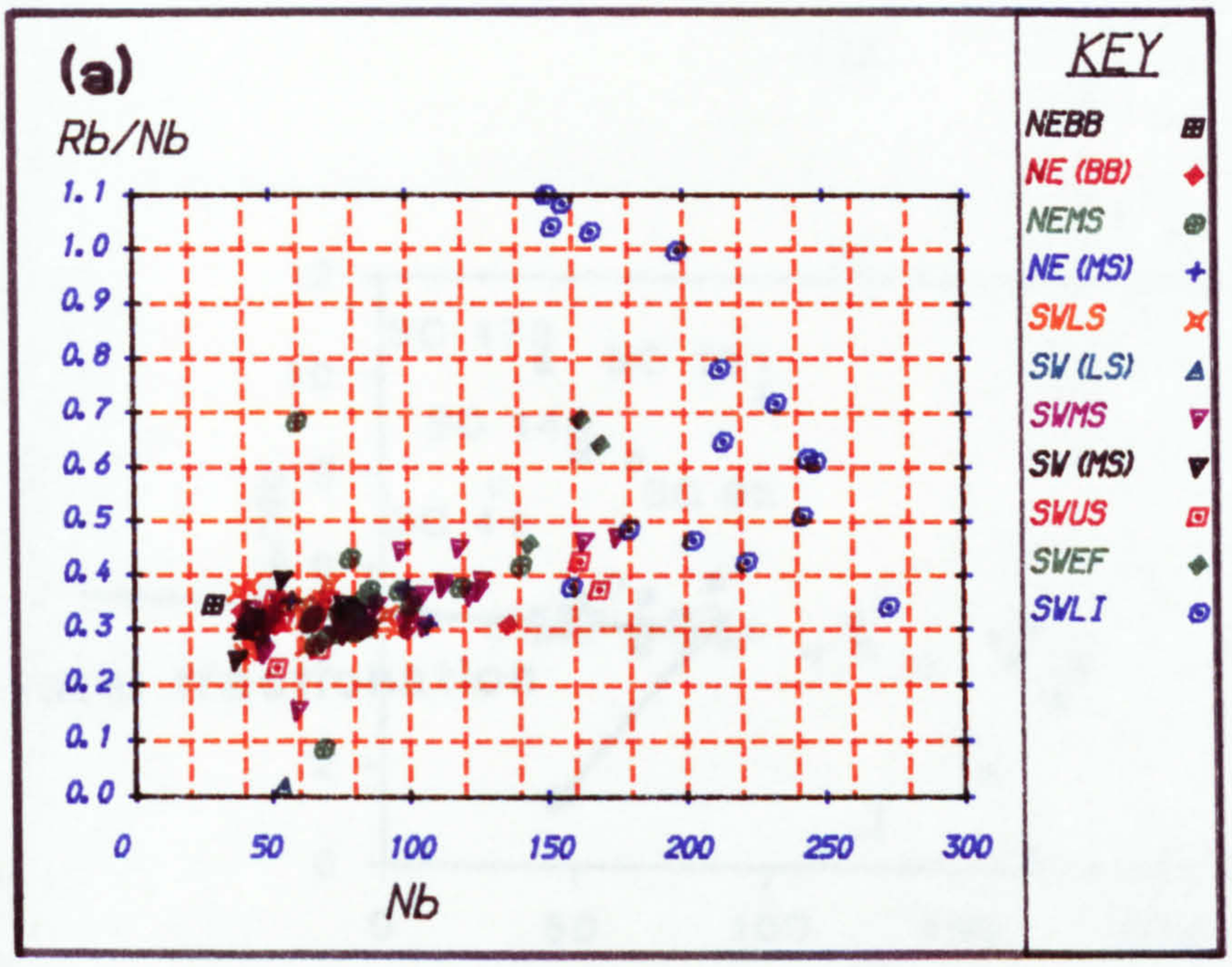
(a)
Rb/Nb
1.1
1.0
0.9
0.8
0.7
0.6
0.5
0.4
0.3
0.2
0.1
0.0
0
50
100
150
200
250
300
Nb
KEY
NEBB
NE (BB)
NEMS
NE (MS)
SWLS
SW (LS)
SWMS
SW (MS)
SWUS
SWEF
SWLI

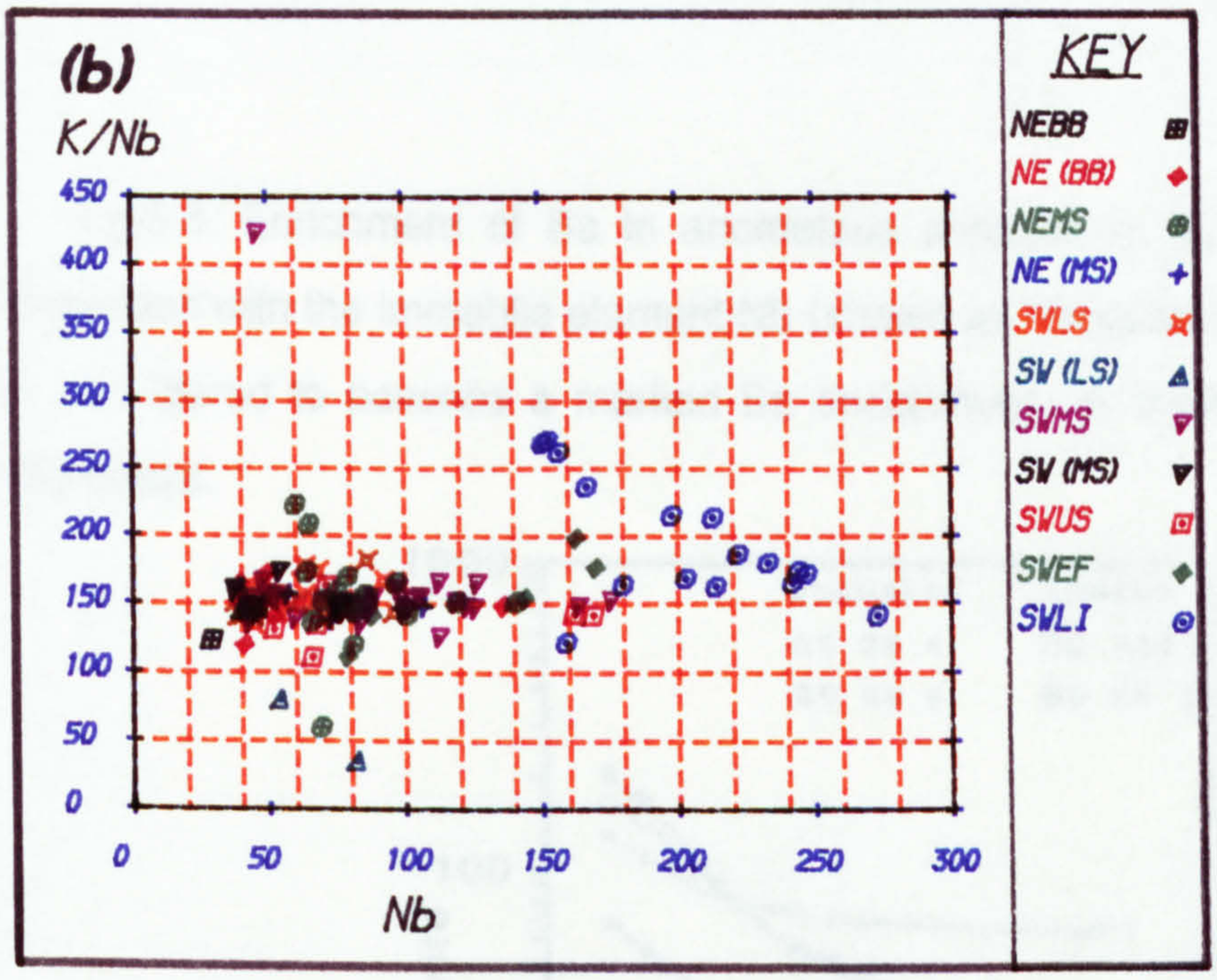
(b)
K/Nb
450
400
350
300
250
200
150
100
50
0
0
50
100
150
200
250
300
Nb
KEY
NEBB
NE (BB)
NEMS
NE (MS)
SWLS
SW (LS)
SWMS
SW (MS)
SWUS
SWEF
SWLI

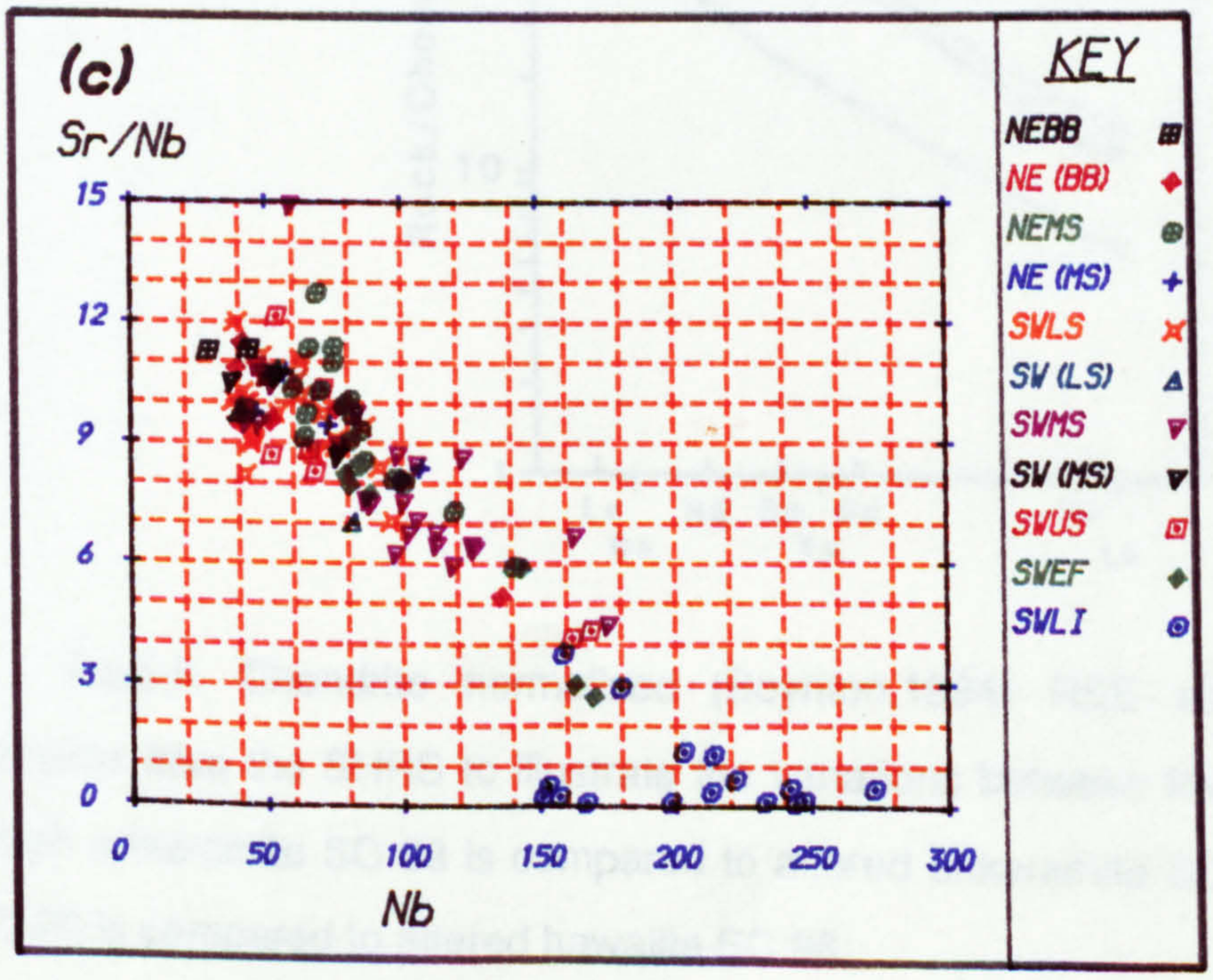
(c)
Sr/Nb
15
12
9
6
3
0
0
50
100
150
200
250
300
Nb
KEY
NEBB
NE (BB)
NEMS
NE (MS)
SWLS
SW (LS)
SWMS
SW (MS)
SWUS
SWEF
SWLI

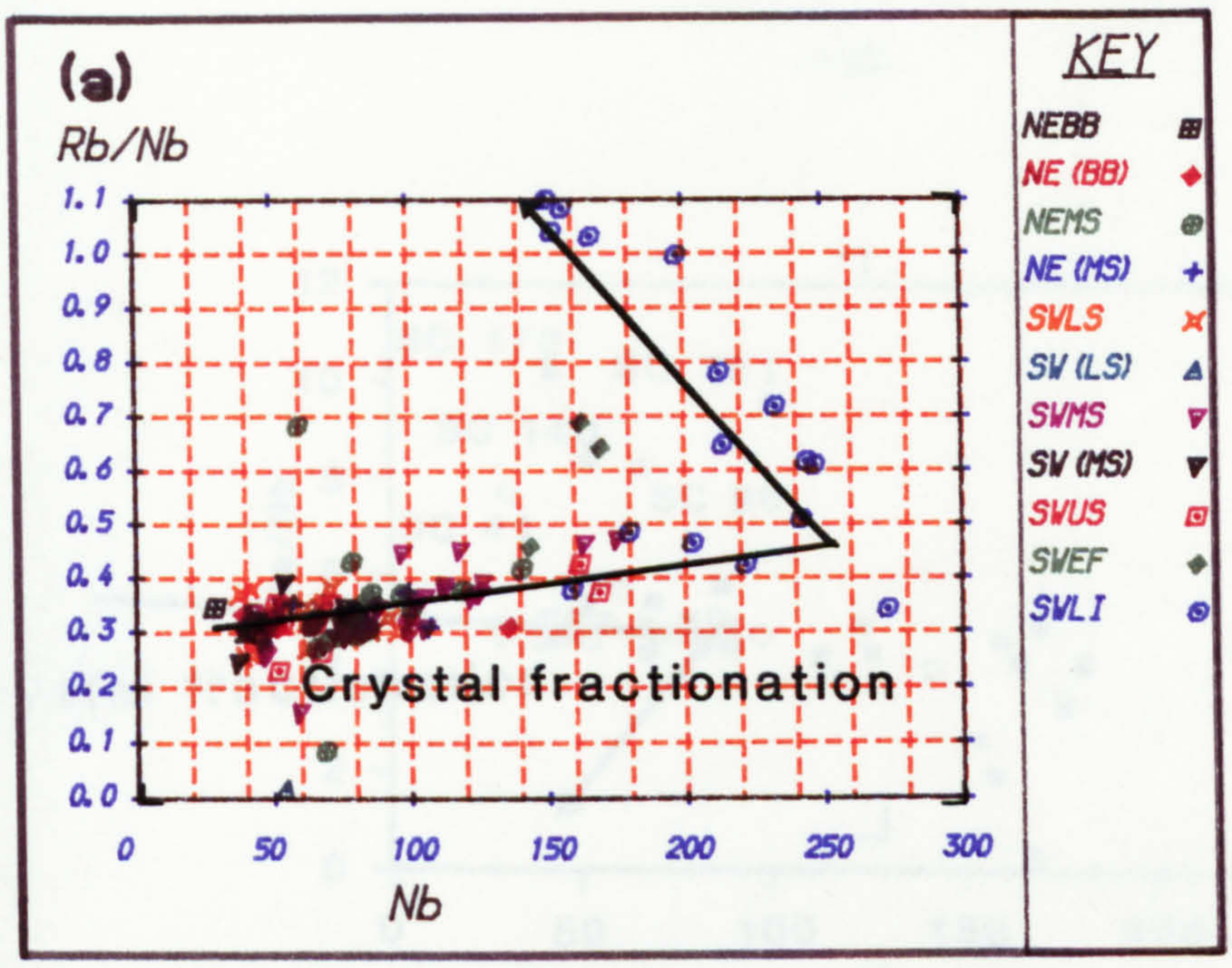
(a)
Rb/Nb
1.1
1.0
0.9
0.8
0.7
0.6
0.5
0.4
0.3
0.2
0.1
0.0
0
50
100
150
200
250
300
Nb
Crystal fractionation
KEY
NEBB
NE (BB)
NEMS
NE (MS)
SWLS
SW (LS)
SWMS
SW (MS)
SWUS
SWEF
SWLI

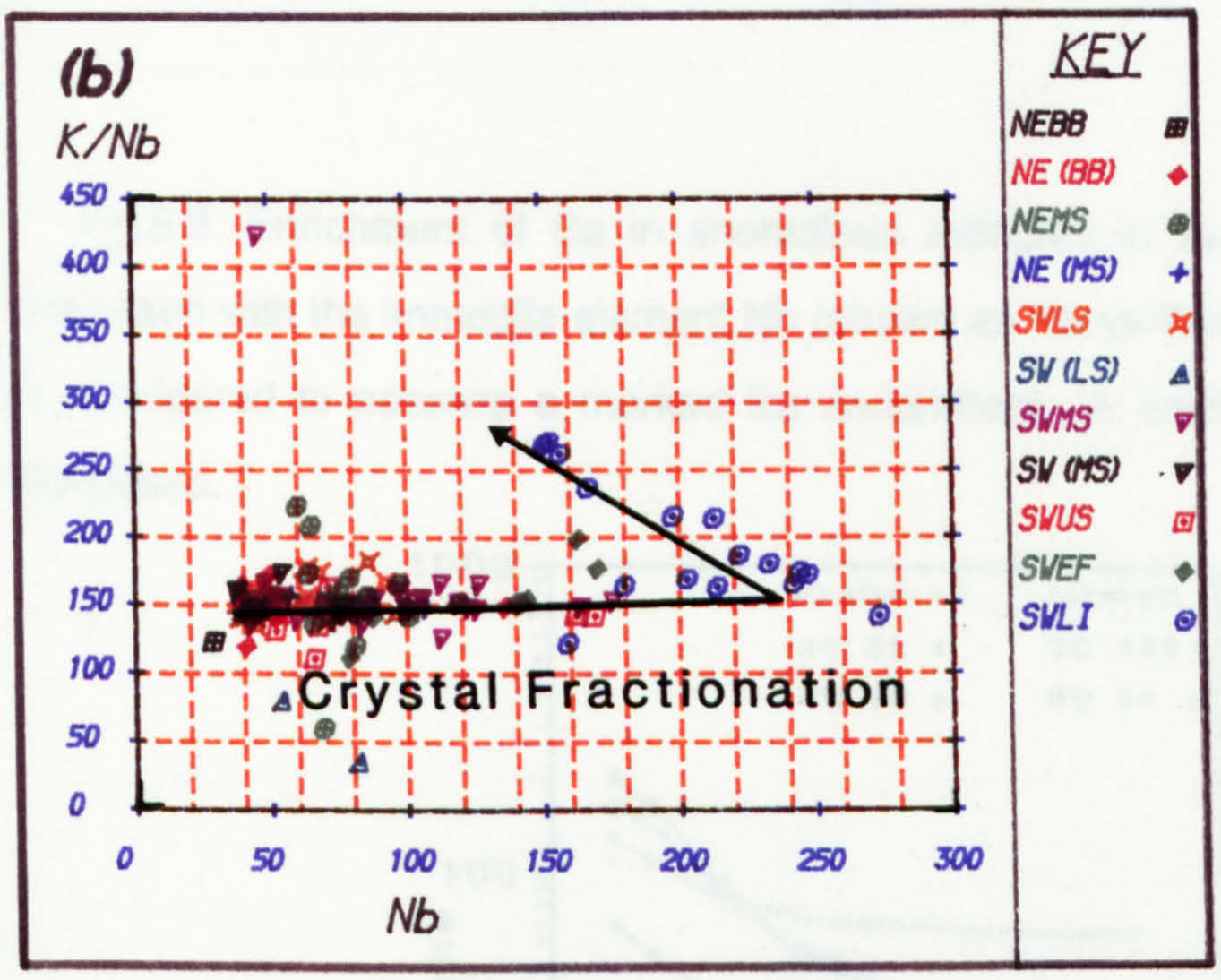
(b)
K/Nb
450
400
350
300
250
200
150
100
50
0
0
50
100
150
200
250
300
Nb
Crystal Fractionation
KEY
NEBB
NE (BB)
NEMS
NE (MS)
SWLS
SW (LS)
SWMS
SW (MS)
SWUS
SWEF
SWLI

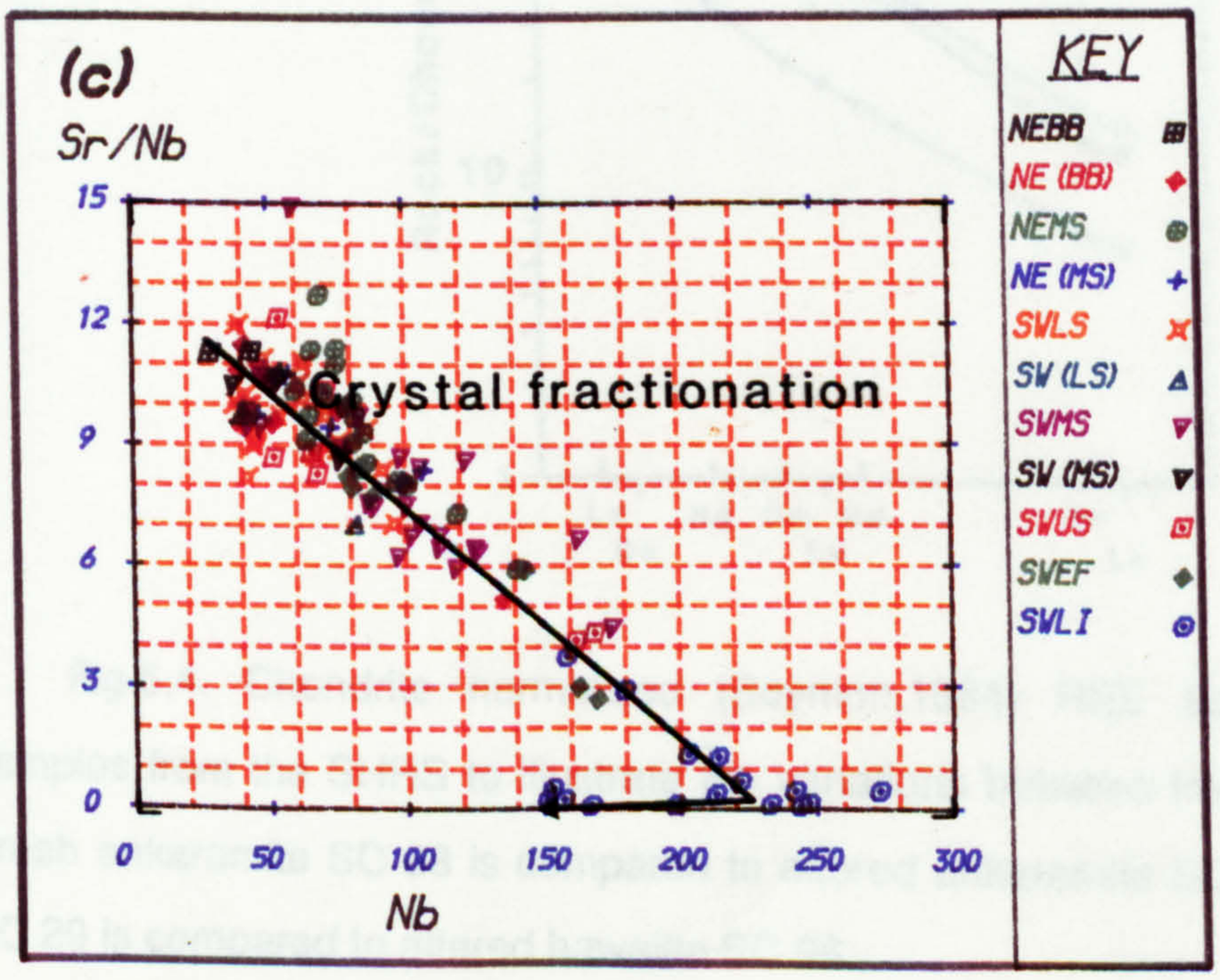
(c)
Sr/Nb
15
12
9
6
3
0
0
50
100
150
200
250
300
Nb
Crystal fractionation
KEY
NEBB
NE (BB)
NEMS
NE (MS)
SWLS
SW (LS)
SWMS
SW (MS)
SWUS
SWEF
SWLI

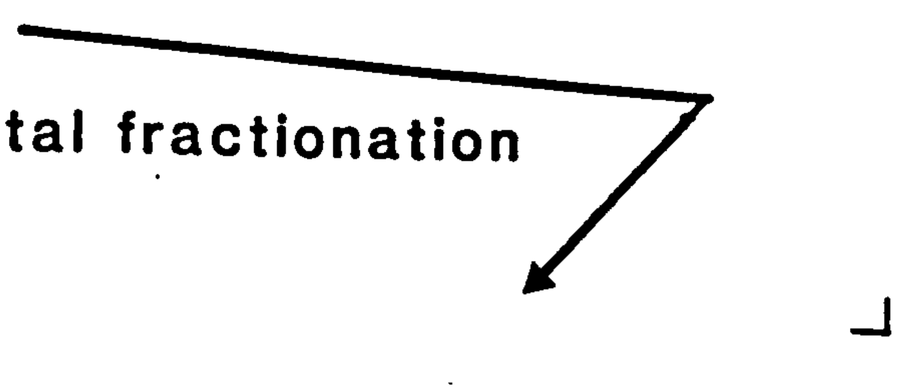

con

are

sup

san

Fre

SC

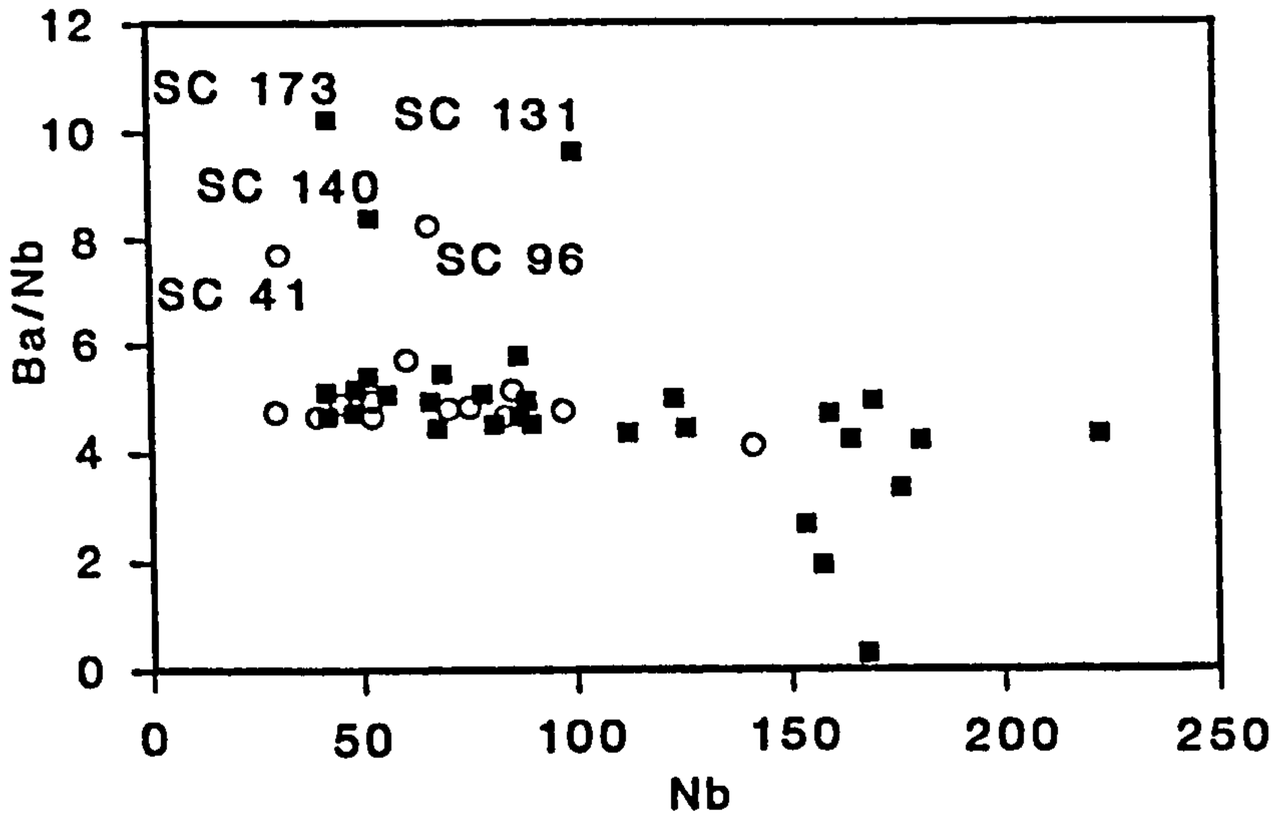

Fig.5.3. Enrichment of Ba in anomalous samples in the SHRS is evident from comparison with the immobile element Nb (shown as Nb vs Ba/Nb). Numbered samples are considered to possess a marked Ba enrichment. A crystal fractionation vector is superposed.

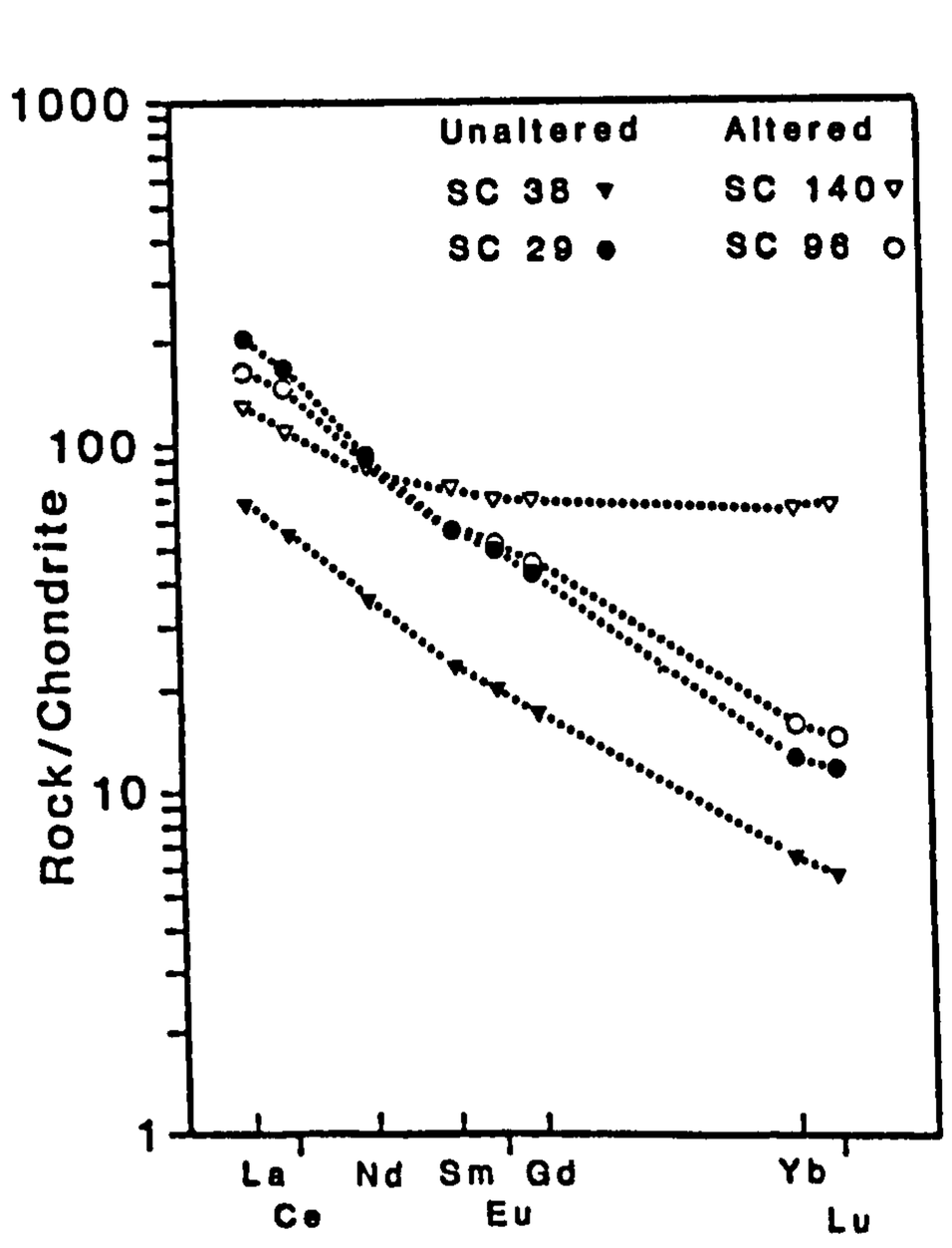

Fig.5.4. Chondrite normalised (Boynton,1984) REE abundances for selected samples from the SHRS to illustrate the variations between fresh and altered samples. Fresh ankaramite SC 38 is compared to altered ankaramite SC 140 and fresh hawaiite SC 29 is compared to altered hawaiite SC 96.

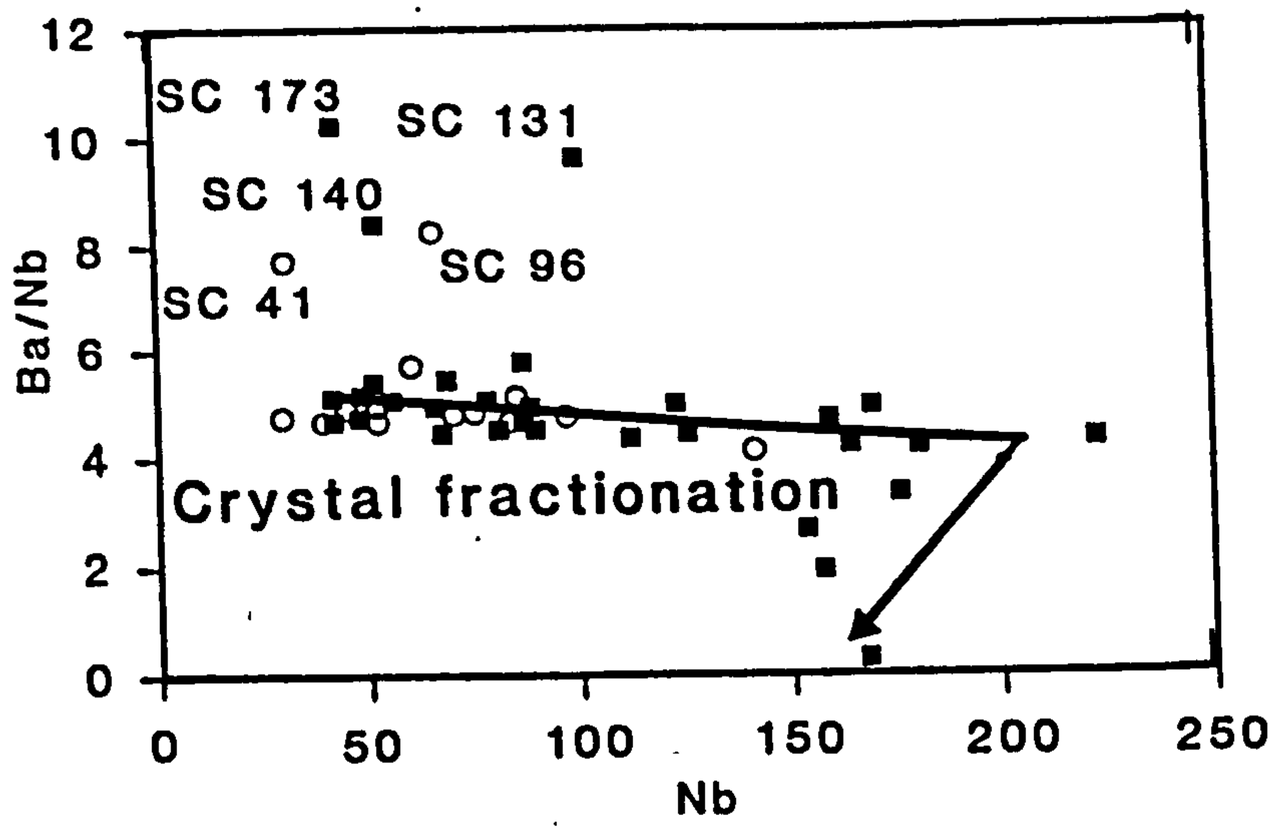

Fig.5.3. Enrichment of Ba in anomalous samples in the SHRS is evident from comparison with the immobile element Nb (shown as Nb vs Ba/Nb). Numbered samples are considered to possess a marked Ba enrichment. A crystal fractionation vector is superposed.

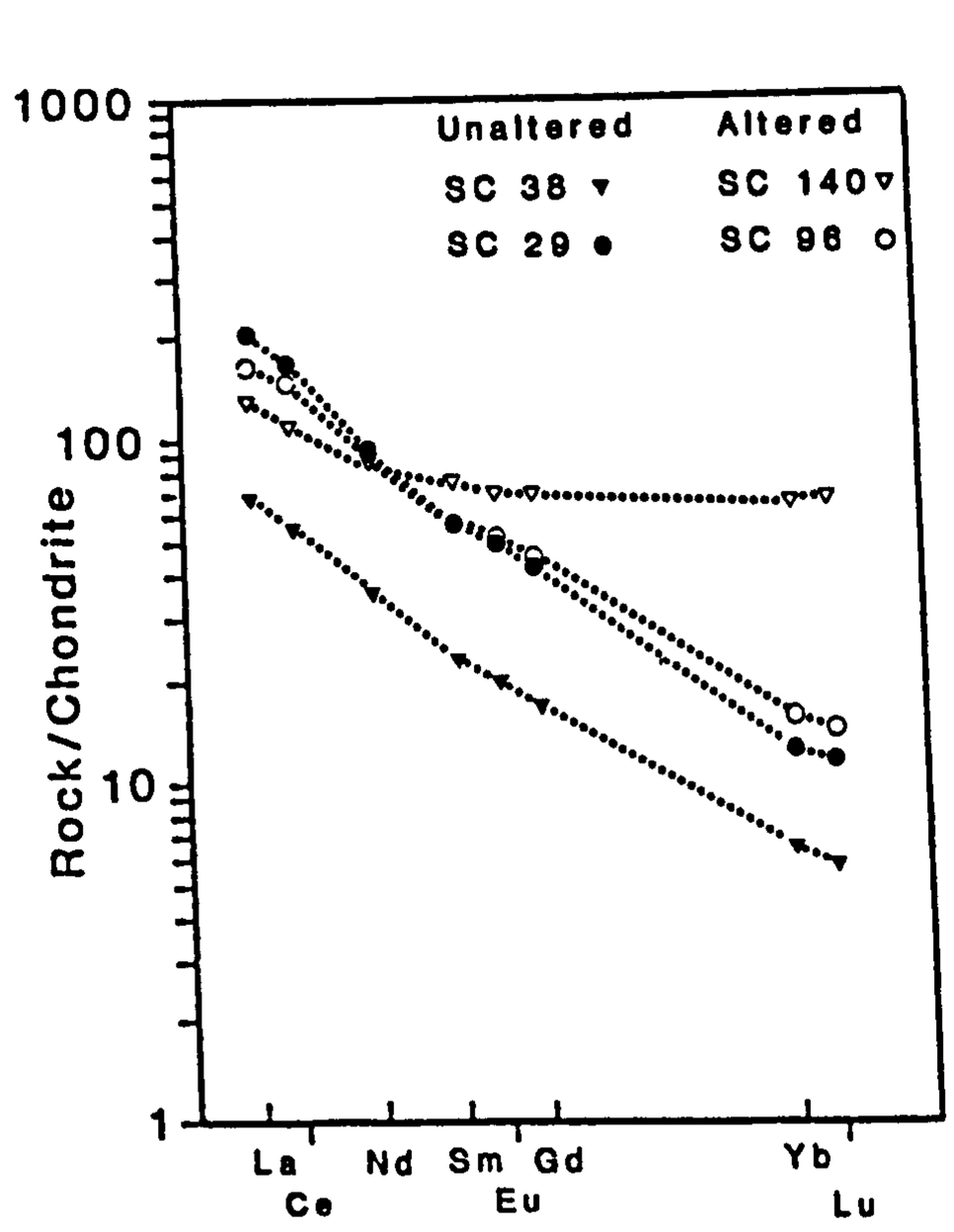

Fig.5.4. Chondrite normalised (Boynton,1984) REE abundances for selected samples from the SHRS to illustrate the variations between fresh and altered samples. Fresh ankaramite SC 38 is compared to altered ankaramite SC 140 and fresh hawaiite SC 29 is compared to altered hawaiite SC 96.

Fig.5.5. Diagrams showing the relationship between Ba, Y and Rb enrichments and depletions in the SHRS.

(a) Ba/Nb vs Y/Nb

(b) Ba/Nb vs Rb/Nb

Crystal fractionation vectors are as shown.

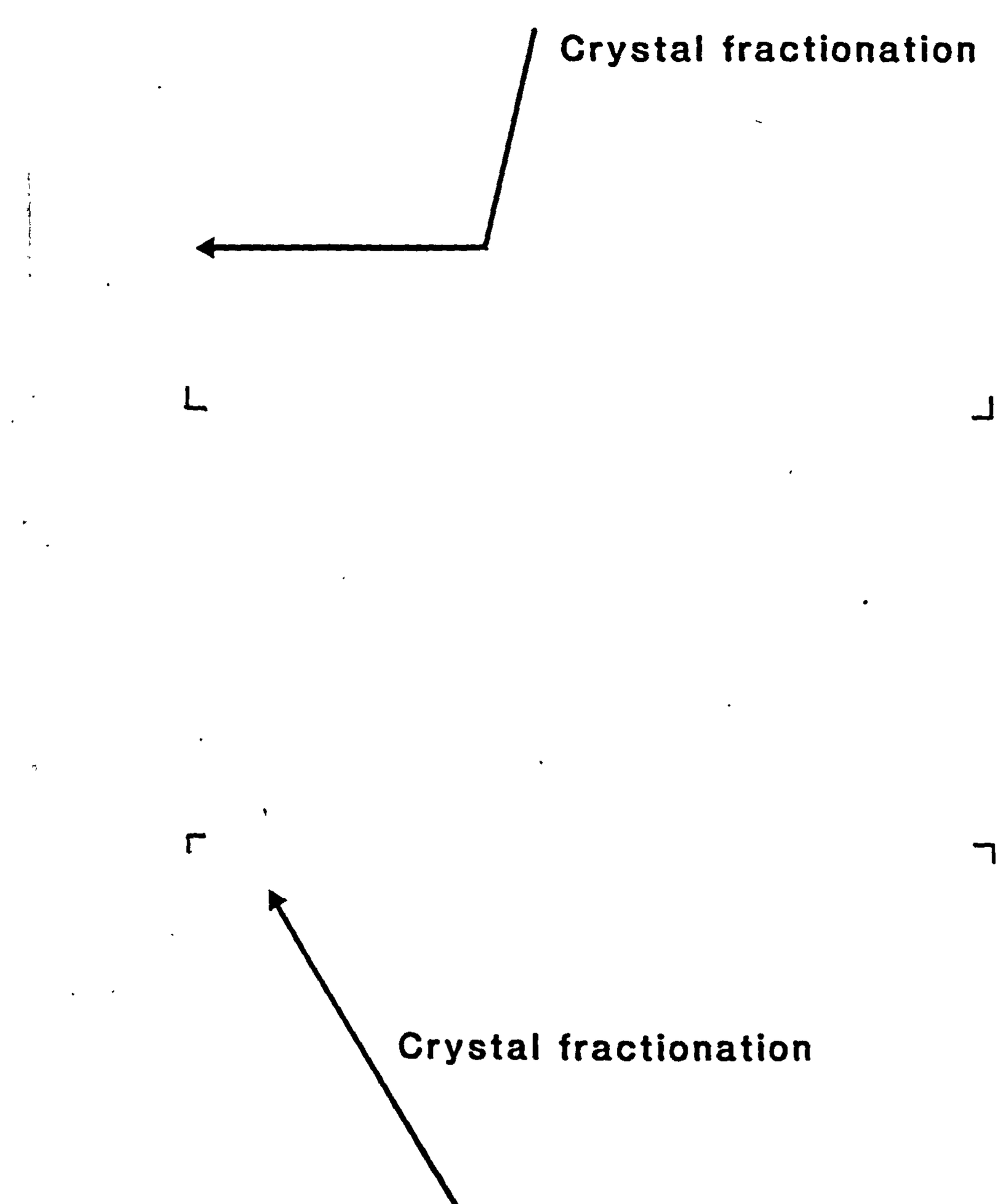
Crystal fractionation
Crystal fractionation

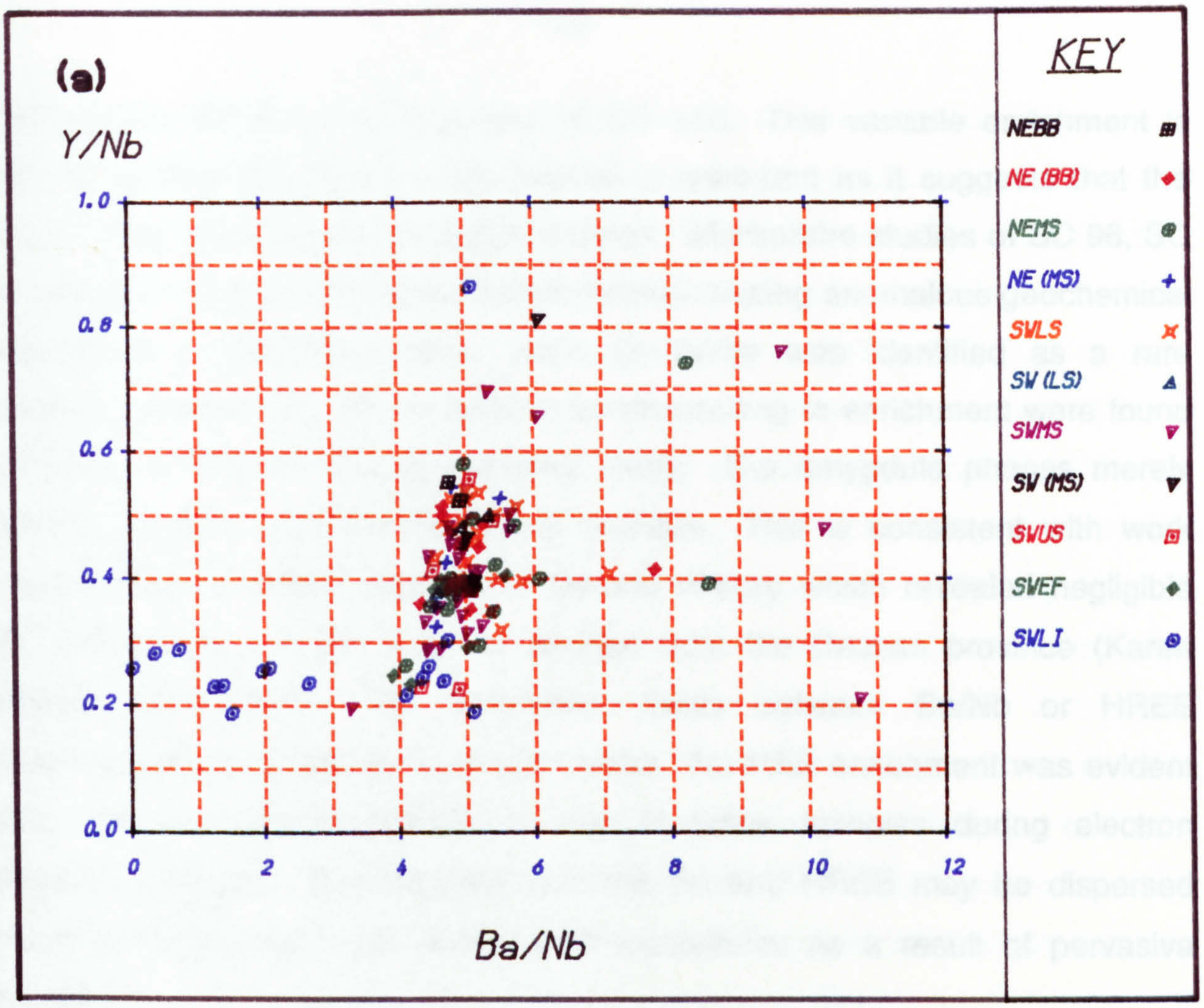
(a)
Y/Nb
1.0
0.8
0.6
0.4
0.2
0.0
0
2
4
6
8
10
12
Ba/Nb
KEY
NEBB
NE (BB)
NEMS
NE (MS)
SWLS
SW (LS)
SWMS
SW (MS)
SWUS
SWEF
SWLI

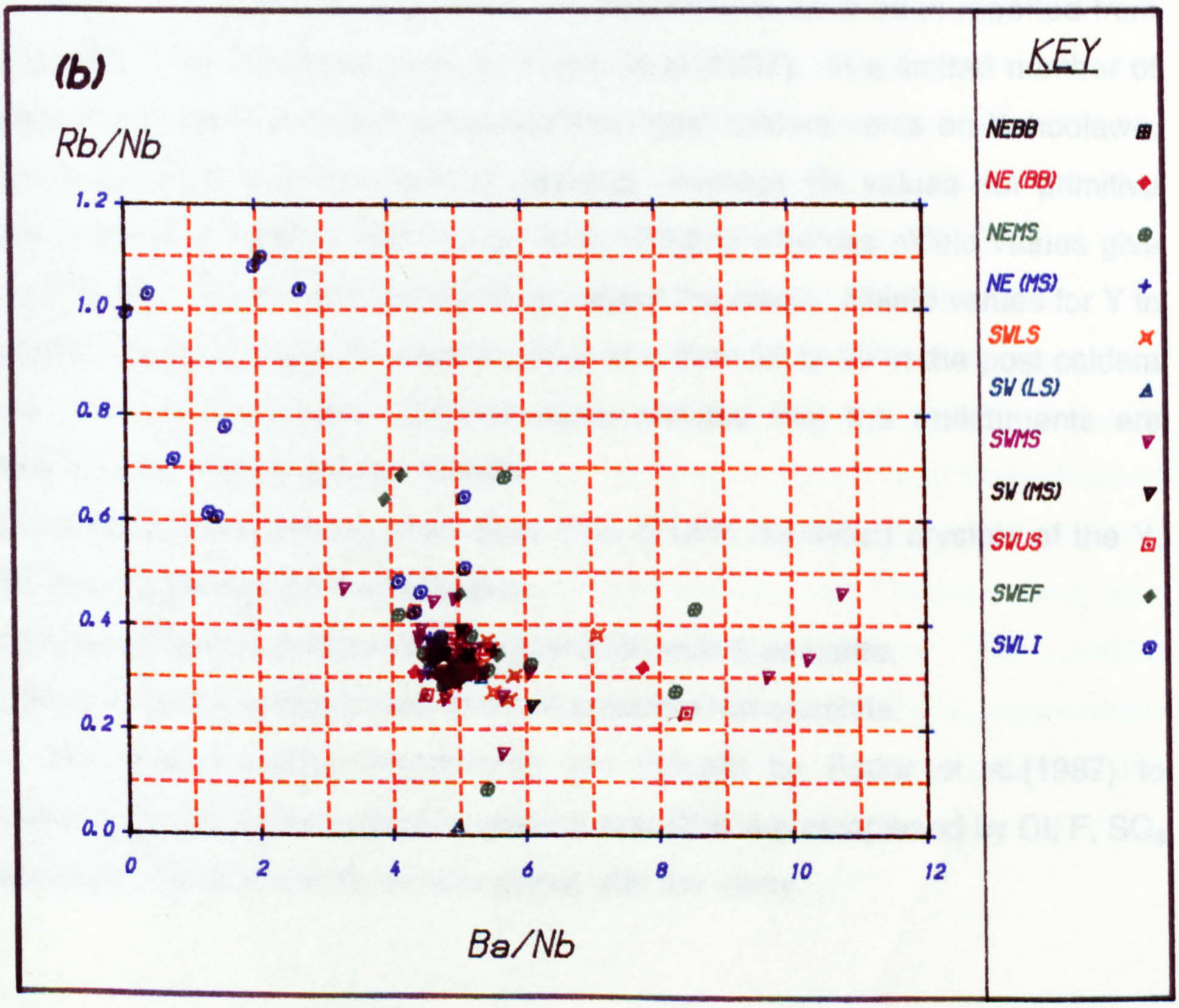
(b)
Rb/Nb
1.2
1.0
0.8
0.6
0.4
0.2
0.0
0
2
4
6
8
10
12
Ba/Nb
KEY
NEBB
NE (BB)
NEMS
NE (MS)
SWLS
SW (LS)
SWMS
SW (MS)
SWUS
SWEF
SWLI

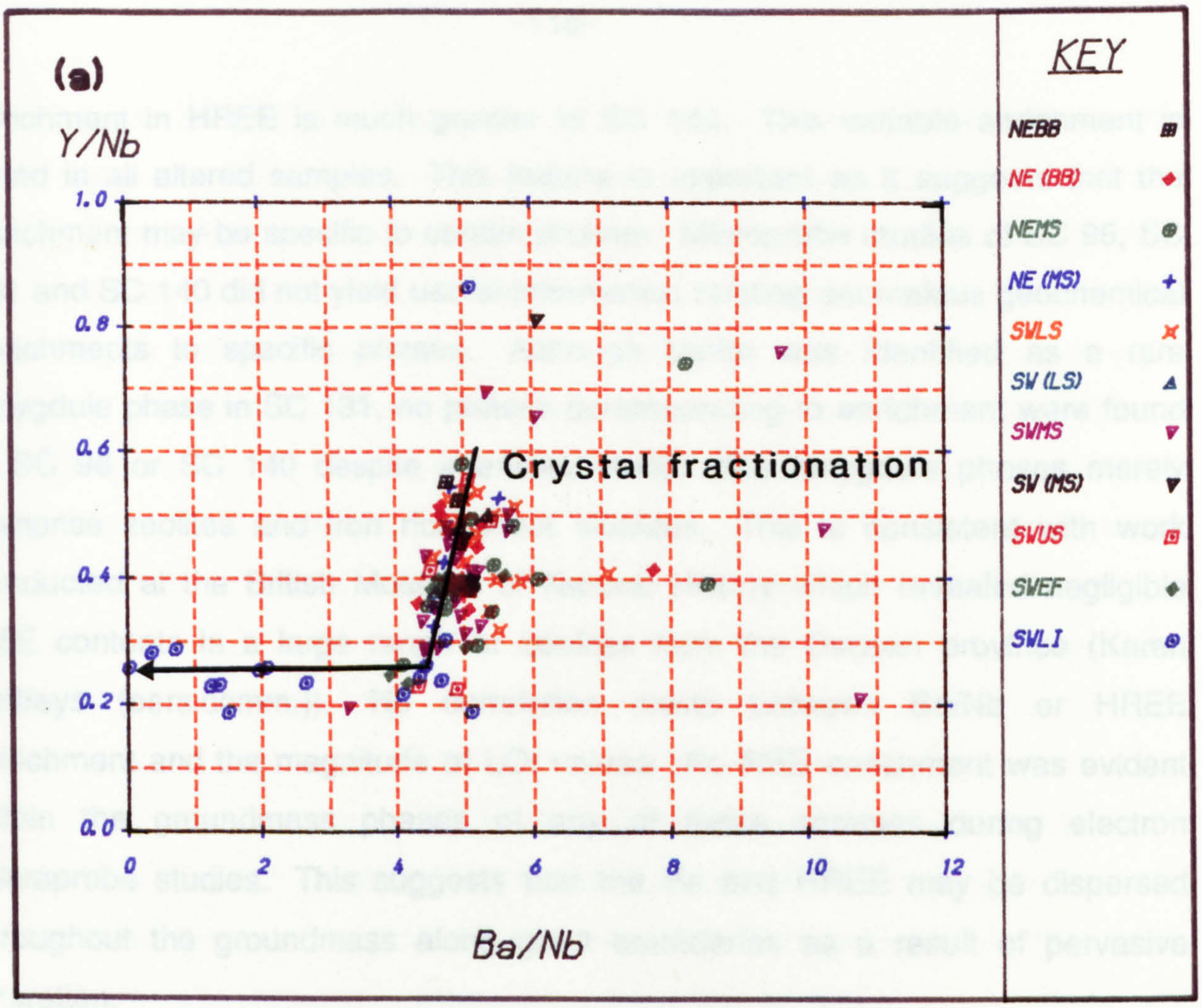
(a)
Y/Nb
1.0
0.8
0.6
0.4
0.2
0.0
0
2
4
6
8
10
12
Crystal fractionation
Ba/Nb
KEY
NEBB
NE (BB)
NEMS
NE (MS)
SWLS
SW (LS)
SWMS
SW (MS)
SWUS
SWEF
SWLI

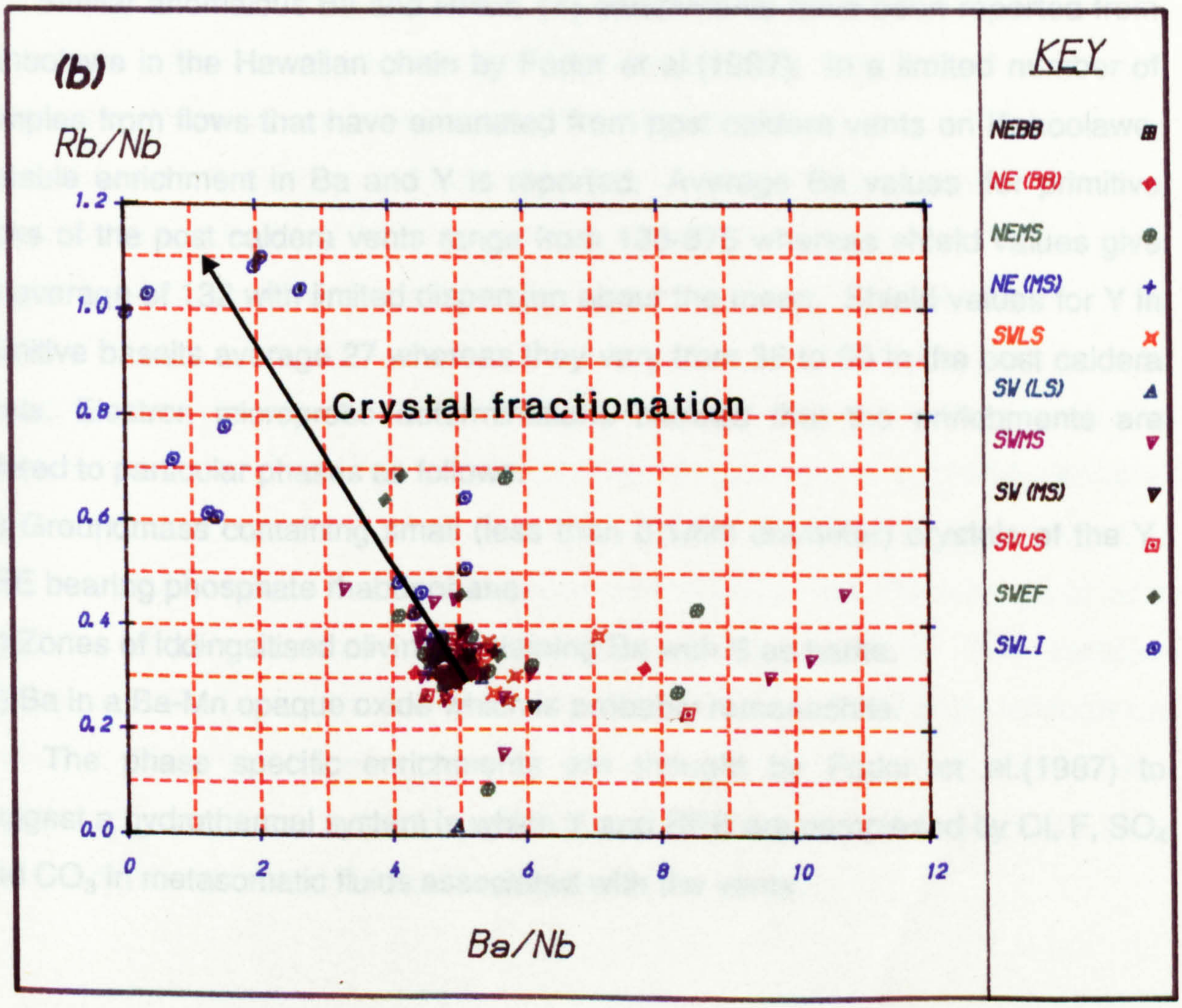
(b)
Rb/Nb
1.2
1.0
0.8
0.6
0.4
0.2
0.0
0
2
4
6
8
10
12
Crystal fractionation
Ba/Nb
KEY
NEBB
NE (BB)
NEMS
NE (MS)
SWLS
SW (LS)
SWMS
SW (MS)
SWUS
SWEF
SWLI

enrichment in HREE is much greater in SC 140. This variable enrichment is found in all altered samples. This feature is important as it suggests that the enrichment may be specific to certain phases. Microprobe studies of SC 96, SC 131 and SC 140 did not yield useful information relating anomalous geochemical enrichments to specific phases. Although barite was identified as a rare amygdule phase in SC 131, no phases corresponding to enrichment were found in SC 96 or SC 140 despite intensive study. The amygdule phases merely comprise zeolites and iron rich sheet silicates. This is consistent with work conducted at the British Museum of Natural History which revealed negligible REE contents in a large range of zeolites from the Deccan province (Karen Jeffreys (pers.comm.)). No correlation exists between Ba/Nb or HREE enrichment and the magnitude of LOI values. No REE enrichment was evident within the groundmass phases of any of these samples during electron microprobe studies. This suggests that the Ba and HREE may be dispersed throughout the groundmass along grain boundaries as a result of pervasive alteration.

Similar anomalous Ba and HREE (Y) enrichments have been reported from Kahoolawe in the Hawaiian chain by Fodor et al.(1987). In a limited number of samples from flows that have emanated from post caldera vents on Kahoolawe, variable enrichment in Ba and Y is reported. Average Ba values for primitive rocks of the post caldera vents range from 138-875 whereas shield values give an average of 132 with limited dispersion about the mean. Shield values for Y in primitive basalts average 27 whereas they vary from 36 to 90 in the post caldera vents. Electron microprobe determinations showed that the enrichments are related to particular phases as follows:

(1) Groundmass containing small (less than 0.1mm diameter) crystals of the Y, REE bearing phosphate rhabdophane.

(2) Zones of iddingsitised olivine containing Ba with S as barite.

(3) Ba in a Ba-Mn opaque oxide which is probably romanechite.

The phase specific enrichments are thought by Fodor et al.(1987) to suggest a hydrothermal system in which Y and REE are complexed by Cl, F, SO_4 and CO_3 in metasomatic fluids associated with the vents.

If the location of altered samples found on St.Helena are related spatially to fresh samples there is no clear evidence to support a causal link between vent and altered samples. This link is more difficult to establish than for the more recent activity on Kahoolawe as volcanic forms such as post caldera vents have been largely buried by subsequent flows on St.Helena. SC 140 occurs in close proximity (less than 50m horizontal distance) to SC 139 and SC 141 which are of a similar primitive composition but remain fresh. In terms of vertical interval these flows are separated by less than 30m. SC 87 occurs within 50m vertically and 150m laterally of SC 85 and 86 which are relatively fresh. Similarly SC 177 occurs within 25m vertically of SC 178 and SC 179 which are not altered. It is thought, therefore that that if hydrothermal fluids have caused anomalous enrichments in Ba, Y and HREE this must occur immediately prior to eruption rather than subsequent to eruption. A similar conclusion was reached by Fodor et al.(1987) based on the areal distribution of anomalous enrichments on Kahoolawe. It seems likely that these anomalous flow units have originated from different vents to underlying and overlying flows that are fresh.

Fig.5.5a; Ba/Nb versus Y/Nb shows that no universal description of the anomalous geochemistry can be made. Whilst some samples possess both high Ba/Nb and Y/Nb others have anomalously high Ba/Nb at low Y/Nb. Similarly Fig.5.5b shows that some samples with Ba/Nb >5.5 also have low Rb/Nb, but some samples with low Rb/Nb do not exhibit correspondingly high Ba/Nb. Thus the Ba and Y enrichments may coincide, but appear to be phase specific. The Rb and K depletions and enrichments are thought to be related to post-eruptive leaching when unrelated to Ba and HREE anomalies. This process is known to operate elsewhere. Studies on Hawaii (e.g. Feigenson et al.(1983), Kohala) have suggested that Rb and K loss through post-eruptive leaching is reduced in lava flows which occur in the rainshadow of the volcanoes. Clearly great care must be taken to remove this extraneous modifying effect. The samples considered in subsequent discussion of source differences all show concordant trends of Rb, K and Ba when plotted against an immobile element such as Nb. Additional precautions to ensure that any remaining alteration products were removed prior to isotopic analysis are described in chapter 7.

CHAPTER 6

TRACE ELEMENT SOURCE CHARACTERISTICS OF THE SHRS : REMOVING THE EFFECTS OF CRYSTAL FRACTIONATION AND PARTIAL MELTING :

6.1; Introduction;

In Chapter 4 the petrographic and geochemical characteristics of the SHRS were shown to be consistent with a cogenetic origin for the St.Helena rock suite. Members of the SHRS were shown to be related by crystal fractionation. In the first part of this chapter an attempt to model in a quantitative manner the effects of crystal fractionation is made. This is necessary as the first stage in inverting the observed compositions to calculate the source compositions. It is also necessary in qualitative discussion of trace element ratios to give an idea of the magnitude of the crystal fractionation effect. The latter effect is often neglected in studies of OIB suites in rocks containing more than 5% MgO e.g. Mattey(1982), Chen and Frey(1983,5), Palacz and Saunders(1986) and Liotard et al.(1986), but nevertheless, it may be important in suites such as St.Helena which have limited trace element variation. An important effect is produced when clinopyroxene fractionation occurs as this mineral has a relatively large range in distribution coefficient in incompatible elements coupled with a high magnitude compared to other likely fractionating phases (Fig.6.1). Thus the fractionation of clinopyroxene can modify La/Yb, for example, significantly (Section.6.3).

Prior to attempting to model the effect of crystal fractionation the basis of the model is critically assessed in terms of the validity of input parameters. Once the trace element abundances have been corrected for crystal fractionation effects it is shown that trace element variations are insufficient to use the commonly used inversion method of Hofmann and Feigenson(1983). Hence the model of Budahn and Schmitt(1985) is used to place constraints on the likely proportion of phases in the source region and the degree of partial melting the source undergoes. In a final discussion section the implications of the degree of melting suggested by the results is considered.

Fig.6.1. Variation in distribution coefficients between mineral and melt for REE in mantle peridotites. Data from Prinzhofer and Allegre(1985), with the exception of kaersutite and phlogopite which are contained in phonolites (Le Marchand et al.(1987)).

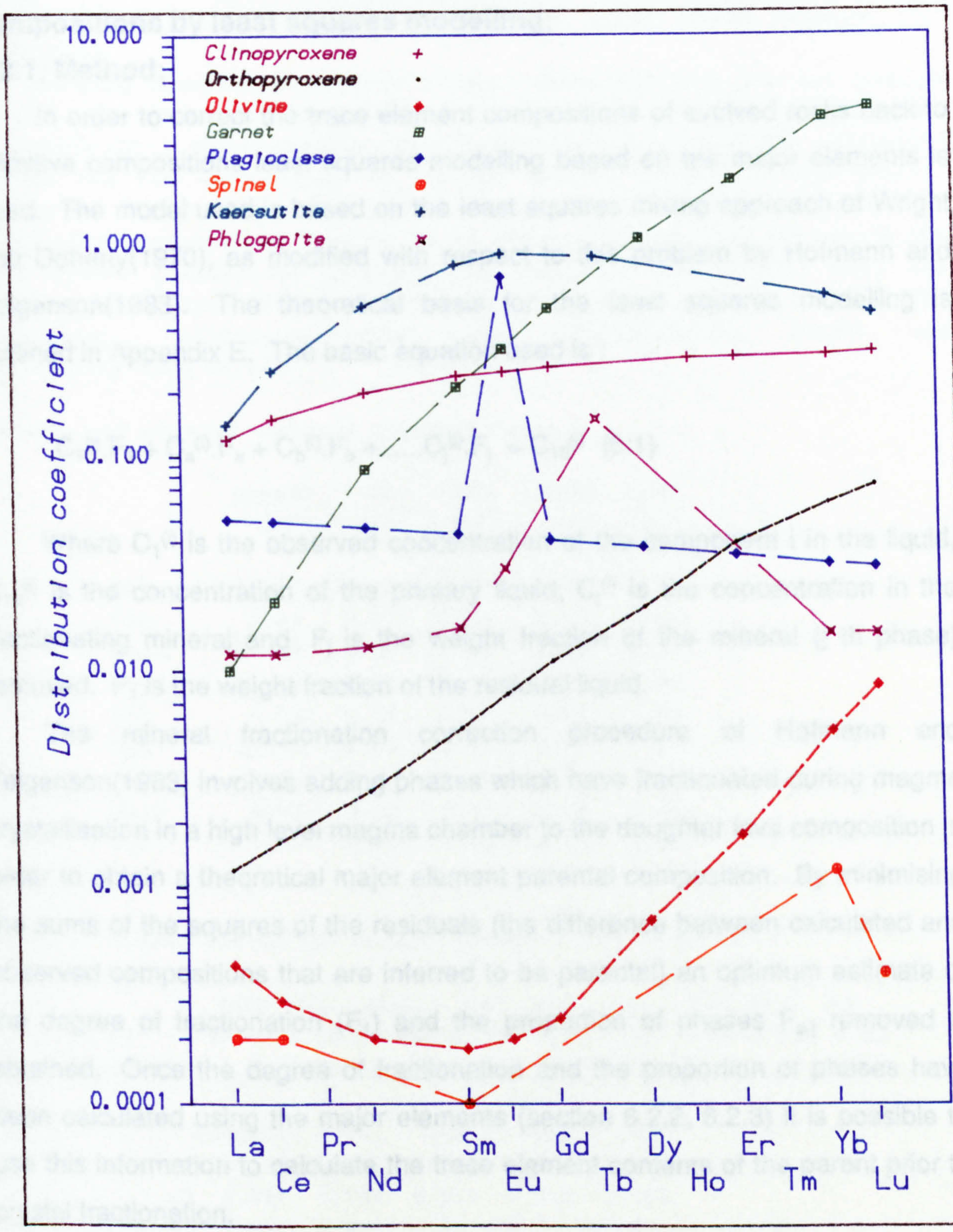
10.000
1.000
0.100
0.010
0.001
0.0001
Distribution coefficient
Clinopyroxene
Orthopyroxene
Olivine
Garnet
Plagioclase
Spinel
Keersutite
Phlogopite
La
Ce
Pr
Nd
Sm
Eu
Gd
Tb
Dy
Ho
Er
Tm
Yb
Lu

6.2; Correction of major element compositions to primitive compositions by least squares modelling;

6.2.1; Method;

In order to correct the trace element compositions of evolved rocks back to primitive compositions least squares modelling based on the major elements is used. The model used is based on the least squares mixing approach of Wright and Doherty(1970), as modified with respect to this problem by Hofmann and Feigenson(1983). The theoretical basis for the least squares modelling is outlined in Appendix E. The basic equation used is :

$$C_1^{(i)}.F_1 + C_a^{(i)}.F_a + C_b^{(i)}.F_b + ...C_j^{(i)}.F_j = C_{10}^{(i)} \quad (6.1)$$

Where $C_1^{(i)}$ is the observed concentration of the component i in the liquid, $C_{10}^{(i)}$ is the concentration of the primary liquid, $C_j^{(i)}$ is the concentration in the fractionating mineral and F_j is the weight fraction of the mineral (j th phase) removed. F_1 is the weight fraction of the residual liquid.

The mineral fractionation correction procedure of Hofmann and Feigenson(1983) involves adding phases which have fractionated during magma crystallisation in a high level magma chamber to the daughter lava composition in order to obtain a theoretical major element parental composition. By minimising the sums of the squares of the residuals (the difference between calculated and observed compositions that are inferred to be parental) an optimum estimate of the degree of fractionation (F_1) and the proportion of phases F_{a-j} removed is obtained. Once the degree of fractionation and the proportion of phases have been calculated using the major elements (section 6.2.2, 6.2.3) it is possible to use this information to calculate the trace element contents of the parent prior to crystal fractionation.

As an illustration of the application of this method, a number of rocks from the St.Helena suite which have been inferred to be cogenetic in terms of major elements (Chapter 4) are compared. The three examples given in Table 6.1 illustrate the derivation of three evolved compositions from a primitive magma SC 113. The simple model is presented at this stage for illustrative purposes only.

The necessary constraints on input parameters are discussed in detail below.

Table 6.1. Derivation of daughter compositions SC 86, SC 175 and SC 149 from parent composition SC 113 using least squares fit modelling.

Scanning electron microprobe mineral determinations for the samples shown. The daughter compositions are actual observed compositions (Appendix C2). The residuals are the differences between the calculated parent and the composition of SC 113 (actual parent in the model). Errors in the analysis are expressed as standard deviation (sd). A plagioclase composition from SC 26 is chosen because this is one of the most calcic plagioclase compositions available and SC 113 does not possess plagioclase (PLAG) phenocrysts. The other mineral compositions olivine(OL), clinopyroxene(CPX) and titanomagnetite (TIMT) are phenocrysts from SC 113.

Parent and mineral extract compositions

	parent 113	OL 113	CPX 113	PLAG 26	TIMT 113
SiO_2	45.47	39.36	49.60	48.08	0.54
TiO_2	2.44	0.00	1.61	0.12	25.83
Al_2O_3	11.47	0.03	4.96	32.99	1.19
FeO	11.49	18.89	6.18	0.70	69.56
MnO	0.16	0.18	0.07	0.01	0.69
MgO	13.09	41.89	14.57	0.15	1.59
CaO	11.36	0.30	22.34	15.83	0.58
Na_2O	2.48	0.00	0.67	2.40	0.00
K_2O	0.77	0.00	0.05	0.08	0.00

Model 1: Ankaramite SC 113 parent, basalt SC 86 daughter

	SiO_2	TiO_2	Al_2O_3	FeO	MnO	MgO	CaO	Na_2O	K_2O
SC 86	47.67	2.89	16.03	11.69	0.18	5.73	9.29	4.03	1.43
Residuals	-0.53	0.05	0.02	-0.28	0.01	0.20	-0.02	0.04	-0.01

	daughter	OL	CPX	PLAG	TIMT
	0.533	0.147	0.250	0.049	0.017
sd	0.017	0.008	0.013	0.013	0.003
%	3.3	5.4	5.3	25.9	17.5

Table 6.1(continued)

Model 2 : Ankaramite SC 113 parent, mugearite SC 175 daughter

	SiO_2	TiO_2	Al_2O_3	FeO	MnO	MgO	CaO	Na_2O	K_2O
SC 175	53.10	0.96	17.16	7.56	0.17	2.02	3.38	6.68	3.19
Residuals	-0.14	0.04	-0.10	-0.20	0.02	0.12	-0.05	0.16	-0.07

	daughter	OL	CPX	PLAG	TIMT
	0.253	0.172	0.353	0.164	0.061
sd	0.008	0.008	0.013	0.010	0.002
%	3.3	4.5	3.8	6.3	3.8

Model 3: Ankaramite SC 113 parent, phonolite SC 149 daughter

	SiO_2	TiO_2	Al_2O_3	FeO	MnO	MgO	CaO	Na_2O	K_2O
SC 149	59.78	0.07	19.25	3.91	0.17	0.00	0.88	9.08	4.95
Residual	0.58	-0.01	-0.22	0.02	0.02	-0.08	-0.09	0.23	-0.10

	daughter	OL	CPX	PLAG	TIMT
	0.169	0.185	0.361	0.199	0.071
sd	0.006	0.008	0.013	0.010	0.002
%	3.3	4.1	3.7	4.9	3.2

Good agreement between the observed and calculated values for the parent is obtained in each example (residuals). The residuals are the normal test of the validity of such models (as sum of the squares of the residuals) (Appendix E). Errors on the percentage of mineral extracted and the degree of crytallisation are also good. *Whilst the model is well constrained mathematically, it is important to consider how close it approaches geological reality.* The examples in Table 6.1 are chosen to illustrate that not too great a reliance should be placed on good fits to the least squares model - the petrographic constraints on input parameters should also be considered carefully. It is noted that the crystallisation interval between SC 113 and SC 175 or SC 149 is too great to be modelled in a single stage. Between 13% MgO and less than 3% MgO the number of phases in the extract will change and phases that are always present may change significantly in composition. This was demonstrated in section 4.5 by the use of element - element variation diagrams. For example, at approximately 3 % MgO an inflection in MgO vs P_2O_5 (Fig.4.15d3) marks the onset of apatite crystallisation which is not considered in the model. This problem is discussed further in

section 6.2.2.

Progressively larger degrees of fractionation are required to produce SC 86 (46%), SC 175 (75%) and SC 149 (83%), (Table 6.1 (as 1 - daughter)). To illustrate the variation in proportions of phases crystallising during crystal fractionation the process has been sequentially modelled. A simple model is adopted in which samples from the SW volcano are derived from ankaramite SC 113 by removal of varying amounts of olivine, clinopyroxene, plagioclase and titanomagnetite. The mineral extract compositions chosen are those given in Table 6.1. The problems of using fixed mineral compositions are discussed in section 6.2.2. The proportions of phases calculated for varying amounts of residual liquid are shown in Fig.6.2. This graph emphasises the conclusions drawn from element-element plots in section 4.5. It is noted that:

(1) The least evolved rocks are formed by fractionation of olivine and clinopyroxene only. Clinopyroxene tends to be be more abundant than olivine.
(2) Plagioclase and titanomagnetite become more important crystallising phases in the hawaiites - phonolites.
(3) In the hawaiites - phonolites clinopyroxene proportions continue to increase whereas olivine remains constant.
(4) The most evolved phonolites are derived by 83% crystal fractionation in this model.

6.2.2; An appraisal of the validity of input parameters to the model;

Prior to utilising least squares modelling techniques to remove the effects of crystal fractionation by the method of Hofmann and Feigenson(1983) a critical appraisal of the validity of the input parameters to the model is vital.

6.2.2.1; Process;

Ideally the method should be used to relate primitive and evolved compositions from a single liquid line of descent. In order to do this very fine scale sampling is required as the conditions of a single liquid line of descent will only be met from within lava flow variations (an example of a closed system). It is usually assumed that the crystal fractionation process is invariant and samples

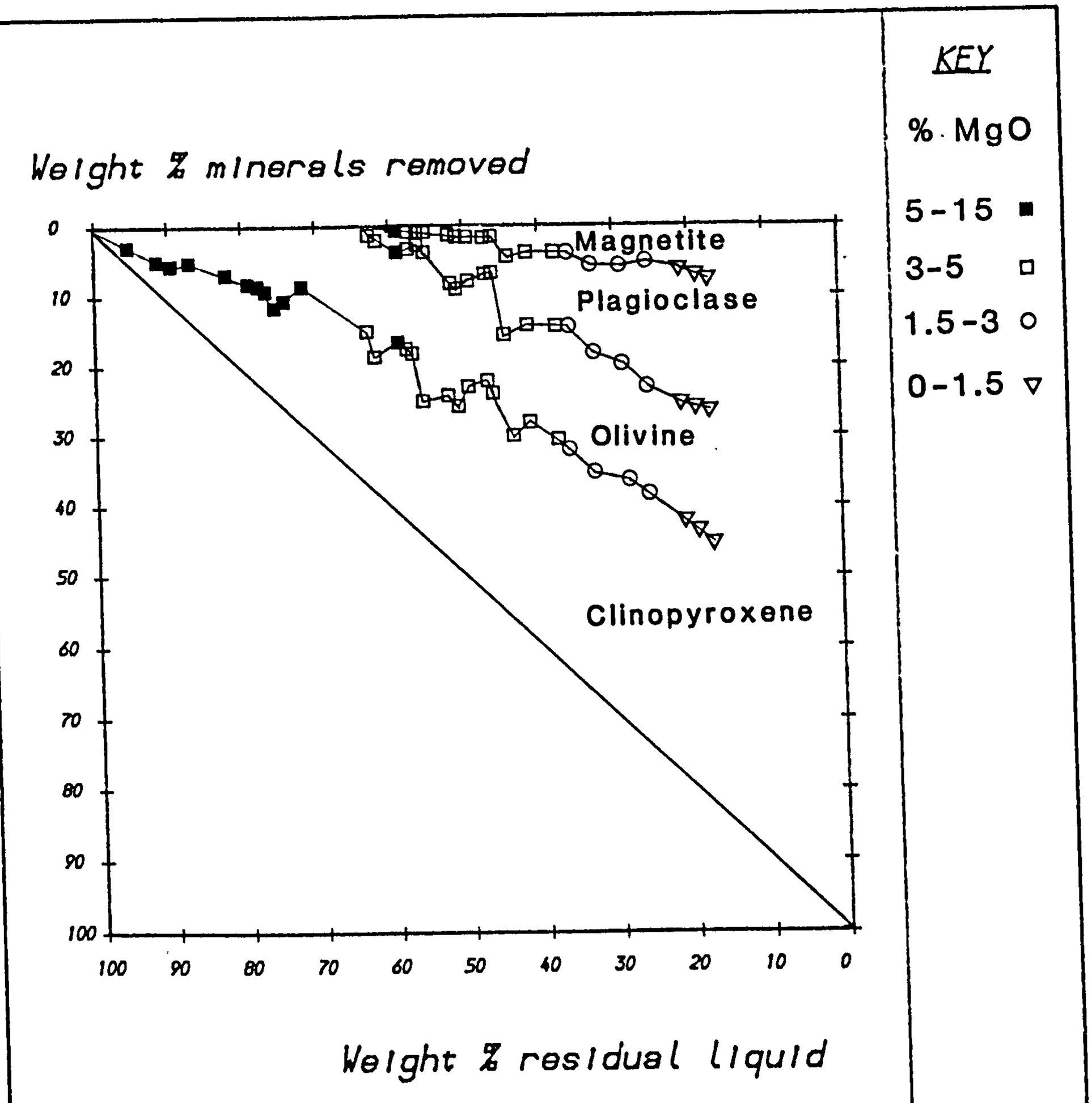

Fig.6.2. Variation in the proportion of mineral phases fractionated during crystallisation as a function of weight % residual liquid. A sequential least squares model is adopted with parental ankaramite SC 113 related to daughter compositions by the removal of varying proportions of the phases shown. The weight % of each mineral removed is shown by the vertical distance between symbols which represent the MgO content of each rock as shown in the key. The mineral extract compositions used in the model are those in table 6.1.

are effectively from the same liquid line of descent (i.e. they have the same parent) (Cox et al.(1979) and Chapter 4. It is shown in section 7.3 that in terms of isotopic composition members of the SHRS vary slightly so they cannot possess the same parent. The trace elements can still be corrected, however, using the modelling based on the major elements in order to minimise the effects of crystal fractionation because the parents are virtually identical in terms of major elements (section 4.5). It is then evident whether the observed isotopic variations are related to trace element variations in the source (section 7.4).

Additionally, modelling is only valid between parents and daughters that are not separated by a large crystallisation interval. For example Wright and Doherty(1970) compare a parental composition of 51.16 SiO_2 and 7.64% MgO and a daughter with 51.12% SiO_2 and 5.35% MgO. In this instance it is possible to neglect the variation in phenocryst composition, whereas the derivation of a phonolite from an ankaramite cannot realistically be modelled in a single stage because the fractionating assemblage will have changed in composition and in terms of the number of components. Thus the derivation of the phonolite SC 149 from the ankaramite SC 113 in this model does not take into account that two-element (Ch 4, Fig.4.13) variation diagrams which suggest the crystallisation of titanomagnetite, apatite, anorthoclase and nepheline in rocks containing less than 4.5% MgO. In addition the composition of olivine, clinopyroxene and plagioclase phenocrysts removed in the extract will vary. This is discussed further in 6.2.2.4.

6.2.2.2; **Parent composition;**

The parent magma composition is difficult to assess because often it does not correspond to the most primitive composition. The most primitive composition observed in a suite of volcanics may not represent the composition of the melt derived from the mantle, if it has fractionated some phases at depth, or if it contains accumulative olivine and clinopyroxene. The high proportion of phenocrysts in samples such as SC 38 and 68 (Fig.4.2) suggest that they may be accumulative. Useful information concerning whether a primitive composition has fractionated or accumulated olivine and clinopyroxene is provided by considering elements compatible in these minerals. Hart and Davis(1978)

consider the case in which olivine crystallises in isolation during the first stages of crystallisation. It was shown that in some basaltic suites olivine accumulation describes a different vector (linear trend) to crystal fractionation (curved trend) when considered in terms of a graph of Mg0 and Ni (Fig.6.3). Thus the inflection point on such a diagram should mark the Ni and MgO composition for the primary magma. The plot of MgO vs Ni (Fig.6.3) for the SHRS shows an inflection at 3-5% MgO at Ni contents below 50 ppm. This feature is however, unlikely to represent a parental composition as melts of the mantle produce 350-400 ppm Ni at 15% MgO (e.g. Hart and Davis(1978), Dupuy et al.(1988)) (Fig.6.3). The apparent enigma is explained because it is known that clinopyroxene is a fractionating phase in the SHRS (Chapter 4). Furthermore, Fig.6.2 and petrographic study show that clinopyroxene is up to twice as common as olivine. Because $Kd_{(Ni)}^{(cpx/l)}$ is less than than $Kd_{(Ni)}^{(ol/l)}$ (Henderson,1982)) it will not produce such a marked curvature in the data set as noted by Dupuy et al.(1988). This effect is illustrated in Fig.6.3. The details of the model are explained in the figure caption. It is apparent that a mixture of olivine and clinopyroxene fractionation can account for the data points in the SHRS A combined fractionation (ol+cpx) model is not adopted because it is critically dependent on $Kd^{(cpx/l)}_{(Ni)}$, which is poorly known. If the trend in Fig.6.3 can be mainly accounted for by crystal fractionation the ankaramites containing 13-14% MgO could represent parental compositions because they contain 350-400 ppm Ni which is consistent with a 5-20% batch melt of the upper mantle (Dupuy et al.(1988)).

An alternative method of calculating the most primitive composition is to use the relationship of Fe and Mg partitioning in olivine derived by Roeder and Emslie(1970). By this method the maximum Fo content can be related to the percentage of MgO and FeO in the liquid if the FeO/Fe_2O_3+FeO ratio is known. The Baker(1968) compilation of FeO and Fe_2O_3 wet chemical determinations for primitive rocks for St.Helena is used. The average $FeO/FeO+Fe_2O_3$ ratio of 0.82 in Baker(1968) in samples containing over 10% MgO is consistent with a Fo content of 83 which is in good agreement with the maximum Fo content observed in mafic St.Helena volcanics containing 14% MgO (section 4.3).

Fig.6.3. Variation of Ni with MgO for the SHRS.

The variations are modelled in terms of crystal fractionation of:

(1) Olivine (solid curves) using the relationship:

$Kd^{(ol/l)}_{(Ni)} = 124.13(1/MgO)-0.897$

(Hart and Davis(1978)).

(2) Clinopyroxene (dashed curves).

Kd values for recommended value of Henderson(1982) ($Kd^{(cpx/l)}_{(Ni)} = 2.6$) and Kd = 1.5 and 1.8 to show the effect of varying this value (the variation in the compilation of Le Marchand et al.(1987) gives a range of 0.8-8).

The MgO contents for different values of Ni are calculated by removing olivine and clinopyroxene mineral compositions from SC 113 (13.1% MgO), (table 6.1)).The Ni contents are calculated using a modified form of equation 6.2 i.e.

$$\frac{C_R}{C_0} = (1-F)^{(D-1)}$$

where F is the degree of crystal fractionation, D is the distribution coefficient, C_R is the concentration in the residue and C_0 is the initial concentration. The ticks on the curve mark the degree of crystal fractionation.

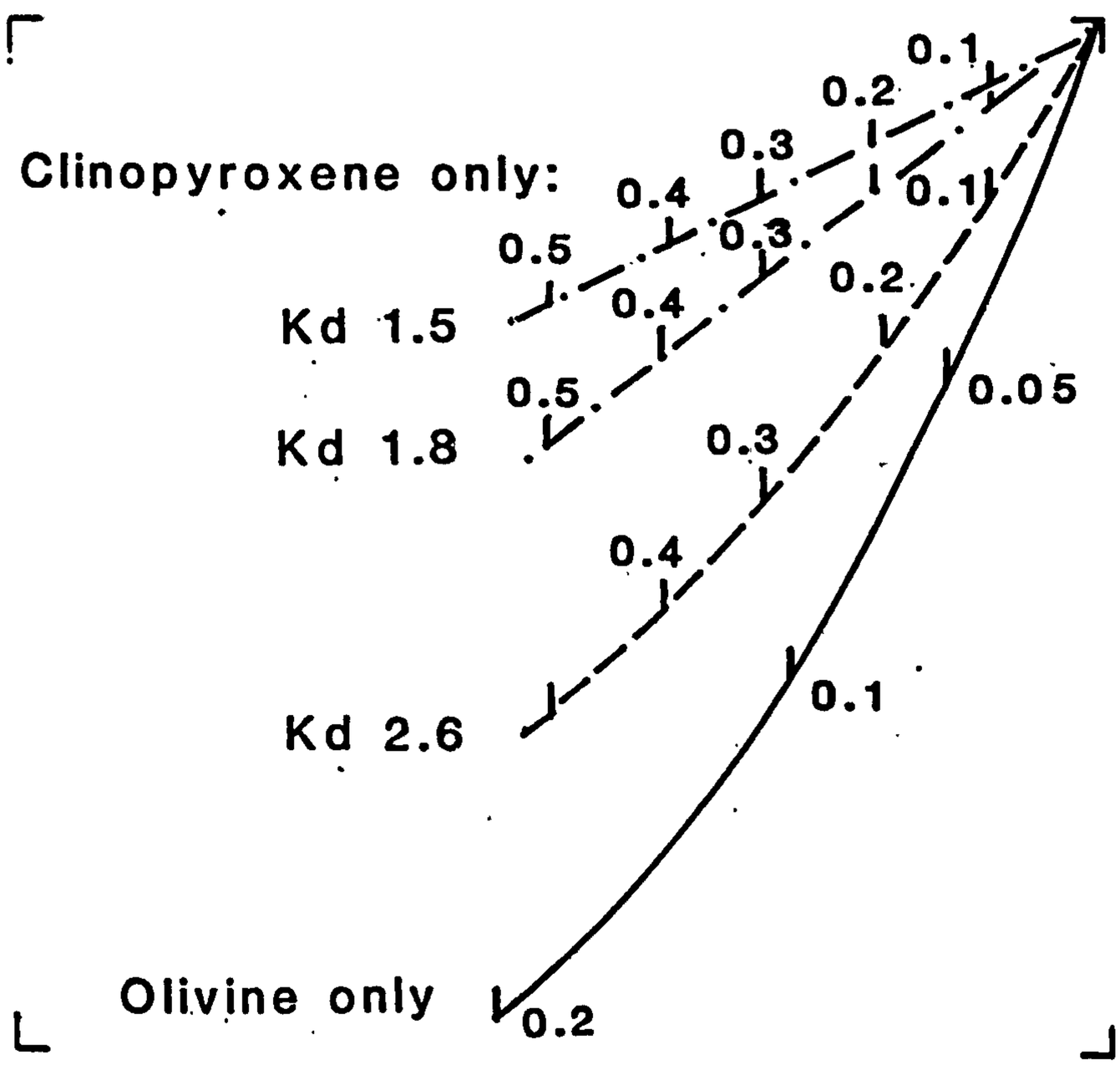
Clinopyroxene only:
Kd 1.5
Kd 1.8
Kd 2.6
Olivine only
0.1
0.2
0.3
0.4
0.5
0.1
0.2
0.3
0.4
0.5
0.05
0.1
0.2

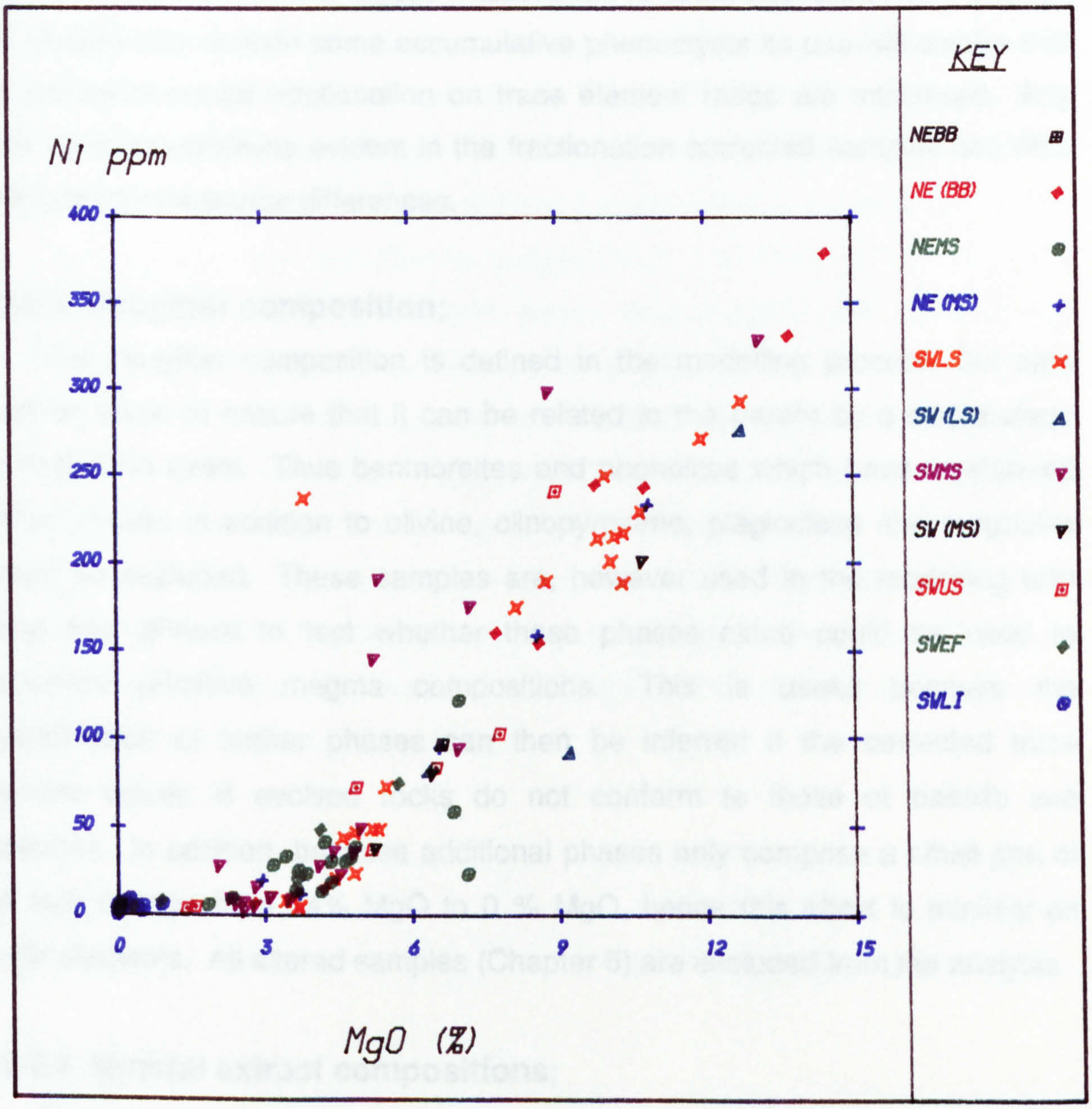
Ni ppm
400
350
300
250
200
150
100
50
0
0
3
6
9
12
15
MgO (%)
KEY
NEBB
NE (BB)
NEMS
NE (MS)
SWLS
SW (LS)
SWMS
SW (MS)
SWUS
SWEF
SWLI

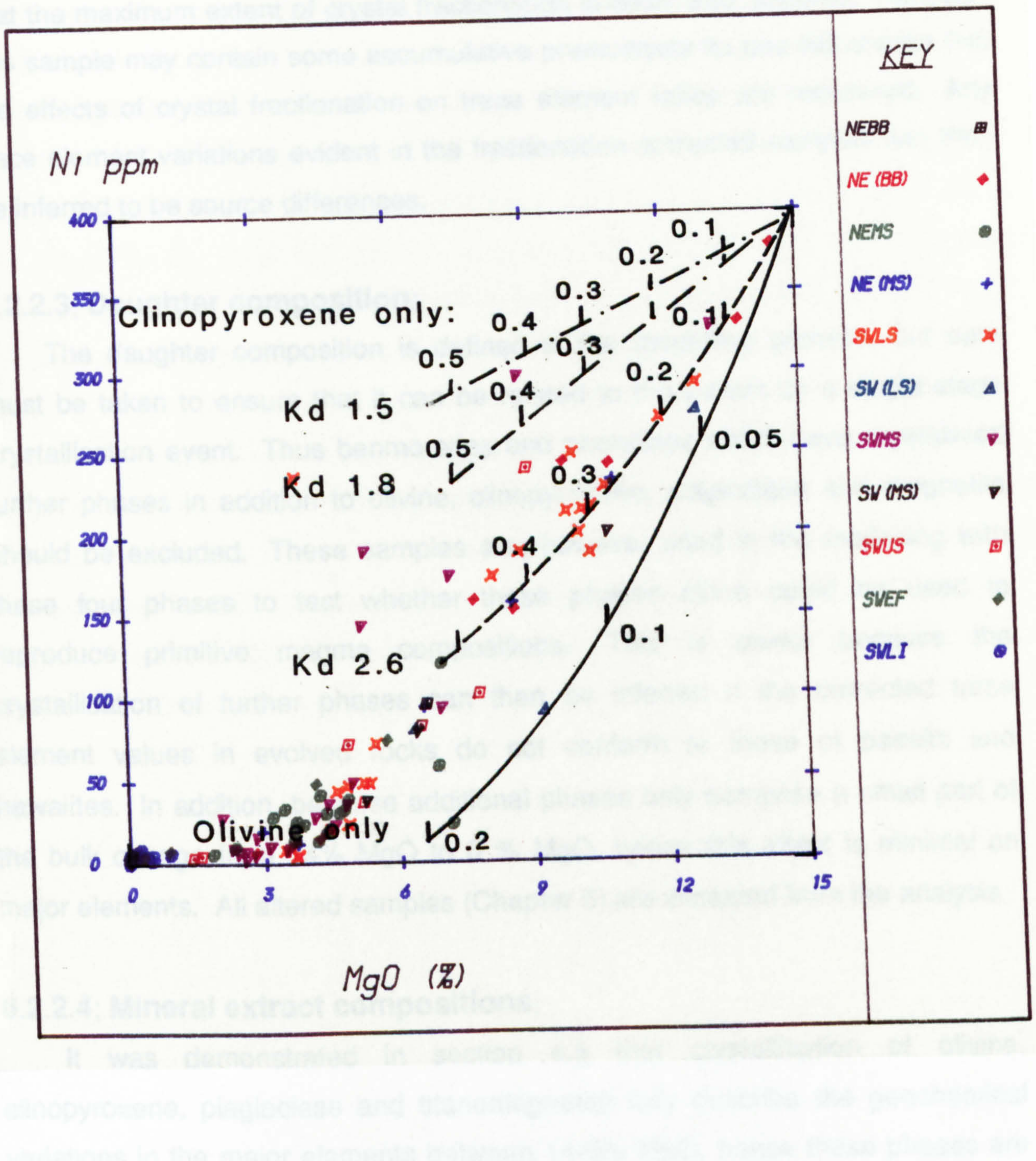
KEY
NEBB
NE (BB)
NEMS
NE (MS)
SVLS
SV (LS)
SVMS
SV (MS)
SVUS
SVEF
SVLI
Ni ppm
400
350
300
250
200
150
100
50
0
0
3
6
9
12
15
MgO (%)
Clinopyroxene only:
Kd 1.5
Kd 1.8
Kd 2.6
Olivine only
0.1
0.2
0.3
0.4
0.5
0.05

Since, the minimisation of the effects of crystal fractionation is required rather than calculation of an exact parent composition the following approach is taken: SC 68 a sample containing 13.69 % MgO is chosen as a parent to ensure that the maximum extent of crystal fractionation is taken into account. Although this sample may contain some accumulative phenocrysts its use will ensure that the effects of crystal fractionation on trace element ratios are minimised. Any trace element variations evident in the fractionation corrected samples can then be inferred to be source differences.

6.2.2.3; Daughter composition;

The daughter composition is defined in the modelling process, but care must be taken to ensure that it can be related to the parent by a single stage crystallisation event. Thus benmoreites and phonolites which have crystallised further phases in addition to olivine, clinopyroxene, plagioclase and magnetite should be excluded. These samples are, however used in the modelling with these four phases to test whether these phases alone could be used to reproduce primitive magma compositions. This is useful because the crystallisation of further phases can then be inferred if the corrected trace element values in evolved rocks do not conform to those of basalts and hawaiites. In addition, because additional phases only comprise a small part of the bulk change from 14% MgO to 0 % MgO, hence this effect is minimal on major elements. All altered samples (Chapter 5) are excluded from the analysis.

6.2.2.4; Mineral extract compositions;

It was demonstrated in section 4.5 that crystallisation of olivine, clinopyroxene, plagioclase and titanomagnetite fully describe the geochemical variations in the major elements between 14-3% MgO, hence these phases are used as the mineral extract components in the model of Hofmann and Feigenson(1983). However, the choice of compositions for the mineral extracts are difficult to assess as an input parameter to the model. Choosing a fixed mineral composition can pose a problem because of the continuous nature of the crystal fractionation process during which the phenocryst composition will be continuously evolving as the magma changes composition (e.g. Wager and

Brown(1968)). A related problem is that it is difficult to define representative probe compositions for phases because of compositional zoning. The simplifying assumption that is made to facilitate modelling is to use a fixed mineral composition from a primitive rock which will maximise the effect of crystal fractionation. It is then possible to assess whether source differences are indicated by the trace element data of the SHRS. To do this the phenocrysts from the most primitive sample (SC 38) are used. It is clear that theoretically this should produce a calculated degree of crystal fractionation which is different from the actual figure. Trial calculations suggest that this effect is not significant because it is the difference between parent and daughter and between the minerals of the extract which govern the least squares fit. Differences in Mg number, within olivine for example, are small compared to major element differences between olivine and plagioclase. To test the validity of using single stage fractionation correction the calculation relating phonolite SC 149 to a parental ankaramite (SC 113) was repeated using a five stage incremental crystallisation model. The mineral extract compositions were varied at each stage according to the phenocryst assemblage in the intermediate rock. The results of this model are shown in Table 6.2.

Table 6.2. Five stage incremental model for derivation of phonolite SC 149 from ankaramite SC 113.

The mineral extract compositions for each stage are average phenocryst values from the intermediate parent (Appendix C1). Fract. is the degree of crystal fractionation at each stage. Mineral abbreviations as in Table 6.1.

Step Parent daughter daughter characteristics:
SC 113 (Ankaramite) --> SC118 (Alkali basalt, 6.6% MgO, 45.2% SiO_2)
SC 118 ----------> SC 168 (Hawaiite, 4.5% MgO, 45.8% SiO_2)
SC 168 ----------> SC 131 (Mugearite, 3.1% MgO, 48.2% SiO_2)
SC 131 ----------> SC 115 (Benmoreite, 2.4% MgO, 51.2% SiO_2)
SC 115 ----------> SC 149 (Phonolite, 0% MgO, 59.9% SiO_2).
SC 113 ----------> SC 149 (Single stage model as in Table 6.1).

		Frac.	OL	CPX	PLAG	TIMT
(1)	SC 113 --> SC 118	0.786	0.123	0.105	-	-
(2)	SC 118 --> SC 168	0.550	0.023	0.108	0.054	0.015
(3)	SC 168 --> SC 131	0.854	0.004	0.035	0.006	0.013
(4)	SC 131 --> SC 115	0.771	-	0.023	0.044	0.044
(5)	SC 115 --> SC 149	0.393	0.037	0.030	0.059	0.015
	Aggregate (1 - 5)	0.135	0.219	0.360	0.192	0.103
	SC 113 --> SC 149	0.169	0.185	0.361	0.199	0.071

It is apparent from Table 6.2 that a quite good agreement exists between the mineral extract compositions and degree of fractionation compared to a single stage derivation of SC 149 to SC 113. This suggests that the use of a single stage rather than multistage crystal fractionation model will not introduce significant errors in back-calculating the trace element concentrations to primitive compositions. It was also found that additional problems are introduced by using an incremental model. Firstly, the interval between parent and daughter at each stage results in larger errors and secondly, these errors are propagated throughout the model.

Adopting the widely used (e.g. Cox et al.(1979)) relationship for incompatible elements: $C_l=C_o*1/F$ (where C_l is the element concentration in the derived magma, C_o is the concentration in the parent and F is the degree of fractionation) places further limits on the validity of the least squares model. For the elements that are incompatible in the range ankaramite to phonolite i.e Zr,

Ta, and Th degrees of crystal fractionation of 85% - 90% are indicated. This is in quite good agreement with the least squares model. The differences probably occur due to the least squares model only considering four phases.

Since it has been shown above that the single stage crystal fractionation model is an adequate approximation of the continuous crystal fractionation approach this is the method used. Feigenson et al.(1983) also considered a *single stage model with fixed mineral extract compositions* to be appropriate. Computation is simplified considerably, and the problems with error propagation of the incremental model do not occur. Thus the use of a fixed mineral composition does not appear detrimental to the model, particularly with respect to correcting samples containing 14 - 4.5% MgO which have only crystallised olivine, clinopyroxene, plagioclase and titanomagnetite. This is in part because of the relatively small range in mineral compositions between 14-4.5% MgO (Fig.4.3). Olivine and clinopyroxene from SC 38 were used together with plagioclase and titanomagnetite from SC 177. Plagioclase was from SC 177 because SC 38 does not contain plagioclase as phenocrysts. The Cr spinels found in the most primitive rocks were not used in modelling because these have no effect on the more evolved rocks from which they are absent and they are volumetrically insignificant in the more primitive rocks (<< 1% overall).

6.2.3; Results of least squares modelling of major elements;

The results for single stage crystal fractionation correction of the major elements using the method of Hofmann and Feigenson(1983) (section 6.2.1) for all members of the SHRS are shown in Fig.6.4. It is evident that the least squares procedure is extremely effective in correcting for the effects of crystal fractionation because a tight cluster of major element compositions occurs. The phonolites and benmoreites are included in this compilation and it is apparent that in terms of major elements their formation can be adequately described in terms of a four phase extract. The effect of additional phases is examined in section 6.3. A good agreement is only obtained once altered samples and primitive samples (> 10 % MgO) have been filtered out.

Fig.6.4. Major element oxide - magnesia variation diagrams for the SHRS to illustrate the efficacy of the crystal fractionation correction procedure described in section 6.2 and 6.3. The corrected compositions (calculated parents) are shown by the overlay.

(a) MgO vs SiO_2

(b) MgO vs Al_2O_3.

(c) MgO vs CaO.

(d) MgO vs FeO.

(e)MgO vs TiO_2.

(f) MgO vs K_2O.

The parental composition is ankaramite SC 68 (13.69% MgO). The mineral extract compositions are olivine and clinopyroxene from SC 38 and plagioclase and titanomagnetite from SC 177. The correction procedure described in the text is undertaken using a modified version of LSQPM PASCAL written by R.Powell.

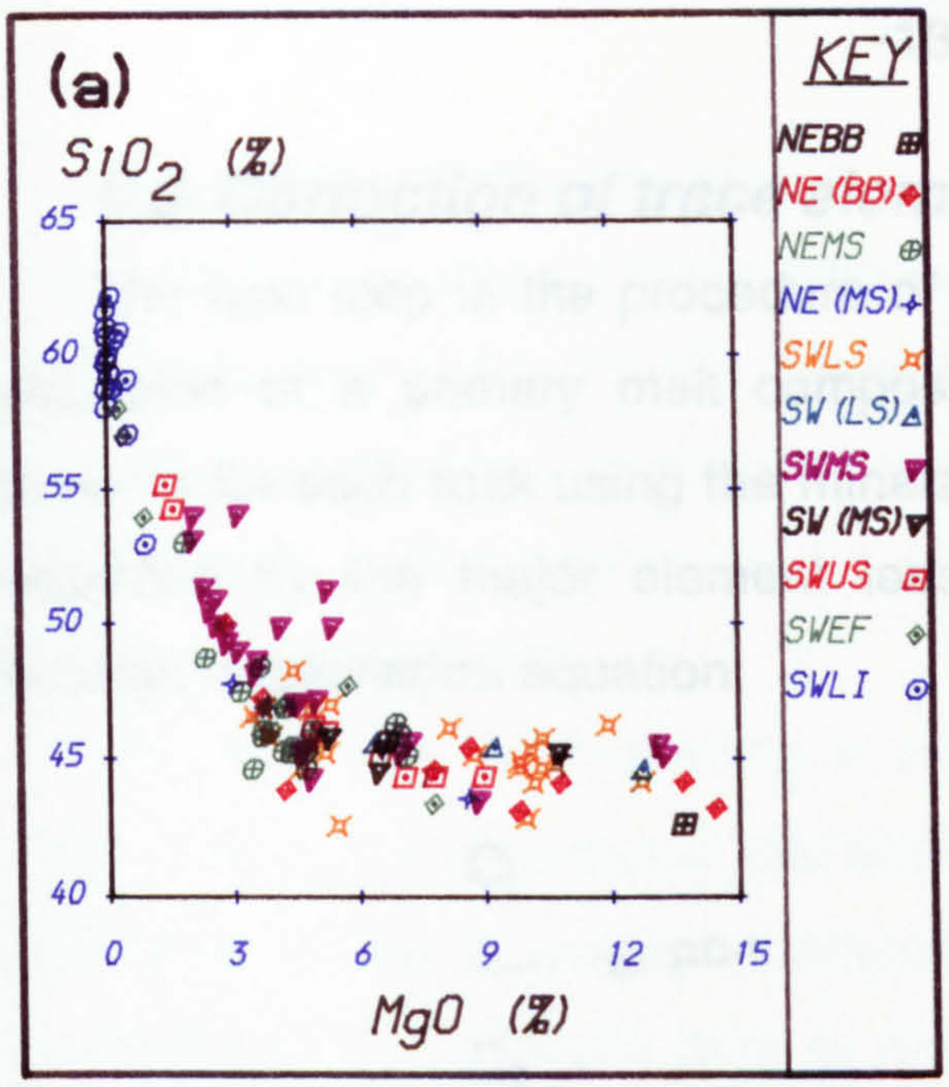
(a)
SiO2 (%)
65
60
55
50
45
40
0
3
6
9
12
15
MgO (%)
KEY
NEBB
NE (BB)
NEMS
NE (MS)
SWLS
SW (LS)
SWMS
SW (MS)
SWUS
SWEF
SWLI

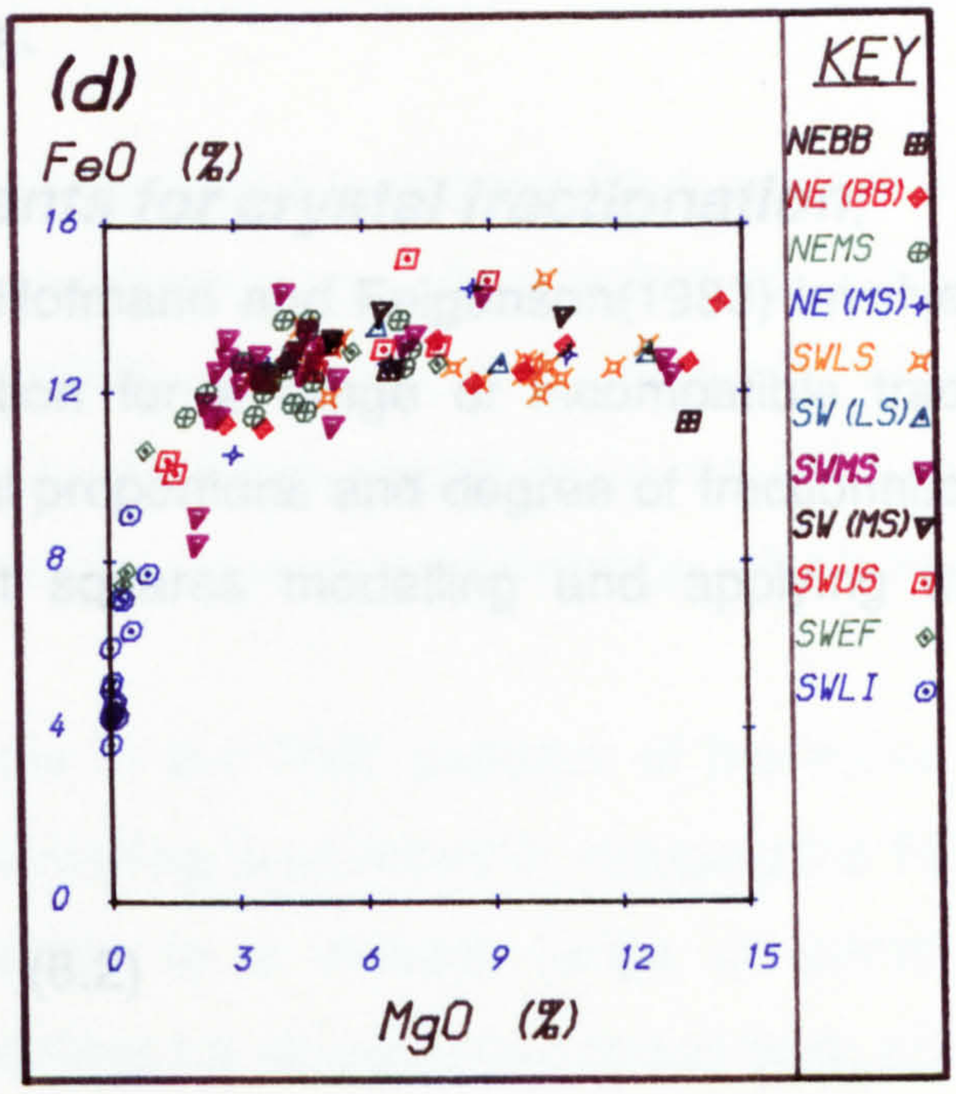
(d)
FeO (%)
16
12
8
4
0
0
3
6
9
12
15
MgO (%)
KEY
NEBB
NE (BB)
NEMS
NE (MS)
SWLS
SW (LS)
SWMS
SW (MS)
SWUS
SWEF
SWLI

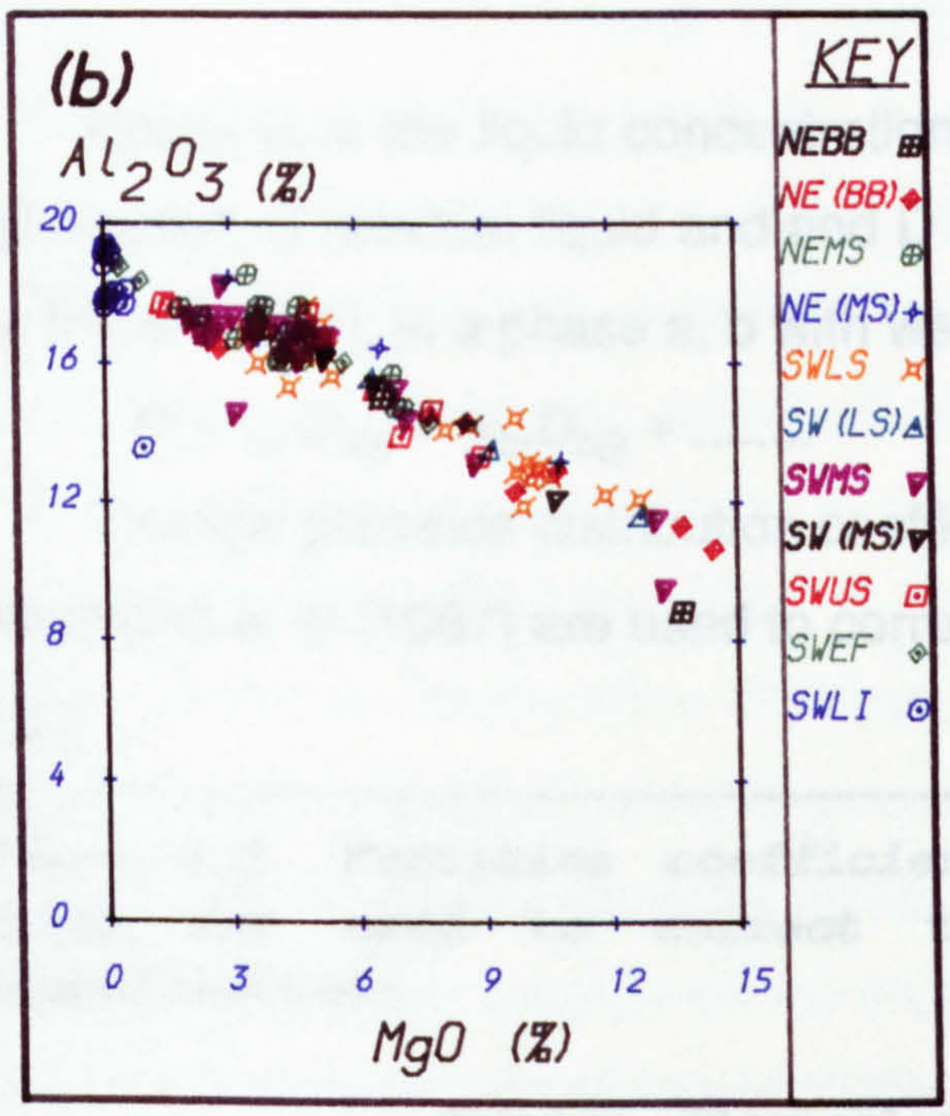
(b)
Al2O3 (%)
20
16
12
8
4
0
0
3
6
9
12
15
MgO (%)
KEY
NEBB
NE (BB)
NEMS
NE (MS)
SWLS
SW (LS)
SWMS
SW (MS)
SWUS
SWEF
SWLI

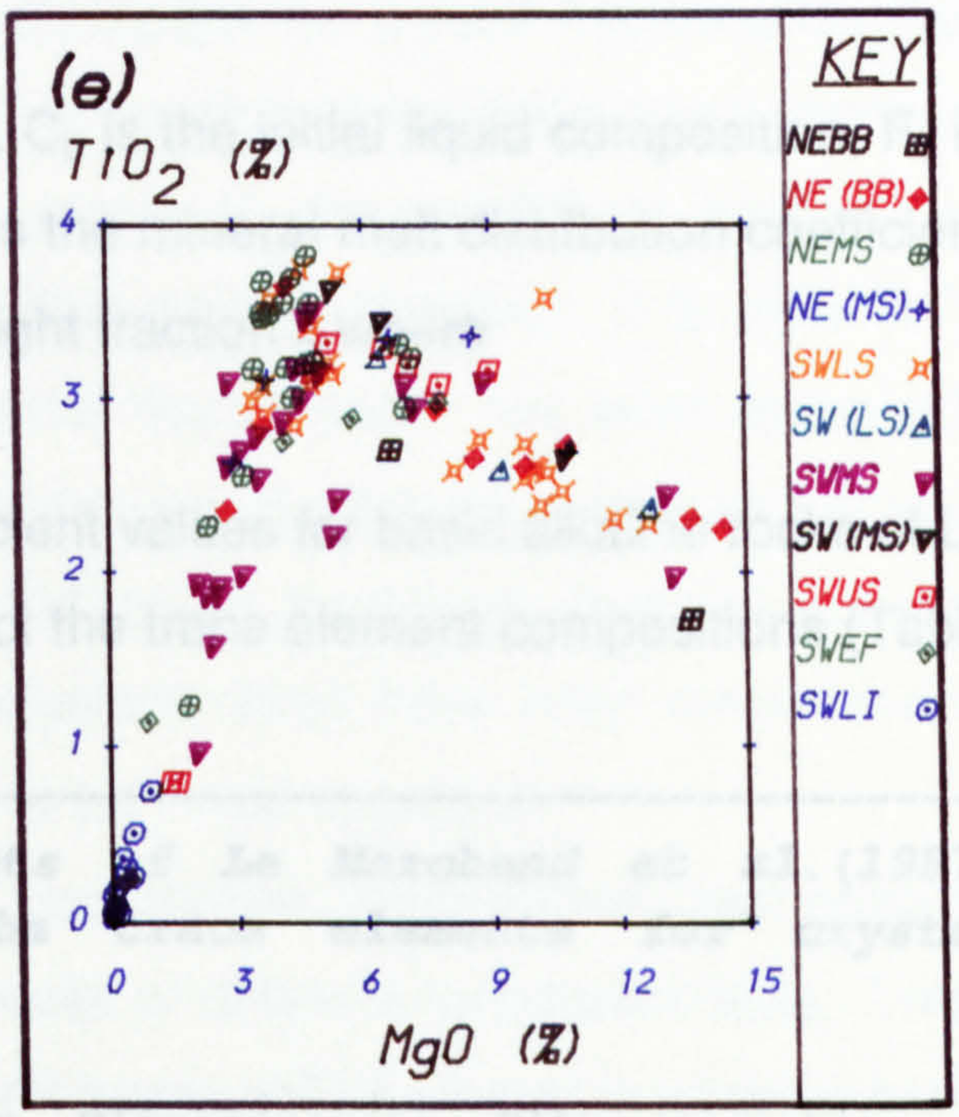
(e)
TiO2 (%)
4
3
2
1
0
0
3
6
9
12
15
MgO (%)
KEY
NEBB
NE (BB)
NEMS
NE (MS)
SWLS
SW (LS)
SWMS
SW (MS)
SWUS
SWEF
SWLI

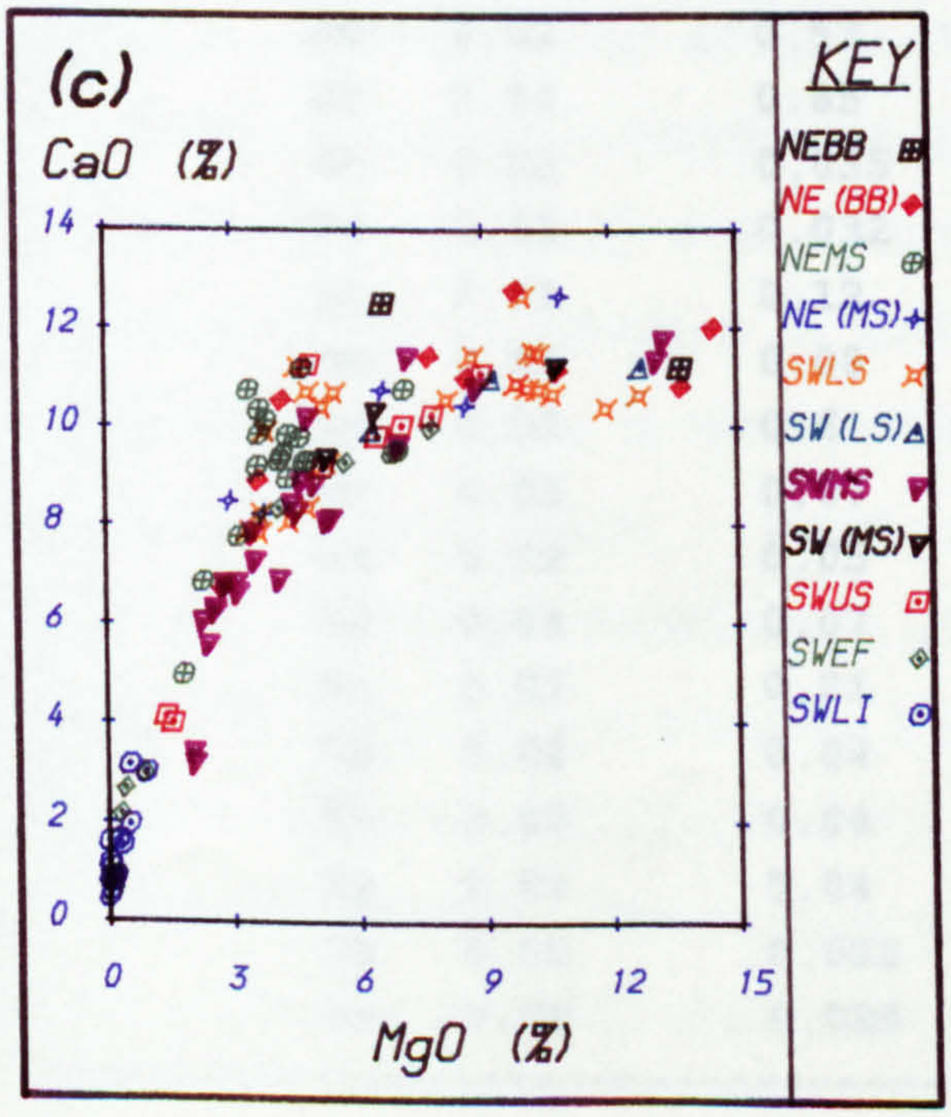
(c)
CaO (%)
14
12
10
8
6
4
2
0
0
3
6
9
12
15
MgO (%)
KEY
NEBB
NE (BB)
NEMS
NE (MS)
SWLS
SW (LS)
SWMS
SW (MS)
SWUS
SWEF
SWLI

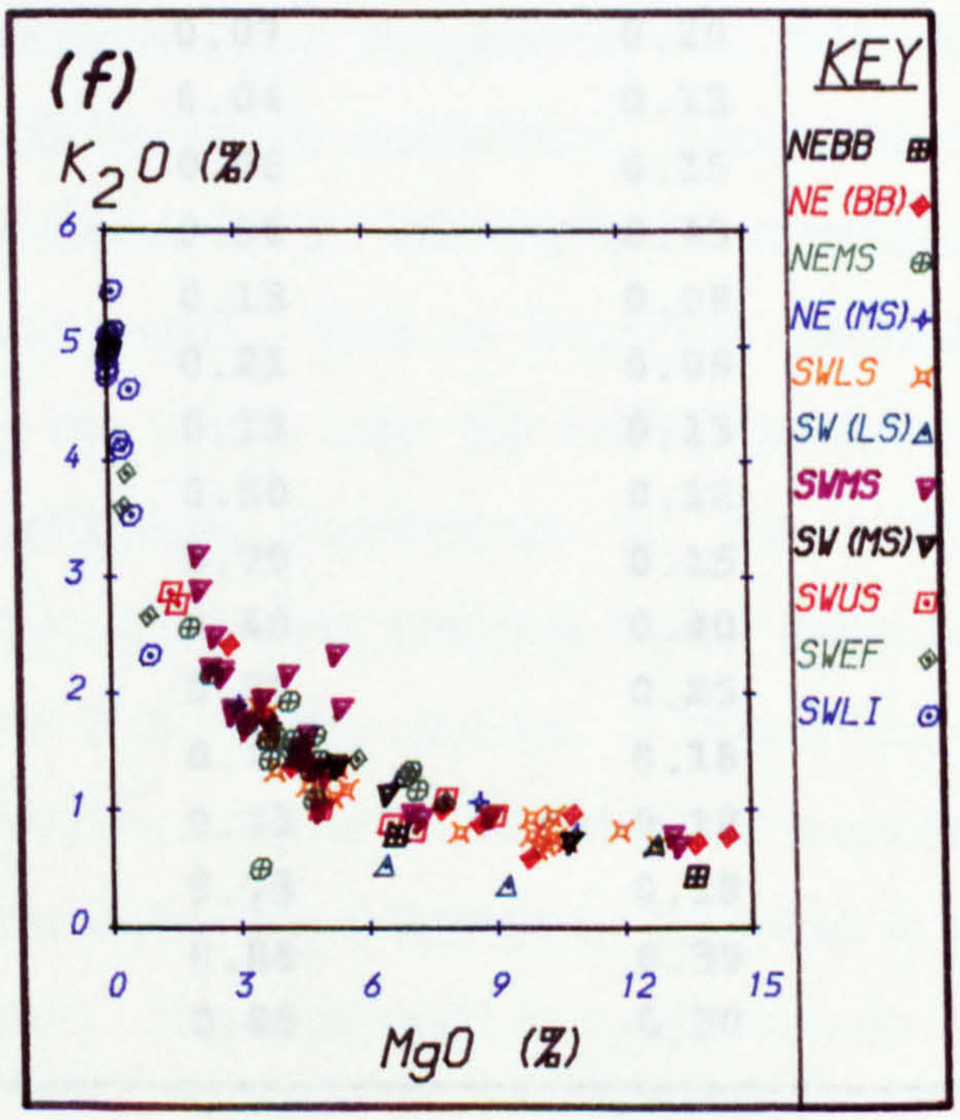
(f)
K2O (%)
6
5
4
3
2
1
0
0
3
6
9
12
15
MgO (%)
KEY
NEBB
NE (BB)
NEMS
NE (MS)
SWLS
SW (LS)
SWMS
SW (MS)
SWUS
SWEF
SWLI

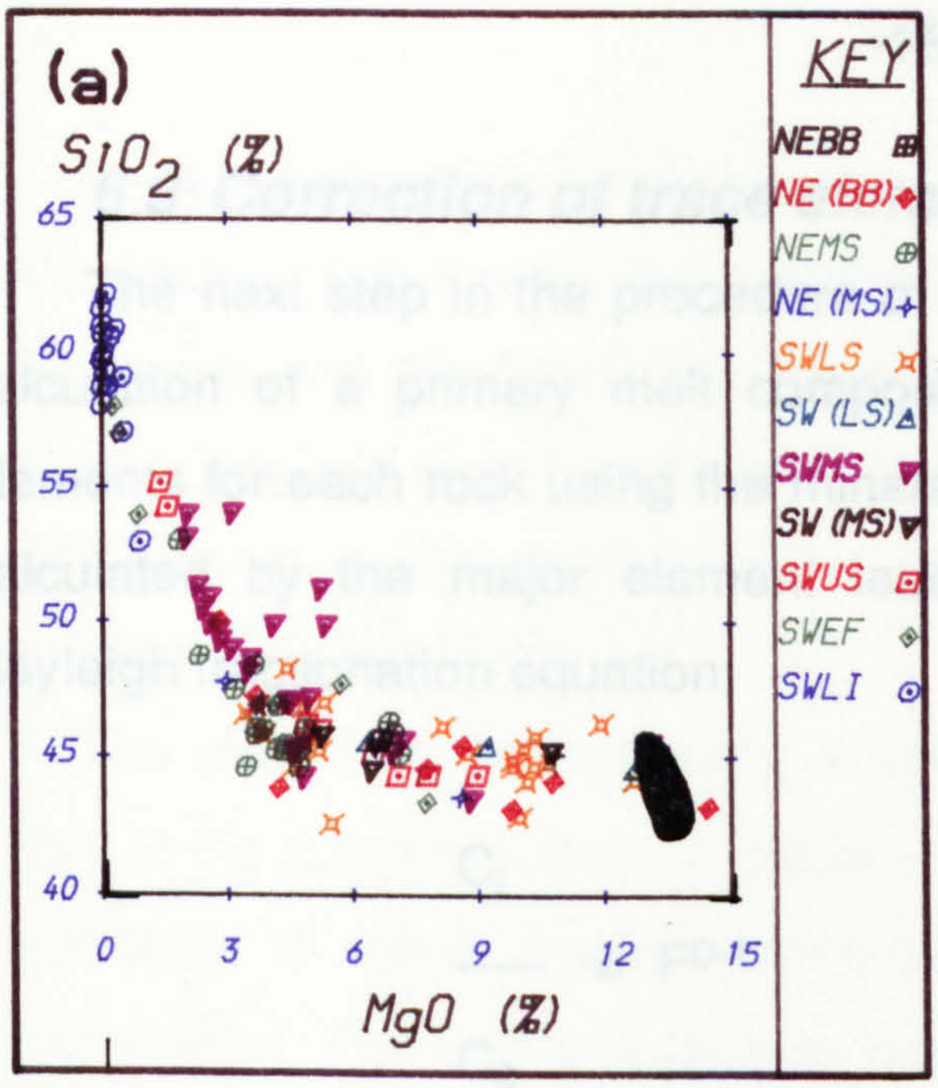
(a)
SiO2 (%)
65
60
55
50
45
40
0
3
6
9
12
15
MgO (%)
KEY
NEBB
NE (BB)
NEMS
NE (MS)
SWLS
SW (LS)
SWMS
SW (MS)
SWUS
SWEF
SWLI

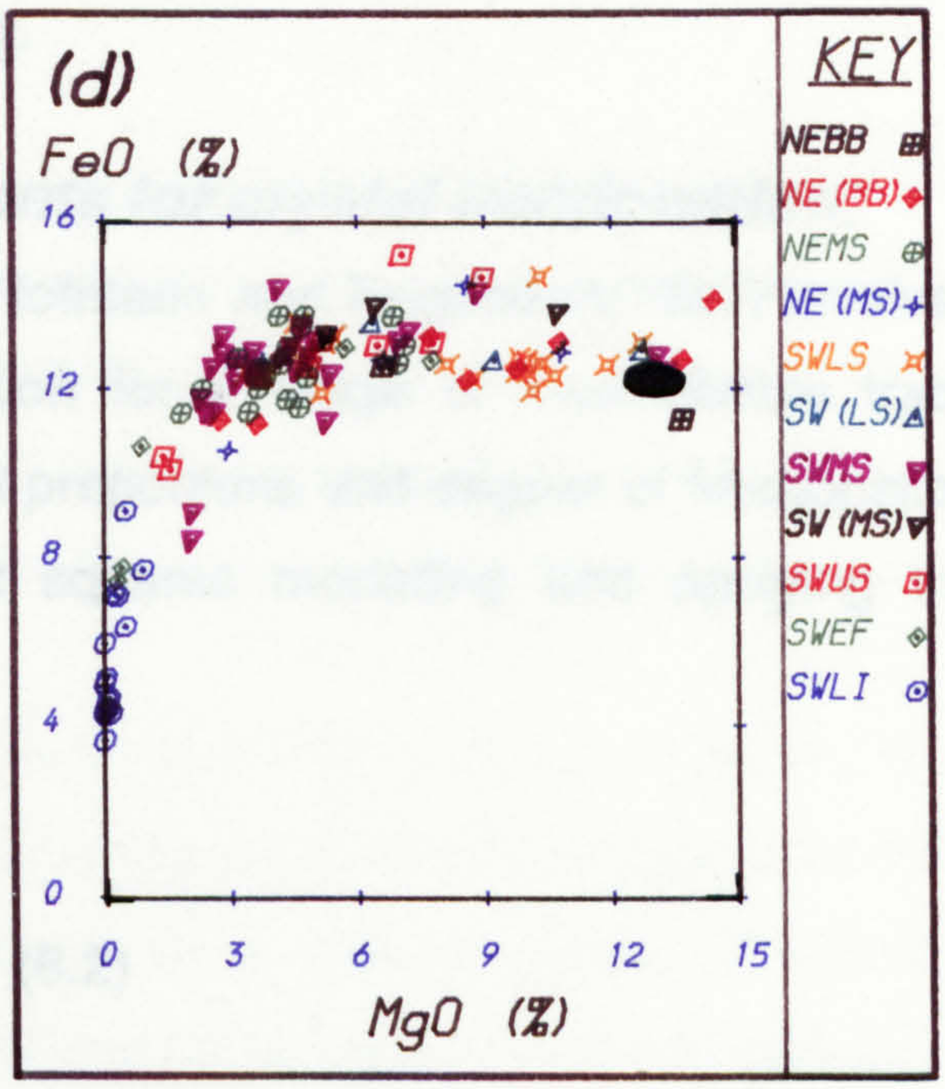
(d)
FeO (%)
16
12
8
4
0
0
3
6
9
12
15
MgO (%)
KEY
NEBB
NE (BB)
NEMS
NE (MS)
SWLS
SW (LS)
SWMS
SW (MS)
SWUS
SWEF
SWLI

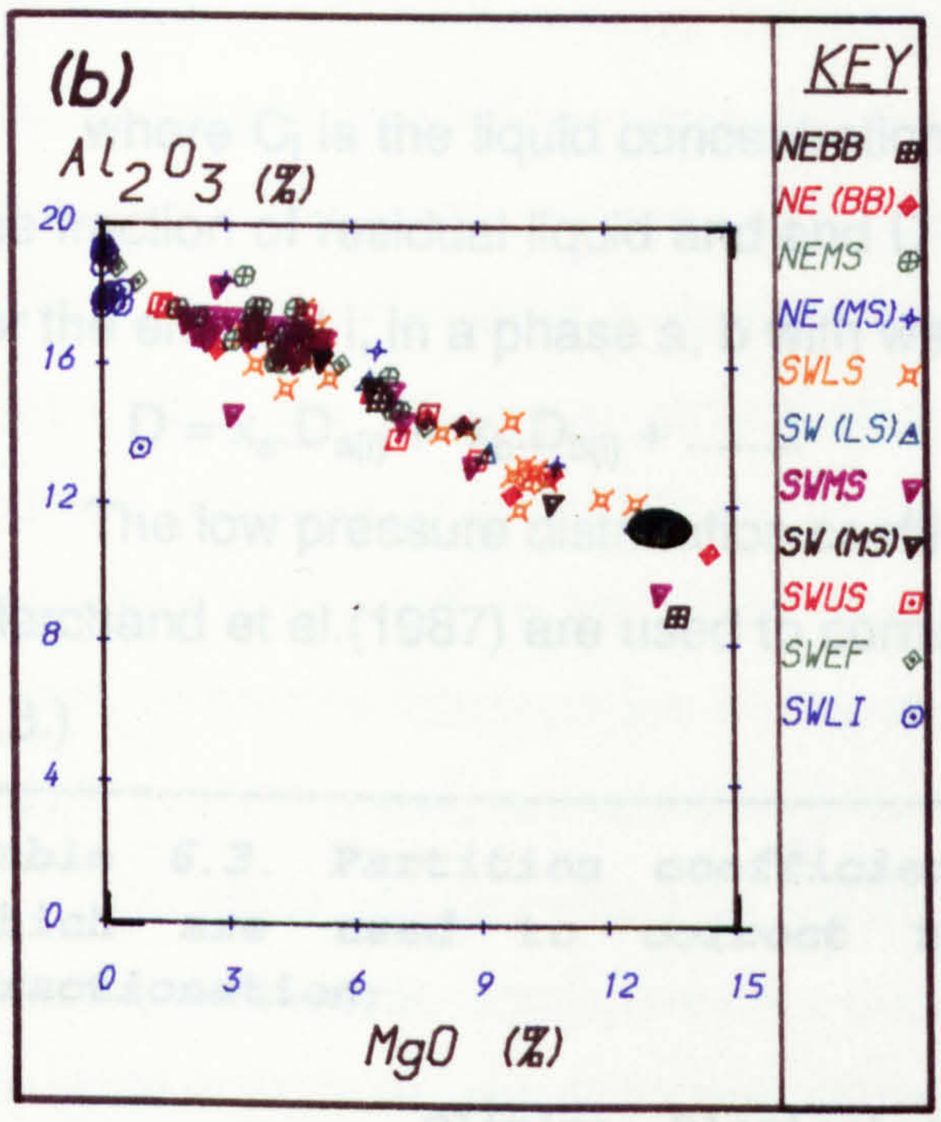
(b)
Al2O3 (%)
20
16
12
8
4
0
0
3
6
9
12
15
MgO (%)
KEY
NEBB
NE (BB)
NEMS
NE (MS)
SWLS
SW (LS)
SWMS
SW (MS)
SWUS
SWEF
SWLI

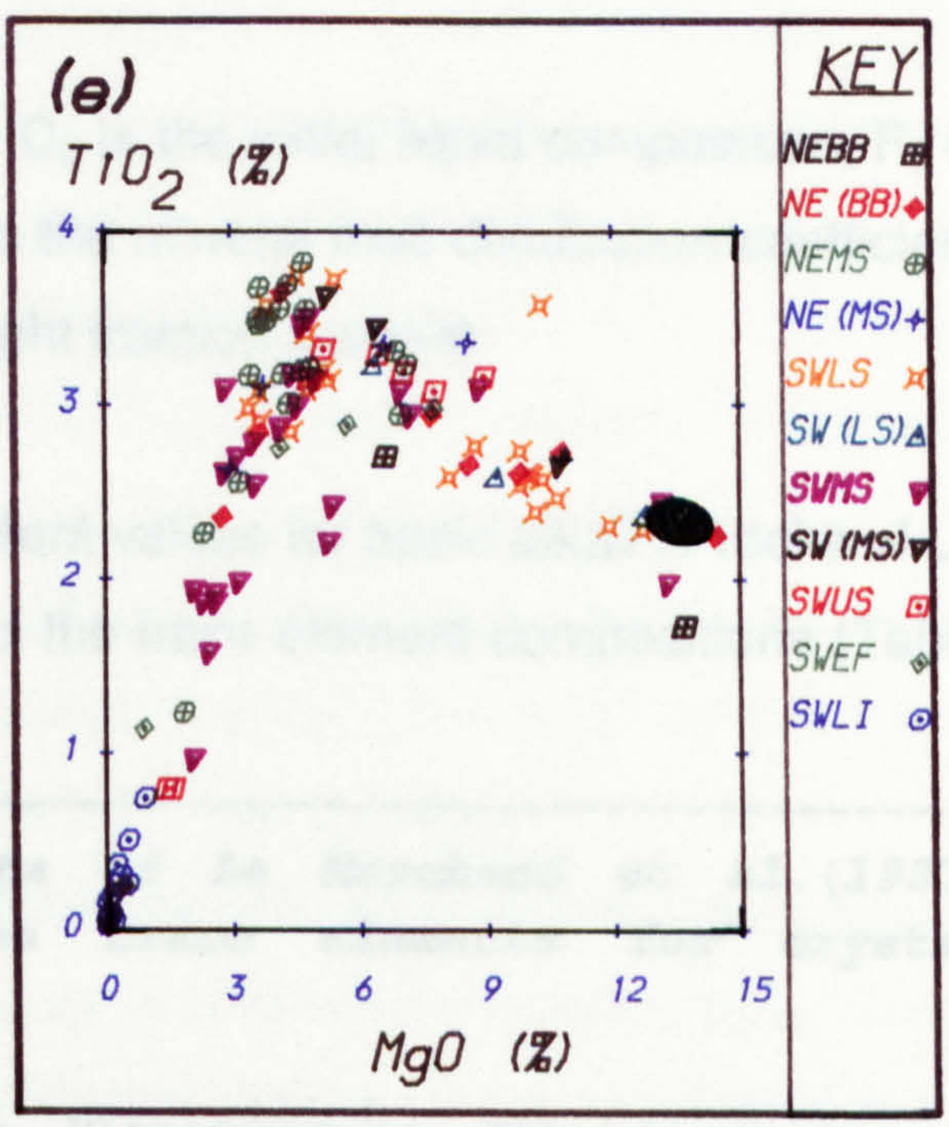
(e)
TiO2 (%)
4
3
2
1
0
0
3
6
9
12
15
MgO (%)
KEY
NEBB
NE (BB)
NEMS
NE (MS)
SWLS
SW (LS)
SWMS
SW (MS)
SWUS
SWEF
SWLI

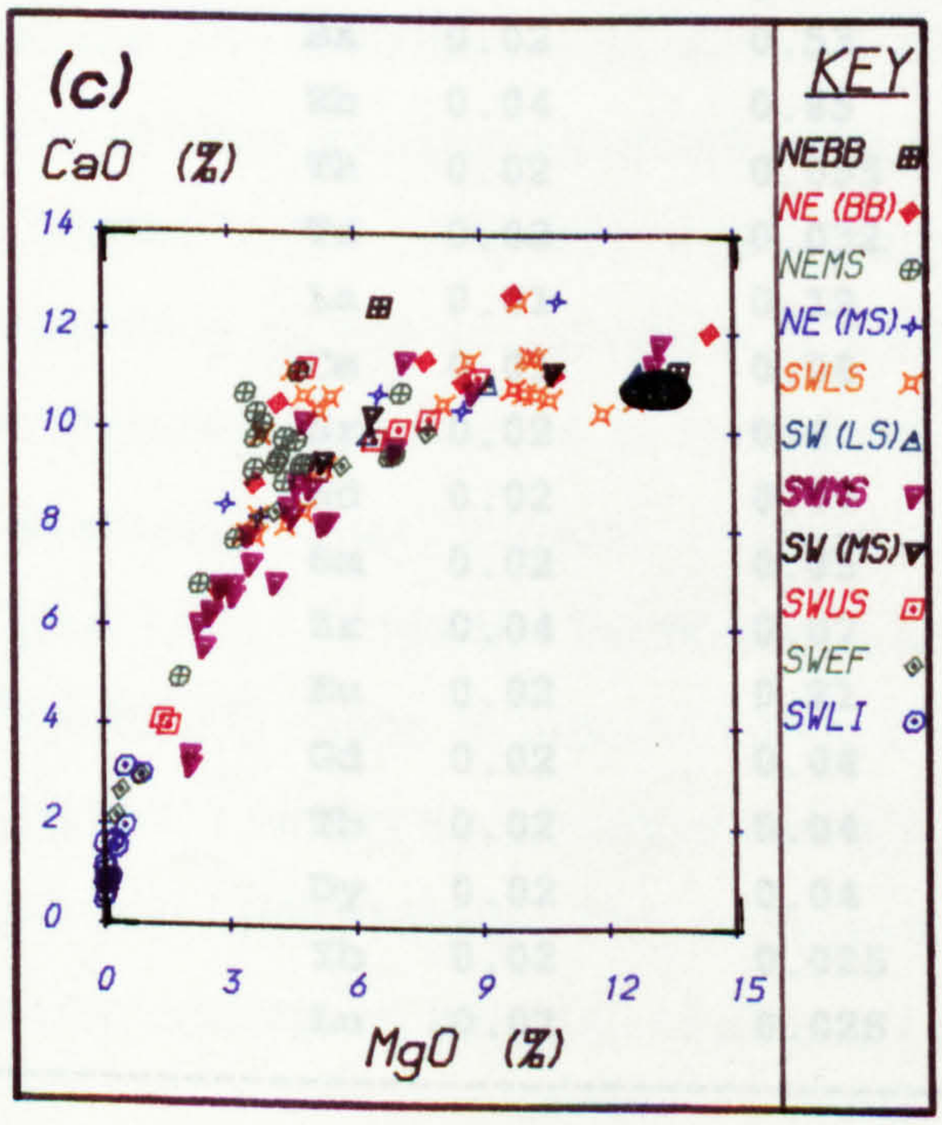
(c)
CaO (%)
14
12
10
8
6
4
2
0
0
3
6
9
12
15
MgO (%)
KEY
NEBB
NE (BB)
NEMS
NE (MS)
SWLS
SW (LS)
SWMS
SW (MS)
SWUS
SWEF
SWLI

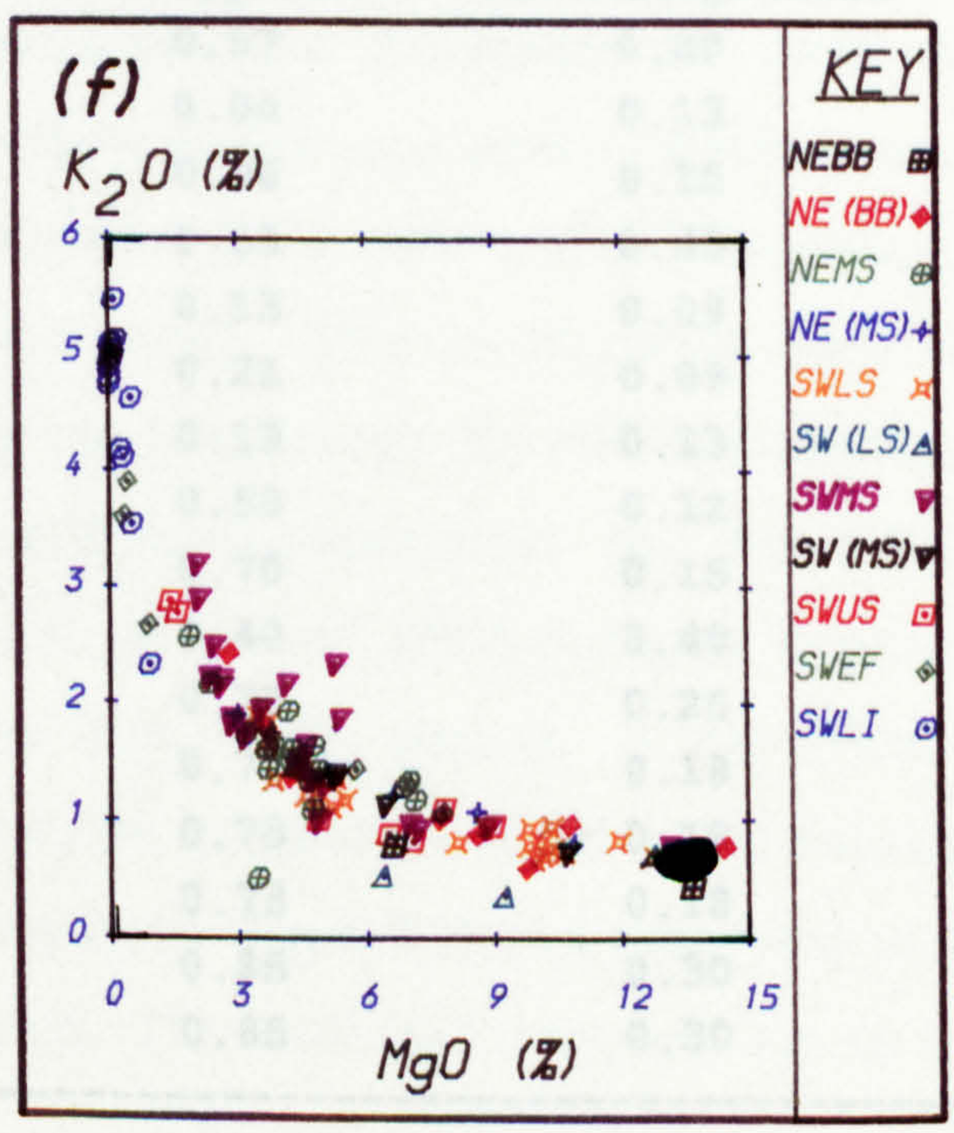
(f)
K2O (%)
6
5
4
3
2
1
0
0
3
6
9
12
15
MgO (%)
KEY
NEBB
NE (BB)
NEMS
NE (MS)
SWLS
SW (LS)
SWMS
SW (MS)
SWUS
SWEF
SWLI

6.3; Correction of trace elements for crystal fractionation;

The next step in the procedure of Hofmann and Feigenson(1983) involves calculation of a primary melt composition for a range of incompatible trace elements for each rock using the mineral proportions and degree of fractionation calculated by the major element least squares modelling and applying the Rayleigh fractionation equation;

$$\frac{C_l}{C_0} = F^{D-1} \qquad (6.2)$$

where C_l is the liquid concentration, C_0 is the initial liquid composition, F_1 is the fraction of residual liquid and and D is the mineral melt distribution coefficient for the element i, in a phase a, b with weight fraction x where

$$D = x_a.D_{a(i)} + x_b.D_{b(i)} + ...$$

The low pressure distribution coefficient values for basic alkaline rocks of Le Marchand et al.(1987) are used to correct the trace element compositions (Table 6.3.)

Table 6.3. Partition coefficients of Le Marchand et al.(1987) which are used to correct the trace elements for crystal fractionation;

	Olivine	Plagioclase	Clinopyroxene	Titanomagnetite
Ba	0.02	0.53	0.07	0.20
Rb	0.04	0.85	0.04	0.13
Th	0.02	0.055	0.06	0.15
Ta	0.02	0.032	0.08	0.45
La	0.01	0.12	0.13	0.09
Ce	0.01	0.08	0.21	0.09
Sr	0.02	0.6	0.13	0.13
Nd	0.02	0.07	0.50	0.12
Sm	0.02	0.05	0.70	0.15
Zr	0.04	0.07	0.40	0.40
Eu	0.02	0.21	0.70	0.25
Gd	0.02	0.04	0.73	0.18
Tb	0.02	0.04	0.73	0.18
Dy	0.02	0.04	0.73	0.18
Yb	0.02	0.025	0.85	0.30
Lu	0.02	0.025	0.85	0.30

In undertaking this correction it is assumed that these partition coefficients are constant. It is known that partition coefficients are composition dependent (e.g. Allegre and Minster(1978), Nielsen(1988). However, the manner by which they vary has not been established and computation would be made unwieldy. Improvements to this model will be possible when our knowledge of partition coefficient data improves.

The results of the modelling in terms of the REE patterns of the rocks is shown in Fig.6.5. It is apparent that the modelling is effective in reducing the REE abundance of more evolved compositions to a narrow range of primitive compositions. For example prior to modelling La abundances range from 65 to 280 times chondrite, whereas following correction for crystal fractionation they vary from 65 to 100 times chondrite. It is not possible to test if the trace elements have been corrected by too large an extent in the modelling, because of uncertainties in the input parameters to the model. However, it is clear from Fig.6.5 that the maximum extent of crystal fractionation has been taken into account because of the similarity of abundances of elements between primitive rocks and corrected rocks. This is important as it ensures that the possible effects of crystal fractionation on trace element ratios have been maximised to enable any remaining source differences to be made apparent.

The rocks are corrected for crystal fractionation using phases that possess different distribution coefficients for elements of different incompatibilities. Thus, the relative abundances of incompatible elements will be altered in addition to the absolute abundances. This effect is investigated by considering the REE, for which relative variations in distribution coefficients are well known. It was shown in section 6.2.1. (Fig.6.2) that clinopyroxene is a volumetrically significant crystallising phase in primitive to evolved rocks. This is important because clinopyroxene is effective at fractionating the LREE from the HREE because it possesses higher mineral - liquid distribution coefficients for the HREE (Figs.6.1,6.6.) Thus the fractionation of this phase will result in higher apparent LREE/HREE ratios in non-primitive lavas than in the source. If this effect is important it would be expected that an inverse correlation would occur between MgO and LREE/HREE. This is indeed the case; Fig.6.7 shows that there is an inverse correlation between MgO and La/Yb. The corrected compositions do not

Fig.6.5. A comparison of the crystal fractionation corrected REE abundances for selected SHRS samples.

Lower figures are corrected for crystal fractionation using the model described in the text.

Upper figures are uncorrected. The samples are from:

(a) NE volcano.

(b) SW volcano.

For the primitive samples SC 37, SC 59, and SC 237 uncorrected compositions are illustrated in the lower figures. Chondrite normalised figures from Boynton(1984).

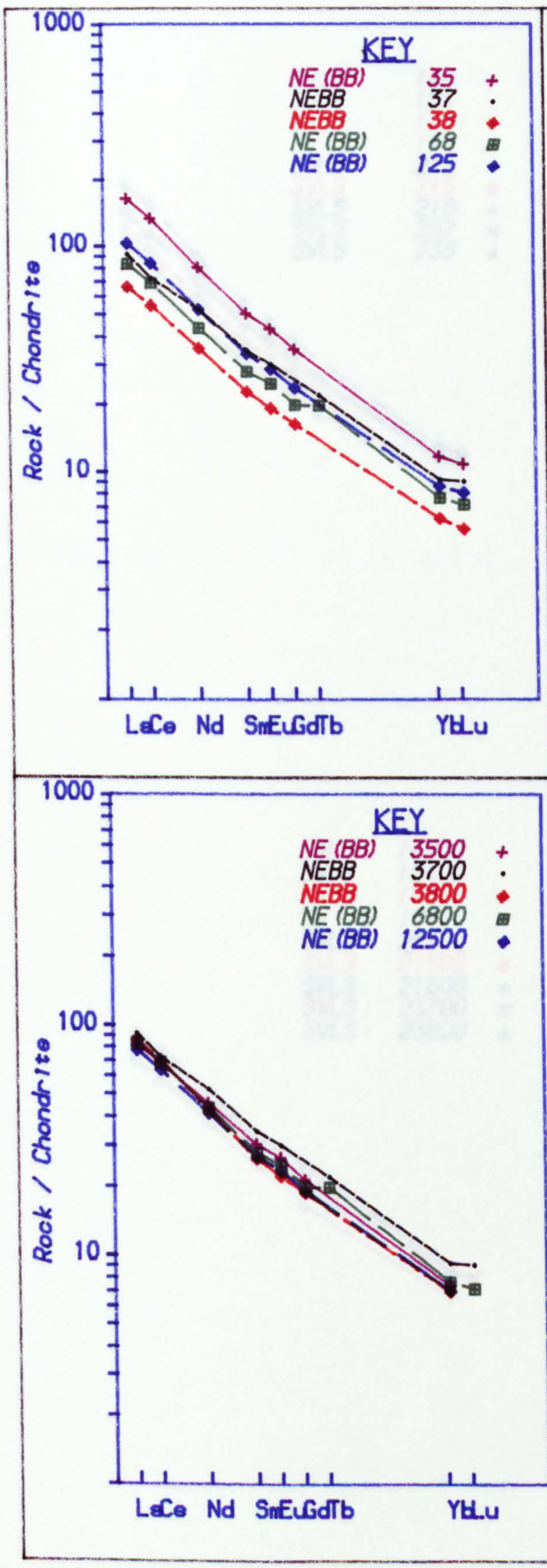
1000
100
10
Rock / Chondrite
KEY
NE (BB) 35
NEBB 37
NEBB 38
NE (BB) 68
NE (BB) 125
LaCe Nd SmEuGdTb YbLu

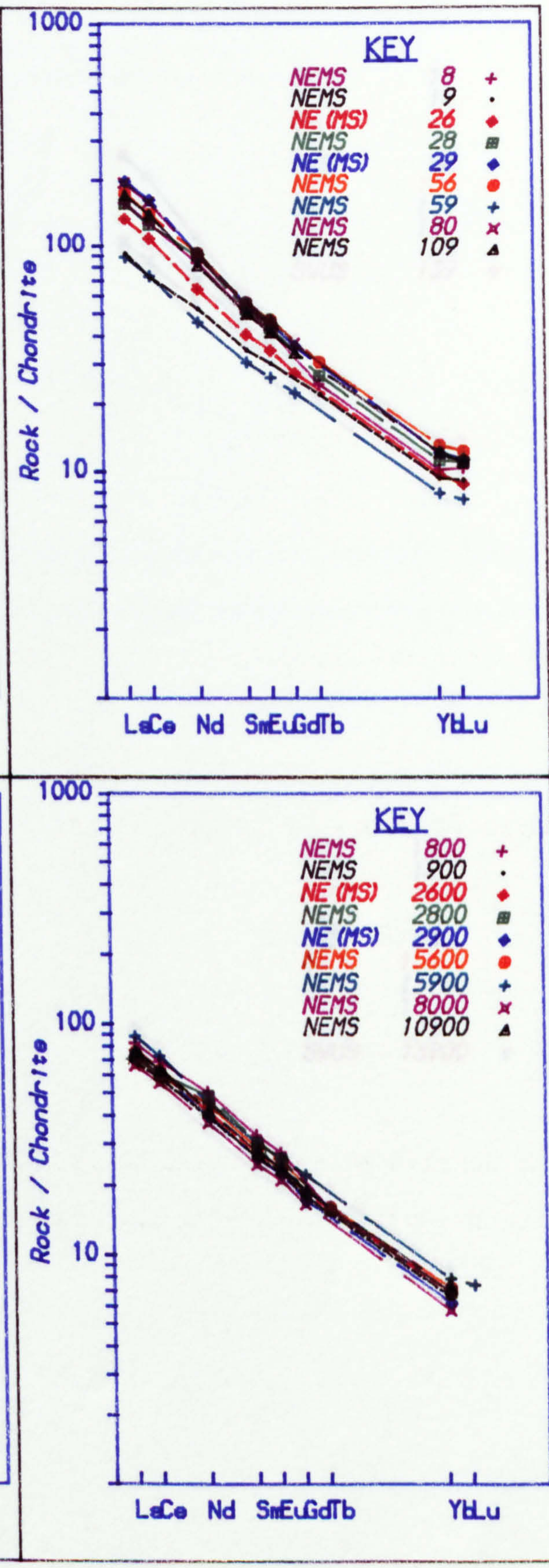
1000
100
10
Rock / Chondrite
KEY
NEMS 8
NEMS 9
NE (MS) 26
NEMS 28
NE (MS) 29
NEMS 56
NEMS 59
NEMS 80
NEMS 109
LaCe Nd SmEuGdTb YbLu

1000
100
10
Rock / Chondrite
KEY
NE (BB) 3500
NEBB 3700
NEBB 3800
NE (BB) 6800
NE (BB) 12500
LaCe Nd SmEuGdTb YbLu

1000
100
10
Rock / Chondrite
KEY
NEMS 800
NEMS 900
NE (MS) 2600
NEMS 2800
NE (MS) 2900
NEMS 5600
NEMS 5900
NEMS 8000
NEMS 10900
LaCe Nd SmEuGdTb YbLu

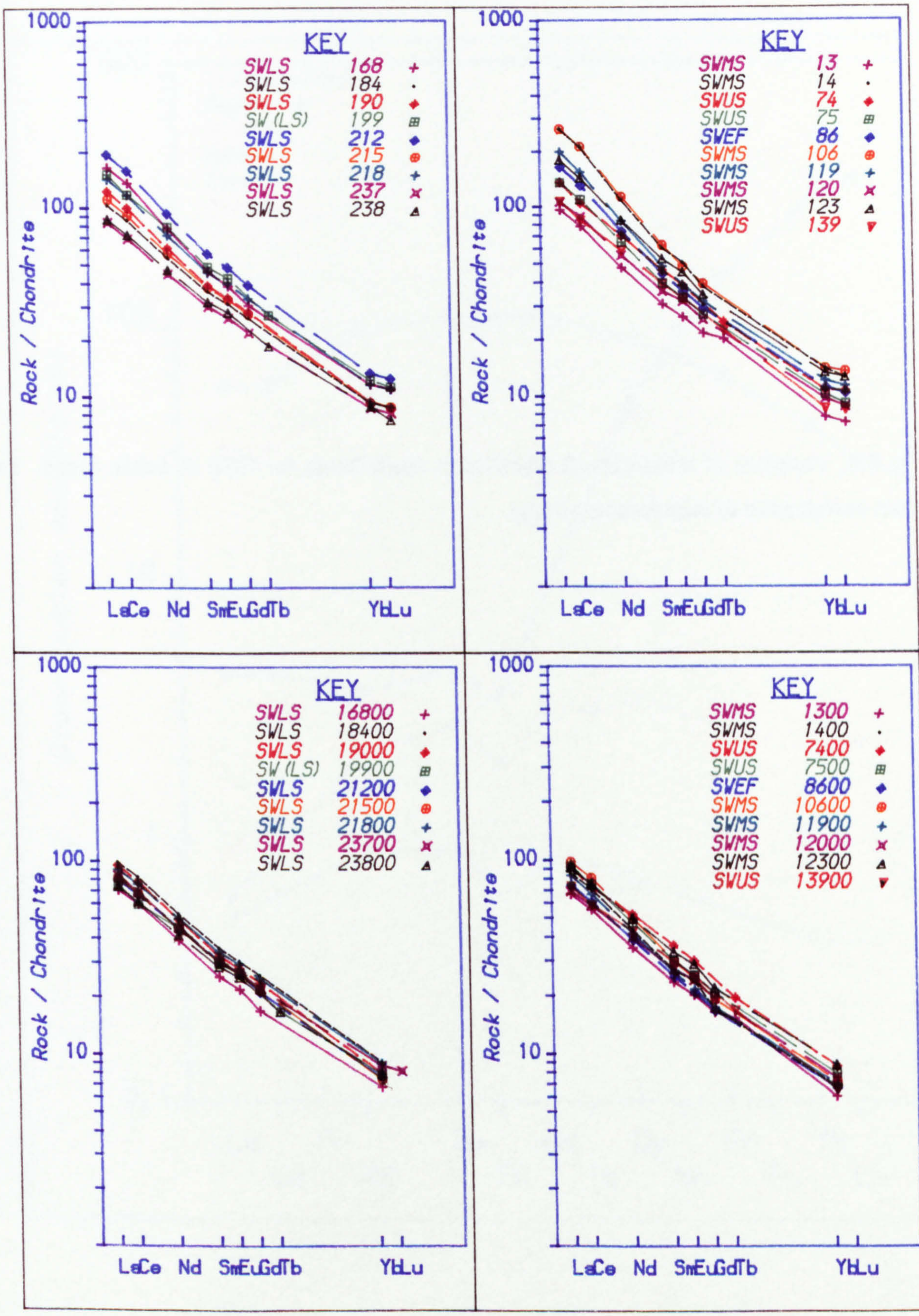
1000
100
10
Rock / Chondrite
KEY
SWLS 168
SWLS 184
SWLS 190
SW (LS) 199
SWLS 212
SWLS 215
SWLS 218
SWLS 237
SWLS 238
LaCe Nd SmEuGdTb YbLu
1000
100
10
Rock / Chondrite
KEY
SWMS 13
SWMS 14
SWUS 74
SWUS 75
SWEF 86
SWMS 106
SWMS 119
SWMS 120
SWMS 123
SWUS 139
LaCe Nd SmEuGdTb YbLu
1000
100
10
Rock / Chondrite
KEY
SWLS 16800
SWLS 18400
SWLS 19000
SW (LS) 19900
SWLS 21200
SWLS 21500
SWLS 21800
SWLS 23700
SWLS 23800
LaCe Nd SmEuGdTb YbLu
1000
100
10
Rock / Chondrite
KEY
SWMS 1300
SWMS 1400
SWUS 7400
SWUS 7500
SWEF 8600
SWMS 10600
SWMS 11900
SWMS 12000
SWMS 12300
SWUS 13900
LaCe Nd SmEuGdTb YbLu

Fig.6.6. Variation of mineral/melt distribution coefficients for REE in acidic rocks. Data from compilation of Henderson(1982)).

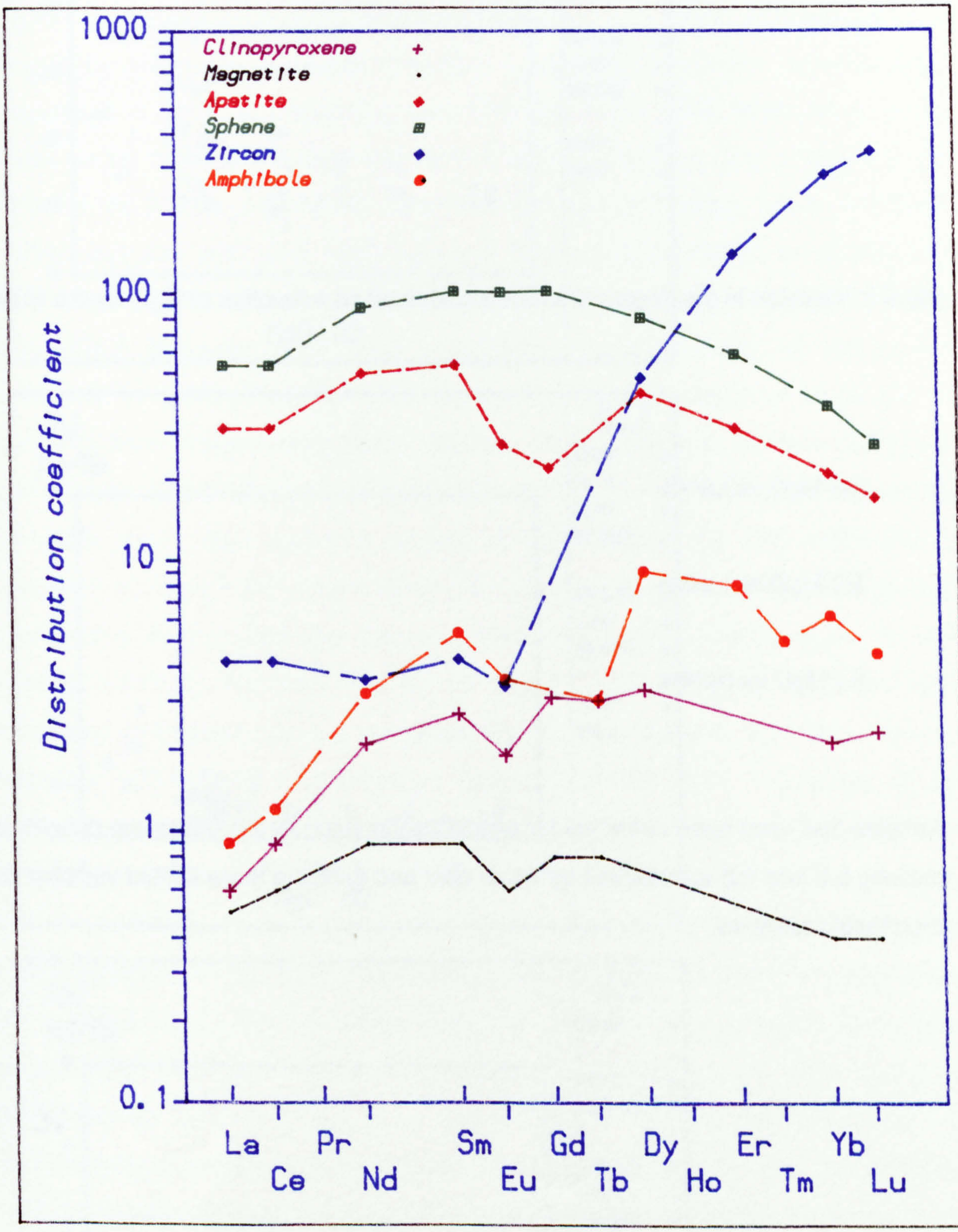
Clinopyroxene
Magnetite
Apatite
Sphene
Zircon
Amphibole
1000
100
10
1
0.1
Distribution coefficient
La
Ce
Pr
Nd
Sm
Eu
Gd
Tb
Dy
Ho
Er
Tm
Yb
Lu

Fig.6.7. Variation in the degree of LREE enrichment as a function of MgO for the SHRS.

(a) MgO vs La/Yb.

(b) MgO vs La/Sm.

(c) MgO vs Nd/Sm

Samples that have been corrected for crystal fractionation by the procedure described in sections 6.2 and 6.3 are marked by *black dots* and exhibit a more limited variation than uncorrected samples.

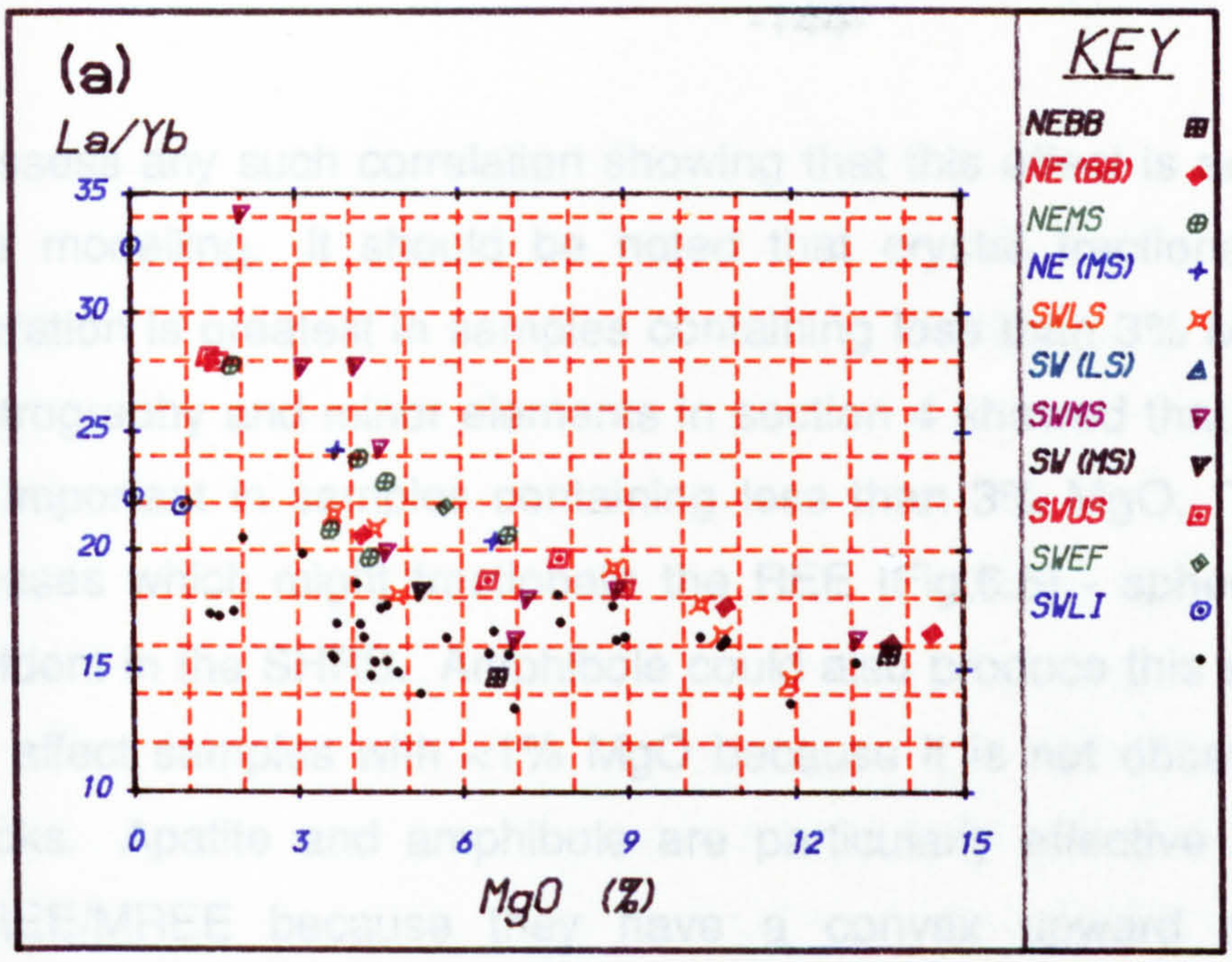
(a)
La/Yb
35
30
25
20
15
10
0
3
6
9
12
15
MgO (%)
KEY
NEBB
NE (BB)
NEMS
NE (MS)
SWLS
SW (LS)
SWMS
SW (MS)
SWUS
SWEF
SWLI

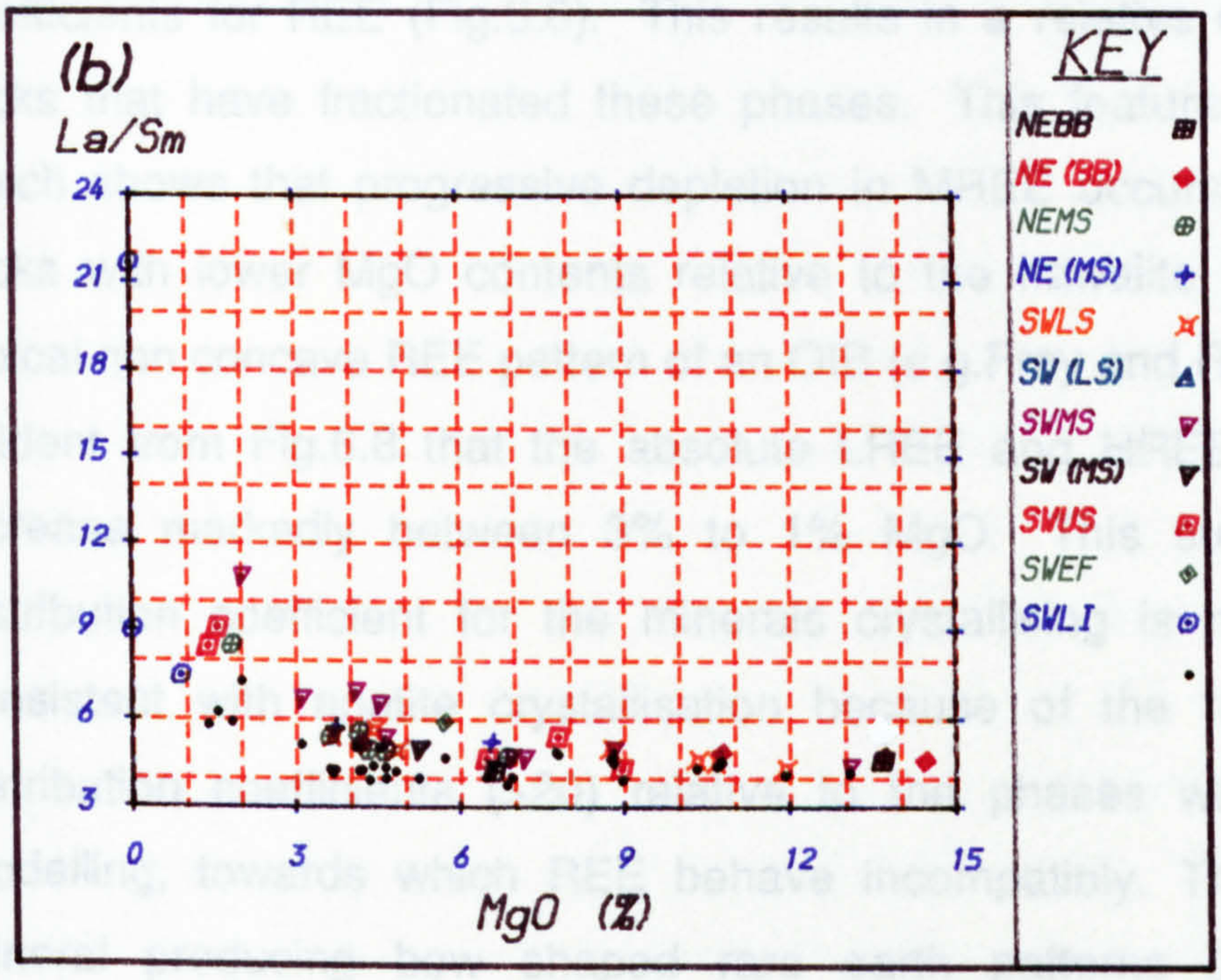
(b)
La/Sm
24
21
18
15
12
9
6
3
0
3
6
9
12
15
MgO (%)
KEY
NEBB
NE (BB)
NEMS
NE (MS)
SWLS
SW (LS)
SWMS
SW (MS)
SWUS
SWEF
SWLI

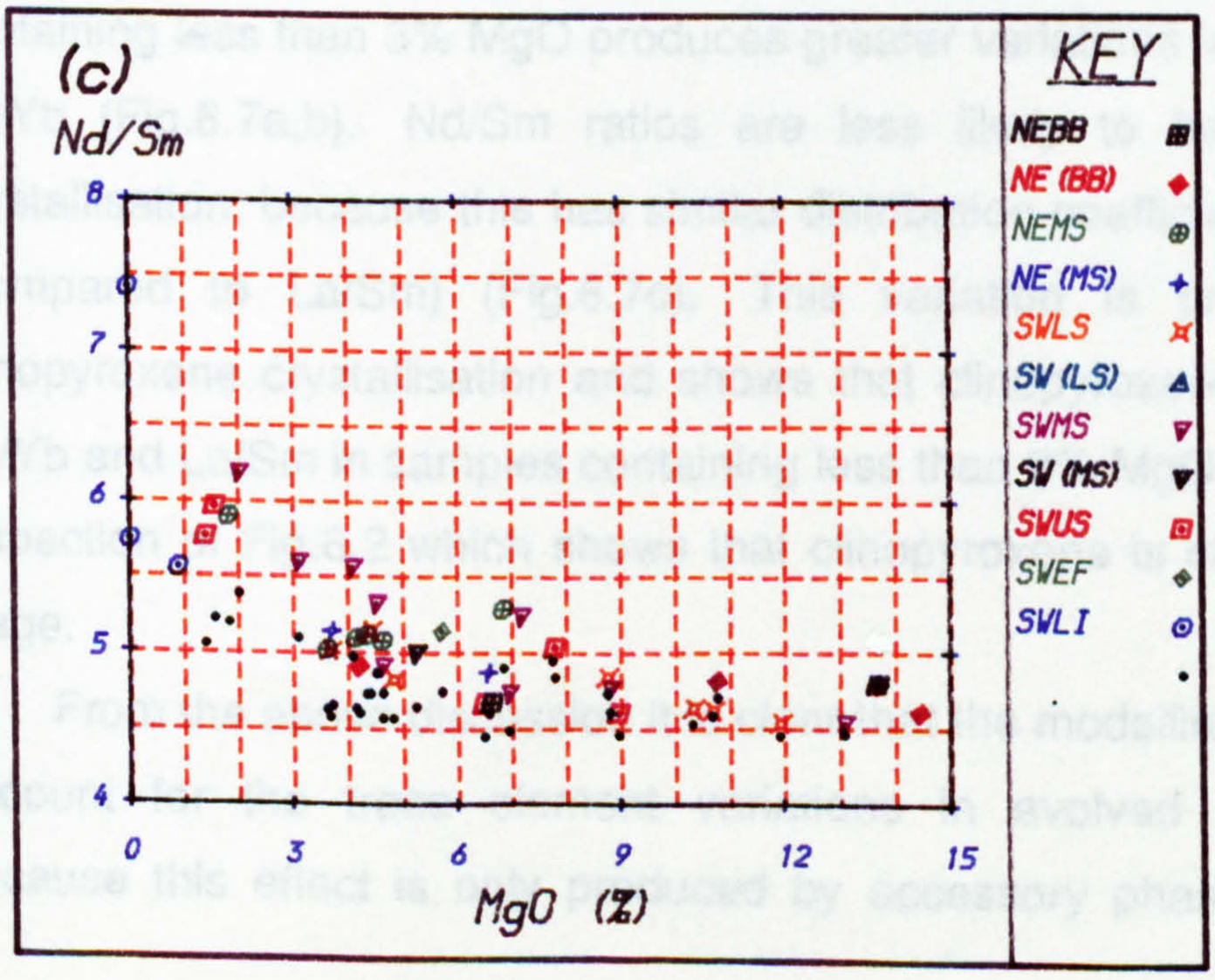
(c)
Nd/Sm
8
7
6
5
4
0
3
6
9
12
15
MgO (%)
KEY
NEBB
NE (BB)
NEMS
NE (MS)
SWLS
SW (LS)
SWMS
SW (MS)
SWUS
SWEF
SWLI

possess any such correlation showing that this effect is adequately removed by the modelling. It should be noted that crystal fractionation corrected La/Yb variation is greatest in samples containing less than 3% MgO. Consideration of petrography and minor elements in section 4 showed that apatite crystallisation is important in samples containing less than 3% MgO. The other likely minor phases which might fractionate the REE (Fig.6.6) - sphene and zircon are not evident in the SHRS. Amphibole could also produce this effect, but is only likely to affect samples with <1% MgO because it is not observed in more primitive rocks. Apatite and amphibole are particularly effective in modifying ratios of LREE/MREE because they have a convex upward pattern of distribution coefficients for REE (Fig.6.6). This results in a relative depletion in MREE in rocks that have fractionated these phases. This feature is evident in Fig.6.8 which shows that progressive depletion in MREE occurs in the more evolved rocks with lower MgO contents relative to the hawaiite SC 168 which has a typical non concave REE pattern of an OIB (e.g.Frey and Roden(1987)). It is also evident from Fig.6.8 that the absolute LREE and HREE abundances do not increase markedly between 3% to 1% MgO. This suggests that the bulk distribution coefficient for the minerals crystallising is near to unity. This is consistent with apatite crystallisation because of the high magnitude of its distribution coefficients (>20) relative to the phases which are used in the modelling, towards which REE behave incompatibly. The crystallisation of a mineral producing bow shaped rare earth patterns (Fig.6.8.) in samples containing less than 3% MgO produces greater variations in terms of La/Sm than La/Yb (Fig.6.7a,b). Nd/Sm ratios are less likely to be affected by apatite crystallisation, because this has similar distribution coefficient for these elements (compared to La/Sm) (Fig.6.7c). This variation is probably produced by clinopyroxene crystallisation and shows that clinopyroxene is also fractionating La/Yb and La/Sm in samples containing less than 3% MgO (this is expected from inspection of Fig.6.2 which shows that clinopyroxene is still fractionating at this stage.

From the above discussion it is clear that the modelling does not adequately account for the trace element variations in evolved rocks. Unfortunately, because this effect is only produced by accessory phases whose abundance

Fig.6.8. REE profiles for evolved rocks which possess variable depletion in the MREE compared to SC 168 - a hawaiite without this feature.

SC 168: hawaiite 4.42% MgO

SC 106: mugearite 3.30% MgO.

SC 62 : benmoreite 2.60% MgO.

SC 93 : trachyte 0.41% MgO.

SC 149: phonolite 0% MgO.

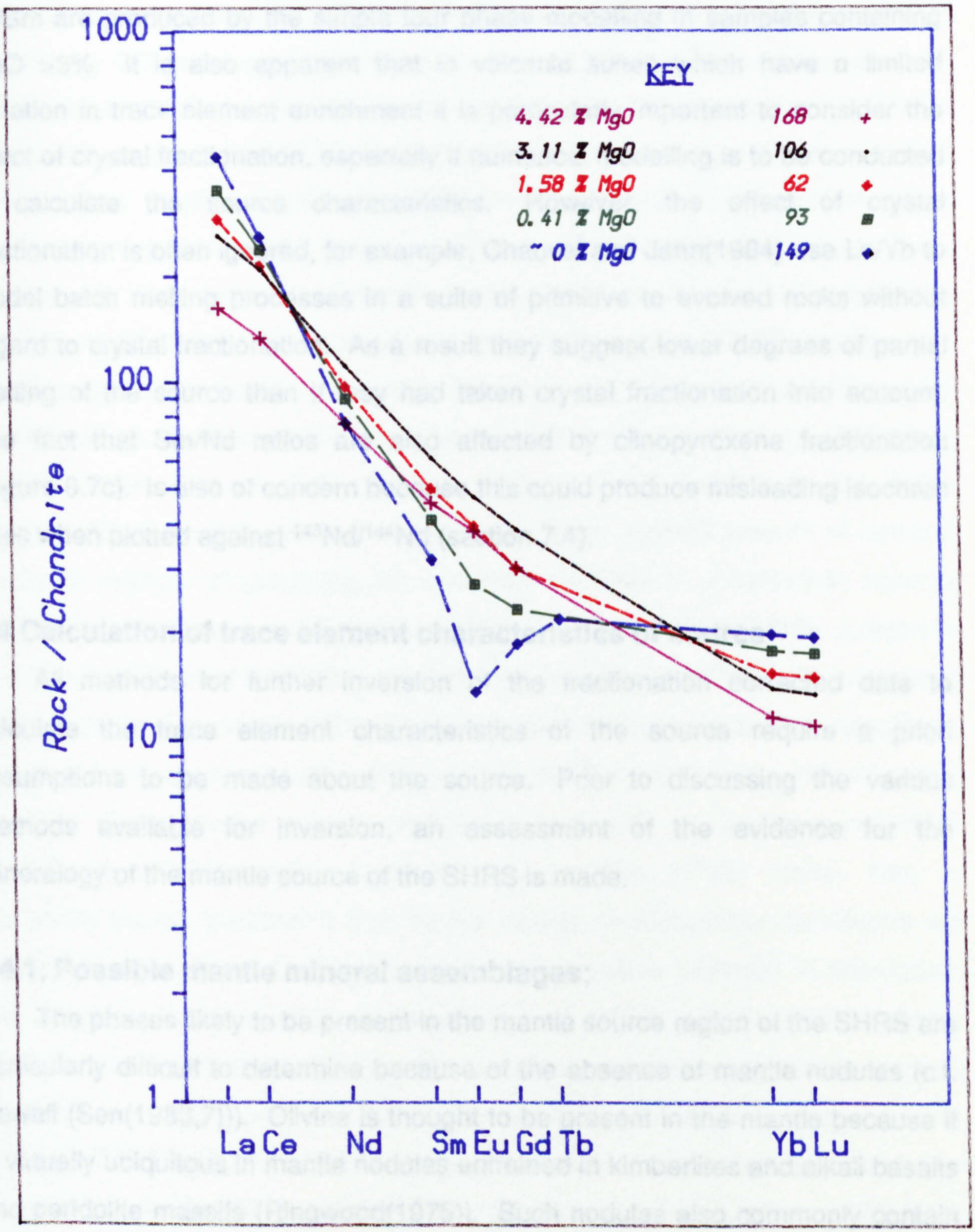
1000
100
10
1
Rock / Chondrite
KEY
4.42 % MgO 168 +
3.11 % MgO 106 •
1.58 % MgO 62 ◆
0.41 % MgO 93 ■
~ 0 % MgO 149 ◆
La Ce Nd Sm Eu Gd Tb Yb Lu

cannot be accurately gauged by least squares calculations, it cannot be removed. It is clear that significant corrections to ratios such as La/Yb and La/Sm are produced by the simple four phase modelling in samples containing MgO >3%. It is also apparent that in volcanic suites which have a limited variation in trace element enrichment it is particularly important to consider the effect of crystal fractionation, especially if numerical modelling is to be conducted to calculate the source characteristics. However, the effect of crystal fractionation is often ignored, for example, Chauvel and Jahn(1984) use La/Yb to model batch melting processes in a suite of primitive to evolved rocks without regard to crystal fractionation. As a result they suggest lower degrees of partial melting of the source than if they had taken crystal fractionation into account. The fact that Sm/Nd ratios are also affected by clinopyroxene fractionation (Figure 6.7c). is also of concern because this could produce misleading isochron ages when plotted against $^{143}Nd/^{144}Nd$ (section 7.4).

6.4 Calculation of trace element characteristics of source

All methods for further inversion of the fractionation corrected data to calculate the trace element characteristics of the source require a priori assumptions to be made about the source. Prior to discussing the various methods available for inversion, an assessment of the evidence for the mineralogy of the mantle source of the SHRS is made.

6.4.1; Possible mantle mineral assemblages;

The phases likely to be present in the mantle source region of the SHRS are particularly difficult to determine because of the absence of mantle nodules (c.f. Hawaii (Sen(1983,7))). Olivine is thought to be present in the mantle because it is virtually ubiquitous in mantle nodules entrained in kimberlites and alkali basalts and peridotite massifs (Ringwood(1975)). Such nodules also commonly contain clinopyroxene, orthopyroxene and spinel or garnet as anhydrous phases. Some nodules also contain hydrous phases such as phlogopite or K-rich amphibole. Thus, all these phases are often adopted in models of mantle melt generation (e.g. Feigenson et al.(1983)). The importance of olivine in the mantle is also consistent with seismic (P) wave anisotropy in the oceanic lithosphere

(Verma(1960)). The determination of whether clinopyroxene and garnet are present in the source is particularly important because of the ability of these phases to fractionation REE (Fig.6.1). Residual clinopyroxene is inferred for the majority of OIB because of its capacity to produce significant fractionation of LREE whilst HREE remain approximately constant (e.g. Feigenson et al.(1983)). These authors point out that this is markedly different from pure garnet control in which strong relative fractionation of both HREE and LREE occurs. The fractionation corrected REE patterns values for St.Helena basalts do not help resolve this issue because of small overall differences in slope (Fig.6.5), but samples such as SC 106 which show a larger difference in LREE compared to HREE suggest that garnet is not a significant control. This is also indicated by the Yb values, because these would be lower if significant amounts of residual garnet (which has a high mineral melt partition coefficient for these elements(Fig.6.1)) occurred in the source However, a small amount of residual garnet is capable of producing the relatively constant Y observed in oceanic basalts (e.g. Hofmann and Feigenson(1983), Hofmann et al.(1987)). Lanphere and Frey(1987) point out that increasing abundances of HREE with increasing incompatibility observed in OIB suggest that such OIB cannot be generated from a garnet free source with chondritic relative HREE abundances. This is stated because clinopyroxene cannot produce a melt with an increase in HREE abundance with increasing incompatibility (positive HREE slope) from a chondritic source because it has similar values of distribution coefficients for HREE (Fig.6.1). Conversely garnet has a progressive increase in distribution coefficients with decreasing incompatibility of HREE (Fig.6.1). For similar reasons crossing REE patterns for different samples between Dy and Lu is good evidence for the presence of garnet in the source (e.g. Budahn and Schmitt(1985)). Olivine and orthopyroxene are unsuitable candidates for producing this variation because the magnitude of the distribution coefficients is relatively low. A recent discussion in the literature of the likelihood of residual garnet occurring in the source of the Kohala volcanics shows that it is not always possible to unequivocally state whether garnet is present or absent in the source of an OIB suite, even when a comprehensive data set is available (Hofmann and Feigenson(1983), Feigenson et al.(1983), Hofmann et al.(1987), Lanphere and

Frey(1987)). Lanphere and Frey(1987) insist that the distribution coefficients of HREE preclude derivation from a garnet free source , whereas the other authors argue that the modelling described above permits derivation of tholeiites from a source slightly depleted in the more incompatible HREE.

This problem is even more difficult to resolve in the SHRS because the degree of fusion appears to be sufficiently similar to not be capable of fractionating REE significantly because of the similarity in slope of the REE patterns in Fig.6.5. The occurrence of garnet bearing xenoliths on Hawaii (Sen,1983,1987) shows that some melts are certainly generated in the garnet stability field (Clague(1987)), section 2.3). A garnetiferous source for OIB is also indirectly indicated by the calculations of McKenzie(1987) who showed that an ascending plume would start to melt at 70-80 km which is within the garnet stability field.

6.4.2; A method of evaluating the source mineral assemblage;

A further estimate of which phases are present in the source can be made by adopting the method of Fitton and Dunlop(1985) and Fitton and James(1986). In this approach a realistic source composition is chosen first and compared to observed melts to calculate distribution coefficients between melt and source.

6.4.2.1; Choice of source;

Fitton and Dunlop(1985)) considered the alkali basalts of the Cameroon line could be related to a N-MORB source. These authors believed N-MORB source to be the source, because this was indicated by the wide areal distribution and homogeneity of these basalts which occur along a 1000km lineament and were erupted over a period of 65 Ma with no clear age progression. This temporal and spatial distribution was thought to be inconsistent with derivation from a localised OIB source plume, but consistent with a homogeneous upper mantle with small scale heterogeneities. The choice of MORB is also followed in this modelling exercise because:

(a) It is known that the St.Helena source is depleted in the LIL Rb, Ba and K relative to other incompatible elements e.g.La, Nb (section 7.3,8.3), hence it is

likely to have undergone multiple partial melting events as has the MORB source mantle. It is argued in Chapter 8 that the composition of the SHRS may be dominated by a component akin to subducted oceanic crust. Such material will possess a depletion in more highly incompatible elements which are intermediate between MORB (subducted oceanic crust) and MORB source (more depleted subducted lithosphere).

(b) The modelling is instructive in indicating the relative Kd variations of the source assemblage and thereby yielding information on the phases present.

(c) The degree of fusion indicated by such models warrants discussion.

The approach of calculating the MORB source follows that of Fitton and Dunlop(1985). They assumed a 15% melt of the MORB source would produce average N-MORB (Sun(1980)). The source and melt are related using a non modal batch partial melting model (Appendix F), (Shaw(1970)):

$$\frac{C_l}{C_0} = \frac{1}{D_0 + F(1-P)} \qquad (6.3)$$

where C_l is the chondrite normalised trace element abundance in the liquid (magma),

C_0 is the chondrite normalised trace element abundance in the solid (source),

D_0 is the bulk distribution of the source assemblage given by

$$D_0 = x_a.D_a + x_b.D_b + \ldots\ldots\ldots\ x_j.D_j,$$

where x_j is the weight fraction of the phase j in the source and D_j is the distribution coefficient between phase j and the melt and P is the bulk distribution coefficient for the liquid sometimes known as the primary melt norm (Hofmann and Feigenson(1983)) and given by:

$$P_j = p_a.D_a + p_b.D_b + \ldots\ldots\ldots\ p_j.D_j \qquad (6.4)$$

here p_j is the weight fraction of phase entering the melt.

A similar approach to that of Fitton and Dunlop(1985) is used here except that the average N-MORB data of Sun and McDonough(1988) are used because a larger sample set for a greater range of elements is available in this compilation. The calculated MORB source is shown in Fig.6.9.

6.4.2.2; Calculation of Kd;

The distribution coefficients between MORB source and primitive St.Helena basalts are generated by a simplified version of equation 6.3 that is used for modelling modal equilibrium partial melting:

$$\frac{C_l}{C_0} = \frac{1}{(D + F(1-D))} \qquad (6.5)$$

equation 6.4 can be rearranged to give:

$$D = \frac{C_0/C_l - F}{1 - F} \qquad (6.6)$$

The resulting D values for various degrees of partial melting are shown in Fig.6.10. The permissible degree of partial melting is constrained by the values of distribution coefficients for Ba remaining positive. Two main points are evident from this modelling. Firstly, the shape of the pattern in relation to published Kd data shows that residual garnet may be required in the source. This is inferred because the distribution coefficients for Gd-Lu are not similar (clinopyroxene control), but $Kd_{Lu} > Kd_{Gd}$ (garnet control) (Fig.6.1). Phlogopite or kaersutite are not capable of producing this feature. (Fig.6.1). Additionally a residual phase rich in K is necessary to account for the unexpectedly high value of Kd_K. Secondly, low degrees of partial melting are implied - the maximum degree of partial melting before negative values for Ba are generated is 0.51%. This is not

Fig.6.9. Results of calculations to infer the MORB source required to produce Sun and McDonough(1988) N-MORB (bold black curve). The source composition is shown as a spidergram of trace elements normalised to Thompson(1982) primitive mantle.

The inferred sources for varying degrees of fusion (5 - 25%) are labelled at the top of figure. This model assumes simple modal batch melting using equation 6.3 (Shaw,1970).

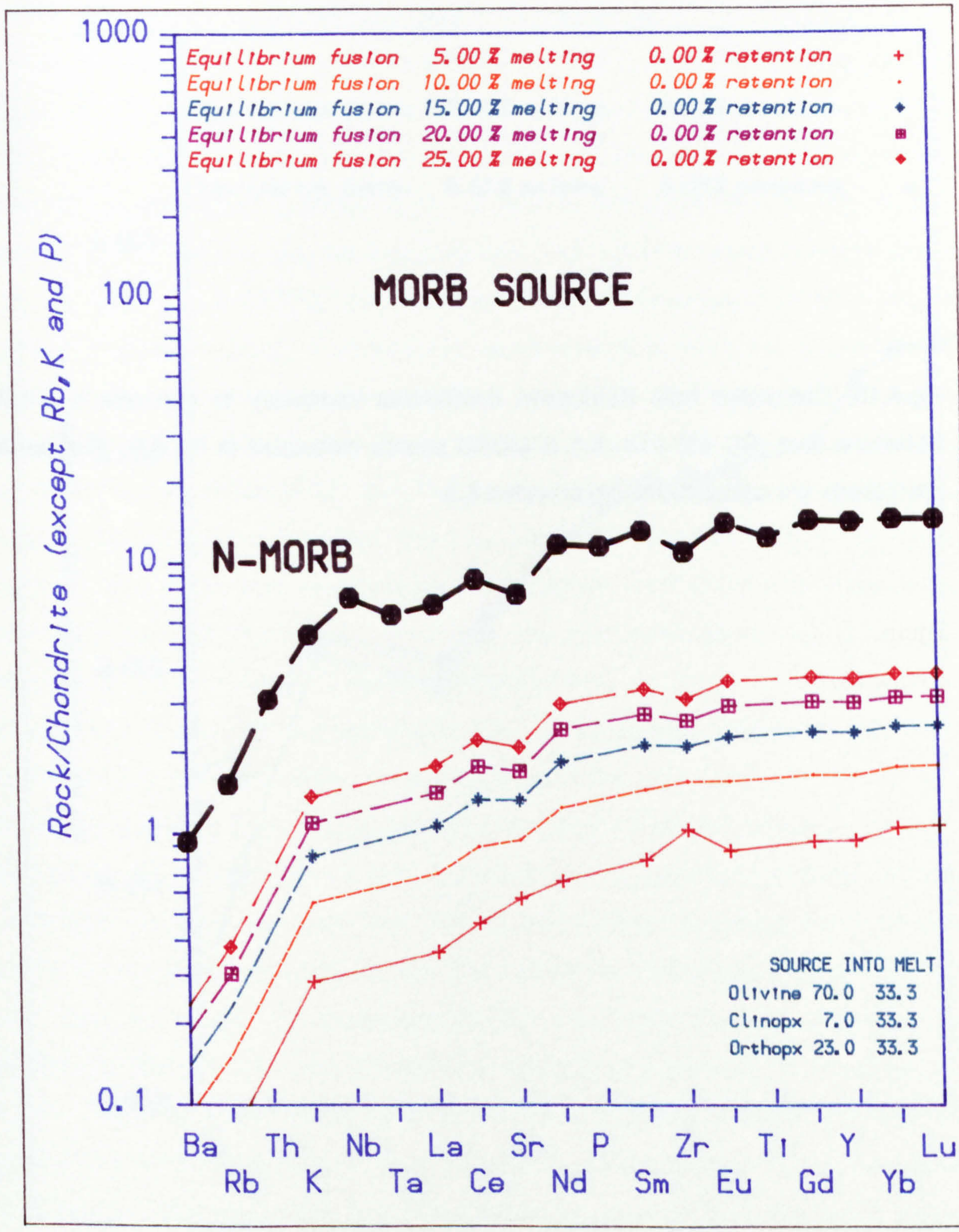
Equilibrium fusion 5.00 % melting 0.00 % retention +
Equilibrium fusion 10.00 % melting 0.00 % retention ·
Equilibrium fusion 15.00 % melting 0.00 % retention ◆
Equilibrium fusion 20.00 % melting 0.00 % retention ⊞
Equilibrium fusion 25.00 % melting 0.00 % retention ◆
MORB SOURCE
N-MORB
Rock/Chondrite (except Rb, K and P)
1000
100
10
1
0.1
SOURCE INTO MELT
Olivine 70.0 33.3
Clinopx 7.0 33.3
Orthopx 23.0 33.3
Ba Th Nb La Sr P Zr Ti Y Lu
Rb K Ta Ce Nd Sm Eu Gd Yb

Fig.6.10. Calculated bulk distribution coefficients necessary to generate a primitive St.Helena lava (SC 68) from the N-MORB source calculated in Fig.6.9. The partition coefficients are calculated using equation 6.3.

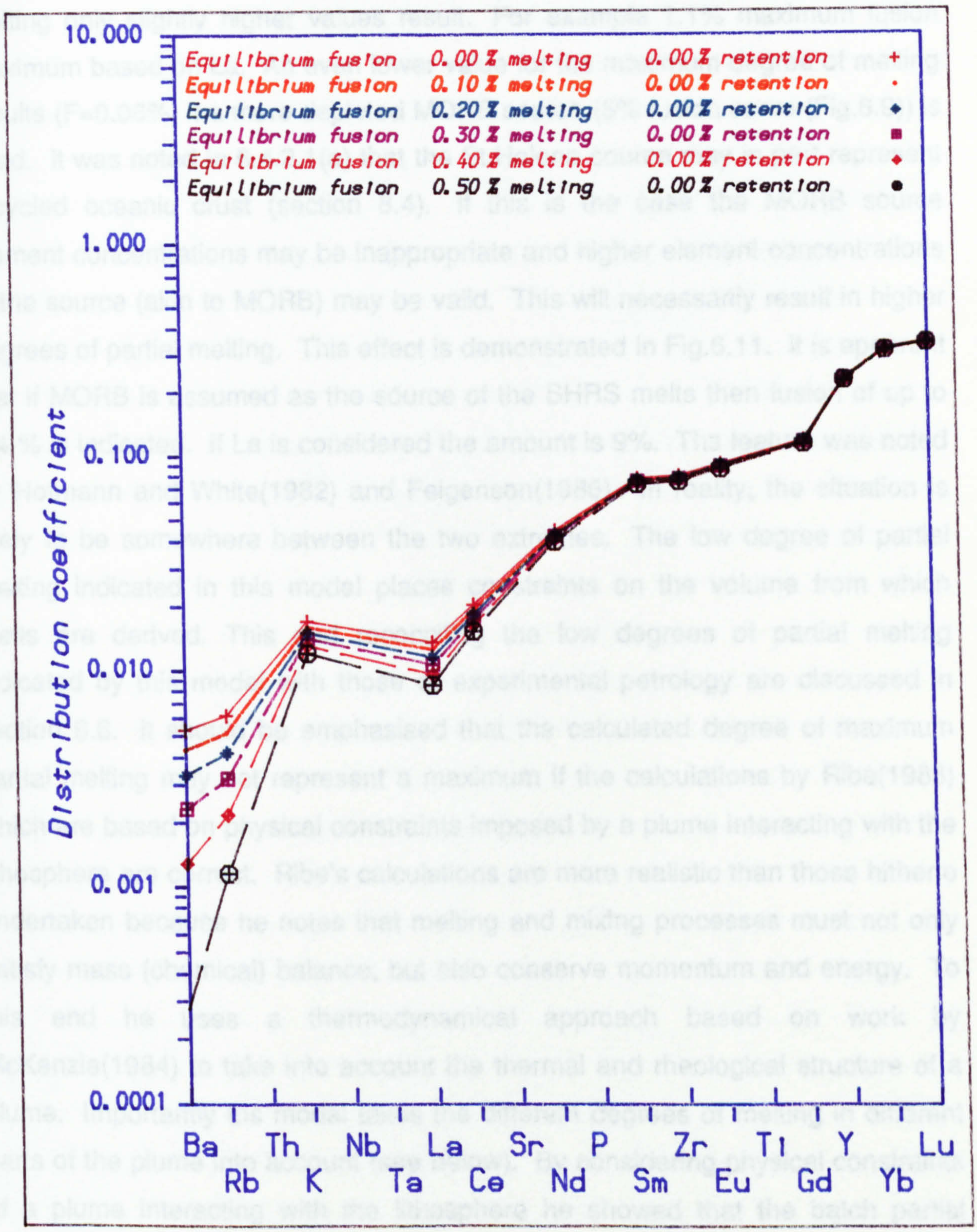
Equilibrium fusion 0.00 % melting 0.00 % retention +
Equilibrium fusion 0.10 % melting 0.00 % retention ·
Equilibrium fusion 0.20 % melting 0.00 % retention ◆
Equilibrium fusion 0.30 % melting 0.00 % retention ■
Equilibrium fusion 0.40 % melting 0.00 % retention ◆
Equilibrium fusion 0.50 % melting 0.00 % retention ●
10.000
1.000
0.100
0.010
0.001
0.0001
Distribution coefficient
Ba Th Nb La Sr P Zr Ti Y Lu
Rb K Ta Ce Nd Sm Eu Gd Yb

critically dependent on the values chosen for the Kd of Ba. If less incompatible elements such as the LREE are used to constrain the maximum degree of partial melting only slightly higher values result. For example 1.1% maximum fusion maximum based on La. An even lower value for the maximum degree of melting results (F=0.06%) if a more depleted MORB source (5% fusion curve (Fig.6.9)) is used. It was noted in 6.4.2.1(a) that the St.Helena source may in part represent recycled oceanic crust (section 8.4). If this is the case the MORB source element concentrations may be inappropriate and higher element concentrations in the source (akin to MORB) may be valid. This will necessarily result in higher degrees of partial melting. This effect is demonstrated in Fig.6.11. It is apparent that if MORB is assumed as the source of the SHRS melts then fusion of up to 3.4 % is indicated. If La is considered the amount is 9%. Ths feature was noted by Hofmann and White(1982) and Feigenson(1986). In reality, the situation is likely to be somewhere between the two extremes. The low degree of partial melting indicated in this model places constraints on the volume from which melts are derived. This and reconciling the low degrees of partial melting indicated by this model with those of experimental petrology are discussed in section 6.6. It should be emphasised that the calculated degree of maximum partial melting may not represent a maximum if the calculations by Ribe(1988) which are based on physical constraints imposed by a plume interacting with the lithosphere are correct. Ribe's calculations are more realistic than those hitherto undertaken because he notes that melting and mixing processes must not only satisfy mass (chemical) balance, but also conserve momentum and energy. To this end he uses a thermodynamical approach based on work by McKenzie(1984) to take into account the thermal and rheological structure of a plume. Importantly ths model takes the different degrees of melting in different parts of the plume into account (see below). By considering physical constraints of a plume interacting with the lithosphere he showed that the batch partial melting equation could overestimate the effect of partial melting by up to 70% in the case of the highly incompatible elements considered here.

Fig.6.11. Calculated bulk distribution coefficients necessary to generate a primitive St.Helena lava from N-MORB (Sun and McDonough(1988)). Calculation performed as in Fig.6.10.

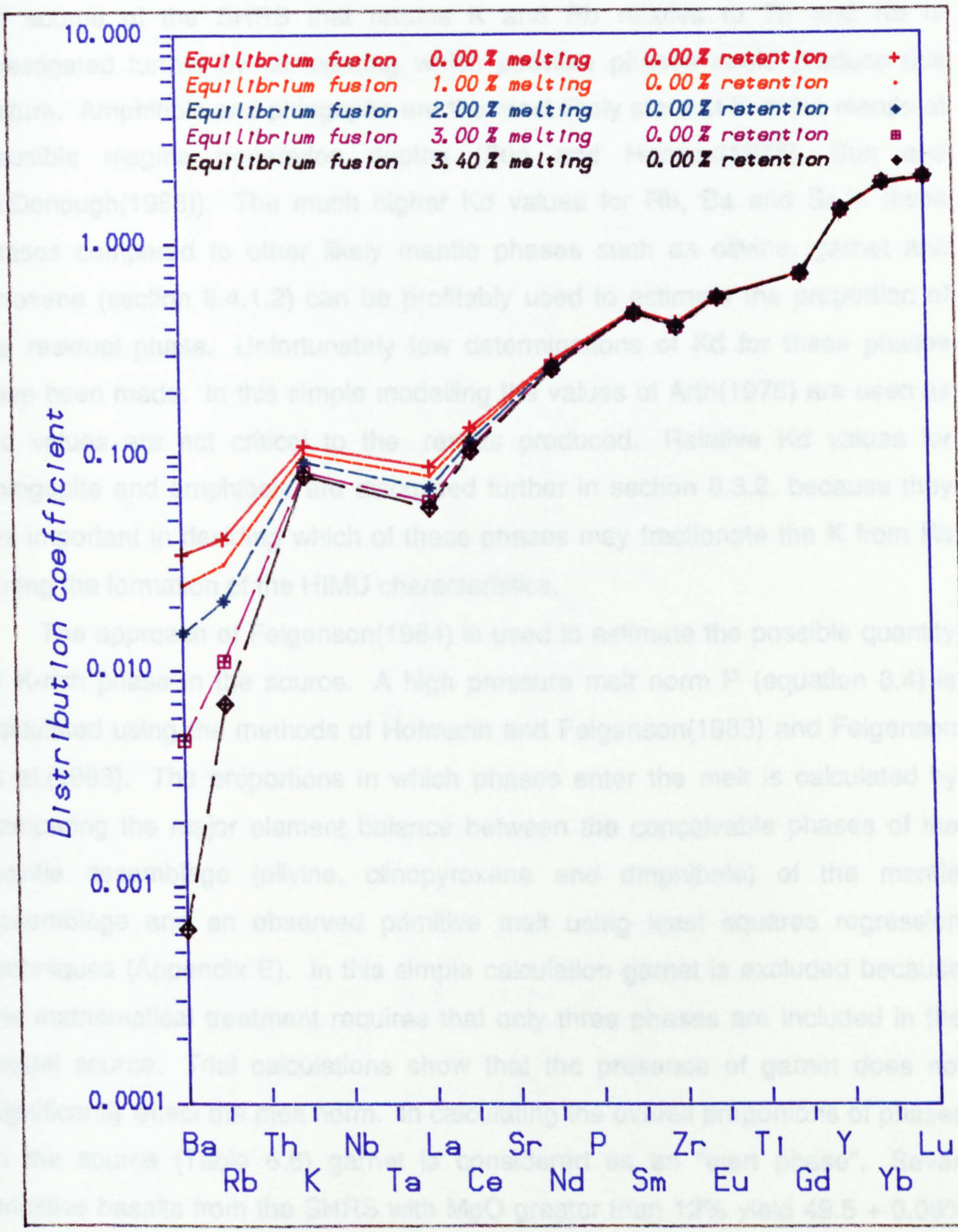
Equilibrium fusion 0.00 % melting 0.00 % retention
Equilibrium fusion 1.00 % melting 0.00 % retention
Equilibrium fusion 2.00 % melting 0.00 % retention
Equilibrium fusion 3.00 % melting 0.00 % retention
Equilibrium fusion 3.40 % melting 0.00 % retention
10.000
1.000
0.100
0.010
0.001
0.0001
Distribution coefficient
Ba Th Nb La Sr P Zr Ti Y Lu
Rb K Ta Ce Nd Sm Eu Gd Yb

6.4.3; Nature and proportion of the K-rich mantle phase;

The implications for melt generation in the presence of a residual phase in the source of the SHRS that retains K and Rb relative to Th and Nb is investigated further by considering which possible phases could produce this feature. Amphibole and phlogopite are the most likely store of K in the mantle at plausible magma generation depths (Sun and Hanson(1975), Sun and McDonough(1988)). The much higher Kd values for Rb, Ba and Sr in these phases compared to other likely mantle phases such as olivine, garnet and pyroxene (section 6.4.1.2) can be profitably used to estimate the proportion of the residual phase. Unfortunately few determinations of Kd for these phases have been made. In this simple modelling the values of Arth(1976) are used as the values are not critical to the results produced. Relative Kd values for phlogopite and amphibole are discussed further in section 8.3.2. because they are important in deciding which of these phases may fractionate the K from Rb during the formation of the HIMU characteristics.

The approach of Feigenson(1984) is used to estimate the possible quantity of K-rich phase in the source. A high pressure melt norm P (equation 6.4) is calculated using the methods of Hofmann and Feigenson(1983) and Feigenson et al.(1983). The proportions in which phases enter the melt is calculated by comparing the major element balance between the conceivable phases of the mantle assemblage (olivine, clinopyroxene and amphibole) of the mantle assemblage and an observed primitive melt using least squares regression techniques (Appendix E). In this simple calculation garnet is excluded because the mathematical treatment requires that only three phases are included in the model source. Trial calculations show that the presence of garnet does not significantly effect the melt norm. In calculating the overall proportions of phases in the source (Table 6.6) garnet is considered as an "inert phase". Seven primitive basalts from the SHRS with MgO greater than 12% yield 49.5 + 0.09% for the proportion of amphibole in the melt norm. Clinopyroxene comprises 45% and olivine the remainder. Typical results for the basalt SC 59 are given in Table 6.4.

Table 6.4. Calculated melt norm for an olivine and clinopyroxene source containing a K-rich phase using an optimum least squares fit to the major element data shown. sd is the standard deviation for the proportion of components. Olivine(OL), amphibole(AMPH) and clinopyroxene(CPX).

(a) *Amphibole*

	Parent SC 59	OL	AMPH	CPX	Calculated parent
SiO_2	43.17	40.20	40.70	47.30	42.97
TiO_2	2.25	0.00	4.00	1.00	2.56
Al_2O_3	10.60	0.10	11.60	11.00	10.77
FeO	12.69	11.43	12.30	8.10	10.40
MnO	0.21	0.20	0.50	0.20	0.36
MgO	14.46	46.50	13.20	14.90	15.09
CaO	11.99	0.30	11.10	14.20	11.83
Na_2O	2.02	0.00	2.60	1.70	2.10
K_2O	0.77	0.00	1.00	0.00	0.54

Proportions of phases in source

	OL	AMP	CPX
	0.040	0.537	0.413
sd	0.008	0.016	0.021
%	19.5	3.1	5.1

(b) *Phlogopite*

	parent SC 59	OL	PHLOG	CPX	Calculated parent
SiO_2	43.17	40.20	35.55	47.30	47.08
TiO_2	2.25	0.00	4.83	1.00	1.44
Al_2O_3	10.60	0.10	15.97	11.00	11.83
FeO	12.69	11.43	7.29	8.10	8.17
MnO	0.21	0.20	0.20	0.20	0.20
MgO	14.46	46.50	18.72	14.90	15.45
CaO	11.99	0.30	0.00	14.20	13.05
Na_2O	2.02	0.00	0.57	1.70	1.62
K_2O	0.77	0.00	8.15	0.00	0.00

Proportions of phases in source

	OL	PHLOG	CPX
	-0.006	0.108	0.919
sd	0.008	0.004	0.012
%	139.4	3.8	1.3

Data sources; Mineral compositions in Feigenson(1984) - Salt Lake crater xenoliths, Hawaii.

It is apparent that phlogopite is not a plausible phase in the mantle assemblage as this produces invalid solutions (negative amounts of olivine in all cases). A similar feature was noted by Feigenson(1984). Since phlogopite has a lower melt norm proportion than amphibole the former phase will indicate lower degrees of melting in the calculations below for the maximum degree of partial melting. Hence only amphibole is considered below in order to calculate the maximum degree of fusion. The norm produced is in agreement with the phase equilibria work of Huckenholz and Gilbert(1983) who showed the presence of Kaersutite in the liquidus composition at pressures as high as 40 Kb during experimental fusion of a K-rich alkali basalt. Similarly, more recent work by Taylor and Green(1988) has shown that a typical OIB source composition (Hawaiian pyrolite) will contain pargasitic amphibole containing up to 30 mole % K-richterite at pressures of less than 20kb (60 km) (in the presence of a C-O-H fluid buffered at an IW+1 oxygen fugacity). Phlogopite occurs at higher pressures.

By substitution in equation 6.3 it is possible to calculate the maximum permissible degree of partial melting if this melt norm is correct. The equations for the elements relating SC 59 to an amphibole bearing source for Rb, Sr and Ba are given in Table 6.5.

Table 6.5. Estimate of the maximum degree of fusion permissible in a source containing amphibole from trace element considerations.

$$\text{Equation 6.3:} \quad \frac{C_l}{C_0} = \frac{1}{(D_0 + F(1 - P)}$$

For SC 59 gives:

$Rb : 1/(D_0 + 0.9.F) = 150$

$Sr : 1/(D_0 + 0.8685F) = 27$

$Ba : 1/(D_0 + 0.8.F) = 258$

The solution for Ba is 0.47%.

Data sources in table.6.6.

It is apparent that the maximum degree of partial melting is limited by the equation for Ba. This gives $F_{maximum}$=0.5% (taking D as 0, if D > 0 the maximum degree of fusion is reduced accordingly). If this degree of melting is assumed it is

then possible to calculate the proportion in which phases are present in the assemblage. This is again possible by further substitution in 6.3 (table 6.6)). The solution is amphibole 1%, clinopyroxene 43% and inert phases 54%. If 1% amphibole exists in the source it is implied that 2% fusion would use up all the amphibole in the source. This is not possible because otherwise the K - retention observed would not occur. It should be remembered that all the models adopted above which consider the LIL are dependent on the assumption that the depletion in LIL occurs in the melting event producing the SHRS. The possibility that LIL depletion could have occurred prior to this is considered in section 8.3. This effect is not considered by Feigenson(1984).

Table 6.6. Estimate of the proportions of phases in source containing a K-rich phase;

Rearranging equation 6.3 gives:

$$D_0 = C_0/C_1 - F(1-P)$$

substituting into this gives:

D_{Sr} : x.(0) + y.(0.07) + z.(0.2) = 0.032
D_{Rb} : x.(0) + y.(0) + z.(0.2) = 0.0024

where x, y and z are the proportion in the source assemblage of inert phases (olivine, orthopyroxene, garnet and spinel), clinopyroxene and amphibole respectively.

These equations may be solved simultaneously. Subtracting equation for Rb from equation for Sr gives

y.(0.007) = 0.0296, y (clinopyroxene) = 45%.

Substitution into equation for Sr gives 0.95% amphibole, 54% inert phases and 45% clinopyroxene.

Constants used in modelling

Feature	Rb	Sr	Ba
Source p.p.m.(*)	0.08	15.5	0.958
Melt p.p.m.(SC 59)	12.0	422.0	247.0
D_{amp}	0.2	0.2	0.4
D_{cpx}	0.0	0.07	0.0
D_{inert}	0.0	0.0	0.0

* The source is that required to form N-MORB by 15% modal melting using equation 6.3. (Fig.6.9).
The Kd values are those of Arth(1976).

6.4.4; Calculating source characteristics by inversion; the method of Hofmann and Feigenson(1983).

Further inversion of the fractionation corrected trace element data is not possible by using the methods of Hofmann and Feigenson(1983) who used a similar preliminary fractionation procedure to that described above. This is due to the limited variation in the degree of trace element enrichment in the St.Helena alkali basalts in comparison to the range observed between tholeiites and alkali basalts of Hawaii (e.g. Frey and Roden(1987)). For example fractionation

corrected Ba abundances vary with two exceptions from 155-220 in the SHRS compared with 30-350 in the Kohala series (Feigenson et al.(1983)). The inversion procedure of Hofmann et al.(1983) is based around interpretation of a process identification diagram (Allegre and Minster(1978)). This diagram is used for discriminating between the effects of crystal fractionation and batch partial melting. Each process describes a different vector when a suite of rocks are plotted on a graph of a highly incompatible element such as Ba (concentration C^H) with a less incompatible element such as Sr or La (C^i) (concentration ratio C^H/C^i) (Fig.6.12.). A graphical solution for the source composition from the process identification diagram is possible by the following method; P_i (the primary melt norm) is obtainable from the slope(S) and intercept(I) on a process identification diagram on which these parameters are described by the equation for a straight line:

$$\frac{C^H}{C^i} = S^i.C^H + I^i \qquad (6.7)$$

where:

$$S^i = D^i_0 / C^i \qquad (6.8)$$

and

$$I^i = \frac{C^H}{C^i}(1 - P^i) \qquad (6.9)$$

If the primary melt norm (equation 6.4) is known, it is then possible to calculate the primary source characteristics relative to C^H. The samples corrected for crystal fractionation from the SHRS do not describe a positive correlation when plotted on such a diagram (Fig.6.12). This indicates that in terms of absolute Ba abundances the trace element variation in the SHRS is

Fig.6.12. Allegre and Minster(1978) discriminant diagram showing variation of a highly incompatible element C^H (Ba) in comparison to a moderately incompatible element C^i (Sr) expressed as;

Ba vs Ba/Sr for the SHRS.

Samples that have been corrected for crystal fractionation are shown by *black dots*. The vectors shown are those for batch partial melting (BPM) and crystal fractionation(CF).

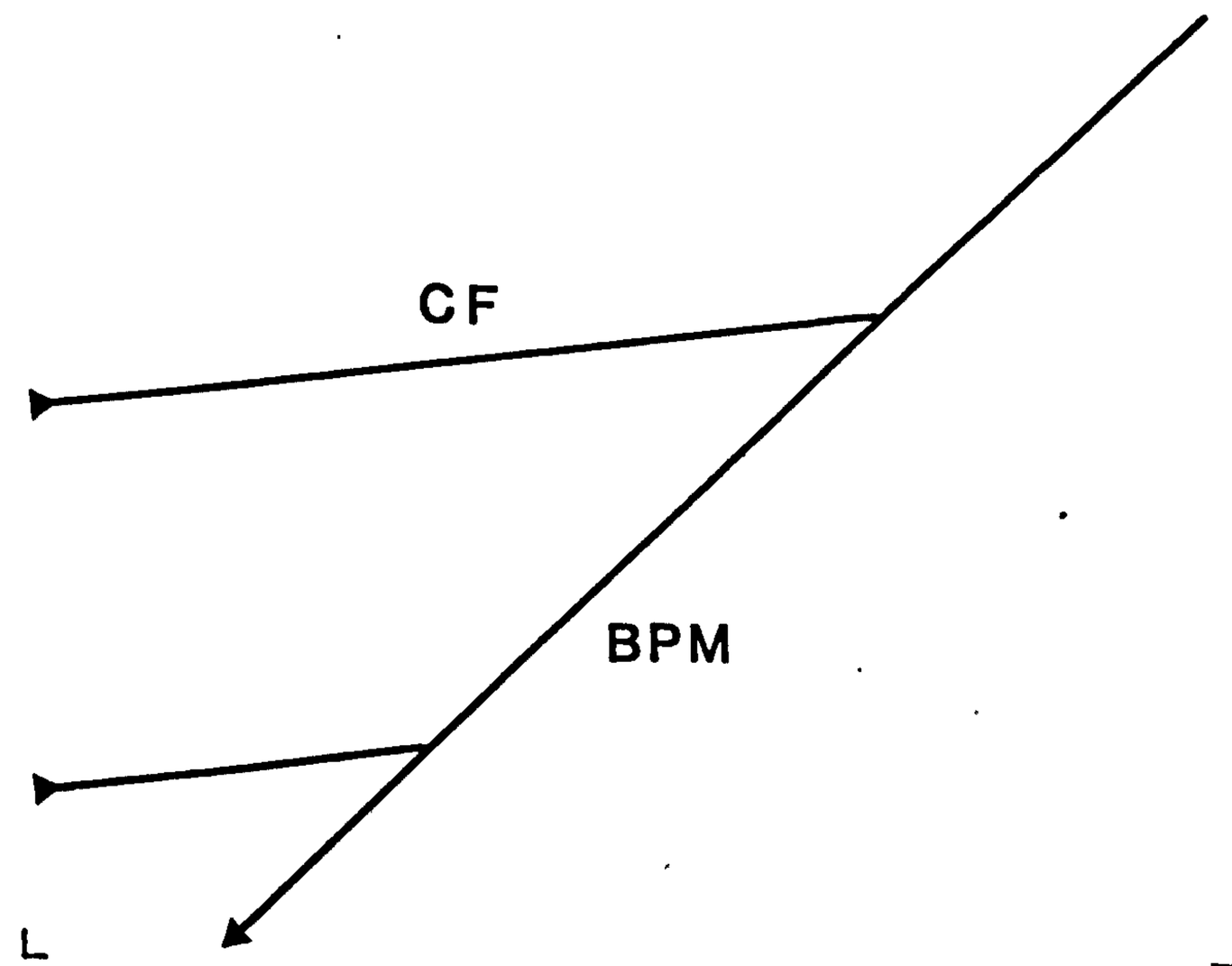
CF
BPM

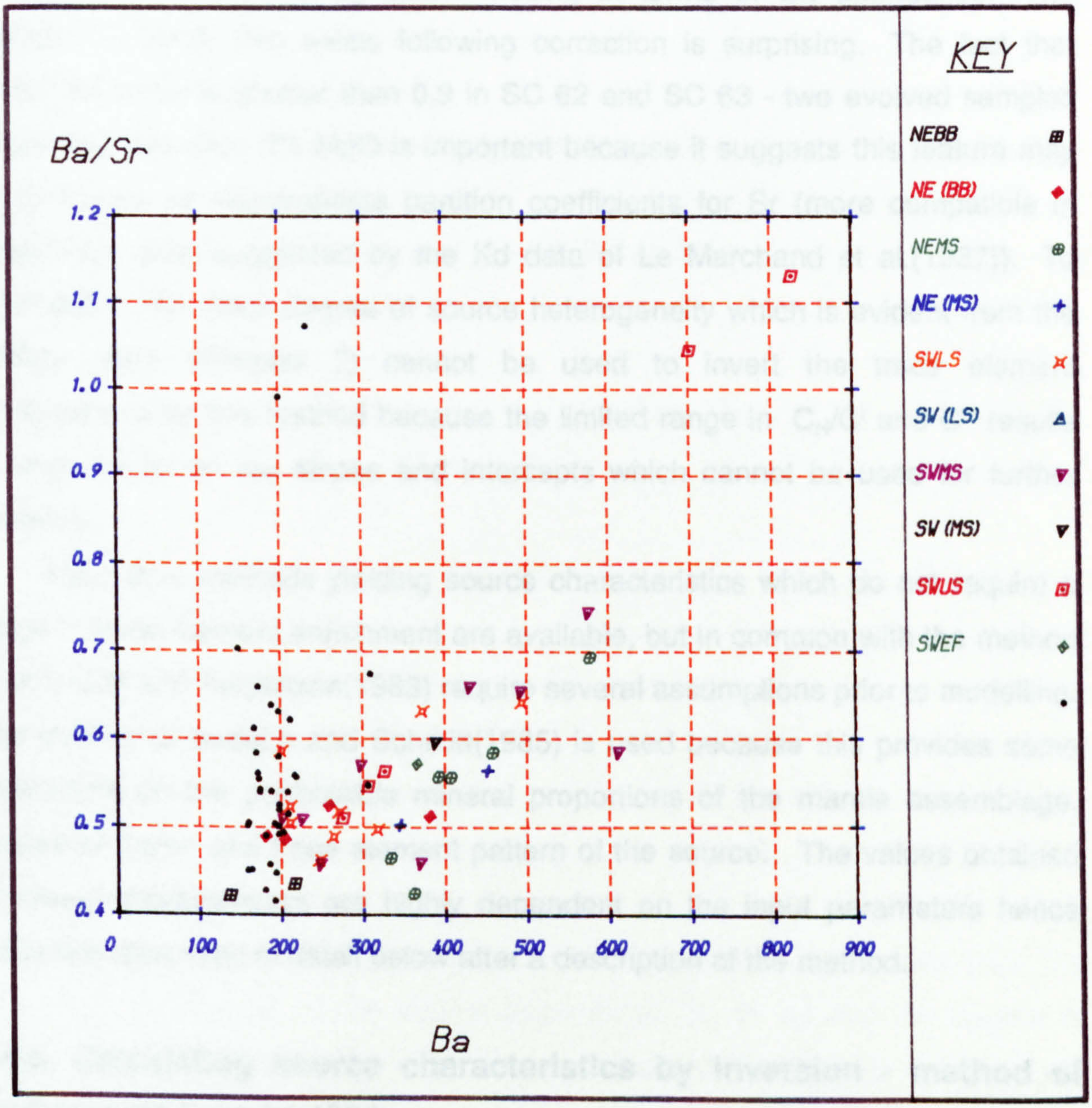
Ba/Sr
1.2
1.1
1.0
0.9
0.8
0.7
0.6
0.5
0.4
0
100
200
300
400
500
600
700
800
900
Ba
KEY
NEBB
NE (BB)
NEMS
NE (MS)
SWLS
SW (LS)
SWMS
SW (MS)
SWUS
SWEF

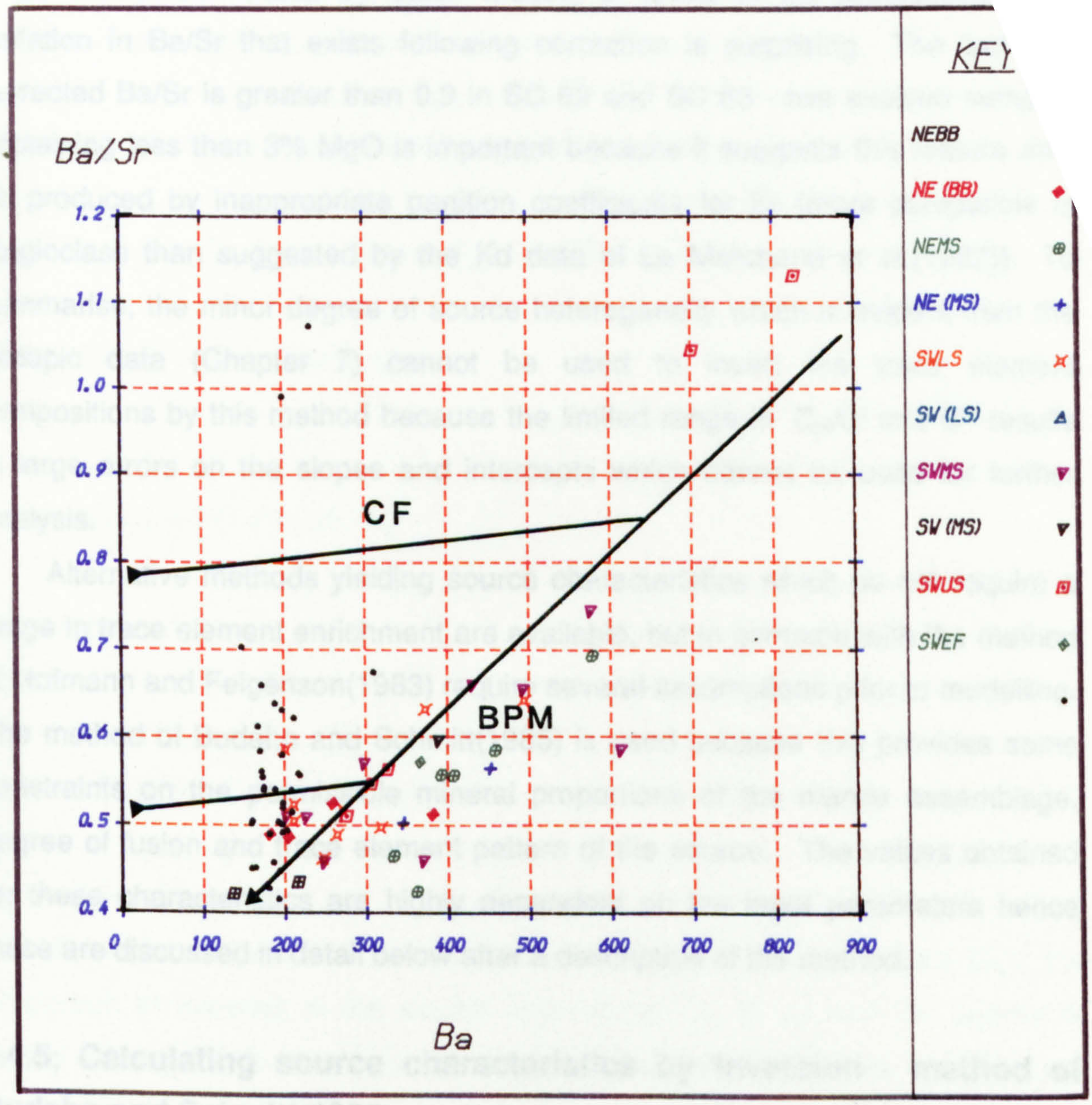
Ba/Sr
1.2
1.1
1.0
0.9
0.8
0.7
0.6
0.5
0.4
0
100
200
300
400
500
600
700
800
900
Ba
CF
BPM
KEY
NEBB
NE (BB)
NEMS
NE (MS)
SWLS
SW (LS)
SWMS
SW (MS)
SWUS
SWEF

adequately described by crystal fractionation processes alone. The occurrence of uncorrected samples from the SHRS lying on the batch melting trend is misleading because the fractionation correction procedure shows that these rocks cannot be related by batch melting in terms of Ba abundance. The variation in Ba/Sr that exists following correction is surprising. The fact that corrected Ba/Sr is greater than 0.9 in SC 62 and SC 63 - two evolved samples containing less than 3% MgO is important because it suggests this feature may be produced by inappropriate partition coefficients for Sr (more compatible in plagioclase than suggested by the Kd data of Le Marchand et al.(1987)). To summarise, the minor degree of source heterogeneity which is evident from the isotopic data (Chapter 7) cannot be used to invert the trace element compositions by this method because the limited range in C_H/C^i and C^H results in large errors on the slopes and intercepts which cannot be used for further analysis.

Alternative methods yielding source characteristics which do not require a range in trace element enrichment are available, but in common with the method of Hofmann and Feigenson(1983) require several assumptions prior to modelling. The method of Budahn and Schmitt(1985) is used because this provides some constraints on the permissible mineral proportions of the mantle assemblage, degree of fusion and trace element pattern of the source. The values obtained for these characteristics are highly dependent on the input parameters hence these are discussed in detail below after a description of the method.

6.4.5; Calculating source characteristics by inversion - method of Budahn and Schmitt(1985);

This technique inverts the observed REE contents of fractionation corrected primitive melts using least squares regression analysis based on the non-modal equilibrium partial melting model given by equation 6.3. Budahn and Schmitt show that equation 6.3 lends itself to solution by least squares analysis. In order to do this it is necessary to reduce the source assemblage to a three phase system. Assumptions about the source assemblage are discussed in 6.4.1.2. The bulk distribution coefficient becomes:

$$D_0 = x_1.D_1 + x_2.D_2 + x_3.D_3 \quad (6.10)$$

where

x_1 = (ol + opx), x_2 = cpx and x_3 = gnt

substituting 6.10 in 6.3 and rearranging gives:

$$C_0/(1/C_l) - (x_1.D_1 + x_2.D_2 + x_3.D_3) = F(1-P) \quad (6.11)$$

substituting $(1 - x_2 - x_3)$ for x_1 gives;

$$C_0/(1/C_l) - (D_1 - D_1.x_2 - D_1.x_3) + x_2.D_2 + x_3.D_3 = F(1-P) \quad (6.12)$$

this simplifies to ;

$$C_0^* (1/C_l) + x_2^*(D_1 - D_2) + x_3^*(D_1 - D_3) = F^*(1-P) + D_1 \quad (6.13)$$

(* = unknown)

The unknowns are the concentration of elements in the source (C_0), the proportion of minerals in the source assemblage (x_1 to x_3) and the degree of partial melting F. In the approach of Budahn and Schmitt(1985) F values are incremented between between 1 - 25% in 1% units. For each degree of partial meting F an array of ($F(1-P) + D_1$) terms is calculated; one for each of the REE used in modelling. This reduces the unknowns to C_0, x_2 and x_3. These values are obtained by using least squares regression conducted utilising a modified version of LSQPM PASCAL. The optimal values for C_0, x_2 x_3 obtained for each increment of partial melting from the constraining elements (REE and Sc) can then be compared. Some solutions are excluded because cpx and garnet components exceed 100% or are negative . Permissible solutions are shown in Fig.6.13 together with the best solution.

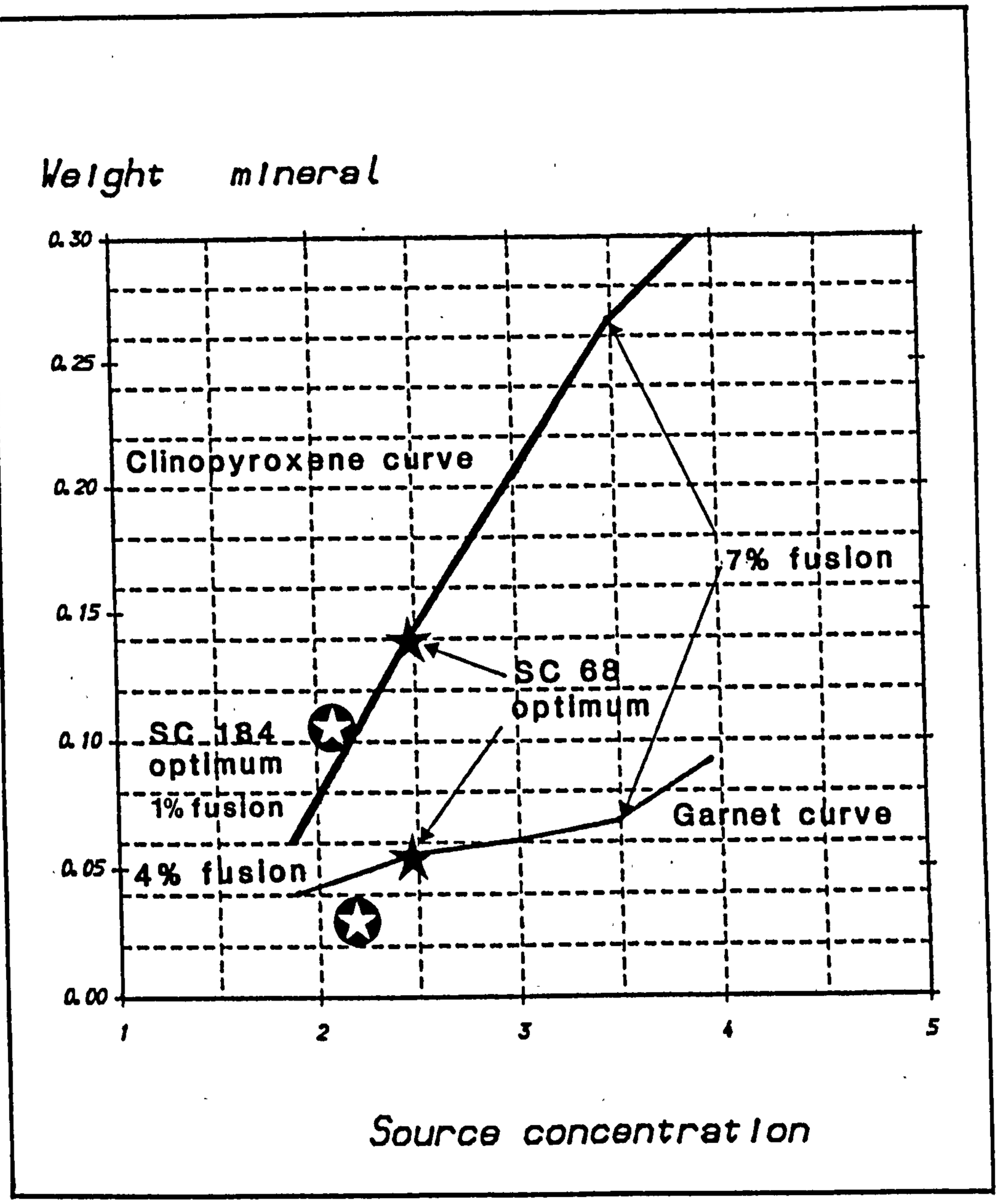

Fig.6.13. Results of source calculations based on the method of Budahn and Schmitt(1985) which are described in section 6.4.5. The trends show the least squares fit for 4-7% mantle fusion for primitive sample SC 68 (13.69 % MgO) in terms of weight% garnet (light curves) and clinopyroxene (bold curves) in the source against the variation in chondrite normalised source concentration shown. The optimum fit for SC 184 (10.7% MgO is also shown).

6.4.5.1; Constraining input parameters - C_l - Chondrite normalised abundances of observed melts;

The fractionation corrected REE and Sc values calculated in section 6.2 and 6.3 were used to represent the composition of observed melts. These are expressed as a chondrite normalised value for the elements above to permit calculation of the average chondritic value of the source. Budahn and Schmitt(1985) applied correction factors to the LREE La, Ce and Nd to account for the assumed LREE depleted source for Hawaiian tholeiites which is indicated (in part) by the downward concavity in LREE on REE patterns, e.g. Frey and Roden(1987). This is necessary because the regression analysis functions by considering the abundance of REE and Sc as identical i.e. a flat chondrite normalised trace element pattern is generated. Because St.Helena alkali basalts do not possess LREE depletion (no downward concavity in La, Ce and Nd) there is no direct evidence for LREE source depletion, but the occurrence of values of $^{143}Nd/^{144}Nd$ greater than than bulk earth in the SHRS (section 7.3) indicates a time integrated Nd/Sm ratio less than chondritic. It is a well known feature of alkali basalts that many have time integrated Nd/Sm higher than chondritic values, despite their Nd isotopic values being more than bulk Earth (Fig.7.4) indicating Nd/Sm ratios in the source being lower than chondritic (e.g. Leeman et al.(1980), Thompson et al.(1984)). For example Leeman et al.(1980) calculated from the range in $^{144}Nd/^{143}Nd$ in the Kilauea - Mauna Kea - Kohala basalts that they had a time integrated $(Nd/Sm)_N$ value of 1.31 this compares to values of < 1.0 observed in the basalts. Possible explanations for this anomaly are discussed further in section 6.6. The approach taken in the modelling is to assume a chondritic parallel REE distribution, because it is not possible to gauge the degree of LREE depletion accurately. It was noted by Budahn and Schmitt that correction is unnecessary in basalts which do not have a chondrite normalised LREE depletion (Fig.6.5).

6.4.5.2; Constraining input parameters - P - the primary melt norm;

The phases likely to be present in the source of the SHRS have been discussed in section 6.4.1. An olivine, clinopyroxene, orthopyroxene, garnet source is preferred. A residual K-bearing phase may also be present. The models considered are a four phase model and a garnet free model. In their model Budahn and Schmitt(1985) use the a melt norm (P equation 6.4) based on experimental petrology results (40 kb) reported by Davis et al.(1965). This suggests orthopyroxene and olivine contribute 20%, clinopyroxene 40% and garnet 40%. This model is adopted here also because it is the simplest mantle assemblage that can be envisaged and it is consistent with the likely depths of genesis indicated by phase equilibria and thermodynamics,. i.e. below the spinel stability field (section 6.6).

6.4.5.3; Partition coefficients;

Partition coefficient data chosen by Budahn and Schmitt(1985) (Table 6.7) are from a compilation by Irving(1978) based on experimental element partitioning between phenocrysts and melts in basalts. Where available data is obtained at T >1300 °C and at P > 20 Kb are used. Whilst the relative values of Kd of the REE are quite well constrained producing regular variations (Fig.6.1.) it is important to remember that the effects of pressure, temperature dependence and concentration are poorly known(Allegre and Minster(1978)). For example Harrison(1981) has shown that REE partitioning between garnet and liquid does not follow Henrys Law at likely melt generation pressures for low concentrations of REE. We must therefore not place too great a reliance on degrees of partial melting, indicated by these models although relative REE fractionations are realistic (Allegre and Minster(1978)).

Table 6.7. Partition coefficient data used in modelling the source composition

Budahn and Schmitt (1985) Kd compilation;

	Olivine	orthopyroxene	garnet	clinopyroxene
La	0.007	0.005	0.0049	0.003
Ce	0.007	0.006	0.098	0.02
Nd	0.008	0.01	0.15	0.09
Sm	0.009	0.013	0.22	0.26
Eu	0.010	0.014	0.26	0.44
Tb	0.011	0.021	0.39	1.60
Dy	0.012	0.025	0.31	2.50
Sc	0.150	0.600	1.60	3.10
Yb	0.014	0.056	0.29	7.40
Lu	0.016	0.068	0.28	8.60

6.4.5.4; Results of the method of Budahn and Schmitt;

Permissible solutions for the primitive sample SC 68 (uncorrected for crystal fractionation) between degrees of fusion of 4 to 8% are shown in Fig.6.13. The best solution (residuals minimised) is also shown, this condition occurs at 5% fusion. It is apparent that the results are consistent with clinopyroxene > garnet in the source at all degrees of fusion. The absolute abundance of REE and Sc in the source govern the degree of partial melting indicated by this model. This is expected intuitively from models dependent on the batch partial melting equation of Shaw(1970) (equation 6.3). It is apparent from this equation that for a given source abundance larger degree partial melts will be required for primitive composition (small C_l/C_0) than more evolved compositions (larger C_l/C_0) because C_l/C_0 is proportional to 1/F. Thus the degree of partial melting indicated by the model is influenced by the choice of the most primitive sample. It was demonstrated in section 6.2.2.2 that SC 68 represents the most valid choice for parent. If, however this sample does contain some accumulative olivine and clinopyroxene, a misleading degree of fusion will be indicated. To test the magnitude of this effect, the modelling was repeated for a slightly less primitive composition (SC 184, 10.7 % MgO). This sample suggested a degree of partial melting of 1% at a similar source concentration to SC 68 (Fig.6.13). Thus small degrees of partial fusion are indicated by this model (1-5 %).

The corrected trace element compositions were not used in this analysis because of their similarity to the primitive composition SC 68 (Fig.7.5). It was thought that errors in correction indicated by uncertainties in the correction procedure would be greater than true source differences.

Whilst the theoretical basis of the model of Budahn and Schmitt(1985) is rigorous, it was found during the course of modelling that a number of fundamental problems exist with this model. Firstly, the method of Budahn and Schmitt(1985) is not robust with respect to using other permutations of source assemblages. When the model was adjusted for a garnet free source, invalid concentrations were produced by this method (negative amounts of olivine in source) and very small source concentrations of chondrite normalised REE and Sc (less than 0.5)). Similarly, an amphibole garnet olivine clinopyroxene source composition was used without success. The problems are thought to arise because the method of Budahn and Schmitt requires large differences between the distribution coefficients of all phases. A further problem with the method of Budahn and Schmitt(1985) which is not discussed by these authors is that Sc abundances are critical to the results and errors. Sc, an element more compatible than the REE in likely mantle phases is used to reduce the errors in the model to acceptable values. To model the effects of Sc abundance uncertainties the Sc abundance in SC 184 was reduced by 5% which is smaller than that caused by analytical error (A.Grey pers.comm). It was found that the degree of partial fusion required by the model was increased to 6% and the source concentrations were changed from 2:1 clinopyroxene to garnet to equal abundances. This suggests that the degree of melting should be treated with extreme caution because:

(1) The absolute abundances of Sc are subject to analytical error.

(2) The chondrite normalised value used for Sc in relation to the REE will affect the result. The omission of this element in the analysis produced a total breakdown of the analysis; higher errors and negative amounts of clinopyroxene required in the source.

6.5; Summary of the modelling exercises;

The modelling exercises conducted above are summarised thus:

(1) The major and trace element variations in absolute abundance caused by crystal fractionation processes are effectively reduced to a narrow range of primitive compositions by the least squares correction method outlined by Hofmann and Feigenson(1983).

(2) The trace element ratios (expressed as more incompatible element/less incompatible element) are significantly lower in the corrected compositions. This is mainly the result of clinopyroxene fractionation.

(3) The trace element ratios in phonolites and trachytes are not reduced to the same extent in crystal fractionation correction. This is thought to be because crystallisation of apatite and amphibole is not considered in the modelling. Any additional difference could be a source difference.

(4) The uniformity of corrected trace element abundances and ratios in the SHRS precludes use of the inversion method of Hofmann and Feigenson(1983).

(5) The method of Budahn and Schmitt(1985) is used to place constraints on the the degrees of partial melting and source concentrations. This technique was found to be highly dependent on Sc abundances used and is not recommended in future studies.

(6) Calculations indicate that the trace element characteristics of the source are consistent with a small amount (< 5%) of a K rich phase in the source.

(7) Models in which OIB are derived from a depleted (MORB) source (e.g. Fitton and Dunlop(1985)) imply very low degree degrees of partial melting of the source.

6.6; Implications of models suggesting small degrees of fusion of source;

Models such as those of Fitton and Dunlop(1985) which suggest low degrees of partial melting, in turn imply a large source volume from which melts are removed, e.g.Frey and Roden(1987). The extent of this problem can be gauged approximately by estimating the total volume of the St.Helena volcanics. Using the minimum degree of fusion calculated by the method of Fitton and Dunlop(1985) in section 6.4.2.2 (0.5%). If a simple cylindrical model of a plume

with a radius of 100km is considered (Courtney and White(1986)) a depth interval of 54km is indicated for the source of St.Helena magmatism (Table 6.8). This is a minimum estimate because non-erupted magmas are not considered. Suyenga(1979) estimated that if non erupted magmas are included this could produce a total volume of 2.5 times the volume of observed erupted Hawaiian volcanics. Using this value gives a depth interval of 135km for melt extraction from a cylinder with a radius of 100 km. Such volumes do not present problems in the case of St.Helena as such a volume could be derived from the asthenosphere. Additionally, larger degree melts (smaller source volumes) may be permissible if the source is less depleted than N-MORB source (section 6.4.2.2). Also this volume of melt was erupted over a period of more than two Ma from a continuously upwelling rather than passive mantle source (section 7.5.2). It has been suggested, however that in the Hawaiian example problems exist because several large volcanoes not only have higher eruption rates, but they may be concurrently active (Frey and Roden(1987). These authors and Feigenson(1986) and Hofmann(1987) do not envisage a scavenging mechanism efficient enough to remove trace elements from this volume.

Table 6.8. Volume estimates of St.Helena magmatism - implications for source region size.

	Model 1:Minimum volume	Model 2: Maximum volume
Volume cone	8400km^3	21000km^3
Source volume	1.6 X 10^{6}km^3	4.2 X 10^{6}km^3
Depth of cylinder (radius 100km)	54km	134km

Minimum volume calculated using 0.5% partial melting - the minimum indicated by the modelling in section 6.4.2.2. Formula for volume of a simple cone and data of Baker(1968) for the St.Helena cone radius 40 km at 4400m depth, height of volcano 5 km are used. Maximum volume calculated using 2.5 times the observed volume to take into account non erupted magma (Suyenga (1979) .

A more significant problem with trace element modelling that suggests small degrees of partial melting is that it is contradictory with the evidence from experimental petrology and thermodynamics which suggest much larger degrees

of partial melting (Thompson et al.(1984), Thompson(1987)). This dilemma was originally outlined during studies of MORB genesis. Experimental studies of various starting mantle assemblages for MORB source are consistent with MORB being produced by up to 25% fusion of lherzolite to leave a harzburgitic residuum (see review by Thompson(1987)). McKenzie(1984,1987) considered the thermodynamic constraints on mantle fusion and estimated that anhydrous mantle upwelling beneath a spreading centre begins to melt at 60 km depth to yield up to 25-30% of aggregated melt from a given mantle volume. O'Hara(1985) reconciled these apparently contradictory pieces of evidence by suggesting that the two disparate degrees of partial melting were accounted for by the "shape" of the melting regime beneath MOR. He suggested that large degrees of partial melting beneath the ridge axis influence the major element chemistry and do not cause trace element fractionation, whilst smaller degrees of partial melting away from the axis are reflected in fractionated ratios of the incompatible elements. This important point was emphasised by McKenzie(1985b) who noted that "If the volume of mantle which passes through the region of extensive melting is small compared with that from which the small melt fractions are extracted then the concentrations of the incompatible elements in the magma will show strong fractionation". Further evidence of this process occurring was provided by the calculations of McKenzie(1984,1985b) who showed that melt can be extracted from the mantle when the melt comprises less than 0.1% and he also showed from Th disequilibria data that only 2% melt could be supported in the melt zone overall (McKenzie(1985a)). The idea that the the different degrees of partial melting indicated by incompatible trace elements and major elements is a consequence of their being derived from different mantle volumes is now widely accepted. For example, Zindler and Jagoutz(1988) consider anhydrous spinel lherzolites which in terms of isotopic characteristics are "among few suitable candidates for N-MORB" collected as nodules (Zindler and Jagoutz(1988)). These have been previously considered as unsuitable as MORB source type material because of the large depletion in elements from Group Two of the periodic table i.e. the LIL elements. Zindler and Jagoutz(1988) suggest that these peridotites may conceivably act as a MORB source if very low (0.2%) degree melts occur at the periphery of the MORB genesis zone.

Alternatively very low degree (0.1%) carbonatitic melts could be produced at greater depths than MORB (i.e. greater than 100km) and then mix with larger degree melts at a higher level (McKenzie(1985), Thompson(1987)). Thompson(1987) notes that very low degree partial melting events during the generation of OIB could explain the dilemma that isotope data usually indicate depleted sources (Rb/Sr, Nd/Sm less than chondritic), whereas observed Rb/Sr and Nd/Sm are usually greater than chondritic in OIB. Thompson(1987) believes that very low degrees of partial melting are capable of fractionating the Rb/Sr and Sm/Nd ratios during OIB genesis. Others believe that metasomatic enrichment prior to eruption can account for this feature (e.g. Chauvel and Jahn(1984)).

The interplay between the zone in which large degrees of partial melts occur and the more extensive zones in which smaller degree melts form can be readily applied to the intraplate oceanic setting. The geometry is similar in as far as a thermal maximum occurs although the geometry is of a point rather than linear source of heat. McKenzie(1985) calculated that for a plume temperature estimated at 1550 °C melting would start to occur at a depth of 100 km to form a 15% aggregate melt fraction. This is again discordant with the trace element data, and can be similarly explained if a maximum degree of partial melting occurs in a small zone beneath the volcano but the trace elements are scavenged from a much larger volume. Such a model is in accord with modelling based on interpretation of geophysical data which shows that a plume may have a hammerhead geometry, with a radius of 300km in which elevated mantle temperatures occur and from which incompatible trace elements could be scavenged (section 2.4) Fig.2.3.).

Wyllie(1988) has suggested a similar model for intraplate oceanic activity based on phase equilibria data. He considers that the two different melting regimes are produced by the presence of the volatiles CH_4 and H_2O in the mantle. In this model the volatile components in the plume have the affect of decreasing the solidus temperature to permit melting at greater depths than in anhydrous peridotite. As the plume ascends it crosses a dehydration boundary at approximately 200km and H_2O is released from the hydrated mantle minerals. This together with CH_4 will cause very small degrees of partial melting once the solidus is exceeded. Trace element fractionation will result, although this effect

is not described in Wyllie's model. High degrees of partial melting will only occur in a narrow central zone in which the solidus for anhydrous garnet lherzolite is exceeded (at temperatures greater than 1500°C at the base of the lithosphere). Trace element fractionation will not occur in this zone. A similar model has been proposed by Green et al.(1987) based on the experimental data of Taylor and Green et al.(1987). In this model the asthenosphere is a fluid absent region in which the C-H-O volatiles are dissolved in very small degree partial melts which carry the incompatible elements upwards. On interacting with the more oxidised lithosphere H_2O rich fluids are released which further lower the solidus of the peridotite and so called redox melting occurs to produce the large volume melts. It should be noted that the models of Green et al.(1987) and to a lesser extent Wyllie(1988) are dependent on a reducing environment below the lithosphere. These ideas are disputed by Eggler(1983) and Mattioli and Wood(1986). However Wyllie's model is mainly dependent on the presence of volatiles in the mantle. In all the models discussed in this section it is necessary that very small degrees of melt can be efficiently transferred to the surface in a convecting mantle matrix. The pioneering work of Ahern and Turcotte(1979) showed that after formation of an incipient melt, the melt becomes buoyant and ascends at a rate greater than that of the convecting mantle. Similar, more recent fluid dynamical modelling has confirmed the efficacy of this process (Stolper et al.(1981), Maaloe and Schie(1982) and McKenzie(1984)). Thus with present knowledge the models in which there is a continuum between high degree (15%) partial melts beneath the plume and smaller degree melts in its periphery and at greater depths seems a viable explanation for both the major and trace element data. A model summarising the thermal regimes thought to exist beneath an oceanic island is shown in Fig.6.14.

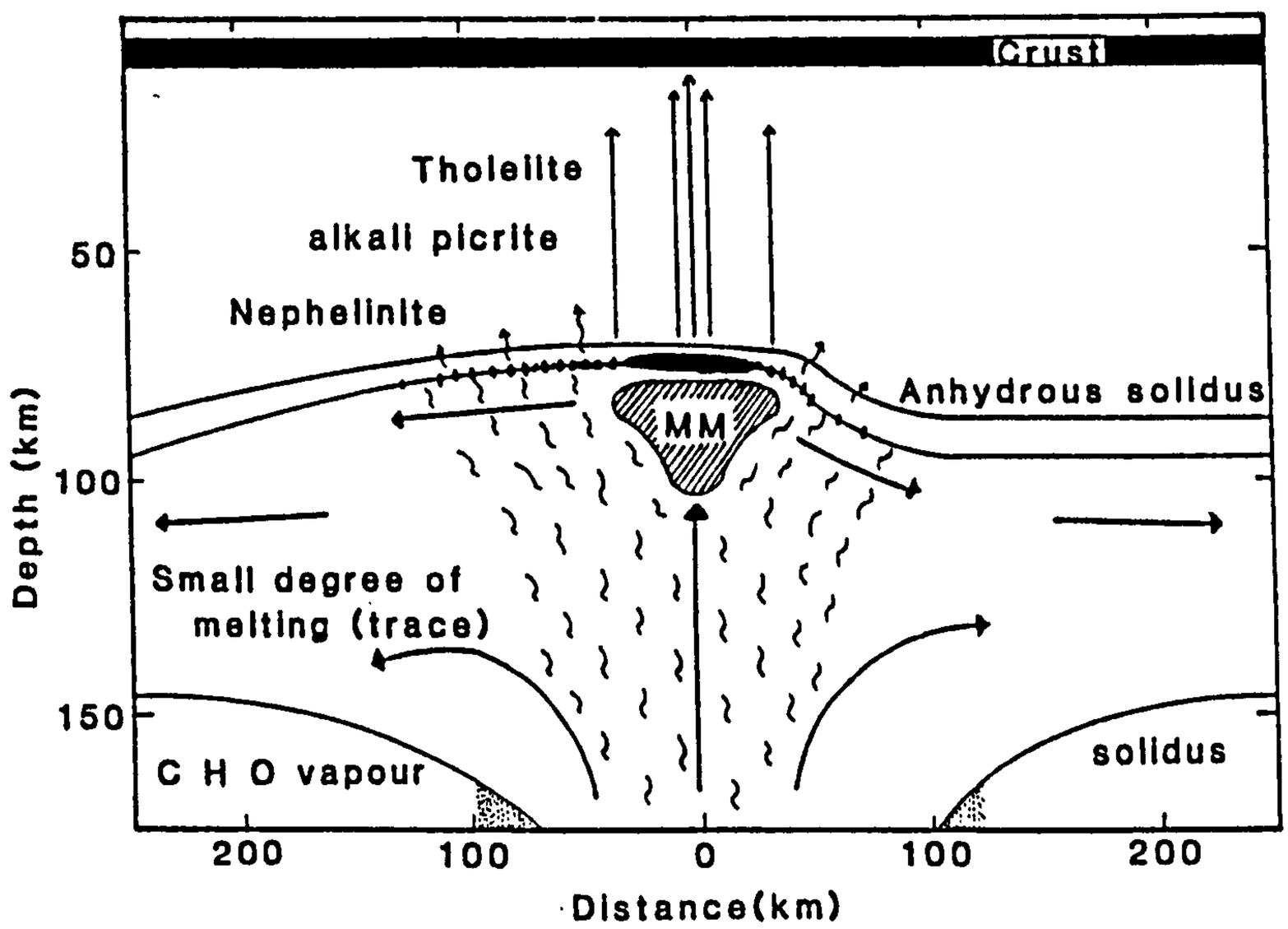

Fig.6.14. Cartoon illustrating the different melting regimes operative beneath an ocean island erupting OIB (after Wyllie(1988)). Material rising in a plume crosses a lower C-H-O lherzolite solidus causing production of small degree melts rich in volatiles. These melts influence the incompatible element budget of the erupted OIB. Larger degree melts (picrites) are produced in the volume MM which is governed by temperatures exceeding the anhydrous solidus. These melts dominate the major element budget of the OIB.

CHAPTER 7

TRACE ELEMENT AND ISOTOPE CONSTRAINTS ON SOURCE REGION CHARACTERISTICS :

7.1; Introduction;

This chapter presents a unified description of the source region characteristics of the St.Helena primary magmas in terms of both isotopes and trace elements. These are considered together because this is necessary for a cogent description of source region characteristics. The temporal variations evident in the concentrations of incompatible elements, corrected for the effects of crystal fractionation (Chapter 6) are used firstly to infer variations in the source region geochemistry over time. The Sr-Nd-Pb isotopic variations are then described and compared with the trace element variations to indicate changes in magma generation processes over time. A discussion section follows in which the implications of the data for source region characteristics and the modification of the primary melts as they ascend through the lithosphere are considered. The isotope data are described in relation to other OIB and MORB suites, but the significance of the isotopic difference between St.Helena and other OIB and MORB is deferred until Chapter 8. In Chapter 8 how the characteristics of the St.Helena magma source may have been acquired is discussed, whereas in the present chapter, the physical and chemical characteristics of the source region at the time of eruption of the magmas are discussed.

7.2; Incompatible trace element variations;

The alkali basalts and hawaiites of the SHRS have approximately parallel chondrite normalised REE distributions (Fig.6.5), but greater degrees of LREE enrichment (70 - 280X chondrite) relative to HREE (6 - 14X chondrite) occur. Although the patterns are subparallel, minor variations in degree of trace element enrichment do occur. For example in the NEBB basalts SC 37 and 38 are less enriched than the basalts of the NE(BB) which intrude them. Similarly SC 56 and SC 59 from the base of the NEMS have slightly less enriched trace element ratios than samples from higher in the NEMS.

It has been demonstrated in Chapter 6 that variation in LREE enrichment is, in part a consequence of crystal fractionation. If the trace element abundances for SHRS basalts and hawaiites, corrected for crystal fractionation using the procedure described in section 6.3 are considered a much smaller variation in the degree of trace element enrichment is evident (Fig.6.5, 6.6). Nevertheless, an increase in the degree of incompatible trace element enrichment in the primitive magmas is apparent through time in each of the volcanoes. For example an increase of REE slope is shown by increasing La/Yb and La/Sm in the NE volcano and in the SWMS-SWLI (Fig.7.1). The SWLS has a more complicated pattern with a discontinuity occurring at its top, apparently representing precursors to the SWMS. The small variations in trace element enrichment in primitive rocks can be explained either by mantle source heterogeneity or by variations in the degree of partial melting or a combination of the two. Source heterogeneity might be expected to produce mixing trends between an OIB component and a more depleted asthenospheric MORB source mantle composition. This is apparent from Fig 1.1 which shows that there are opportunities for the enriched melts from a plume to interact with its envelope and the lithosphere both of which are likely to be depleted if it is assumed that the MORB reservoir occurs above the OIB reservoir in the mantle. This is a widely held assumption because of the widespread occurrence of MORB at MOR, indicating a shallow source. This reasoning has given rise to the models of mantle dynamics in which the OIB source is overlain by the MORB source (Wasserburg and De Paolo(1979), Allegre et al.(1980), McKenzie and O'Nions(1983) and Thompson et al.(1984)). The consensus reached by these authors is disputed by Anderson(1981) who envisages enriched plume source material overlying source MORB in the upper mantle. This idea is unlikely given the paucity of enriched mantle xenoliths in comparison with MORB like xenoliths in OIB (Menzies and Hawkesworth(1987), section 2.3). The data of Schilling et al.(1985) and Hanan et al.(1986) provide evidence for MORB source acting as a widespread sink for point sources of OIB such as St.Helena. These data can only be explained by "point sources" of OIB penetrating a MORB source matrix from below and subsequently mixing with it. The upper part of the oceanic lithosphere is also likely to be of a depleted type composition given that it

Fig.7.1. Variation in degree of LREE enrichment through time in the SHRS expressed as:

(a) La/Yb versus stratigraphic height.

(b) La/Sm versus stratigraphic height.

Black dots are samples corrected for crystal fractionation using the procedure described in sections 6.2 and 6.3.

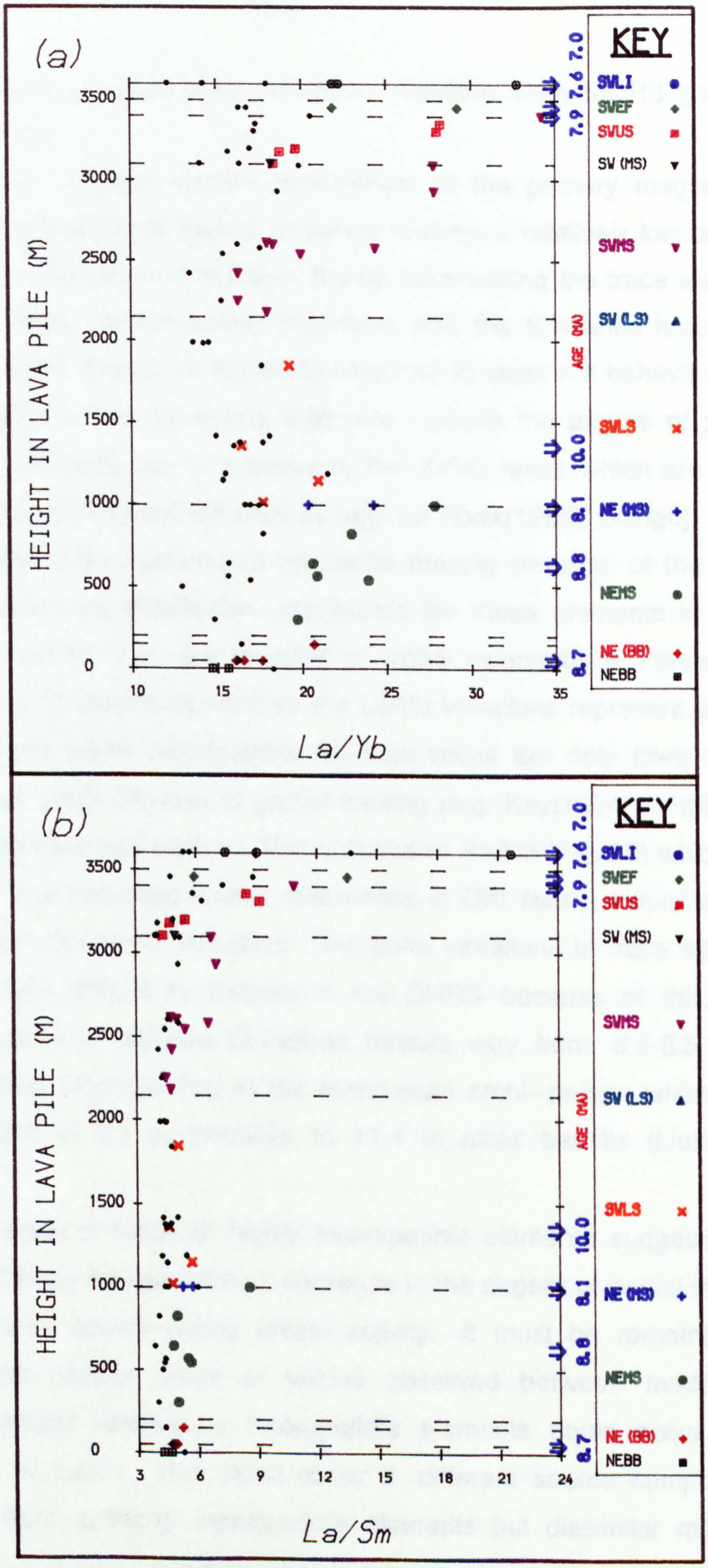
(a)
HEIGHT IN LAVA PILE (M)
3500
3000
2500
2000
1500
1000
500
0
10
15
20
25
30
35
La/Yb
7.9 7.6 7.0
10.0
8.1
8.8
8.7
AGE (Ma)
KEY
SVLI
SVEF
SVUS
SW (MS)
SVMS
SW (LS)
SVLS
NE (NS)
NEMS
NE (BB)
NEBB
(b)
HEIGHT IN LAVA PILE (M)
3500
3000
2500
2000
1500
1000
500
0
3
6
9
12
15
18
21
24
La/Sm
7.9 7.6 7.0
10.0
8.1
8.8
8.7
AGE (Ma)
KEY
SVLI
SVEF
SVUS
SW (MS)
SVMS
SW (LS)
SVLS
NE (NS)
NEMS
NE (BB)
NEBB

represents the depleted harzburgitic residuum resulting from MORB genesis (e.g.Ringwood(1975)).

If the variation in trace element enrichment of the primary magmas is caused solely by differences in degree of partial melting, a relatively low degree of partial melting is necessary to achieve this by fractionating the trace element ratios (e.g. Kay(1984)). In comparing St.Helena with the S.Atlantic islands of Bouvet and Ascension Weaver et al.(1988) note that Zr does not behave as an incompatible element in the St.Helena volcanics. Hence the degree of partial melting may be sufficiently low to fractionate the Zr/Nb ratios which are often used to characterise OIB source differences (e.g. Le Roex(1985), Gough). Thus La/Yb is also likely to be fractionated by partial melting because of the large difference in mineral-melt distribution coefficients for these elements in likely mantle phases (Fig.6.1). The use of ratios of highly incompatible elements is therefore necessary to determine whether the La/Yb variations represent source differences, because highly incompatible element ratios are only likely to be fractionated at very small degrees of partial melting (e.g. Kay(1984)). Ratios of highly incompatible elements such as Th/Ta, Ba/La or Ba/Nb (Fig.5.5) which are commonly used to demonstrate source differences in OIB suites, exhibit a very limited range in the St.Helena volcanics. Temporal variations in trace element enrichment are very difficult to discern in the SHRS because of this. For example Ba/La ratios in primitive St.Helena basalts vary from 6.5-8.5 when compared to basalts from Ua Pou in the Marquesas archi-pelago which vary from a Ba/La ratio of 3.1 in tholeiites to 11.4 in alkali basalts (Liotard et al.(1986)).

The small range in ratios of highly incompatible elements suggests that increases in La/Yb may be caused by a decrease in the degree of partial melting of an homogeneous source during shield activity. It must be remembered, however, that the greater range of values observed between moderately incompatible elements relative to incompatible elements could occur at a constant degree of fusion. This could occur if different source components contain similar ratios of highly incompatible elements but dissimilar ratios of moderate to slightly incompatible elements. In this case interactions between the components would be very difficult to distinguish using highly incompatible

elements. There is a likelihood that this effect is important in St.Helena magmatism as it is known from comparative studies of S.Atlantic OIB suites (Weaver et al.(1987) that St.Helena is depleted in highly incompatible LIL elements relative to other S.Atlantic OIB. Thus, if mixing is occurring between an OIB component and a depleted component with similar ratios of highly incompatible elements (e.g. St.Helena Ba/Nb = 5-6, N-MORB =4-5) then it cannot be easily discerned by use of ratios of these elements, especially if the depleted component is more akin to E-MORB. Fig.7.2 shows spidergrams of S.Atlantic OIB analysed by Weaver et al.(1987) normalised to N-MORB. This representation is useful for discerning which incompatible element ratios may be readily used to distinguish between OIB and MORB. It is evident that between the elements Y to Ta element abundance compared to MORB vary between 2 and 20, hence ratios such as La/Yb are likely to exhibit relatively large variations between OIB and MORB and be useful in illustrating mixing between the two.

It is also important to remember that in addition to the variations in the magnitude of the element ratios between the two components, the absolute abundance of elements in the two components also determines how clearly mixing is evident (Langmuir et al.(1978), Schilling et al.(1985)). Thus although a large difference in La/Yb between MORB and St.Helena is apparent on Fig.7.2, the La content in MORB is much lower than that for St.Helena so that there is not a direct correspondence between the proportion of depleted material in the mixture and difference in ratios between the components. This effect becomes more marked with the highly incompatible elements (large difference in absolute abundance compared to moderately incompatible elements).

It is apparent from Fig.7.2 that the ratios of highly incompatible elements in MORB and St.Helena are similar apart from K. This indicates that ratios of incompatible elements involving K offer the greatest prospect for deducing source characteristics. Fig.7.3a and b show a comparison of K/Nb and uncorrected La/Yb, the latter is used to emphasise the difference between the two ratios. It is evident that K is behaving more compatibly than elements that are normally considered to be more compatible than K. This is apparent because samples that have the lowest K/Nb also have the highest La/Yb. For example, 237 and 238 at the top of the SWLS have high values of K/Nb at low

Fig.7.2. Spidergrams of primitive (>5% MgO) S.Atlantic basalts normalised to N-MORB (Sun,1980). These basalts are shown normalised to chondrite in Fig.4.12. Data from Weaver et al.(1988).

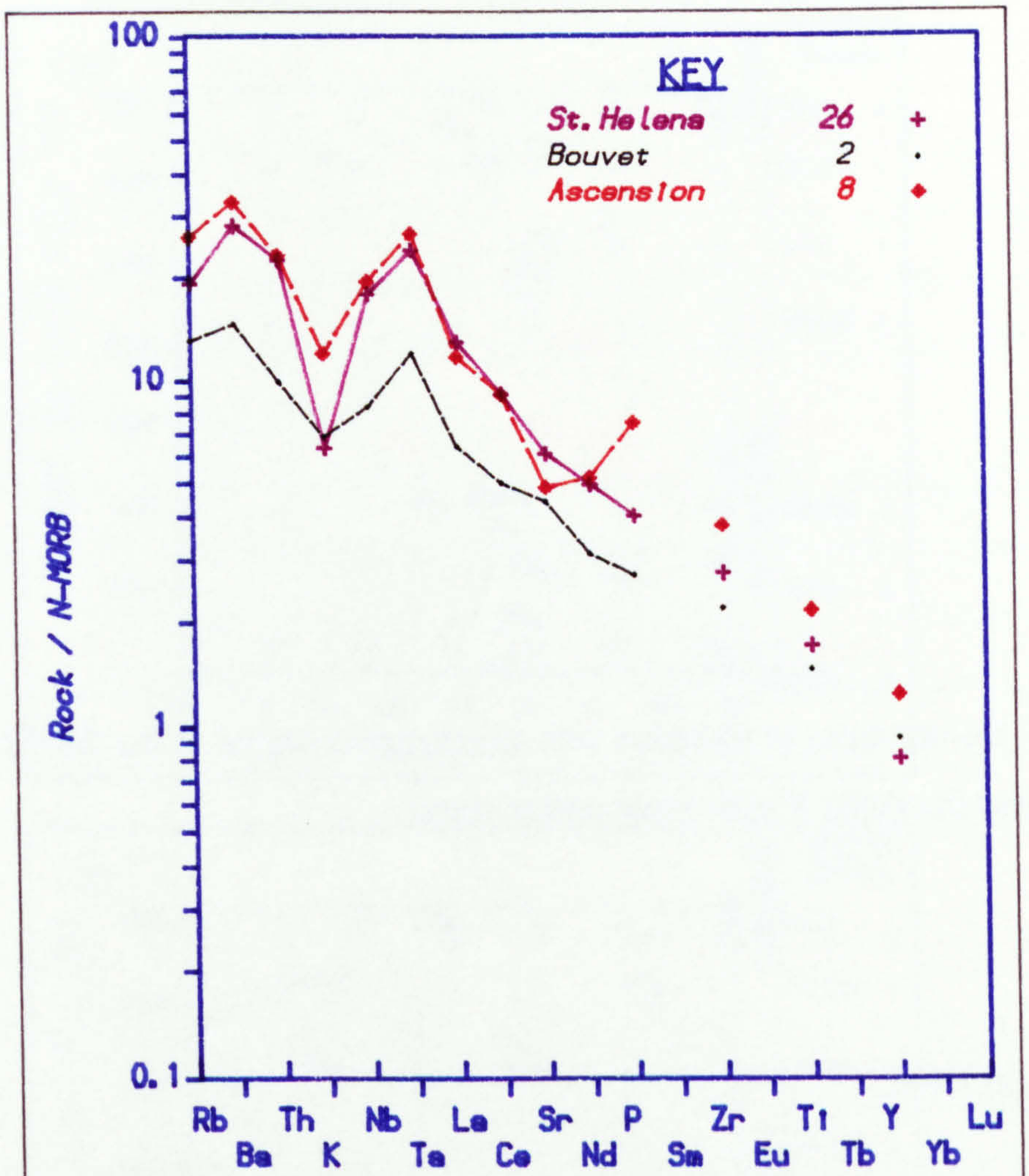
100
10
1
0.1
Rock / N-MORB
KEY
St. Helena 26
Bouvet 2
Ascension 8
Rb Th Nb La Sr P Zr Ti Y Lu
Ba K Ta Ce Nd Sm Eu Tb Yb

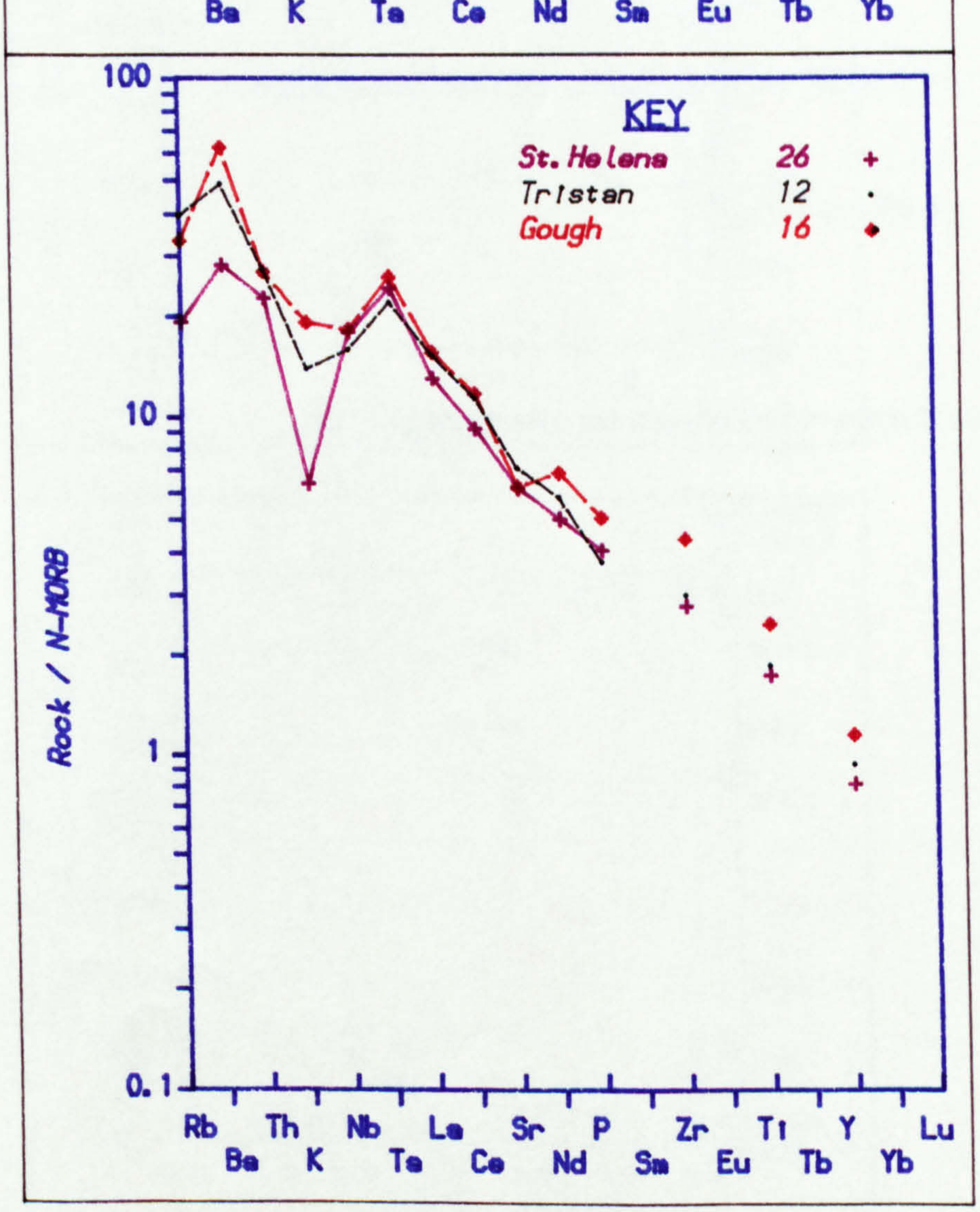
100
10
1
0.1
Rock / N-MORB
KEY
St. Helena 26
Tristan 12
Gough 16
Rb Th Nb La Sr P Zr Ti Y Lu
Ba K Ta Ce Nd Sm Eu Tb Yb

Fig.7.3. Comparison of variation with stratigraphic height in the SHRS for a geochemical parameter involving K with other parameters:

(a) K/Nb.

(b) La/Yb (uncorrected for crystal fractionation).

(c) $^{207}Pb/^{204}Pb$.

Samples numbers are shown for references in text.

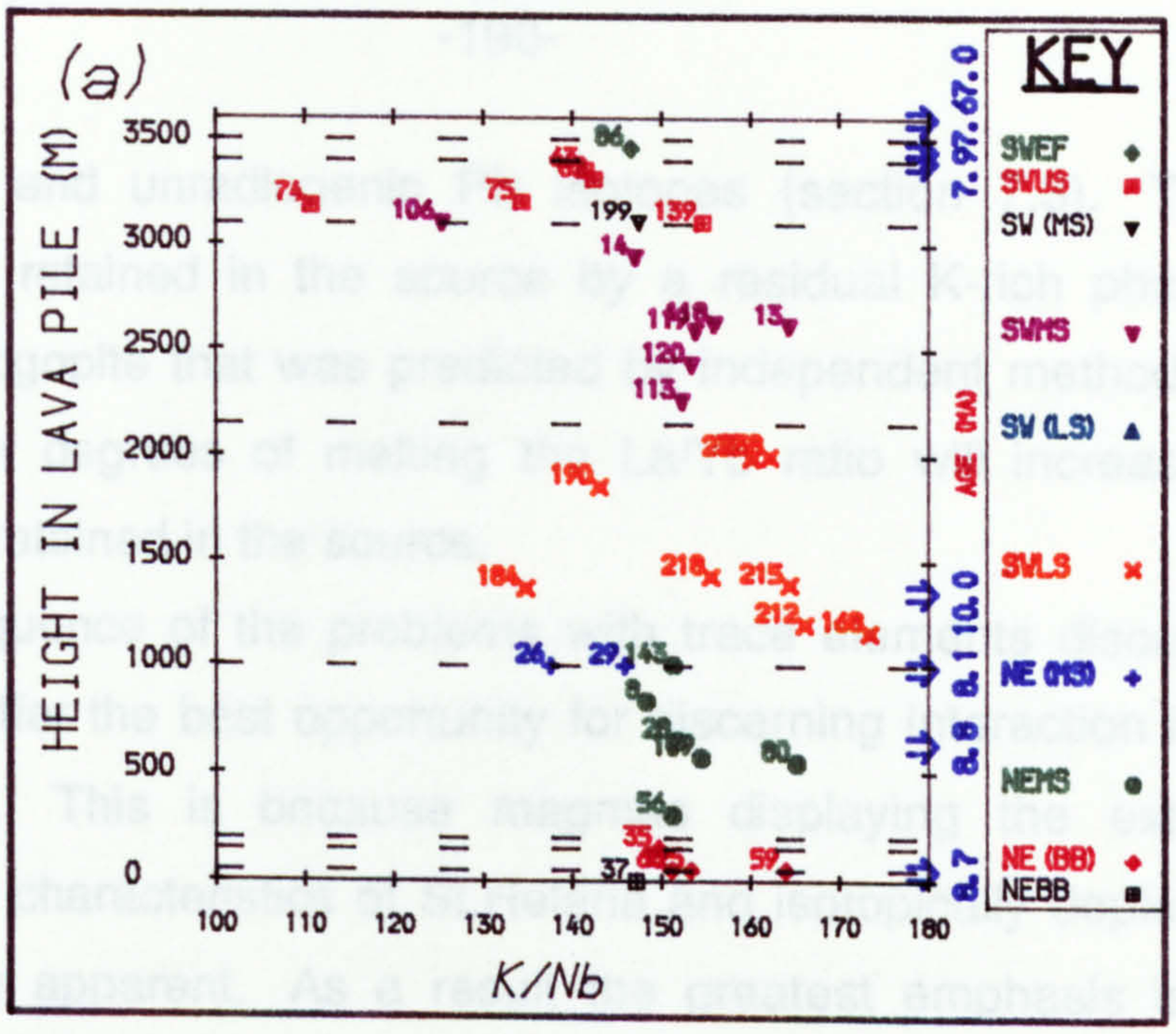
(a)
HEIGHT IN LAVA PILE (M)
3500
3000
2500
2000
1500
1000
500
0
100
110
120
130
140
150
160
170
180
K/Nb
KEY
SVEF
SVUS
SW (MS)
SVMS
SW (LS)
SVLS
NE (BB)
NEBB
NEMS
AGE (MA)
7.97.67.0
8.1 10.0
8.8
8.7

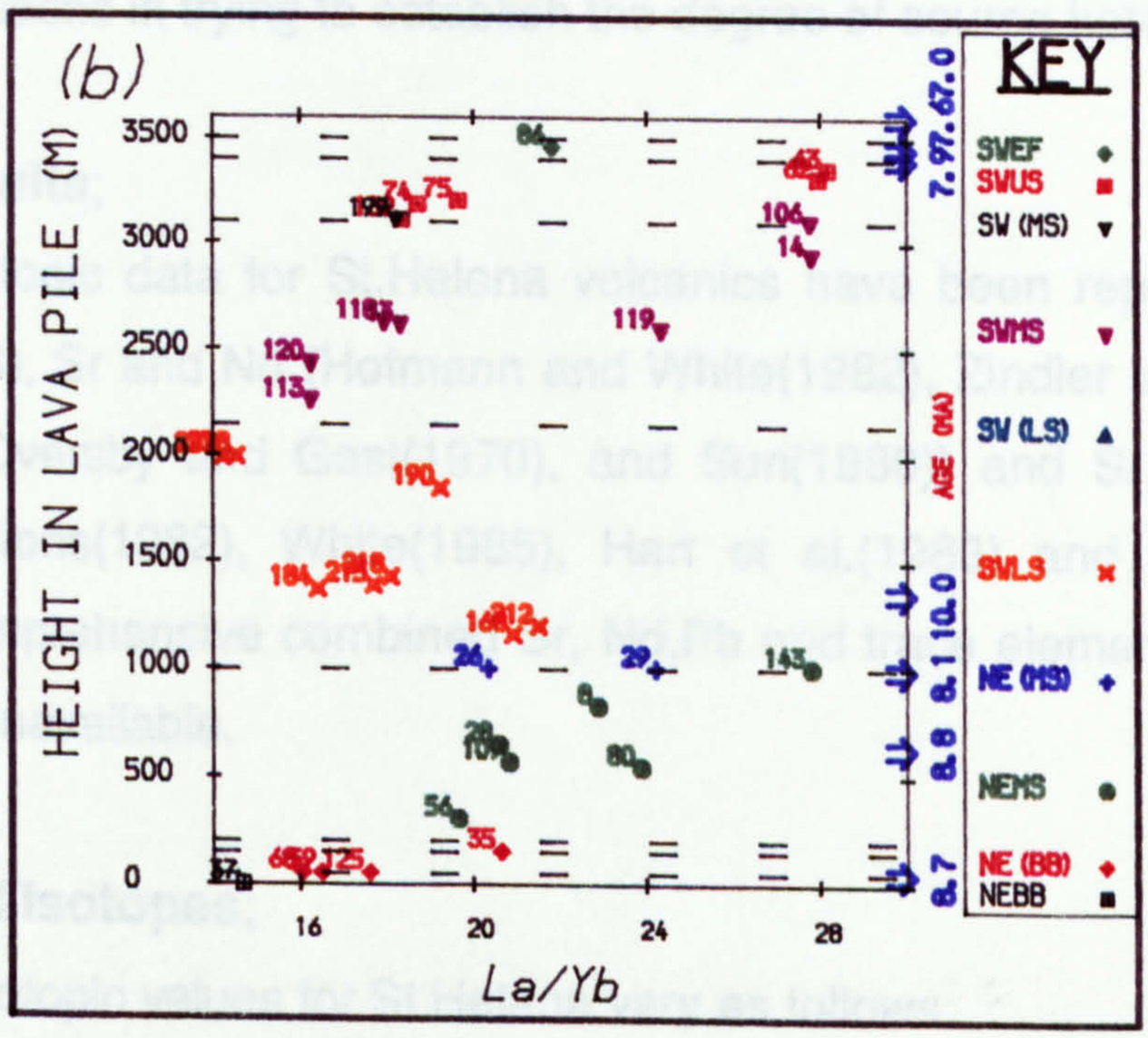
(b)
HEIGHT IN LAVA PILE (M)
3500
3000
2500
2000
1500
1000
500
0
16
20
24
28
La/Yb
KEY
SVEF
SVUS
SW (MS)
SVMS
SW (LS)
SVLS
NE (BB)
NEBB
NEMS
AGE (MA)
7.97.67.0
8.1 10.0
8.8
8.7

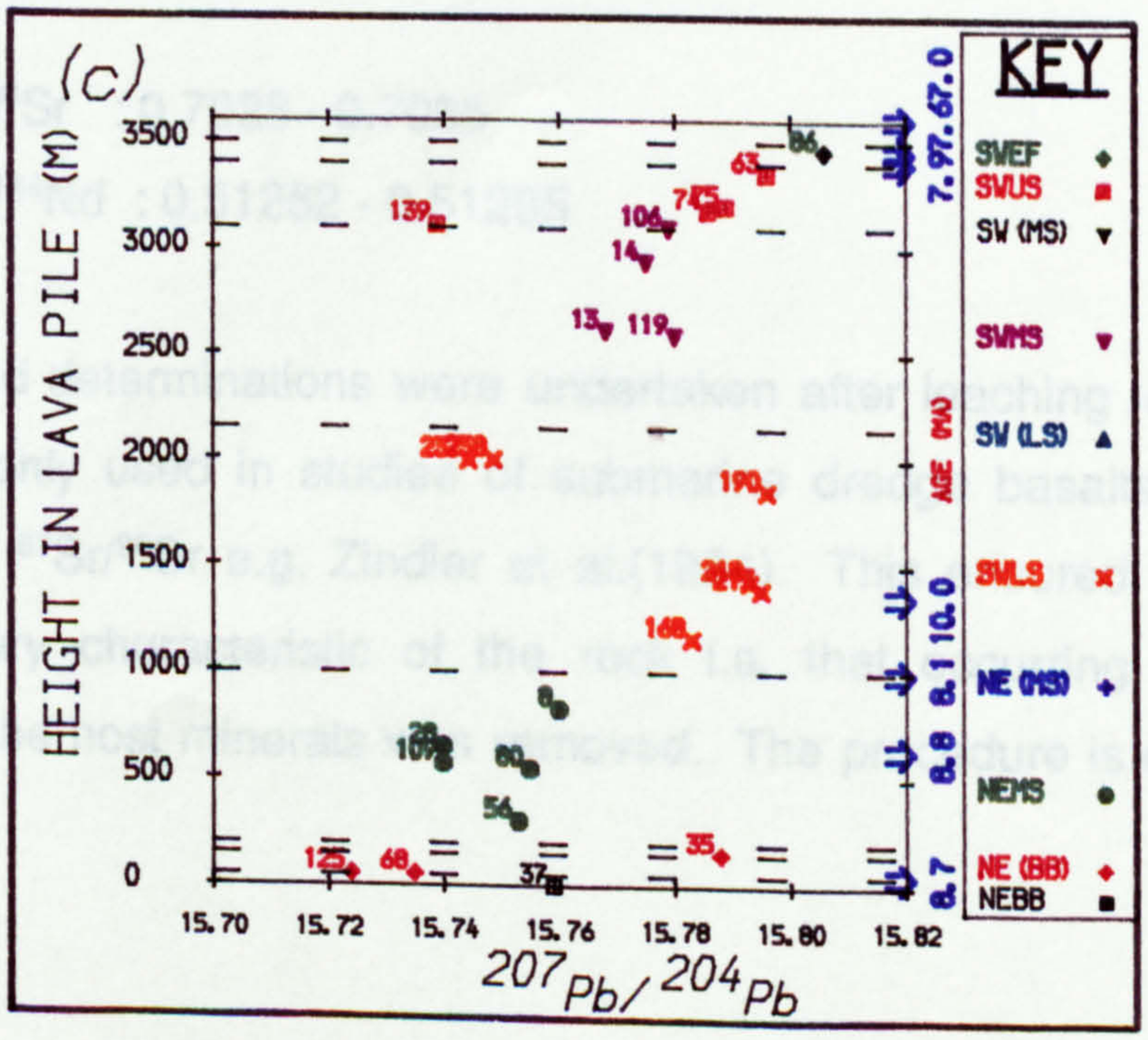
(c)
HEIGHT IN LAVA PILE (M)
3500
3000
2500
2000
1500
1000
500
0
15.70
15.72
15.74
15.76
15.78
15.80
15.82
207Pb/204Pb
KEY
SVEF
SVUS
SW (MS)
SVMS
SW (LS)
SVLS
NE (BB)
NEBB
NEMS
AGE (MA)
7.97.67.0
8.1 10.0
8.8
8.7

values of La/Yb and unradiogenic Pb isotopes (section 7.3). This can be explained if K is retained in the source by a residual K-rich phase such as amphibole or phlogopite that was predicted by independent methods in section 6.4. With smaller degrees of melting the La/Yb ratio will increase but K/Nb decrease as K is retained in the source.

As a consequence of the problems with trace elements discussed above isotopic studies offer the best opportunity for discerning interaction between the two components. This is because magmas displaying the extreme (end-member) isotopic characteristics of St.Helena and isotopically depleted material should be readily apparent. As a result the greatest emphasis is placed on isotopic determinations in trying to establish the degree of source heterogeneity.

7.3; Isotope results;

Previous isotopic data for St.Helena volcanics have been reported for Sr (Grant et al.(1976), Sr and Nd (Hofmann and White(1982), Zindler et al.(1982)), Pb(Gast(1969), Oversby and Gast(1970), and Sun(1980)) and Sr,Nd and Pb (Cohen and O'Nions(1982), White(1985), Hart et al.(1986) and Newsom et al.(1986)) but comprehensive combined Sr, Nd,Pb and trace element data have been previously unavailable.

7.3.1; Sr and Nd isotopes;

Sr and Nd isotopic values for St.Helena vary as follows:

$^{87}Sr/^{86}Sr$: 0.7028 - 0.7065

$^{143}Nd/^{144}Nd$: 0.51282 - 0.51295

All Sr and Nd determinations were undertaken after leaching in 6M Hcl, a procedure commonly used in studies of submarine dredge basalts to remove seawater derived $^{87}Sr/^{86}Sr$ e.g. Zindler et al.(1984). This ensured that Sr that was not a primary characteristic of the rock i.e. that occurring as a grain boundary film to the host minerals was removed. The procedure is described in Appendix B6.1

Fig.7.4. $^{87}Sr/^{86}Sr$ vs $^{143}Nd/^{144}Nd$ isotope diagram for the SHRS showing field of analyses relative to other OIB and MORB. Data sources referenced in Zindler and Hart(1986).

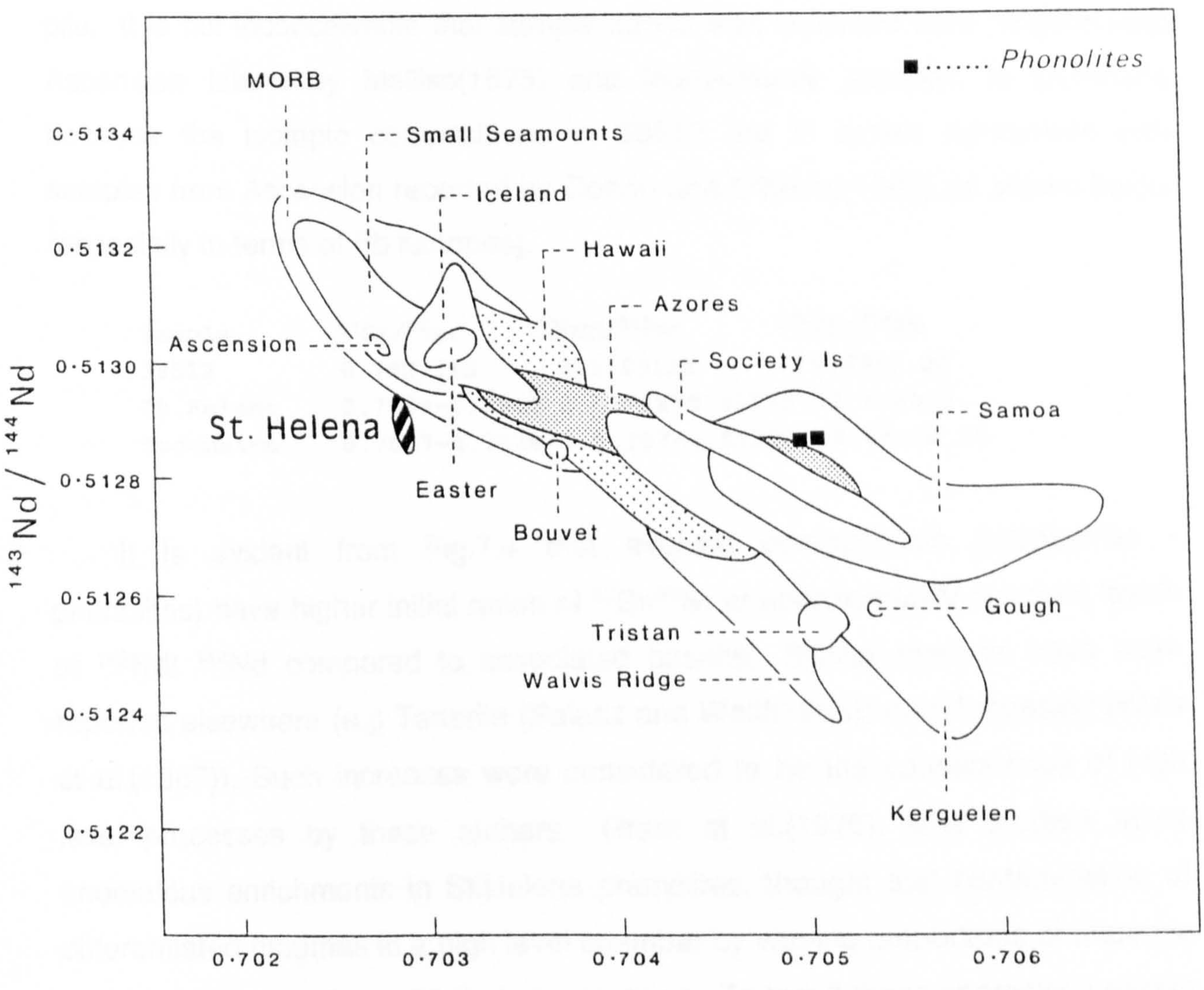
■ ..... Phonolites
MORB
Small Seamounts
Iceland
Hawaii
Azores
Ascension
Society Is
Samoa
St. Helena
Easter
Bouvet
Gough
Tristan
Walvis Ridge
Kerguelen
0·5134
0·5132
0·5130
0·5128
0·5126
0·5124
0·5122
143Nd / 144Nd
0·702
0·703
0·704
0·705
0·706
87Sr / 86Sr

Fig.7.4 shows the new Sr-Nd isotope data from this study relative to fields for other oceanic basalts. It is apparent that $^{143}Nd/^{144}Nd$ is more variable compared to the age corrected $^{87}Sr/^{86}Sr$ when considered in relation to the range of oceanic magmas. The new results are in good agreement with previously reported values. However isotopic compositions as extreme as those reported for trachyte 39512 in Cohen and O'Nions(1982) were not found ($^{206}Pb/^{204}Pb$ - 19.68±0.02,$^{87}Sr/^{86}Sr$ - 0.70277, $^{143}Nd/^{144}Nd$ - 0.51296±2). This discrepancy occurs despite the analysis of a range of compositions from throughout the lava pile. It is not inconceivable that sample 39512 was collected from neighbouring Ascension Island by Melliss(1875) and inadvertently ascribed to St.Helena because the isotopic compositions in 39512 are in closer agreement with samples from Ascension reported by Cohen and O'Nions(1982) as shown below (especially in terms of Pb isotopes).

Sample	$^{87}Sr/^{86}Sr$	$^{143}Nd/^{144}Nd$	$^{206}Pb/^{204}Pb$
39512	0.70277±3	0.51296±2	19.68±0.02
St.Helena	0.7028-0.7065	0.51282-0.51295	20.4-20.9
Ascension	0.7027-0.7028	0.51297-0.51305	19.43-19.56

It is evident from Fig.7.4 that evolved compositions (mugearites - phonolites) have higher initial ratios of $^{87}Sr/^{86}Sr$ at approximately constant levels of $^{143}Nd/^{144}Nd$ compared to associated basalts. Similar features have been reported elsewhere (e.g Tenerife (Palacz and Wolff(1988)) and Ascension (Weis et al.(1987)). Such increases were considered to be the consequence of high level processes by these authors. Grant et al.(1976), who studied these anomalous enrichments in St.Helena phonolites, thought that contamination of differentiated magmas in a high level chamber by varying proportions of meteoric and seawater was the most likely explanation. To test if these anomalous values are a primary magmatic characteristic, leaching experiments were conducted, the results of which are given in Table 7.1.

Table 7.1; Results of leaching experiments conducted on 5 phonolites.

The samples were leached by leaving in 6M Hcl for 15 minutes and then placing the beakers in an ultrasonic bath for 15 minutes. This is the routine leach. Two sigma errors are better than 0.000025.

Rock	*Unleached rock*	*Leached rock*	*Leachant*
SC 83	0.703585	0.703040	0.704369
SC 116	0.703308	0.703088	0.704891
SC 151	0.705479	0.704670	0.705876
SC 172	0.705484	0.704630	0.706140
SC 231	0.705759	0.705439	0.705876

It is apparent that the leachant tends to have a higher $^{87}Sr/^{86}Sr$ than the unleached rock and the leached rock. In addition the unleached rock has a higher value than the leached rock. The fact that the leachant possesses higher values of $^{87}Sr/^{86}Sr$ suggests that it is likely that Sr with excess radiogenic Sr has been added to the phonolites after their crystallisation. A detailed mass balance study of Rb and Sr in the phonolites is required to definitively determine this. This was not conducted as it is not of direct relevance to the source of the SHRS. A similar feature was noted by Palacz and Wolff(1988) in phonolitic tuffs from Tenerife. They thought this to be due to meteoric water entering a largely solidified magma chamber prior to eruption. This was inferred because separated feldspars did not possess the anomalously high $^{87}Sr/^{86}Sr$ registered in the whole rock. Thus it seems likely that in the St.Helena phonolites the enrichments in Sr are grain boundary effects caused subsequent to solidification of the magma chamber. As these differences have no bearing on source region geochemistry, these Sr isotopic enrichments are not discussed in detail and general descriptions of $^{87}Sr/^{86}Sr$ variations in the source region do not consider these rocks.

A weak negative correlation of isotopic ratios in less evolved rocks exists in Sr - Nd isotopic space (Fig.7.5). This trend occurs between samples with low $^{87}Sr/^{86}Sr$ and high $^{143}Nd/^{144}Nd$ and samples with higher $^{87}Sr/^{86}Sr$ and lower $^{143}Nd/^{144}Nd$. A poor correlation exists because of the small range in $^{143}Nd/^{144}Nd$ in relation to the errors. This is likely to be the main reason for a vertical array in Fig.7.4.

Fig.7.5. $^{87}Sr/^{86}Sr$ vs $^{143}Nd/^{144}Nd$ in fresh samples for the SHRS. Average error as shown. Error represented by symbol size for $^{87}Sr/^{86}Sr$.

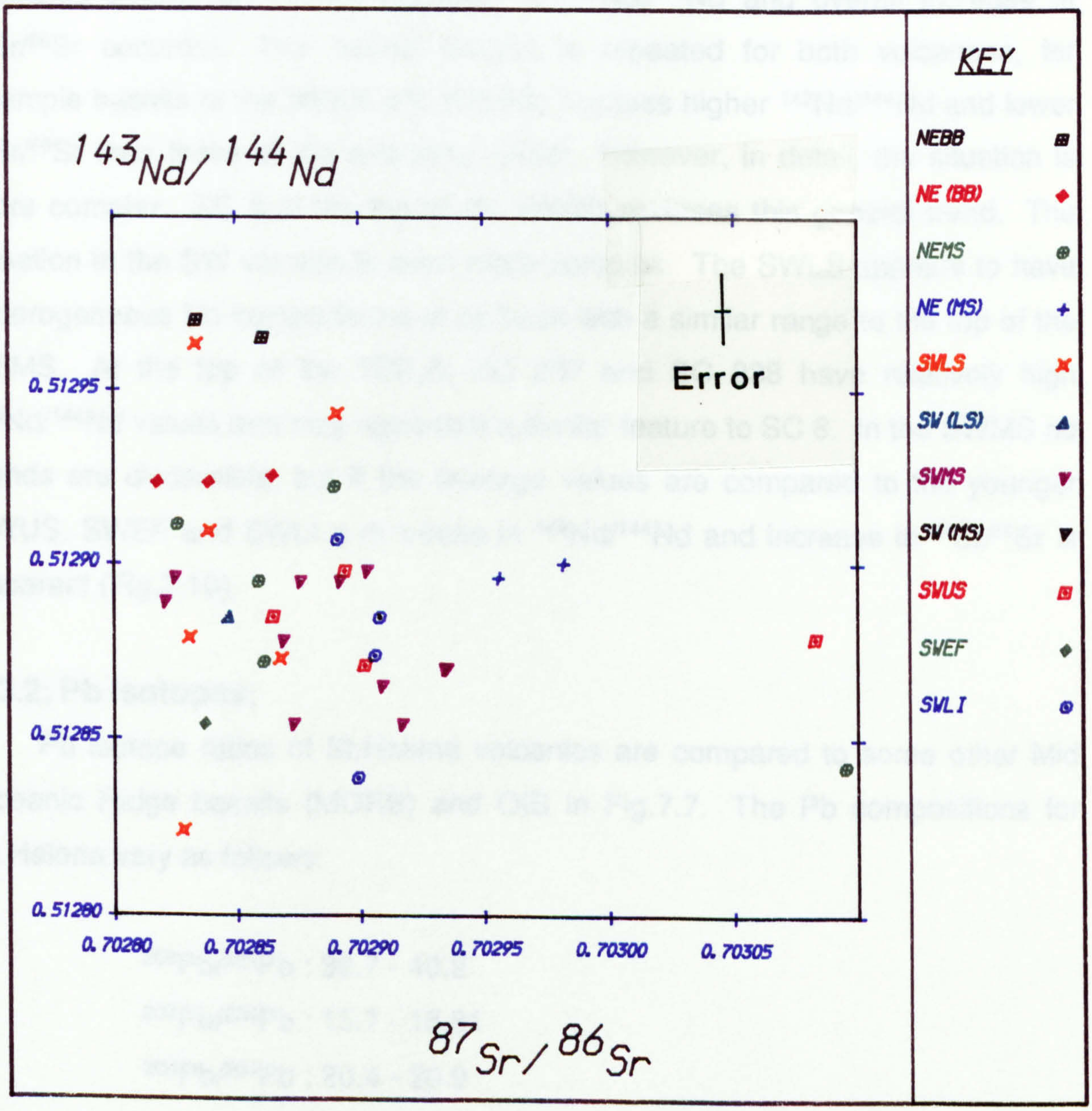
KEY
NEBB
NE (BB)
NEMS
NE (MS)
SWLS
SW (LS)
SWMS
SW (MS)
SWUS
SWEF
SWLI
143Nd/144Nd
Error
0.51295
0.51290
0.51285
0.51280
0.70280
0.70285
0.70290
0.70295
0.70300
0.70305
87Sr/86Sr

The temporal variations in Sr and Nd isotopic compositions of the SHRS are shown in Fig.7.6a and 7.6b respectively. It should be noted that the range of variations are small compared to the analytical error. It is evident that during subaerial activity an overall decrease in $^{143}Nd/^{144}Nd$ and overall increase in $^{87}Sr/^{86}Sr$ occurred. This overall pattern is repeated for both volcanoes, for example basalts of the NEBB and NE(BB) possess higher $^{143}Nd/^{144}Nd$ and lower $^{87}Sr/^{86}Sr$ than those of the overlying shield. However, in detail, the situation is more complex. SC 8 at the top of the NEMS reverses this general trend. The situation in the SW volcano is even more complex. The SWLS appears to have heterogeneous Nd compositions at its base with a similar range to the top of the NEMS. At the top of the SWLS, SC 237 and SC 238 have relatively high $^{143}Nd/^{144}Nd$ values and may represent a similar feature to SC 8. In the SWMS no trends are discernible, but if the average values are compared to the younger SWUS, SWEF and SWLI a decrease in $^{143}Nd/^{144}Nd$ and increase in $^{87}Sr/^{86}Sr$ is apparent (Fig.7.10).

7.3.2; Pb isotopes;

Pb isotope ratios of St.Helena volcanics are compared to some other Mid Oceanic Ridge basalts (MORB) and OIB in Fig.7.7. The Pb compositions for St.Helena vary as follows:

$^{208}Pb/^{204}Pb$: 39.7 - 40.2

$^{207}Pb/^{204}Pb$: 15.7 - 15.81

$^{206}Pb/^{204}Pb$: 20.4 - 20.9

A larger range is reported than that of Sun(1980), who mainly analysed rocks from the upper part of the SW volcano which were collected by Baker. It is evident that the St.Helena suite has extremely radiogenic Pb isotope compositions in comparison with other oceanic magmas. The reasons why St.Helena may possess such characteristics are considered in Chapter 8. It is also evident that good correlations exist between different Pb isotopic compositions (Fig.7.8). This may be ascribed to a number of processes that are described below. Temporal variations in Pb isotopes occur (Fig.7.9) - the least

Fig.7.6. Variation of Sr and Nd isotopes with height in the St.Helena lava pile:

(a) $^{87}Sr/^{86}Sr$.

(b) $^{143}Nd/^{144}Nd$.

Error

H

Error

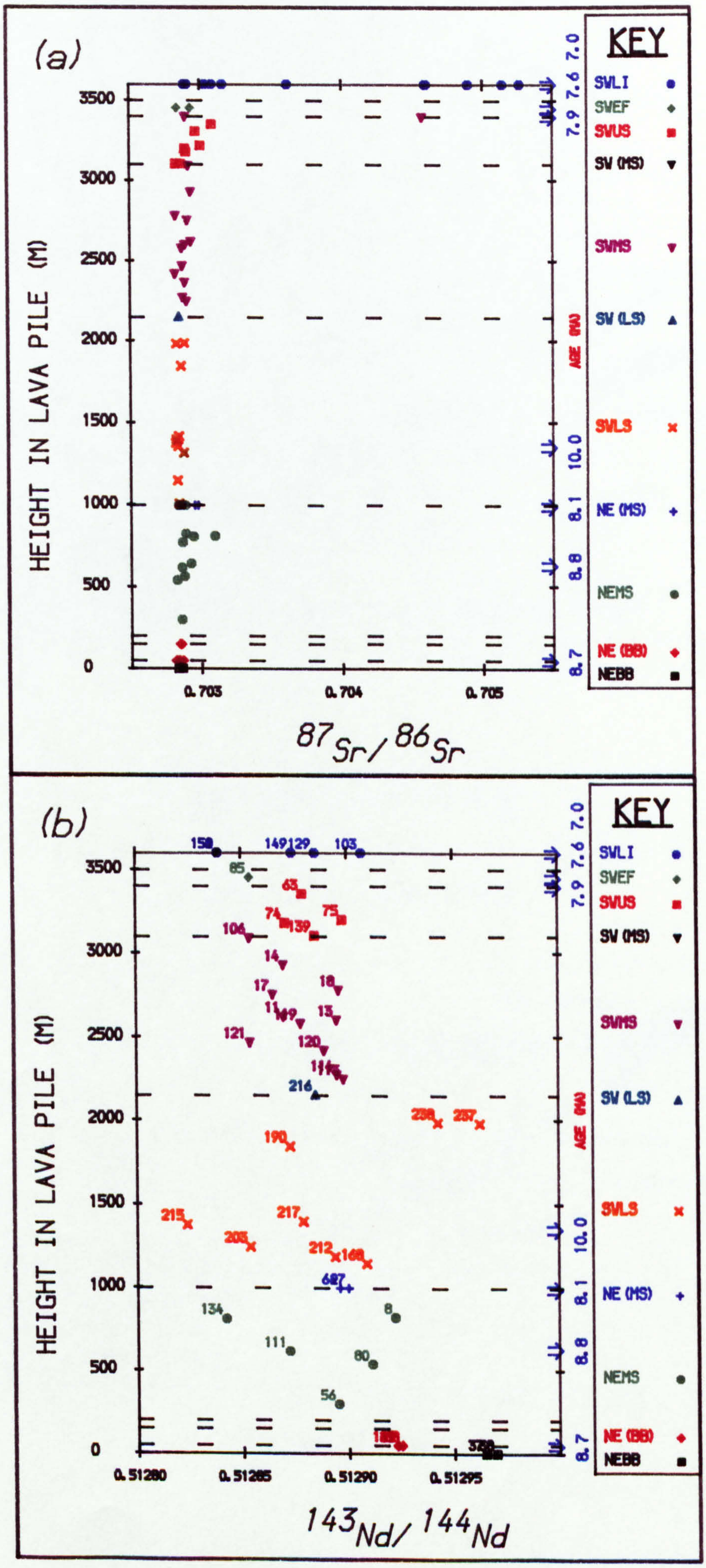
(a)
HEIGHT IN LAVA PILE (M)
3500
3000
2500
2000
1500
1000
500
0
0.703
0.704
0.705
87Sr/86Sr
7.9 7.6 7.0
10.0 8.1 8.8 8.7
AGE (MA)
KEY
SVLI
SVEF
SVUS
SV (MS)
SVMS
SV (LS)
SVLS
NE (MS)
NEMS
NE (BB)
NEBB
(b)
0.51280
0.51285
0.51290
0.51295
143Nd/144Nd

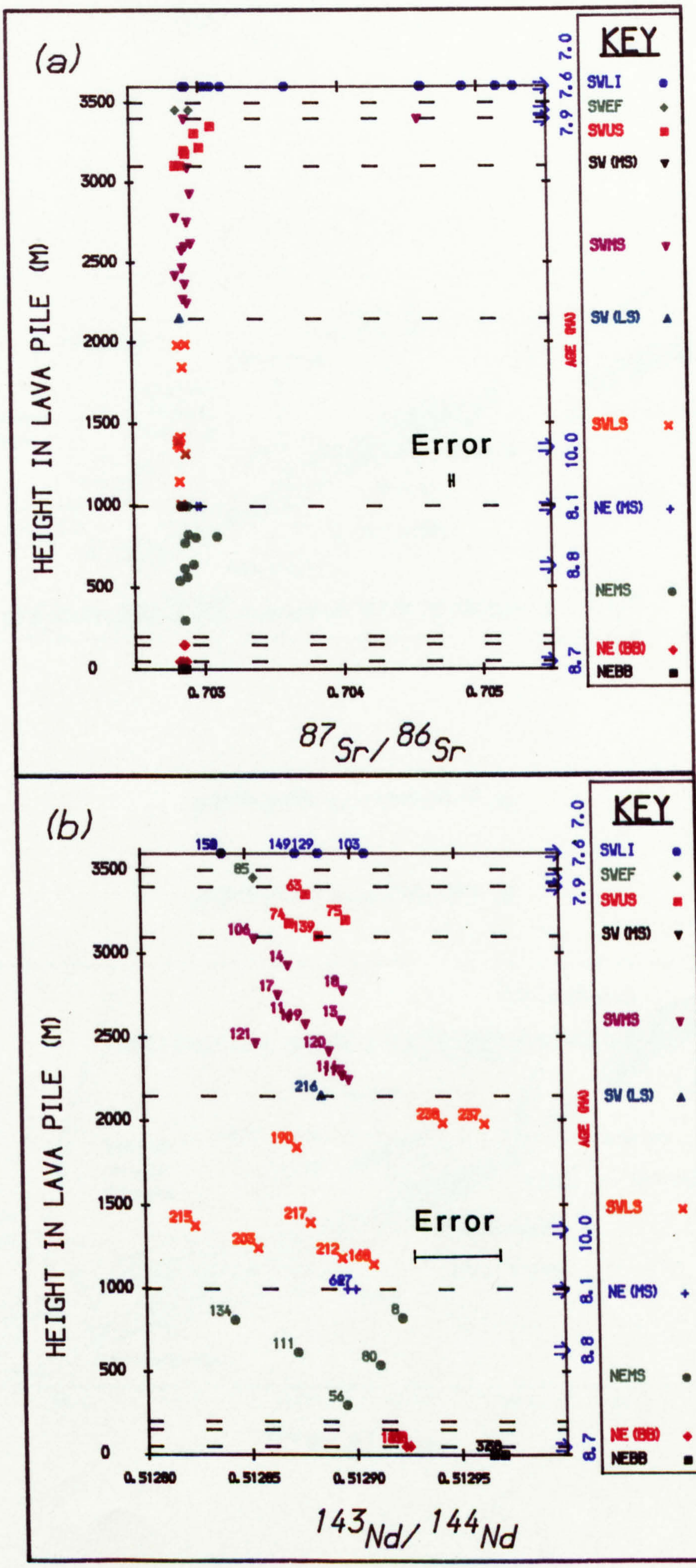
(a)
HEIGHT IN LAVA PILE (M)
3500
3000
2500
2000
1500
1000
500
0
0.703
0.704
0.705
87Sr/86Sr
Error
KEY
SVLI
SVEF
SVUS
SV (MS)
SVMS
SV (LS)
SVLS
NE (MS)
NEMS
NE (BB)
NEBB
AGE (MA)
7.9 7.6 7.0
10.0
8.1
8.8
8.7
(b)
158
149 129
103
85
63
74
139
75
106
14
17
18
11
13
121
120
216
256
257
190
215
217
205
212
168
87
134
8
111
80
56
0.51280
0.51285
0.51290
0.51295
143Nd/144Nd

Fig.7.7. Comparison of Pb isotopes in the SHRS relative to other OIB and MORB.

(a) $^{206}Pb/^{204}Pb$ vs $^{208}Pb/^{204}Pb$.

(b) $^{206}Pb/^{204}Pb$ vs $^{207}Pb/^{204}Pb$.

Data sources referenced in Zindler and Hart(1986).

(a)

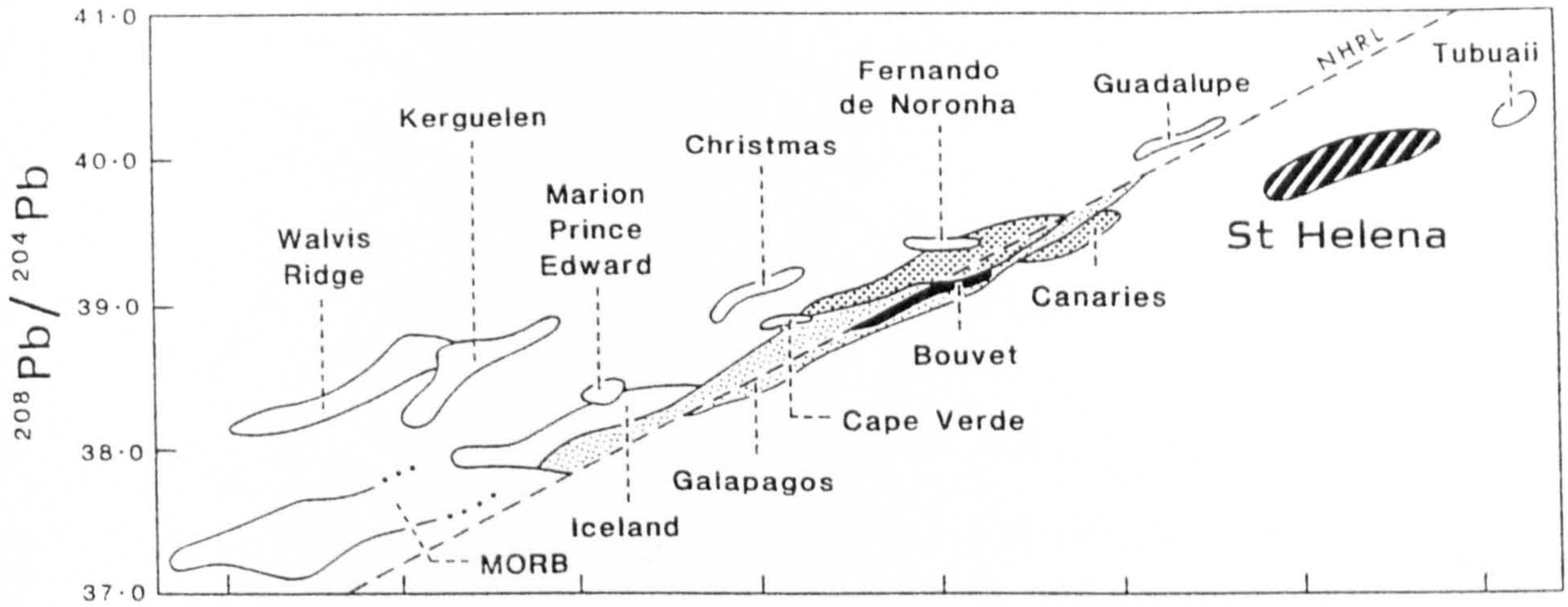
41·0
40·0
39·0
38·0
37·0
208Pb/204Pb
Kerguelen
Christmas
Fernando
de Noronha
Guadalupe
NHRL
Tubuaii
Marion
Prince
Edward
Walvis
Ridge
St Helena
Canaries
Bouvet
Cape Verde
Galapagos
Iceland
MORB

(b)

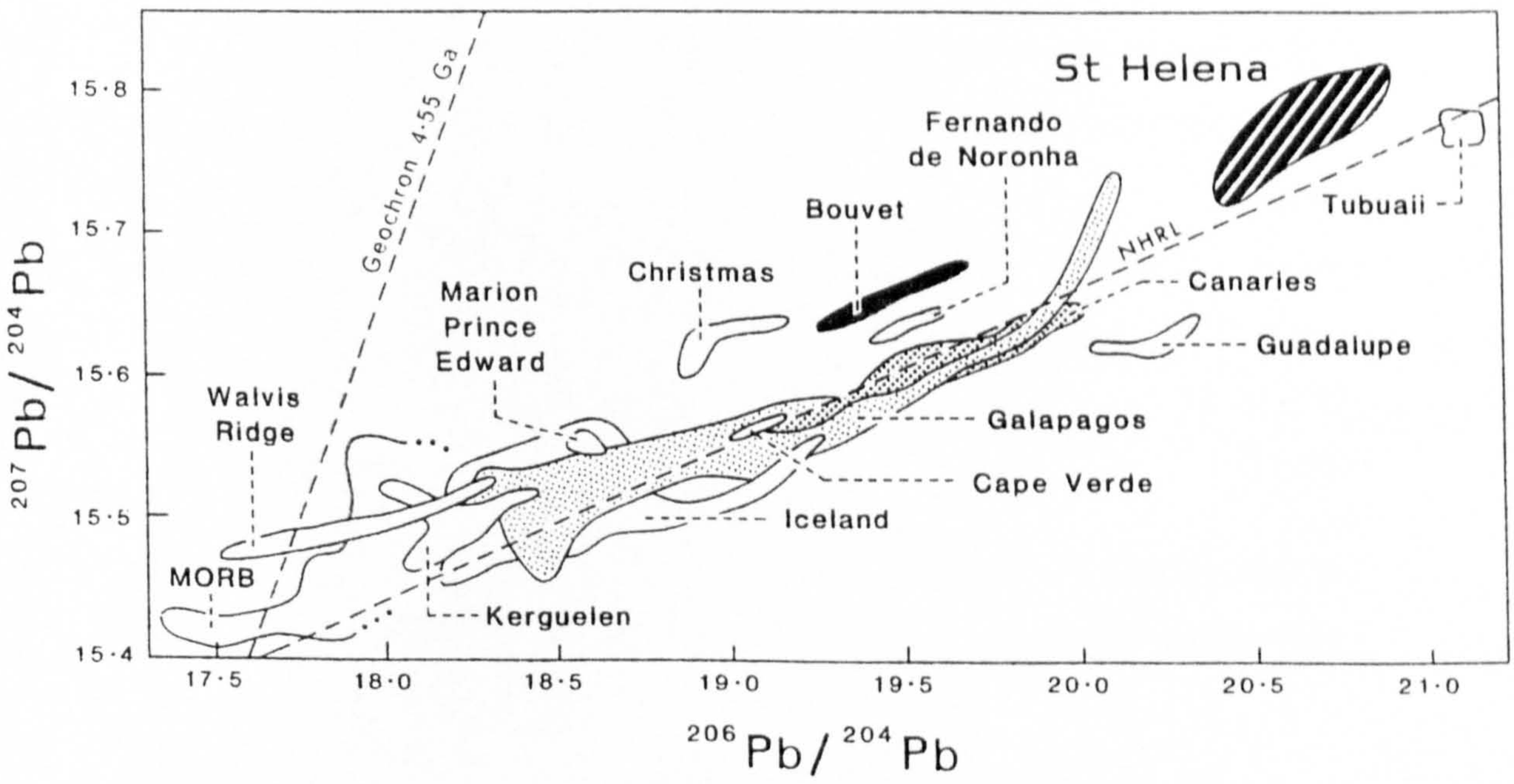
Geochron 4·55 Ga
St Helena
Fernando
de Noronha
Bouvet
Tubuaii
NHRL
Christmas
Canaries
Marion
Prince
Edward
Guadalupe
Walvis
Ridge
Galapagos
Cape Verde
Iceland
MORB
Kerguelen
15·8
15·7
15·6
15·5
15·4
207Pb/204Pb
17·5
18·0
18·5
19·0
19·5
20·0
20·5
21·0
206Pb/204Pb

Fig.7.8. Pb isotope correlations in the SHRS:

(a) $^{206}Pb/^{204}Pb$ vs $^{208}Pb/^{204}Pb$.

(b) $^{206}Pb/^{204}Pb$ vs $^{207}Pb/^{204}Pb$.

Regression analysis of the curves gives the following diagnostics:

(a) $^{206}Pb/^{204}Pb$(x) vs $^{208}Pb/^{204}Pb$(y)

All points: y= 0.7597x(±0.0481x) + 24.2731(±0.9941).

Correlation coefficient = 0.94

Points shown excluded: y = 0.7702x(±0.0337x) + 24.0552(±0.6960).

Correlation coefficient = 0.97

(b) $^{206}Pb/^{204}Pb$(x) vs $^{207}Pb/^{204}Pb$(y);

All points: y = 0.1525x(±0.0337x) + 12.6133(±0.4093)

Correlation coefficient = 0.81

Points shown excluded: y = 0.1594x(±0.0139x) + 12.471(±0.2874)

Correlation coefficient = 0.9023

By using well established techniques (e.g. Chase(1981)) applied to equations D1 to D4 the following characteristics are indicated for the fractionation event forming the "isochron":

(a) Age of separation event: 2.4±0.2 Ga.

(2.37 Ga for full data set, 2.45 if three points excluded).

(b) Primary mu (before fractionation) : 7.7. Secondary mu (in 2nd stage of Pb evolution) : 15.3

(c) Primary kappa : 5.2, Secondary kappa : 2.8.

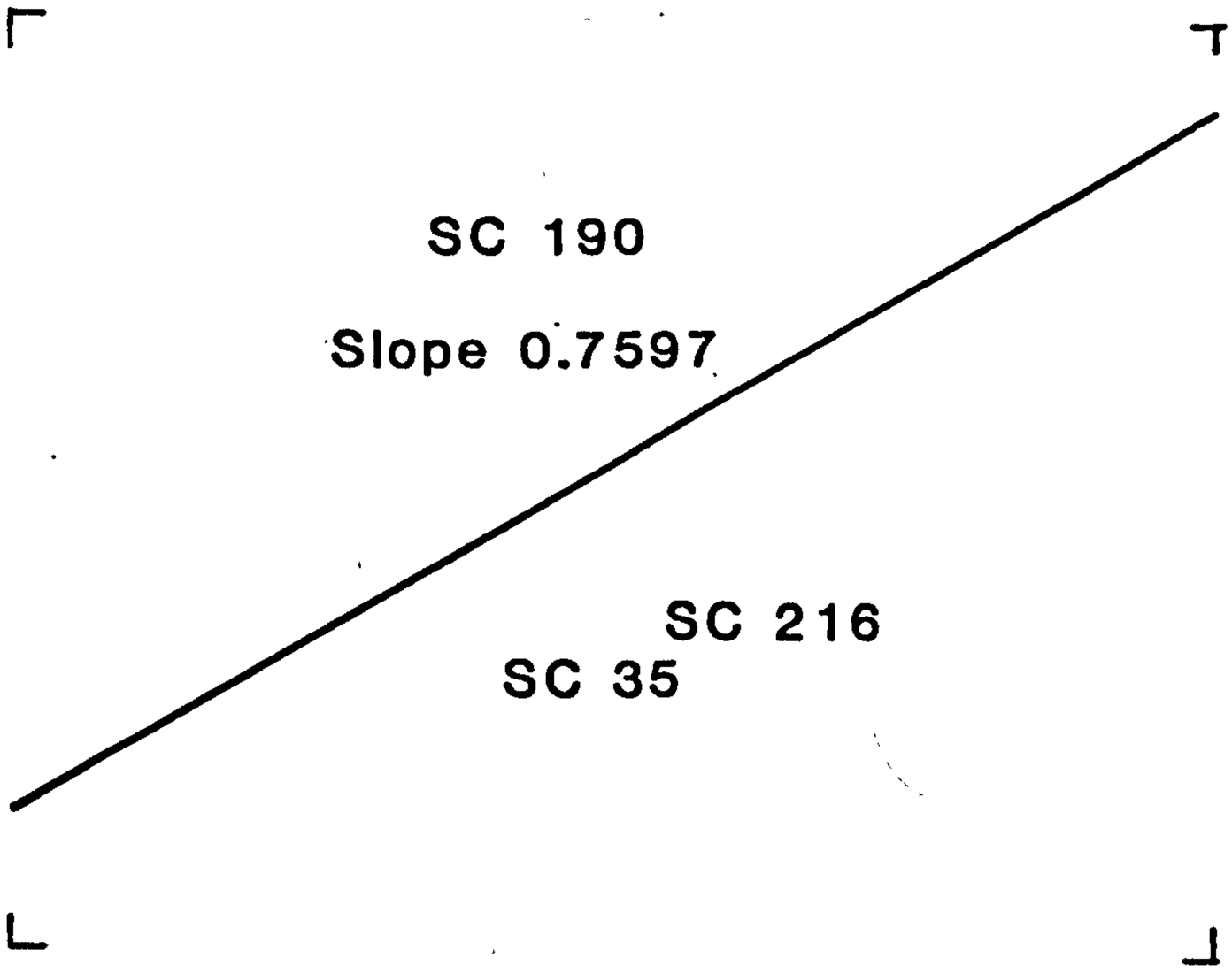
SC 190
Slope 0.7597
SC 216
SC 35

SC 190
SC 35
Slope 0.1525
SC 216

(a)

$^{208}Pb/^{204}Pb$

40.2
40.1
40.0
39.9
39.8
39.7

20.4 20.5 20.6 20.7 20.8 20.9

$^{206}Pb/^{204}Pb$

KEY

NEBB
NE (BB)
NEMS
NE (MS)
SWLS
SW (LS)
SWMS
SW (MS)
SWUS
SWEF
SWLI

(b)

$^{207}Pb/^{204}Pb$

15.82
15.80
15.78
15.76
15.74
15.72
15.70

20.4 20.5 20.6 20.7 20.8 20.9

$^{206}Pb/^{204}Pb$

KEY

NEBB
NE (BB)
NEMS
NE (MS)
SWLS
SW (LS)
SWMS
SW (MS)
SWUS
SWEF
SWLI

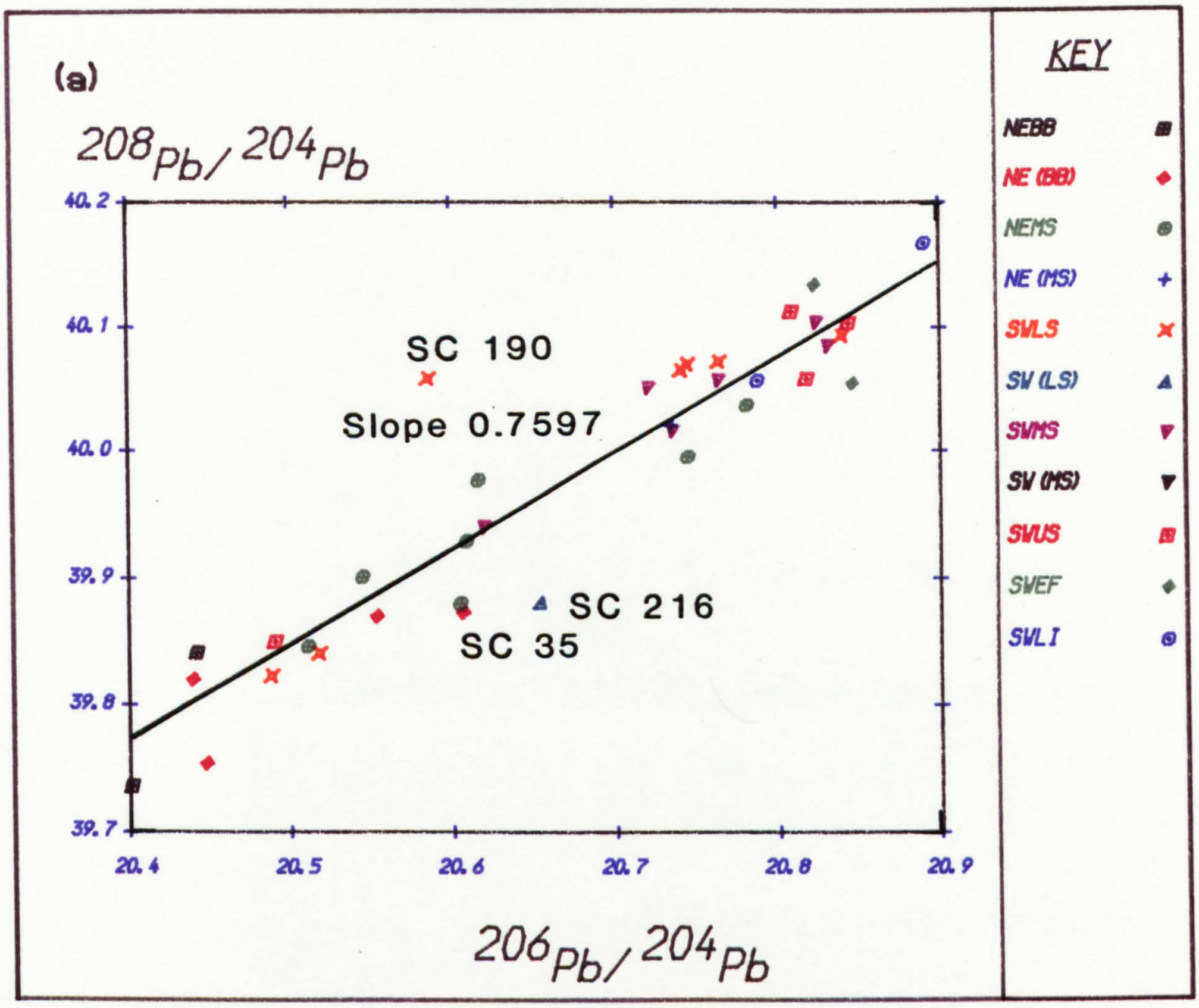
(a)
208Pb/204Pb
40.2
40.1
40.0
39.9
39.8
39.7
SC 190
Slope 0.7597
SC 216
SC 35
20.4
20.5
20.6
20.7
20.8
20.9
206Pb/204Pb
KEY
NEBB
NE (BB)
NEMS
NE (MS)
SWLS
SW (LS)
SWMS
SW (MS)
SWUS
SWEF
SWLI

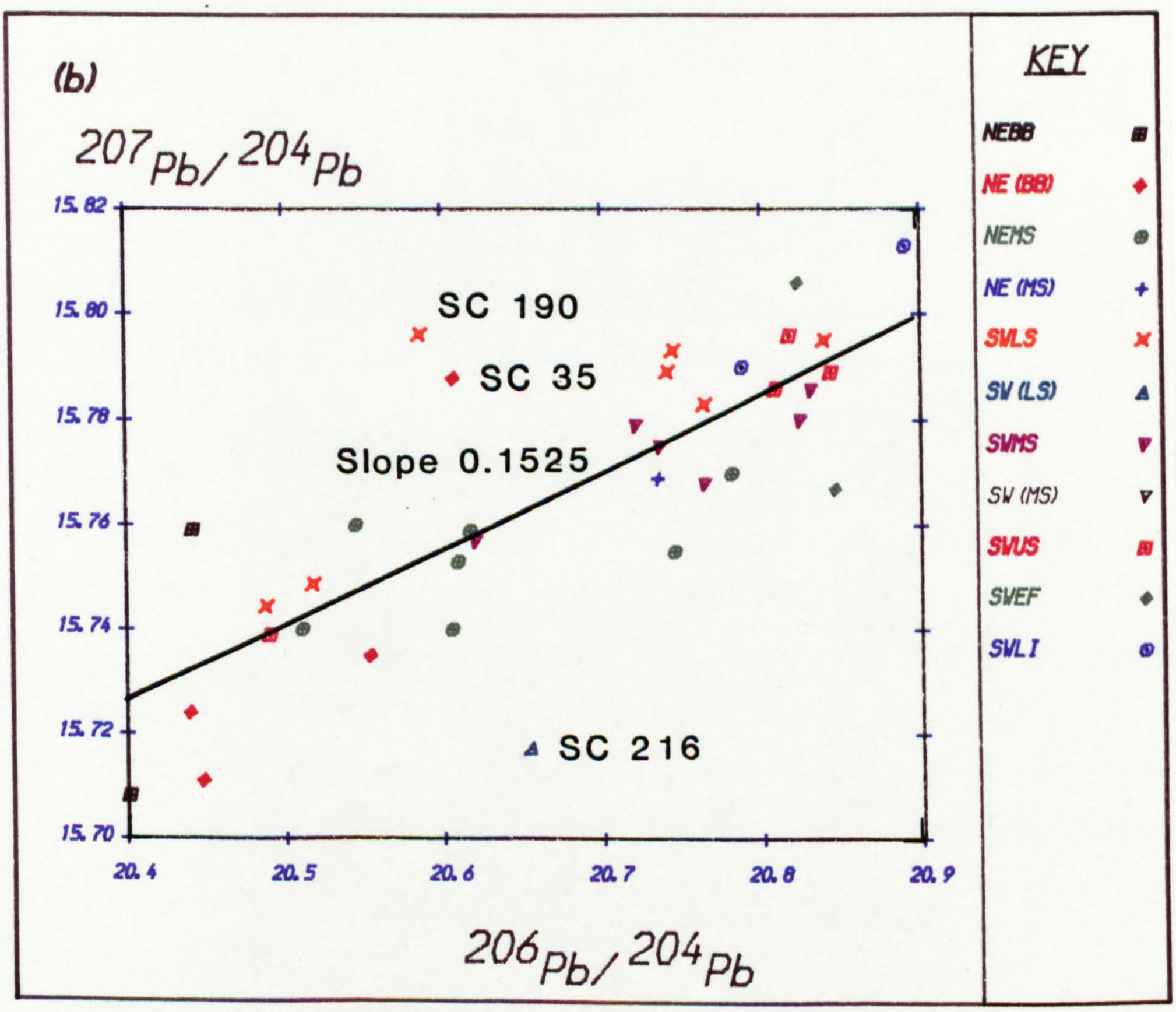
(b)
207Pb/204Pb
15.82
15.80
15.78
15.76
15.74
15.72
15.70
SC 190
SC 35
Slope 0.1525
SC 216
20.4
20.5
20.6
20.7
20.8
20.9
206Pb/204Pb
KEY
NEBB
NE (BB)
NEMS
NE (MS)
SWLS
SW (LS)
SWMS
SW (MS)
SWUS
SWEF
SWLI

Fig.7.9. Temporal variations in Pb isotopes in the SHRS:

(a) $^{208}Pb/^{204}Pb$ versus height in the lava pile.

(b) $^{207}Pb/^{204}Pb$ " "

(c) $^{206}Pb/^{204}Pb$ " "

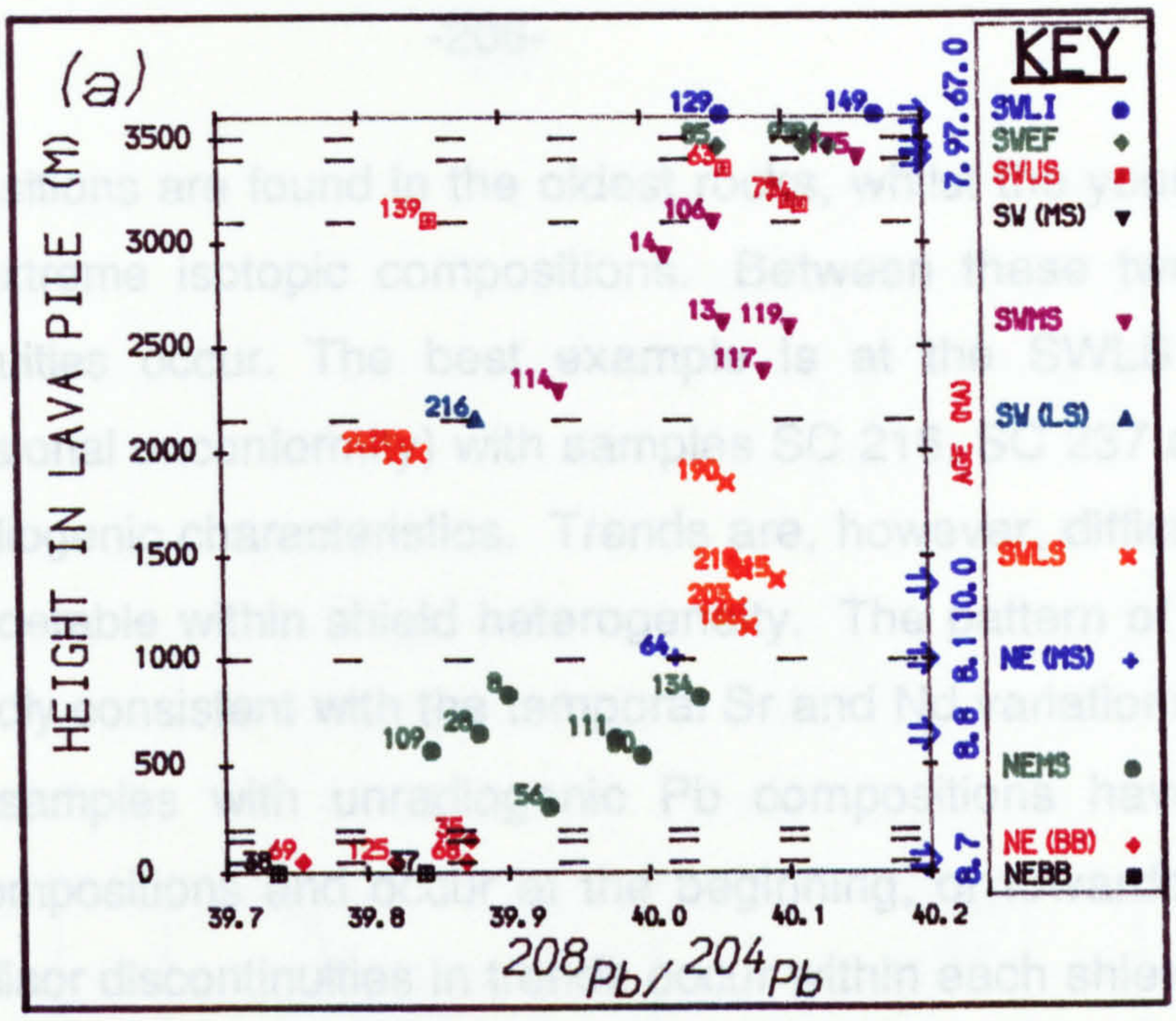
(a)
HEIGHT IN LAVA PILE (M)
3500
3000
2500
2000
1500
1000
500
0
39.7
39.8
39.9
40.0
40.1
40.2
208Pb/204Pb
7.9 7.6 7.0
AGE (MA)
10.0
8.8 8.1
8.7
KEY
SWLI
SWEF
SWUS
SW (MS)
SWMS
SW (LS)
SWLS
NE (MS)
NEMS
NE (BB)
NEBB

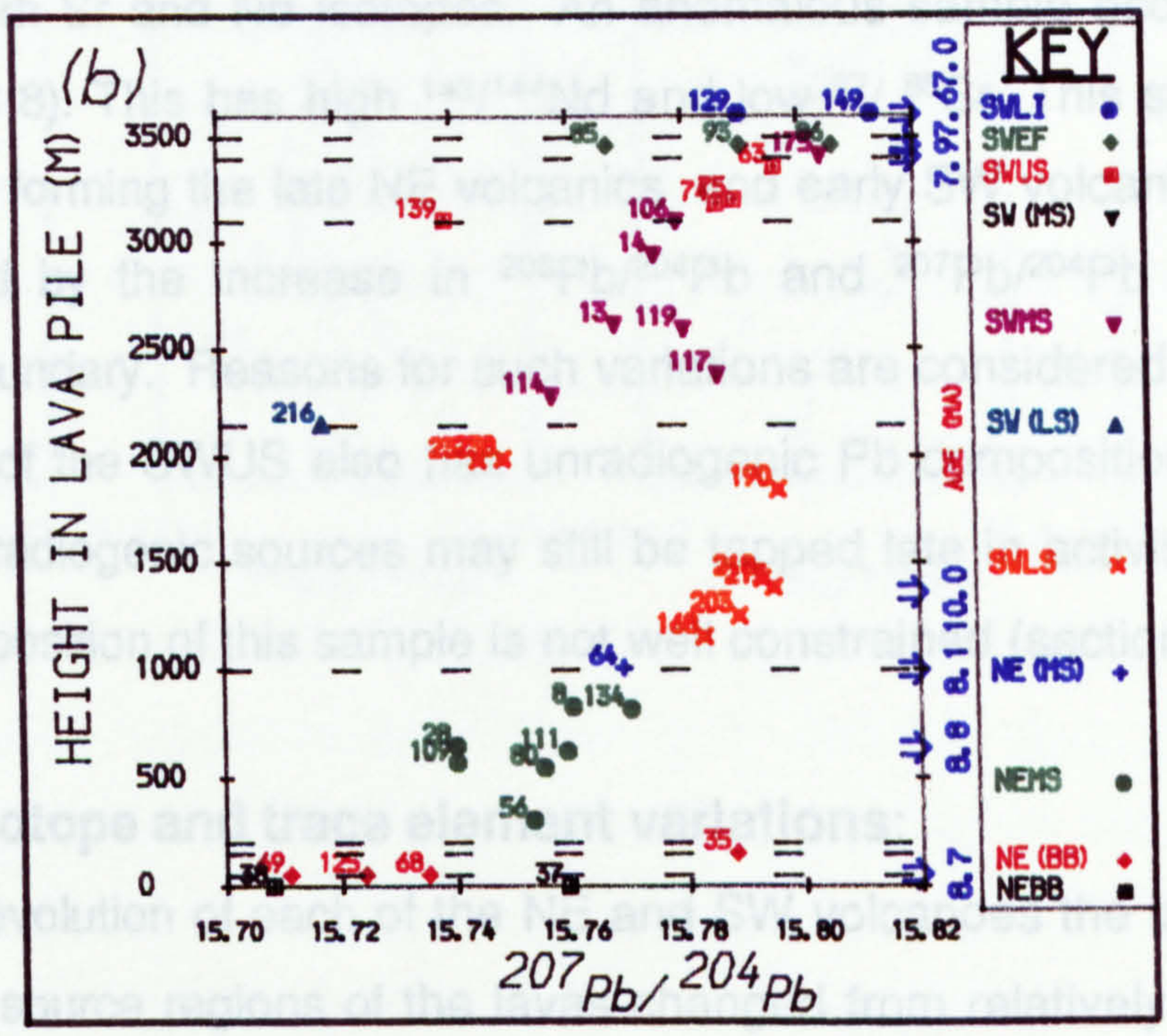
(b)
HEIGHT IN LAVA PILE (M)
3500
3000
2500
2000
1500
1000
500
0
15.70
15.72
15.74
15.76
15.78
15.80
15.82
207Pb/204Pb
7.9 7.6 7.0
AGE (MA)
10.0
8.8 8.1
8.7
KEY
SWLI
SWEF
SWUS
SW (MS)
SWMS
SW (LS)
SWLS
NE (MS)
NEMS
NE (BB)
NEBB

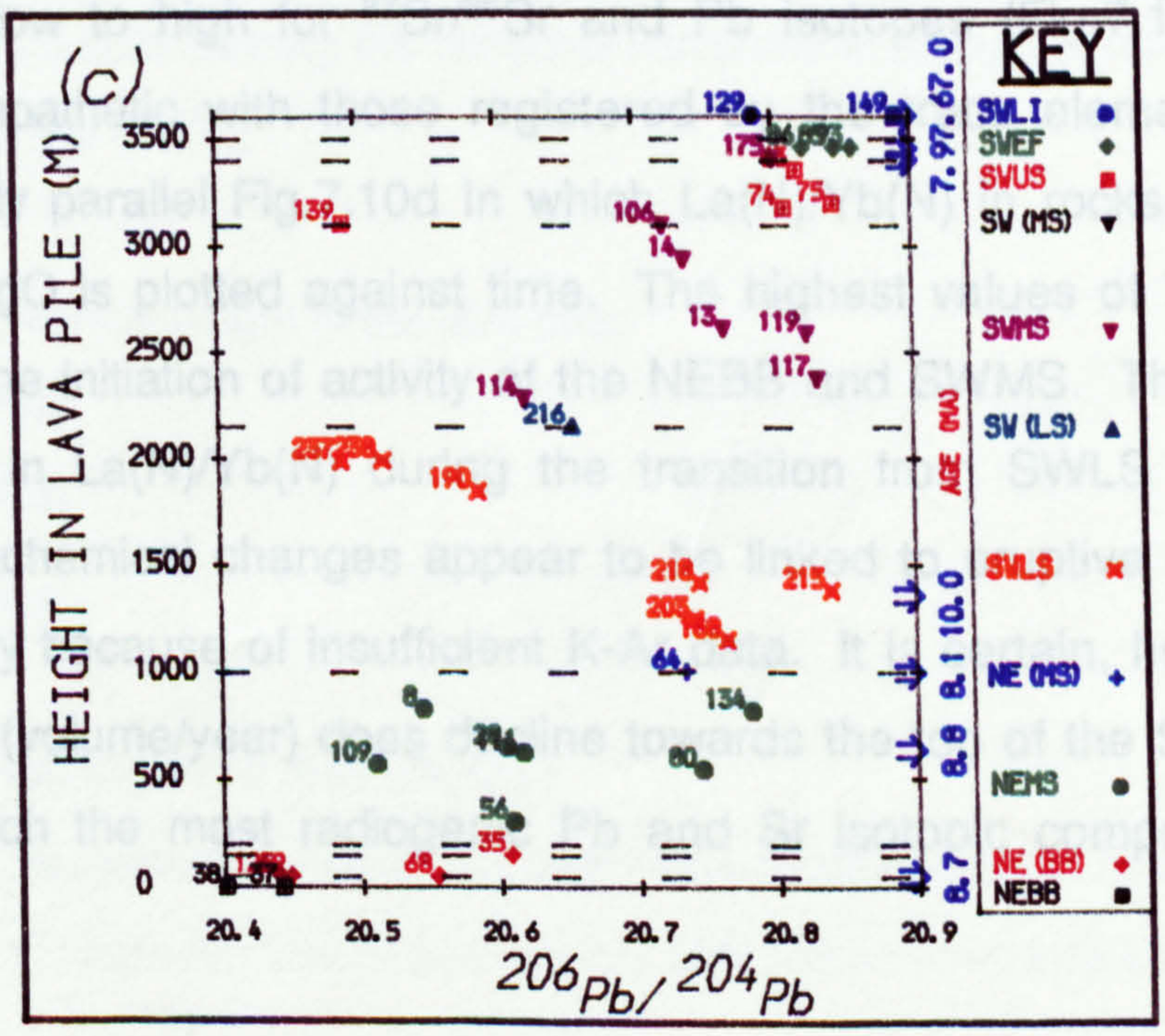
(c)
HEIGHT IN LAVA PILE (M)
3500
3000
2500
2000
1500
1000
500
0
20.4
20.5
20.6
20.7
20.8
20.9
206Pb/204Pb
7.9 7.6 7.0
AGE (MA)
10.0
8.8 8.1
8.7
KEY
SWLI
SWEF
SWUS
SW (MS)
SWMS
SW (LS)
SWLS
NE (MS)
NEMS
NE (BB)
NEBB

radiogenic compositions are found in the oldest rocks, whilst the youngest rocks have the most extreme isotopic compositions. Between these two extremes several discontinuities occur. The best example is at the SWLS to SWMS discontinuity (erosional unconformity) with samples SC 216, SC 237 and SC 238 possessing unradiogenic characteristics. Trends are, however, difficult to define because of considerable within shield heterogeneity. The pattern of Pb isotopic variations is broadly consistent with the temporal Sr and Nd variations (Fig.7.10). It is seen that samples with unradiogenic Pb compositions have the most radiogenic Nd compositions and occur at the beginning, or towards the end of shield activity. Minor discontinuities in trends occur within each shield, which are not discernible with Sr and Nd isotopes. An anomalous sample occurs high in the NE shield(SC 8). This has high $^{143}/^{144}$Nd and low $^{87}/^{86}$Sr. This suggests an overlap in activity forming the late NE volcanics and early SW volcanics. This is further suggested by the increase in $^{208}Pb/^{204}Pb$ and $^{207}Pb/^{204}Pb$ across the NEMS /SWLS boundary. Reasons for such variations are considered below. SC 139 at the base of the SWUS also has unradiogenic Pb composition indicating that relatively unradiogenic sources may still be tapped late in activity (although the stratigraphic position of this sample is not well constrained (section 3.4.1.3)).

7.4; Coupled isotope and trace element variations;

During the evolution of each of the NE and SW volcanoes the isotopic data indicate that the source regions of the lavas changed from relatively high to low $^{143}Nd/^{144}Nd$ and low to high for $^{87}Sr/^{86}Sr$ and Pb isotopes (Fig.7.10). These changes are sympathetic with those registered by the trace elements. Thus Fig.7.10a-c closely parallel Fig.7.10d in which La(N)/Yb(N) in rocks containing more than 5% MgO is plotted against time. The highest values of $^{143}Nd/^{144}Nd$ are recorded at the initiation of activity of the NEBB and SWMS. This parallels the discontinuity in La(N)/Yb(N) during the transition from SWLS to SWMS. Although the geochemical changes appear to be linked to eruptive rate, this is difficult to quantify because of insufficient K-Ar data. It is certain, however that the eruptive rate (volume/year) does decline towards the top of the SW volcano (Fig.3.7), for which the most radiogenic Pb and Sr isotopic compositions are recorded.

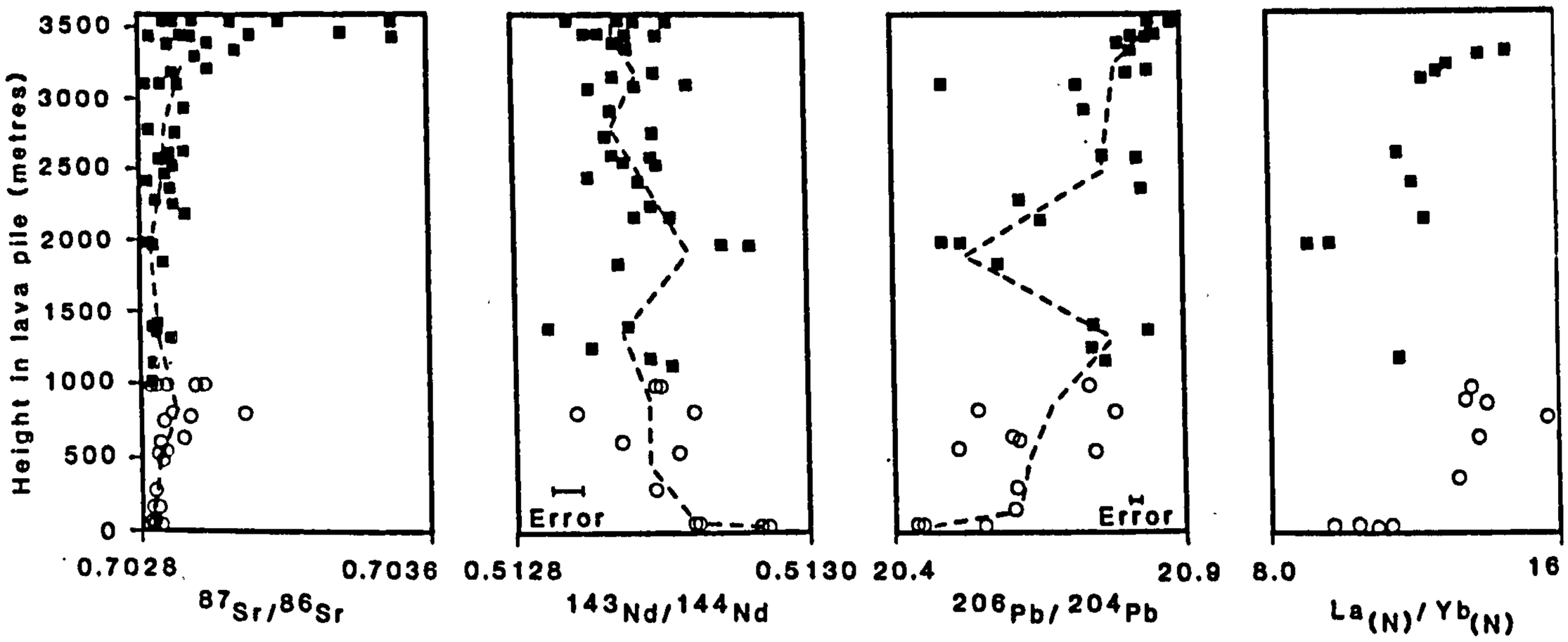

Fig.7.10. Diagram summarising the temporal variations in isotope and trace element geochemistry in the SHRS:

(a) $^{87}Sr/^{86}Sr$ versus height in the lava pile.

(b) $^{143}Nd/^{144}Nd$ " "

(c) $^{206}Pb/^{204}Pb$ " "

(d) $La_{(N)}/Yb_{(N)}$ " "

((d) Is for rocks containing more than 5% MgO.)

The dashed line represents a moving average of the values obtained by subdivision of the shield units. Error bars represented by symbol size unless otherwise stated.

In analogous situations elsewhere, where coupled trace element and isotope variations occur, correlations also occur between parent/daughter ratios and isotopes. For example Chen and Frey(1985) find a good correlation between Sm/Nd and $^{143}Nd/^{144}Nd$, in Haleakala volcanics, Hawaii. A poor positive correlation exists between Sm/Nd and $^{143}Nd/^{144}Nd$ in the SHRS. (Fig.7.11a). This correlation may result in part from crystallisation of phases that can fractionate REE. In section 6.3 clinopyroxene was shown to be particularly effective at fractionating REE and effecting ratios such as Sm/Nd. However, $^{143}Nd/^{144}Nd$ does vary beyond error in Fig.7.11a, hence some of this effect may be real. However, because of the small range in $^{143}Nd/^{144}Nd$ in relation to error and the effect of crystal fractionation no age significance can be attached to such a trend.

A correlation between $^{87}Sr/^{86}Sr$ and Rb/Sr does not exist (Fig.7.11b). Reasons for a poor correlation may include the susceptibility of Rb and Sr to alteration (Chapter 5). In addition Rb/Sr ratios are fractionated during crystal fractionation because $Kd_{(Sr)} > Kd_{(Rb)}$ between melt and plagioclase. In addition it is possible that Rb and Sr abundances in the source may be affected by the presence of a residual phase retaining Rb (section 7.2, 8.3.3). Positive correlations between parent/daughter ratios and isotopes (e.g. Sm/Nd and $^{143}Nd/^{144}Nd$) are consistent with two component mixing, but do not exclude the possibility that the trends could represent mantle isochrons. In the latter case the trends represent a previous separation of the components from a homogeneous parent. The age of separation of these components is given by the slope on a diagram of Sm/Nd vs $^{143}Nd/^{144}Nd$. Correlations on a Pb-Pb isotope diagram (Fig.7.8) could similarly be explained as a secondary isochron resulting from a previous mixing event as suggested by Chase(1981). Whether these variations result from ancient element fractionation events or recent mixing is discussed in 7.5.2. The correlation in Fig.7.8. gives an age of 2.4±0.2 Ga for the U/Pb fractionation event if the correlation of Fig.7.8 is interpreted as an isochron. The effect of an ancient (ca. 2.4 Ga) fractionation event in producing the U-Th-Pb isotopic systematics of the SHRS is modelled further in section 8.2. Further correlation between trace elements and isotopes are not evident because of the limited variation in ratios of incompatible elements together with large differences

Fig.7.11a. Sm/Nd versus $^{143}Nd/^{144}Nd$. *Black dots* represent samples corrected for crystal fractionation.

Fig.7.11b. (p211) Rb/Sr versus $^{87}Sr/^{86}Sr$. Possible vectors for crystal fractionation and alteration are shown.

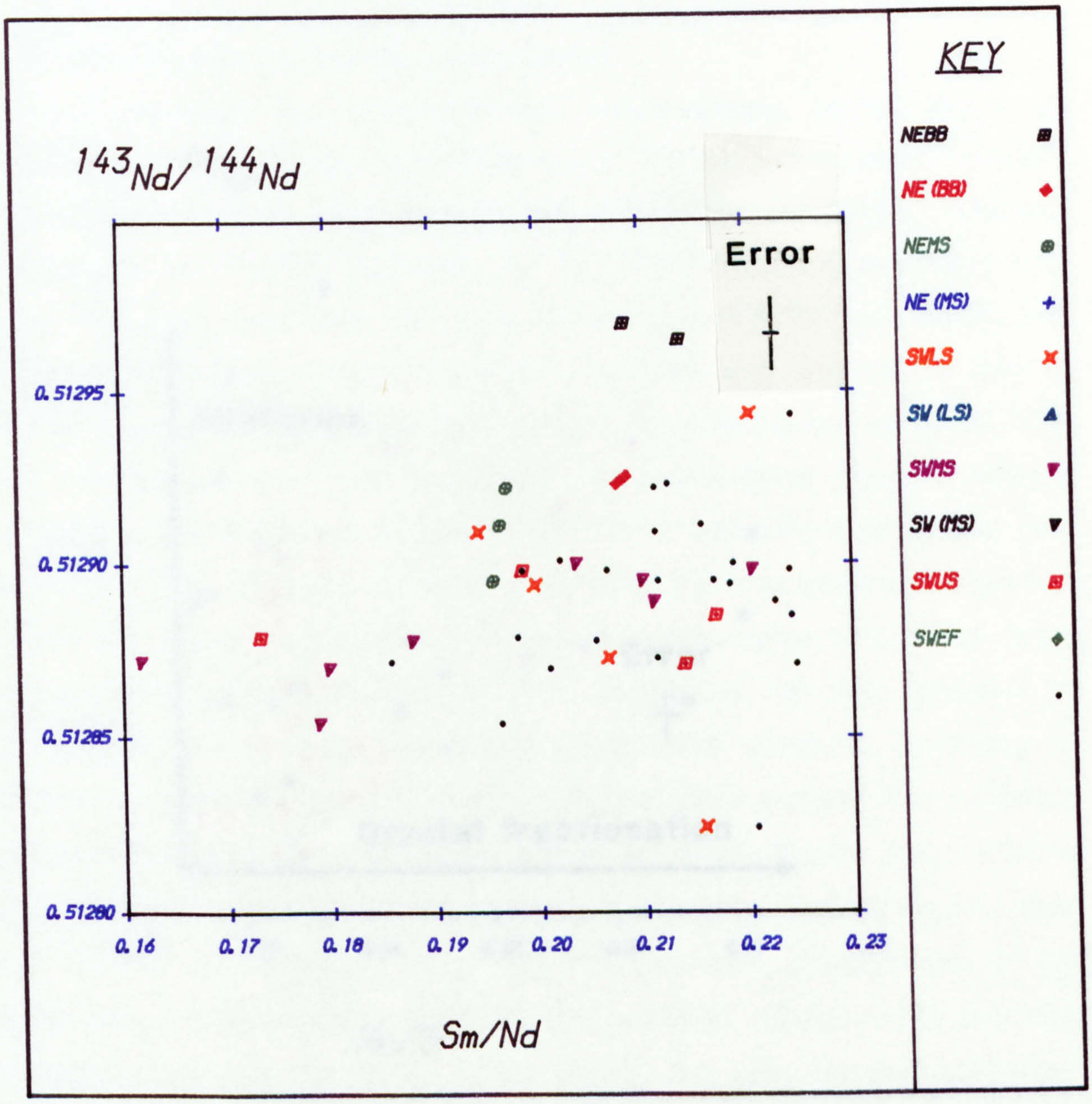
KEY
NEBB
NE (BB)
NEMS
NE (MS)
SVLS
SV (LS)
SVMS
SV (MS)
SVUS
SWEF
Error
143Nd/144Nd
0.51295
0.51290
0.51285
0.51280
0.16
0.17
0.18
0.19
0.20
0.21
0.22
0.23
Sm/Nd

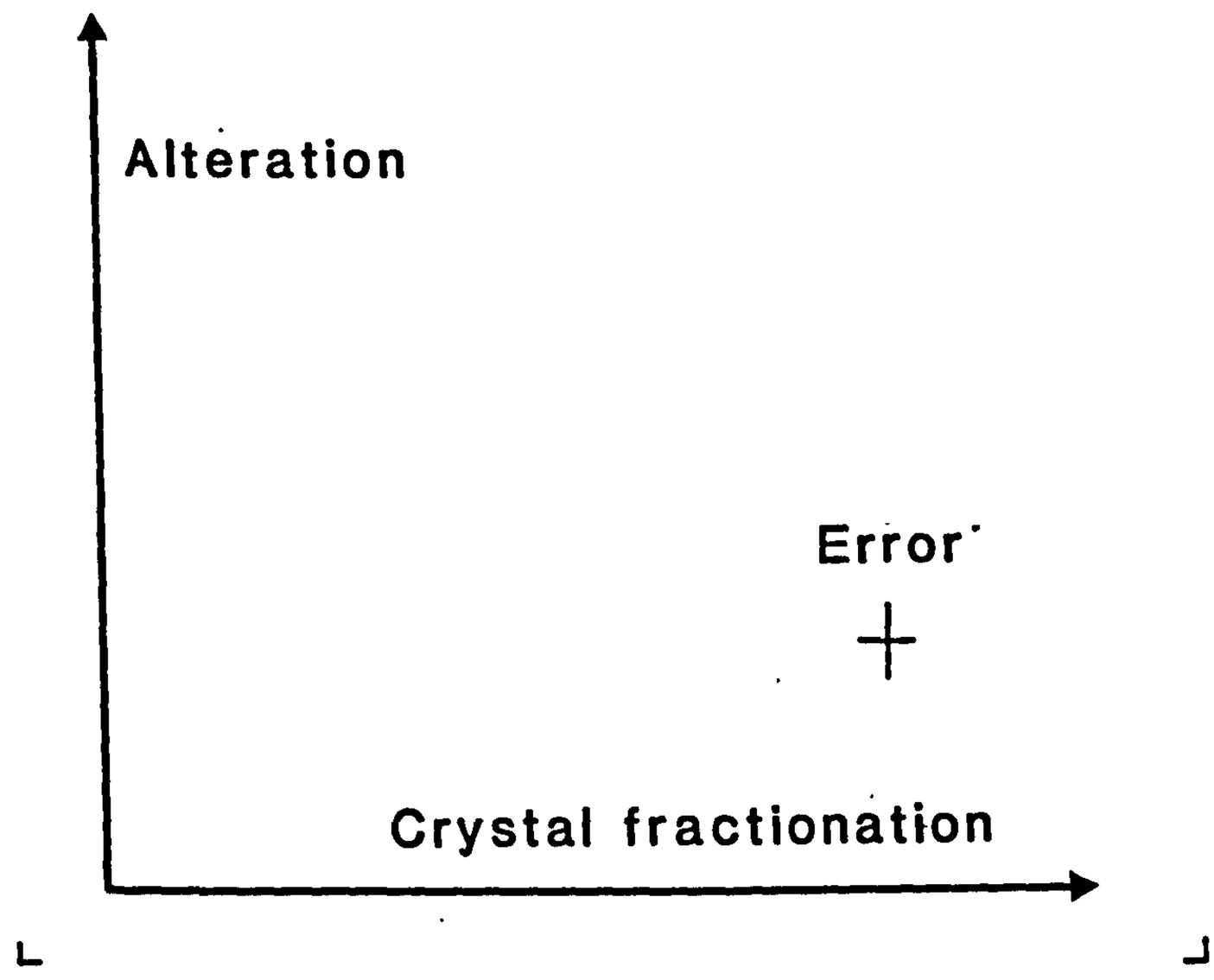
Alteration
Error
Crystal fractionation

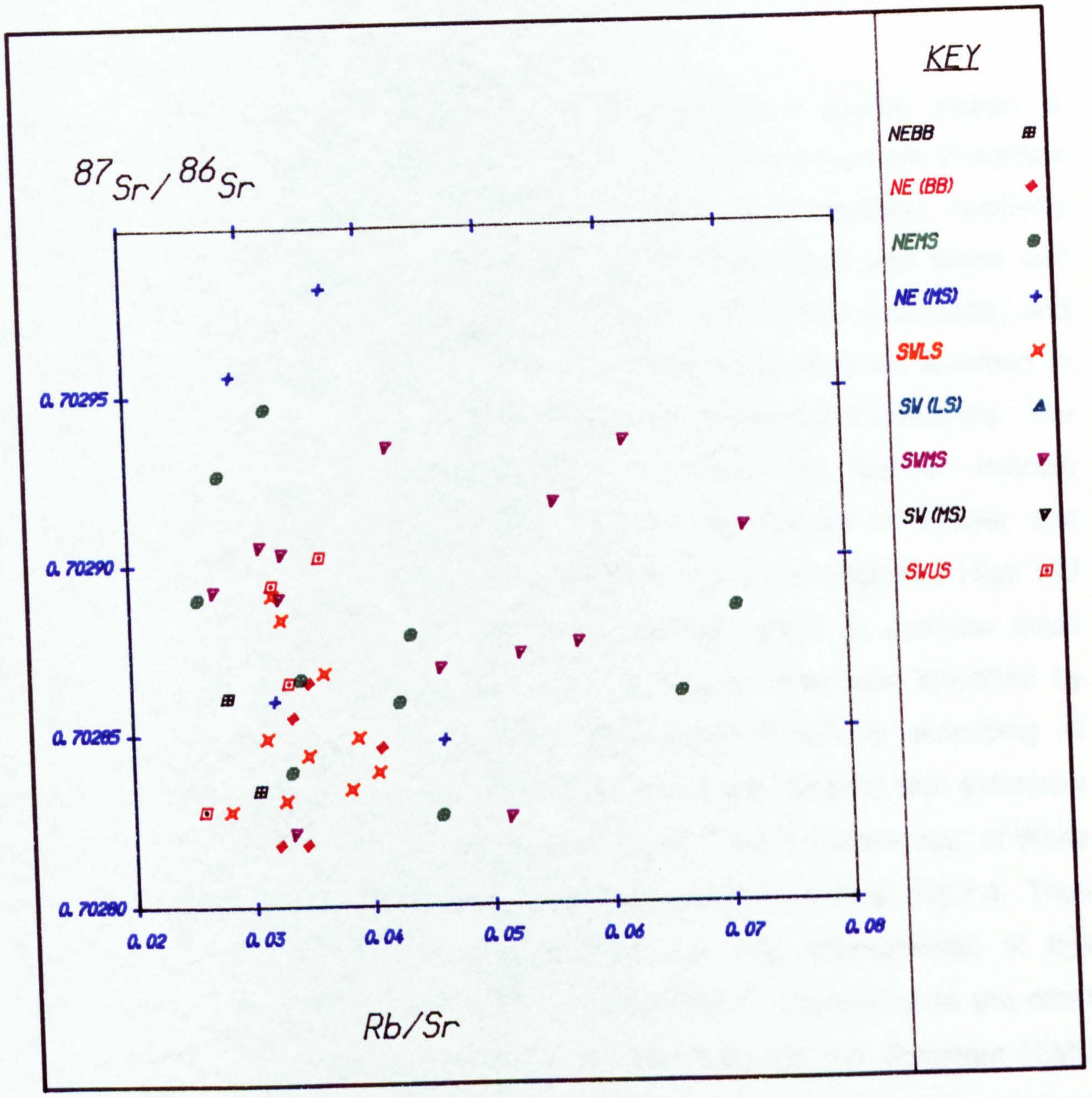
KEY
NEBB
NE (BB)
NEMS
NE (MS)
SWLS
SW (LS)
SWMS
SW (MS)
SWUS
87Sr/86Sr
0.70295
0.70290
0.70285
0.70280
0.02
0.03
0.04
0.05
0.06
0.07
0.08
Rb/Sr

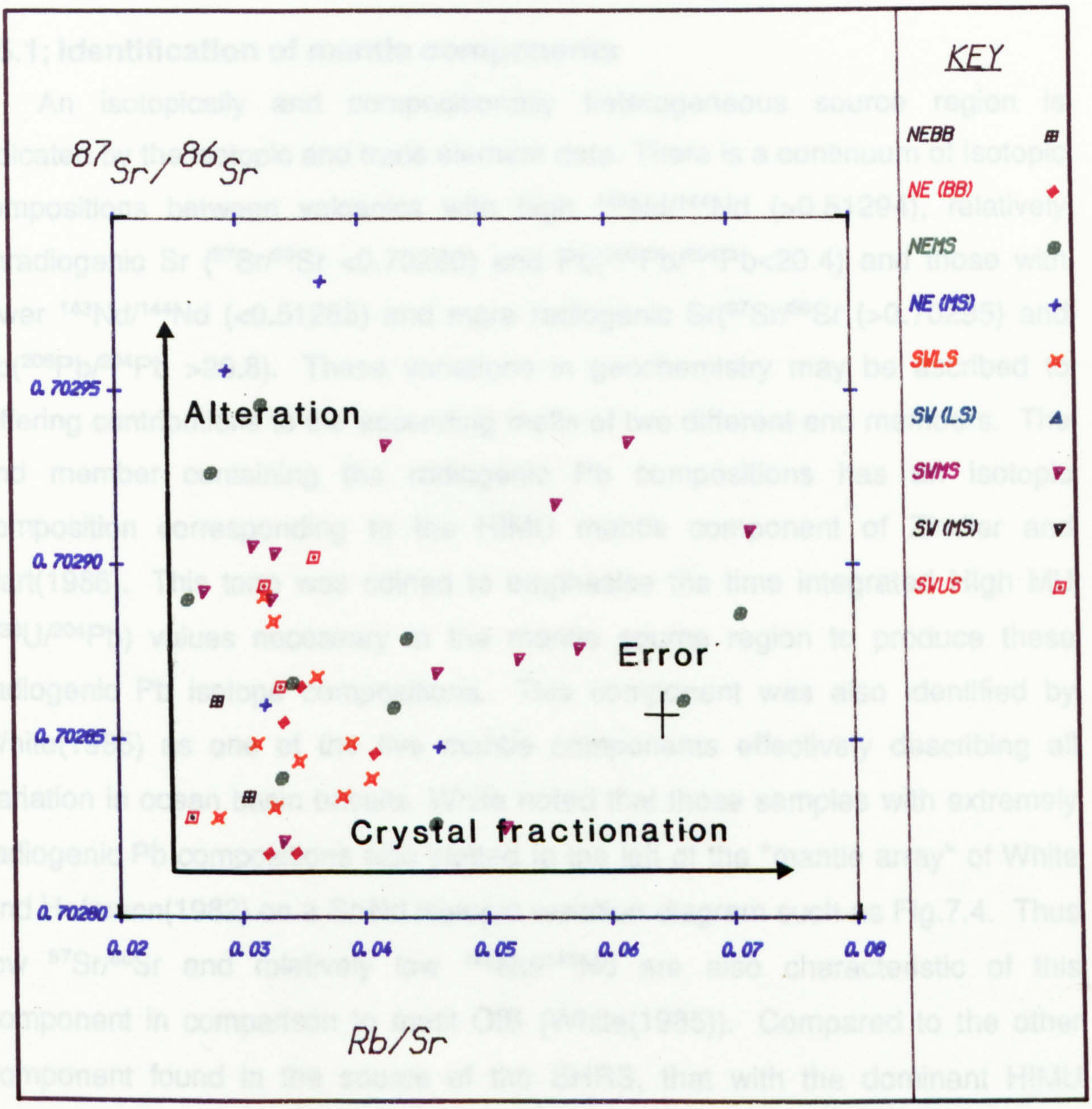
KEY
NEBB
NE (BB)
NEMS
NE (MS)
SWLS
SW (LS)
SWMS
SW (MS)
SWUS
87Sr/86Sr
0.70295
0.70290
0.70285
0.70280
Alteration
Error
Crystal fractionation
0.02
0.03
0.04
0.05
0.06
0.07
0.08
Rb/Sr

in trace element abundance in the two conceivable sources (sections 7.2, 7.5.1).

7.5; Interactions between mantle components beneath St.Helena.

7.5.1; Identification of mantle components

An isotopically and compositionally heterogeneous source region is indicated by the isotopic and trace element data. There is a continuum of isotopic compositions between volcanics with high $^{143}Nd/^{144}Nd$ (>0.51294), relatively unradiogenic Sr ($^{87}Sr/^{86}Sr$ <0.70280) and Pb($^{206}Pb/^{204}Pb$<20.4) and those with lower $^{143}Nd/^{144}Nd$ (<0.51285) and more radiogenic Sr($^{87}Sr/^{86}Sr$ (>0.70295) and Pb($^{206}Pb/^{204}Pb$ >20.8). These variations in geochemistry may be ascribed to differing contributions to the ascending melts of two different end members. The end member containing the radiogenic Pb compositions has an isotopic composition corresponding to the HIMU mantle component of Zindler and Hart(1986). This term was coined to emphasise the time integrated HIgh MU ($^{238}U/^{204}Pb$) values necessary in the mantle source region to produce these radiogenic Pb isotope compositions. This component was also identified by White(1985) as one of the five mantle components effectively describing all variation in ocean basin basalts. White noted that those samples with extremely radiogenic Pb compositions also plotted to the left of the "mantle array" of White and Hofmann(1982) on a Sr-Nd isotopic variation diagram such as Fig.7.4. Thus low $^{87}Sr/^{86}Sr$ and relatively low $^{143}Nd/^{144}Nd$ are also characteristic of this component in comparison to most OIB (White(1985)). Compared to the other component found in the source of the SHRS, that with the dominant HIMU component has relatively low ^{143}Nd and high $^{87}Sr/^{86}Sr$ and also has the greatest degree of incompatible trace element enrichment. The second component is relatively depleted and has less radiogenic Sr and Pb compositions. In isotopic space this lies on a vector between the HIMU component and the depleted MORB source mantle end member (DMM) of Zindler and Hart(1986) (Fig.7.12). The exact position of the second component on the vector towards DMM is difficult to establish. As stated in section 7.2. the relatively depleted component may be MORB source or it may be a mixture of MORB source and St.Helena OIB source formed in a previous melting event. An overall intermediate

Fig.7.12. Pb-Sr and Pb-Nd isotopic variations in MORB and OIB.

(a) $^{206}Pb/^{204}Pb$ vs $^{87}Sr/^{86}Sr$.

(b) $^{206}Pb/^{204}Pb$ vs $^{143}Nd/^{144}Nd$.

Data from compilation of Zindler and Hart(1986).

The mixing proportions shown are calculated using equations from Faure(1986). The bold tick marks for the St.Helena - DMM 1 mixing array in the preferred model (see text) are calculated using a trace element concentration ratio in the source of 2XDMM=HIMU. The DMM element concentrations are from Zindler and Hart(1986) who adopted a ratio of 10XDMM=HIMU. The DMM isotope values are from Zindler and Hart(1986), the HIMU values are suggested by the maximum reported values for this component. The end member compositions for the preferred model are as follows:

End member	Sr	Nd	Pb
HIMU	0.70310(24ppm)	0.51280(1.30ppm)	21.500(0.04ppm)
DMM1	0.70216(12ppm)	0.51335(0.65ppm)	17.397(0.04ppm)

In the model of Zindler and Hart values are similar except for source concentration of HIMU. 120ppm Sr, 6.5 ppm Nd and 0.4 ppm Pb.

(a)

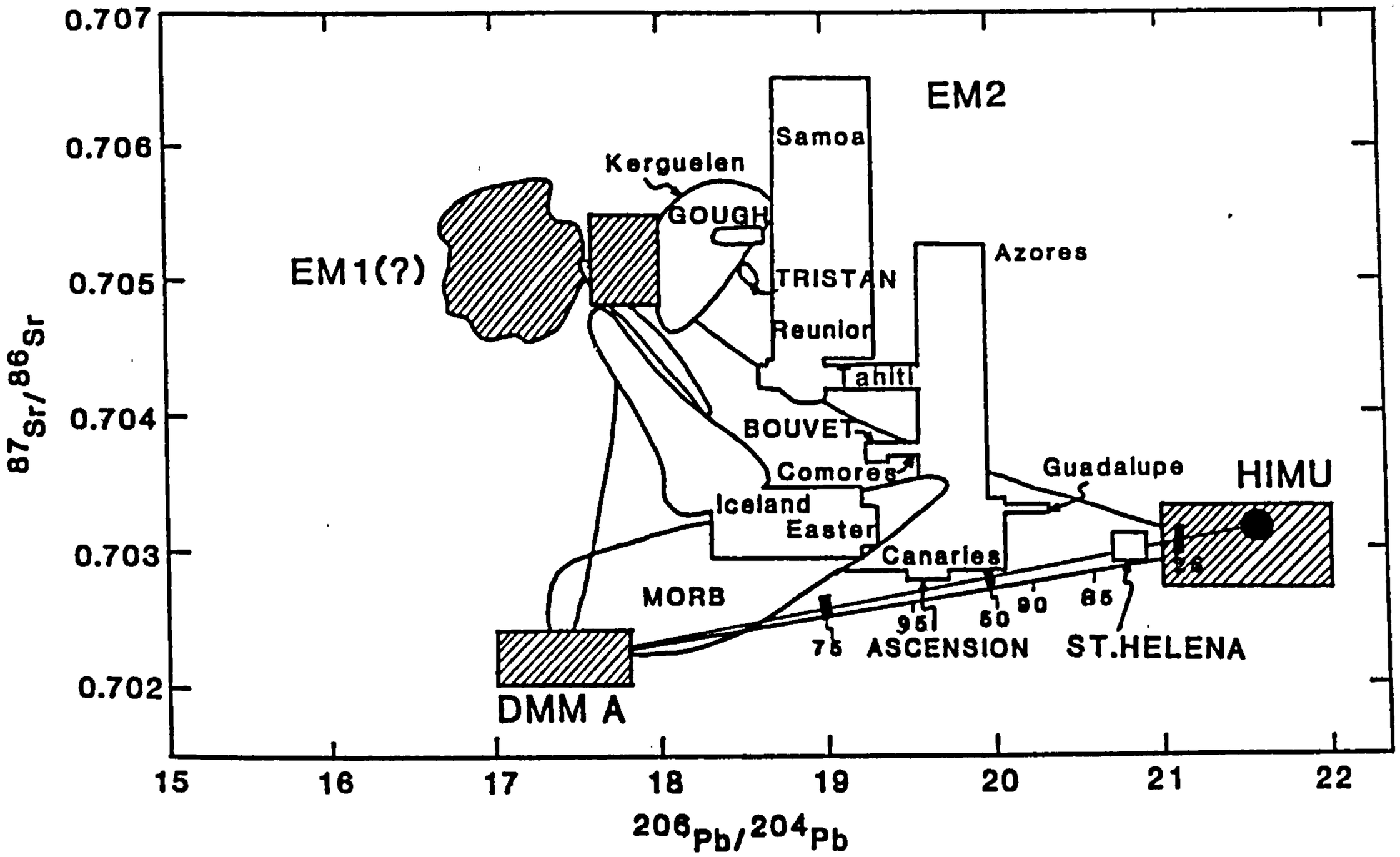
0.707
0.706
0.705
0.704
0.703
0.702
$^{87}Sr/^{86}Sr$
EM1(?)
EM2
Samoa
Kerguelen
GOUGH
Azores
TRISTAN
Reunion
Tahiti
BOUVET
Comores
Guadalupe
HIMU
Iceland
Easter
Canaries
MORB
95
50
90
85
75
ASCENSION
ST.HELENA
DMM A
15
16
17
18
19
20
21
22
$^{206}Pb/^{204}Pb$

(b)

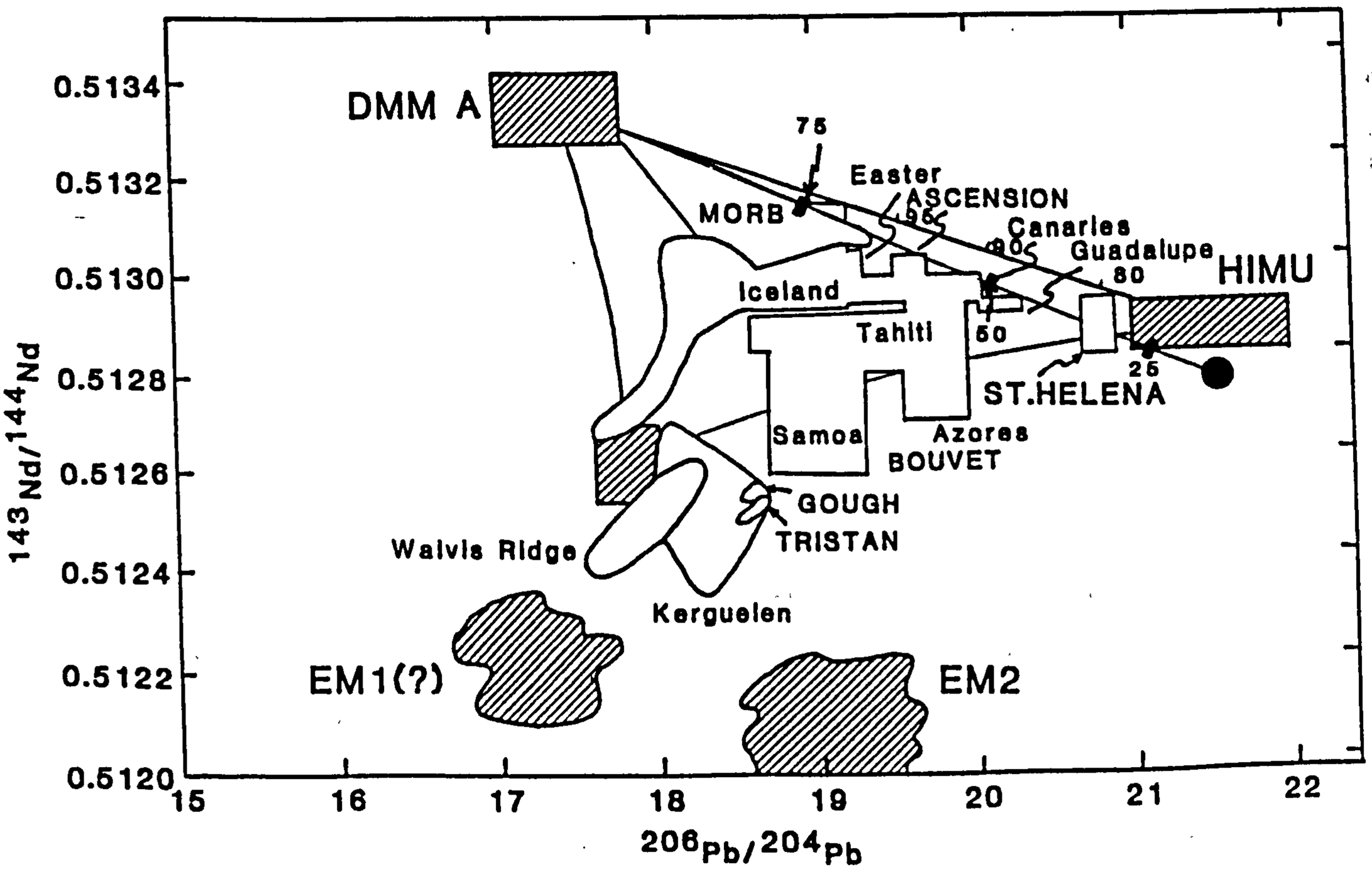
0.5134
0.5132
0.5130
0.5128
0.5126
0.5124
0.5122
0.5120
$^{143}Nd/^{144}Nd$
DMM A
75
Easter
ASCENSION
MORB
95
Canarles
90
Guadalupe
80
HIMU
Iceland
Tahiti
50
25
ST.HELENA
Samoa
Azores
BOUVET
GOUGH
TRISTAN
Walvis Ridge
Kerguelen
EM1(?)
EM2
15
16
17
18
19
20
21
22
$^{206}Pb/^{204}Pb$

composition could exist in the lithosphere if it has been impregnated by OIB magmatism (Duncan et al.(1986)). Alternatively, it could exist in the plume envelope which is likely to be a mixture of OIB and MORB (section 7.2).

7.5.2; When did mixing of the components occur?

Two alternatives to account for positive correlations between parent daughter ratio and isotopic composition were recognised as possible end member scenarios by Zindler et al.(1979) who erected a useful classification to explain them. This is outlined in Table 7.2. The LOM model involves *large* scale (>30 km), *old* heterogeneities which become mixed as *melts.* SYS denotes *small* scale heterogeneities that are *young* and mix in the *solid* state. The principal difference between these models is that in the SYS model the end members have segregated from a common parent, whereas in the LOM model the two end members are not related by a single fractionation event.

Table 7.2; Mantle mixing scenarios (after Zindler et al.(1979))

Model	*Scale*	*Age*	*Nature of mixing*
LOM	Large(>30 km)	Old (>errorchron)	Mixing of melts
SYS	Small (<10m)	Young(<errorchron)	Solid state

In the SYS model a mantle melting event fractionates the parent daughter ratio at the age given by the isochron. The melt then solidifies to exist as an intimate mixture of melt and parent on a scale of less than 10m. The host and daughter then evolve separately and produce different isotopic compositions dependent on their parent daughter ratios. When this heterogeneous mantle portion is subsequently melted Zindler et al.(1979) suggest that random correlations of geochemical parameters with time or that a *decrease in LREE enrichment* with time could occur as the daughter melt is likely to be the low temperature melting component which will become more depleted through time. In the LOM model two ancient mantle components evolve separately after an independent formation. The mixing trend is produced immediately prior to eruption. According to Zindler et al.(1979) an *increase in the degree of LREE enrichment* is likely to occur through time as a primary picrite melt becomes progressively more contaminated by a LREE fluid which percolates up from

below. According to Zindler et al.(1979) chemostratigraphic variations should be of value in resolving the question of whether correlations such as that of Fig.7.8 represent mixing lines or mantle isochrons. However, these authors did not consider the physical framework of mixing. They state that the SYS model will produce random correlations of geochemical parameters with time, but this is not thought to be true by this author. It is now recognised that it is not possible to distinguish whether trends such as those on Fig.7.8 represent mixing lines or isochrons, especially if independent evaluation of the date of separation by Rb-Sr or Sm-Nd systematics is unavailable (e.g. Zindler et al.(1984)). A similar conclusion was drawn by White et al.(1987). One means of achieving temporal variation in an OIB suite with a source comprising two interdependent components representing an isochron is by chemical zonation of an ascending plume. Chemical zoning of a plume has been suggested by (Duncan et al.(1986)) to explain the geochemical features observed at Ua Pou, Marquesas islands. Chemical zoning has been modelled by Griffiths(1986) who envisages a toroidal circulation developing within the rising diapir which causes entrainment of depleted material from the plume envelope to occur. The toroidal circulation causes a zoned plume to develop with the more depleted material in the centre, and the original diapir material forming an outer torus. This model may account for the spatial variation in a group of islands such as the Galapagos (Geist et al.(1988)). For a single island such as St.Helena this model is difficult to reconcile with the data because it is necessary to invoke preferential removal of the depleted component from the plume early in activity when it has become coincident with the zone of highest temperature. Fortuitous repetition of this zoning would be necessary during the activity of each shield unit. It is difficult to account for the repeated, regular geochemical variations with this alternative and the simpler model in which correlation reflects mixing of independent sources is favoured.

7.5.3; The geometric framework of magma production;

Clearly a more satisfactory description of the recent mixing event is required than the LOM model of Zindler et al.(1979). Their explanation is implausible because of its simplicity - the fact that two mantle components are considered to melt in total isolation. It will be demonstrated that there are a number of zones in which mixing can occur. In the following sections the physical characteristics of the components, how they become mixed and how these processes may vary over time will be considered.

Some constraints on the geometric relationship of the two components are provided by integrated studies of S.Atlantic magmatism based on dredged rocks from along the adjacent Mid Atlantic Ridge (MAR). Schilling et al.(1984) identified an enriched component indicated by high La/Sm and Nb/Zr in MORB 700km from and at a similar latitude to St.Helena. More recent studies by Graham et al.(1988) have similarly shown the existence of low $^{3}He/^{4}He$ values in MORB at the same latitude as St.Helena. These values are 25% lower than those in average MORB for adjacent ridge segments. More significantly Hanan et al.(1986) showed that a radial decline in radiogenic Pb content of recent MAR basalts occurred with distance from St.Helena (once the effect of mixing between the MAR basalts and other OIB sources such as Tristan da Cunha had been removed). This component can be identified over a distance of 3000km . Studies by Fitton et al.(1983) and Halliday et al.(1988) have indicated the presence of a HIMU component in the basalts of the Cameroon line which occurs 1000km to the NE of St.Helena ($^{206}Pb/^{204}Pb$ >20.2). The most radiogenic samples analysed by Halliday et al.(1988) are obtained from Mount Cameroon which is on the continental/oceanic divide and not in the oceanic sector which is closest to St.Helena. This has led these authors to suggest that the St.Helena component in these basalts may be derived from lithosphere rather than the asthenosphere. They suggest that the HIMU characteristics may have been conferred on the lithosphere when the St.Helena hotspot was under the Niger delta 130 Ma ago. This position is part of the calculated hotspot track of Morgan(1983)). Similarly a HIMU component has been reported in the Cape Verde island volcanics (Davies et al.(1988)). Whilst it is not certain whether these HIMU domains are independent or spatially related to St.Helena, these studies indicate the

widespread nature of the St.Helena component. The data of Hanan et al.(1986) suggest that a regional maximum occurs in the vicinity of St.Helena. Thus a geochemically anomalous mantle source region existed beneath St.Helena during the volcanic activity. This anomaly was coincident with the thermal anomaly responsible for the volcanism. The chemically anomalous material was supplied throughout the eruptive history of St.Helena suggesting that the diapir was continually replenished rather than being an isolated passive "blob" that was passively heated. The studies of Halliday et al.(1988) and calculated hotspot tracks Morgan(1981) further support the longevity of a plume.

The suggestion that OIB melts can be principally generated from within the lithosphere has also been made (Wright(1984)). This idea is now examined to assess whether it could be be applicable to the genesis of the SHRS. This model was developed specifically to account for the origin of Hawaiian tholeiites, but could be more widely applicable. In this model the depleted lithosphere (MORB source composition) is modified through time by isotopic evolution in the Rb-Sr, Sm-Nd and U-Th-Pb systems since formation at the East Pacific Rise and subsequent metasomatic additions to form the source of Hawaiian tholeiites. Wright calculated that 35-42% melting of a MORB source with an addition of 15-20% highly alkalic melt that precipitates amphibole followed by substantial olivine fractionation is necessary to form the tholeiites. A similar model has been proposed by Sen(1983) who thought that the sequence of enrichment observed in Hawaiian volcanoes could be explained by progressively smaller degrees of partial melting of the lithosphere. Both of these models encounter a similar problem, namely that what Sen(1983) terms metasomatic additions are required to replenish the highly incompatible elements lost from the source during each partial melting event. This is a considerable problem. Feigenson(1986) pointed out that some alkali basalts capping the volcanoes are isotopically indistinguishable from the tholeiites of the shields (Stille et al.(1987)). This would require the metasomatic fluid to possess identical isotopic composition to the lithosphere. Feigenson(1986) considers this to be fortuitous. In addition because tholeiites from different shields have different compositions (Stille et al.(1986)), a different metasomatic composition would be required for each volcano. Frey and Roden(1987) point out that the small degree of partial melting

required to produce the metasomatic fluid which infiltrates the lithosphere would require scavenging of trace elements from a large mantle volume. They calculate that for a 35km depth an area with a radius of 150km would be required. They consider scavenging from this volume is not realistic, especially if two shields are active concurrently. The partial melting models discussed in section 6.7 may indicate that this is not a problem, however. A final problem with models that require large degrees of partial fusion followed by olivine fractionation (Wright(1984)) or garnet and clinopyroxene fractionation (Anderson,1985) is that of transition metal abundances. Feigenson(1986) calculates that erupted basalts should contain three to four times lower Ni abundance than that actually observed in Hawaiian basalts. Thus although a similar model could be proposed for St.Helena OIB insuperable objections exist. A plume would still be necessary to supply the isotopic charactersitics of St.Helena which are shown to be maximised in the area of St.Helena and sustained for a considerable period.

7.5.4; Mechanism for mixing of components;

If the presence of a plume is accepted the potential zones in which mixing of the two components may occur can conveniently be divided into those that are primary and a direct consequence of the plume's presence and those that are secondary and occur subsequent to the segregation of melts from the source region. In considering both these interactions it is important to remember that the efficiency of mixing is likely to decline through time in response to a declining thermal flux. The decreasing volume of magmatic products during the transition from shield building to minor parasitic activity is the surface expression of this.

Interaction between the two end members in the plume is likely to be influenced by the proportion of each component and its melting characteristics. The plume may possess either a high proportion of HIMU domains to surrounding matrix (small (metre) scale heterogeneity within the plume) or complete internal isolation of HIMU domains (large (kilometre) scale heterogeneity between the plume and its envelope). This is essentially the difference between what has been termed a "thermal plume" and "chemical plume" by Zindler et al.(1984). In a "thermal plume" the ascending diapir is

similar in composition to the passive surrounding mantle. Both have small scale heterogeneities. The thermal high in the vicinity of the plume causes melting over a greater depth interval and enhancement of the enriched "blob" component within the melt (Sleep(1984)). A "chemical plume" is composed of material that is different from the passive mantle. It must also be remembered that this is a simplistic view because although in a "chemical plume" large scale heterogeneity occurs between plume and envelope, a different scale of heterogeneity can occur within the plume itself. The difference in overall composition of the plume and mantle may simply be because there is a higher blob/matrix ratio in the plume than the surrounding mantle. In the instance of St.Helena, however the regional data of Hanan et al.(1986) leave no doubt that large scale mantle heterogeneity does occur around St.Helena. The decline in HIMU signature along the MAR to the N and S of the latitude of St.Helena in dredge basalts is most easily accounted for by a reduction in the proportion of HIMU domains in the mantle source as the melting regime is liable to remain similar along the ridge. Thus, a chemical maximum of the HIMU signature is indicated in the St.Helena area and a "chemical plume" in which large scale heterogeneity between the plume and its envelope appears likely to exist. Because the HIMU signature associated with the plume increases with time it is not thought that variations in the volumetric proportions of the two components in the plume can account for the observed temporal variations. An increase in the proportion of HIMU to DMM domains in time would be required to produce the observations, but this is counterintuitive to the decline in thermal flux, which is liable to be coupled to a decreasing HIMU chemical flux. It is suggested, therefore, that preferential fusion of the HIMU component occurs under the influence of a waning heat supply. If it is assumed that the trace element enriched HIMU component has the lowest solidus temperature then this alternative satisfies the observations most readily.

A primary interaction may also occur between HIMU mantle within the diapir and the surrounding envelope of relatively depleted material. At the inception of activity of a shield, a high heat flux would cause melting of the surrounding envelope. Clearly as the heat flux decreases the contribution to ascending melts will become largely restricted to the enriched mantle within the diapir. In addition, continued melt extraction from the plume envelope will cause

the envelope to become relatively refractory and more depleted through time. Thus the contribution of depleted material in the envelope to melts is likely to decrease for both reasons.

The fact that the ascending diapir is not passive must also be considered, hence direct assimilation of depleted components from the lithosphere may occur. Erosive thinning and sub-solidus incorporation of the lithosphere have been suggested as efficient processes when modelling the effect of secondary convection cells associated with an ascending plume (e.g. Yuen and Fleitout(1985)). The importance of this process is difficult to establish, but it is evident that the efficacy of this process is likely to decrease with time, which is again consistent with the results.

Secondary interactions can occur as melts formed by the combination of primary processes ascend. These interactions will occur at the base of and within the lithosphere. As melts ascend through the lithosphere incompatible elements may be scavenged from the surrounding depleted lithosphere as described by Navon and Stolper(1987) for example. If the melt pathways possess a fixed geometry during the activity of a shield unit it is likely that chemical exchange will decrease as the elements in the adjacent lithosphere become progressively depleted or the composition of the wall rocks approaches that of the ascending melt. Such a model is strongly dependent on the scale of the pathways and whether they are of a transient nature. If the speed of ascent of magma batches following segregation is rapid compared to the time necessary for equilibration to occur between melt and wall rock, the effect of Navon and Stolper(1987) may not be significant. Spera(1984) (section 2.3) reviews magma ascent rates and states that magmas ascend at the rate of cm/s to m/s which suggests that insufficient time for equilibration within the lithosphere may occur, (except at the base before melt ascent by crack propagation commences)

An additional factor that must considered in explaining the temporal variations is that the oceanic crust and lithosphere are likely to be moving relative to the stationary plume. The new K-Ar age data for St.Helena indicate subaerial activity over a period of approximately 2Ma. In this time a relative movement of approximately 20 km would have occurred assuming a half spreading rate of 2cm/year (e.g.Mitchell-Thome(1971)). This simple calculation is made by

assuming the movement of the MAR relative to a fixed hotspot is negligible. This is suggested by plate motion reconstructions made by Morgan(1983). This figure is not well constrained, but the magnitude of the result is sufficiently large to indicate that significant movement of the plate will occur relative to the fixed plume. It is suggested that the plate motion is responsible for the shift of volcanic activity from the NE to SW volcano. This is broadly consistent with the direction of plate motion which would be expected to be moving approximately from W to E away from the MAR which is oriented N - S. It was argued in section 2.5 that this process was likely due to the existence of two seamount volcanoes to the W of St.Helena. This is thought consistent with the continued existence of a hotspot subsequent to activity on St.Helena (and continued movement of the plate relative to this hotspot). If this situation has occurred it may be possible that the two volcanoes were simultaneously active. Establishing whether this process has operated is largely dependent on our understanding of plume geometry. If a point source of heat exists below the island there is no difficulty in producing transfer of activity. If a hammerhead geometry as described by Courtney and White(1986) occurs the above explanation is not valid because the maximum temperature of the plume will cover a wide area. It is then necessary to account for the shift in activity by high level changes in the magma conduits. However high level changes are likely to be the result of changes at greater depth and as Courtney and White(1986) point out the plume has a narrow central jet where temperatures are maximised. For these reasons it is thought that the shift in activity is a response to the change in relative position of the heat source beneath the island due to plate motion.

7.5.5; Relative contribution of components in relation to the geometric framework of magma generation;

Quantitative estimates of the relative contribution of the two components to ascending melts are possible by consideration of the variation in isotopic and trace element ratios. Such exercises must be conducted within the geometric framework of magma generation that is discussed above. A simple estimate of the proportions of components in the source (integrated over all the zones where interactions occur) can be obtained by considering the magnitude and range of

isotopic values for the the SHRS in relation to the proportions calculated by applying a mixing model to the two components. The proportion of the components in the mixture is calculated by using a standard mixing equation (Langmuir et al.(1978), Faure(1986)) and assuming that mixing of 100% melts from each source component occurs (i.e. no trace element fractionation occurs during melting to increase the incompatible element concentrations in the source). The isotopic composition of the end members used are those that represent the most extreme compositions observed in erupted volcanics. DMM1 is from Zindler and Hart(1986) and the HIMU composition is adjusted to the most extreme isotopic values evident in the literature (other HIMU OIB sources are discussed in section 8.2). Clearly both end members may be more extreme than the values chosen, but the simplest case must be considered to illustrate the effect of varying the ratios of trace elements in the components. Zindler and Hart(1986) attempt to model the composition of all oceanic basalts in terms of mixing between DMM, HIMU and other mantle components. In their model they prefer a non magmatic origin for HIMU (section 8.5) and adopt HIMU source concentrations that are ten times greater than those in DMM. The results of this model are shown in Pb-Sr and Pb-Nd isotopic space in Fig.7.12 and in terms of the range of isotopic values between the two end members in Fig.7.13 (curve A). It is apparent that the proportion of the DMM component varies from *43-80%* of the mixture, for the range of observed Sr, Nd or Pb isotopic compositions. The range varies for each element because it depends on the position of the chosen end member. The high proportion of DMM is a consequence of Zindler and Hart(1986) adopting a high DMM/HIMU (HIMU/DMM) source element ratio. It is likely that Zindler and Hart used such a high value in order for only small proportions of HIMU to be necessary in the source of OIB intermediate in isotopic composition between the end members, such as Guadalupe (Fig.7.12) for which no HIMU signature is indicated by variations within the lavas. It is thought that a DMM/HIMU source element ratio of 10 is unrealistically high for two reasons. Firstly, the trace element modelling using the method of Budahn and Schmitt(1985) is consistent with a source concentration of two - four times chondrite. It is argued in section 8.2. and 8.3. that the isotopic and trace element ratios of the SHRS indicate a source that has undergone a previous melt

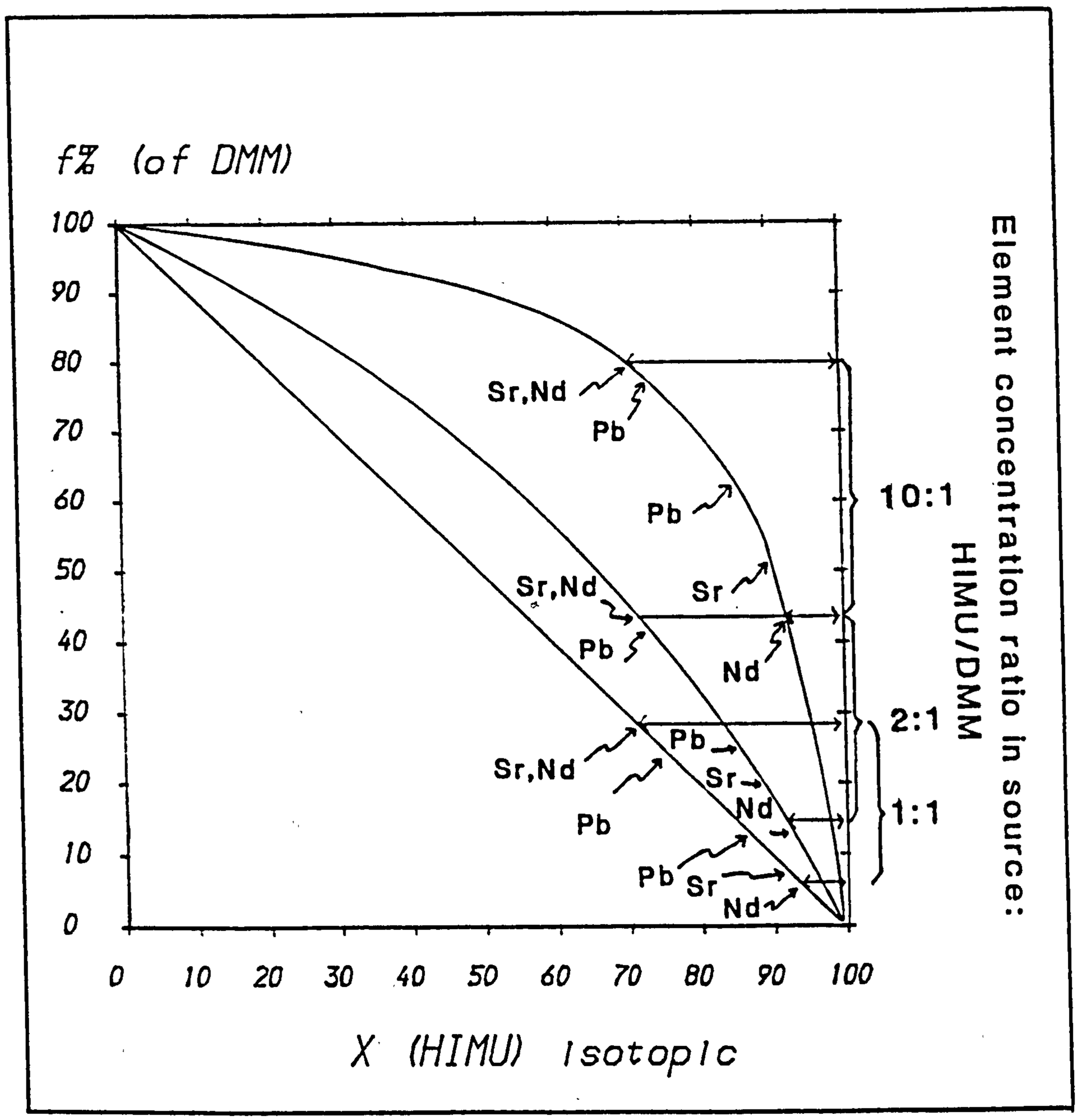

Fig.7.13 Diagram showing the effect of varying the HIMU:DMM element concentration in the source region. The x-axis represents the observed Sr,Nd and Pb isotope compositions (marked on curves) expressed as a proportion of the difference in isotopic compositions between the HIMU and DMM endmembers (as a fraction of HIMU). The y-axis represents the contribution of DMM required in the mixture to generate these isotopic values. The characteristics of the end members are given in Fig.7.12.

extraction event. This would not produce such high values of element concentrations. However, if such a high value is used it implies a significant contribution oF DMM to the the SHRS. This would imply a plume dominated by DMM component with streaks of HIMU component in it (e.g. Fitton and James(1986)). If a lower HIMU/DMM source element concentration ratio is adopted, it is evident from Fig.13 (curve B) and Fig.7.12 that a much smaller contribution of DMM is required *(15-40%).* A still smaller ratio results if a 1:1 ratios is adopted. Thus the simple mixing calculation conducted above is strongly dependent on the source concentrations of DMM and HIMU. These values are poorly constrained, but the ratio of 10 adopted by Zindler and Hart(1986) produces surprisingly high proportions of DMM. These high proportions result because this type of calculation does not take into account the physical constraints placed on magma generation, namely that 100% melts will not be derived from each component. The result of smaller degrees of partial melting will be to increase the concentrations of the elements involved in mixing. This effect will be particularly important if different degrees of partial melting of the different components occur, as the relative element concentrations will change. A more realistic model is adopted below in which a plume impinges on the lithosphere to produce small degrees of partial melting of DMM/MORB source material in the lithosphere and/or in the plume envelope. This can occur either by direct transfer of heat at the plume/host boundary or by heat transfer resulting from the the passage of plume melts in the lithosphere or asthenosphere. A similar model was adopted by Chen and Frey(1983,5) to explain the coupled isotope and trace element variations in Haleakala basalts, Hawaii. In their model a 100% melt of an enriched mantle plume occurred accompanied by small degree (2 - 0.1%) melts of the lithosphere (MORB composition). The results for a similar model in which different degrees of partial melting in the plume and its envelope produce a series of mixing curves between melts derived from the two end members. The effect of this variation on an incompatible element pair compared to an isotopic ratio is illustrated in Fig.7.14a, in which La/Sm ratios are plotted against $^{143}/^{144}Nd$ for 1.0-0.01% partial melts of MORB source and 100% melts of the plume source. It is apparent from Fig.7.14a that for 100% plume melting the crystal fractionation corrected La/Sm

Fig.7.14. Modelling of the variation of crystal fractionation corrected La/Sm with $^{143}Nd/^{144}Nd$ in the SHRS (shaded field).

(a) The variation in the position of the melt envelope for 1.0% to 0.1% melting of the MORB source at various degrees of partial melting of the plume source (100%, 10%, 5%, 2%, 1%). The 0.01% fusion curve is shown for the 100% plume melt. The position of the 80:20 plume:MORB source line of constant mixing proportion is shown for reference.

The data for Haleakala, Hawaii (Chen and Frey(1985)) are also plotted to show the difference in temporal progression between the two suites.

(b) Modelling of the effect of varying the degree of fusion of the MORB source at constant degrees of fusion of the plume source (2%).

Input parameters to the model:

Plume source(ppm): La,0.656. Nd,1.26. Sm,0.406.

MORB source (ppm): La,0.328. Nd,1.15. Sm,0.406.

The ratios of $^{143}Nd/^{144}Nd$ of the components are those from Fig.7.12. The MORB source is calculated from Fig.6.9. (The source required to generate Sun and McDonough(1988) N-MORB from 15% fusion of a MORB source). The curves are calculated using general mixing equations from Faure (1986).

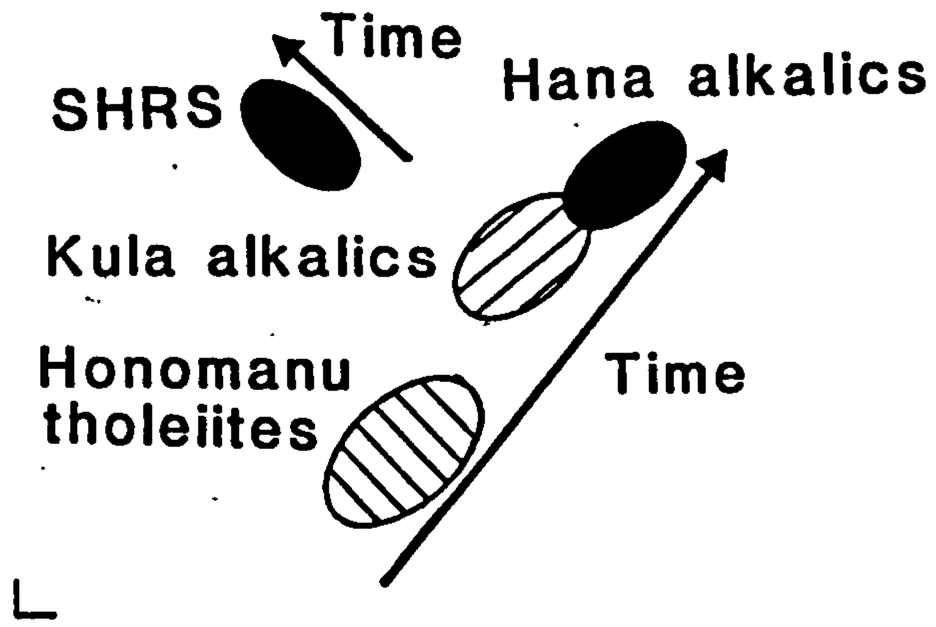
Time
SHRS
Hana alkalics
Kula alkalics
Honomanu
tholeiites
Time

SHRS

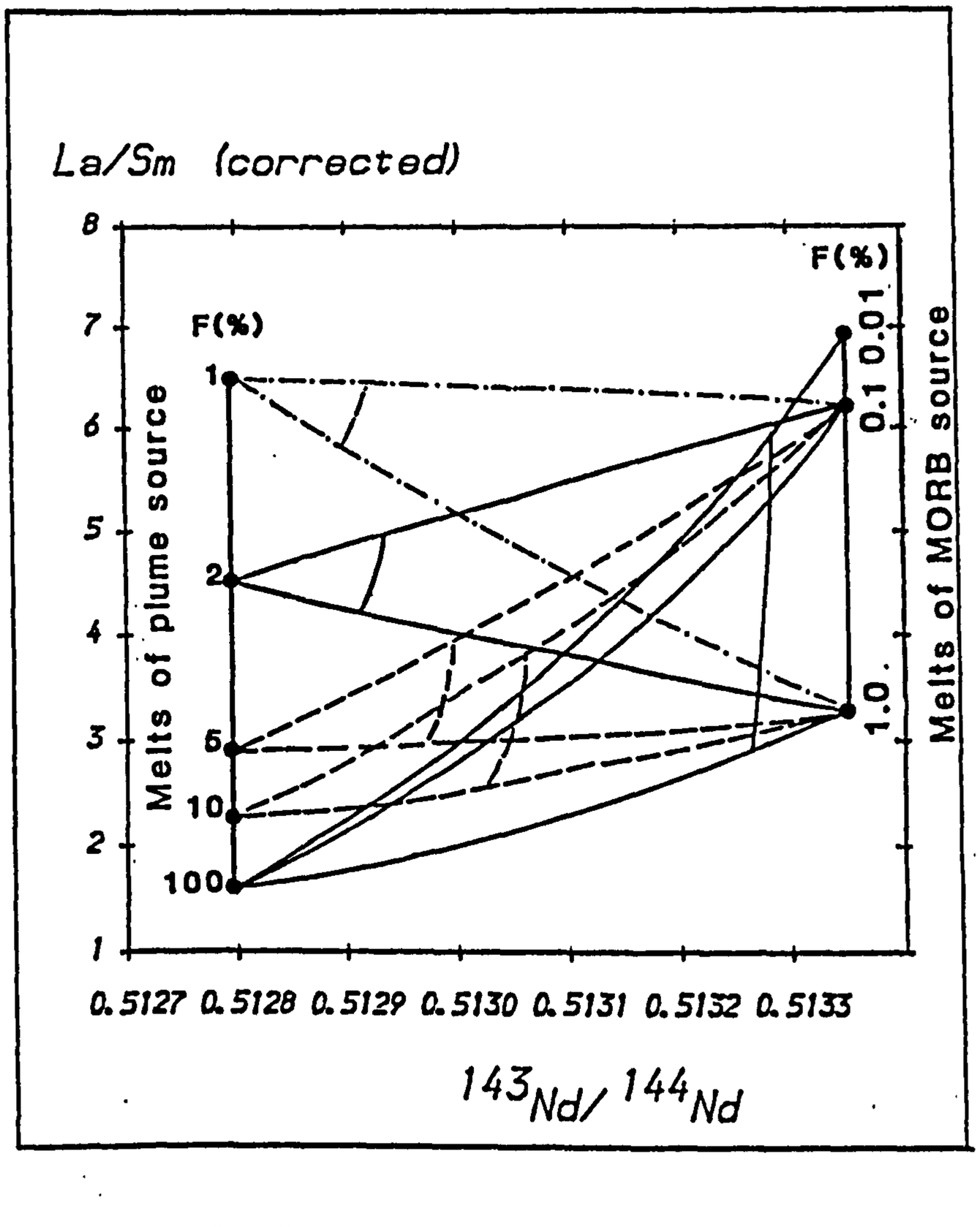
La/Sm (corrected)
8
7
6
5
4
3
2
1
F(%)
1
2
5
10
100
Melts of plume source
0.1 0.01
1.0.
Melts of MORB source
0.5127 0.5128 0.5129 0.5130 0.5131 0.5132 0.5133
143Nd/144Nd

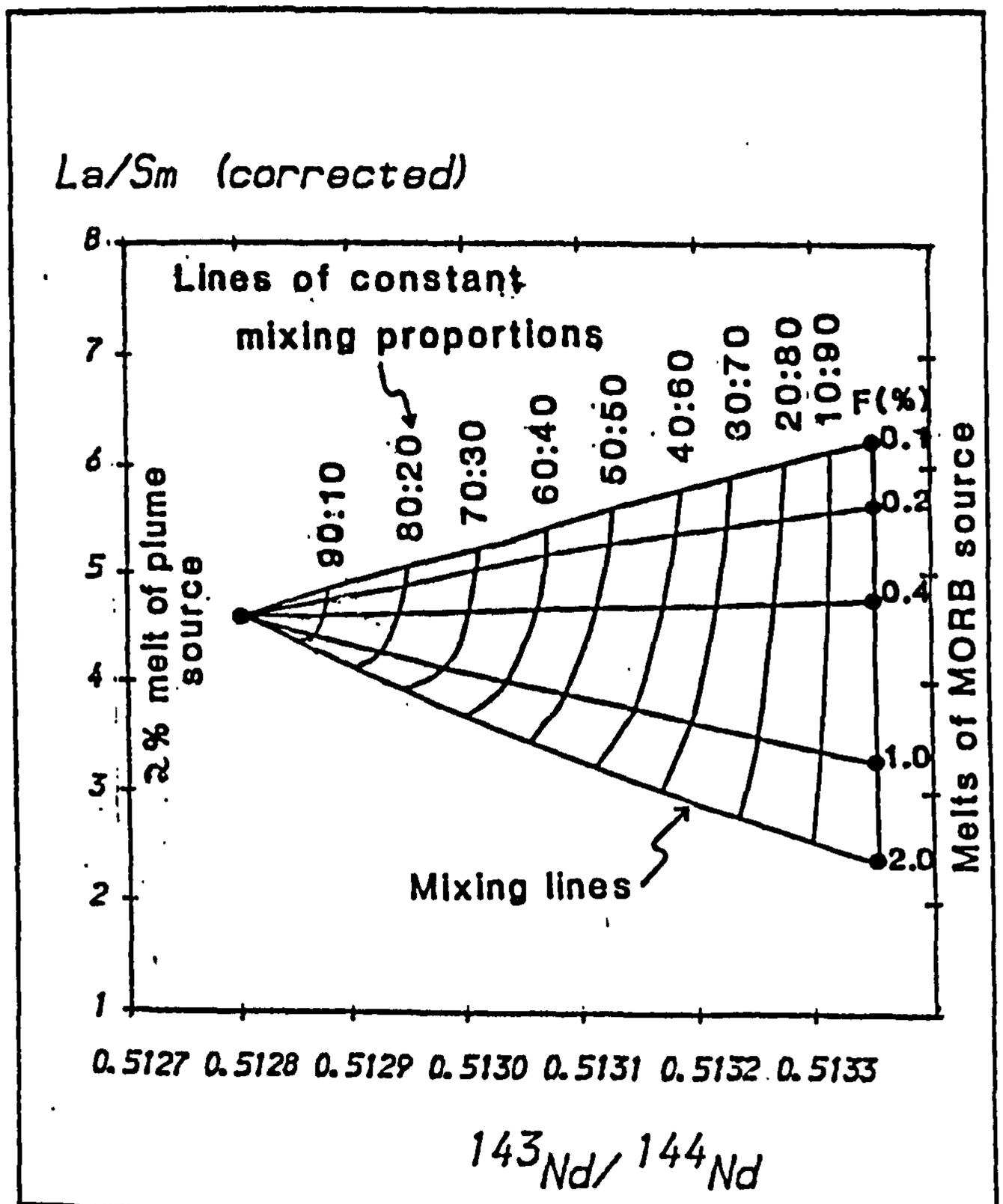
La/Sm (corrected)
8
7
6
5
4
3
2
1
Lines of constant
mixing proportions
90:10
80:20
70:30
60:40
50:50
40:60
30:70
20:80
10:80
F(%)
0.1
0.2
0.4
1.0
2.0
2% melt of plume source
Mixing lines
Melts of MORB source
0.5127 0.5128 0.5129 0.5130 0.5131 0.5132 0.5133
143Nd/144Nd

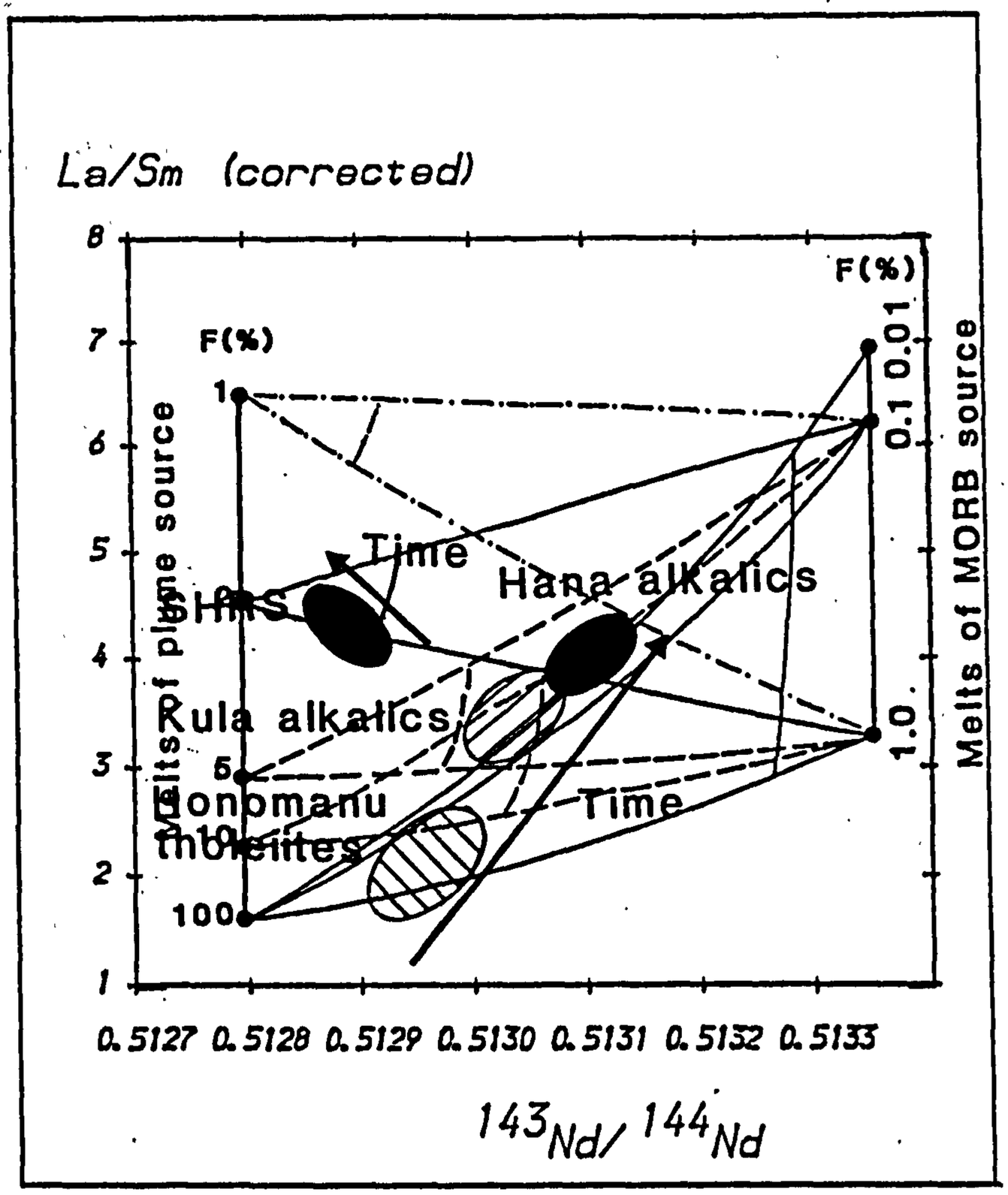
La/Sm (corrected)
8
7
6
5
4
3
2
1
F(%)
1
5
10
100
Melts of plume source
Time
SHRS
Hana alkalics
Rula alkalics
Honomanu tholeiites
Time
0.1 0.01
1.0
Melts of MORB source
0.5127 0.5128 0.5129 0.5130 0.5131 0.5132 0.5133
143Nd/144Nd

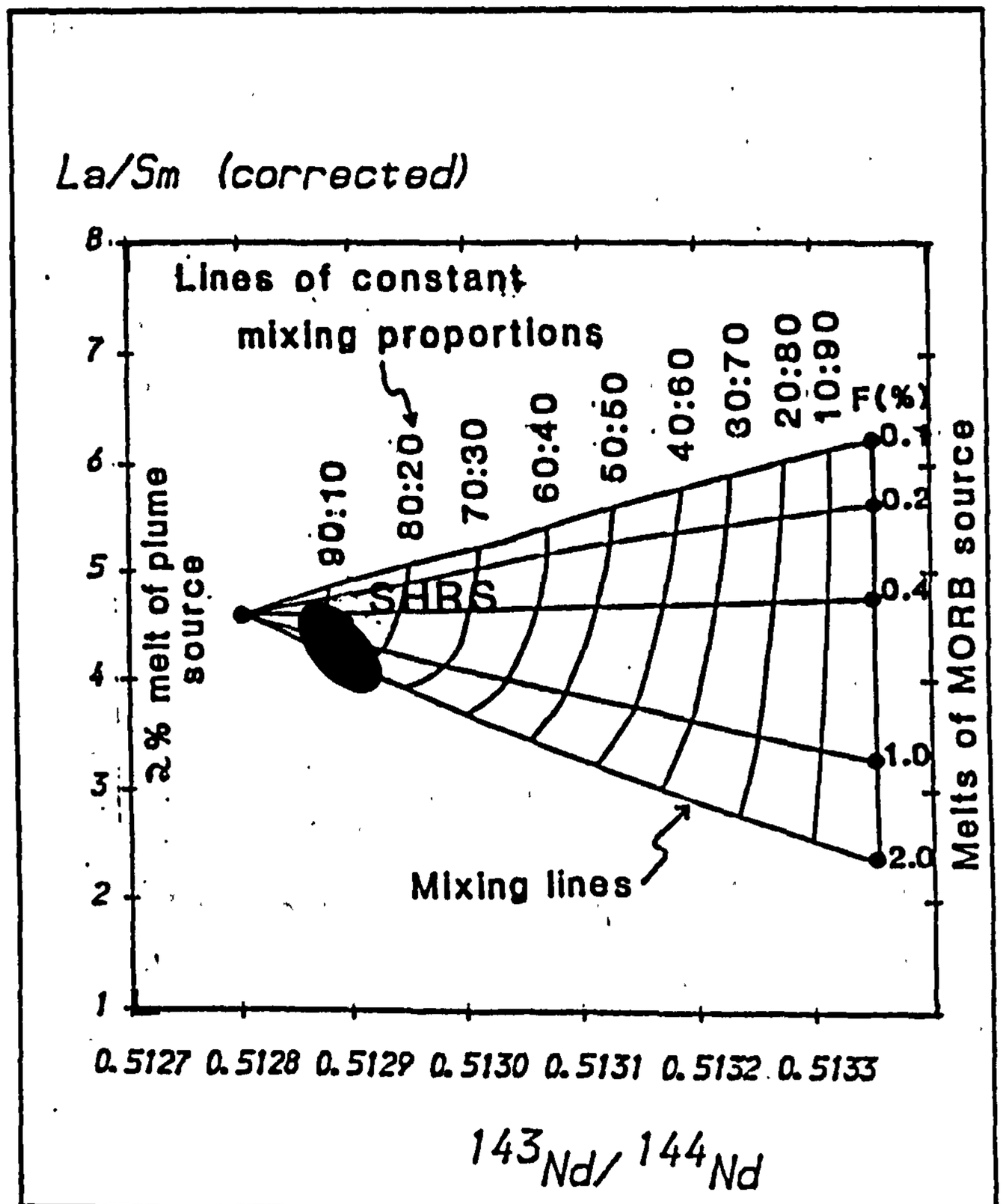
La/Sm (corrected)
8
7
6
5
4
3
2
1
Lines of constant mixing proportions
90:10
80:20
70:30
60:40
50:50
40:60
30:70
20:80
10:90
F(%)
0.1
0.2
0.4
1.0
2.0
2% melt of plume source
SHRS
Mixing lines
Melts of MORB source
0.5127 0.5128 0.5129 0.5130 0.5131 0.5132 0.5133
143Nd/144Nd

ratios in the SHRS are too high to be accounted for by this model even if very low degrees of partial melting of MORB source are invoked (<0.01%). This discrepancy is thought to occur because the plume itself will undergo partial melting which will fractionate the La/Sm ratio. It is found that for the source concentrations used 3% fusion of the HIMU component is compatible with the the observed values of La/Sm and $^{143}Nd/^{144}Nd$ (Fig.7.14b). It is emphasised that this degree of melting and the mixing proportions have no physical significance as they are directly dependent on the estimated source concentrations which are poorly known. The important points to note from Fig.7.14b are that:

(1) Smaller proportions of components are possible in models invoking different degrees of melting of the components in the source.
(2) The degree of trace element enrichment is remarkably constant. This indicates that the degree of fusion in the plume remains approximately constant (2-5%). Different degrees of fusion of the MORB source have a limited effect on trace element ratios because the SHRS are near to the the plume end member composition.
(3) The samples which have the greatest trace element enrichment and lowest values of $^{143}Nd/^{144}Nd$ are produced by smaller degree partial melts of the MORB source, and these melts contribute a smaller proportion to the mixture than melts with lower trace element ratios. This is consistent with temporal variations - lavas erupted at a late stage in the NE and SW volcano evolution are most enriched in terms of trace elements and have the largest HIMU signature. Such temporal effects would be expected with a waning heat flux causing less fusion of the depleted component.

It is apparent from Fig.7.14a that the lavas from Haleakala, Hawaii described by Chen and Frey(1983,5) which are typical of Hawaiian volcanism, possess a different geochemical age progression from those of St.Helena. Notably, other OIB suites tend to possess a similar geochemical age progression to St.Helena, for example; more radiogenic Pb and Sr compositions and less radiogenic Nd compositions occur in the youngest, trace element enriched volcanics in each suite e.g. Ua Pou, Marquesas (Duncan et al.(1986), Principe

(Cameroon line (Halliday et al.(1988)) and the Marquesas islands (Dupuy et al.(1986)). In OIB suites where good age constraints are unavailable positive correlations in parent/daughter with isotopic ratios are the norm e.g. Iceland (Zindler et al.(1979), small Pacific seamounts (Zindler et al.(1984)). In other cases no temporal trends are discernible despite considerable isotopic heterogeneity e.g. Galapagos (Geist et al.(1988), Cape Verde Islands (Davies et al.(1988)). The isotope - trace element correlations in islands such as St.Helena are readily explicable by a *declining thermal flux* causing *lower* lower degrees of fusion of a MORB lithosphere/asthenosphere component through time. Hawaiian volcanics, which appear to be an exception to the rule are less easy to explain. Chen and Frey(1983,5) explained the trend evident in Fig.7.14a by a *decrease* in the *contribution of the plume component* in the mixture coupled with a *decrease in the degree of partial melting of MORB source. The decrease* in the contribution of the plume component in the source is thought to occur as the island moves away from the plume. Thus, the essential difference between these two models is that in the St.Helena situation there is no requirement to vary the proportion of end members in the source, whereas in the Hawaiian example a decline in fusion is coupled to a decline in the enriched blob/matrix ratio in the plume.

7.6; Summary;

The general model that is envisioned (Fig.7.15) for the temporal variations in geochemistry in the SHRS draws upon all of the alternatives outlined above, but particular emphasis is placed on primary effects. It is believed that the principal effect generating the mixing trends are interactions within the plume and with its surrounding envelope. This produces the clearest causal link between a declining thermal flux and the time related geochemical variations. Following segregation of melts from the source region a secondary interaction between ascending melt and lithosphere may occur. These effects are superposed on the mixing trends which tend to obscure the main variations. This is believed to be a less important process as it does not satisfactorily explain the temporal geochemical variations unless lithospheric melt pathways are established throughout the activity of a shield and the geochemical contribution of the

Fig.7.15. General model of genesis of SHRS.

Zones of mixing between components.

A : Within plume.
B : Plume/envelope.
C : Plume/lithosphere (direct).
D : Melt pathway interactions.
E : Subcrustal magma chambers.
F : High level magma chambers.

▲ = Thermal and chemical flux

▶ = Movement of oceanic plate relative to plume.

Bold arrows represent melts ascending through lithosphere
Smaller arrows represent smaller degree melts freezing into lithosphere.

(a) 10 Ma - Initial stage. The plume is shown as impinging on a lithosphere unaffected previously by magmatism. However, some failed OIB melts may exist in the lithosphere. Magmatic activity associated with the plume necessarily existed prior to 10 Ma, to account for the 4400m of volcanics built up from the seafloor. During this time some depletion of the MORB component in the lithosphere to form more refractory material may have occurred as passing melts scavenged elements from the lithosphere. As a result it is likely that the unsampled submarine samples possessed more depleted compositions than the subaerial ones.

(b) 9 Ma - The development of the NE shield. Early volcanics (NEBB, NE(BB)) have the highest proportion of DMM component because of large degrees of fusion in the plume causing fusion of the depleted plume envelope and lithosphere. During activity the thermal flux beneath the volcano declines, either as a deep seated effect or because of the relative plate motion. This results in smaller degree melts from the plume periphery with higher greater trace element enrichment and smaller degrees of melts in the plume envelope. If the melt pathways in the lithosphere remain constant with earlier activity only refractory material will remain, again resulting in an increased HIMU signature with time.

(c) 8 Ma: SW volcano - Larger degree melts produce greater degrees of fusion in in envelope/lithosphere and a higher DMM component than in the NEMS. However at the base of the SW volcano the geochemistry is a combination of enriched material from the edge of the plume (beneath the NE volcano) and depleted material from the centre of the plume (beneath the SW volcano). Overlapping high level melt conduits are necessary to achieve this.

(d) Waning stages of activity - Declining thermal flux causes an increase in the signature of the HIMU component for similar reasons to those at the top of the NEMS. The development of well established magma chambers permit more time for evolved compositions to be produced by crystal fractionation resulting in homogenisation of material ascending from the mantle to produce a relatively constant isotopic composition in the SWUS, SWEF and SWLI.

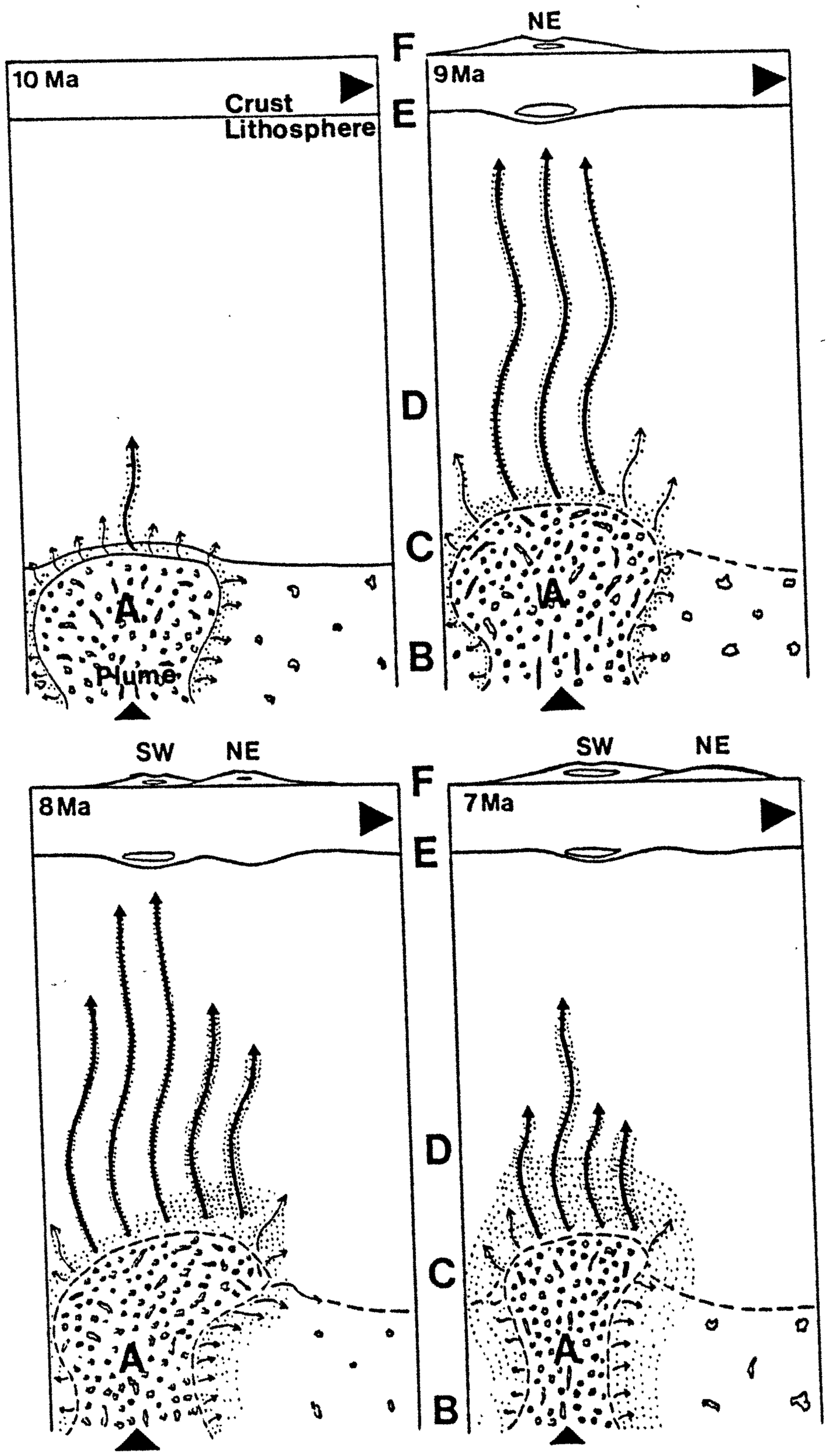
10 Ma
Crust
Lithosphere
A
Plume
NE
9Ma
A
F
E
D
C
B
SW
NE
8Ma
A
SW
NE
7Ma
A

wallrock decreases throughout this time. It is also uncertain that magma ascent rates are low enough for this process to operate. It is thought that the occurrence of samples which reverse the geochemical trends at the top of shield units (e.g. SC 8 (NEMS) and SC 237,238 (SWLS)) can most easily be explained as precursors to the next shield unit. It is necessary to invoke an overlap of high level (crustal) magma conduits and mixing between the last melts of one phase of activity and and the first of the next. Alternatively, if switching of melt pathways with renewed incorporation of adjacent depleted material is an important process, this could be invoked to produce the anomalous isotope compositions. This process may be aided by the motion of the plate relative to the heat source. In the example at the top of the NEMS/base of the SWLS the observed melts will be a combination of those from the centre plume (depleted) and the edge of the plume (enriched) (Fig.7.15b,c). Another factor is that the eradication of heterogeneities could be effected by the establishment of long-lived high level magma chambers. Thus, the difference between the relatively uniform SWUS and SWEF in which evolved lavas occur and heterogeneous NEMS and SWLS in which primitive types dominate could be explained by magma chambers in the NEMS and SWLS being more transient and with a more rapid throughput of material from depth to the surface occurring. This difference also corresponds to a difference in style of activity of the two shields; the SWUS has fewer discontinuities and pyroclastic horizons than the SWLS, which represents less stable shield activity.

CHAPTER 8

THE ORIGIN OF THE HIMU MANTLE COMPONENT :

8.1;Introduction;

The value of the SHRS isotopic characteristics in providing an illustration of source region interactions has already been discussed in Chapter 7. The isotopically extreme nature of the St.Helena magma source is also of great intrinsic interest. The St.Helena mantle component has been defined as one of the five principal mantle components which contribute towards virtually all oceanic magmatic products in terms of isotopic composition (White(1985)). The term "HIMU component" (Zindler and Hart(1986)) is currently in vogue because this is more descriptive of the source characteristics (HIgh time integrated MU ($^{238}U/^{204}Pb$)) than the term "St.Helena mantle component" (White(1985)). Because of this the former term is used throughout this chapter. The processes by which these characteristics are generated are clearly of fundamental importance to our understanding of chemical geodynamics, yet they have remained enigmatic. Ideas of how these characteristics were acquired may only be gleaned by an integrated study of the full range of ocean basin volcanics. Such studies have produced a great diversity of alternatives to account for the HIMU characteristics. The questions that must be posed to help resolve this issue are, firstly which elements were fractionated in events producing the HIMU component and secondly how and when did this occur. This chapter firstly describes the characteristics of the HIMU component that sets it apart from other principal mantle components. This is achieved by comparison of its isotopic characteristics within a global framework. An isotopic criterion to distinguish basalts with a significant HIMU component in their source is defined to enable comparison of the trace element characteristics of HIMU source OIB. The trace element features are initially described by comparison with trace element characteristics of S.Atlantic OIB, which encompasses a large range of global oceanic magmatic compositions. Comparisons are then made with other HIMU OIB suites to investigate whether any common features exist. The various alternatives that have been proposed to account for the creation of the St.Helena

component are considered from a critical viewpoint. The possible mechanisms by which the characteristics could be produced are then evaluated. This is followed by consideration of how and where the St.Helena component could be stored and how it may become mobilised to become part of the OIB reservoir.

8.2; Isotopic characteristics of HIMU;

The extreme isotope characteristics of St.Helena compared to other oceanic volcanic suites are evident in the diagrams used to investigate source interactions in Chapter 7. Thus compared to MORB and the vast majority of other OIB St.Helena has extremely radiogenic Pb compositions (Fig.7.7) The location of St.Helena basalts to the left of the "mantle array" in Sr-Nd isotopic space (Fig.7.4) may be a result of relatively low $^{143}Nd/^{144}Nd$ or low $^{87}Sr/^{86}Sr$, or a combination of both. Comparisons of variations of Sr and Nd isotopes versus Pb isotopes (Fig.7.12) suggest that the displacement to the left of the mantle array may mainly be accounted for by St.Helena magmas possessing relatively low $^{87}Sr/^{86}Sr$. This is deduced from the lower abundance of OIB possessing $^{87}Sr/^{86}Sr$ lower than St.Helena compared with OIB which contain higher $^{143}Nd/^{144}Nd$ than St.Helena. For example Guadalupe (Fig.7.12) has a higher $^{87}Sr/^{86}Sr$ than St.Helena but also has a higher $^{143}Nd/^{144}Nd$, i.e. St.Helena is more MORB like than Guadalupe in terms of $^{87}Sr/^{86}Sr$ but not $^{143}Nd/^{144}Nd$. Further evidence for the relative degree of Rb-Sr and Sm-Nd fractionations is given below.

To enable comparison of the trace element characteristics of St.Helena with other OIB containing a significant HIMU component an arbitrary definition of basalts containing a significant HIMU component is now given. *HIMU source basalts are considered to be those with $^{206}Pb/^{204}Pb$ >20.0.* This value is chosen because Pb isotopes are the sole feature that uniquely distinguishes HIMU source basalts from other OIB and MORB. Sr and Nd isotopic values are unsuitable as discriminants because MORB possesses a more depleted radiogenic character and some OIB are more enriched relative to St.Helena (e.g. Gough and Tristan da Cunha islands, Fig.7.4). The position of HIMU source basalts below the Sr-Nd isotope "mantle array" of White and Hofmann(1982) is well known, but it cannot be used to discriminate from other basalts because

basalts with relatively unradiogenic Pb also plot below this (e.g basalts of the LoNd array of Hart et al.(1986) such as Walvis Ridge (Fig.7.4)). The $^{206}Pb/^{204}Pb$ value is chosen rather than the $^{208}Pb/^{204}Pb$ or $^{207}Pb/^{204}Pb$ ratios as high values of these ratios may be recorded in arc basalts with a sediment subduction component (e.g. South Sandwich arc - Cohen and O'Nions(1982)). The arbitrary value of 20 rather than a value of 19.5 that was chosen by White(1985) is used to exclude all E-type MORB and OIB that may result from recent mixing between HIMU and MORB components in the source region (Fig.7.7). The NE seamounts are not excluded however, but these seamounts clearly possess a substantial HIMU component in their source (Taras and Hart(1983)). The NE seamounts and Guadalupe (Sun(1980)) are not considered further below, because of insufficient data on LIL elements. The location of islands meeting this criterion for HIMU are shown in Fig.8.1.

Within the S.Atlantic framework (section 8.3.1) Gough and Tristan da Cunha are nearer to the Enriched Mantle end members (EM) of Zindler and Hart(1986). They possess Sr and Nd compositions near to that deduced for Bulk Earth. The possible explanations for the formation of these islands which are examples of the so-called DUPAL OIB are beyond the aegis of this chapter, and are not considered further below. Ascension OIB occurs on a mixing trend between St.Helena and MORB and Bouvet lies on a mixing trend between St.Helena and Tristan da Cunha and Gough islands (Fig.7.12).

The isotope characteristics described above show that in terms of parent/daughter ratios the St.Helena magma source must have possessed a high U/Pb ratio and low Rb/Sr ratio to evolve to its present isotopic compositions. These isotopic characteristics may be used to estimate the time for which the St.Helena source has possessed the trace element characteristics which are necessary for the source to evolve by radioactive decay towards the radiogenic HIMU compositions observed in the erupted volcanics. These ages are very valuable in placing constraints on the process by which the HIMU component was produced and how it was stored and transported to the source region of OIB. The ages calculated for separation using the two - stage Pb evolution model of Chase(1981) yield a separation period of approximately 2.4 Ga for the HIMU component in St.Helena OIB (section 7.4.). Sr and Nd isotopes do not produce

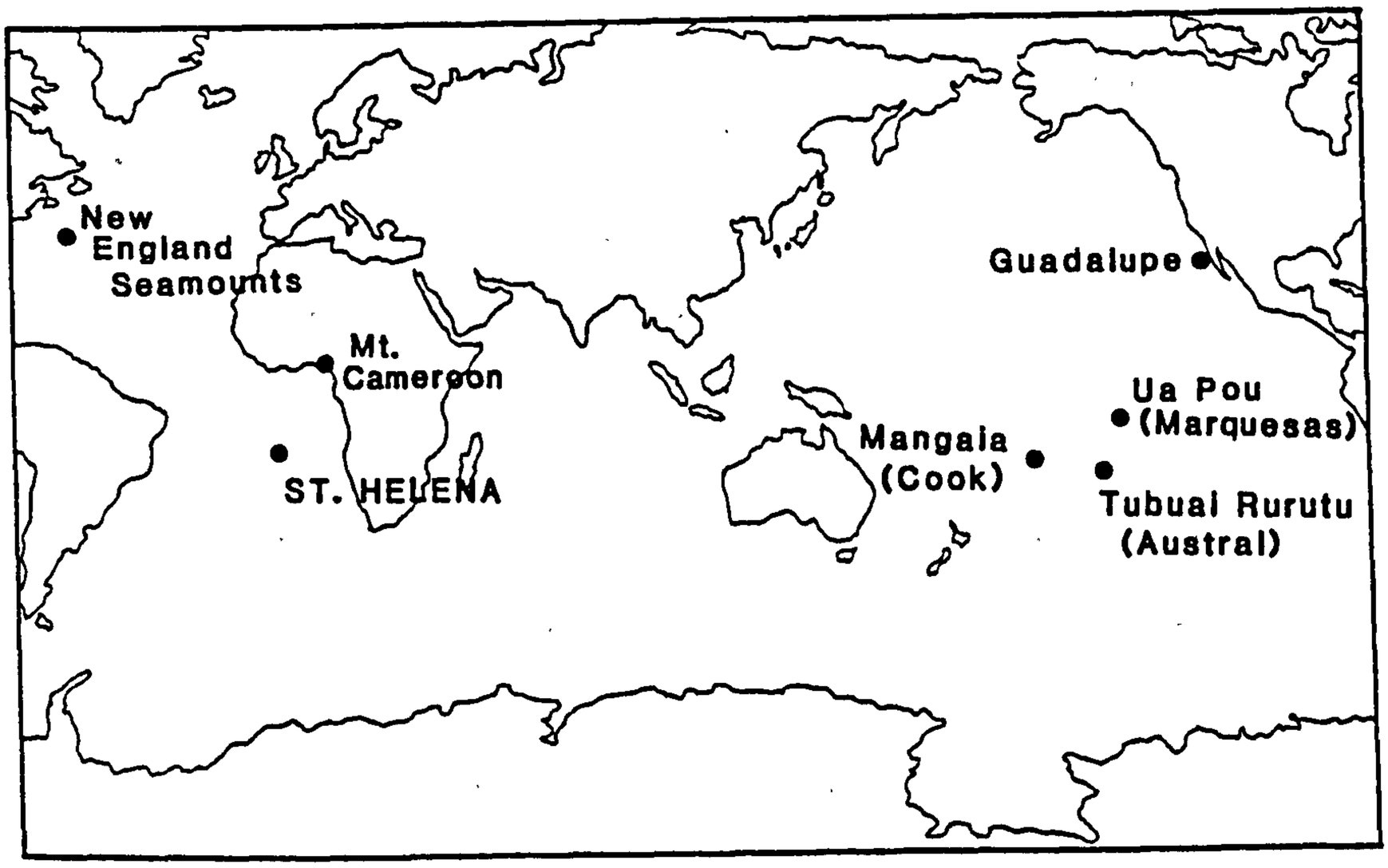

Fig.8.1. Location map of HIMU OIB discovered to date.

The criterion for inclusion as HIMU OIB is $^{206}Pb/^{204}Pb > 20.0$ (see text for discussion of this choice).

good constraints on the age of formation of these characteristics (section 7.4).

The 2.4 Ga separation time calculated in section 7.4 is based on the interpretation of the Pb-Pb correlation for the SHRS as an isochron (Fig.7.8). However, this may not be a valid assumption for the reasons discussed in section 7.5.2. Independent methods for calculating the likely source separation time are also available. The method of Sun and McDonough(1988) is used to derive the separation age from a comparison of ^{235}U evolution and ^{238}U evolution. In this method secondary mu in a two stage Pb evolution model is calculated by a comparison of the observed $^{206}Pb/^{204}Pb$ ratios in the SHRS with first stage $^{206}Pb/^{204}Pb$ values derived from models of Archaean and Proterozoic mantle evolution. The version II Pb isotopic growth curves of Zartmann and Doe(1981) are used because these are consistent with the Pb isotope data available from Archaean and Proterozoic komatiites (e.g. Brevart et al.(1986)) and Phanerozic ophiolites (e.g. Chen and Pallister(1981)) according to Sun and McDonough(1988). The variation of calculated secondary mu required to produce the $^{206}Pb/^{204}Pb$ characteristics of sample SC 149 (that with the most extreme radiogenic Pb of the SHRS) from the $^{206}Pb/^{204}Pb$ curves of Zartmann and Doe(1981) for various separation ages are shown in Fig.8.2a. These curves are calculated from equation D5, Appendix D. A minimum possible separation time of 1 Ga is indicated by the observed value of mu in a member of the SHRS (from Sun and McDonough(1988)) with a similar value of $^{206}Pb/^{204}Pb$ (20.9) to SC 149 (20.89) (Fig.8.2a). This is a minimum separation period because any variations in U/Pb through partial melting would cause an increase in U/Pb because U is more incompatible than Pb (section 8.4), (Sun and McDonough(1988)). Further constraints are placed on the separation age by calculating the theoretical $^{207}Pb/^{204}Pb$ values for the mu_2 values shown in Fig.8.2a. The curve produced by solving equation (D6), Appendix D, for these values of mu is shown in Fig.8.2c. This indicates a separation time of approximately 2 Ga because this corresponds to the measured $^{207}Pb/^{204}Pb$ in SC 149. *Secondary values of mu and kappa of 16 and 3.5 respectively are indicated for a 2 Ga separation period* (from Fig.8.2a and 8.2b). The secondary mu value calculated in section 7.4 by assuming correlations in Pb-Pb isotopic space represent mantle isochrons (mu_2=15.5) is in good agreement with this method.

Fig.8.2. Modelling of the U-Th-Pb systematics of the HIMU component over the past 3.2 Ga.

(a) Variation in the $^{238}U/^{204}Pb$ ratio necessary to develop the radiogenic Pb compositions observed in the SHRS. A two stage model is adopted in which the $^{206}Pb/^{204}Pb$ ratio at the time of the fractionation event (x-axis) is given by the Pb mantle evolution curve (version II) of Doe and Zartman(1981). The second stage mu value (y-axis) necessary to produce the observed composition of $^{206}Pb/^{204}Pb$ in the most radiogenic of the SHRS compositions (SC 149=20.89) are calculated using the standard equation for decay of ^{238}U to ^{206}Pb (equation(D5), appendix,D) The point marked by the asterisk is the observed value of $^{238}U/^{204}Pb$ in the SHRS basalt SB 2882 (Sun and McDonough(1988). SB 2882 possesses identical (within error) Pb isotopic compositions to SC 149.

(b) Variation in the $^{232}Th/^{238}U$ ratio necessary to produce the observed $^{208}Pb/^{204}Pb$ values in SC 149 (40.1672) using a similar model to that in (a). Equation D7, appendix D is used.

(c) The variation in the present day $^{207}Pb/^{204}Pb$ produced by assuming mu values calculated in (a). First stage $^{207}Pb/^{204}Pb$ values are derived from Doe and Zartman(1981). The observed $^{207}Pb/^{204}Pb$ value in SC 149 corresponds to an age of 2 Ga.

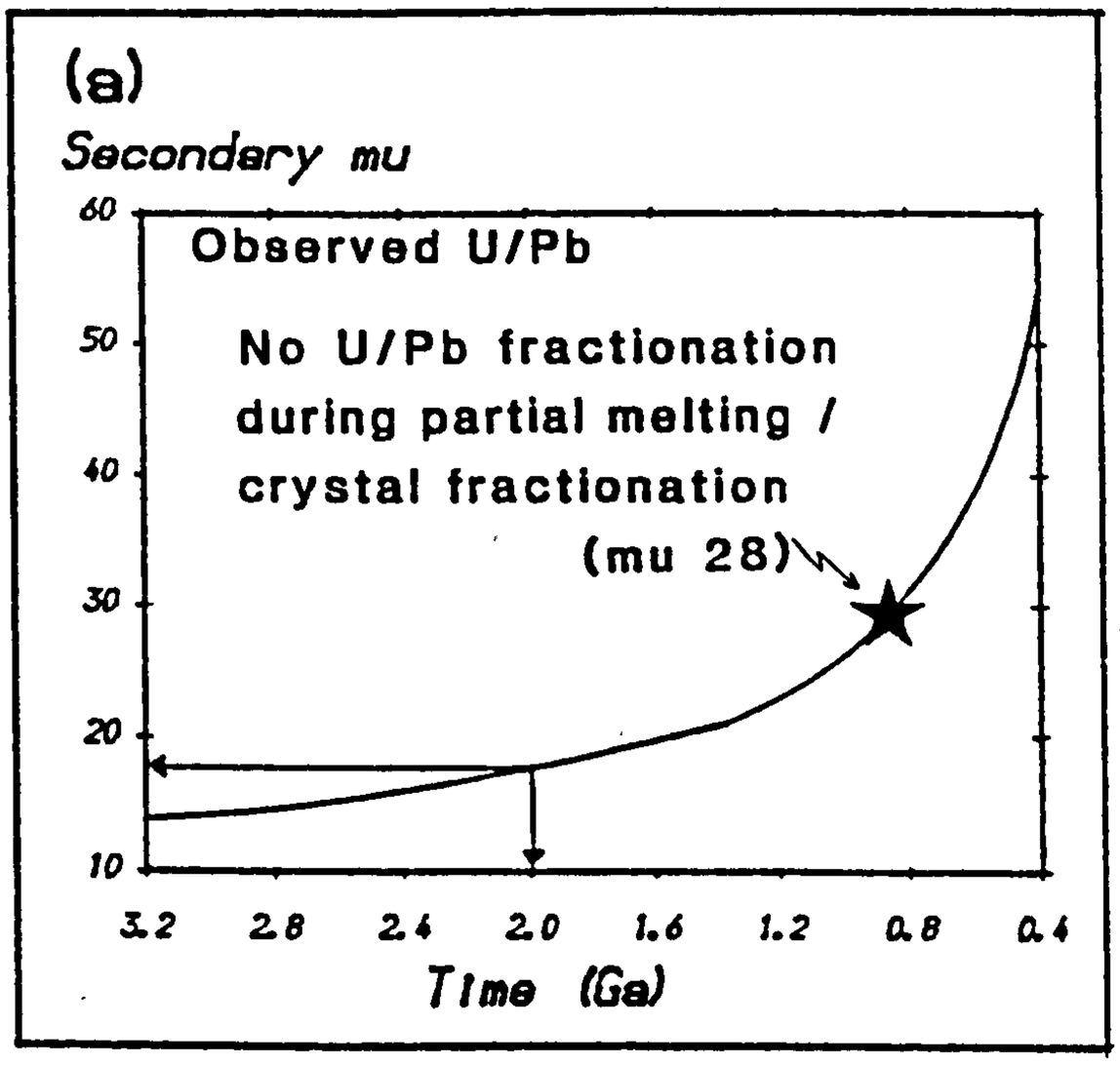
(a)
Secondary mu
Observed U/Pb
No U/Pb fractionation
during partial melting /
crystal fractionation
(mu 28)
60
50
40
30
20
10
3.2
2.8
2.4
2.0
1.6
1.2
0.8
0.4
Time (Ga)

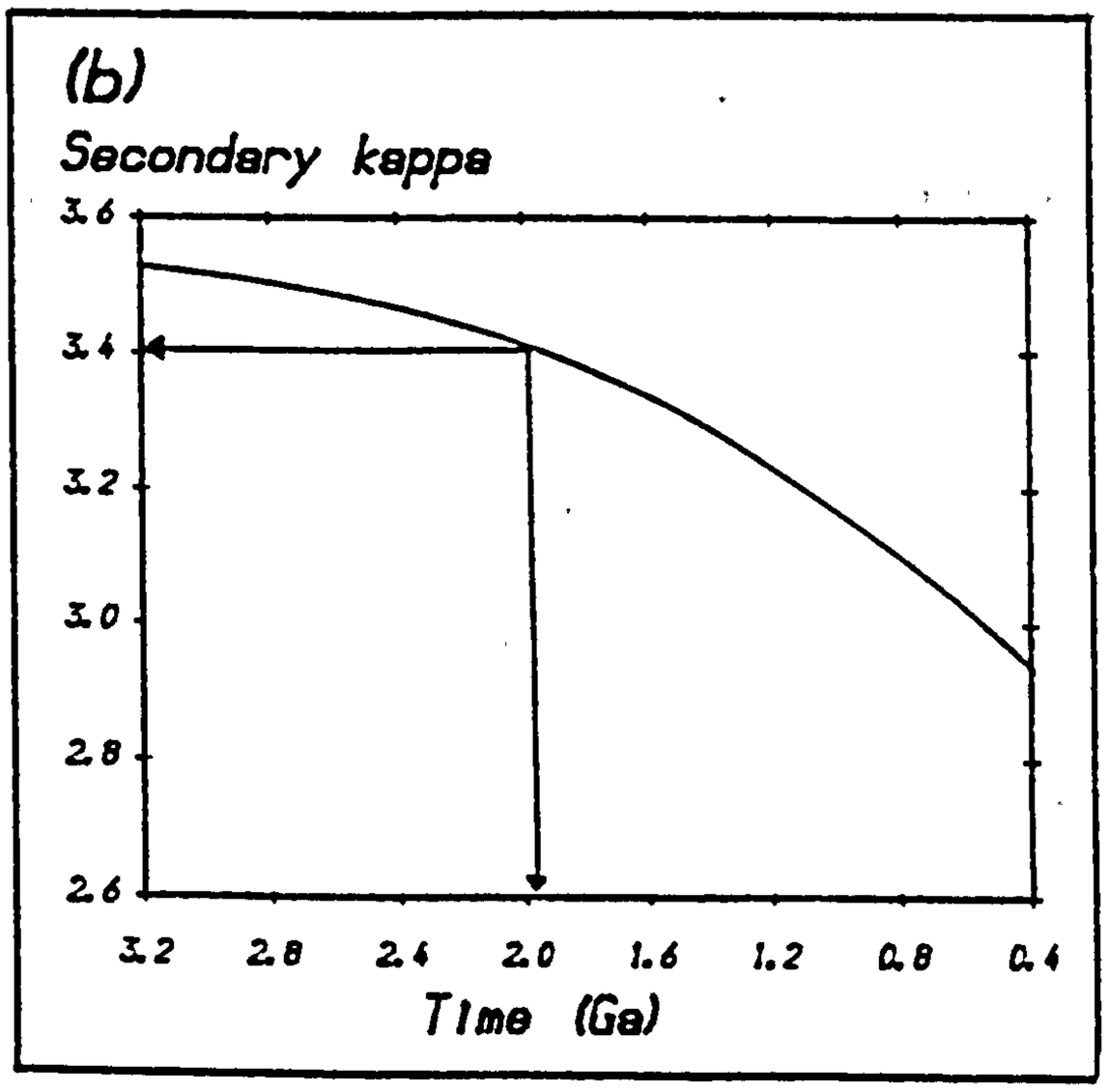
(b)
Secondary kappa
3.6
3.4
3.2
3.0
2.8
2.6
3.2
2.8
2.4
2.0
1.6
1.2
0.8
0.4
Time (Ga)

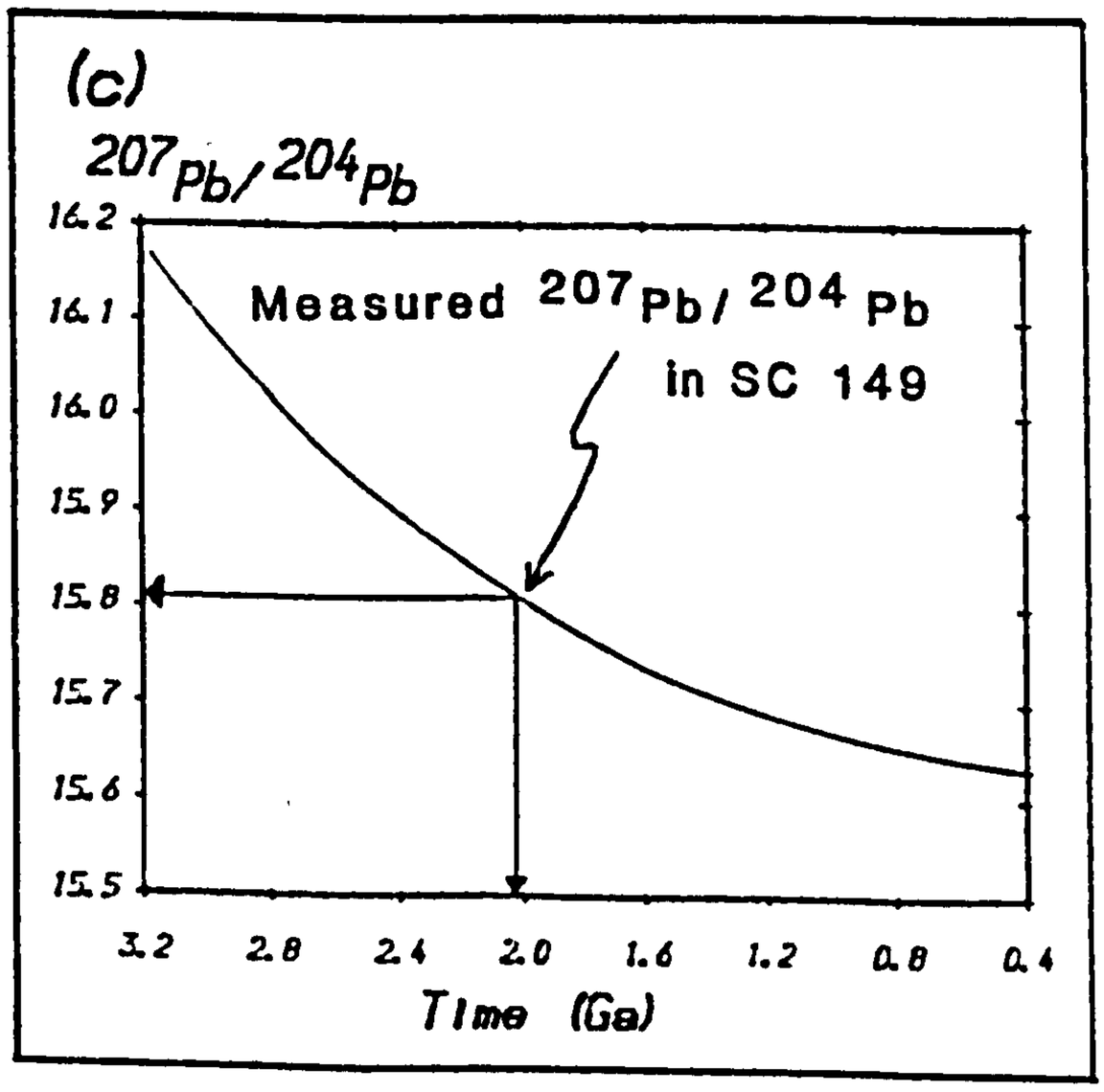
(c)
207Pb/204Pb
16.2
16.1
16.0
15.9
15.8
15.7
15.6
15.5
Measured 207Pb/204Pb
in SC 149
3.2
2.8
2.4
2.0
1.6
1.2
0.8
0.4
Time (Ga)

This may be fortuitous because calculations in section 7.4. indicate a lower secondary kappa (2.5) and an unrealistically high primary kappa (>5) (compared to other OIB and other methods of calculating primary kappa (Allegre et al.(1986c)). Sun and McDonough(1988) noted that a similar isolation time is indicated for other HIMU OIB by this technique. For example Tubuai and Mangaia (Palacz and Saunders(1986)) give 1.7 Ga. Sun and McDonough(1988) also noted that Ua Pou gives an isolation time of 1 Ga, which is the youngest separation time for the HIMU OIB.

A recent contribution by Galer and O'Nions(1985) has cast doubt on the likelihood of material present in the upper mantle retaining Pb (and by implication Sr and Nd) isotope characteristics for a period as great as that suggested by Pb-Pb isotope correlations such as Fig.7.8 or the calculation above. They considered kappa values derived from the radiogenic $^{208}Pb^*/^{206}Pb^*$ ratio. This is given by the difference between measured Pb isotope values and primordial values given by the Canyon Diablo meteorite calculated as:

$$\frac{^{208}Pb^*}{^{206}Pb^*} = \frac{(^{208}Pb/^{204}Pb)_{meas} - (^{208}Pb/^{204}Pb)_{Canyon\ Diablo}}{(^{206}Pb/^{204}Pb)^{meas} - (^{206}Pb/^{204}Pb)_{Canyon\ Diablo}} \qquad (8.1)$$

Thus $^{208}Pb^*/^{206}Pb^*$ gives the time integrated Th/U ratio over the age of the earth (termed $kappa_{(Pb)}$). Galer and O'Nions(1985) pointed out that the average $kappa_{Pb}$ for MORB (3.75) was only slightly smaller than their assumed *planetary kappa value of 3.9*. They suggested that this was because there was a steady state flux of Pb (and other incompatible elements) from a lower primitive reservoir to a depleted reservoir caused by entrainment at the upper mantle - lower mantle boundary. The residence time of Pb in the upper reservoir was calculated as 0.6 Ga. This figure was calculated by assuming a simple two stage Pb evolution model similar to that adopted by Sun and McDonough(1988) as explained above, except that the model Pb growth curves of Zartmann and Doe(1981) were not used. First stage Pb evolution is based on equation D4 and D7. Galer and O'Nions(1985) used first stage kappa and mu values of *3.9* and *8* respectively. A secondary kappa value of *2.5* was used because because this is the average value calculated from measured values of $^{232}Th/^{230}Th$ in studies of MORB. This

Fig.8.3. Modelling of the evolution of radiogenic $^{208}Pb^*/^{206}Pb^*$ (equation 8.1) with time assuming various permutations of first and second stage kappa values in a simple two stage model of Pb evolution commencing at 4.55 Ga.

(a) Second stage evolution curves for radiogenic $^{208}Pb^*/^{206}Pb^*$ for:

$mu_1 = 8.0$, $kappa_2 = 2.5$, $mu_2 = 4\text{-}20$ for:

(1) Light lines $kappa_1 = 3.9$ (after Galer and O'Nions(1985))

(2) Bold lines $kappa_1 = 4.2$ (value from Allegre et al.(1986c)).

(b) Second stage Pb evolution curves as in (a) showing the effect of varying $kappa_2$ (2.5-3.5) with other parameters given by:

$mu_1 = 8.0$, $mu_2 = 20$, $kappa_1 = 4.2$

(a) Two stage Pb evolution curves for:

mu_1=8.0, mu_2=variable as shown, $kappa_1$=4.2 (bold lines), $kappa_1$= 3.9(light lines), $kappa_2$= 2.5

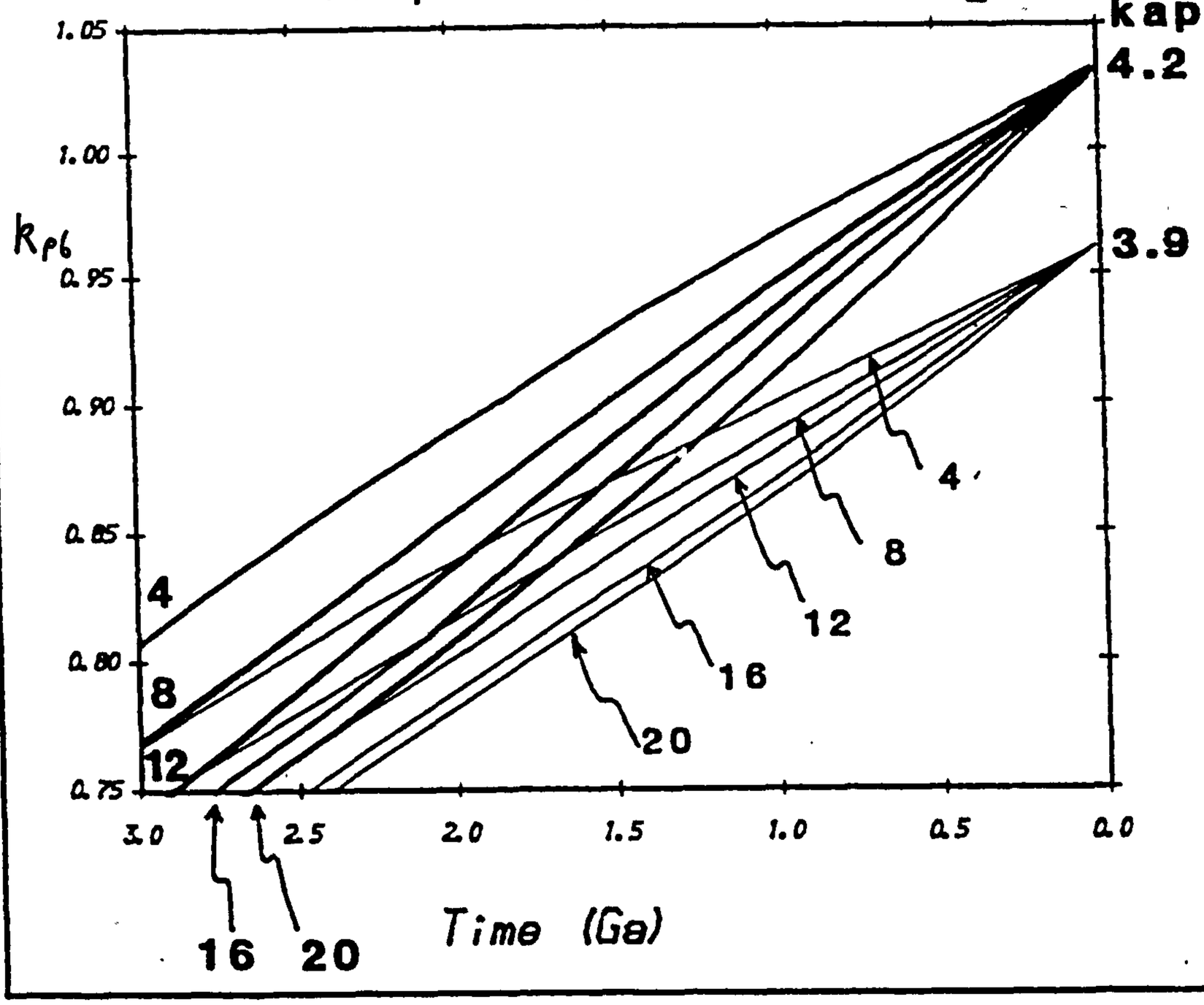

(b) Two stage Pb evolution curves for:

mu_1=8.0, mu_2=20.0, $kappa_1$=4.2, $kappa_2$= variable as shown

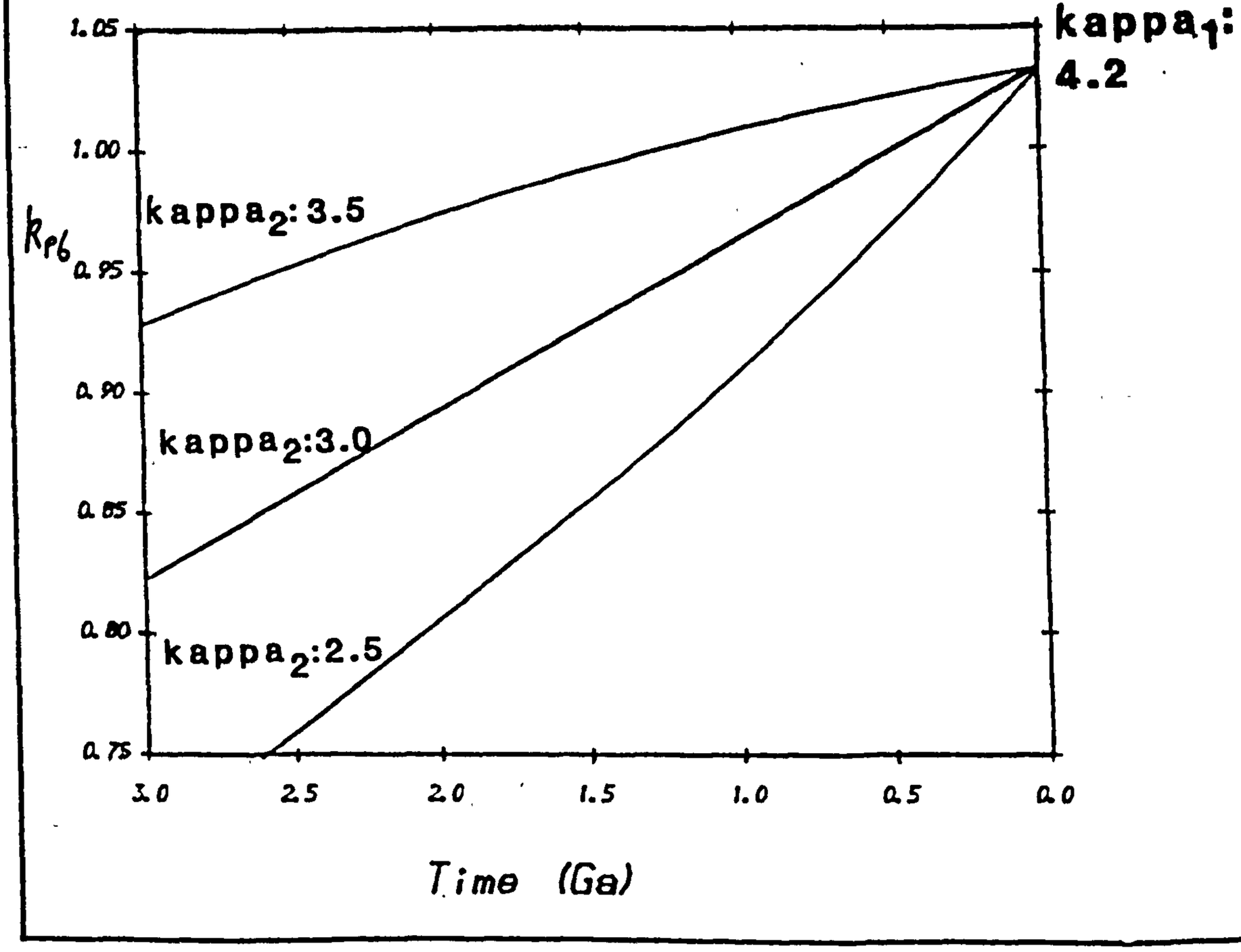

is termed $kappa_{Th}$. The model is shown in Fig.8.3a. Secondary mu ranges from 4 to 20 . It is apparent that for an average value of mu of 8 to 12 which is required to generate isotopic Pb values in MORB which lie to the right of the geochron (Fig.7.7), Tatsumoto(1978), *a residence time for Pb in the upper mantle of 0.6 Ga* is indicated for the average MORB value for $kappa_{Pb}$ of 3.75. This is at variance with the separation time calculated for both MORB and OIB suites including the sample calculation above. This enigma may not exist as such if the results of Allegre et al.(1986c) are correct. They derive a *planetary kappa value of 4.2* using data from both Archaean komatiites and recent basalts. This is important because a two stage model will then produce a separation time consistent with that described above. This effect is illustrated in Fig.8.3a. The bold curves are derived from the same model as those for primary kappa =3.9, except that primary kappa is assumed to be 4.2. It is clear that the permissible residence age of Pb is almost doubled for the small increase in primary kappa values. The fact that the residence age is critically dependent on the value of primary kappa was not stressed by Galer and O'Nions(1985). Similarly they did not illustrate the effect of varying secondary kappa values. This effect is illustrated in Fig.8.3b which shows that the residence ages are again critically dependent on the secondary kappa values. A mu_2 value of 20 is used as a maximum value for HIMU; the method of Sun and McDonough(1988) gives mu_2 = 17. A separation age consistent with that calculated by the method of Sun and McDonough(1988) i.e. 2 Ga is feasible if a second stage kappa of more than 3 occurs for the SHRS source. Unfortunately no $kappa_{Th}$ determinations have been made which would indicate the present kappa value in the SHRS assuming this ratio is not fractionated during partial melting. Measured $kappa_{Th}$ varies from 2.6 - 3.7 in OIB, Allegre et al.(1986c). Thus the assumed $kappa_{Th}$ value in the model of Galer and O'Nions(1985) is an absolute minimum for OIB source regions. Further independent support for a residence time greater than that calculated by Galer and O'Nions(1985) is that the secondary kappa value of more than 3 calculated using the method of Sun and McDonough (Fig.8.2b) yields a separation age of more than 2 Ga from Fig.8.3b. These inconsistencies with the model of Galer and O'Nions(1985) which occur if primary kappa is greater than 3.9 have also been noted by White et al.(1987) who consider EPR

basalts for which separation ages of 1.4 Ga are indicated by the Pb-Pb isochron. White et al.(1987) did not consider the effect of secondary kappa variations because this is approximately constant at 2.5 in MORB (Allegre et al.(1986c)). An additional problem with the Galer and O'Nions model is that compilations of MORB data do not suggest derivation from a primitive reservoir (Ito et al.(1987)) because Pacific and Atlantic MORB samples with high $kappa_{Pb}$ correlate poorly with $^{206}Pb/^{204}Pb$. Thus MORBs which are primitive in terms of $kappa_{Pb}$ are *least* primitive in terms of $^{206}Pb/^{204}Pb$. This is the opposite to the prediction of the Galer and O'Nions model.

If the source separation event is assumed to be 2Ga it is possible to calculate the element fractionations for the Rb-Sr, Sm-Nd and U-Th-Pb systems required to produce the isotopic characteristics observed in the SHRS. A simple 2 stage model is adopted in which the fractionation event occurred at 2 Ga which is consistent with the Pb modelling adopted above (e.g. Hart et al.(1986)). The starting compositions are obtained from Allegre et al.(1983b)) and Faure(1986). It is found that a *decrease in Rb/Sr of 72%* is required, together with an *increase in Sm/Nd, U/Pb and Th/Pb of 5%, 112% and 61% respectively.* This implies a Th/U decrease of 36%. These results are presented in Table.8.2. The remainder of this chapter will enquire how such fractionations and others indicated by the trace element data may be produced.

8.3; Trace element characteristics of HIMU source;

8.3.1; Comparison of trace element geochemistry of S.Atlantic OIB;

An integrated study of S.Atlantic OIB magmatism from a trace element perspective has previously been made by Wood et al.(1981) and Weaver et al.(1986,7). In such studies it has been demonstrated that the isotopic diversity of these islands is matched by a diversity in their incompatible trace element ratios. Hence S.Atlantic magmatism provides a useful framework in which to compare the St.Helena source characteristics. This section draws extensively on the data of Weaver et al.(1986,7) in supplementing the data of the present study.

A chondrite normalised multi-element plot for a range of S.Atlantic oceanic OIB is shown in Fig.4.8. The spidergrams are typical for OIB in that an increase in highly incompatible element abundance occurs with increasing incompatibility

from Y to Nb with relatively low abundances of the most highly incompatible elements (with the exception of Th). A distinctive peak occurs at Nb and Ta which is absent in volcanics from destructive plate margins (Thompson et al.(1984)). A plot normalising the OIB compositions from the S.Atlantic islands to that of a primitive Bouvet island basalt is shown in Fig.8.4 This diagram emphasises the differences between these islands more effectively than a conventional plot normalised to modified chondrite. A Bouvet island basalt is chosen for normalisation because in terms of S.Atlantic OIB it is intermediate in trace element (Fig.7.2) (Weaver et al.(1987)) and isotopic composition (Fig.7.4). Trends subparallel to the Bouvet values may be accounted for by crystal fractionation effects. Non-parallel slopes are of interest as they may suggest variations in source compositions or variations in the degree of partial melting. If the trace element enrichment as registered by ratios of moderately incompatible elements (e.g. La) to less incompatible elements (e.g. Yb) is considered it is seen that St.Helena, Tristan da Cunha and Gough islands have greater degrees of trace element enrichment than Bouvet and Ascension. Such differences (as registered by Ce(n)/Y(n) variations) were ascribed to smaller degrees of partial melting producing the St.Helena, Tristan da Cunha and Gough island magmas by Weaver et al.(1987). The highly incompatible elements are more valuable in indicating source variations as they are only likely to be fractionated at very small degrees of partial melting (e.g. Kay(1984)). In considering these elements, the main differences are between Gough and Tristan da Cunha and the other islands. *Gough and Tristan da Cunha are more enriched in Rb, Ba, Th and K relative to Ta* whereas in the other islands the abundances are similar to Nb and Ta (Fig.8.4). In Gough and Tristan da Cunha islands this difference appears to be a combination of a relative increase in alkalis and a depletion in Nb and Ta. An additional difference specific to *Ascension and St.Helena is the occurrence of a marked K depletion.* This K depletion is *accompanied by depletion of Rb and to a lesser extent Ba relative to Nb.* This variation is apparent by comparison of selected moderately - highly incompatible trace element ratios Fig.8.5 and Table.8.1. It is clear that the lowest values for Rb/Th, K/Th and Ba/Nb amongst S.Atlantic OIB are recorded for St.Helena. Relatively constant values for ratios of Ce/Pb (table 8.1) and Nb/U are found in all oceanic basalts (Hofmann et

Fig.8.4. Spidergrams of S.Atlantic OIB normalised to Bouvet OIB, represented by basalt 1972,0 148(4) (Weaver et al.(1987)). Other primitive basalts analysed by Weaver et al.(1987). Chondrite normalising values are from Thompson(1982).

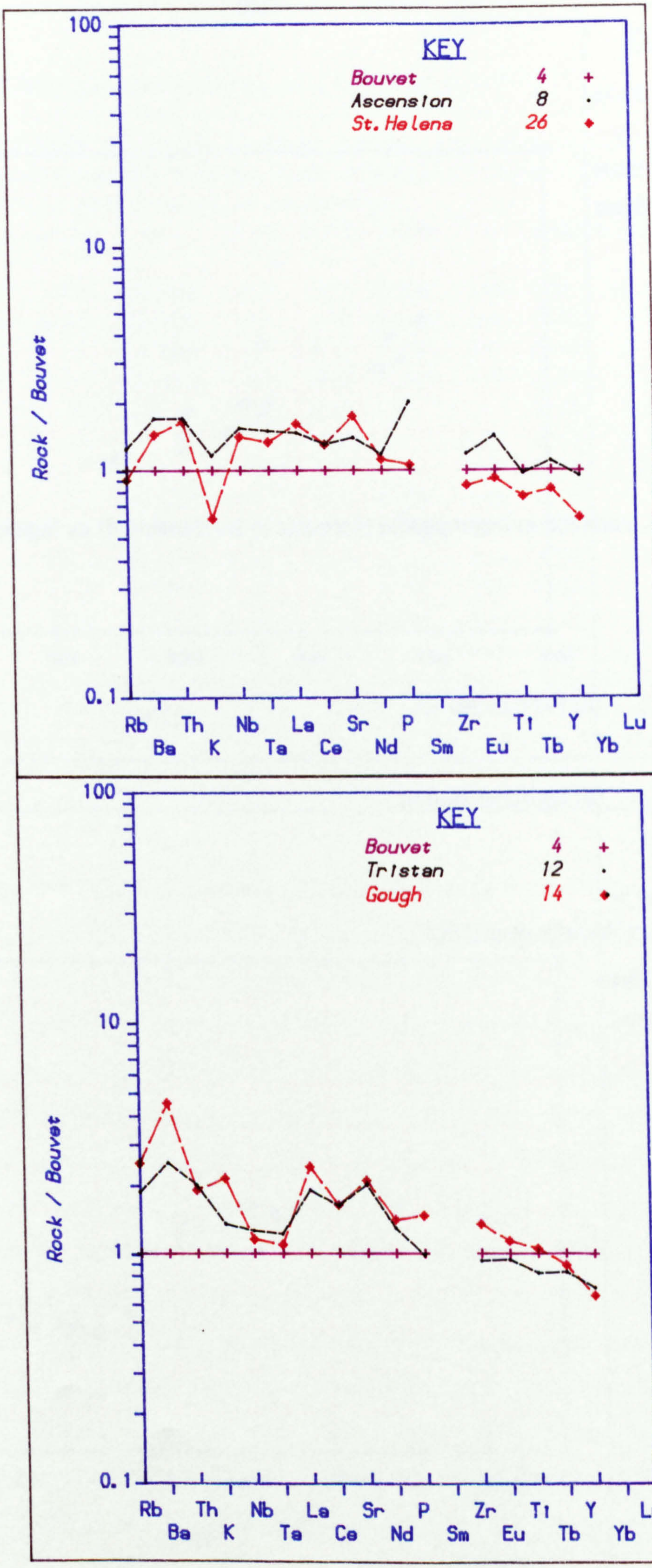
KEY
Bouvet 4 +
Ascension 8 ·
St. Helena 26 ◆
100
10
1
0.1
Rock / Bouvet
Rb Ba Th K Nb Ta La Ce Sr Nd P Sm Zr Eu Ti Tb Y Yb Lu
KEY
Bouvet 4 +
Tristan 12 ·
Gough 14 ◆
100
10
1
0.1
Rock / Bouvet
Rb Ba Th K Nb Ta La Ce Sr Nd P Sm Zr Eu Ti Tb Y Yb Lu

Fig.8.5. Variation in incompatible elements in S.Atlantic OIB as registered by:

(a) K/Th vs Rb/Th.

(b) La/Nb vs Ba/Nb.

Data from Weaver et al.(1987).

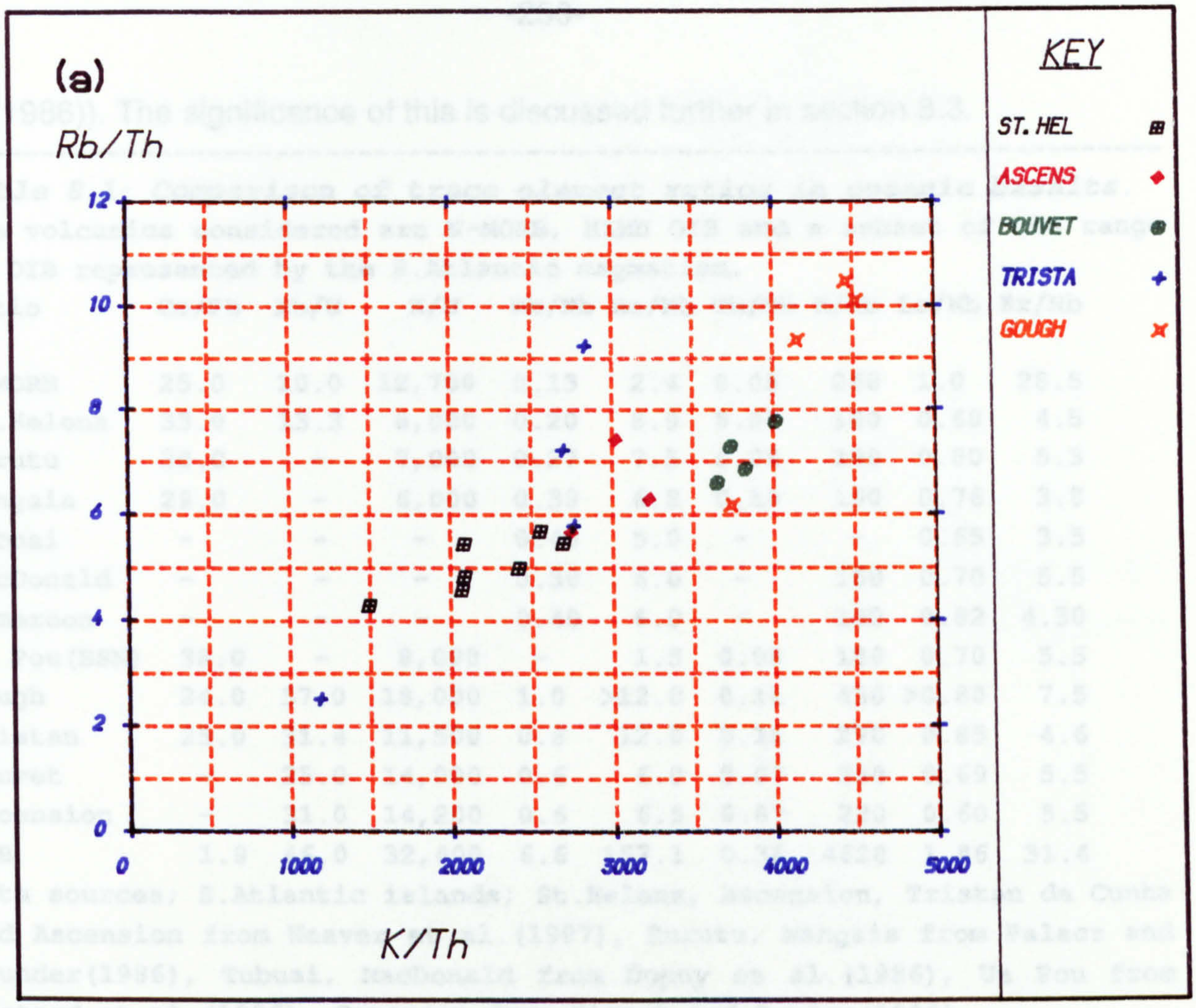
(a)
Rb/Th
12
10
8
6
4
2
0
0
1000
2000
3000
4000
5000
K/Th
KEY
ST. HEL
ASCENS
BOUVET
TRISTA
GOUGH

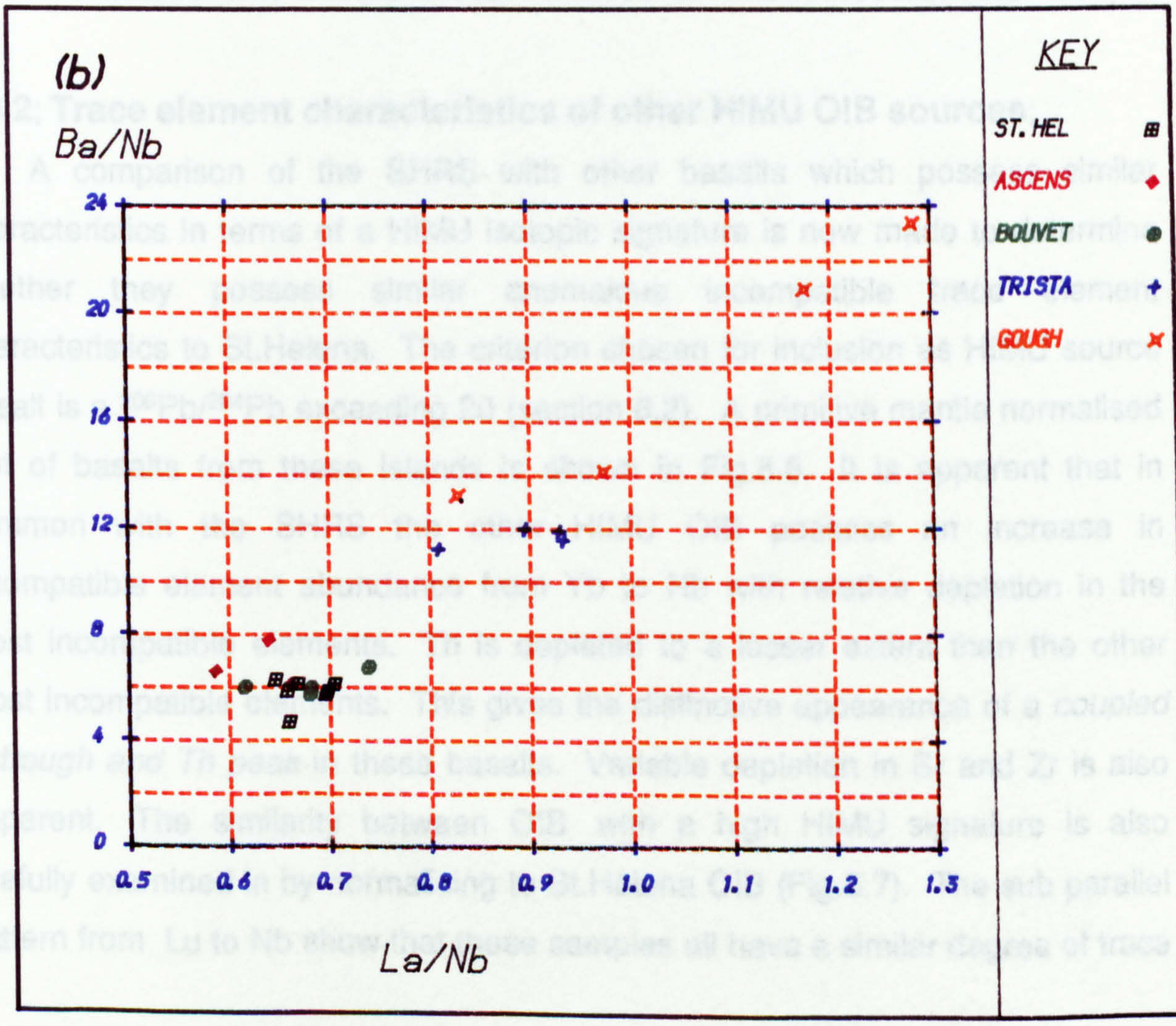
(b)
Ba/Nb
24
20
16
12
8
4
0
0.5
0.6
0.7
0.8
0.9
1.0
1.1
1.2
1.3
La/Nb
KEY
ST. HEL
ASCENS
BOUVET
TRISTA
GOUGH

al.(1986)). The significance of this is discussed further in section 8.3.

Table 8.1; Comparison of trace element ratios in oceanic basalts.
The volcanics considered are N-MORB, HIMU OIB and a subset of the range of OIB represented by the S.Atlantic magmatism.

Ratio	Ce/Pb	Rb/U	K/U	Rb/Nb	Ba/Nb	Th/Nb	K/Nb	La/Nb	Zr/Nb
N-MORB	25.0	10.0	12,700	0.13	2.4	0.05	260	1.0	28.5
St.Helena	33.0	13.3	8,000	0.20	5.9	0.08	180	0.68	4.5
Rurutu	30.0	-	7,000	0.27	7.5	0.08	180	0.80	5.3
Mangaia	29.0	-	6,000	0.38	6.2	0.10	160	0.76	3.8
Tubuai	-	-	-	0.40	5.0	-	-	0.65	3.5
MacDonald	-	-	-	0.30	6.0	-	150	0.70	5.5
Cameroon	-	-	-	0.40	6.0	-	150	0.82	4.30
Ua Pou(BSN)	38.0	-	8,000	-	1.5	0.08	180	0.70	5.5
Gough	24.0	37.0	18,000	1.0	>12.0	0.11	430	>0.80	7.5
Tristan	25.0	31.4	11,500	0.8	12.0	0.11	270	0.85	4.6
Bouvet	-	25.0	14,000	0.6	6.0	0.08	260	0.69	5.5
Ascension	-	31.0	14,200	0.6	6.5	0.07	220	0.60	5.5
VAB	1.9	46.0	32,400	6.6	157.1	0.36	4628	1.86	31.4

Data sources; S.Atlantic islands; St.Helena, Ascension, Tristan da Cunha and Ascension from Weaver et al.(1987), Rurutu, Mangaia from Palacz and Saunder(1986), Tubuai, MacDonald from Dupuy et al.(1986), Ua Pou from Liotard et al.(1986), Cameroon from Fitton and Dunlop(1985).

8.3.2; Trace element characteristics of other HIMU OIB sources;

A comparison of the SHRS with other basalts which possess similar characteristics in terms of a HIMU isotopic signature is now made to determine whether they possess similar anomalous incompatible trace element characteristics to St.Helena. The criterion chosen for inclusion as HIMU source basalt is a $^{206}Pb/^{204}Pb$ exceeding 20 (section 8.2). A primitive mantle normalised plot of basalts from these islands is shown in Fig.8.6. It is apparent that in common with the SHRS the other HIMU OIB possess an increase in incompatible element abundance from Yb to Nb with relative depletion in the most incompatible elements. Th is depleted to a lesser extent than the other most incompatible elements. This gives the distinctive appearance of a *coupled K trough and Th peak* in these basalts. Variable depletion in Sr and Zr is also apparent. The similarity between OIB with a high HIMU signature is also usefully examined in by normalising to St.Helena OIB (Fig.8.7). The sub parallel pattern from Lu to Nb show that these samples all have a similar degree of trace

Fig.8.6. Spidergrams of HIMU OIB normalised to chondrite. The data are from the following sources:

Mangaia, 28 : MAN 96A, Palacz and Saunders(1986).

Rurutu, 29 : 199(6), " "

Ua Pou, 31 : 6600, Liotard et al.(1986).

Ua Pou, 33 : 6604, " "

Macdonald, 35 : MC 2 - 201 6983 AB, Dupuy et al.(1988).

Macdonald, 37 : MCD 079 6974 BSN, " "

Tubuai, 39 : TBA-036 7288 AB, " "

Tubuai, 41 : TBA-102 7290 AB " "

Cameroon, 45 : C 195, from Fitton et al.(1983).

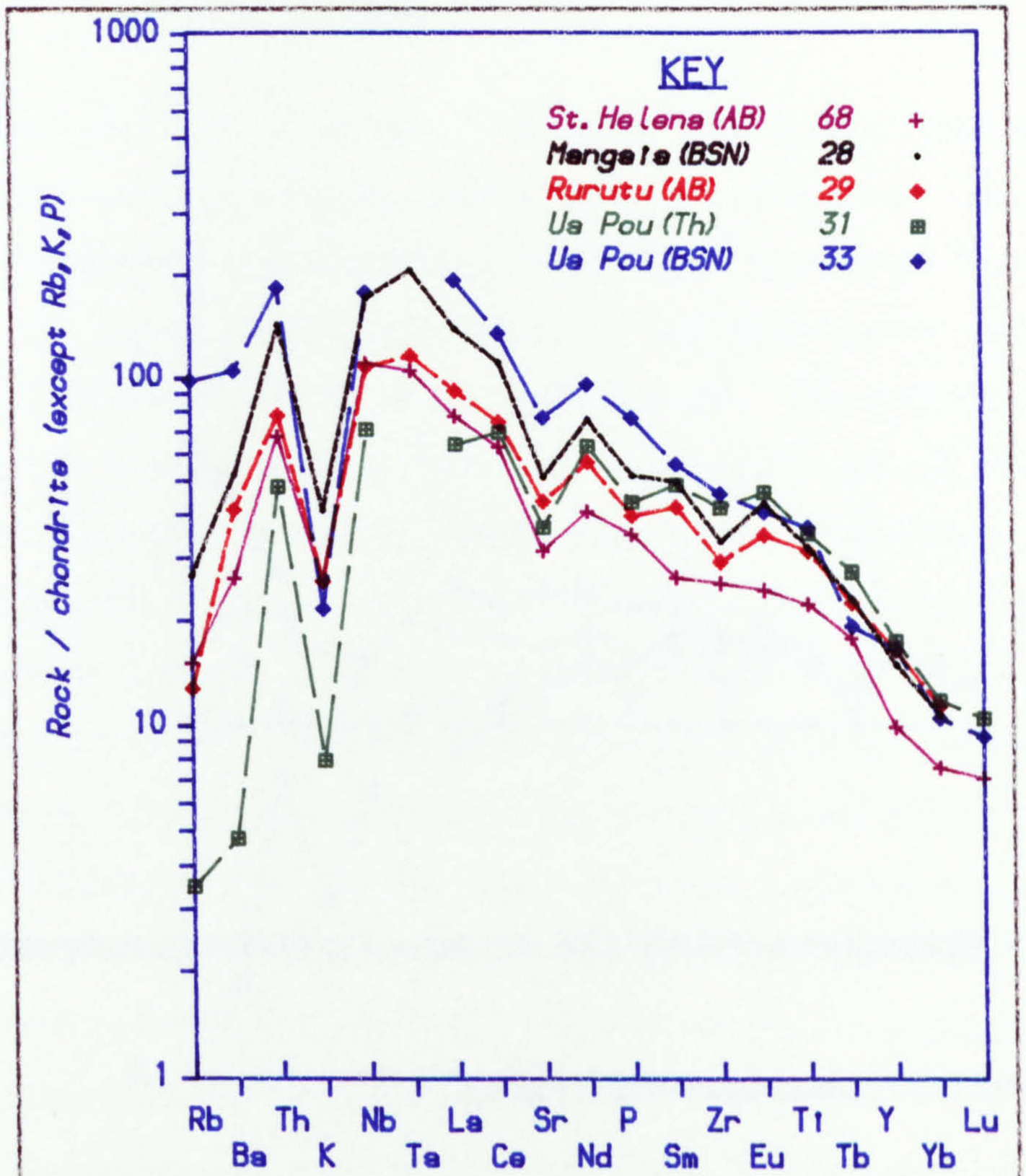
KEY
St. Helena (AB) 68
Mangaia (BSN) 28
Rurutu (AB) 29
Ua Pou (Th) 31
Ua Pou (BSN) 33
Rock / chondrite (except Rb,K,P)
1000
100
10
1
Rb Th Nb La Sr P Zr Ti Y Lu
Ba K Ta Ce Nd Sm Eu Tb Yb

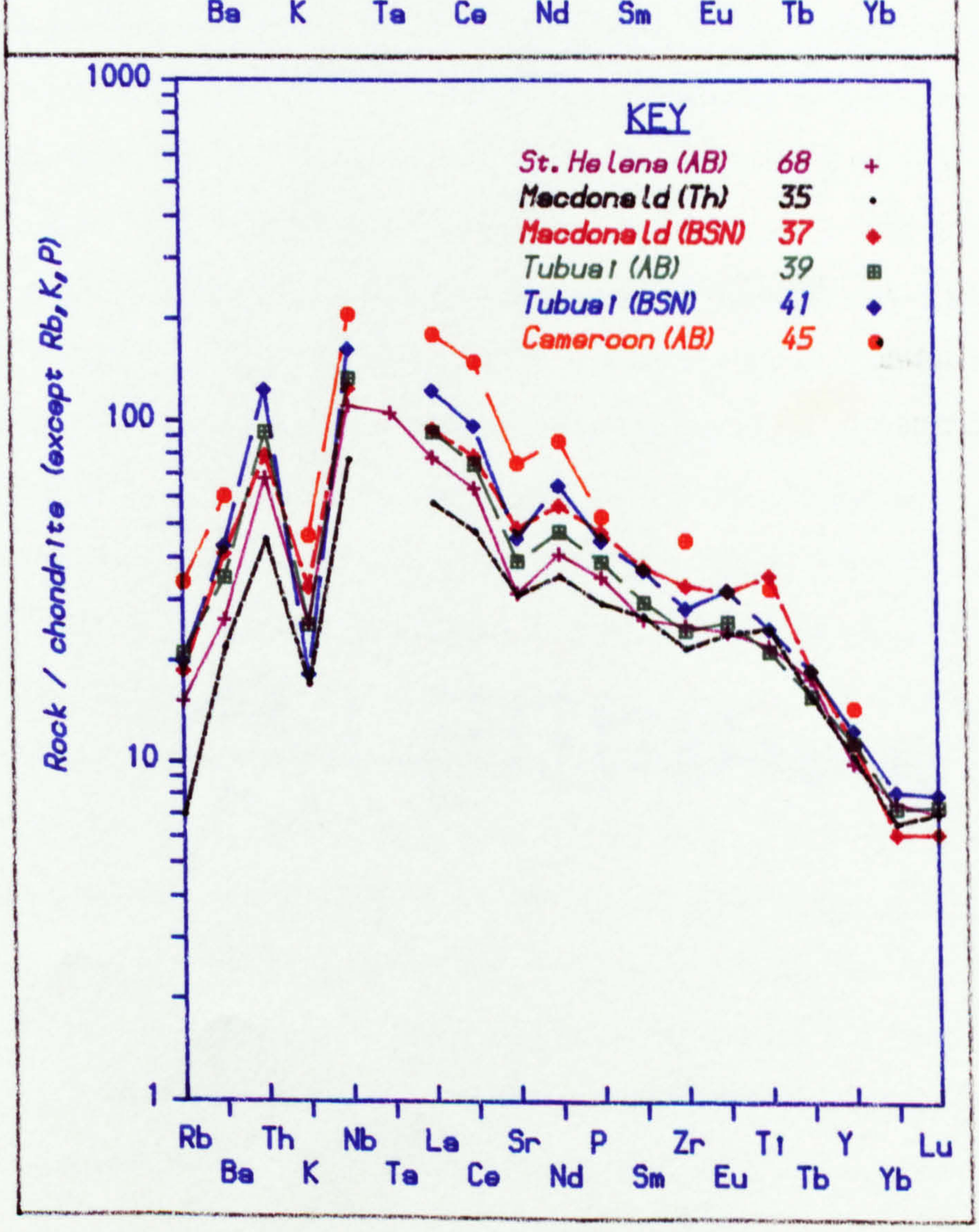
KEY
St. Helena (AB) 68
Macdonald (Th) 35
Macdonald (BSN) 37
Tubuai (AB) 39
Tubuai (BSN) 41
Cameroon (AB) 45
Rock / chondrite (except Rb,K,P)
1000
100
10
1
Rb Th Nb La Sr P Zr Ti Y Lu
Ba K Ta Ce Nd Sm Eu Tb Yb

Fig.8.7. Spidergrams of HIMU OIB normalised to St.Helena compositions SC 68.

Samples from references cited in Fig.8.6.

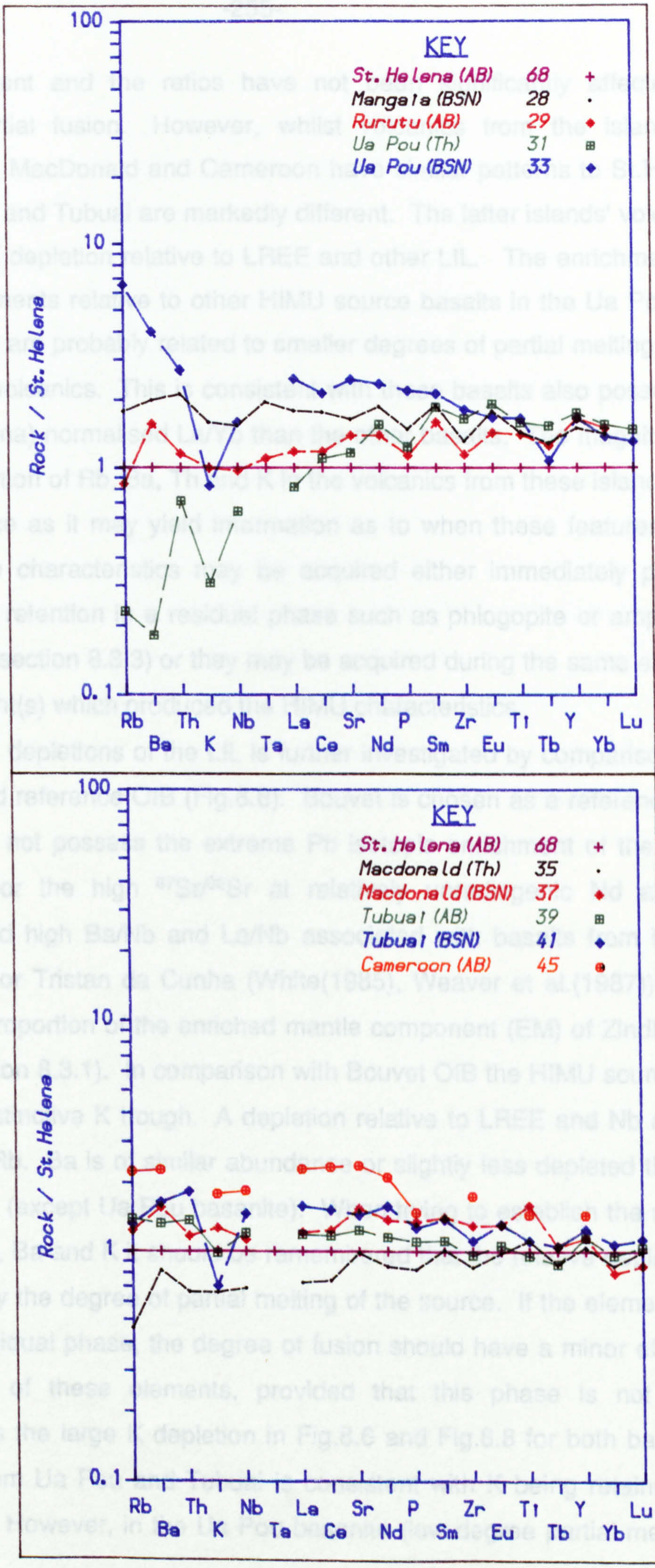
KEY
St. Helena (AB) 68 +
Mangaia (BSN) 28 ·
Rurutu (AB) 29 ◆
Ua Pou (Th) 31 ⊞
Ua Pou (BSN) 33 ◆
100
10
1
0.1
Rock / St. Helena
Rb Th Nb La Sr P Zr Ti Y Lu
Ba K Ta Ce Nd Sm Eu Tb Yb
KEY
St. Helena (AB) 68 +
Macdonald (Th) 35 ·
Macdonald (BSN) 37 ◆
Tubuai (AB) 39 ⊞
Tubuai (BSN) 41 ◆
Cameroon (AB) 45 ●
100
10
1
0.1
Rock / St. Helena
Rb Th Nb La Sr P Zr Ti Y Lu
Ba K Ta Ce Nd Sm Eu Tb Yb

element enrichment and the ratios have not been significantly affected by variations in partial fusion. However, whilst volcanics from the islands of Mangaia, Rurutu, MacDonald and Cameroon have similar patterns to St.Helena those for Ua Pou and Tubuai are markedly different. The latter islands' volcanics have a marked K depletion relative to LREE and other LIL. The enrichments in incompatible elements relative to other HIMU source basalts in the Ua Pou and Tubuai basanites are probably related to smaller degrees of partial melting in the source of these volcanics. This is consistent with these basalts also possessing a higher (St.Helena) normalised La/Yb than the other basalts. The magnitude of the relative depletion of Rb, Ba, Th and K in the volcanics from these islands is of crucial importance as it may yield information as to when these features were acquired. These characteristics may be acquired either immediately prior to eruption through retention in a residual phase such as phlogopite or amphibole (as discussed in section 8.3.3) or they may be acquired during the same element fractionation event(s) which produced the HIMU characteristics.

The relative depletions of the LIL is further investigated by comparison with the Bouvet island reference OIB (Fig.8.8). Bouvet is chosen as a reference OIB because it does not possess the extreme Pb isotopic enrichment of the HIMU source basalts or the high $^{87}Sr/^{86}Sr$ at relatively unradiogenic Nd and Pb compositions and high Ba/Nb and La/Nb associated with basalts from islands such as Gough or Tristan da Cunha (White(1985), Weaver et al.(1987)) which contain a high proportion of the enriched mantle component (EM) of Zindler and Hart(1986) (section 8.3.1). In comparison with Bouvet OIB the HIMU source OIB all possess a distinctive K trough. A depletion relative to LREE and Nb and Ta also occurs for Rb. Ba is of similar abundance or slightly less depleted than Th in most samples (except Ua Pou basanite). When trying to establish the relative depletions of Rb, Ba and K it should be remembered that the relative depletion is also governed by the degree of partial melting of the source. If the elements are retained in a residual phase, the degree of fusion should have a minor effect on the abundance of these elements, provided that this phase is not totally consumed. Thus the large K depletion in Fig.8.6 and Fig.8.8 for both basanites and tholeites from Ua Pou and Tubuai is consistent with K being retained in a residual phase. However, in the Ua Pou basanite (low degree partial melts) Rb

Fig.8.8. Spidergrams of HIMU OIB normalised to Bouvet island basalt (Fig.8.4).

Samples from references cited in Fig.8.6.

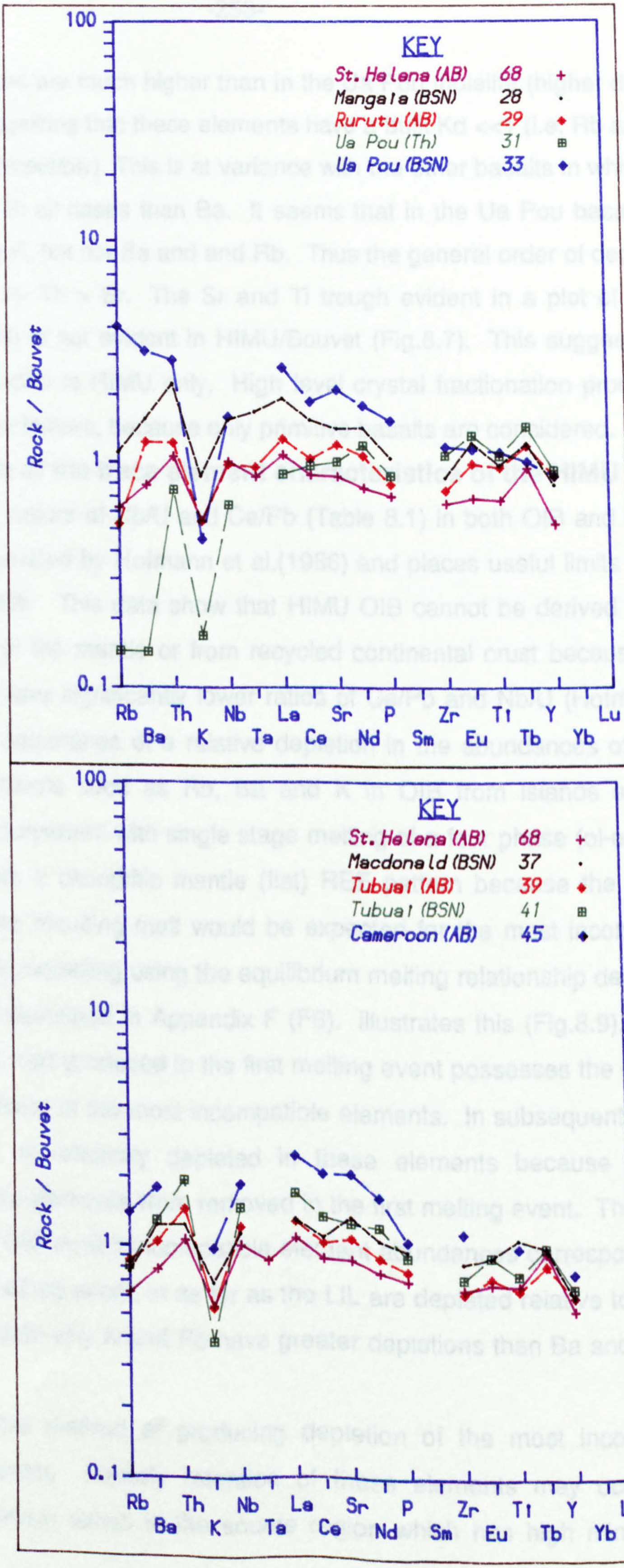
KEY
St. Helena (AB) 68 +
Mangaia (BSN) 28 ·
Rurutu (AB) 29 ◆
Ua Pou (Th) 31 ⊞
Ua Pou (BSN) 33 ◆
100
10
1
0.1
Rock / Bouvet
Rb Ba Th K Nb Ta La Ce Sr Nd P Sm Zr Eu Ti Tb Y Yb Lu
KEY
St. Helena (AB) 68 +
Macdonald (BSN) 37 ·
Tubuai (AB) 39 ◆
Tubuai (BSN) 41 ⊞
Cameroon (AB) 45 ◆
100
10
1
0.1
Rock / Bouvet
Rb Ba Th K Nb Ta La Ce Sr Nd P Sm Zr Eu Ti Tb Y Yb Lu

and Ba abundances are much higher than in the Ua Pou tholeiite (higher degree partial melts), suggesting that these elements have a bulk Kd <<1 (i.e. Rb and Ba are behaving incompatibly). This is at variance with the other basalts in which Rb is more depleted in all cases than Ba. It seems that in the Ua Pou basanite a phase is retaining K, but not Ba and and Rb. Thus the general order of depletion is K > Rb > Ba >= Th > Sr. The Sr and Ti trough evident in a plot of HIMU /chondrite (Fig.8.6) is not evident in HIMU/Bouvet (Fig.8.7). This suggests this feature is not specific to HIMU only. High level crystal fractionation processes cannot explain this feature, because only primitive basalts are considered.

8.3.3; Formation of the trace element characteristics of the HIMU OIB;

The uniform nature of Nb/U and Ce/Pb (Table 8.1) in both OIB and MORB has been demonstrated by Hofmann et al.(1986) and places useful limits on the origin of HIMU OIB. This data show that HIMU OIB cannot be derived from a primitive portion of the mantle or from recycled continental crust because both these reservoirs have significantly lower ratios of Ce/Pb and Nb/U (Hofmann et al.(1986)). The occurrence of a relative depletion in the abundances of highly incompatible elements such as Rb, Ba and K in OIB from islands such as St.Helena is not consistent with single stage melting of a four phase (ol-opx-cpx-gnt) lherzolite with a chondritic mantle (flat) REE pattern because the highest abundances in the resulting melt would be expected for the most incompatible elements. Simple modelling using the equilibrium melting relationship derived by Shaw(1970) and described in Appendix F (F6). illustrates this (Fig.8.9). In this simple model the melt produced in the first melting event possesses the greatest degree of enrichment of the most incompatible elements. In subsequent melting events the melt is relatively depleted in these elements because a large proportion of these elements were removed in the first melting event. The SHRS and other HIMU OIB exhibit incompatible element abundances corresponding to more than one melting event, in as far as the LIL are depleted relative to La, but this does not explain why K and Rb have greater depletions than Ba and Th (c.f. Fig.8.8).

An alternative method of producing depletion of the most incompatible elements also exists. Namely retention of these elements may occur in a residual phase which exists in the source region which has high mineral/melt

Fig.8.9. Modelling of effect of repeated batch melting events on incompatible trace elements. A simple batch melting model of the two times chondrite source composition is conducted in which incremental melting (in units of 1% fusion) occurs with no melt retention in source (equation 6.3, Shaw,(1970)). The chondritic source composition and melt norm (P, equation 6.4) are those of Thompson et al.(1984)).

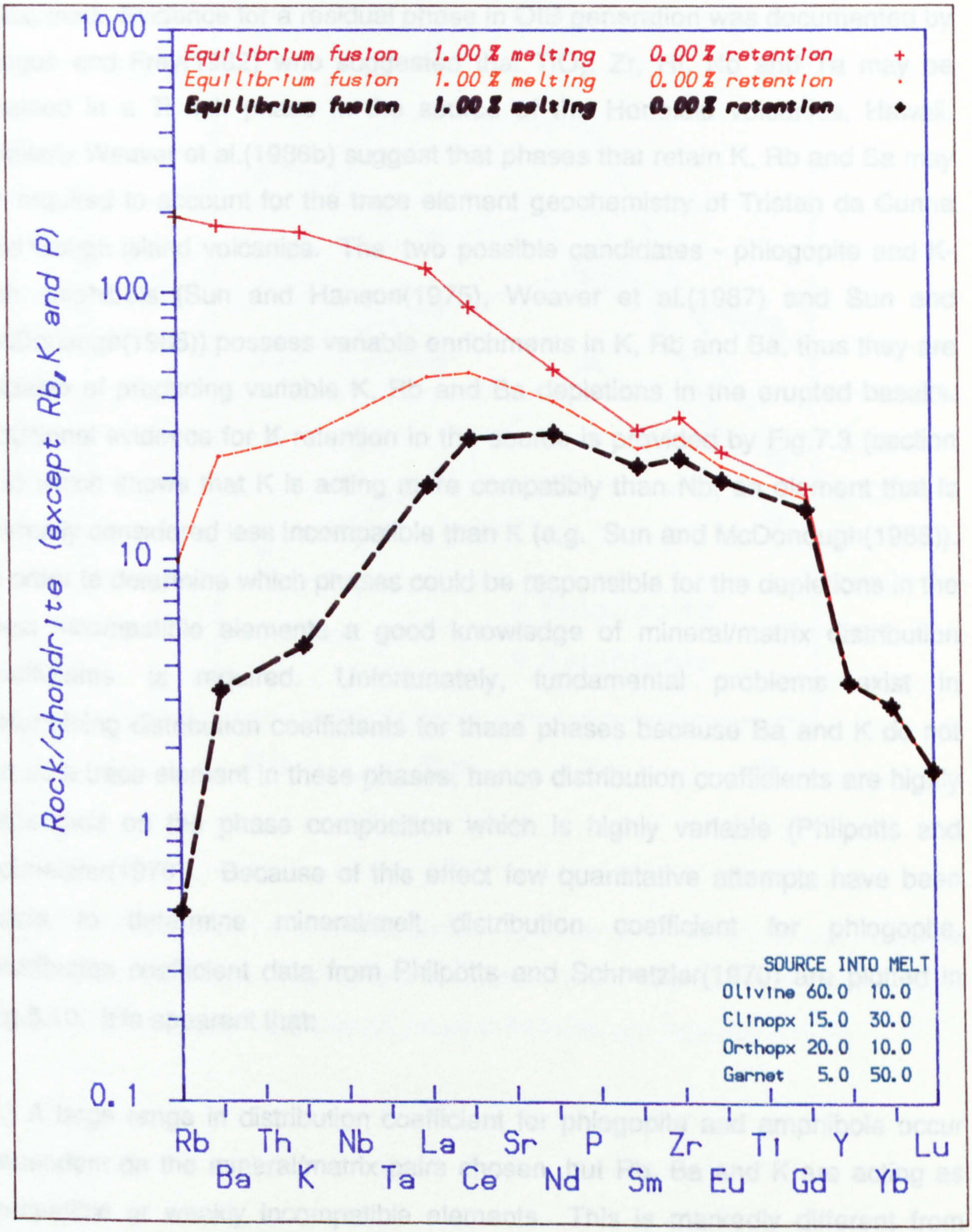
Equilibrium fusion 1.00 % melting 0.00 % retention +
Equilibrium fusion 1.00 % melting 0.00 % retention ·
Equilibrium fusion 1.00 % melting 0.00 % retention ◆
1000
100
10
1
0.1
Rock/chondrite (except Rb, K and P)
SOURCE INTO MELT
Olivine 60.0 10.0
Clinopx 15.0 30.0
Orthopx 20.0 10.0
Garnet 5.0 50.0
Rb Th Nb La Sr P Zr Ti Y Lu
Ba K Ta Ce Nd Sm Eu Gd Yb

partition coefficients for these elements (section 6.4.2 and 6.4.3). This effect is accentuated at low degrees of partial melting at which this phase is not consumed. Evidence for a residual phase in OIB generation was documented by Clague and Frey(1982) who suggested that TiO_2, Zr, Hf, Nb and Ta may be retained in a Ti rich phase in the source of the Honolulu volcanics, Hawaii. Similarly Weaver et al.(1986b) suggest that phases that retain K, Rb and Ba may be required to account for the trace element geochemistry of Tristan da Cunha and Gough island volcanics. The two possible candidates - phlogopite and K-rich amphibole (Sun and Hanson(1975), Weaver et al.(1987) and Sun and McDonough(1988)) possess variable enrichments in K, Rb and Ba, thus they are capable of producing variable K, Rb and Ba depletions in the erupted basalts. Additional evidence for K retention in the source is provided by Fig.7.3 (section 7.2) which shows that K is acting more compatibly than Nb, an element that is normally considered less incompatible than K (e.g. Sun and McDonough(1988)). In order to determine which phases could be responsible for the depletions in the most incompatible elements a good knowledge of mineral/matrix distribution coefficients is required. Unfortunately, fundamental problems exist in determining distribution coefficients for these phases because Ba and K do not act as a trace element in these phases, hence distribution coefficients are highly dependent on the phase composition which is highly variable (Philpotts and Schnetzler(1970)). Because of this effect few quantitative attempts have been made to determine mineral/melt distribution coefficient for phlogopite. Distribution coefficient data from Philpotts and Schnetzler(1970) are plotted in Fig.8.10. It is apparent that:

(1) A large range in distribution coefficient for phlogopite and amphibole occur dependent on the mineral/matrix pairs chosen, but Rb, Ba and K are acting as compatible or weakly incompatible elements. This is markedly different from their highly incompatible behaviour towards likely mantle phases (Fig.6.1).

(2) $"Kd"_{(Ba,Rb,K)}^{(phlogopite)} > "Kd"_{(Ba,Rb,K)}^{(amphibole)}$

(3) $"Kd"_{(K)}^{(amphibole,phlogopite)} > "Kd"_{(Ba,Rb)}^{(amphibole,phlogopite)}$. This is not consistent with the observation that K and Rb depletions are of greater magnitude than Ba in most cases (Figs.8.6,8.8)).

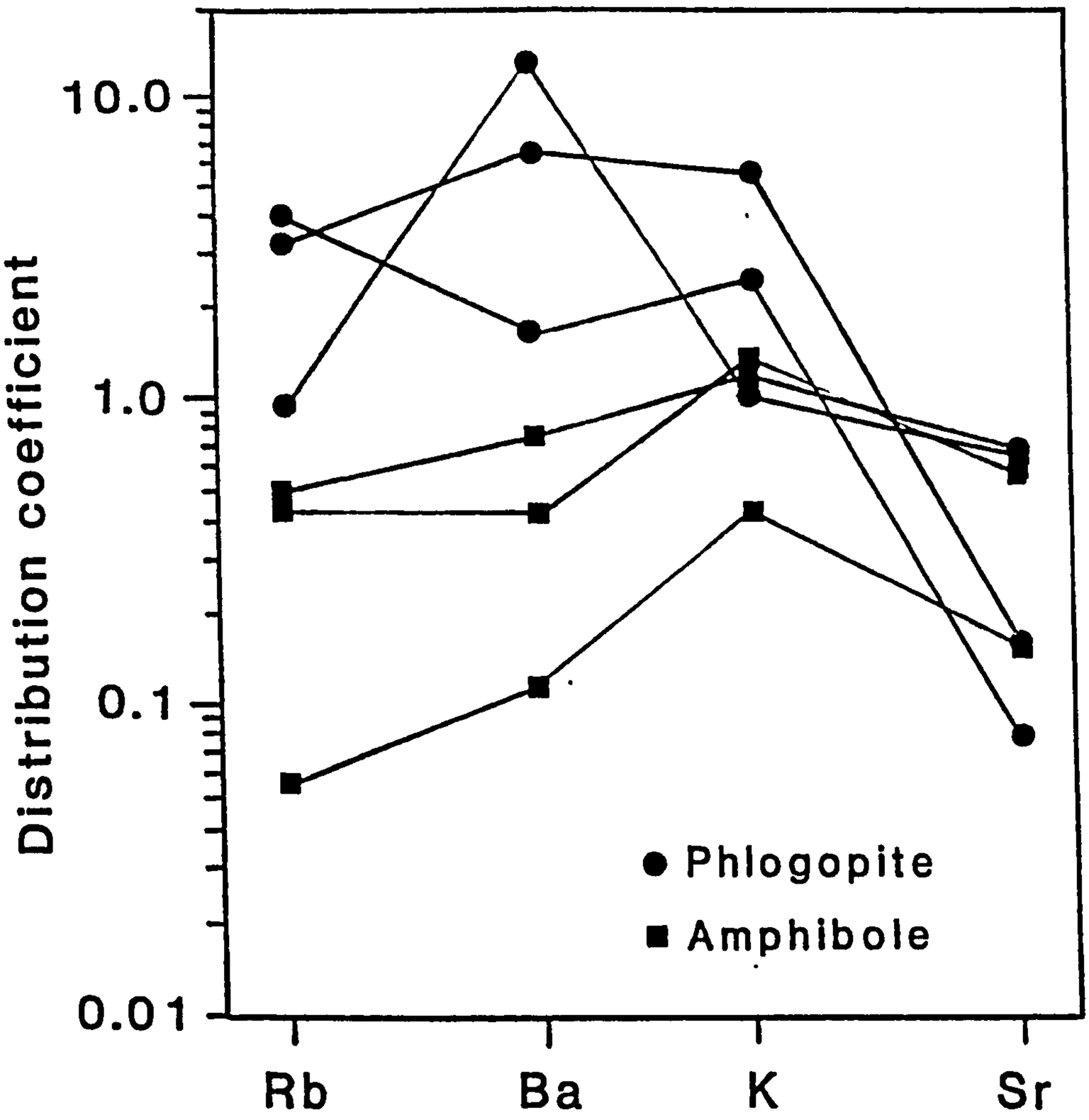

Fig.8.10. Comparison of mineral/melt partition coefficients for phlogopite and amphibole in volcanics. Data from Philpotts and Schnetzler(1970). The curves for each mineral are for different mineral separates described in Philpotts and Schnetzler(1970)

The occurence of a similar distribution coefficient for Ba relative to K and Rb could be explained because these distribution coefficients are unrepresentative; the Kd values shown in Fig.8.10 have been determined at low pressures in evolved volcanics (Philpotts and Schnetzler(1970)), hence they may not provide sound constraints on the Kd under mantle conditions, for which no determinations have been made.

An alternative method of assessing the likely effect of phlogopite and amphibole in the source on the Rb, Ba and K abundances in volcanics is to assess the relative abundances of these elements in mantle xenoliths that contain a K-rich phase. These xenoliths belong to the Phlogopite Peridotite (PP) and Phlogopite K Richterite Peridotite (PKP) suites. Although these minerals are of small volumetric importance in the xenoliths their enrichments in Rb, Ba and K compared to phases such as olivine and clinopyroxene tend to dominate the whole rock budget (Menzies et al.(1987)). A selection of spidergrams for xenoliths from the Kimberley group of pipes, S.Africa (Erlank et al.(1987)) is shown in Fig.8.11. The main points evident are:

(1) In all samples the K abundances are approximately equal to Rb abundances and Ba abundances are significantly lower. Since, K is a major structural constituent of phlogopite, it should be remembered that the differences in K abundance will largely reflect the proportion of phlogopite in a particular xenolith.

(2) Sr abundances are more variable than Rb, Ba and K, but tend to be lower than Rb and K.

(3) Zr is enriched relative to similar moderately incompatible elements such as P.

(4) Some samples contain anomalous enrichments in other elements e.g. Nb in JJG 360A, P in AJE 18.

These relative enrichments in the xenoliths suggest that the amphibole and phlogopite they contain could produce the features of LIL depletion observed in HIMU source OIB if they occurred in the source. This is evident because the relative enrichments are the inverse of the depletions observed in Fig.8.6 and Fig.8.8. The enrichments in Nb, Zr, P and Ba (e.g. Nb and Zr in JJG 360A) in some of the xenoliths is inconsistent with the phases that produce these features occurring as a residual phase in the HIMU OIB sources. Possible phases that could produce these anomalous features in the xenoliths are discussed further in

Fig.8.11. Spidergrams of a range of mantle nodules containing metasomatic phases from the Kimberley pipes, S.Africa.

(a) Phlogopite K-richterite peridotites (PKP).

(b) Phlogopite peridotites (PP).

Data from Erlank et al.(1987). Data normalised to chondrite values of Thompson(1982).

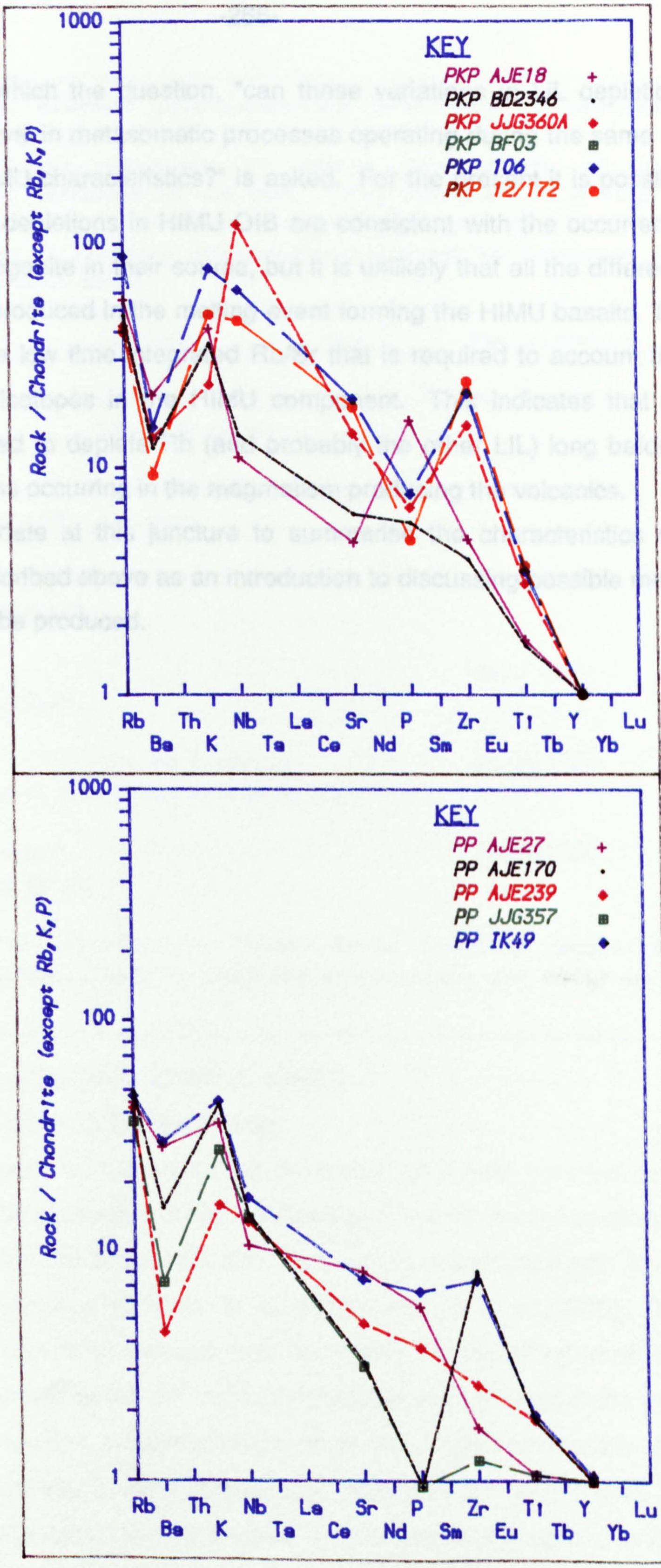
KEY
PKP AJE18
PKP BD2346
PKP JJG360A
PKP BF03
PKP 106
PKP 12/172
Rock / Chondrite (except Rb,K,P)
1000
100
10
1
Rb Th Nb La Sr P Zr Tt Y Lu
Ba K Ta Ce Nd Sm Eu Tb Yb
KEY
PP AJE27
PP AJE170
PP AJE239
PP JJG357
PP IK49
Rock / Chondrite (except Rb,K,P)
1000
100
10
1
Rb Th Nb La Sr P Zr Tt Y Lu
Ba K Ta Ce Nd Sm Eu Tb Yb

section 8.4.5 in which the question, "can these variations in LIL depletion be attributed to removal in metasomatic processes operating during the same event producing the HIMU characteristics?" is asked. For the present it is possible to note that the LIL depletions in HIMU OIB are consistent with the occurrence of amphibole or phlogopite in their source, but it is unlikely that all the different LIL depletions were produced in the melting event forming the HIMU basalts. This is apparent from the low time integrated Rb/Sr that is required to account for the unradiogenic Sr isotopes in the HIMU component. This indicates that some process is required to deplete Rb (and probably the other LIL) long before the possible depletions occurring in the magmatism producing the volcanics.

It is appropriate at this juncture to summarise the characteristics of the HIMU source described above as an introduction to discussing possible methods by which it could be produced.

Table 8.2. Main element fractionations necessary to produce the HIMU component.

The calculations necessary to derive the amount of element fractionation are explained in the text. They are based on a simple two stage growth model with the element fractionations occurring at 2 Ga. Minus signs refer to relative decreases and plusses to increases in the absolute abundance or ratio.

Feature	Evidence	Age	Fractionation
LIL depleted	Low ratios of LIL/LREE or Nb	-	Rb-,Ba-,Th-,K-
High time integrated U/Pb	Radiogenic Pb isotopes	2.0 Ga	U/Pb +112%
High time integrated Th/Pb	" "	2.0 Ga	Th/Pb +37%
Low time integrated Th/U			Th/U -36%
Low time integrated Rb/Sr	Sr,Nd isotopes below mantle array		Rb/Sr -72%
Slightly high? integrated Sm/Nd	" "		Sm/Nd +5%

Data sources for calculations; Rb-Sr, Sm-Nd starting compositions - Allegre et al.(1986c), U-Th-Pb starting compositions and decay constants - Faure (1986).

8.4; Mechanisms for production of HIMU;

8.4.1; Methods of U/Pb fractionation;

Early explanations relevant to the production of a HIMU component were concerned with the production of high U/Pb ratios. The method of fractionation of U from Pb is enigmatic because it does not vary in accordance with the Rb-Sr and Sm-Nd systematics (O'Nions et al.(1979), Allegre et al.(1980)). Isotope systematics in these latter systems may be readily explained by trace element fractionation events in which the most incompatible element enters the melt and evolution of a residue relatively enriched in the more compatible element produces the observed isotopic composition (Appendix D). In the U-Pb system the opposite is the case. Most terrestrial basalts plot to the right of a 4.55 Ga

isochron on a plot of $^{207}Pb/^{204}Pb$ vs $^{206}Pb/^{204}Pb$ (Fig.7.7) which passes through the primordial Pb composition (Tatsumoto(1978)). The fact that most mantle derived volcanics plot to the right side of this line which is known as the geochron necessitate that mantle U/Pb has increased in the past (Tatsumoto(1978)). Because U and Pb are of similar incompatiblity which is most incompatible is of crucial importance in explaining the production of high U/Pb in terrestrial basalt sources. Assessing the charge/radius characteristics of these elements is inconclusive because of difference in their characteristic oxidation state. Limited experimental data (Tatsumoto(1978) and Watson et al.(1986)) suggest that U is indeed more incompatible than Pb. Newsom et al.(1986) point out that U/Pb ratios in the majority of MORB are greatly in excess of those in primitive mantle. This gives a crude indication that U/Pb are higher in melt than source. Positive correlation of U/Pb and Pb in MORB would appear to confirm this (Newsom et al.(1986)). Since U is thought to be more incompatible than Pb an increase in U/Pb cannot be achieved by a simple melt extraction event. The occurrence of basalts to the right of the geochron requires a reservoir to the left to balance it and a mechanism for forming these reservoirs that does not involve fractionation of U/Pb by partial melting. Because no suitable reservoir is immediately obvious this is known as the Pb paradox (Allegre et al.(1980). Hence in order to understand the high time integrated U/Pb evident in the St.Helena source we need to investigate some of the models that have been suggested to resolve the Pb paradox and attempt to identify the reservoir complementary to that producing OIB. Some of the possible alternatives to balancing the radiogenic Pb in OIB can be immediately discounted. Although some MORB do have Pb isotopic compositions to the left of the geochron (Fig.7.7), those lying to the right are predominant. Volume constraints also exclude DMM as a likely store of unradiogenic Pb (Zindler and Hart (1986)) because they suggest that MORB source comprises only 11% of the silicate Earth. This proportion is small compared to the continental crust which dominates the Pb budget of the Earth. The lower mantle is also an unlikely reservoir because on the basis of rare gas data it appears to possess primitive signature (section 8.3.2).

8.4.2; Continuous core growth through earth history;

Early explanations for the U/Pb fractionation implicated the growth of the core in the loss of Pb, a chalcophilic element. The removal of Pb in a sulphide phase with core growth continuing through Earth history was suggested by Vollmer (1977) and Vidal and Dosso(1978) as a means of creating high U/Pb ratios in the mantle. More recent studies by Newsom and Palme (1984) and Newsom et al.(1986) have effectively demonstrated that such fractionation is highly unlikely. Newsom et al.(1986) consider OIB and MORB abundances of elements that have a strongly chalcophilic nature (e.g.Mo) or a siderophile nature (e.g.W) similar to, but greater than that for Pb. From comparisons with elements of similar incompatibilities, but without marked chalcophile or siderophile characteristics (Ba and Pr) it was shown that continuous core formation could not have occurred. This was apparent because ratios of W/Ba and Mo/Pr were found to be similar in both crust and mantle, thus the mantle values have not been modified since the fractionation event producing the bulk of the crust. Similarly no correlation between Pb content in the mantle and radiogenic Pb (as registered by second stage U/Pb in a two-stage Pb growth model) was apparent. Both these factors mitigate against continued core growth after accretion and depletion of Pb by this means.

8.4.3; Recycling of altered oceanic crust via subduction zones - seawater alteration processes (SAP);

The model of OIB genesis involving recycling altered oceanic crust via subduction zones provides another method by which U can be fractionated from Pb. This model was first proposed by Hofmann and White(1980,2). They proposed that the basaltic oceanic crust generated at MOR is modified by hydrothermal alteration and low temperature alteration as it spreads away from the ridge. Upon subduction further changes in composition occur through dehydration, decarbonation and partial melting. The oceanic crustal unit which forms cool, dense eclogite with increasing pressure is thought to become detached from the mantle part of the lithosphere during subduction due to density contrasts and it then sinks into the "deep mantle". This was also suggested by Ringwood(1982,5) who envisaged large thicknesses of eclogite and residual

harzburgite (the upper part of the oceanic lithosphere) piling up at the 670km discontinuity as a "megalith". The layer of stored, subducted crust was thought to increase in temperature through internal radioactive heat production and heat transfer by Hofmann and White(1982) resulting in a density decrease giving rise to plumes which feed OIB volcanism.

Hofmann and White(1982) noted additional consequences for OIB volcanism, implicit to OIB representing recycled oceanic crust. They suggested that evidence of a previous melt extraction event should be clearly evident in OIB derived from recycled oceanic crust. It was demonstrated in section 6.4.2. and 8.3.3. that the trace element characteristics of primitive members of the SHRS are consistent with derivation from a source that has undergone more than one melting event. It was also shown in section 6.4.2 that if the depleted material melting to form the members of the SHRS were MORB (oceanic crust) rather than MORB source , then higher degree partial melts are permissible (3-9%) compared to values of less than 1% when extraction of melts from the mantle is less plausible (section 6.6). This point was also made by Hofmann and White(1982) who modelled the REE abundances in OIB resulting from fusion of MORB. These authors also pointed out that the concentrations of the compatible elements Ni and Cr should be low (compared to MORB source mantle) in OIB derived from recycled oceanic crust. It, has been shown, however in section 6.2.2.2. that the more primitive magmas in the SHRS have Ni abundances that are compatible with derivation from melting of normal upper mantle. Hofmann and White(1982) attributed the occurrence of "normal" concentrations of Ni and Cr in other OIB (which mitigated against their model) to buffering of these compatible elements by mantle peridotite during ascent of a diapir of recycled oceanic crust (this process was also suggested to operate for independent reasons by Ringwood(1982,1985)). More recently Dupuy et al.(1988) have ascribed low Ni contents in HIMU OIB from the Marquesas islands to their source being a mixture of recycled oceanic crust and mantle peridotite.

At the time this model was developed the problems with the removal of lead by core growth were not recognised, so Hofmann and White(1982) appealed to this for the required fractionation of U from Pb. They noted, however that the absorbtion of U into the oceanic crust during hydrothermal circulation might

account for the increase of U/Pb in HIMU sources. They also noted that subduction of U-bearing sediments could also produce this effect. It is now known that deep sea sediments are enriched in Pb relative to U (White et al.(1984)), thus recycling of this material to the mantle via subduction zones would have the opposite to the desired effect (Newsom et al.1986). The enrichment of Pb in deep sea sediments is thought to be related to hydrothermal processes involving circulation of seawater in a convective system related to the MAR. These seawater hydrothermal alteration processes (SAP) have also been suggested as a means of affecting the LIL budget of the oceanic crust. Since this mechanism was first suggested by Hofmann and White(1982) much attention has been focussed on ridge centred hydrothermal processes to establish whether the necessary fractionation of the U-Th-Pb, Rb-Sr and Sm-Nd systems can be achieved by this method.

The efficacy of SAP in increasing U/Pb and decreasing Th/U has been demonstrated by numerous studies of hydrothermal vent waters and dredged basalts. Preliminary studies of vent waters at 21 degrees N on the EPR by Michard et al.(1983) demonstrated that deposition of U from the circulating hydrothermal fluid occurred to produce a 20% increase in U in the oceanic crust. However, it was shown by Michard et al.(1985) that this U increase alone was insufficient to produce the mu increases envisaged in the two stage Pb evolution models as described by Chase(1981) (section 8.3). A depletion in Pb was clearly also required. The evidence for Pb depletion at this stage was limited to the low mu values recorded in deep sea oceanic sediments (White et al(1984)). Further direct evidence of Pb loss was provided by studies of the Black Smokers at 21 degrees N on the EPR by Chen et al.(1986) and Chen(1987). It was shown that exchange between the circulating water and oceanic crust had occurred to produce an increase in U/Pb and decrease in Th/U in the crust. The magnitude of these variations is model dependent according to the estimated water rock ratio which varies from 1 to 5. It is also possible to calculate theoretical variations in these ratios from mass balance calculations based on the rate of crust production, and the continental fluxes of these elements. The results for this modelling are given in Table 8.3 where they are compared to the values calculated by the Chase(1981) model for two stage enrichment of the U/Pb of

OIB sources. It is evident that Pb depletion is more important than U deposition as predicted by Michard et al.(1985). The figures are also broadly consistent with the results of Chase(1981). A problem with this model is that no direct observations of crust have been made to assess this problem. The approach of Chen and Pallister(1981) was to study a 7km reconstructed section through oceanic crust which now forms the Samail ophiolite. This study produced results contradictory to those from hydrothermal vent fluids in that an increase in abundance of U, Th and Pb was apparent in the uppermost 2km that had been most subject to hydrothermal alteration. Further studies of ophiolite suites could clearly be of value.

Table 8.3. Summary of U, Th, Pb modelling conducted by Chen et al.(1986)

Models 1 and 2 are based on the observed variations in the U-Th-Pb system in hydrothermal vent fluids from the 21 degrees N EPR site. W/R denotes the water / rock ratio used in the model. Model 3 is based on mass balance calculations of the global U-Th-Pb system from the known fluxes of these elements in hydrothermal fluids, rivers and their contents in MORB and seawater. The element fractionations are based on isotopic data from Table 8.2.

Model	U	Pb	Th	U/Pb	Th/U
1. W/R=1	+5%	-10%	0%	+15%	-5%
2. W/R=5	+23%	-227%	0%	+250%	-23%
3.Mass balance	+10%	-28%	0%	+40%	-11%
4.Isotopic	-	-	-	+112%	-36%

If other isotopic systems are considered this scenario is not fully consistent. Alteration of oceanic crust may also produce decoupling of Th and U isotopes (Chen et al.(1986)). There is, however no evidence for this decoupling as OIB suites show good correlations between 208 Pb/204 Pb and 206 Pb /204 Pb (Fig.8.3). These correlations are also found in MORB (e.g. White et al.(1987), Ito et al.(1987)).

A further contradiction exists, however, because it is known that alteration of oceanic crust results in an increase in $^{87}Sr/^{86}Sr$ ratios from studies of dredge basalts (Hart et al.(1974), O'Nions et al.(1977) and Zindler et al.(1984)) and also

from studies of vent fluids. This is not expected from the low values of $^{87}Sr/^{86}Sr$ recorded in volcanics with a HIMU signature (Fig.7.12a). Albarede et al.(1981) showed that hydrothermal fluid had interacted with oceanic crust to produce a mixing curve between MORB and seawater. Piepgras and Wasserburg(1985) similarly showed that large scale equilibration had occurred between Sr in fluid and basalt. This interaction may not be important if, as Zindler and Hart(1986) suggest, the crust underwent alteration processes when the isotopic value of Sr in seawater was more akin to that of the mantle early in Earth history. The alteration may however produce a decrease in Rb/Sr ratios in the oceanic crust which is important in generating low Sr isotopic values. This is suggested because the Rb content of hydrothermal fluids is greater than that in seawater, suggesting leaching of Rb from the crust (Michard et al.(1984)). This is at variance with the results of Staudigel and Hart(1983) which showed a net increase in LIL in dredge basalts. Michard et al.(1984) suggested that this discrepancy could be resolved because the dredge samples are only affected by Low T interaction with seawater just below the seafloor. The averaging effect of the hydrothermal waters are thought to be more representative of the crust as a whole.

A depletion in K is also suggested by the data of Michard et al.(1984). It was also found that the K/Rb of the hydrothermal fluids was lower than that of the seawater. This suggests that Rb may be extracted more efficiently than K. This is inconsistent with the depletion order evident in HIMU source basalts in which K is the most depleted of the LIL. Further modifications subsequent to SAP may be necessary to achieve this.

In the alteration process it appears that Nd isotopes and the Sm/Nd ratios are unlikely to be greatly fractionated. This is apparent from the study of REE content of hydrothermal fluids by Michard et al.(1983) who found no appreciable leaching effect. Piepgras and Wasserburg(1985) found that the Nd isotopic content of hydrothermal fluids was more heterogeneous than that of Sr suggesting less efficient exchange between fluid and crust. This indicates that HIMU may tend to lie to the left of the mantle array because of variations in Rb/Sr rather than Sm/Nd (this is suggested on independent grounds in section 8.2).

8.4.4; Recycling of altered oceanic crust via subduction zones - Subduction zone processing (SZP);

Zindler et al.(1982) argued that the effects of seawater and hydrothermal SAP could be completely removed during subduction zone processing (SZP). This idea arose to counter the problem of Th/U fractionation during SAP (section 8.4.3). They suggested that a substantial increase in U/Pb during MORB generation is required to produce the high time integrated U/Pb seen in HIMU source basalts. Zindler and Hart(1986) point out that this is unlikely due to the relatively low mu values recorded for MORB glasses. They point out that this U/Pb increase could be achieved in SZP whilst retaining the Th/U coherence. Alternatively White et al. (1987) argue that the greater coherence of U, Th and Pb isotopes in Pacific N-MORB (which they consider to be a mix of DMM and HIMU components) is evidence that this group of elements behave coherently during SAP.

Thus a general dilemma exists in models requiring SAP followed by SZP, namely that after both processes have operated it is difficult to attribute the observed features to a particular environment or a combination. The nature of the partial melting processes/slab dehydration processes that operate in a subduction zone are as important as they are difficult to establish. Non magmatic processes are required to account for the fractionation of U/Pb because the distribution coefficient for Pb is thought to be greater than that for U (section 8.4.1). The presence of nebulous metasomatic fluids were thought by Hofmann and White(1982) to possibly affect the LIL budget, but they considered this process insignificant in comparison to SAP. Insufficient experimental data on processes operating at this depth are available, so arc lavas must be examined for evidence of LIL enrichments relative to other mantle derived products. The characteristically high abundances of Ba, Sr and Pb have been attributed to SZP. These features were noted by Hawkesworth and Powell(1980) (high Sr/Ce), De Paulo and Johnson(1979) (High Sr/Nd) and Kay(1980) (high Pb/La and Ba/La). Comparisons of basalts from a number of tectonic settings enabled Pearce(1983) to state that high Rb, K, Ba, Th and Sr formed a subduction component. The relatively low mu values recognised in arc volcanics (Tatsumoto(1978)) provide additional evidence that SZP is capable of producing the required fractionation of

U/Pb (Zindler and Hart(1986)). Palacz and Saunders(1986) have suggested that volatile elements such as K, Rb, Ba and possibly LREE and Pb may be driven off from a slab of oceanic crust during subduction to account for the LIL depletion in HIMU source basalts. Dupuy et al.(1988) have also pointed out that in terms of LIL and Sr spidergrams of basalts with a HIMU signature are "antipathic images" of VAB. The implication being that they are conjugates formed during subduction. This feature is illustrated in Fig. 8.12. The St.Helena basalt is compared to an average arc tholeiite from Sun(1980). It is apparent that the depletion in LIL in HIMU corresponds to an enrichment in LIL in arc basalts. There is a good correspondence between the maximum depletions and enrichments. It is noted that the order of enrichment in Island arc volcanics (Fig.8.12). i.e. Ba>K>Rb is not consistent with small degree melts of a depleted source such as MORB source (Fig.8.9) black curve) because the the order expected would be K>Ba>Rb. It seems that some other process is increasing K abundances relative to Ba and Rb.

Phase equilibria studies of the system $KAlSiO_4$ - Mg_2SiO_4 - SiO_2 - H_2O by Wyllie and Sekine(1982) have suggested that mantle phlogopite may form as a consequence of slab subduction. This would be significant as phlogopite could provide a means of fractionating K from other LIL to produce the K trough seen in HIMU volcanics (Section 8.3). In their model Wyllie and Sekine(1982) envisaged that phlogopite forms by interaction between cool siliceous magma rising from melting oceanic crust and the hotter overlying mantle wedge peridotite. The aqueous fluids produced during this hybridisation could be important in transport of LIL (Fyfe and McBirney(1973)). Wyllie further suggested that the phlogopite clinopyroxenites formed were stable at the depths they were generated and could melt on crossing a deeper solidus to produce the alkalic magmas erupted behind volcanic arcs. The phlogopite pyroxenites occur directly above the subducted crust in this model. If these phlogopite pyroxenites then melt in close proximity to and interact with subducted oceanic crust this could explain the conjugate nature of HIMU OIB and arc basalts suggested by Dupuy et al.(1988). It is uncertain whether the spatial occurrence of the phlogopite masses and the crust is suitable for this to occur, as the two could remain discrete.

Fig.8.12. Spidergram of an average arc basalt (Sun(1980)) in comparison with N-MORB (Sun(1980)) and a member of the SHRS (SC 68).

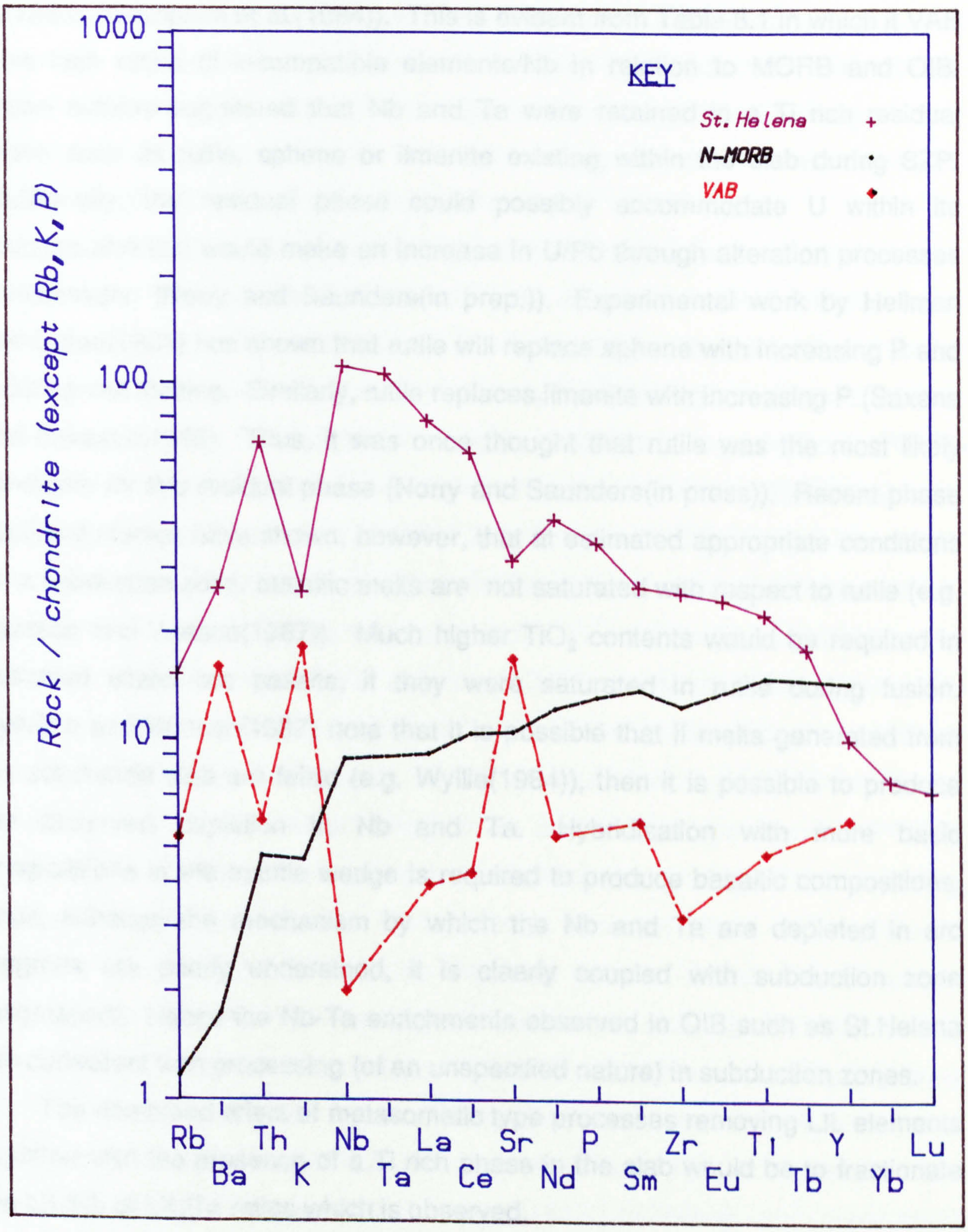
KEY
St. Helena +
N-MORB •
VAB ◆
1000
100
10
1
Rock / chondrite (except Rb, K, P)
Rb Th Nb La Sr P Zr Ti Y Lu
Ba K Ta Ce Nd Sm Eu Tb Yb

Another well known feature of arc magmas is the depletion of Nb and Ta in comparison with elements of similar incompatibility such as La (Saunders et al.(1980), Thompson et al.(1984)). This is evident from Table 8.1 in which it VAB have high ratios of incompatible elements/Nb in relation to MORB and OIB. These authors suggested that Nb and Ta were retained in a Ti rich residual phase such as rutile, sphene or ilmenite existing within the slab during SZP. Additionally, the residual phase could possibly accommodate U within its structure and this would make an increase in U/Pb through alteration processes unnecessary (Norry and Saunders(in prep.)). Experimental work by Hellman and Green(1981) has shown that rutile will replace sphene with increasing P and T during wet melting. Similarly, rutile replaces ilmenite with increasing P (Saxena and Eriksson,1985). Thus, it was once thought that rutile was the most likely candidate for this residual phase (Norry and Saunders(in press)). Recent phase equilibria studies have shown, however, that at estimated appropriate conditions for a subduction zone, basaltic melts are not saturated with respect to rutile (e.g. Ryerson and Watson(1987)). Much higher TiO_2 contents would be required in observed island arc basalts, if they were saturated in rutile during fusion. Ryerson and Watson(1987) note that it is possible that if melts generated from the subducted slab are felsic (e.g. Wyllie(1984)), then it is possible to produce the observed depletion in Nb and Ta. Hybridisation with more basic compositions in the mantle wedge is required to produce basaltic compositions. Thus, although the mechanism by which the Nb and Ta are depleted in arc magmas are poorly understood, it is clearly coupled with subduction zone magmatism. Hence the Nb-Ta enrichments observed in OIB such as St.Helena are consistent with processing (of an unspecified nature) in subduction zones.

The combined effect of metasomatic type processes removing LIL elements together with the presence of a Ti rich phase in the slab would be to fractionate the LIL/Nb or LIL/Ta ratios which is observed.

The production of HIMU characteristics by recycling of ancient oceanic crust is now widely favoured by geochemists as a "distinct possibility" (White et al.(1987), Allegre and Turcotte(1986a), Palacz and Saunders(1987), Dupuy et al.(1988), Saunders et al.(1988) and Sun and McDonough(1988). As is pointed out above, however it is dangerous to favour a model that is essentially

untestable. If the events in the mantle - oceanic crust - subduction zone - mantle cycle are considered it is evident that because two consecutive reprocessing stages are involved it is difficult to test this hypothesis. Until alteration processes are more fully understood the material entering the subduction zone will be poorly constrained. Even if our knowledge of the average geochemistry of such material did improve, subduction zone processing provides the opportunity to obliterate any of these processes to fit the model.

A further insight into the possibility that HIMU represents recycled oceanic crust is given by the Roberts Victor eclogites (S.Africa) which have also been interpreted as recycled oceanic crust. The compelling evidence for this is based on O isotopes. The most comprehensive study by MacGregor and Manton(1986) has shown that the Roberts Victor eclogites possess a large range in $^{18}0/^{16}O$ (2-7), with the lowest values being significantly lower than the mantle value for non eclogitic nodules which is $^{18}0/^{16}O$ = 5.5 - 6 (Kyser(1986)). These low values are interpreted by MacGregor and Manton(1986) as resulting from hydrothermal alteration of oceanic crust prior to subduction. In addition (Kyser(1986)) states that *"it is highly unlikely that the very low $^{18}O/^{16}O$ values of these eclogites can result from the small, high temperature fractionations that are thought to occur in the mantle."* Supportive evidence of this interpretation comes from studies of ophiolites such as the Samail, which show a similarly large range in $^{18}0/^{16}O$, extending to $^{18}0/^{16}O$ values of below 2. (McCulloch et al.(1981)). Thus according to the model of Hofmann and White(1980,2) in which HIMU OIB represents recycled oceanic crust, it would be expected that the SHRS should contain anomalously low $^{18}O/^{16}O$. Although it should be remembered that mixing interaction in the SHRS source region between a HIMU component possessing low $^{18}O/^{16}O$ and MORB with higher $^{18}O/^{16}O$ (5-6) would diminish the evidence of this effect observed in the SHRS. Efficient subsolidus mixing of different parts of the oceanic crust in a "megalith" (Ringwood(1982)) (following subduction) could also average the range of values of $^{18}O^{16}O$ observed in ophiolites or the Roberts Victor eclogite.

$^{18}0/^{16}O$ determinations for whole rock samples from the SHRS have been made by Grant et al.(1976). The lowest values that they report are 6.5, which is typical for OIB (e.g.Kyser(1986)). Ascension island, which has similar radiogenic

Pb compositions to St.Helena ($^{206}Pb/^{204}Pb>19.5$) also possesses normal values for $^{18}O/^{16}O$ in OIB. These results are important since if low $^{18}0/^{16}O$ values are indicative of low temperature hydrothermal processes in the oceanic crust and they cannot be modified at higher temperatures then the HIMU component sampled in the SHRS cannot have undergone interaction with a hydrothermal system in the oceanic crust. One scenario which could be invoked to explain this is if the upper few kilometres of oceanic crust that experiences hydrothermal processes are scraped off (obducted) or consumed by partial melting in subduction zones with the lower oceanic crust forming the HIMU reservoir. This is consistent with the occurrence of Group I eclogites from the Roberts Victor locality that possess normal mantle values of $^{18}0/^{16}O$ (> 6). It is argued by Jagoutz et al.(1984) that these represent deeper parts of the oceanic crust whereas the Group II eclogites that contain the heterogeneous $^{18}0/^{16}O$ ratios represent upper oceanic crust that has undergone hydrothermal alteration. This is also consistent with studies of the Samail ophiolite (McCulloch et al.(1981)) which has an upper zone heterogeneous in $^{18}0/^{16}O$ ratios and a more uniform lower zone. If this scenario is realistic a corrolary of it is that the Rb-Sr, Sm-Nd and U-Th-Pb fractionations that are required to produce the HIMU isotopic characteristics (section 8.2) must all have occurred in the subduction zone if a recycling model is adopted. The mechanism for the loss of the upper oceanic crust remains speculative.

8.4.5; Continental lithosphere processes;

Some authors (Zindler and Hart(1986), Hart et al.(1986) have argued that the required fractionations of U/Pb, Th/Pb and Rb/Sr in HIMU OIB cannot be produced by the combined effect of SAP and SZP. Hart et al.(1986) point out that the element fractionation that needs to be considered is that between U and Rb. Hart et al.(1986) suggest that if the relative proportions of Sr, Nd and Pb are kept approximately constant at bulk earth values during recycling an order of magnitude increase in U/Rb is required. It should be noted that the Rb/U fractionation calculated by this method is highly misleading because it assumes that Sr, Nd and Pb are kept constant during recycling. The evidence reviewed in section 8.4.3. showed that Pb could be leached from the oceanic crust and Sr is

exchanged in the oceanic crust. Although the addition of Sr and depletion of Pb from the crust cannot be constrained numerically, it is clear that the consequence of this is that the U/Rb ratio need not be increased by as much as an order of magnitude. Hart et al.(1986) argue that the requirement for a large increase in U/Rb invalidates the model of recycling oceanic crust to form HIMU OIB because the two processing stages do not produce fractionation of Rb from U in either altered oceanic crust or in continental crust. The basis of this is the work by Staudigel and Hart(1983) which they believe indicates that Rb is not fractionated from U in SAP. However, this is far from certain (section 8.4.3.). The hydrothermal fluid data of Michard et al.(1983,1984) suggest that U may be deposited in the oceanic crust whereas Rb is leached from it. Hart et al.(1986) further argue that because U is unfractionated from Rb in the average continental crust this cannot represent a complementary reservoir to HIMU. However, the use of the average continental crust as a conjugate to HIMU is not a very good test because it is an average; it is better to study arc basalts. Unfortunately, few studies have been made of VAB, in which U has been determined. A compilation by Sun(1980) shows that contrary to the statement by Hart et al.(1986), U/Rb may be possibly fractionated by SAP / SZP. This is evident from Table 8.1, which shows that Rb/U are significantly higher in VAB than in MORB from which they may be derived (46.0 and 10.0 respectively). This suggests an increase in Rb and a decrease in U (if this IAT were derived directly from MORB) which is compatible with the element fractionations indicated by the isotope systematics (Table 8.2). Rb/U ratios in the SHRS are approximately 13.0, hence this value is lower than arc basalts as would be expected if element fractionation had occurred in the subduction zone. Hart et al.(1986) suggest that such fractionations can be produced if melt generation involves phlogopite occurring in the lithosphere through metasomatic processes because this is capable of producing Rb/U fractionations of several orders of magnitude. Hawkesworth et al.(1987) also note that phlogopite is capable of fractionating U from Pb.

To investigate whether the trace element features in HIMU can be accounted for by mantle metasomatism processes operating in the continental lithosphere relevant mantle nodule compositions are briefly reviewed. The distinctive K and Rb depletion in HIMU requires a conjugate K,Rb-rich phase

recording a complementary metasomatic fluid. It was shown in section 8.3.3 that nodules known as metasomatised PKP mantle nodules (Phlogopite K-richterite peridotites) and Phlogopite peridotites (PP) have the order of enrichment of; *Rb>=K>Ba > Sr.* This is broadly the opposite to what is found in HIMU (depletion order K>=Rb>Ba>Sr). While some of the anomalous LIL abundances of HIMU source basalts could be accounted for by depletions associated with metasomatic processes some problems remain unanswered. Firstly, a greater depletion in the HFS elements Nb, Zr and Ti would be expected to accompany the LIL depletion. Secondly, a problem with such models is that the wide variation in metasomatic phases suggested by Fig.8.22 is difficult to reconcile with the broadly similar features of the HIMU source basalts. A group of minerals has recently been recognised which could explain the enrichments observed in Nb in HIMU type OIB if they were incorporated into the HIMU source (they would necessarily not form a residual phase during magma generation). It is not then necessary to invoke the retention of Nb in a Ti rich phase during the subduction of recycled oceanic crust (section 8.4.4). These Nb-Zr-Ti rich phases are known as the crichtonite minerals of the $AM_{21}O_{38}$ structural type (Haggerty(1983), Haggerty et al.(1986)). Here M are small cations, but importantly A may contain Ba in lindsleyite or K in mathiasite (hence the name LIMA). It is very difficult to assess the volumetric importance of such minerals within the mantle because of their low abundance and because they may have been wrongly identified (Haggerty et al(1986)).

8.5; Storage and transport mechanisms for HIMU;

Of all the models described above a problem exists which is common to all. This is that the mantle segment with the HIMU characteristics has to be stored for a period of at least two Ga in order for the Pb isotopes to evolve to the observed extreme values. (Tatsumoto(1978), section 8.3). Following this period of storage a transport mechanism to the magma generation zone must be available.

8.5.1; Storage of the HIMU component;

The data indicate that the HIMU component must remain physically separate from other mantle components with different isotopic characteristics to enable evolution to the unusual isotopic compositions observed today. The problem is how can the HIMU component remain discrete for 2 Ga (section 8.2) in a mantle that is vigorously convecting? The processes that have the potential to destroy mantle heterogeneities that need to be considered are chemical diffusion and physical mixing. Hofmann and Hart(1978) concluded that over the age of the Earth diffusion would not eradicate heterogeneities over a distance of more than 1km, even in the presence of 5% basaltic melt. Given that a maximum period of evolution of 2 Ga is required and that the proportion of melt in the mantle is liable to be much less than 5% (McKenzie(1985a)), there appears to be no difficulty in preserving large scale heterogeneities. Indeed if simple solid state (atomic) diffusion models are considered the distance over which diffusive interactions would occur are even smaller. Hofmann and Hart(1978) suggest diffusion coefficients in the range $D=10^{-14}$ to 10^{-16} cm^2 sec^{-1}. A diffusion length of only 6cm to 6.3m over the period of required separation of the HIMU component (2 Ga) is obtained.

Eradication of large scale heterogeneities by convection may be possible over much shorter periods of time. Numerical modelling by Olson et al.(1984) and Hoffman and McKenzie(1985) has shown that mantle heterogeneities may be homogenised in periods shorter than the separation times required by the isotopic data. Such modelling is strongly dependent on input parameters, in particular convection mode, viscosity, layer depth and magma extraction process (Hoffman and McKenzie(1985)). Despite variation of these parameters these authors suggested that a convecting layer would become well mixed on a lateral scale of 2000km minimum after 0.5 to 1.0 Ga. An original equidimensional heterogeneity of original layer thickness is stretched and thinned to an average thickness of 1/50 th of layer depth over this period. It is important to remember that if these processes could destroy heterogeneities it is necessary to store the proto-HIMU component elsewhere before it becomes part of the convective system. Thus, the models of Hanson(1977), Wood(1979) and Zindler et al.(1984) in which streaks of enriched mantle enclosed in a convecting depleted

matrix are supposed to evolve to the end member compositions over a period of Ga would be untenable. Where the proto HIMU component could be stored separately from the convective system is investigated in the transport models described in the next section.

With respect to how these two processes may effect the St.Helena source two observations are pertinent. Firstly, although the HIMU component may be broken down into smaller units i.e. a change from km scale heterogeneity to metre scale heterogeneity, the melting behaviour of such a unit might produce a HIMU signature if the preferential melting models of Sleep(1984) were operative, i.e. if the HIMU component has a lower solidus than the matrix. Secondly the time period over which the HIMU would be subject to convective mixing is likely to be less than the maximum age indicated by U/Pb systematics. This is because whatever the method of formation of the HIMU characteristics the mantle segment is not likely to become immediately involved in the convective cycle. For example, if the HIMU component represents subducted oceanic crust, it will be isolated from convection at the mesosphere boundary layer. Alternatively, if it is formed in the subcontinental lithosphere, it may reside there before it is delaminated. However, the results of Hoffman and McKenzie(1985) have been criticised by Zindler and Hart(1986) for not taking into account the different rheologies between blob and matrix. They suggest that these differences may foster the survival of heterogeneities. Similarly numerical modelling on convective systems by Gurnis and Davies(1986) leads them to suggest that this process is relatively inefficient at homogenising the mantle. The present consensus of such models is that *"convective thinning alone is insufficient to homogenise the mantle"* (Kellogg and Turcotte(1986)). These authors consider the effect of normal strain together with diffusion processes acting on a boundary layer. They conclude that diffusion can only operate on the scale of a few centimetres or less and that when combined with deformation produces layers of a minimum thickness of 2cm. They relate this model to pyroxenite layers in high temperature peridotites which they consider to be stretched and thinned oceanic crust. These ideas have culminated in the marble cake mantle model of Allegre and Turcotte(1986a) in which the upper mantle comprises thin (1m thick maximum) streaks of subducted crust in a convecting

DMM matrix.

8.5.2; Transport of the HIMU component;

Prior to investigating the method by which the HIMU component may be transported from its zone of formation to its position as an OIB source it is necessary to study the areal distribution of the HIMU component. If a widespread occurrence is apparent it is necessary to invoke a large scale process that could affect large areas of mantle. The radiogenic compositions of the SHRS were originally thought to be an unusual occurrence that was not recorded elsewhere. (e.g. compilation of Sun(1980)). Current thinking is that the HIMU component is a globally ubiquitous magma source (e.g. White(1985)), Zindler and Hart(1986), Saunders et al.(1988)). This change in ideas has mainly been caused by additional data acquisition and the recognition that mixing with a HIMU component and DMM is necessary to account for the Sr, Nd and Pb isotopic variations exhibited by many oceanic basalts (White(1985), Zindler and Hart(1986)). In addition, regional studies such as those in the S.Atlantic by Hanan et al.(1986) have shown that evidence of a HIMU component can be recorded over distances of several thousand kilometres. Thus any suitable mechanisms involving the transport of HIMU component from its zone of origin to the magma source region must be compatible with large scale processes of global dynamics.

The mechanism of formation of HIMU characteristics by subduction of altered oceanic crust readily leads to a mechanism for storage and transport of the material with HIMU characteristics. Ringwood's(1982,5) model for recycling dealt with the mechanistic concept of recycling. Ringwood created a model in which the processed oceanic crust is subducted to the 670km seismic discontinuity and then becomes ponded at the boundary and spreads out laterally. Owing to the density difference between the lower lithosphere and the colder upper part which comprises crust and residual harzburgite, the lower lithosphere becomes separated from the upper lithosphere and is recirculated into the convective upper mantle. The cooler oceanic crust and harzburgite undergo phase changes which enhance their negative buoyancy relative to the surrounding mantle which causes them to be continue down to the 670km

discontinuity, (Irifune and Ringwood(1986)). At this depth the harzburgite becomes buoyant relative to the ambient mantle and forms a *"megalith containing disrupted pieces of oceanic crust".* Heating of the megalith occurs as it thermally equilibrates with the surrounding mantle. This causes fusion of the lower temperature melting component, i.e. the oceanic crust which interacts with the surrounding harzburgite to confer its isotopic and trace element signature on it. Further heating causes diapirs of harzburgitic material to ascend and form hotspots. Hofmann and White(1982) suggested that decay of K and U within the oceanic crust may be effective in providing the heat input necessary for diapiric ascent. They also suggest that a characteristic time for this process to occur may account for the long residence times required in the mantle. A similar model has also been developed by Allegre and Turcotte(1985), this is known as the mesosphere boundary layer model. In this model the inherently unstable thermal boundary layer between the lower and upper mantle is stabilised by the cool subducted lithosphere.

Much recent discussion has focussed on whether a descending slab can penetrate the 670km discontinuity. Tomographic interpretation of seismic data (e.g. Creager and Jordan(1986)), has indicated anomalously fast travel times beneath the downgoing slab of the Marianas Trench which he suggests is a continuation of the slab. Although it is possible that it could merely be the downwelling limb of a lower mantle convection cell induced by the overlying cold slab. Although the existence of a layered mantle is fundamental to many ideas in geochemistry, it is not of fundamental importance to the present model as the descending slab could be mobilised by internal heat supply or an external plume influence whether it was at the base of the upper mantle or the core mantle boundary.

Rare gas data provide further constraints on the geodynamic models proposed to account for the formation of the HIMU source. He isotope data for MORB and OIB (Kurz et al.(1982), Allegre et al.(1983a)) has shown two populations in terms of $^{3}He/^{4}He$. This is significant as it suggests different proportions of primordial ^{3}He and radiogenic ^{4}He in these basalts. Ratios of $^{3}He/^{4}He$ (R) are expressed relative to the atmospheric $^{3}He/^{4}He$ ratio (Ra) as R/Ra. MORB contains R/Ra of 7 - 9 and contains only 12% primordial R/Ra

component (O'Nions and Oxburgh(1983)). The loss of ^{3}He suggests its source has been degassed (Allegre et al.(1986a). This is substantiated by Xe data which suggests an early outgassing of the MORB reservoir in Earth history because of the presence of a the daughter ^{129}Xe derived from the short lived isotope ^{129}I in MORB but not the atmosphere (Allegre et al.(1986a)). Some basalts such as those of Loihi, Hawaii and Iceland (Kurz et al.(1982)) possess a significant primordial He signature (R/Ra > 20). This is consistent with a two layer mantle model in which the primordial He is from a lower undegassed reservoir. A two layer mantle is is also required by O'Nions and Oxburgh(1983) to account for a discrepancy between the thermal and He flux. He is preferentially retained in the lower mantle. OIB with a substantial EM component (Zindler and Hart(1986) such as Tristan da Cunha da Cunha and Gough contain R/Ra 5-6 (Kurz et al.(1982), this suggests they are not obtained from this primitive reservoir. Recent determinations on the St.Helena basalts by Graham et al.(1988) show that St.Helena has a very low R/Ra compared with the majority of OIB (R/Ra =5.1-5.9) This is consistent with the St.Helena HIMU source component representing recycled oceanic crust. It may have derived this He isotope character from either low R/Ra MORB from which it would be generated or it may have been subject to high ^{4}He production rates because of a high U content (indicated by high time integrated U/Pb). Hart(1984) has suggested that following eruption at the MOR oceanic crust may develop low R/Ra due to loss of mantle He during subsolidus cooling as spreading occurs. The He data are also inconsistent with HIMU being directly derived from the lower mantle. However, Saunders et al.(1988) suggest that oceanic crust may have been recycled into the lower mantle They suggest that it has not acquired a primordial He signature because they believe that unradiogenic ^{3}He is being degassed from the core. This is inconsistent with the models of O'Nions and Oxburgh(1983) and Allegre et al.(1986a) who support the existence a two layer mantle with the lower mantle containing a significant primordial He signature. It may be conceivable that the HIMU component has resided in the lower mantle following subduction if either the diffusion rate of He is insufficient to affect the megalith or if excess ^{4}He production occurs through the high U content of the megalith. Allegre and Turcotte (1985) consider that subducted slabs will form irregular massess at the

670 km discontinuity and that their thickness will be sufficient that they will be unaffected by the ^3He flux from below. Basalts with high values of R/Ra such as those of Loihi, Hawaii will form in areas where the boundary layer is not coated by slabs and this causes instabilties to develop that result in entrainment of pristine mantle with a high ^3He signature.

If the model proposed by Hart et al.(1986) in which metasomatic processes play an important role in forming oceanic crust is correct the subcontinental lithosphere could act as a storage zone for HIMU. Alternatively a remobilised megalith which had formed a plume could penetrate the lithosphere and confer HIMU characteristics on it. By either means the subcontinental lithosphere could possess HIMU characteristics. It is thought possible that by overthickening the cold root of the lithosphere pieces could be delaminated to sink into the convecting oceanic reservoir (McKenzie and O'Nions(1983)). Evidence that the base of continental lithosphere may be negatively buoyant is provided by a study beneath California by Clayton (unpublished) who demonstrated a discrete zone of cold material detached from main part of lithosphere.

8.6; Summary;

It is apparent that a multitude of origins have been suggested to account for the formation of the HIMU source. These ideas were mainly developed to account for the U-Pb fractionation required from the Pb isotope data. It has been demonstrated in section 8.3.3 that HIMU basalts also possess a consistent depletion in other LIL. This must also be taken into consideration. The order of depletion K > Rb > Ba > Th is not in accord with their order of incompatiblities : D K > D Th > D Rb > D Ba. This mitigates against an origin of the depletion in LIL by multiple melting events. This and the fractionation of U from Pb show that mechanisms of LIL fractionation involving silicate melts are untenable. Whilst some of the LIL depletion may be accounted for by residual phases occurring in the source of HIMU, this does not account for the low time integrated Rb/Sr indicated by unradiogenic Sr isotopes. This suggests that some other mechanism for LIL depletion is required. The continuous core growth model for removal of Pb is no longer tenable in isolation as core growth cannot produce the required depletions in non siderophilic LIL. The work by Newsom et al.(1986)

supports this because no evidence exists to show that highly chalcophile and siderophile elements such as Pr and Mo are depleted (section 8.4.3). A further constraint on the process producing HIMU is that it must be capable of producing large volumes of HIMU because of its importance in producing the mixing arrays found in oceanic basalts (Zindler and Hart(1986)). The recycling model of Hofmann and White satisfies this prerequisite well and is, therefore superficially attractive. Unfortunately, this model is also difficult to test because it involves two stages of processing. The data currently available on hydrothermal alteration of the crust are consistent with each of the U-Th-Pb, Sm-Nd and Rb-Sr systematics of HIMU, but it is possible that it may not produce the required fractionation of U from Rb (Hart et al.(1986)). The required fractionation of K from Rb also seems unlikely (section 8.3). Therefore whilst these data provides some supportive evidence to the model it is apparent that either a further stage of processing or a different model is required. SZP provides the opportunity for further processing. Although the mechanisms for SZP are poorly understood the geochemistry of oceanic arc lavas is consistent with this. They are enriched in LIL (Kay(1984)) and may possess a marked enrichment in K and do not have high mu values (Tatsumoto(1978)). Because of this there is no apparent requirement to invoke other models for generating HIMU. The reasons put forward by Hart et al. (1986) to discount the oceanic crustal recycling model for HIMU genesis have been shown to be poorly founded. In addition it is difficult to envisage how processes operating within the heterogeneous lower continental lithosphere can produce the relatively uniform features evident in HIMU. It may be possible to reconcile the two separate models if the phases found in the subcontinental lithosphere are also stable within the subduction zone environment. The phlogopite hybridisation model of Wyllie and Sekine(1982) may be important in this respect because it provides a means of producing a K rich phase which would possess a fairly uniform chemistry. The likelihood of our being able to resolve the problem of producing HIMU characteristics is discussed further in Chapter 9.

CHAPTER 9

SUMMARY :

9.1; Introduction;

In this chapter the contribution of the present study to our understanding of OIB genesis is assessed. This acts as a summary of this study and enables joint consideration of the disparate aspects of OIB genesis discussed. These aspects are firstly the OIB source region characteristics and the modification of magmas as they ascend through the lithosphere and secondly, the validity of models developed to account for the formation of the geochemical characteristics of the source. The principal remaining objectives required to advance our knowledge of the role of HIMU genesis in chemical geodynamics are identified and the means by which they may be achieved discussed. In addition, various precautions necessary in the rigorous interpretation of a comprehensive data set from a single volcanic suite are described.

9.2; High level modifications of magmas and volcanics;

It has been shown in Chapters 4 and 6 that the volcanics and intrusives of St.Helena which vary from picrobasalts to phonolites represent mantle derived melts which have experienced differing degrees of crystal fractionation. Accompanying this range in major element composition is a corresponding trace element variation, both in terms of absolute abundance and relative differences (trace element ratios). The relative differences result from the variable incompatibilities of different elements in members of the fractionating assemblage. Clinopyroxene is particularly capable of fractionating trace element ratios. Coupled petrologic study and least squares modelling shows that clinopyroxene is a significant phase in the mineral extract at all stages of crystallisation and that it produces variation in ratios of LREE/HREE or LREE/MREE such as La/Yb. Although source heterogeneity may render these differences insignificant, this is not the case in the St.Helena volcanics. It is thought that these effects have been previously underestimated in other OIB suites and that in similar studies a simple quantitative estimate of the magnitude

of this effect should be made to constrain the maximum possible variation which may be caused by crystal fractionation. Such estimates are preferable to ignoring the effect of crystal fractionation in samples containing more than 5% MgO. For example Palacz and Saunders(1986) actually state that samples containing >5% MgO can be considered to be unaffected by appreciable amounts of Low P fractionation. Such ideas have been shown to be patently false by this study. It is recognised that detailed studies will be necessary in the future to enable these corrections to be made. Consideration of the effect of Low P fractionation is especially necessary if petrogenetic melting models are developed which involve ratios of elements of differing incompatibility in the fractionating assemblage. For example Chauvel and Jahn(1984) argue on the basis of modelling of uncorrected La_N/Yb_N that an enriched source is required for the Massif Central alkali basalts. In fact, some apparent source enrichment may be simply be accounted for by the effect of crystal fractionation, which has been neglected.

Assessing the extent of alteration is another precaution which must be taken when trying to infer source characteristics from a volcanic suite, and the importance of doing this has been highlighted by this study. It has been shown in Chapter 5 that post eruptive alteration may influence the incompatible trace element ratios that are often used to characterise magma sources, e.g. Ba/Nb. This effect is not simply that of leaching Rb and K which has been identified in other studies (e.g. Chen and Frey(1985)), although this does occur. More significant variations in trace element ratios are caused by the presence of secondary phases which have high trace element abundance of a certain element. Two styles of alteration induced enrichment are observed; one involves high Ba, the other high REE (particularly HREE and Y). These two styles do not always occur in unison. Recognising such features is important because of the value of Ba and REE in assessing source characteristics. It is thought that this effect may not have been identified in other studies, for example, Weaver et al.(1987), present an analysis from St.Helena which has an anomalous Ba enrichment. In regional studies such as that of Weaver et al.(1987) the magnitude of such variations may be small compared to inter-island variations. Thus only in a detailed study of an OIB suite is it possible to recognise such

effects. The effect of alteration may be also be unrecognised because these anomalous enrichments do not correspond to traditional indices of alteration such as the proportion of zeolites and the percentage loss on ignition because these secondary phases are dispersed throughout the groundmass rather than being localised in zeolites and volatile rich.

Some samples, particularly phonolitic intrusives possess enrichments of $^{87}Sr/^{86}Sr$ at approximately constant levels of Nd and Pb isotopes (Chapter 7). This is also believed to be related to the migration of fluids interacting with rocks after crystallisation of the primary phases. The phonolites are probably more susceptible to this because of their low Sr concentrations. This effect may be more common than previously realised since several recent detailed studies of OIB phonolites have illustrated a similar effect (Weis et al.(1987) and Palacz and Wolff(1988)). In the light of this extreme care is required when using non-primitive rocks to obtain source characteristics such as the approximate proportion of end members mixtures. Examples of using phonolites for this purpose do, however, exist (Vidal et al.(1984), Duncan et al.(1986)).

9.3; Source characteristics of the SHRS;

Fresh, primitive basalts from the St.Helena lava pile have small, but significant differences in their trace element and isotope geochemistry. These variations suggest mixing between a trace element enriched plume and a depleted MORB source mantle which occurs either in the lithosphere or asthenosphere. This study has been valuable in demonstrating this because well constrained stratigraphic sampling provides time constraints which show that geochemical parameters do not vary randomly with time. This must be the result of high level mixing processes occurring at the base of, or within the lithosphere. Detailed studies of this type are surprisingly rare except for that of Chen and Frey(1983,5) who consider the Hualalai sequence, Hawaii in some detail. More studies of this type are required because the results can be used to model source interaction more effectively.

It was noted in section 7.5 that Hawaii appeared unusual compared to most other OIB in that an inverse rather than positive correlation occurs between parent daughter ratios and isotope compositions. Further studies are likely to

reveal that no general rule is applicable to the geochemical evolution of OIB suites, because of the number of independent variables which control their geochemistry. These variables are:

(1) Degree of fusion in the plume and lithosphere (each of which are dependent on a number of other variables).
(2) Scale of chemical heterogeneity within the plume and between the plume and its envelope.
(3) Relative movement between lithosphere and plume.
(4) Extent of the plume in terms of the dimension of the zone of chemical and thermal anomaly in relation to the area of eruption.
(5) Occurrence of toroidal circulation within plume.
(6) Degree of lithospheric incorporation through erosional delamination by the plume.
(7) Extent of interaction of ascending magmas with lithosphere.

An interesting tangential question is whether the evolutionary sequences evident in OIB suites are similar. Fig.9.1 shows the well established evolutionary sequence from Hawaii following the interpretation of Clague(1987). If this sequence is compared to either of the shield volcanoes on St.Helena there are major differences. Firstly, the alkalic pre-shield and tholeiitic shield are absent on St.Helena. It is possible that these may be absent because they were erupted as submarine flows. The sequence, is however similar in that the oldest rocks that occur on St.Helena (below the erosional unconformity in the NE volcano) have the lowest normative nepheline content (<1%). Secondly, the alkalic rejuvenated stage is also absent from St.Helena as there is no appreciable time interval before the intrusion of the SWLI which are not dissimilar to the slightly older lavas of the SWUS. It is likely that more alkalic magmas were generated subsequent to the isolation of activity when the perimeter of the plume was below the island (Fig.7.15). They did not, however reach the surface.

Detailed studies on other oceanic islands will undoubtedly provide further information on source interactions. Previously many studies have effectively demonstrated the mixing of different source materials (e.g. Chen and

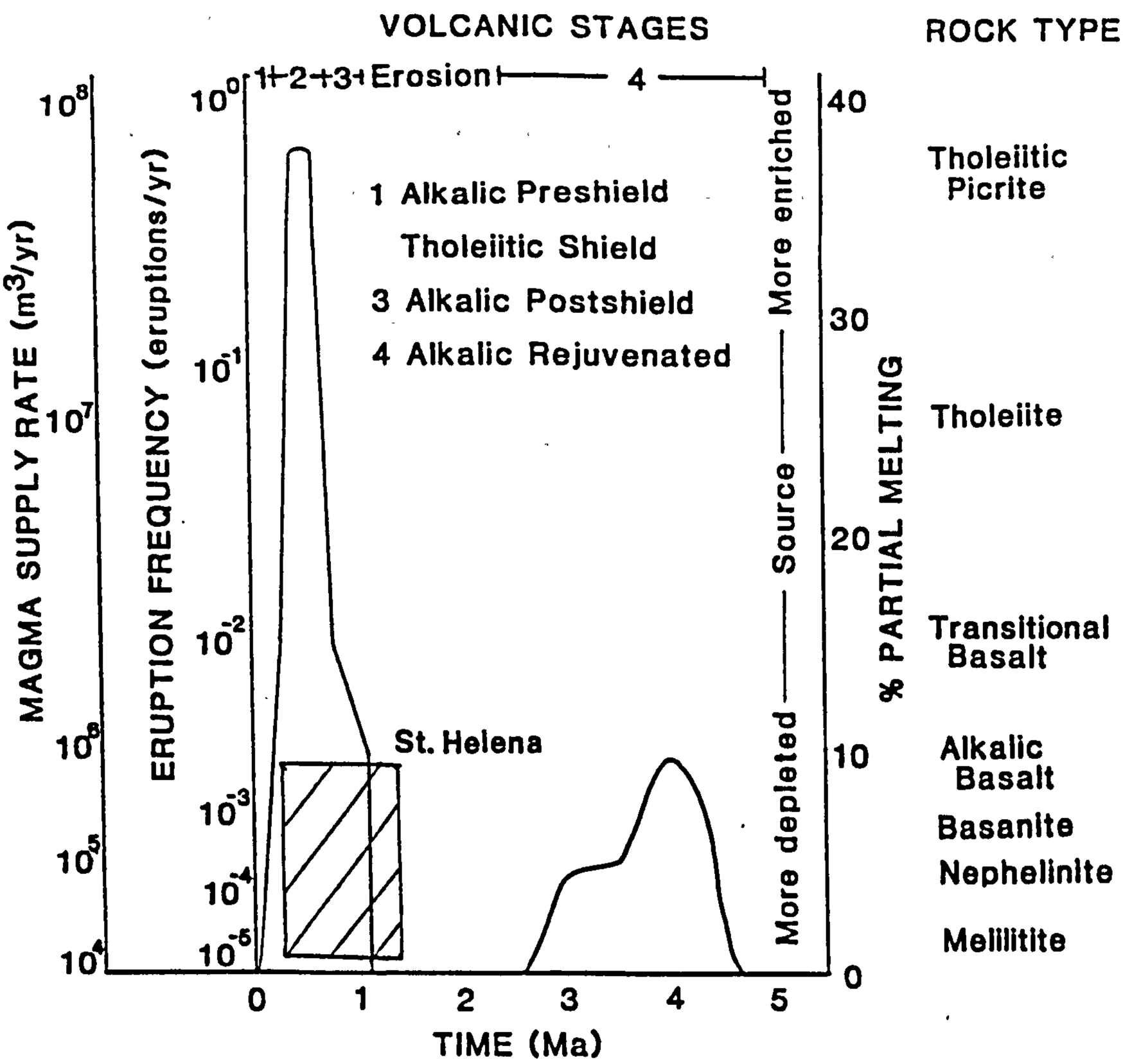

Fig.9.1. Evolutionary characteristics of a typical Hawaiian volcano (from Clague(1987)). The magma supply rate and subduction frequency cannot be portrayed for St.Helena because of insufficient K-Ar data. The stages of shield development for the NE volcano of St.Helena and the predicted degree of partial melting (Chapter 6) are therefore shown as a field. The form of the curve for St.Helena is thought to be akin to that for Hawaii (within the area defined by the box).

Frey(1983,1985), Mattey(1982), Liotard et al.(1985), but understanding of the mechanical processes has been incomplete. These processes are, however, important because, as Ribe(1988) points out mixing processes are not simply geochemical balances, but must also conserve energy and momentum as well. By considering such features he shows that the batch melting equations of Shaw(1970) may underestimate the degree of trace element enrichment due to partial melting by up to 70%. This will result in unrealistically low values of fusion in models that use these equations(e.g. Fitton and Dunlop(1985), section 6.3). Models of mantle melting at present also do not consider the effect of small scale (m - cm) heterogeneity of materials which may have different rheologies and melting behaviour (solidi). The possible existence of such small scale heterogeneity has been indicated by studies of alpine lherzolite masses which exhibit extreme isotopic heterogeneity on a small scale (e.g. Allegre and Turcotte(1986a), Jagoutz(1988), Pearson et al.(in preparation)). Modelling of the melting behaviour of such "marble cake" material being undertaken by Lewin and Allegre (Paris) will undoubtedly place further constraints on the fusion of small scale heterogeneities in OIB and MORB sources.

Other processes such as the interactions between melt and lithosphere as the melts ascend may also affect this budget. The model of Navon and Stolper(1987) in which the mantle part of the lithosphere acts as a chromatographic column may be extreme in as far as geochemical fronts for particular elements do not occur which would be expected if this were the case (Hofmann(1987)). In addition melts may ascend at rates of cm/s to m/s (Spera(1984)) which may not permit opportunity for interaction between the melt and column.

Only once such effects have been considered will it be possible to realistically gauge the source characteristics. At present ideas on this are model dependent particularly with regard to whether an enriched source or depleted source is chosen. The Kohala, Hawaii example is informative because this is a tightly controlled data set, yet, two groups of workers - Hofmann et al.(1987) and Lanphere and Frey(1987) cannot even agree on the likely presence or absence of garnet in the source. Petrogenetic modelling conducted in this study has shown that the trace element abundances in the SHRS are compatible with

derivation from an olivine - clinopyroxene - orthopyroxene - garnet source, in which a K-rich residual phase may be present. Small degrees of partial melting (1 - 10%) are indicated. The simple models used are liable to be far short of reality. Further progress is likely to be made by considering the physical characteristics of plume melting (Ribe(1988)) However, no true inversions of the source are likely to be possible in the future because significant a priori assumptions will be necessary, with a limited basis for them. For example, it has been shown that the evidence available in volcanic suites does not permit unique models of depleted, primitive, enriched, garnetiferous or garnet free sources to be adopted. Thus, even when the physical constraints on melt genesis are better understood and when other input parameters such as partition coefficient data is more reliable, fundamental assumptions will still be necessary.

9.4; Acquisition of the HIMU isotopic characteristics;

The unusual isotopic characteristics of the SHRS have been stressed throughout this study. The new isotopic determinations have reaffirmed the existence of the St.Helena volcanics as extreme, near end member compositions in terms of their Pb isotopes. The limited amount of mixing with a depleted component enables the isotopic characteristics of this component to be clearly defined. The extremely radiogenic Pb compositions indicate high time integrated U/Pb ratios. The position of St.Helena volcanics to the left of the Sr-Nd "mantle array" indicates a complementary low time integrated Rb/Sr ratio. A new contribution to the discussion on the origin of the HIMU mantle component is the recognition that OIB suites with HIMU isotopic characteristics also possess shared trace element features. The notable feature that all HIMU OIB share is depletion in the LIL Rb, K and to a lesser extent Ba relative to Th and Nb. The depletion of K relative to Th which has a similar incompatibility indicates that this feature cannot solely be produced by multiple melting events which produce depletion in the highly incompatible LIL elements (section 8.3). The specific study of St.Helena is useful as it is used to show whether a phase that might be retaining these elements exists in the source region at present or whether it is a consequence of the event producing the proto HIMU characteristics. It is suggested that the HIMU OIB may all possess a K, Rb rich phase in their

sources which accounts for some of the depletion evident, but that previous extraction of LIL is necessary to account for the low time integrated Rb/Sr. The ideas put forward to account for HIMU isotopic characteristics have been critically reviewed in the light of the trace element characteristics. It has been noted that any model put forward to account for the origin of HIMU must also take into account the volumetric importance of HIMU in MORB and OIB genesis (Zindler and Hart(1986)). This critical feature makes the recycling of ancient altered oceanic crust to form HIMU characteristics an attractive one (Hofmann and White(1980,2), Ringwood(1982,5)). It has been shown that ridge centred hydrothermal alteration processes are capable of producing the isotope characteristics of HIMU if the isotope systems are considered separately. However, if they are considered together it seems that the required fractionation of U from Rb may possibly not be achieved by this method (Hart et al.(1986)). A means of producing the relative differences in K and Rb is also not available. Hence subduction zone processing is also required in addition to hydrothermal alteration of subducted oceanic crust. It is also uncertain whether the upper part of the oceanic crust which is involved in hydrothermal circulation is ultimately incorporated into the the HIMU component. Information on this aspect of the recycling model is provided by ophiolites which possess a much wider range of oxygen isotope compositions than that observed in the SHRS in their upper part, but not their lower part.

Although the subcontinental lithosphere has been suggested as a suitable zone in which HIMU can be generated and stored, this is not required by the data. The argument used by Hart et al.(1986) to invoke production of HIMU in the lithosphere is weak because these authors categorically state that the U/Rb fractionations cannot be produced by either hydrothermal alteration of the oceanic crust or subduction zone processing without recourse to the full range of available data. This was reviewed in Chapter 8 and it was shown that it is far from certain that these features could not be produced in the oceanic crust recycling model of Hofmann and White(1980,2). In addition, the requirement for such a significant U/Rb fractionation stated by Hart et al.(1986) is not necessary if the behaviour of Sr and Pb is taken into account (section 8.4.5.)

It is possible that HIMU features could solely be produced in subduction zones. It will probably never be possible to resolve the issue of whether HIMU can be derived by recycling of oceanic crust because two consecutive processes occur. It is thought that more detailed consideration of the relationship between HIMU and arc volcanics could yield useful information on the production of the trace element characteristics of HIMU. The possible presence of a K - rich phase in the subduction zone in the vicinity of the slab should be investigated further because of its ability to produce K-depletion. This is possible by more phase equilibria work following the pioneering studies reviewed by Wyllie(1984). In addition the stability of LIL rich phases which are found in mantle nodules should be further investigated to ascertain whether they are stable at magma generation depths in subduction zones, and if they can produce the required element fractionations in either subduction zones or subcontinental lithosphere. Further work is required to identify recently discovered phases such as the crichtonite series that can contain large quantities of LIL and HFSE, and in particular to gain an appreciation of their relative importance and stability fields. This presents problems because these volumetrically insignificant phases are not only difficult to identify, but they can contain a significant quantity of the LIL in the mantle. Thus the work on nodules should be awaited with keen interest by scholars of OIB. Further data on HIMU OIB themselves are also desirable, particularly with respect to $^{18}O/^{16}O$ and rare gas data (e.g. $^{3}He/^{4}He$). Hydrothermal alteration of the upper oceanic crust is capable of fractionating $^{18}O/^{16}O$ beyond the range observed in OIB as discussed in Chapter 8. However, insufficient data for HIMU OIB are available at present. Future data may indicate that the upper part of the subducted oceanic crust cannot be incorporated into the HIMU reservoir, if a recycling model is invoked. Further $^{3}He/^{4}He$ data are also necessary. Preliminary data from St.Helena indicate a non-primitive, degassed source for the SHRS source components which is compatible with derivation from recycled MORB. It will be interesting to compare the He isotope systematics with Sr-Nd-Pb systematics in other HIMU OIB.

It is apparent that several avenues of research are available from which information pertinent to the formation of the enigmatic HIMU component may be obtained. A thorny and possibly insurmountable problem is presented because if

HIMU has been formed by several stages of geochemical processing it will be difficult to distinguish their effects. Attempting to decipher the limited evidence available should provide a formidable challenge to future geochemists.

Albarede, F., Michard, A., Minster, J.F. and Michard, G., 1981, $^{87}Sr/^{86}Sr$ ratios in hydrothermal waters and deposits from the East Pacific Rise at 21 degrees N, *Earth Planet. Sci. Letts.*, **55**, 229-236.

Ahern, C.J. and Turcotte, D.L., 1979, Magma migration beneath an ocean ridge, *Earth Planet. Sci. Letts.*, **45**, 115-22.

Allegre, C.J., 1982, Chemical geodynamics, *Tectonophys.*, **81**, 109-32.

Allegre, C.J. and Minster, J.F., 1978, Quantitative models of trace element behaviour in magmatic processes, *Earth Planet. Sci. Letts.*, **38**, 1-25.

Allegre, C.J., Brevart, O., Dupre, B. and Minster, J.F., 1980, Isotopic and chemical effects produced in a continuously differentiating convecting earth mantle, *Phil Trans R. Soc. Lond.*, **Ser A 297**, 447-77.

Allegre, C.J., Staudacher, T., Sarda, P. and Kurz, M., 1983a, Constraints on the evolution of the Earth's mantle from rare gas systematics, *Nature, Lond.*, **303**, 762-6.

Allegre, C.J., Hart, S.R. and Minster, J.F., 1983b, Chemical structure and evolution of the mantle and continents determined by inversion of Nd and Sr isotopic data, II: Numerical experiments and diffusion, *Earth Planet. Sci. Letts.*, **66**, 191-213.

Allegre, C.J. and Turcotte, D.L., 1985, Geodynamic mixing in the mesosphere boundary layer and the origin of oceanic islands, *Geophys. Res. Letts.*, **12**, 207-10.

Allegre, C.J. and Turcotte, D.L., 1986a, Implications of a two-component marble cake mantle, *Nature, Lond.*, **323**, 123, 7.

Allegre, C.J. and Staudacher, T. and Sarda, P., 1986 b, Rare gas systematics: Formation of the atmosphere, evolution and structure of the Earth's mantle, *Earth Planet. Sci. Letts.*, **81**, 127-50.

Allegre, C.J., Dupre, B. and Lewin, E., 1986c, Thorium /Uranium ratio of the Earth, *Chem. Geol.*, **56**, 219-27.

Anderson, D.L., 1981, Hotspots, basalts and the evolution of the mantle, *Science*, **213**, 82-9.

Anderson, D.L., 1982, Isotopic evolution of the mantle: the role of magma mixing, *Earth Planet. Sci. Letts.*, **57**, 1-12.

Anderson, D.L., 1985, Hotspot magmas can form by fractionation and contamination of mid-ocean ridge basalts, *Nature, Lond.*, **318**, 145-9.

Arth, J.G., 1976, Behaviour of trace elements during magmatic processes - a summary of theoretical models and their applications, *J. Res. U.S. G. S.*, **4**, 41-7.

Baker, B.H. and McBirney, A.R., 1985, Liquid fractionation, Part III: geochemistry of zoned magmas and the compositional effects of liquid fractionation, *J. Volcanol. Geotherm. Res.*, **24**, 55-81.

The geology of St. Helena Island, S. Atlantic.
Baker, I., 1968, Unpubl PhD thesis, Univ of London.

Baker, I., 1969, Petrology of the volcanic rocks of St.Helena Island, South Atlantic, *Bull. Geol. Soc. Am.*, **80**, 1283-310.

Baker, I., Gale, N.H. and Simmons, J., 1967, Geochronology of the St.Helena volcanoes, *Nature, Lond.*, **215**, 1451-4.

Batiza, R., 1982, Abundance, distribution and size of volcanoes in the Pacific Ocean and implications for the origin of non-hotspot volcanoes, *Earth Planet. Sci. Letts.*, **60**, 197-206.

Bott, M.H.P., 1982, *The interior of the Earth: its structure, constitution and evolution*, (Publ. Edward Arnold).

Boynton, W.V., 1984, Cosmochemistry of the rare earth elements; meteorite studies, In: Henderson, P., *Rare earth element geochemistry*, Elsevier, Amsterdam.

Brevart, O., Dupre, B. and Allegre, C.J., 1986, Lead-lead age of komatiitic lavas and limitations on the structure and evolution of the Precambrian mantle, *Earth Planet. Sci. Letts.*, **77**, 293-302.

Briden, J.C., Rex, D.C., Faller, A.M. and Tomblin, J.F., 1979, K-Ar geochronology and paleomagnetism of volcanic rocks in the lesser Antilles volcanic arc, *Phil. Trans. R. Soc. London*, **A291**, 485-528

Brooks, C., Hart, S.R., Hofmann, A.W. and James, D.E., 1976, Rb-Sr mantle isochrons from oceanic regions, *Earth Planet. Sci. Letts.*, **32**, 51-.

Bryan, W.B., Finger, L.W. and Chayes, F., 1969, Estimating proportions in petrographic mixing equations by least squares approximation, *Science*, **163**, 926-9.

Budahn, J.R. and Schmitt, R.A., 1985, Petrogenetic modeling of Hawaiian tholeiitic basalts: A geochemical approach, *Geochim. Cosmochim. Acta*, **49**, 67-87.

Calmant, S. and Cazenave, A., 1987, Anomalous elastic thickness of the oceanic lithosphere in the south central Pacific, *Nature, Lond.*, **328**, 236-238.

Chase, C.G., 1981, Ocean island Pb: 2 stage histories and mantle evolution, *Earth Planet. Sci. Letts.*, **52,** 277-84.

Chayes, F., 1963, Relative abundance of intermediate members of the oceanic basalt-trachyte association - reply to discussions, *J. Geophys. Res.*, **68,** 5108-9.

Chauvel, C. and Jahn, B.M., 1984, Nd-Sr isotope and REE geochemistry of alkali basalts from the Massif Central, France, *Geochim. Cosmochim. Acta*, 48, 93-110.

Chen, C.Y. and Frey, F.A., 1983, Origin of Hawaiian tholeiite and alkalic basalt, *Nature, Lond.*, **302,** 785-9.

Chen, C.Y. and Frey, F.A., 1985, Trace element and isotopic geochemistry of lavas from Haleakala volcano, East Maui, Hawaii. Implications for the origin of Hawaiian basalts, *J.Geophys.Res.*, **B10,** 8743-68.

Chen, J.H., 1987, U, Th and Pb, Isotopes in Hot Springs on the Juan de Fuca Ridge, *J. Geophys. Res.*, **92,** 11411-15.

Chen, J.H. and Pallister, J.S., 1981, Lead isotopic studies of the Samail ophiolite, Oman, *J. Geophys. Res.*, **86,** 2699-708.

Chen, J.H., Wasserburg, K.L., Von Damm, K.L. and Edmond, J.M., 1986, The U-Th-Pb systematics in hot springs on the East Pacific Rise at 21 degrees N and Guaymas basin, *Geochim. Cosmochim. Acta*, **50,** 2467-79.

Chen, W.P. and Molnar, P., 1983, Focal depths of intracontinental and intraplate Earthquakes and their implications for the thermal and mechanical properties of the lithosphere, *J. Geophys. Res.*, **88,** 4183-214.

Clague, D.A. and Frey, F.A., 1982, Petrology and trace element geochemistry of the Honolulu volcanics, Oahu: implications for the oceanic mantle below Hawaii, *J. Petrol.*, **23,** 447-501.

Clague, D.A., 1987, Hawaiian xenolith populations, magma supply rates, and development of magma chambers, *Contrib. Mineral Petrol.*, **96,** 577-58.

Cohen, R.S., and O'Nions, R.K., 1982, Identification of recycled continental material from Sr, Nd and Pb isotope investigations, *Earth Planet. Sci. Letts.*, **61,** 73-84.

Courtney, R.C. and White, R.S., 1986, Heat flow and geoid across the Cape Verde Rise: evidence for dynamic support from a thermal plume in the mantle, *Geophys. J. R. Astron. Soc.*, **87,** 815-67.

Cox, K.G., Bell, J.D. and Parkhurst, R.J., 1979, *The interpretation of igneous rocks*, (George Allen and Unwin Ltd.).

Creager, K.C. and Jordan, T.H., 1984, Slab penetration into the lower mantle beneath the Mariana and other island arcs of the N.W. Pacific, *J. Geophys. Res.*, **91**, 3573-89.

Crock, J.G., Licte, F.E., Riddle, G.O. and Beechs, C.L., 1986, Separation and preconcentration of the REE and Y from geological materials by ion exchange and sequential acid elution, *Talanta*, **33**, 601-6.

Daly, R.A., 1927, The geology of St.Helena Island, *Proc. Am. Ac. Sci.*, 62 No 2.

Darwin, C., 1873, *Naturalist's voyage around the world*, (John Murray, London).

Darwin, C., 1876, *Geological observations*, Second edition, (publ. Smith, Elder and Co., London).

Davis, B.T.C. and Schairer, J.F., 1965, Melting relations in the join diopside forsterite pyrope at 40 kilobars and at one atmosphere, *Carnegie Inst. Wash. Yearb.*, 64, 123-5.

De Paolo, D.J., 1981, Trace element and isotopic effects of combined wall rock assimilation and fractional crystallisation, *Earth Planet. Sci. Letts.*, **53**, 189-902.

De Paolo, D.J. and Johnson, R.W., 1979, Magma genesis in the New Britain island arc: constraints from Nd and Sr isotopes and trace element patterns, *Contrib. Mineral. Petrol.*, **70**, 367-379.

Detrick, R.S. and Crough, S.T., 1978, Island subsidence, hot spots and lithospheric thinning, *J. Geophys. Res.*, **83**, 1236-44.

Downes, H., 1983, The petrogenesis of coexisting saturated and undersaturated continental alkaline magma series, Leeds Univ. unpubl. PhD thesis.

Duncan, R.A., McCulloch, M.T., Barsczus, H.G. and Nelson, D.R., 1986, Plume versus lithospheric sources for the melts at Ua Pou, Marquesas Is., *Nature, Lond.*, **322**, 534-8.

Dupuy, C., Vidal, P., Barsczus, H.G. and Chauvel, C., 1987, Origin of basalts from the Marquesas Archipelago (south central Pacific Ocean): isotope and trace element constraints, *Earth Planet. Sci. Letts.*, **82**, 145-52.

Dupuy, C., Barsczus, H.G., Liotard, J.M. & Dostal, J., 1988, Trace element evidence for the origin of ocean island basalts: an example from the Austral Islands

(French Polynesia), *Contrib. Min. Petrol.*, **98**, 293-302.

Eggler, D.H., 1983, Upper mantle oxidation state: evidence from olivine - orthopyroxene - ilmenite assemblages, *Geophys. Res. Letts.*, 10, 365-8.

Erlank, A.J., Waters, F.G., Hawkesworth, C.J., Haggerty, S.G., Allsopp, H.L., Rickard, R.S. and Menzies, M., 1987, Evidence for mantle metasomatism in peridotite nodules from the Kimberley pipes, South Africa, In: *Mantle metasomatism*, (eds., Menzies, M.A. and Hawkwesworth, C.J., Academic Press, inc.), p 221-313.

Emery, K.O. and Uchupi, E., 1984, *The Geology of the Atlantic Ocean*, (Springer Verlag N.Y. inc.)

Ewing, M., 1965, The sediments of the Argentine basin, *Q. J. R. Astr. Soc.*, **6**, 10-27.

Faure, G., 1986, *Principles of isotope geology*, (John Wiley and Sons, inc.)

Feigenson, M.D., 1984, Geochemistry of Kauai volcanics and a mixing model for the origin of Hawaiian alkali basalts, *Contrib. Mineral Petrol.*, **87**, 109-19.

Feigenson, F.D., Hofmann, A.W. and Spera, J.F., 1983, Case studies on the origin of basalt: II. The transition from tholeiitic to alkalic volcanism on Kohala volcano, Hawaii, *Contrib. Mineral. Petrol.*, **84**, 390-405.

Feigenson, M.D., 1986, Constraints on the origin of Hawaiian lavas, *J. Geophys. Res.*, **91**, 9383-93.

Fitton, J.G., Kilburn, C.R.J., Thirlwall, M.F. & Hughes, D.J., 1983, The 1982 eruption of Mount Cameroon, West Africa, *Nature, Lond.*, **306**, 327-332.

Fitton, J.G. and Dunlop, H.M., 1985, The Cameroon Line, West Africa,and its bearing on the origin of oceanic and continental alkali basalt, *Earth Planet. Sci. Letts.*, **72**, 23-38.

Fitton, J.G. and James, D., 1986, Basic volcanism associated with intraplate linear features, *Phil. Trans. R. Soc. Lond.*, **A 317**, 253-66.

Fodor, R.V., Bauer, G.R., Jacobs, R.S. and Bornhorst, T.J., 1987, Anomalous hydrothermal? enrichments in tholeiites and alkali basalts of Kahoolawe, Hawaii, *J. Volc. Geotherm. Res.*, **31**, 171-6.

Forsyth, D.W., 1977, The evolution of the upper mantle beneath mid-ocean ridges, *Tectonophys.*, **38**, 89-118.

Frey, F.A. and Roden, M.F., 1987, The mantle source for the Hawaiian Islands: constraints from the lavas and ultramafic inclusions, In: Menzie & Hawkesworth, eds., *Mantle Metasomatism*, (Academic Press Inc.) p 423-63.

Frey, F.A. and Clague, D.A., 1983, Geochemistry of diverse basalt types from Loihi Seamount, Hawaii: petrogenetic implications, *Earth Planet. Sci. Letts.*, 66, 337-55.

Galer, S.J.C. and O'Nions, R.K., 1985, Residence time of Thorium, Uranium, and Lead in the mantle with implications for mantle convection, *Nature, Lond.*, 316, 778-82.

Gast, P.W., 1969, The isotopic composition of lead from St.Helena and Ascension islands, *Earth Planet. Sci. Letts.*, 5, 353-55.

Geist, D.J., White, W.M. and McBirney, A.R. 1988, Plume asthenosphere mixing beneath the Galapagos archipelago, *Nature*, 333, 657-660

Graham, D.W., Jenkins, W.J. and Schilling, J.G., 1988, He-Pb isotope relationships in the South Atlantic, *Trans. Am. Union. Geophys. EOS.*, 69, 510.

Grant, N.K, Powell, J.L., Burkholder, F.R., Walther, J.V. and Coleman, M.L., 1976, The isotope composition of Strontium and Oxygen in lavas from St.Helena, South Atlantic, *Earth Planet. Sci. Letts.*, 31, 209-23.

Green, D.H., 1971., Composition of basaltic magmas as indicators of origin: Application to oceanic volcanism, *Phil. Trans. R. Soc.*, A268, 707-25.

Green, D.H., Fallon, T.J. and Taylor, W.R., 1987, Mantle derived magma, roles of variable source peridotite and variable C-H-O fluid composition, In: *Magmatic Processes*: *Physiochemical principles*, The Geochemical Society, special publication No 1, (ed., B.O. Myson), p 139-54.

Griffiths, R.W. 1986, Dynamics of mantle thermals with constant buoyancy or anomalous internal heating, *Earth Planet. Sci. Letts.*, 78, 435-46.

Gurnis, M. and Davies, G.F., 1986, Mixing in numerical models of mantle convection incorporating plate kinematics, *J. Geophys. Res.*, 91, 6375-95.

Haggerty, S.E., 1983, Lindsleyite (Ba) and Mathiasite (K) two new chromium titanites in the crichtonite series from the Upper Mantle, *Amer. Mineral.*, 68, 494-505.

Haggerty, S.E., Erlank, A.J. and Grey, I.E., 1986, Metasomatic mineral titanite in the upper mantle, *Nature. Lond.*, 319, 761-3.

Haggerty, S.E., 1986, Diamond genesis in a multiply constrained model, *Nature*, **320**, 34-8.

Halliday, A.N., Dickin, A.P., Fallick, A.E. and Fitton, J.G., 1988, Mantle Dynamics: A Nd, Sr, Pb and O isotopic study of the Cameroon Line Volcanic Chain, *J. Petrol.*, **29**, 181-211.

Hanan, B.B., Kingsley, R.H. and Schilling, J.-G., 1986, Pb isotope evidence in the South Atlantic for migrating ridge-hotspot interactions, *Nature, Lond.*, **322**, 137-44

Hanson, G.N., 1977, Geochemical evolution of the sub oceanic mantle, *J. Geol. Soc. Lond.*, **134**, 235-53.

Harris, C., 1983, The petrology of lavas and associated plutonic inclusions of Ascension Island, *J. Petrol.*, **24**, 425-70.

Harrison, W.J., 1981, Partition coefficient for REE between garnets and liquids: implications of non-Henry's Law behaviour for models of basalt origin and evolution, *Geochim. Cosmochim. Acta*, **45**, 1529-44.

Hart, S.R., 1984a, A large-scale isotope anomaly in the Southern Hemisphere mantle, *Nature, Lond.*, **309**, 753-57.

Hart, S.R., 1984b, He diffusion in Olivine, *Earth Planet. Sci. Letts.*, **70** 297-302.

Hart, S.R., Erlank, A.J. and Kable, E.J.D., 1974, *Contrib. Mineral Petrol.*, **44**, 219-30

Hart, S.R. and Davis, K., 1978, Partitioning between olivine and silicate melt, *Earth Planet. Sci. Letts.*, **40**, 203-19.

Hart, S.R., Gerlach, D.C. and White, W.M., 1986, A possible new Sr-Nd-Pb array and consequences for mantle mixing, *Geochim. Cosmochim. Acta*, **50**, 1551-7.

Hawkesworth, C.J., Van Calsteren, P., Rogers, N.W., and Menzies, M.A., 1987, Isotope variations in recent volcanics: a trace element perspective In: *Mantle Metasomatism*, (eds., Menzies, M.A. and Hawkesworth, C.J., Academic Press inc.,), p 365-88.

Hawkesworth, C.J. and Powell, B.M., 1980, Magma genesis in the Lesser Antilles island arc, *Earth Planet. Sci. Letts.*, **51**, 297-308.

Hellman, P.L. and Green, T.H., 1979, The role of sphene as an accessory phase in the high pressure partial melting of hydrous mafic compositions, *Earth Planet. Sci. Letts.*, **42**, 191-201.

Hellman, P.L., Smith, R.E. and Henderson, P., 1979, The mobility of the REE: Evidence and implications from selected terrains affected by burial metamorphism, *Cont. Min. Petrol.*, **71**, 23-44.

Henderson, P., 1982, *Inorganic Chemistry*, (Pergamon Press).

Hofmann, A.W., 1987, Nb in Hawaiian Magmas: Constraints on source composition and evolution, *Chem. Geol.*, **57**, 17-30.

Hofmann, A.W. and Hart, S.R., 1978, An assessment of local and regional isotopic equilibrium in the mantle, *Earth Planet. Sci. Letts.*, **38** 44-62.

Hofmann, A.W. and White, W.M., 1980, The role of subducted oceanic crust in mantle evolution, *Carnegie Inst. Wash. Yearb.*, **79**, 477-83.

Hofmann, A.W. and White, W.M., 1982, Mantle plumes from ancient oceanic crust, *Earth Planet. Sci. Letts.*, **57**, 421-36.

Hofmann, A.W. and Feigenson, M.D., 1983, Case studies on the origin of basalt I: Theory and reassessment of Grenada lavas, *Contrib. Mineral. Petrol.*, **84**, 380-392.

Hofmann, A.W., Jochum, K.P., Seufert, M. and White, W.M., 1986, Nb and Pb in Oceanic basalts: new constraints on mantle evolution, *Earth Planet. Sci. Letts*, **76**, 33-45.

Hofmann, A.W., Feigenson, F.D. and Raczek, I., 1987, Kohala revisited, *Contrib. Mineral. Petrol.*, **95**, 114-22.

Hoffman, N.R.A. and McKenzie, D.P., 1985, The destruction of geochemical heterogeneities by differential fluid motions during mantle convection, *Geophys. J. R. Astr. Soc.*, **82**, 163-206.

Huckenholz, H.D. and Gilbert, M.C., 1983, Melting relations of a kaersutite bearing olivine nephelenite from the Hocheifel, F.R.G., *Trans. Am. Geophys. Union. EOS.*, **64**, 898.

Humphris, S.E., Morrison, M.A. and Thompson, R.N., 1978, Influence of rock crystallisation history upon subsequent lanthanide mobility during hydrothermal alteration of basalts, *Chem. Geol.*, **23**, 125-37.

Humphris, S.E., 1984, The mobility of REE in the crust, In: *Rare Earth element geochemistry*, (ed. P. Henderson, Elsevier).

Ito, E., White, W.M. and Gopel, C., 1987, The O, Sr, Nd and Pb isotope geochemistry of MORB, *Chem. Geol.*, **62**, 157-76.

Irifune, T. and Ringwood, A.E., 1986, The eclogite garnetite transformation at high pressure and some geophysical implications, *Earth Planet. Sci. Letts.* **77,** 245-6

Irvine, T.N. and Baragar, W.R.A., 1971, A guide to the chemical classification of the common volcanic rocks, *Can. J. Earth Sci.*, **8,** 523-48.

Irvine, T.N., 1978, Density current structure and magmatic sedimentation, *Carnegie Inst. Wash. Yearb.*, **77,** 743-51.

Jackson, E.D., and Shaw, H.R., 1975, Stress fields in central portions of the Pacific plate: delineated in time by linear volcanic chains, *J. Geophys. Res.*, **80,** 1861-74.

Jagoutz, E.J., Dawson, B., Hores, S., Spettel, B. and Wanke, H., 1984, Anorthositic oceanic crust in the Archaean, *Lunar Planet Scl.*, **15,** 395-6.

Kanasewich, E.R. and Gutawaski, P.R., 1975, Detailed seismic analysis of a lateral mantle inhomogeneity, *Earth Planet. Sci. Letts.*, **66,** 427-37.

Kaneoka, I. and Takaoka, N., 1980, Rare gas isotopes in Hawaiian ultramafic nodules and volcanic rocks: constraints on genetic relationships, *Science*, **208,** 1366-8.

Kay, R.W., 1980, Volcanic arc magmas: implications of a melting-mixing model for element recycling in the upper mantle, *J. Geol.*, **88,** 497-522.

Kay, R.W., 1984, Elemental abundances relevant to the identification of magma sources, *Phil. Trans. R. Soc. Lond.*, **A310,** 535-47.

Klein, F.W., 1982, Earthquakes at Loihi submarine Volcano and the Hawaiian hot spot, *J. Geophys. Res.*, **87,** 7719-26.

Kellogg, L.H. and Turcotte, D.L., 1986, Homogenisation of the mantle by convective mixing and diffusion, *Earth Planet. Sci. Letts.*, **81,** 371-8.

Kyser, T.K., 1986, Stable isotope variations in the mantle, In: *Stable Isotopes in high temperature geological processes, Reviews in Mineralogy Volume 16 Mineral. Soc. America.*, (eds., J.W. Valley, Taylor, H.P. and O'Neil, J.R.).

Kurz, M.D., Jenkins, W.J. and Hart, S.R. 1982, He isotopic systematics of ocean islands and mantle heterogeneity, *Nature, Lond.*, **297,** 43-6.

LaBrecque, J.L., Kent, D.V. and Cande, S.C., 1971, Revised magnetic polarity time scale for the Late Cretaceous to Cenozoic, *Geology*, **5,** 330-35.

Langmuir, C.H., Bender, J.F., Bence, A.E. and Hanson, G.N., 1977, Petrogenesis of basalts from the FAMOUS area: Mid-Atlantic Ridge, *Earth Planet. Sci. Letts.*, **36**, 133-56.

Langmuir, C.H., Vocke, R.D. and Hanson, J.N., 1978, A general mixing equation with applications to Icelandic basalts, *Earth Planet. Sci. Letts.*, **87**, 380-92.

Lanphere, M.A. and Frey, F.A., 1987, Geochemical evolution of Kohala Volcano, Hawaii, *Contrib. Mineral. Petrol.*, **95**, 100-113.

Leake, B.E., 1978, Nomenclature of amphiboles, *Amer. Mineral.*, **63**, 1023-52.

Le Bas, M.J., Le Maitre, R.W., Streckheisen, A. and Zanettin, B. 1986, A chemical classification of volcanic rocks based on the total alkalis-silica diagram, *J. Petrol.*, **27**, 745-50.

Le Maitre, R.W., 1962, Petrology of the volcanic rocks, Gough Island, South Atlantic, *Bull. Geol. Soc. Am.* 73, **1309-40.**

Le Marchand, F., Benoit, U. and Calas, G., 1987, Trace element distribution coefficients in alkalic series, *Geochim. Cosmochim. Acta*, **51**, 1071-81.

Le Roex, A.P. and Erlank, A.J., 1982, Quantitative evaluation of fractional crystallisation N in Bouvet Island lavas, *J. Volcan. Geotherm. Res.* **13**, 309-19.

Le Roex, A.P. 1985, Geochemistry, Mineralogy and magmatic evolution of the basaltic and trachytic lavas from Gough Island, South Atlantic, *J. Petrol.*, **26**, 149-86.

Leeman, W.P., Budahn, J.R., Gerlach, D.C., Smith, D.R. and Powell, B.N., 1980, Origins of Hawaiian tholeiites: trace element constraints, *Amer. J. Sci.*, **280a**, 794-819.

Liotard, J.M., Barsczus, H.G., Dupuy, C. & Dostal, J., 1986, Geochemistry and origin of basaltic lavas from the Marquesas Archipelago, French Polynesia, *Contrib. Mineral. Petrol.*, **92**, 260-8.

Ludden, J.N., and Thompson, G.T., 1979, An evaluation of the behaviour of the REE during the weathering of sea-floor basalts, *Earth Planet. Sci. Letts.*, **43**, 85-92.

Maaloe, S. and Schie, A., 1982, The permeability controlled accumulation of primary magma, *Contrib. Mineral Petrol.*, **81**, 35-7.

Maaloe, S., Sorensen, I., and Hertogen, J., 1986, The Trachybasaltic Suite of Jan Mayen, *J. Petrol.*, **27**, 439-66.

MacDonald, K.A. and Katsura, T., 1964, Chemical composition of Hawaiian lavas, *J. Petrol.*, **5**, 82, 133.

MacGregor, I.D. and Manton, W.I., 1986, Robert Victor eclogites: ancient oceanic crust, *J. Geophys. Res.*, **91**, 14603-79.

Manhes, Minster and Allegre, C., 1978, Comparative U - Th - Pb and Rb - Sr study of the Saint Severin Amphoterite: Consequences for early Solar System chronology, *Earth Planet. Sci. Letts.*, **39**, 14-24.

Mattey, D.P., 1982, The minor and trace element geochemistry of volcanic rocks from Truk, Ponape and Kusaie, Eastern Caroline Islands; the evolution of a young hot spot trace across old Pacific Ocean crust, *Contrib. Mineral. Petrol.*, **80**, 1-13.

McCulloch, M.T., Gregory, R.T., Wasserburg, G.J. and Taylor, H.P., 1981, Sm-Nd, Rb-Sr in $^{18}O/^{16}O$ isotopic systematics on Ocean crustal section: evidence from the Samail Ophiolite, *J. Geophys. Res.*, **86**, 2721-35.

Mattioli, G.S. and Wood, B.J., 1986, Upper mantle fO_2 recorded by spinel lherzolites, *Trans. Am. Soc. Union EOS.*, **67**, 375.

McKenzie, D.P., 1984, The generation and compaction of partially molten rock, *J. Petrol.*, **25**, 713-65.

McKenzie, D.P., 1985 a, ^{230}Th - ^{238}U disequilibrium and the melting process beneath ridge axes, *Earth Planet. Sci. Letts.*, **72**, 149-57.

McKenzie, D.P., 1985 b, The extraction of magma from the crust and mantle, *Earth Planet. Sci. Letts.*, **74**, 81-91.

McKenzie and O'Nions, R.K., 1983, Mantle reservoirs and ocean island basalts, *Nature*, **301**, 229-31.

McNutt, M.K., 1984, Lithospheric structure and thermal anomalies, *J. Geophys. Res.*, **89**, 11180-94.

Melliss, J.C., 1875, St. Helena: A physical, historical and topographical description of the island, (L. Reeve and Co., London.)

Menzies, M. and Murthy, V.R., 1980, Nd and Sr isotope geochemistry of hydrous mantle nodules and their host alkali basalts: implications for local heterogeneities in metasomatically veined mantle, *Earth Planet. Sci. Letts.*, 46, 323-34.

Menzies, M.A. and Hawkesworth, C.J., 1987, Upper mantle process and composition. In: *Mantle Xenolith*, (ed. P. Nixon, publ. John Wiley and sons, Ltd.).

Menzies, M., Rogers, N., Tindle, A. & Hawkesworth, C.J., 1987, Metasomatic and enrichment processes in lithospheric peridotites an affect of asthenosphere-lithosphere interaction, In: *Mantle metasomatism*, (eds., Menzies, M.A. and Hawkwesworth, C.J., Academic Press, inc.). p 313-61.

Meschede, M., 1986, A method of discriminating between different types of mid-ocean ridge basalts and continental tholeiites with the Nb-Zr-Y diagram, *Chem. Geol.*, 56, 207-18.

Michard, A. and Albarede, F., 1985, Hydrothermal uranium uptake at ridge crest, *Nature, Lond.*, **317**, 244-6.

Michard, A., Albarede, F., Michard, G., Minster, J.F. and Charlou, J.L., 1983, Rare earth elements and uranium in high temperature solutions from the East Pacific Rise hydrothermal vent field (13 degrees N), *Nature, Lond.*, **303**, 795-7.

Michard, G., Albarede, F., Michard, A., Minster, J.F., Charlou, J.L. & Tan, N., 1984. Chemistry of solutions from the 13 degree N East Pacific hydrothermal site, *Earth Planet. Sci. Letts.*, **67**, 297-307.

Michard, A. and Albarede, F., 1986, The REE content of some hydrothermal fluids, *Chem. Geol.*, **55**, 51-60.

Michard, A., Becaire, C. & Michard, G., 1987, Uranium and rare earth elements in CO_2rich fluids from Val-les-Bains (France), *Geochim. Cosmochim. Acta*, **51**, 901-11.

Mitchell-Thome, 1971, *Geology of the South Atlantic Islands*, (Beitrage Zur Regionale Geologie der Erde, Gebruder Bortraeger. Berlin.)

Molnar, P. and Stock, J., 1987, Relative motions of hotspots in the Pacific and Indian Oceans since Late Cretaceous time, *Nature*, **327**, 587-91.

Moore, J.G., 1987, Subsidence of the Hawaiian ridge, In: *Volcanism in Hawaii, V1* (eds. Decker, R.W, Wright, T.L. and Staucher, P.H.).

Morgan, W.J., 1971, Convection plumes in the lower mantle, *Nature, Lond.*, **230**, 42-3.

Morgan, W.J., 1983, Hotspot tracks and the early rifting of the Atlantic, *Tectonophys.*, **94**, 123-39.

Morrison, M.A., 1978, The use of immobile trace elements to distinguish the paleotectonic affinities of metabasalts: Applications to the Paleocene basalts of Mull and Skye, Northwest Scotland, *Earth Planet. Sci. Letts.*, **39**, 407-16.

Mullen, E.D., 1983, $MnO/TiO_2/P_2O_5$: a minor element discriminant for basaltic rocks of oceanic environments and its implications for petrogenesis, *Earth Planet. Sci. Letts.*, **62**, 52-62.

Navon, O. and Stolper, E., 1987, Geochemical consequences of melt percolation: the upper mantle as a chromatographic column, *J. Geol.*, **95**, 285-309.

Newsom, H.E. and Palme, H., 1984, The depletion of siderophile elements in the Earth's mantle: new evidence from molybdenum and tungsten, *Earth Planet. Sci. Letts.*, **69**, 354-64.

Newsom, H.E., White, W.M., Jochum, K.P. and Hofmann, A.W., 1986, Siderophile and chalcophile element abundances in oceanic basalts, Pb isotope evolution and growth of the Earth's core, *Earth Planet. Sci. Letts.*, **80**, 299-313.

Nielsen, R.L., 1988, A model for the simulation of combined major and tra element liquid lines of descent, *Geochim. Cosmochim. Acta*, **52**, 27-39.

Nicolas, A. and Poirier, J.P., 1976, *Crystalline plasticity and solid state flow in metamorphic rocks*, (John Wiley and Sons; London, New York, Sydney and Toronto).

Norry, M.J. and Saunders, A.D., The significance and consequences of Nb and Ta anomalies in terrestrial magmas, (In preparation).

O'Hara, M.J. and Matthews, R.E., 1981, Geochemical evolution in advancing, periodically replenished, continuously fractionated magma chamber, *J. Geol. Soc.*, **138**, 237-77.

O'Hara, M.J., 1985, Importance of the shape of the melting regime during partial melting of the mantle, *Nature, Lond.*, **314**, 58-62.

Oliver, J.R., 1869, *The geology of St. Helena*, (Benjamin Grant, St. Helena).

Olson, P., Yuen, D.A. and Balsiger, D., 1984, Convective mixing and the fine structure of mantle heterogeneity, *Phys. Earth Planet. Inter.*, **36**, 291-304.

O'Nions, R.K., Carter, S.R., Cohen, R.S., Evenson, N.M. and Hamilton, P.J., 1978, Pb, Nd and Sr isotopes in oceanic ferromangenese deposits and ocean floor basalts, *Nature*, **273**, 435-8.

O'Nions, R.K., Evenson, N.M. and Hamilton, P.J., 1979, Geochemical modelling of mantle differentiation and crustal growth, *J. Geophys. Res.*, 84 6091-6101,

O'Nions, R.K. and Oxburgh, E.R., 1983, Heat and He in the earth, *Nature, Lond.*, 306, 429-31.

Oversby, V.R. and Gast, P.W., 1970, Lead from oceanic islands, *J. Geophys. Res.*, 75, 2097-114.

Palacz, Z.A. and Saunders, A.D., 1986, Coupled trace element and isotope enrichment in the Cook-Austral-Samoa Islands, South West Pacific, *Earth Planet. Sci. Letts.*, **79**, 270-80.

Palacz, Z.A. and Wolff, J.A., (in press) Sr, Nd and Pb isotopic characteristics of the Grandilla pumice deposit, Tenerife: a study of the causes of Sr- isotope variations in felsic pyroclastics, In *Magmatism in the ocean basins*, (Geol. Soc. London Spec. Publn.)

Pearce, J.A. and Cann, J.R., 1973, Tectonic setting of basic volcanic rocks determined using trace element analyses, *Earth Planet. Scl. Letts.*, 19, 290-300.

Pearce, J.A. and Norry, M.J., 1979, Petrogenetic implications of Tl, Zr, Y and Nb variations in volcanic rocks, *Contrib. Mineral. Petrol.*, 69, 33-47.

Philpotts, J.A. and Schnetzler, C.C., 1970, Phenocryst matrix partition coefficients for K, Rb, Sr and Ba, with applications to anorthosite and basalt genesis, *Geochim. Cosmochim. Acta*, 34, 307-22.

Piepgras, D.J. and Wasserburg, G.J., 1985, Strontium and neodymium isotopes in hot springs on the East Pacific Rise and Guaymas basin, *Earth Planet. Scl. Letts.*, 72, 341-56.

Potts, P.J., Thorpe, O.W., Isaacs, M.C. and Wright, D.W., 1985, High precision instrumental neutron activation analysis of geological samples employing simultaneous counting with both planar and coaxial detectors, *Chem. Geol.*, 48, 145-55.

Presnall, D.C. and Helsley, C.E., 1982, Diapirism of depleted peridotite - A model for the origin of hotspots, *Phy. Earth Planet. Inter.*, 29, 148-60.

Prinzhofer, A. and Allegre, C.J., 1985, Residual peridotites and the mechanisms of partial melting, *Earth Planet. Sci. Letts.*, 74, 251-65.

Reid, M.J., Gancarz, A.L. and Albee, A.L., 1973, Constrained least-squares analysis of petrologic problems with an application to lunar sample 1204, *Earth Planet.*

Sci. Letts., **17**, 433-45.

Richard, P., Shimizu, N. and Allegre, C.J., 1976, $^{143}Nd/^{144}Nd$, a natural tracer an application to oceanic basalts, *Earth Planet. Sci. Letts.*, **31**, 269-78.

Ribe, M.N., 1988, Dynamical geochemistry of the Hawaiian plume, *Earth Planet. Sci. Letts.*, **88**, 37-46.

Ribe, N.M. and Smooke, M.D., 1987, A stagnation point flow model for melt extraction from a mantle plume, *J. Geophys. Res.*, **92**, 6437-43.

Ringwood, 1975, *Composition and petrology of the Earth's mantle*, (McGraw-Hill, New York).

Ringwood, A.E., 1982, Phase transformations and differentiations in subducted lithosphere: implications for mantle dynamics and salt petrogenesis and crustal evolution, *J. Geol.*, **90** 611-43.

Ringwood, A.E., 1985, Mantle dynamics and basalt petrogenesis, *Tectonophys*, **122**, 17-34.

Roden, M.K., Hart, S.R., Frey, F.A. and Melson, W.G., 1986, Sr, Nd, and Pb Isotopic and REE geochemistry of St Paul's Rocks: the metamorphic and metasomatic development of an alkali basalt mantle source, *Contrib. Mineral. Petrol.*, **85**, 376-90.

Roedder, E., 1965, Liquid CO_2 inclusions in olivine bearing modules and phenocrysts from basalts, *Am. Mineral*, **50**, 1740-82.

Roedder, P.L. and Emslie, R.F., 1970, Olivine liquid equilibrium, *Contrib. Mineral Petrol.*, **29**, 275-98.

Ryan, M.P., 1987, Neutral buoyancy and the mechanical evolution of magmatic systems, In: *Magmatic Processes*: *Physiochemical principles*, The Geochemical Society, special publication No 1, (ed., B.O. Myson), p 258-85.

Ryerson, F.J. and Watson, E.B., 1987, Rutile saturation in magmas: Implications for Ti - Nb - Ta depletion in island arc basalts, *Earth Planet. Sci. Letts.*, **86**, 225-39.

Saunders, A.D., Tarney, J. and Weaver, S.D., 1980, Transverse geochemical variations across the Antarctic peninsula: implications for the genesis of calc - alkaline magmas, *Earth Planet. Sci. Letts.* **46**, 334-60.

Saunders, A.D., Norry, M.J. and Weaver, S.D., 1988, Mantle trace elements, (in press).

Saggerson, E.P. and Williams, L.A.J., 1984, Ngurumanite from Southern Kenya and its bearing on the origin of rocks in Northern Tanganyika alkaline district, *J. Petrol.*, **5**, 50-81.

Schilling, J.G., Thompson, G., Kingsley, R. and Humphris, S., 1984, Hotspot-migrating ridge interaction in the S. Atlantic, *Nature. Lond.*, **313**, 187-191

Schilling, J.G., 1985, Upper Mantle Heterogeneities and dynamics, *Nature, Lond.*, **314**, 62-7.

Sen, G., 1983, A petrologic model for the constitution of the upper mantle and crust of Kohala shield, Oahu, Hawaii and Hawaiian magmatism, *Earth Planet. Sci. Letts.*, **62**, 215-28.

Sen, G., 1987, Xenoliths associated with the Hawaiian hot-spot, In: *Mantle Xenoliths*, ed., P.H. Nixon, (John Wiley and Sons Ltd.).

Shaw, D.M., 1970, Trace element fractionation during anatexis, *Geochim. Cosmochim. Acta*, **34**, 237-42.

Sleep, N.H., 1984, Tapping of magmas from ubiquitous mantle heterogeneities: an alternative to mantle plumes? *J. Geophys. Res.*, **89**, 10029-41.

Spera, F.J., 1984, Carbon dioxide in petrogenesis III: Role of volatiles in the ascent of alkaline magma with special reference to xenolith bearing mafic lavas, *Contrib. Mineral Petrol.*, **88**, 217-32.

Staudigel, H. and Hart, S.R., 1983, Alteration of basaltic glass: mechanisms and the significance for the oceanic crust seawater budget, *Geochim. Cosmochim. Acta*, **47**, 337-50.

Staudigel, H., Zindler, A., Hart, S.R., Leslie, T., Chen, C.Y. and Clauge, D., 1984, The isotope systematics of a juvenile intraplate volcano: Pb, Nd, and Sr isotope ratios of basalts from Loihi Seamount, Hawaii, *Earth Planet. Sci. Letts.*, **69**, 13-29.

Stille, P., Unruh, D.M. and Tatsumoto, M., 1986, Pb, Sr, Nd and Hf isotopic constraints on the origin of Hawaiian basalts and evidence for a unique mantle source, *Geochim. Cosmochim. Acta*, **50**, 2303-3219.

Streckheisen, A., 1976, To each plutonic rock its proper name, *Earth. Sci. Rev.*, **12**, 1-33.

Stolper, E., Walker, P., Hager, B.H. and Hays, J.F., 1981, Melt segregation from partially molten source regions: the importance of melt density and source region size, *J. Geophys. Res.*, **86**, 6261-73.

Sun, S.S., 1980, Lead isotopic study of young volcanic rocks from mid-ocean ridges, ocean islands and island arcs, *Phil. Trans. R. Soc. Lond.*, **A297,** 409-445.

Sun, S.S. and Hanson, G.N., 1975, Origin of Ross Island basanitoids and limitations upon the heterogeneity and mantle sources for alkali basalts and nephelinites, *Contrib. Mineral. Petrol.*, **52,** 77-106.

Sun, S.S. and Nesbitt, P.W., 1978, Petrogenesis of Archaean ultrabasic and basic volcanics: Evidence from REE, *Contrib. Mineral. Petrol.*, **65,** 301-25.,

Sun, S.S., Nesbitt, R.N. and Saraskin, A.Y., 1979, Geochemical characteristics of mid-ocean ridge basalts, *Earth Planet. Sci. Letts.*, 44, 119-38.

Sun, S.S. and McDonough, W.F., (in press) Chemical and isotopic systematics of oceanic basalts: implications for mantle composition and processes, In: *Magmatism in the ocean basins*, (Geol. Soc. London Spec. Publn., eds., Saunders, A.D. and Norry, M.J.)

Suyenga, J., 1979, Isostasy and flexure of the lithosphere under the Hawaiian Islands, *J. Geophys. Res.*, **84, 5599-5604.**

Taras, B.D. and Hart, S.R., 1983, Geochemical evolution of the New England Seamount Chain: isotopic and trace element constraints, *Trans. Am. Geophys. Union. EOS.*, **64, 907.**

Tatsumoto, M., 1978, Isotopic composition of lead in oceanic basalts and its implication to mantle evolution, *Earth Planet. Sci. Letts.*, **38,** 63-87.

Taylor, W.R. and Green, D.H., 1987, The petrogenetic role of methane: effect on liquidus phase relations and the solubility mechanisms of reduced C-H volatiles, In: *Magmatic Processes*: *Physiochemical principles*, The Geochemical Society, special publication No 1, (ed., B.O. Myson). p 129-38.

Taylor, W.R. and Green, W.H., 1988, Measurement of reduced peridotite C - O - H Solidus and implications for redox melting of the mantle, *Nature*, *Lond.*, **332,** 349-52.

Ten Brink, S.U. and Brocher, T.M., 1988, Multichannel seismic evidence for a subcrustal intrusive complex under Oahu and a model for Hawaiian volcanism, *J. Geophys. Res.*, **B13,** 13687-708.

Thompson, R.N., 1982, Magmatism of the British Tertiary volcanic province, *Scott. J. Geol.*, **18,** 50-107.

Thompson, R.N., Morrison, R.A., Hendry, G.L. and Parry, S.J., 1984, An assessment of the relative roles of crust and mantle in magma genesis: an elemental approach, *Phil. Trans. R. Soc. Lond.*, **A310**, 549-590.

Thompson, R.N., 1987, Phase-equilibria constraints on the genesis and magmatic evolution of oceanic basalts, *Earth Science Reviews*, **24**, 161-210.

Vidal, P. and Dosso, L., 1978, Core formation: catastrophic or continuous? Sr and Pb isotope geochemistry constraints, *Geology*, **13**, 15-8.

Vidal, Ph., Chauvel, C. and Brousse, R., 1984, Large mantle heterogeneity beneath French Polynesia, *Nature, Lond.*, **307**, 536-8.

Verma, F., 1960, Elasticity of some high density crystals, *J. Geophys. Res.*, **65**, 757-806.

Vollmer, R., 1977, Terrestrial lead isotopic evolution and formation time of the Earth's core, *Nature, Lond.*, **270**, 144-7.

Wager and Brown, 1968, *Layered igneous rocks*, (Oliver and Boyd).

Walsh, J.N., Buckley, F. and Barker, 1981, The simultaneous determination of the rare earth elements in rocks using ICP Source Spectometry, *Chem. Geol.*, **33**, 141-53.

Wasserburg, G.J. and De Paulo, D.J., 1979, Models of earth structure inferred from neodymium and strontium isotopic abundances, *Proc. Nat. Acad. Sciences*, **76**, 3594-98.

Watts, A.B., 1978, An analysis of isostasy in the world's oceans, 1: Hawaiian-Emperor seamount chain, *J. Geophys. Res.*, **83, B12**, 5989-6004.

Watson, E.B., Ben Othmann, D.B., Luck, J.M. and Hofmann, A.W., 1987, Partitioning of U, Pb, Cs, Yb, Hf, Re and Os between chromium diopsidic pyroxene and haploblastic liquid, *Chem. Geol*, **62**, 191-208.

Weaver, B.L., Wood, D.A., Tarney, J. and Joron, J.L., 1986, Role of subducted sediment in the genesis of ocean island basalts: evidence from South Atlantic Ocean islands, *Geology*, **14**, 275-8.

Weaver, B.L., Wood, D.A., Tarney, J. and Joron, J.L., 1987, Geochemistry of ocean island basalts from the South Atlantic: Ascension, Bouvet, St.Helena, Gough and Tristan da Cunha, *In*: *Alkaline magmatism.* (Eds G.J. Fitton and B.R. Upton).

Weis, D., Demaiffe, D., Cauet, S. and Javoy, M., 1987, Sr, Nd, and H isotopic ratios in Ascension Island lavas and plutonic inclusions; cogenetic origin, *Earth*

Planet. Sci. Letts., **82**, 225-68.

White, W.M. and Hofmann, A.W., 1982, Sr and Nd isotope geochemistry of oceanic basalts and mantle evolution *Nature*, **296**, 821-5.

White, W.M., Patchett, P.J., and Othmann, D.B., 1984, U, Th and Pb in deep sea sediments, crustal recycling and the evolution of the mantle, *Trans. Am. Geophys. Union EOS.*, **65**, 296.

White, W.M., 1985, Sources of oceanic basalts: radiogenic isotopic evidence, *Geology*, **13**, 115-8.

White, W.M, Hofmann, A.W. and Puchelt, H., 1987, Isotope geochemistry of Pacific MORB. *J. Geophys. Res.*, **92**, 4881-93.

Wood, D.A, Gibson, I.L. and Thompson, R.N., 1976, Elemental mobility during zeolite facies metamorphism of the Tertiary basalts of E. Iceland, *Contrib. Min. Petrol.*, **55**, 241-54.

Wood, D.A., Joron, J.L. and Treuil, M., 1979, A reappraisal of the use of trace elements to classify and discriminate between magma series erupted in different tectonic settings, *Earth Planet. Scl. Letts.*, **45**, 326-36.

Wood, D.A., Tarney, J. and Weaver, B.L., 1981, trace element variations in Atlantic ocean basalts and Proterozoic dykes from north west Scotland: their bearing upon the nature and geochemical evolution of the upper mantle, *Tectonophys.*, **75**, 91-112.

Wilson, J.T., 1963, A possible origin of the Hawaiian Islands, *Canadian J. Phys.*, **41**, 863-70.

Wright, C., 1975, Comment on seismic array evidence of a core boundary source for the Hawaiian linear volcanic chain by E.R. Kanasewich and others, *J. Geophys. Res.*, **80**, 1915-19.

Wright, T.L. and Doherty, P.C., 1970, A Linear Programming and Least Square Computer Method for Solving Petrologic Mixing Problems, *Bull. Geol. Soc. Am.*, **81**, 1995-2007.

Wright, T.L. and Fiske, R., 1971, Origin of the differentiated and hybrid lavas of Kilauea volcano, Hawaii, *J. Petrol.*, **12**, 1-65.

Wright, T.L., 1984, Origin of Hawaiian tholeiite: A metasomatic model, *J. Geophys. Res.*, **89**, 3233-52.

Wyllie, P.J., 1978, Mantle fluid compositions buffered in peridotite CO_2-H_2O- by carbonates, amphibole and phlogopite, *J. Geol.*, **86**, 687-713.

Wyllie, P.J., 1984, Constraints imposed by experimental petrology on possible and impossible magma sources and products, *Phil. Trans. R. Soc. Lond.*, **A 310**, 439-56.

Wyllie, P.J., 1988, Solidus Curves, mantle plumes, and magma generation beneath Hawaii, *J. Geophys. Res.*, **93**, 4171-81.

Wyllie, P.J. and Sekine, T., 1982, The formation of mantle phlogopite in subduction zone hybridisation, *Contrib. Mineral. Petrol.*, **79**, 375-80.

Yuen and Fleitout, Thinning of the lithosphere by small-scale convective destabilisation, *Nature, Lond.*, **313**, 125-8.

Zartman, R.E., and Doe, B.R., 1981, Plumbotectonics - the model, *Tectonophys.*, **75** 135-62.

Zindler, A. and Jagoutz, E., 1988, Mantle cryptology, *Geochim. Cosmochim. Acta*, **52**, 319-33.

Zindler, A., Jagoutz, E. and Goldstein, S., 1982, Nd, Sr and Pb isotopic systematics in a three component mantle: a new perspective, *Nature, Lond.*, **58**, 519-23.

Zindler, A., Staudigel, H. and Batiza, R., 1984, Isotope and trace element geochemistry of young Pacific seamounts: implications for the scale of upper mantle heterogeneities, *Earth Planet. Scl. Letts.*, **70, 1** 75-95.

Zindler, A., Hart, S.R., Frey, F.A. and Jakobsson, S.P., 1979, Nd and Sr isotope ratio and rare earth element abundances in Reykjanes Peninsula basalts: evidence for mantle heterogeneity beneath Iceland, *Earth Planet. Scl. Letts.*, **45**, 249-62.

Zindler, A. and Hart, S.R., 1986, Chemical Geodynamics, *Ann. Rev. Earth Planet Scl.*, **14**, 493-571.

Appendix A:

Sample localities and characteristics:

Table A1 lists the locality and characteristics of all samples collected during the field season on St.Helena. The grid references are based on Directorate of Overseas Survey (DOS) 1:25000 sheet G891, edition 6, 1983. Accurate positions were obtained from 1:10,000 sheets. The location of samples within the geological framework is shown in Fig.A1.

Abbreviations, Table A1:

(1) Stratigraphic height;

The abbreviations used for stratigraphic units are as follows;

NEBB : NE volcano, basal breccias.
NE(BB) : NE volcano, dykes intruded into NEBB.
NEMS : NE volcano, main shield.
NE(MS) : NE volcano, dykes intruded into high levels of NEMS.

SWLS : SW volcano, lower shield.
SW(LS) : Dykes intruded into SWLS.
SWMS : SW volcano, main shield.
SW(MS) : SW volcano, dykes intruded into SWMS.
SWUS : SW volcano, upper shield.
SWEF : SW volcano, E. flank eruptions.
SWLI : SW volcano, late intrusions.

A dot after a shield name denotes a flow from a parasitic cone.

(2) Rock type;

Abbreviations for rock types are as follows:

BAS : Alkali basalt.
TBAS : Hawaiite.
TAND : Mugearite.
TRAC : Trachyte.
PHON : Phonolite.

(3) Texture;

AP : Aphyric.
MP : < 10 % phenocrysts.
P : > 10 % phenocrysts.

(4) *Alteration;*

A field classification of the degree of alteration was used. The detailed basis of this is described in more detail in section 3.5. In brief the abbreviations are:

F : Fresh
MF : Moderately fresh
MA : Moderately altered
A : Altered

(5) *Height;*

The basis for ascribing an overall height to each sample is given in Section 3.7.

(6) *Position;*

The following abbreviations are given to enable location of samples in Fig A1 by using the relevant place names; Fig.3.2;

For the NE volcano:
BARN : The Barn.
FISH : Fisher's Valley.
FLAG : Flagstaff Hill.
SUGAR : Sugarloaf hill.
TURK : Turk's Cap.
RUPERTS: Rupert's Valley.

For the SW volcano:
BLUE: Blue Hill.
BROAD : Broad Gut.
CHAOS : Gates of Chaos.
FORT : High Knoll Fort.
HIGH : High Hill.
HOOPER : Hooper's Hill.
LEMON : Lemon Valley.
LOTS : Lot's Wife.
PV : Powell's Valley.
RIDING : Riding Stones Hill.
SANDY E : Sandy Bay E.
SANDY W : Sandy Bay W.
SHARK : Shark's Valley.
WHITE : White Point.

(7) *Analysis;*

The analysis column describes which methods of analysis were used to investigate each sample. The following abbreviations are used :

XRF : X-Ray Fluorescence Spectrometry (Appendix B2).
ICP : XRF and Inductively Coupled Plasma Spectrometry (Appendix B3).

St. Helena

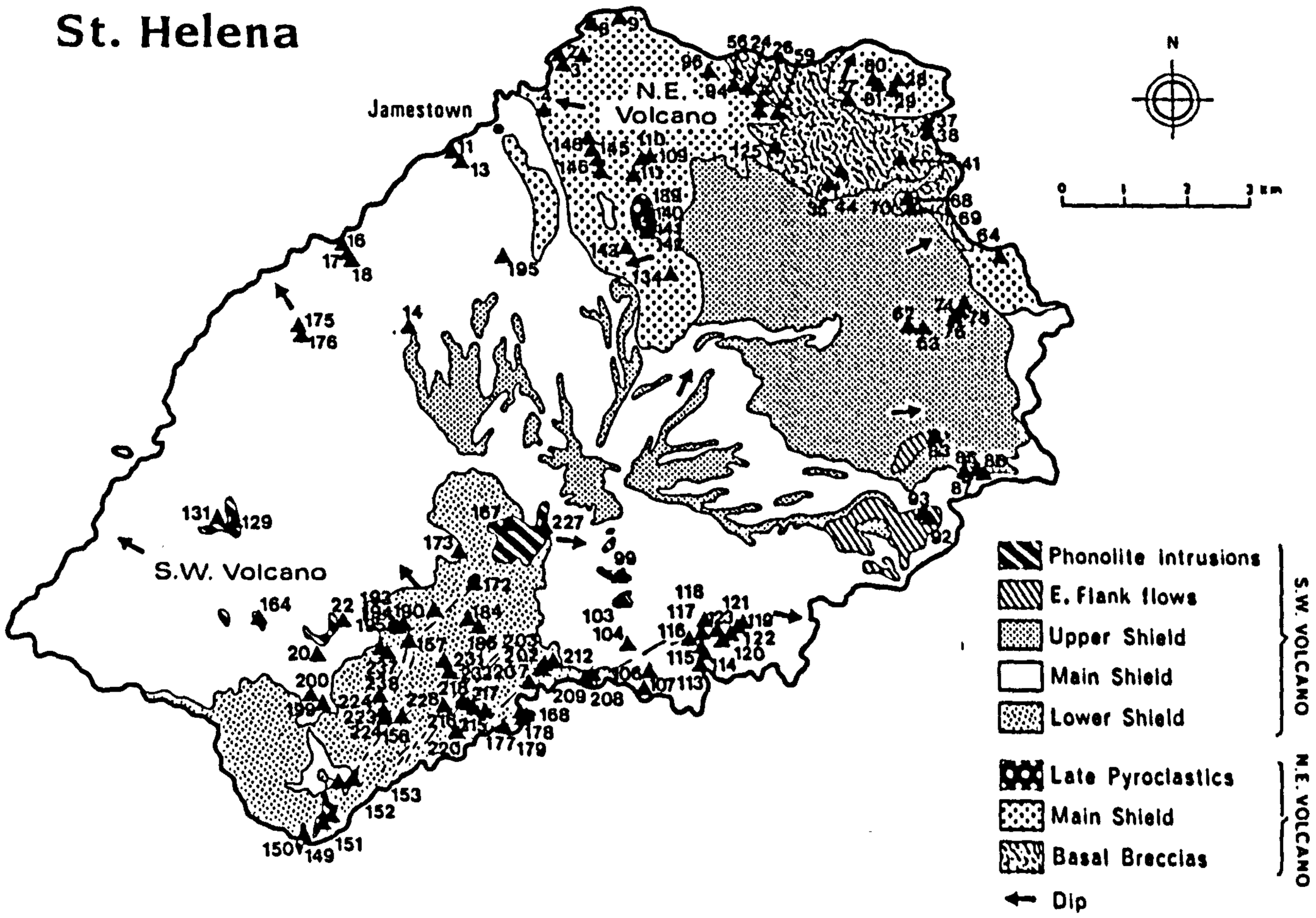

Fig.A1; Sample location map: St.Helena.

INA : XRF and Neutron Activation Analysis (Appendix B4).
Sr, Nd, Pb : Geologically significant isotopes of these elements evaluated.

The number following the above descriptions refers to the departmental thin section number. Numbers start as follows;

78 : Polished thin section.
48 : Standard thin section.

Table A1; Details of the samples collected during the field season:
Abbreviations are described above.

Rock No	*Strat unit*	*Rock type*	*Text*	*Alt*	*Height*	*G.R.*	*Posn*	*Analysis*
SC 1	NEMS	TBAS	AP	A	856m	1038 3959	SUGAR	/
SC 2	NEMS	TBAS	P	MA	773m	0918 3901	SUGAR	XRF.Sr.
SC 3	NEMS	BAS	P	MA	807m	0924 3903	SUGAR	XRF
SC 4	NEMS	BAS	P	MA	800m	0902 3866	SUGAR	XRF.Sr.
SC 5	NE(MS)	BAS	AP	MA	1000m	0899 3850	SUGAR	/
SC 6	NE(MS)	TBAS	AP	MA	1000m	0893 3857	NR	/
SC 7	NE(MS)	TBAS	P	MA	1000m	0953 3938	NR	/
SC 8	NEMS	BAS	P	F	824m	0978 3985	SUGAR	INA.Sr,Nd,Pb.7512.
SC 9	NEMS	BAS	P	F	1000m	1023 4000	SUGAR	ICP.Sr.
SC 10	SWMS	TBAS	AP	A	2700m	0770 3743	LEMON	/
SC 11	SWMS	TBAS	AP	MA	2623m	0761 3700	LEMON	XRF.Sr.Nd.7506.
SC 12	SWMS	TBAS	P	MA	2560m	0747 3744	LEMON	/
SC 13	SWMS	BAS	P	F	2603m	0758 3758	LEMON	INA.Sr.Nd.Pb.7508.
SC 14	SWMS	BAS	AP	MA	2930m	0697 3537	LEMON	ICP.Sr.Nd.Pb
SC 15	SWMS	TBAS	AP	MA	-	0872 3797	LEMON	/
SC 16	SWMS	TBAS	P	F	2697m	0596 3610	LEMON	XRF.
SC 17	SWMS	BAS	P	A	2756m	0617 3574	LEMON	XRF.Sr.Nd.
SC 18	SWMS	TBAS	AP	F	2783m	0620 3571	LEMON	XRF.Sr.Nd.7509
SC 19	SWMS	TBAS	AP	A	2816m	0624 3572	LEMON	/
SC 20	SW(MS)	BAS	P	F	3150m	0576 2968	HOOP	XRF
SC 21	SWLI	TRAC	AP	A	3600m	0613 3001	HOOP	/
SC 22	SWMS	TBAS	P	F	3600m	0594 3033	HOOP	XRF
SC 23	NE(MS)	BAS	P	F	1000m	1253 3858	FLAG	XRF
SC 24	NE(MS)	BAS	P	F	1000m	1281 3831	FLAG	/
SC 25	NE(BB)	BAS	P	F	50m	1307 3821	FLAG	XRF
SC 26	NE(MS)	BAS	P	P	1000m	1287 3828	FLAG	ICP.Sr.7722.
SC 27	NE(MS)	BAS	P	F	1000m	1382 3851	BARN	XRF.Sr.7774.Nd
SC 28	NEMS	BAS	P	F	642m	1473 3865	BARN	XRF.Sr.Pb.
SC 29	NE(MS)	BAS	P	MF	547m	1452 3854	BARN	ICP.Sr.7775.
SC 30	NEMS	TBAS	P	MA	617m	1381 3888	BARN	/
SC 31	NE(BB)	BAS	P	MA	50m	1337 3838	BARN	/
SC 32	SWUS	TAND	AP	MF	3350m	1438 3713	TURK	/
SC 33	SWUS	TAND	AP	F	3335m	1484 3727	TURK	/

No	Unit	Rock	Text	Alt	Height	G.R.	Posn	Analysis
SC 34	NE(BB)	BAS	P	A	50m	1389 3704	TURK	/
SC 35	NE(BB)	TBAS	P	MA	150m	1378 3701	TURK	ICP.Sr.Pb.7777.
SC 36	SWUS	TBAS	P	MA	-	1375 3699	TURK	/
SC 37	NEBB	BAS	P	F	0m	1524 3830	TURK	INA.Nd.Pb
SC 38	NEBB	BAS	P	F	0m	1524 3831	TURK	ICP.Sr.Nd.Pb.7510.
SC 39	NEBB	BAS	P	A	0m	1523 3833	TURK	/
SC 40	NEBB	BAS	P	A	0m	1523 3833	TURK	/
SC 41	NE(BB)	BAS	P	F	50m	1477 3761	TURK	XRF.Sr.Nd.
SC 42	NE(BB)	TBAS	P	MF	150m	1477 3761	TURK	/
SC 43	NE(BB)	BAS	P	F	50m	1324 3758	TURK	/
SC 44	NE(BB)	TBAS	P	MF	150m	1363 3747	TURK	XRF.Sr
SC 45	NEBB	BAS	P	MF	0m	1425 3772	TURK	/
SC 46	NE(BB)	TBAS	P	MA	150m	1399 3796	TURK	/
SC 47	NEBB	BAS	P	A	0m	1403 3795	TURK	/
SC 48	NEBB	BAS	P	A	0m	1403 3795	TURK	/
SC 49	NEBB	TBAS	P	MA	0m	1405 3789	TURK	/
SC 50	NE(BB)	BAS	P	MA	50m	1418 3778	TURK	/
SC 51	NE(BB)	BAS	P	MF	50m	1424 3772	TURK	/
SC 52	NEBB	BAS	P	A	0m	1412 3783	TURK	/
SC 53	NEBB	BAS	P	A	0m	1412 3783	TURK	/
SC 54	NE(BB)	TBAS	P	F	150m	1320 3911	TURK	/
SC 55	NEMS	BAS	P	A	300m	1281 3860	FLAG	/
SC 56	NEMS	BAS	P	F	300m	1282 3858	FLAG	INA.Sr.NdPb.
SC 57	NEMS	BAS	P	MA	300m	1286 3845	FLAG	/
SC 58	NE(MS)	BAS	AP	MF	1000m	1288 3842	FLAG	/
SC 59	NEMS	BAS	P	F	400m	1288 3839	FLAG	ICP
SC 60	NE(MS)	BAS	P	MF	1000m	1289 3832	FLAG	/
SC 61	SWUS	TAND	P	MA	3395m	1589 3840	FISH	/
SC 62	SWUS	TAND	P	F	3305m	1529 3490	FISH	ICP.Sr.7776.
SC 63	SWUS	TAND	AP	F	3350m	1521 3491	FISH	INA.Sr.Nd.Pb.
SC 64	NE(MS)	BAS	P	F	450m	1624 3628	FISH	XRF
SC 65	NEMS	TBAS	P	A	-	1621 3614	FISH	/
SC 66	NEMS	BAS	AP	MF	-	1603 3578	FISH	/
SC 67	SWUS	BAS	P	A	3105m	1613 3569	FISH	/
SC 68	NE(BB)	BAS	P	F	50m	1479 3672	TURK	INA.Sr.Nd.7881.
SC 69	NE(BB)	BAS	P	F	50m	1479 3672	TURK	ICP.Sr.Nd.7890.
SC 70	NE(BB)	TBAS	AP	F	150m	1477 3675	TURK	XRF
SC 71	NE(BB)	BAS	P	MF	50m	1475 3672	TURK	/
SC 72	SWUS	TBAS	A	A	3245m	1571 3499	FISH	/
SC 73	SWUS	TBAS	AP	A	3155m	1586 3555	FISH	/
SC 74	SWUS	BAS	P	F	3175m	1585 3535	FISH	INA.Sr.Nd.Pb.
SC 75	SWUS	BAS	AP	MF	3195m	1585 3520	FISH	ICP.Sr.Nd.Pb.
SC 76	SWUS	TBAS	AP	MF	3215m	1582 3516	FISH	XRF.Sr.
SC 77	SWUS	TBAS	AP	A	3225m	1575 3509	FISH	/
SC 78	NEMS	BAS	AP	A	630m	1382 3912	BARN	/
SC 79	NEMS	TBAS	P	F	637m	1389 3904	BARN	/
SC 80	NEMS	BAS	P	F	541m	1425 3860	BARN	ICP.Sr.Nd.Pb.
SC 81	NEMS	BAS	AP	MA	493m	1423 3855	BARN	XRF
SC 82	NEMS	BAS	AP	MF	445m	1423 3855	BARN	/

No	Unit	Rock	Text	Alt	Height	G.R.	Posn	Analysis	xliv
SC 83	SWEF	TRAC	P	MF	3450m	1540 3332	SHARK	ICP.Sr.Nd.	
SC 84	SWEF	TRAC	AP	MA	3450m	1552 3303	SHARK	/	
SC 85	SWEF	TBAS	P	MF	3450m	1590 3279	SHARK	XRF.Sr.Nd.Pb.	
SC 86	SWEF	BAS	P	F	3450m	1592 3278	SHARK	ICP.Sr.Nd.Pb.48104	
SC 87	SWEF	BAS	P	MF	3450m	1618 3275	SHARK	INA.Nd.	
SC 88	SWEF	TAND	AP	MA	3450m	1406 3190	SHARK	/	
SC 89	SWEF	TAND	AP	F	3450m	1412 3296	SHARK	/	
SC 90	SWEF	TRAC	AP	MA	3450m	1455 3211	SHARK	/	
SC 91	SWEF	TAND	AP	F	3450m	1466 3207	SHARK	/	
SC 92	SWEF	TRAC	AP	F	3450m	1546 3192	SHARK	XRF.Sr.Nd.7778	
SC 93	SWEF	TAND	AP	F	3450m	1507 3194	SHARK	ICP.Sr.Nd.Pb.48083.	
SC 94	NEMS	BAS	MP	MA	450m	1251 3867	FLAG	XRF	
SC 95	NEMS	BAS	P	MF	480m	1216 3879	FLAG	/	
SC 96	NEMS	BAS	MP	MA	500m	1170 3896	FLAG	ICP.Sr.7505.	
SC 97	NELP	BAS	P	MA	3100m	1139 3575	FISH	/	
SC 98	SWLI	TRAC	AP	MA	3600m	1052 3102	PV	/	
SC 99	SWLI	TRAC	AP	F	3600m	1051 3105	PV	XRF	
SC 100	SWLI	TRAC	AP	MA	3600m	1028 3144	PV	/	
SC 101	SWLI	TRAC	AP	MF	3600m	1031 3150	PV	/	
SC 102	SWMS	BAS	AP	MA	-	1049 3191	PV	/	
SC 103	SWLI	PHON	AP	F	3600m	1032 3058	PV	ICP.Sr.Nd.48084.	
SC 104	SWMS	BAS	AP	MF	2977m	1050 2991	SWMS	XRF	
SC 105	SWMS	TBAS	AP	MA	3020m	1066 2989	PV	/	
SC 106	SWMS	BAS	MP	F	3091m	1096 2949	PV	ICP.Sr.Nd.Pb.48085	
SC 107	SWMS	BAS	AP	MF	2950m	1082 2944	PV	XRF	
SC 108	NEMS	BAS	P	MA	557m	1120 3679	RUPERTS	/	
SC 109	NEMS	BAS	P	MF	565m	1092 3686	RUPERTS	ICP.Sr.Pb.48086	
SC 110	NEMS	TBAS	P	MF	573m	1081 3680	RUPERTS	XRF	
SC 111	NEMS	BAS	P	F	618m	1043 3708	RUPERTS	XRF.Sr.Nd.Pb.7717.	
SC 112	SWMS	BAS	P	F	2180m	1184 2971	PV	/	
SC 113	SWMS	BAS	P	F	2250m	1175 2987	PV	ICP.Sr.Nd.7719.	
SC 114	SWMS	BAS	P	F	2275m	1169 2991	PV	XRF.Sr.Nd.Pb.7718.	
SC 115	SWMS	BAS	AP	MF	2298m	1162 2999	PV	XRF.7720.	
SC 116	SW(MS)	TRAC	AP	MA	3600m	1159 3009	PV	XRF.Sr.	
SC 117	SWMS	BAS	P	MF	2370m	1159 3015	PV	XRF.Sr.Pb.7728.	
SC 118	SWMS	BAS	P	MF	2613m	1221 3034	PV	XRF.7726.	
SC 119	SWMS	BAS	MP	MF	2581m	1219 3029	PV	ICP.Sr.Nd.Pb.7723.	
SC 120	SWMS	BAS	MP	MF	2421m	1201 3003	PV	ICP.Sr.Nd.Pb.7721.	
SC 121	SWMS	BAS	P	MF	2470m	1208 3017	PV	XRF.Sr.Nd.7724.	
SC 122	SWMS	BAS	MP	MF	2428m	1201 3005	PV	XRF.7727.	
SC 123	SWMS	BAS	AP	F	2543m	1216 3023	PV	ICP.7725.	
SC 124	NE(BB)	BAS	P	MF	50m	1280 3753	FLAG	/	
SC 125	NE(BB)	BAS	P	F	50m	1278 3752	FLAG	ICP.Sr.Nd.Pb.48091	
SC 126	NELP	BAS	P	A	3100m	1127 3607	FISH	/	
SC 127	NELP	BAS	P	A	3100m	1127 3607	FISH	/	
SC 128	NELP	BAS	P	A	3100m	1127 3607	FISH	/	
SC 129	SWLI	TRAC	AP	F	3600m	0455 3153	HIGH	XRF.Sr.Nd.Pb.48092.	
SC 130	SWLI	TRAC	AP	MF	3600m	0443 3168	HIGH	/	
SC 131	SWMS.	BAS	AP	F	3395m	0442 3179	HIGH	ICP.Sr.7504.	

No	Unit	Rock	Text	Alt	Height	G.R.	Posn	Analysis	xlv
SC 132	SWLI	TRAC	AP	F	3600m	0446 3149	HIGH	/	
SC 133	NEMS	BAS	P	MA	791m	1051 3706	RUPERTS	/	
SC 134	NEMS	BAS	P	MF	812m	1049 3707	RUPERTS	XRF.Sr.Nd.Pb.7882.	
SC 135	SWMS	TBAS	AP	MA	-	1029 3765	RUPERTS	/	
SC 136	NEMS.	BAS	AP	A	1000m	1030 3735	RUPERTS	/	
SC 137	NELP	BAS	P	MA	3100m	1139 3575	FISH	/	
SC 138	NELP	BAS	P	MA	3100m	1138 3578	FISH	/	
SC 139	NELP	BAS	P	MF	3100m	1134 3579	FISH	XRF.Sr.Nd.Pb.48094.	
SC 140	NELP	BAS	P	MF	3100m	1131 3578	FISH	ICP.Sr.Nd.7503.	
SC 141	NELP	BAS	P	MF	3100m	1128 3578	FISH	XRF.Sr.48096.	
SC 142	NELP	BAS	P	A	3100m	1125 3576	FISH	/	
SC 143	NEMS.	TBAS	AP	F	1000m	1014 3621	RUPERTS	ICP.Sr.	
SC 144	NEMS.	BAS	AP	MF	1000m	1021 3619	RUPERTS	/	
SC 145	NEMS	BAS	P	F	1000m	0990 3720	RUPERTS	XRF	
SC 146	NEMS.	TBAS	MP	MF	1000m	0978 3743	RUPERTS	XRF	
SC 147	NEMS.	TBAS	AP	A	1000m	0975 3748	RUPERTS	/	
SC 148	NEMS	BAS	AP	MF	718m	0982 3764	RUPERTS	XRF	
SC 149	SWLI	PHON	AP	F	3600m	0594 2750	BLUE	ICP.Sr.Nd.Pb.7779.	
SC 150	SWLI	PHON	AP	MF	3600m	0560 2700	BLUE	XRF.Sr.Nd.	
SC 151	SWLI	PHON	AP	MF	3600m	0609 2721	BLUE	XRF.Sr.Nd.	
SC 152	SWLI	TAND	AP	MF	3600m	0606 2791	BLUE	ICP.Sr.Nd.7780	
SC 153	SWLI	PHON	AP	MF	3600m	0636 2780	LOTS	XRF.Sr.	
SC 154	SWLI	PHON	X	MF	3600m	0681 2807	LOTS	7891	
SC 155	SWLI	PHON	X	MF	3600m	0686 2809	LOTS	7892	
SC 156	SWLI	PHON	AP	MF	3600m	0698 2860	LOTS	XRF.Sr.	
SC 157	SWLI	TRAC	AP	F	3600m	0720 2978	LOTS	XRF.Sr.	
SC 158	SWLS	BAS	P	MF	-	0712 2970	CHAOS	/	
SC 159	SWLS	BAS	P	MF	-	0705 2975	CHAOS	/	
SC 160	SWLS	TBAS	AP	MA	-	0700 2978	CHAOS	/	
SC 161	SWLS	TBAS	AP	MA	-	0682 2978	CHAOS	/	
SC 162	SWLS	BAS	AP	MA	-	0679 2991	CHAOS	/	
SC 163	SWLS	BAS	MP	MA	-	0677 2991	CHAOS	/	
SC 164	SWLI	PHON	AP	F	3600m	0492 3012	WHITE	XRF	
SC 165	SWMS	BAS	P	A	-	0385 3005	WHITE	/	
SC 166	SWLI	TRAC	AP	F	3600m	0444 3019	WHITE	/	
SC 167	SWLI	PHON	AP	F	3600m	0874 3145	RIDING	XRF.Sr.	
SC 168	SWLS	TBAS	AP	MF	1150m	0910 2922	SANDY E	ICP.Sr.Nd.Pb.7781.	
SC 169	SWLS	BAS	MP	MA	-	0915 2921	SANDY E	/	
SC 170	SWLS	BAS	P	MA	-	0971 2951	SANDY E	/	
SC 171	SWLS	BAS	AP	MF	2155m	0772 3111	LOT	/	
SC 172	SWLI	PHON	AP	MF	3600m	0822 3090	LOT	XRF.Sr.	
SC 173	SWMS	BAS	P	MF	2180m	0782 3117	LOT	ICP.Sr.Pb.	
SC 174	SWMS	BAS	AP	MF	3400m	0565 3462	SADDLE	/	
SC 175	SWMS.	TAND	AP	F	3400m	0565 3464	SADDLE	ICP.Sr.Nd.Pb.7783	
SC 176	SWMS.	TBAS	AP	A	3400m	0565 3458	SADDLE	XRF	
SC 177	SWLS	BAS	P	F	1118m	0895 2877	SANDY W	ICP.Sr.7784.	
SC 178	SWLS	BAS	P	MF	1010m	0905 2884	SANDY W	XRF.Sr.	
SC 179	SWLS	BAS	P	MF	1030m	0891 2869	SANDY W	XRF	
SC 180	SWLS	TBAS	AP	MA	1040m	0889 2865	SANDY W	/	

No	Unit	Rock	Text	Alt	Height	G.R.	Posn	Analysis
SC 181	SWLS	BAS	AP	MA	-	0873 2874	BROAD	/
SC 182	SWLS	TBAS	AP	MF	-	0879 2881	BROAD	/
SC 183	SWLI	PHON	AP	MF	3600m	0800 3941	BROAD	/
SC 184	SWLS	BAS	P	F	1360m	0840 3019	BROAD	ICP.Sr.
SC 185	SWLS	BAS	AP	MA	-	0840 3019	BROAD	/
SC 186	SWLS	BAS	P	MF	1340m	0828 3010	BROAD	XRF.Nd.7893
SC 187	SWLS	BAS	P	MA	1345m	0829 3015	BROAD	/
SC 188	SWLS	TBAS	AP	MA	1885m	0698 3046	BROAD	/
SC 189	SWLS	BAS	AP	MA	1860m	0700 3041	BROAD	/
SC 190	SWLS	BAS	MP	MF	1845m	0702 3039	BROAD	ICP.Sr.Nd.Pb.
SC 191	SWLS	TBAS	AP	A	1835m	0712 3040	BROAD	/
SC 192	SWLS	BAS	P	MA	-	0719 3039	BROAD	/
SC 193	SW(LS)	BAS	P	F	2100m	0728 3032	BROAD	XRF
SC 194	SWLS	BAS	P	F	2050m	0699 3051	BROAD	XRF
SC 195	SWMS.	TBAS	AP	F	3400m	0860 3571	FORT	XRF
SC 196	SWMS.	TBAS	AP	F	3400m	0868 3602	FORT	/
SC 197	SWMS.	TBAS	AP	F	3400m	0873 3465	FORT	/
SC 198	SW(MS)	TBAS	AP	F	3150m	0537 2861	BLUE	/
SC 199	SW(MS)	BAS	P	F	3150m	0565 2872	BLUE	XRF.7883.
SC 200	SWMS	BAS	P	F	-	0587 2879	BROAD	XRF
SC 201	SWLI	PHON	AP	MF	3600m	0671 2892	BROAD	/
SC 202	SWLS	BAS	AP	MA	1265m	0965 2962	SANDY E	XRF
SC 203	SWLS	BAS	AP	F	1248m	0960 2960	SANDY E	XRF.Pb.Nd.
SC 204	SWLS	TBAS	AP	F	1203m	0953 2952	SANDY E	/
SC 205	SWLS	BAS	AP	MA	-	0953 2952	SANDY E	/
SC 206	SWLS	BAS	AP	MA	1209m	0950 2950	SANDY E	/
SC 207	SW(LS)	BAS	P	F	2100m	0944 2943	SANDY E	XRF
SC 208	SWLS	BAS	P	MF	1320m	1020 2951	SANDY E	XRF.Sr.7884.
SC 209	SWLS	BAS	P	MF	1330m	1022 2951	SANDY E	XRF.
SC 210	SWLS	BAS	AP	MA	1340m	1023 2953	SANDY E	/
SC 211	SWLS	BAS	MP	MA	1270m	1011 2944	SANDY E	/
SC 212	SWLS	BAS	AP	MA	1190m	0983 2941	SANDY W	ICP.Nd.
SC 213	SWLS	BAS	MP	MA	1203m	0965 2944	SANDY W	/
SC 214	SWLS	TBAS	AP	MF	-	0855 2874	SANDY W	/
SC 215	SWLS	BAS	P	F	1380m	0845 2874	SANDY W	ICP.Sr.Nd.Pb.
SC 216	SW(LS)	BAS	MP	MF	2100m	0830 2880	SANDY W	XRF.Sr.Nd.Pb.7894.
SC 217	SWLS	BAS	P	F	1400m	0811 2884	SANDY W	XRF.Sr.Nd.7785.
SC 218	SWLS	BAS	P	MF	1420m	0810 2886	SANDY W	ICP.Sr.Pb.
SC 219	SWLS	BAS	P	MF	1410m	0801 2883	SANDY W	/
SC 220	SWLS	BAS	P	MA	1415m	0801 2883	SANDY W	XRF
SC 221	SWLI	PHON	AP	MF	3600m	0698 2939	CHAOS	/
SC 222	SWLS	BAS	P	MF	1900m	0651 2953	CHAOS	XRF
SC 223	SWLS	TBAS	AP	F	1940m	0642 0651	CHAOS	XRF
SC 224	SWLS	BAS	P	F	1958m	0639 2931	CHAOS	XRF.7895.
SC 225	SWLI	PHON	AP	MF	3600m	0909 3162	RIDING	/
SC 226	SWLI	PHON	AP	F	3600m	0885 3157	RIDING	/
SC 227	SWLI	PHON	AP	F	3600m	0885 2123	RIDING	XRF.Sr.
SC 228	SWLI	PHON	AP	MF	3600m	0870 2892	RIDING	/
SC 229	SWLS	TBAS	AP	MA	-	0803 2891	SANDY W	/

No	Unit	Rock	Text	Alt	Height	G.R.	Posn	Analysis
SC 230	SWLS	BAS	P	MA	-	0819 2908	SANDY W	/
SC 231	SWLI	PHON	AP	MF	3600m	0823 2293	SANDY W	XRF.Sr.
SC 232	SWLS	BAS	P	MF	1963m	0856 2923	SANDY W	XRF.7885.
SC 233	SWLI	PHON	AP	MA	3600m	0870 2951	SANDY W	/
SC 234	SWLS	BAS	AP	MA	-	0773 2813	SANDY W	/
SC 235	SWMS.	TBAS	AP	A	3150m	0266 2978	WHITE	/
SC 236	SW(MS)	TBAS	AP	A	3150m	0400 2977	WHITE	/
SC 237	SWLS	BAS	P	F	1983m	0635 2930	CHAOS	ICP.Sr.Nd.Pb.48103.
SC 238	SWLS	BAS	P	F	1988m	0635 2930	CHAOS	INA.Sr.Nd.7886.
SC 239	SWLS	TBAS	MP	A	1993m	0634 2932	CHAOS	/
SC 240	SWLS	BAS	P	A	1990m	0636 2928	CHAOS	/
SC 241	SWLS	BAS	AP	A	1996m	0632 2927	CHAOS	/

Appendix B: Sample preparation, analytical techniques and precision;

B1; Sample preparation;

Prior to analysis samples were reduced to a powder in a 3 stage process. Representative samples were chosen according to the proportion of phenocrysts. A large volume of porphyritic sample was used (> 1 kg), whereas a smaller volume was sufficient to represent aphyric samples. Firstly the samples were placed in a hydraulic splitter and reduced to chips suitable for the second stage, a mechanical jaw crusher. Throughout these stages surface weathering veneer, altered fracture surfaces and zeolites were removed by hand picking. Finally, 70g of chips of less than 2mm diameter were placed in an agate swing mill and reduced to less than 100 mesh. An agate tema rather than a tungsten carbide tema was used to minimise contamination by Cr, Nb and Ta. The grain size was checked firstly by sieving to gain an appreciation of how smooth powder of less than 100 mesh felt to the touch. Powder grain size was then checked qualitatively by making a smooth paste with water. The grinding process took 6-8 minutes. The tema barrel was then rigorously cleaned with water to avoid cross contamination.

B2; XRF analysis;

B2.1; Major element analysis: preparation of fusion beads;

Major elements were determined on 46mm diameter beads. These were produced by weighing 0.400g of dried powder into a platinum crucible. The powder was diluted by 4.00g of lithium borate flux (Johnson and Matthey Spectroflux 110). The powder and flux were then mechanically mixed to ensure dispersion of the rock powder. The crucible was then placed in a furnace for 30 minutes at 1000 °C. Once cool the mixture was made up to 4.4g with flux with the assumption that any weight loss could be accounted for by loss of water from the slightly hydroscopic flux. The crucible was then directly heated in a flame until the contents were molten and homogenised. The glass was cast in a copper ring that rested on a steel die, which in turn was on a hotplate. The disk was formed by pressing firmly down on the molten material with a heated Al press. After cooling, the samples were labelled and put in an air tight plastic bag to prevent rehydration. A crude idea of the amount of non-structurally bound water and other volatiles in each sample was obtained by determining the loss on ignition of the powder

when placed in a furnace at 1000 °C for one hour. Approximately 1g of powder was weighed accurately into a ceramic container. The difference in weights measured before and after putting in the furnace was divided by the initial sample weight to gain an estimate of the amount of volatiles in the sample.

B2.2; Trace element analysis: preparation of pressed powder pellets;

46mm diameter briquettes of 15g rock bound with 4ml of Moviol P.V.A. were placed between polished steel die at 10 p.s.i. for 10 seconds. The pellet was then dried at 110 °C for 1 hour in an oven and placed in a vacuum dessicator prior to analysis. The pellets were held in the sample holder by a mylar film which is effectively transparent to X-Ray radiation.

B2.3; Machine operating conditions;

Beads were analysed in a Phillips PW 1400 XRF at Leeds University. Operating conditions are shown in Table B1. Machine drift is corrected by reference to a lab standard which is always present in one of the four sample positions. The data produced is read via magnetic tape onto a mainframe computer. Data processing to account for mass absorbtion and matrix effects is then undertaken by a suite of programs written by Mr A.Grey. Analytical error varies between 5-10% (A.Grey pers.comm.). A detailed appraisal of operator precision and precision for the PW 1400 XRF is given by Downes(1983).

B3; Inductively Coupled Plasma determinations of REE;

Sample preparation;

To ensure that REE determinations were within analytical range, 2g of basaltic material was weighed accurately into a Pt crucible, whilst only 1.0g of evolved material was weighed out. The powder was digested in 5ml of 60% perchloric acid followed by 20ml of 40% HF. The crucibles were placed on a water bath for one hour and periodically stirred with a Pt rod to increase the area of reaction. The mixture was then dried down beneath a teflon coated heating element. A second dissolution with 20ml of perchloric acid was then conducted. 20ml of 20% Hcl are added and solute partially dissolved by heating over a water bath. Dissolution is completed by direct heating of the beaker with a bunsen burner.

Anion exchange columns of 100-200 mesh resin were primed by distilled water. 20ml Sample solution was added to the columns down a glass rod to avoid disturbing the resin. The remainder of the 125ml solution is then added. The rod is washed with 0.4 M Hcl to ensure total transfer. Likewise the beaker is rinsed out 3 times to ensure that all material enters column. 550ml 1.75 M Hcl is used to wash the solution onto the column, initially in small amounts. REE are eluted using 500ml of 4M Hcl. The material is collected and then dried down to 10ml and it is filtered to remove any resin. The solution is finally made up to 10ml of 4m Hcl.

Sample analysis;

The solutions were analysed for REE with a Phillips PV 8210 1.5m ICP operating at 1.0kW. An appraisal of the technique, analytical error and precision is given by Walsh et al.(1981).

Table B1. Operating conditions for the PW 1400 XRF Spectrometer.

Measuring program 1. Rhodium target with power set at 40 kV by 60 mA

Element	line	Collimator	Detector	Crystal	2-theta	offsets +	offsets -	time (secs)
Na	Ka	Coarse	Flow	PX 1	23.65	1.6	1.6	160
Mg	Ka	Coarse	Flow	PX 1	28.60	1.2	1.2	80
Al	Ka	Coarse	Flow	PET	144.90	---	---	30
Si	Ka	Coarse	Flow	InSb	144.56	---	---	20
P	ka	Coarse	Flow	Ge	141.03	---	---	20
K	Ka	Fine	Flow	LiF 200	136.69	---	---	8
Ca	Ka	Fine	Flow	LiF 200	113.09	---	---	8
Ti	Ka	Fine	Flow	LiF 200	86.14	---	---	8
Mn	Ka	Fine	Flow	LiF 200	62.97	---	---	8
Fe	Ka	Fine	Flow	LiF 200	57.52	---	---	4

Measuring program 2. Rhodium target with power set at 80 kV by 30 mA

Element	line	Collimator	Detector	Crystal	2-theta	offsets +	offsets -	time (secs)
Cr	Ka	Fine	Flow	LiF 200	69.38	1.0	1.0	80
Co	Ka	Fine	Flow	Lif 220	77.89	0.5	---	80
Ni	Ka	Fine	Flow	LiF 200	48.67	1.0	---	80
Cu	Ka	Fine	Flow	LiF 200	45.03	0.6	1.0	80
Zn	Ka	Fine	Scint	LiF 200	41.76	1.0	---	80
Rb	Ka	Fine	Scint	LiF 200	26.62	0.5	0.8	80
Sr	Ka	Fine	Scint	LiF 200	25.15	0.6	0.6	80
Y	Ka	Fine	Scint	LiF 200	23.80	0.8	0.8	80
Zr	Ka	Fine	Scint	LiF 200	22.55	0.4	0.8	80
Nb	Ka	Fine	Scint	LiF 220	30.39	0.6	0.6	80
Ba	Ka	Fine	Scint	LiF 220	15.54	0.5	0.3	80
Pb	Lb	Fine	Scint	LiF 200	28.26	0.5	1.0	80

Measuring program 3. ~ Rhodium target with power set at 80 kV by 30 mA

Element	line	Collimator	Detector	Crystal	2-theta	offsets +	offsets -	time (secs)
Th	La	Fine	Scint	LiF 220	39.19	0.9	0.5	400
U	La	Fine	Scint	LiF 200	26.11	1.0	0.4	400

Measuring program 4. Rhodium target with power set at 50 kV by 50 mA

Element	line	Collimator	Detector	Crystal	2-theta	offsets +	offsets -	time (secs)
Sc	Ka	Fine	Flow	LiF 200	97.73	0.6	0.6	400
V	Ka	Fine	Flow	LiF 220	123.12	---	1.1	160

B4; INAA determination of REE, Th,Pb, Hf and Ta;

Selected samples were analysed by instrumental neutron activation analysis (INAA) for La, Ce, Nd, Sm, Eu, Tb, Yb, Lu, Hf, Ta, Th and U. Detailed descriptions of the analytical technique are given in Potts et al.(1985).

0.3g of sample powder was dried overnight at 110 °C and loaded into polythene capsules that were heat sealed. Laquered iron foils were placed between samples to monitor the neutron flux.

Samples were irradiated in the 270 degree core tube facility at the Silwood Park Reactor Centre (Imperial College). After one week of cooling samples were counted at the Open University using a low energy photon spectrometer and a coaxial Ge(Li) detector. An EG and G ORTEC multichannel analyser was used to calculate peak areas and online corrections were made for neutron flux variations and sample weight.

B5; Mineral analyses conducted by Electron microprobe;

Mineral analyses were determined on the Jeol JXA-50A which is fitted with an energy dispersive system (Link 860 series 2). Operating conditions were a beam current of 1 nA, accelerating voltage of 20kV and a count time of 100 secs. The calibration standards used are:

Si : Wollastonite.
Ti : Rutile (synthetic).
Al : Corundum (synthetic).
Fe : Fe metal.
Mn : Rhodonite.
Mg : Periclase.
Ca : Wollastonite.
Na : Jadeite.
K : Orthoclase.
Cr : Pure Cr metal.
Ni : Pure Ni metal.

A ZAF data reduction program for the energy dispersive data corrects for mean atomic number, absorbtion and fluorescence of sample.

B6; Isotopic analytical techniques;

B6.1; Sr Isotopic analysis ($^{87}Sr/^{86}Sr$);

Samples were analysed in batches of 6. 30ml teflon beakers were cleaned in concentrated SB HNO_3 and left for two days. Beakers were then stored in DD H_2O until required. Immediately before use, they were boiled twice in distilled water. To each clean, dry beaker which had been treated by an anti-static gun, approximately 200mg of powder was added. All samples were leached to remove non primary Sr. The leachant was 6M Hcl which was added to the samples in teflon beakers, left to stand for 30 minutes and then placed in an ultrasonic device for 15 minutes. The leachant was then decanted off. The samples were then digested overnight in 1ml of conc HNO_3 and 8ml of 40% HF. The liquid was then evaporated off and 1ml conc HNO_3 added to drive off

any remaining HF. This was dried down and 8ml 6M Hcl were added and evaporated to convert to chloride. The sample was dissolved in 2ml of 2.5 M Hcl and placed in a clean centrifuge tube. Solutions were centrifuged at 2800 r.p.m for 10 minutes to remove any suspended solid. 1ml of solution was taken from the centrifuge tubes without disturbing the solid and the solution was added to anion exchange columns containing Biorad AG 50W-X8 resin which was pretreated with 2.5 M Hcl. The solution was washed on with two 1ml additions of 2.5 M Hcl. Elution was conducted using 42ml of 2.5 M Hcl and the Sr collected in 12ml of 2.5 M Hcl. The sample was then dried and redissolved in 2.5 M Hcl and the procedure repeated in order to minimise Rb interference. Samples were then evaporated and stored under Parafilm in micro-beakers prior to loading.

The sample was loaded onto a Ta filament bead which had been outgassed at 4.5 amps under a vacuum of $< 10^{-6}$ Torr. Prior to loading, a drop of H_3PO_4 was added to the filament and evaporated until flat. The sample, held in a pipette previously cleaned in HNO_3 and DD H_2O was then loaded in a small drop of DD H_2O. The sample was evaporated at 1.2 amps until nearly dry and excess H_3PO_4 driven off by increasing the current to 2.4 amps at which temperature the filament started to glow.

Sr analyses were performed on a VG isomass 54-E mass spectrometer operating at an accelerating voltage of 8 kV and 2kG magnetic field. Peak switching across masses 88, 87 and 86 was conducted automatically. Rb interference was corrected by reference to peak 85. The ^{86}Sr tail was measured at peak 87.3 and the background at 84.5. 200 scans were measured using a 2 second delay and a 5 second count time. Two Sr isotopes standards (NBS 987) were included in each turret for which Sr ratios were being measured. $^{87}Sr/^{86}Sr$ is normalised to E&A = 0.70800, NBS 987 = 0.71023. Errors on Sr were typically 0.002%. Over the period of study the average value of standard NBS 987 was 0.71029. Sr total procedure blanks were less than 2ng.

B6.2; Determination of Sr concentrations by isotope dilution;

In the phonolites, in which the age correction $^{87}Sr/^{86}Sr$ (present) to initial ratios was highly dependent on the Rb/Sr ratio spiking was necessary to determine Sr concentrations which were below 10 ppm. A similar procedure was adopted to that above, with the exception that a known weight of $^{87}Rb/^{84}Sr$ spike was added before digestion. The Rb is collected from the anion exchange resins after elution of 24ml of 2.5M Hcl. Collection is in 6ml of 2.5 M Hcl.

The Sr samples are loaded as described above and Sr concentrations calculated on line to the VG Isomass 54-E.

B6.3; Neodymium isotopic analysis (^{143}Nd / ^{144}Nd);

The dissolution stage and initial elution to collect Sr was conducted as described in the previous section. Nd was then collected in teflon beakers reserved for Nd chemistry, which were cleaned in a similar manner to the Sr teflon beakers. Collection was by 30ml of 6M Hcl after Ba had been removed by elution with 60ml of 2M HNO_3. REE were converted to nitrate form by evaporating in concentrated HNO_3. Nd of sufficient purity for analysis was then produced by passing the sample through two further columns. The first column set were based on pre-treatment of anion resin with 5ml of 90% 8M CH_3COOH (acetic acid) and 10 % 5M HNO_3. The sample was loaded in a 75 : 25 ratio of these acids (1-2ml) and washed on with 2 further additions of 1ml. Elution was with

50ml of 90:10 acetic : Nitric. The REE were collected in 10ml of 0.05M HNO_3. After evaporation to dryness conversion to chloride anions was made by evaporating to dryness with 0.125 M SB Hcl. Nd was separated from the other REE on PTFE columns. The sample was firstly, dissolved in 1ml of 0.125 M SB Hcl and washed on using 2 further 1ml additions. Elution was conducted for a further 2.5 hours and the eluent (0.125 M Hcl) was removed from the columns. Collection with SB 0.25 M Hcl was made according to a temperature controlled callibration which was checked every month. The sample was then dried down and stored in Parafilmed microbeakers prior to analysis.

The sample was loaded onto a triple filament bead assembly comprising a central Re filament and two adjacent Ta filaments. Samples were loaded in clean pipettes (rinsed twice with DD H_2O) in a drop of DD H_2O. Half of the sample was added to each Ta filament and dried down at 1.2 A.

Nd isotopic determinations were made on a VG MM30 mass spectrometer under operating conditions of 8 kV accelerating voltage and 3 kG magnetic field. Peaks were automatically switched across masses 146, 144 and 143. Background was measured at 146.5 and Sm interference was corrected for at peak 147. Upwards of 500 scans across the spectrum were made in total. ^{143}Nd / ^{144}Nd was normalised to $^{146}Nd/^{144}Nd$ of 0.7219 for BCR-1 (which is constant as its constituents are not part of a radioactive decay series). 18 analyses of La Jolla standard gave $^{143}Nd/^{144}Nd$ = 0.5119046 . $^{143}Nd/^{144}Nd$ isotope ratios were normalised to BCR-1 0.512665. Average standard two sigma error of Nd isotopic data typically 0.004%. Nd total procedure blanks were < 0.2 ng.

B6.4; Pb Isotope analysis;

Teflon beakers were cleaned by leaving for more than 2 days each in concentrated QD HNO_3, 10% QD Hcl and DD H_2O. 200 mg of rock powder were weighed into a teflon beaker and then digested for at least 2 days in 2ml HNO_3 and 6ml 40% HF. To ensure dissolution the beaker was then placed in an ultrasonic bath for 15 minutes. After evaporating to dryness, the residue was converted to bromide by drying down in 6ml of 1M HBr. The sample was then redissolved in 2ml 1M HBr and left for > 2 hours. The solution was then placed in a centrifuge tube cleaned by rinsing with 6M Hcl and left overnight containing 1M HBr. Samples were then centrifuged and the supernatant liquid added to the anion exchange columns, which had been cleaned by twice passing 4ml of 6M Hcl and DD H_2O through alternately before pretreatment with 3ml of 1M HBr. The samples were washed on with 3ml of 1M HBr and collected in cleaned beakers by eluting with 4ml of DD 6M Hcl. The sample was then evaporated and dried down again in a drop of phosphoric acid and one drop of nitric acid to drive off the Br_2.

Pb in phosphoric acid was loaded onto a single Re filament outgassed as for single Ta beads. Before loading Pb, silica gel was added and virtually dried down to act as an inhibitor for Pb ionisation in the mass spectrometer. The Pb was dried until flat and the phosphoric then driven off by increasing the current to 2.2 amps.

Pb isotopic measurements were made on a VG MM30 at operating conditions of an accelerating voltage of 8.0 kV and a magnetic field of 3.5 kG. Pb data was collected at a temperature of 1150 - 1400 °C. Peaks were switched between masses 204, 206, 207 and 208. 203.5 acted as the baseline and 207.5 as the tail.

The precision of Pb isotopic determinations is mainly governed by determinations of standards, which are used to correct for mass fractionation. 15 analyses of SRM 981 indicated Pb fractionation of 1.1 per mill per atomic mass unit. Pb total procedure blanks were < 1ng.

Appendix C : Analytical data:

C1.1; Microprobe data of mineral phases;

Table C1 presents representative probe analyses for 45 samples from the SHRS. The samples are arranged in mineral groups, with ascending sample number within each group. The compositions chosen represent a typical average composition of either a groundmass or phenocryst phase in a particular sample. In some sample phenocryst compositions only are given. This is due to a lack of fresh groundmass crystals within the sample (this applies particularly to olivine analyses). Because of the large variability in feldspar composition within a particular sample a maximum and minimum value is presented for each sample.

Abbreviations:

ol: Olivine analyses.
Fo: Percentage Forsterite.

cpx: Clinopyroxene analyses
En: Enstatite.
Wo: Wollastonite.
Fs: Ferrosillite.

plag: Plagioclase analyses.
kf: K - feldspar analyses.
An: Anorthite component in plagioclase.
Ca: Anorthite component in feldspar.
Na: Albite component in feldspar.
K: Orthoclase component in feldspar.

op: Opaque mineral analyses.

Table C1: Probe analyses (OLIVINE) liv

Rock	17 ol Phen	26 ol Phen	28 ol Phen	28 ol Gmass	29 ol Gmass	38 ol Phen	68 ol Phen	68 ol Gmass	69 ol Phen	113 ol Phen
SiO2	38.44	37.96	37.43	37.11	37.31	39.39	39.19	35.85	38.41	39.36
TiO2	0.09	0.00	0.00	0.07	0.13	0.01	0.00	0.05	0.00	0.00
Al2O3	0.17	0.00	0.29	0.08	0.75	0.05	0.05	0.15	0.24	0.03
Fe2O3	20.12	21.86	25.66	27.71	29.69	16.50	18.95	34.35	19.68	18.89
MnO	0.29	0.34	0.25	0.74	1.09	0.35	0.26	0.46	0.32	0.18
MgO	40.95	38.96	35.86	34.59	31.48	43.23	41.58	28.56	40.73	41.89
CaO	0.32	0.25	0.23	0.47	0.30	0.32	0.27	0.50	0.27	0.30
NiO	0.00	0.10	0.10	0.00	0.00	0.00	0.08	0.00	0.08	0.18
Cr2O3	0.00	0.00	0.05	0.00	0.00	0.00	0.05	0.00	0.04	0.02
Total	100.39	99.47	99.87	100.77	100.75	100.02	100.43	99.92	99.77	100.85
Fo	78.10	74.10	71.20	68.90	64.60	82.10	79.60	59.30	78.40	79.70

Rock	113 ol Gmass	115 ol Gmass	117 ol Phen	117 ol Gmass	118 ol Phen	119 ol Phen	119 ol Gmass	120 ol Gmass	122 ol Phen	123 ol Gmass
SiO2	36.12	33.03	35.82	35.48	36.88	37.78	34.56	36.68	39.34	35.45
TiO2	0.04	0.51	0.00	0.09	0.05	0.04	0.16	0.07	0.03	0.66
Al2O3	0.00	0.18	0.19	0.11	0.45	0.17	0.00	0.30	0.06	0.36
Fe2O3	33.08	47.08	35.41	39.17	31.21	24.37	37.01	34.26	17.46	0.07
MnO	0.63	1.44	0.81	1.03	0.51	0.40	1.10	0.83	0.28	32.88
MgO	28.94	17.13	27.71	24.02	31.11	37.17	25.79	26.72	43.47	0.69
CaO	0.47	1.05	0.40	0.53	0.52	0.23	0.44	0.48	0.25	29.30
NiO	0.06	0.00	0.03	0.01	0.07	0.04	0.00	0.00	0.19	0.55
Cr2O3	0.06	0.00	0.00	0.06	0.03	0.02	0.00	0.00	0.08	0.00
Total	99.40	100.42	100.37	100.50	100.83	100.22	99.06	99.68	101.16	99.96
Fo	60.50	38.60	57.70	46.00	77.70	74.30	54.70	65.70	81.40	60.90

Rock	131 ol Gmass	134 ol Gmass	168 ol Phen	173 ol Phen	173 ol Gmass	177 ol Phen	177 ol Gmass	186 ol Phen	186 ol Gmass	199 ol Gmass
SiO2	36.49	36.67	34.75	38.72	34.53	38.64	36.40	38.54	35.64	34.80
TiO2	0.07	0.08	0.05	0.02	0.06	0.05	0.06	0.01	0.07	0.14
Al2O3	0.17	0.09	0.29	0.00	0.33	0.24	0.05	0.25	0.00	0.23
Fe2O3	36.60	31.35	37.01	18.17	43.57	19.75	31.42	19.76	36.10	36.24
MnO	0.62	0.87	0.97	0.27	0.93	0.38	0.72	0.18	0.62	0.90
MgO	24.34	30.04	26.11	42.09	19.23	40.53	31.42	41.12	27.50	26.51
CaO	0.39	0.49	0.39	0.23	0.81	0.41	0.46	0.19	0.45	0.54
NiO	0.44	0.05	0.05	0.22	0.00	0.09	0.04	0.08	0.00	0.38
Cr2O3	0.00	0.02	0.05	0.00	0.02	0.10	0.00	0.08	0.00	0.04
Total	99.12	101.07	99.67	99.72	99.48	100.19	100.57	100.21	100.38	99.78
Fo	53.80	62.40	55.10	80.30	43.50	78.20	63.50	78.60	57.20	56.00

Rock	208 ol Phen	208 ol Gmass	224 ol Phen	224 ol Gmass	232 ol Phen	232 ol Gmass	238 ol Phen	238 ol Gmass	51 ol Gmass	51 ol Phen
SiO2	38.92	36.26	38.75	35.59	38.22	36.13	38.53	35.97	36.62	37.89
TiO2	0.05	0.07	0.00	0.00	0.02	0.11	0.00	0.26	0.22	0.03
Al2O3	0.50	0.19	0.00	0.15	0.30	0.00	0.00	0.16	0.46	0.57
Fe2O3	16.31	33.46	18.30	34.56	19.59	31.60	19.12	35.56	0.04	22.90
MnO	0.28	0.72	0.24	0.68	0.34	0.53	0.17	0.72	31.33	0.35
MgO	43.53	29.54	42.32	28.16	41.14	30.23	41.82	27.89	0.59	38.24
CaO	0.25	0.50	0.29	0.56	0.36	0.55	0.25	0.31	31.20	0.21
NiO	0.17	0.20	0.08	0.11	0.03	0.00	0.15	0.13	0.46	0.16
Cr2O3	0.00	0.00	0.00	0.00	0.00	0.00	0.00	0.00	0.04	0.05
Total	100.01	100.94	99.98	99.81	100.00	99.15	100.04	101.00	100.96	100.40
Fo	82.40	60.60	80.30	58.20	78.60	62.60	79.40	57.80	63.50	74.50

Table C1: Probe analyses (CLINOPYROXENE) lv

Rock	8 cpx Gmass	11 cpx Gmass	17 cpx Phen	17 cpx Gmass	18 cpx Gmass	26 cpx Phen	26 cpx Gmass	28 cpx Phen	28 cpx Gmass	29 cpx Gmass
SiO2	51.99	50.34	49.28	51.31	50.95	48.61	49.77	48.61	44.85	49.74
TiO2	0.81	1.34	2.16	1.34	1.13	2.23	2.42	1.58	4.23	2.23
Al2O3	1.20	2.30	3.91	1.15	1.53	5.49	4.64	6.69	6.33	4.60
Fe2O3	9.47	13.43	8.89	11.46	11.07	7.14	8.14	6.91	9.57	8.02
MnO	0.46	0.42	0.20	0.29	0.45	0.11	0.16	0.16	0.32	0.23
MgO	13.47	10.45	13.31	12.34	13.27	13.89	12.98	13.71	11.72	12.12
CaO	21.36	20.21	21.09	21.04	19.97	21.96	21.20	21.12	21.06	21.27
Na2O	1.26	0.73	0.80	0.63	0.78	0.91	0.79	0.44	1.18	1.56
K2O	0.05	0.10	0.50	0.06	0.14	0.02	0.06	0.05	0.07	0.38
NiO	0.01	0.00	0.00	0.00	0.00	0.01	0.03	0.02	0.12	0.00
Cr2O3	0.00	0.00	0.00	0.00	0.00	0.02	0.00	0.31	0.00	0.07
Total	100.08	99.32	100.14	99.62	99.29	100.39	100.19	99.60	99.45	100.22
Mg No	70.70	57.30	72.30	65.20	67.20	77.40	73.60	77.70	67.90	72.30
En	44.60	44.14	45.20	44.40	42.10	46.80	46.40	46.10	46.70	47.70
Wo	39.20	31.90	39.60	36.20	38.90	41.20	39.50	41.90	36.20	37.80
Fs	16.20	23.70	15.20	19.40	19.00	12.10	14.20	12.00	17.10	14.50

Rock	35 cpx Gmass	38 cpx Phen	38 cpx Gmass	62 cpx Gmass	68 cpx Phen	68 cpx Gmass	69 cpx Phen	69 cpx Gmass	92 cpx Gmass	96 cpx Phen
SiO2	50.63	49.95	47.20	48.89	48.96	47.40	47.83	46.75	49.32	44.90
TiO2	1.74	1.44	3.19	0.54	1.40	2.88	2.28	2.98	0.15	3.60
Al2O3	2.33	5.82	5.38	1.92	5.94	6.51	6.83	4.75	1.73	8.50
Fe2O3	10.44	5.79	9.29	18.99	5.77	7.37	6.26	11.08	21.61	8.00
MnO	0.34	0.17	0.24	0.60	0.14	0.11	0.00	0.15	1.13	0.14
MgO	11.99	13.93	12.67	6.14	14.51	12.81	13.49	10.68	4.22	12.10
CaO	21.98	21.71	20.92	21.33	22.35	22.24	22.26	21.41	20.54	21.97
Na2O	0.40	0.32	0.35	1.26	0.56	0.67	0.57	1.14	1.60	0.69
K2O	0.04	0.03	0.04	0.14	0.01	0.03	0.00	0.07	0.06	0.05
NiO	0.04	0.12	0.06	0.00	0.00	0.00	0.00	0.15	0.00	0.10
Cr2O3	0.00	0.08	0.00	0.00	0.82	0.24	0.00	0.00	0.00	0.00
Total	99.93	99.36	99.34	99.81	100.46	100.26	99.52	99.16	100.36	100.05
Mg No	66.50	80.60	70.30	35.90	81.40	75.30	79.30	62.90	24.80	72.60
En	46.70	47.50	45.50	47.20	47.40	48.40	48.50	47.50	46.50	48.70
Wo	35.40	42.40	38.30	18.90	42.80	38.80	40.90	33.00	13.30	37.20
Fs	17.90	10.20	16.20	33.90	9.80	12.70	10.60	19.50	40.20	14.10

Rock	96 cpx Gmass	111 cpx Gmass	113 cpx Phen	113 cpx Gmass	114 cpx Gmass	115 cpx Gmass	117 cpx Gmass	118 cpx Phen	118 cpx Gmass	119 cpx Gmass
SiO2	44.78	46.01	49.60	48.20	49.94	49.71	51.27	47.53	48.07	47.60
TiO2	4.15	4.26	1.61	2.55	1.76	0.97	1.63	1.95	2.71	2.84
Al2O3	7.10	5.93	4.96	5.46	3.29	2.34	2.44	6.99	4.89	4.36
Fe2O3	9.36	9.31	6.18	8.64	11.30	10.67	8.62	6.68	9.42	9.47
MnO	0.24	0.16	0.07	0.11	0.40	0.35	0.22	0.18	0.25	0.33
MgO	11.51	11.14	14.57	12.42	11.14	12.00	13.87	13.06	12.24	12.72
CaO	21.47	22.03	22.34	22.14	21.83	22.08	21.86	21.50	21.87	21.13
Na2O	0.78	0.77	0.67	0.14	1.04	0.90	0.37	0.61	0.85	0.84
K2O	0.04	0.05	0.05	0.04	0.19	0.10	0.06	0.04	0.04	0.04
NiO	0.00	0.05	0.00	0.00	0.00	0.00	0.00	0.61	0.00	0.00
Cr2O3	0.00	0.00	0.06	0.08	0.00	0.00	0.03	0.00	0.00	0.00
Total	99.43	99.71	100.11	99.78	100.89	99.12	100.37	99.15	100.34	99.33
Mg No	68.10	67.70	80.60	71.70	63.00	66.00	73.70	77.30	69.30	69.80
En	47.70	49.00	47.00	47.70	47.00	46.60	45.50	47.70	47.10	45.50
Wo	35.60	34.50	42.70	37.40	33.40	35.20	40.10	40.40	36.70	38.10
Fs	16.70	16.50	10.30	14.80	19.60	18.20	14.40	11.90	16.20	16.50

Rock	120 cpx Gmass	122 cpx Gmass	123 cpx Gmass	131 cpx Gmass	140 cpx Phen	140 cpx Gmass	149 cpx Gmass	152 cpx Gmass	153 cpx Gmass	168 cpx Gmass
SiO2	49.79	49.10	46.51	48.85	46.79	48.17	49.08	51.72	52.00	50.19
TiO2	2.60	2.57	3.50	2.64	2.13	2.76	0.07	0.32	0.96	1.52
Al2O3	3.71	3.50	5.60	3.87	8.17	5.00	0.80	1.19	1.99	2.83
Fe2O3	9.70	10.01	9.74	10.62	7.16	8.34	25.49	13.47	8.49	8.62
MnO	0.24	0.21	0.14	0.27	0.10	0.06	2.02	1.01	0.43	0.29
MgO	13.23	12.84	12.59	12.28	12.50	13.07	1.35	10.24	13.84	13.92
CaO	20.73	20.72	21.40	20.41	21.58	21.90	18.91	21.46	22.14	21.76
Na2O	0.56	0.22	0.78	0.73	0.43	0.15	3.07	0.81	1.15	0.79
K2O	0.04	0.06	0.11	0.01	0.02	0.06	0.05	0.03	0.00	0.07
NiO	0.01	0.00	0.00	0.00	0.00	0.02	0.00	0.07	0.00	0.09
Cr2O3	0.00	0.00	0.05	0.00	0.00	0.20	0.00	0.01	0.00	0.00
Total	100.61	99.23	100.42	99.68	98.88	99.73	100.84	100.33	101.00	100.08
Mg No	70.30	69.10	69.40	66.80	75.50	73.50	8.00	42.00	73.40	73.60
En	44.20	44.50	45.90	44.40	48.30	46.90	44.70	48.00	45.80	45.30
Wo	39.20	38.40	37.60	37.20	39.00	39.00	4.40	23.00	39.80	40.30
Fs	16.60	17.10	16.50	18.50	12.70	14.10	50.80	30.00	14.40	14.50

Rock	173 cpx Phen	173 cpx Gmass	175 cpx Gmass	177 cpx Phen	177 cpx Gmass	186 cpx Phen	199 cpx Gmass	208 cpx Phen	208 cpx Gmass	216 cpx Phen
SiO2	48.69	44.76	51.90	47.68	45.79	47.18	49.44	48.73	47.49	47.01
TiO2	1.48	4.08	0.63	1.88	3.24	1.86	2.49	1.28	2.84	2.45
Al2O3	5.58	6.68	1.96	6.26	6.47	7.85	3.35	5.86	5.67	7.05
Fe2O3	5.84	10.97	11.75	5.84	8.68	7.21	8.31	5.63	8.58	7.45
MnO	0.10	0.21	0.45	0.13	0.14	0.21	0.30	0.15	0.01	0.12
MgO	14.30	12.29	11.64	13.81	12.18	13.51	13.75	14.69	12.97	13.26
CaO	22.37	20.74	21.08	22.65	22.17	21.30	22.03	21.90	21.37	22.29
Na2O	0.70	0.85	1.27	0.50	1.08	0.67	1.02	0.63	0.32	0.31
K2O	0.00	0.05	0.00	0.37	0.02	0.04	0.03	0.00	0.10	0.03
NiO	0.01	0.05	0.00	0.00	0.00	0.00	0.07	0.09	0.00	0.00
Cr2O3	0.10	0.06	0.27	0.00	0.00	0.00	0.00	0.00	0.00	0.12
Total	99.17	100.74	100.95	99.12	99.77	99.83	100.79	98.96	99.35	100.09
Mg No	81.10	66.20	62.90	80.50	71.10	76.40	74.00	81.90	72.90	75.70
En	47.70	44.50	45.00	48.70	48.20	46.40	46.00	46.80	46.30	47.80
Wo	42.40	36.70	34.60	41.30	36.80	41.00	40.00	43.60	39.10	39.50
Fs	9.90	18.70	20.40	10.00	15.00	12.60	14.00	9.60	14.50	12.50

Table C1: Probe analyses (CLINOPYROXENE) lvi

Rock	217 cpx Phen	217 cpx Gmass	224 cpx Phen	224 cpx Gmass	232 cpx Phen	232 cpx Gmass	238 cpx Phen	238 cpx Gmass	51 cpx Gmass
SiO2	47.54	48.18	48.52	47.44	50.04	49.73	49.31	48.44	50.56
TiO2	2.35	2.45	1.86	2.56	1.56	1.76	1.40	2.43	2.09
Al2O3	6.74	4.29	5.99	4.89	4.25	4.08	5.15	3.80	2.41
Fe2O3	7.33	8.59	6.04	8.91	6.35	6.57	5.67	8.90	8.95
MnO	0.17	0.25	0.14	0.17	0.12	0.02	0.07	0.16	0.19
MgO	13.54	13.07	13.94	13.17	14.45	14.23	14.53	13.29	13.51
CaO	22.40	21.97	22.44	21.46	22.56	22.13	22.72	21.27	21.98
Na2O	1.25	0.30	0.49	0.77	0.18	0.98	0.64	0.76	0.40
K2O	0.01	0.09	0.01	0.03	0.00	0.03	0.00	0.03	0.02
NiO	0.07	0.13	0.00	0.00	0.04	0.00	0.56	0.13	0.04
Cr2O3	0.24	0.00	0.57	0.18	0.34	0.21	0.00	0.00	0.02
Total	101.64	99.32	100.00	99.58	99.89	99.73	100.05	99.21	100.17
Mg No	76.30	72.70	80.10	72.10	76.80	79.10	81.90	72.30	72.50
En	47.60	46.80	48.10	45.80	0.80	46.90	47.90	45.40	45.90
Wo	40.00	38.70	41.60	39.10	54.10	42.50	42.60	39.50	39.20
Fs	12.40	14.60	10.30	15.10	45.00	11.10	9.40	15.10	14.90

Plagioclase analyses:

Rock	8 plag Phen	8 plag Gmass	11 plag Gmass	11 plag Gmass	17 plag Gmass	17 plag Gmass	18 plag Gmass	26 plag Phen	26 plag Gmass	28 plag Phen
SiO2	53.76	62.46	55.80	64.10	52.33	56.91	58.35	48.08	58.89	50.43
TiO2	0.04	0.17	0.16	0.15	0.14	0.22	0.14	0.12	0.01	0.12
Al2O3	28.55	21.60	28.15	22.10	29.50	26.87	25.41	32.99	25.08	31.04
Fe2O3	0.71	0.53	0.78	0.69	0.80	0.72	0.90	0.70	0.61	0.76
MnO	0.01	0.02	0.00	0.12	0.03	0.01	0.07	0.01	0.00	0.00
MgO	0.07	0.22	0.31	0.11	0.16	0.18	0.05	0.15	0.32	0.07
CaO	11.60	3.36	9.99	2.99	12.57	9.02	7.49	15.83	6.52	13.95
Na2O	4.52	8.21	5.13	7.98	3.96	5.67	5.94	2.40	7.09	3.31
K2O	0.32	2.51	0.38	2.63	0.29	0.80	1.35	0.08	0.92	0.20
BaO	0.00	0.00	0.01	0.25	0.18	0.00	0.00	0.01	0.16	0.00
Total	99.58	99.08	100.71	101.12	99.96	100.40	99.70	100.37	99.60	99.88
An	56.60	16.80	51.00	16.50	63.00	45.20	38.20	79.40	34.10	69.50
Ca	57.70	17.10	51.70	28.70	65.50	50.10	38.10	78.30	33.20	69.30
Na	40.40	68.70	46.10	62.10	32.90	45.20	53.90	21.20	61.20	29.50
K	1.90	13.50	2.20	15.50	1.60	4.70	8.00	0.50	5.60	1.20

Rock	28 plag Gmass	29 plag Phen	29 plag Gmass	35 plag Phen	35 plag Gmass	38 plag Gmass	38 plag Gmass	62 plag Phen	68 plag Gmass	69 plag Phen
SiO2	53.64	52.21	55.66	48.35	55.37	50.13	52.58	57.89	52.38	50.64
TiO2	0.29	0.10	0.19	0.02	0.13	0.18	0.27	0.00	0.16	0.08
Al2O3	28.67	29.85	27.42	32.46	26.80	30.91	30.03	25.50	29.47	31.04
Fe2O3	0.93	0.68	1.08	0.68	0.39	0.98	0.93	0.60	0.65	0.65
MnO	0.00	0.00	0.00	0.03	0.07	0.00	0.05	0.05	0.00	0.06
MgO	0.11	0.13	0.12	0.04	0.00	0.12	0.28	0.00	0.28	14.42
CaO	11.68	12.97	9.78	16.28	9.65	13.98	12.44	7.88	12.51	2.89
Na2O	4.40	4.51	6.23	2.14	5.79	3.09	3.91	6.36	4.10	0.21
K2O	0.33	0.22	0.41	0.10	0.58	0.15	0.22	0.46	0.34	0.07
BaO	0.00	0.03	0.00	0.00	0.20	0.00	0.00	0.29	0.05	0.00
Total	100.05	100.70	100.89	100.10	98.98	99.54	100.71	99.03	99.94	100.06
An	57.70	62.10	60.30	79.20	46.40	70.60	63.30	38.70	61.80	70.50
Ca	58.40	60.90	59.60	80.40	46.30	71.00	63.70	39.40	62.20	72.40
Na	39.70	37.80	37.90	19.00	50.00	28.18	35.30	57.30	35.80	26.20
K	1.90	1.20	2.50	0.60	3.70	0.90	1.40	3.20	2.00	1.40

Rock	92 plag Gmass	96 plag Phen	96 plag Gmass	111 plag Phen	111 plag Gmass	113 plag Gmass	114 plag Gmass	115 plag Gmass	115 plag Gmass	117 plag Gmass
SiO2	62.13	47.65	51.21	47.61	53.65	52.60	57.29	56.94	59.44	62.40
TiO2	0.00	0.00	0.07	0.00	0.33	0.33	0.08	0.02	0.07	0.06
Al2O3	23.21	32.20	29.75	33.14	29.39	29.40	26.82	26.42	24.55	23.52
Fe2O3	0.25	0.65	1.08	0.49	0.91	0.69	0.98	0.88	0.89	0.41
MnO	0.05	0.00	0.11	0.08	0.00	0.00	0.04	0.00	0.07	0.00
MgO	0.32	0.15	0.16	0.00	0.00	0.00	0.00	0.00	0.00	0.15
CaO	4.23	16.03	12.86	16.90	12.41	13.04	9.11	8.57	6.77	4.55
Na2O	8.98	2.22	3.75	1.69	4.35	3.78	5.62	6.32	7.39	7.29
K2O	1.07	0.09	0.40	0.11	0.39	0.33	0.40	0.45	0.73	1.89
BaO	0.16	0.09	0.20	0.22	0.00	0.03	0.19	0.10	0.15	0.21
Total	100.40	99.08	99.59	100.24	101.43	100.20	100.53	99.70	100.06	100.48
An	22.40	79.30	64.70	82.40	59.86	62.60	45.30	42.50	32.60	24.10
Ca	21.10	79.60	64.20	83.80	59.80	64.30	46.00	41.70	32.20	23.50
Na	72.90	19.00	33.10	15.20	37.90	33.80	51.20	55.50	63.40	65.10
K	6.00	0.70	2.70	1.00	2.30	2.00	2.80	2.80	4.40	11.50

Rock	117 plag Gmass	118 plag Gmass	119 plag Phen	119 plag Gmass	119 plag Gmass	120 plag Gmass	120 plag Gmass	121 plag Phen	121 plag Gmass	122 plag Phen
SiO2	57.23	49.87	48.34	51.15	60.33	53.05	59.52	52.99	62.53	52.96
TiO2	0.04	0.12	0.12	0.18	0.13	0.08	0.14	0.00	0.07	0.13
Al2O3	26.33	31.78	32.86	30.05	23.32	29.52	25.27	28.83	22.19	28.89
Fe2O3	0.41	0.92	0.52	0.82	0.62	0.84	0.58	0.55	0.69	0.79
MnO	0.01	0.00	0.00	0.00	0.00	0.08	0.00	0.00	0.00	0.09
MgO	0.37	0.03	0.00	0.00	0.04	0.00	0.00	0.02	0.00	0.00
CaO	8.19	14.68	16.51	13.33	4.53	12.60	7.29	11.36	3.55	12.13
Na2O	6.89	2.99	2.17	3.97	7.42	4.38	7.29	4.84	8.04	4.14
K2O	0.65	0.20	0.07	0.26	3.49	0.34	0.78	0.37	2.78	0.32
BaO	0.27	0.00	0.00	0.00	0.24	0.28	0.00	0.23	0.19	0.25
Total	100.39	100.59	100.59	99.76	100.12	101.17	100.87	99.19	100.04	99.70
An	40.40	72.80	80.00	65.70	22.80	60.30	34.40	56.00	17.70	59.40
Ca	39.50	72.30	80.50	64.00	20.60	60.00	34.00	55.10	16.50	60.50
Na	56.50	26.50	19.10	34.50	60.30	37.60	61.63	42.40	67.70	37.20
K	4.00	1.20	0.40	1.50	19.10	2.40	4.40	2.50	15.70	2.30

Table C1: Probe analyses (PLAGIOCLASE)

Rock	122 plag Gmass	123 plag Gmass	123 plag Gmass	131 plag Gmass	131 plag Gmass	134 plag Phen	134 plag Gmass	140 plag Gmass	140 plag Gmass	152 plag Gmass
SiO2	56.88	53.17	58.34	54.95	56.91	51.55	53.39	53.20	58.48	54.17
TiO2	0.13	0.18	0.25	0.09	0.28	0.11	0.16	0.25	0.12	0.14
Al2O3	25.95	28.32	25.66	28.11	26.04	30.63	28.88	29.13	25.70	28.09
Fe2O3	0.93	0.86	0.66	0.57	0.95	0.66	0.82	1.02	1.00	1.16
MnO	0.00	0.09	0.00	0.00	0.09	0.00	0.00	0.04	0.00	0.04
MgO	0.00	0.08	0.11	0.31	0.00	0.10	0.10	0.30	0.12	0.15
CaO	8.72	11.22	7.38	10.13	8.35	13.93	11.77	12.00	7.54	10.62
Na2O	6.28	4.80	6.49	5.41	6.27	3.60	4.78	4.27	6.29	5.16
K2O	0.67	0.36	1.29	0.47	0.67	0.21	0.30	0.32	0.85	0.32
BaO	0.00	0.08	0.25	0.04	0.04	0.00	0.09	0.00	0.20	0.15
Total	99.56	99.16	100.43	100.08	99.60	100.79	100.29	100.53	100.30	100.00
An	42.00	56.00	37.30	51.20	40.90	67.00	57.40	60.00	38.70	53.60
Ca	41.80	55.50	36.00	50.50	44.90	67.40	56.80	60.60	38.20	52.60
Na	54.40	42.30	56.20	52.50	51.70	31.40	41.30	37.60	56.40	45.30
K	3.80	2.20	7.80	3.60	3.40	1.20	1.90	1.80	5.40	2.10

Rock	168 plag Gmass	168 plag Gmass	173 plag Gmass	175 plag Phen	177 plag Phen	177 plag Gmass	186 plag Gmass	186 plag Gmass	199 plag Phen	199 plag Gmass
SiO2	63.16	52.35	52.32	59.88	46.33	53.73	51.99	57.65	47.24	55.61
TiO2	0.18	0.12	0.06	0.00	0.06	0.08	0.08	0.26	0.07	0.42
Al2O3	22.30	29.20	29.71	24.08	33.35	28.33	29.30	23.99	33.09	26.79
Fe2O3	0.45	0.27	0.64	1.15	0.55	0.93	0.81	2.20	0.60	1.32
MnO	0.00	0.09	0.05	0.09	0.12	0.02	0.05	0.00	0.00	0.01
MgO	0.00	0.00	0.00	0.39	17.51	0.16	0.00	1.10	0.00	0.00
CaO	3.88	12.43	12.73	5.58	1.53	11.32	12.88	6.55	17.14	9.56
Na2O	7.86	4.27	4.03	7.67	0.11	4.48	3.69	5.83	1.81	5.98
K2O	2.41	0.31	0.28	0.63	0.00	0.87	0.33	1.30	0.11	0.64
BaO	0.08	0.00	0.02	0.37	0.00	0.00	0.15	0.00	0.00	0.00
Total	100.32	99.04	99.84	99.84	99.56	99.92	99.28	98.88	100.06	100.33
An	18.80	73.50	62.20	30.30	85.70	55.70	62.80	38.80	83.10	46.90
Ca	18.50	73.00	62.60	29.60	85.90	55.90	64.40	40.10	83.40	45.20
Na	67.70	25.00	35.80	66.20	13.50	38.50	33.40	52.20	15.90	51.10
K	13.80	2.00	1.60	4.20	0.60	5.60	2.20	7.71	0.60	3.60

Rock	208 plag Gmass	208 plag Gmass	216 plag Phen	216 plag Gmass	216 plag Gmass	217 plag Phen	217 plag Gmass	224 plag Gmass	232 plag Gmass	238 plag Gmass
SiO2	60.56	51.72	47.69	62.46	52.42	47.62	51.72	52.36	50.61	53.27
TiO2	0.31	0.06	0.00	0.18	0.29	0.03	0.78	0.18	0.05	0.25
Al2O3	22.33	28.22	32.81	23.11	28.54	32.56	21.85	29.28	30.37	26.56
Fe2O3	0.98	2.73	0.47	0.63	0.84	0.61	6.80	0.87	0.74	2.89
MnO	0.00	0.03	0.05	0.10	0.07	0.00	0.01	0.00	0.01	0.00
MgO	0.64	1.30	0.06	0.00	0.19	0.00	2.33	0.00	0.00	1.83
CaO	3.86	11.54	16.88	4.70	12.08	16.66	8.23	12.95	13.95	9.26
Na2O	6.83	3.68	2.11	7.55	4.15	1.78	5.68	4.09	3.67	4.26
K2O	3.14	0.30	0.14	2.13	0.34	0.15	2.46	0.29	0.23	0.61
BaO	0.18	0.18	0.28	0.17	0.00	0.05	0.01	0.00	0.03	0.00
Total	98.83	99.76	100.49	101.03	98.92	99.46	99.87	100.02	99.66	98.93
An	23.30	64.00	80.90	23.10	59.90	81.30	49.00	61.90	67.30	56.60
Ca	22.70	65.50	80.60	22.70	61.00	83.00	46.50	62.60	66.80	58.20
Na	59.10	32.60	18.10	64.90	37.00	16.00	41.60	35.70	31.80	38.20
K	18.20	2.00	1.30	12.30	2.00	1.00	11.90	1.70	1.40	3.60

Rock	51 plag Phen	51 plag Gmass
SiO2	53.11	60.27
TiO2	0.29	0.29
Al2O3	28.53	23.45
Fe2O3	1.00	0.76
MnO	0.00	0.00
MgO	0.00	0.49
CaO	11.60	5.92
Na2O	4.72	7.59
K2O	0.40	1.26
BaO	0.10	0.09
Total	99.75	100.12
An	70.20	41.50
Ca	69.40	40.00
Na	28.20	51.00
K	2.40	8.50

Table C1: Probe analyses (K - FELDSPAR) lviii

Rock	8 kf Gmass	17 kf Gmass	18 kf Gmass	26 kf Gmass	62 kf Gmass	92 kf Gmass	114 kf Gmass	120 kf Gmass	121 kf Gmass	122 kf Gmass
SiO2	63.25	63.71	61.76	63.25	63.35	66.32	62.58	64.67	63.37	64.36
TiO2	0.07	0.22	0.07	0.22	0.11	0.33	0.23	0.17	0.03	0.17
Al2O3	21.43	19.11	22.95	22.05	21.65	18.40	19.57	20.16	21.29	20.86
Fe2O3	0.58	0.81	0.62	0.74	1.51	0.36	1.80	0.36	0.97	0.54
MnO	0.00	0.03	0.10	0.03	0.06	0.01	0.00	0.00	0.00	0.00
MgO	0.03	0.51	0.20	0.20	0.03	0.00	0.26	0.00	0.29	0.17
CaO	1.74	5.38	4.57	3.13	2.73	0.02	2.99	1.53	1.93	2.26
Na2O	7.40	8.28	7.02	7.31	7.48	6.32	6.02	6.38	7.04	6.65
K2O	5.20	0.54	2.52	3.99	2.30	8.43	6.34	7.07	5.24	5.17
BaO	0.13	0.00	0.17	0.18	0.32	0.25	0.11	0.29	0.09	0.17
TOTAL	99.83	99.49	99.98	101.10	99.54	100.44	99.90	100.63	100.25	100.37
Ca	8.30	7.50	23.70	16.00	14.70	21.10	15.50	7.10	59.60	11.50
Na	62.30	45.90	42.70	61.60	70.40	72.90	50.00	53.50	29.40	55.40
K	29.40	46.50	50.30	22.40	14.90	6.00	34.90	39.50	73.00	33.00

Rock	131 kf Gmass	149 kf Gmass	149 kf Gmass	152 kf Gmass	153 kf Gmass	175 kf Gmass	177 kf Gmass	217 kf Gmass	232 kf Gmass	238 kf Gmass
SiO2	62.74	66.33	65.78	64.67	66.25	65.51	62.98	59.46	63.45	63.37
TiO2	0.08	0.00	0.05	0.11	0.00	0.11	0.23	1.83	0.05	0.14
Al2O3	22.19	18.66	19.58	19.22	18.77	19.07	22.18	19.22	19.83	21.43
Fe2O3	0.47	0.85	0.42	0.28	0.31	0.34	0.34	4.40	0.86	0.31
MnO	0.00	0.00	0.06	0.02	0.00	0.00	0.13	0.02	0.00	0.00
MgO	0.15	0.00	0.00	0.00	0.00	0.00	0.00	0.15	0.52	0.04
CaO	4.04	0.18	0.63	1.26	0.34	6.18	3.56	2.09	1.88	2.93
Na2O	6.60	6.42	6.93	5.24	5.51	6.66	6.48	5.96	4.74	6.82
K2O	3.68	8.14	5.70	8.51	8.08	0.01	3.42	6.75	7.12	3.96
BaO	0.13	0.04	0.15	0.02	0.47	0.07	0.07	0.19	0.47	0.35
TOTAL	100.08	100.62	99.30	99.33	99.73	97.95	99.39	100.13	98.92	99.35
Ca	57.90	0.80	3.40	5.80	1.70	2.40	18.60	11.50	13.10	14.84
Na	21.50	54.10	62.50	45.50	49.80	57.00	60.30	53.90	43.30	61.20
K	38.00	45.00	34.10	48.70	48.50	40.51	21.11	34.60	43.70	24.00

Table C1: Probe analyses (OPAQUES) lix

Rock	8 opq Phen	11 opq Gmass	17 opq Gmass	18 opq Gmass	18 opq Gmass	26 opq Gmass	28 opq Gmass	29 opq Gmass	35 opq Gmass	38 opq Gmass
SiO2	0.59	0.26	0.47	54.66	0.62	0.32	0.33	0.36	3.27	0.77
TiO2	21.25	20.54	29.50	0.12	23.67	16.49	20.72	20.74	29.81	26.03
Al2O3	1.66	3.06	1.45	28.61	1.99	7.54	2.27	2.14	2.32	1.44
Fe2O3	71.88	73.74	65.68	1.12	69.09	67.45	69.36	70.99	60.34	69.17
MnO	0.90	0.87	0.76	0.06	0.86	0.19	0.82	0.94	0.75	0.68
MgO	2.27	1.86	2.17	0.44	2.12	5.67	4.24	3.63	2.03	1.11
CaO	0.13	0.01	0.13	10.42	0.13	0.00	0.06	0.08	0.46	0.28
NiO	0.00	0.00	0.00	4.91	0.00	0.00	0.10	0.00	0.02	0.16
ZnO2	0.31	0.40	0.27	0.52	0.00	0.00	0.12	0.20	0.00	0.00
V2O3	0.13	0.08	0.19	0.05	0.19	0.40	0.17	0.23	0.40	0.18
Cr2O3	0.00	0.07	0.00	0.00	0.00	1.58	2.11	0.38	1.58	0.05
Total	99.12	100.89	100.62	100.91	98.67	99.64	100.30	99.69	100.98	99.87

Rock	62 opq Gmass	68 opq Gmass	96 opq Gmass	113 opq Gmass	113 opq Gmass	114 opq Gmass	115 opq Gmass	117 opq Gmass	118 opq Gmass	118 opq Gmass
SiO2	0.43	0.34	0.44	0.54	0.54	0.41	0.69	0.87	1.41	1.28
TiO2	18.32	2.89	26.42	25.83	25.83	15.96	20.80	24.18	3.56	25.82
Al2O3	1.87	21.71	1.43	1.19	1.19	1.31	1.03	1.93	18.55	1.67
Fe2O3	77.32	32.29	68.12	69.56	69.56	78.86	73.79	68.96	43.15	68.05
MnO	0.69	0.15	0.60	0.69	0.69	0.96	0.72	0.53	0.09	0.54
MgO	0.85	11.62	2.40	1.59	1.59	1.38	0.90	1.67	8.58	1.38
CaO	0.00	0.05	0.25	0.58	0.58	0.50	0.78	0.13	0.10	0.97
NiO	0.01	0.16	0.02	0.00	0.00	0.00	0.05	0.10	0.15	0.00
ZnO2	0.45	0.31	0.03	0.00	0.00	0.24	0.24	0.12	0.18	0.01
V2O3	0.23	0.26	0.23	0.22	0.22	0.10	0.04	0.25	0.14	0.00
Cr2O3	0.00	30.18	0.02	0.07	0.07	0.00	0.02	0.04	24.70	0.00
Total	100.17	99.96	99.96	100.27	100.27	99.72	99.06	98.78	100.61	99.72

Rock	119 opq Gmass	120 opq Gmass	121 opq Gmass	122 opq Gmass	123 opq Gmass	131 opq Gmass	131 opq Gmass	134 opq Gmass	140 opq Gmass	140 opq Gmass
SiO2	0.32	0.40	0.47	0.32	0.40	0.13	0.42	0.23	0.42	0.19
TiO2	24.46	24.44	21.20	24.75	24.30	30.10	28.70	26.31	24.70	14.20
Al2O3	2.11	1.93	1.88	1.46	1.57	0.77	1.48	1.47	2.51	9.81
Fe2O3	69.65	68.69	72.48	70.06	70.28	65.82	65.50	68.76	68.22	62.38
MnO	0.88	0.75	0.80	0.86	0.57	0.87	0.81	0.48	0.55	0.55
MgO	2.96	3.37	2.88	2.88	2.93	1.61	2.59	1.56	2.09	4.57
CaO	0.01	0.31	0.00	0.09	0.44	0.13	0.10	0.25	0.47	0.00
NiO	0.00	0.04	0.00	0.00	0.03	0.00	0.12	0.00	0.10	0.00
ZnO2	0.01	0.11	0.00	0.19	0.22	0.00	0.05	0.00	0.31	0.10
V2O3	0.29	0.09	0.41	0.18	0.36	0.11	0.41	0.21	0.51	0.42
Cr2O3	0.36	0.06	0.02	0.10	0.07	0.07	0.00	0.01	0.00	9.00
Total	101.05	100.19	100.14	100.89	101.17	99.61	100.18	99.28	99.88	101.22

Rock	149 opq Gmass	152 opq Gmass	168 opq Gmass	173 opq Gmass	175 opq Gmass	199 opq Gmass	208 opq Gmass	217 opq Gmass	232 opq Gmass	238 opq Gmass
SiO2	0.84	0.34	0.53	0.37	0.43	0.62	0.47	0.59	0.27	0.17
TiO2	4.04	20.84	24.53	29.15	18.74	25.35	26.22	27.28	26.29	24.14
Al2O3	0.91	0.83	2.08	2.42	1.42	1.93	1.67	1.98	3.51	1.33
Fe2O3	91.58	76.03	69.56	64.34	77.48	0.27	67.29	64.76	65.77	69.78
MnO	0.89	0.18	0.84	0.61	0.89	0.02	0.60	0.29	0.60	0.68
MgO	0.00	1.86	1.54	2.08	0.77	68.96	2.99	2.65	3.91	2.41
CaO	0.34	0.70	0.06	0.19	0.00	1.02	0.14	0.12	0.06	0.18
NiO	0.09	0.06	0.02	0.00	0.00	1.61	0.14	0.03	0.10	0.00
ZnO2	0.00	0.00	0.09	0.08	0.28	0.23	0.00	0.00	0.00	0.21
V2O3	0.00	0.05	0.35	0.47	0.25	0.00	0.32	0.43	0.00	0.31
Cr2O3	0.00	0.00	0.00	0.10	0.10	0.16	0.37	0.40	0.00	0.21
Total	98.69	100.89	99.60	99.81	100.36	100.17	100.21	98.53	100.51	99.42

Rock	51 opq Gmass
SiO2	0.35
TiO2	26.25
Al2O3	3.37
Fe2O3	62.14
MnO	0.46
MgO	3.04
CaO	0.02
NiO	0.00
ZnO2	0.00
V2O3	0.00
Cr2O3	0.00
Total	95.63

Appendix C1.2; Analytical data for whole rocks;

The samples are grouped in order of ascending height in the stratigraphy. To search for a particular sample, therefore, the relevant height should be found in Table A1. Samples with the same height are grouped in ascending numerical order.

Analytical techniques and errors for the determinations are described in Appendix B2.

Samples that have been determined for REE using INAA techniques also have data for U and Th. Samples analysed for REE using ICP do not possess U and Th analyses.

Table C2 Whole rock analyses

	37	38
	NEBB 0	NEBB 0
SiO2	45.65	42.63
TiO2	2.71	1.73
Al2O3	14.99	8.83
Fe2O3	12.55	11.29
MnO	0.17	0.16
MgO	6.64	13.69
CaO	12.51	11.22
Na2O	2.71	1.25
K2O	0.78	0.43
P2O5	0.38	0.21
L.o.I.	2.36	2.82
Cr	194.00	922.00
Co	46.00	67.00
Ni	97.00	420.00
Cu	47.00	33.00
Zn	88.00	75.00
Rb	14.00	10.00
Sr	498.0	327.0
Y	23.0	16.0
Zr	173.0	130.0
Nb	44.0	29.0
Ba	217.0	138.0
U	1.0	0.0
Th	3.0	0.0
Ta	2.5	0.0
V	29.0	20.0
Sc	39.0	45.0
Hf	4.5	0.0
La	28.2	20.3
Ce	57.8	43.8
Pr	0.0	5.9
Nd	31.1	21.1
Sm	6.6	4.4
Eu	2.2	1.4
Gd	0.0	4.2
Dy	0.0	3.3
Ho	0.0	0.6
Er	0.0	1.7
Yb	1.9	1.3
Lu	0.3	0.2
SrI	0.702861	0.000000
NdI	0.512965	0.000000
Pb 8/4	39.841	0.000
Pb 7/4	15.759	0.000
Pb 6/4	20.442	0.000

	25	41	68	69	125	35	44	70
	NE(BB) 50	NE(BB) 50	NE(BB) 50	NE(BB) 50	NE(BB) 50	NE(BB) 150	NE(BB) 150	NE(BB) 150
SiO2	44.57	43.09	44.14	45.40	44.11	43.85	47.21	50.02
TiO2	2.94	2.61	2.31	2.66	2.73	3.64	2.84	2.36
Al2O3	14.50	12.31	11.28	14.30	12.89	16.33	17.28	16.41
Fe2O3	13.23	12.46	12.67	12.19	13.10	12.77	11.16	11.25
MnO	0.20	0.18	0.19	0.18	0.17	0.19	0.18	0.24
MgO	7.73	9.78	13.71	8.61	10.78	4.22	3.65	2.78
CaO	11.44	12.77	10.81	10.99	11.14	10.51	8.88	6.69
Na2O	3.02	2.04	1.85	2.31	2.38	3.61	4.16	4.94
K2O	1.01	0.59	0.71	0.88	0.96	1.37	1.79	2.43
P2O5	0.47	0.37	0.37	0.46	0.45	0.65	0.95	0.87
L.o.I.	1.57	4.88	1.83	2.05	1.32	2.62	3.43	1.68
Cr	241.00	542.00	928.00	359.00	457.00	0.00	8.00	0.00
Co	53.00	56.00	66.00	53.00	68.00	43.00	36.00	26.00
Ni	161.00	245.00	331.00	155.00	243.00	16.00	13.00	7.00
Cu	76.00	94.00	62.00	86.00	83.00	37.00	23.00	14.00
Zn	99.00	83.00	94.00	102.00	104.00	106.00	114.00	146.00
Rb	16.00	13.00	13.00	16.00	17.00	25.00	33.00	42.00
Sr	524.0	470.0	372.0	498.0	494.0	746.0	807.0	702.0
Y	22.0	17.0	20.0	26.0	24.0	29.0	35.0	49.0
Zr	208.0	166.0	175.0	217.0	199.0	271.0	351.0	497.0
Nb	49.0	41.0	39.0	52.0	52.0	76.0	100.0	136.0
Ba	255.0	318.0	182.0	243.0	259.0	382.0	507.0	589.0
U	0.0	0.0	1.0	0.0	0.0	0.0	0.0	0.0
Th	0.0	0.0	2.9	0.0	0.0	0.0	0.0	0.0
Ta	0.0	0.0	2.4	0.0	0.0	0.0	0.0	0.0
V	36.0	28.0	25.0	33.0	39.0	46.0	59.0	73.0
Sc	34.0	45.0	37.0	37.0	40.0	25.0	12.0	17.0
Hf	0.0	0.0	4.3	0.0	0.0	0.0	0.0	0.0
La	0.0	0.0	25.7	0.0	31.7	50.6	0.0	0.0
Ce	0.0	0.0	55.0	0.0	67.5	107.0	0.0	0.0
Pr	0.0	0.0	7.1	0.0	8.7	12.1	0.0	0.0
Nd	0.0	0.0	25.9	0.0	31.3	48.1	0.0	0.0
Sm	0.0	0.0	5.4	0.0	6.5	9.8	0.0	0.0
Eu	0.0	0.0	1.8	0.0	2.1	3.2	0.0	0.0
Gd	0.0	0.0	5.1	0.0	6.1	9.1	0.0	0.0
Dy	0.0	0.0	4.2	0.0	4.7	6.6	0.0	0.0
Ho	0.0	0.0	0.7	0.0	0.8	1.2	0.0	0.0
Er	0.0	0.0	2.0	0.0	2.3	3.3	0.0	0.0
Yb	0.0	0.0	1.6	0.0	1.8	2.4	0.0	0.0
Lu	0.0	0.0	0.2	0.0	0.3	0.4	0.0	0.0
SrI	0.000000	0.702839	0.702865	0.702818	0.702818	0.702855	0.702846	0.000000
NdI	0.000000	0.512923	0.512925	0.512923	0.512923	0.000000	0.000000	0.000000
Pb 8/4	0.000	0.000	39.870	39.754	39.820	39.873	0.000	0.000
Pb 7/4	0.000	0.000	15.735	15.711	15.724	15.788	0.000	0.000
Pb 6/4	0.000	0.000	20.554	20.448	20.440	20.607	0.000	0.000

	59	56	94	81	96	80	109	110	111	28
	NEMS 400	NEMS 300	NEMS 450	NEMS 493	NEMS 500	NEMS 541	NEMS 565	NEMS 573	NEMS 618	NEMS 642
SiO2	43.17	45.21	45.10	46.05	44.63	45.28	48.37	44.63	45.98	46.28
TiO2	2.25	3.68	3.23	3.67	3.81	3.54	3.49	3.17	3.48	3.30
Al2O3	10.60	16.03	14.68	17.04	16.87	16.06	17.34	18.49	17.56	15.64
Fe2O3	14.10	12.98	13.01	12.50	13.47	13.73	12.28	11.46	12.26	13.71
MnO	0.21	0.20	0.19	0.20	0.20	0.22	0.17	0.17	0.15	0.18
MgO	14.46	4.35	7.13	3.67	4.71	4.16	3.63	3.43	3.84	6.86
CaO	11.99	9.82	10.78	9.84	11.18	9.30	9.18	10.75	10.12	9.47
Na2O	2.02	4.25	3.05	3.30	3.00	4.96	3.89	3.82	3.63	4.01
K2O	0.77	1.53	1.17	1.61	1.09	1.93	1.60	0.50	1.61	1.28
P2O5	0.35	0.75	0.67	0.75	0.63	0.82	0.76	0.63	0.66	0.68
L.o.I.	1.17	0.70	1.15	1.64	0.49	0.79	1.19	1.47	2.11	0.08
Cr	579.00	0.00	27.00	11.00	23.00	13.00	22.00	93.00	39.00	79.00
Co	67.00	40.00	41.00	40.00	103.00	39.00	45.00	36.00	47.00	43.00
Ni	379.00	19.00	24.00	22.00	50.00	14.00	15.00	34.00	24.00	59.00
Cu	67.00	8.00	31.00	29.00	61.00	4.00	23.00	31.00	30.00	29.00
Zn	100.00	119.00	114.00	123.00	112.00	126.00	123.00	94.00	105.00	107.00
Rb	12.00	30.00	24.00	34.00	18.00	36.00	32.00	6.00	41.00	20.00
Sr	422.0	706.0	732.0	786.0	748.0	786.0	734.0	878.0	621.0	719.0
Y	19.0	32.0	47.0	31.0	49.0	34.0	33.0	24.0	29.0	28.0
Zr	156.0	311.0	296.0	292.0	229.0	344.0	305.0	246.0	338.0	260.0
Nb	39.0	84.0	81.0	79.0	66.0	97.0	86.0	69.0	60.0	70.0
Ba	205.0	393.0	404.0	675.0	544.0	459.0	408.0	373.0	343.0	334.0
U	0.0	2.2	0.0	0.0	0.0	0.0	0.0	0.0	0.0	1.9
Th	0.0	5.8	0.0	0.0	0.0	0.0	0.0	0.0	0.0	5.0
Ta	0.0	4.6	0.0	0.0	0.0	0.0	0.0	0.0	0.0	4.1
V	28.0	0.0	62.0	50.0	56.0	56.0	57.0	43.0	50.0	41.0
Sc	36.0	2.0	24.0	21.0	35.0	21.0	27.0	25.0	26.0	27.0
Hf	0.0	6.9	0.0	0.0	0.0	0.0	0.0	0.0	0.0	6.5
La	27.4	52.9	0.0	0.0	50.1	59.7	52.1	0.0	0.0	47.6
Ce	58.7	111.0	0.0	0.0	116.0	126.6	110.5	0.0	0.0	99.7
Pr	6.9	0.0	0.0	0.0	13.6	14.6	13.2	0.0	0.0	0.0
Nd	27.3	54.7	0.0	0.0	50.8	54.5	48.2	0.0	0.0	53.4
Sm	5.9	10.7	0.0	0.0	10.5	10.7	9.6	0.0	0.0	10.1
Eu	1.9	3.4	0.0	0.0	3.4	3.3	3.0	0.0	0.0	3.1
Gd	5.7	0.0	0.0	0.0	10.3	9.5	8.6	0.0	0.0	0.0
Dy	4.3	0.0	0.0	0.0	8.1	6.9	6.4	0.0	0.0	0.0
Ho	0.8	0.0	0.0	0.0	1.5	1.2	1.4	0.0	0.0	0.0
Er	2.2	0.0	0.0	0.0	4.2	3.4	3.3	0.0	0.0	0.0
Yb	1.7	2.7	0.0	0.0	3.3	2.5	2.5	0.0	0.0	2.3
Lu	0.2	0.4	0.0	0.0	0.5	0.4	0.4	0.0	0.0	0.4
SrI	0.000000	0.702859	0.000000	0.000000	0.702884	0.702826	0.702879	0.000000	0.702861	0.702926
NdI	0.000000	0.512895	0.000000	0.000000	0.000000	0.512911	0.000000	0.000000	0.512872	0.000000
Pb 8/4	0.000	39.929	0.000	0.000	0.000	39.995	39.846	0.000	39.977	39.880
Pb 7/4	0.000	15.753	0.000	0.000	0.000	15.755	15.740	0.000	15.759	15.740
Pb 6/4	0.000	20.609	0.000	0.000	0.000	20.745	20.511	0.000	20.617	20.605

	148	145	2	3	4	134	8	9	143	146
	NEMS 718	NEMS 758	NEMS 773	NEMS 800	NEMS 807	NEMS 812	NEMS 824	NEMS 1000	NEMS 1000	NEMS 1000
SiO2	48.73	46.05	45.87	45.82	45.45	46.86	45.11	45.28	53.06	47.47
TiO2	2.27	3.21	2.95	3.46	3.01	3.18	3.19	3.54	1.23	2.56
Al2O3	17.30	16.74	14.72	17.59	16.84	16.61	17.57	16.06	17.52	16.66
Fe2O3	11.99	12.27	12.59	12.00	11.75	12.58	11.56	13.73	11.42	12.74
MnO	0.21	0.19	0.20	0.19	0.19	0.18	0.15	0.22	0.26	0.25
MgO	2.32	4.84	6.97	3.68	4.35	4.22	4.65	4.75	1.84	3.17
CaO	6.86	9.31	9.53	10.35	8.96	9.43	9.76	9.30	4.95	7.77
Na2O	4.29	3.77	3.17	3.72	3.95	3.50	3.53	4.05	5.84	3.97
K2O	2.17	1.42	1.33	1.43	1.46	1.60	1.34	1.63	2.57	1.73
P2O5	1.10	0.83	0.64	0.82	0.78	0.80	0.73	0.62	0.67	1.20
L.o.I.	1.86	1.99	2.08	2.00	1.77	1.29	2.05	1.48	0.65	1.68
Cr	0.00	60.00	271.00	14.00	37.00	68.00	43.00	38.00	0.00	31.00
Co	37.00	40.00	49.00	36.00	37.00	60.00	37.00	40.00	30.00	39.00
Ni	10.00	39.00	122.00	26.00	31.00	42.00	31.00	33.00	6.00	29.00
Cu	32.00	35.00	46.00	24.00	38.00	45.00	40.00	29.00	20.00	39.00
Zn	147.00	105.00	102.00	100.00	106.00	231.00	97.00	82.00	151.00	129.00
Rb	45.00	25.00	20.00	25.00	26.00	26.00	22.00	21.00	59.00	35.00
Sr	869.0	796.0	584.0	825.0	815.0	790.0	853.0	631.0	834.0	809.0
Y	35.0	32.0	27.0	29.0	32.0	42.0	28.0	26.0	37.0	36.0
Zr	433.0	296.0	240.0	281.0	305.0	296.0	267.0	235.0	593.0	392.0
Nb	119.0	82.0	64.0	75.0	81.0	85.0	75.0	65.0	141.0	101.0
Ba	617.0	412.0	348.0	385.0	402.0	435.0	362.0	395.0	578.0	452.0
U	0.0	0.0	0.0	0.0	0.0	0.0	1.7	0.0	0.0	0.0
Th	0.0	0.0	0.0	0.0	0.0	0.0	5.2	0.0	0.0	0.0
Ta	0.0	0.0	0.0	0.0	0.0	0.0	4.2	0.0	0.0	0.0
V	68.0	55.0	46.0	48.0	54.0	52.0	46.0	42.0	67.0	66.0
Sc	12.0	24.0	26.0	25.0	21.0	31.0	21.0	21.0	6.0	16.0
Hf	0.0	0.0	0.0	0.0	0.0	0.0	6.2	0.0	0.0	0.0
La	0.0	0.0	0.0	0.0	0.0	0.0	48.3	49.3	83.4	0.0
Ce	0.0	0.0	0.0	0.0	0.0	0.0	102.0	106.4	167.3	0.0
Pr	0.0	0.0	0.0	0.0	0.0	0.0	0.0	12.8	15.5	0.0
Nd	0.0	0.0	0.0	0.0	0.0	0.0	50.0	47.4	57.8	0.0
Sm	0.0	0.0	0.0	0.0	0.0	0.0	9.9	9.5	9.8	0.0
Eu	0.0	0.0	0.0	0.0	0.0	0.0	3.1	3.0	3.0	0.0
Gd	0.0	0.0	0.0	0.0	0.0	0.0	0.0	8.5	7.9	0.0
Dy	0.0	0.0	0.0	0.0	0.0	0.0	0.0	6.3	6.1	0.0
Ho	0.0	0.0	0.0	0.0	0.0	0.0	0.0	1.1	1.1	0.0
Er	0.0	0.0	0.0	0.0	0.0	0.0	0.0	3.2	3.5	0.0
Yb	0.0	0.0	0.0	0.0	0.0	0.0	2.1	2.4	3.0	0.0
Lu	0.0	0.0	0.0	0.0	0.0	0.0	0.3	0.3	0.4	0.0
SrI	0.000000	0.000000	0.702866	0.000000	0.702946	0.703095	0.702890	0.702839	0.702886	0.000000
NdI	0.000000	0.000000	0.000000	0.000000	0.000000	0.512842	0.512922	0.000000	0.000000	0.000000
Pb 8/4	0.000	0.000	0.000	0.000	0.000	40.037	39.901	0.000	0.000	0.000
Pb 7/4	0.000	0.000	0.000	0.000	0.000	15.770	15.760	0.000	0.000	0.000
Pb 6/4	0.000	0.000	0.000	0.000	0.000	20.781	20.545	0.000	0.000	0.000

Table C2 Whole rock analyses

	23	26	27	29	64
	NE(MS) 1000	NE(MS) 1000	NE(MS) 1000	NE(MS) 1000	NE(MS) 1000
SiO2	43.55	45.34	47.75	46.88	45.11
TiO2	3.35	3.33	2.63	3.10	2.69
Al2O3	14.28	16.41	18.36	16.74	13.17
Fe2O3	14.47	12.65	10.53	12.61	12.85
MnO	0.19	0.19	0.18	0.21	0.19
MgO	8.57	6.59	2.94	3.73	10.83
CaO	10.43	10.73	8.47	8.20	12.66
Na2O	2.97	3.29	4.02	4.91	2.20
K2O	1.07	1.21	1.90	1.74	0.80
P2O5	0.54	0.58	1.05	0.92	0.43
L.o.I.	0.73	0.78	2.08	0.23	0.00
Cr	327.00	187.00	0.00	13.00	566.00
Co	60.00	50.00	30.00	35.00	58.00
Ni	159.00	95.00	20.00	12.00	233.00
Cu	51.00	34.00	32.00	30.00	89.00
Zn	112.00	108.00	107.00	121.00	94.00
Rb	20.00	22.00	33.00	37.00	13.00
Sr	611.0	687.0	894.0	802.0	447.0
Y	30.0	31.0	38.0	32.0	25.0
Zr	227.0	280.0	375.0	352.0	194.0
Nb	57.0	73.0	107.0	99.0	46.0
Ba	315.0	345.0	488.0	452.0	222.0
U	0.0	0.0	0.0	0.0	0.0
Th	0.0	0.0	0.0	0.0	0.0
Ta	0.0	0.0	0.0	0.0	0.0
V	40.0	44.0	56.0	55.0	36.0
Sc	33.0	30.0	20.0	18.0	43.0
Hf	0.0	0.0	0.0	0.0	0.0
La	0.0	40.7	0.0	60.5	52.2
Ce	0.0	86.3	0.0	129.4	110.0
Pr	0.0	10.5	0.0	14.8	13.0
Nd	0.0	38.0	0.0	54.5	49.0
Sm	0.0	7.8	0.0	10.6	10.0
Eu	0.0	2.5	0.0	3.3	3.2
Gd	0.0	7.0	0.0	9.2	9.5
Dy	0.0	5.3	0.0	6.7	6.8
Ho	0.0	0.9	0.0	1.2	1.3
Er	0.0	2.6	0.0	3.3	3.4
Yb	0.0	2.0	0.0	2.5	2.5
Lu	0.0	0.3	0.0	0.4	0.4
SrI	0.000000	0.702860	0.702982	0.702848	0.702956
NdI	0.000000	0.000000	0.512900	0.000000	0.512896
Pb 8/4	0.000	0.000	0.000	0.000	40.020
Pb 7/4	0.000	0.000	0.000	0.000	15.769
Pb 6/4	0.000	0.000	0.000	0.000	20.735

	178	177	179	232	168	212	203	202	208	209
	SWLS 1010	SWLS 1018	SWLS 1030	SWLS 1032	SWLS 1150	SWLS 1190	SWLS 1248	SWLS 1265	SWLS 1320	SWLS 1330
SiO2	44.62	44.85	46.97	44.15	48.22	46.82	46.53	45.54	45.33	45.74
TiO2	3.74	2.74	3.14	2.29	2.85	2.91	2.98	3.09	2.60	2.58
Al2O3	16.21	14.40	16.34	12.05	15.29	16.93	16.77	16.18	13.15	13.02
Fe2O3	13.56	12.73	13.07	13.08	12.99	12.31	12.37	12.79	12.40	12.60
MnO	0.19	0.17	0.22	0.18	0.19	0.23	0.21	0.20	0.18	0.19
MgO	4.59	9.81	5.32	12.72	4.42	3.68	3.42	4.83	10.07	10.34
CaO	11.20	10.86	9.25	10.65	8.05	7.82	7.85	8.35	10.79	10.77
Na2O	3.71	2.34	3.61	1.85	4.07	3.80	3.71	3.79	2.36	2.26
K2O	1.21	0.93	1.36	0.69	1.42	1.84	1.88	1.38	0.81	0.76
P2O5	0.56	0.43	0.68	0.36	0.60	0.81	0.79	0.68	0.41	0.41
L.o.I.	1.64	1.37	0.39	2.80	1.90	1.88	2.34	1.97	1.26	1.81
Cr	46.00	395.00	80.00	530.00	30.00	4.00	0.00	14.00	570.00	573.00
Co	45.00	62.00	46.00	66.00	47.00	41.00	39.00	41.00	58.00	53.00
Ni	44.00	174.00	49.00	293.00	21.00	4.00	8.00	24.00	201.00	217.00
Cu	52.00	77.00	56.00	73.00	31.00	24.00	21.00	49.00	86.00	82.00
Zn	111.00	98.00	107.00	98.00	85.00	113.00	107.00	101.00	93.00	92.00
Rb	23.00	17.00	23.00	14.00	24.00	30.00	26.00	25.00	14.00	13.00
Sr	590.0	540.0	678.0	380.0	591.0	770.0	809.0	674.0	427.0	407.0
Y	29.0	24.0	30.0	19.0	27.0	32.0	34.0	29.0	22.0	22.0
Zr	257.0	186.0	276.0	153.0	257.0	319.0	309.0	303.0	195.0	186.0
Nb	67.0	51.0	75.0	38.0	68.0	92.0	86.0	76.0	46.0	45.0
Ba	305.0	264.0	366.0	206.0	373.0	494.0	501.0	384.0	221.0	223.0
U	0.0	1.4	0.0	0.0	0.0	0.0	0.0	0.0	0.0	0.0
Th	0.0	3.6	0.0	0.0	8.0	0.0	0.0	0.0	0.0	0.0
Ta	0.0	2.8	0.0	0.0	13.0	0.0	0.0	0.0	0.0	0.0
V	41.0	32.0	45.0	28.0	43.0	54.0	54.0	48.0	0.0	0.0
Sc	33.0	40.0	27.0	36.0	23.0	16.0	16.0	26.0	0.0	0.0
Hf	0.0	4.7	0.0	0.0	0.0	0.0	0.0	0.0	0.0	0.0
La	0.0	31.8	0.0	0.0	50.2	59.8	0.0	0.0	0.0	0.0
Ce	0.0	66.7	0.0	0.0	107.7	127.0	0.0	0.0	0.0	0.0
Pr	0.0	0.0	0.0	0.0	12.4	15.1	0.0	0.0	0.0	0.0
Nd	0.0	32.3	0.0	0.0	45.8	55.6	0.0	0.0	0.0	0.0
Sm	0.0	6.8	0.0	0.0	8.9	11.1	0.0	0.0	0.0	0.0
Eu	0.0	2.3	0.0	0.0	2.8	3.5	0.0	0.0	0.0	0.0
Gd	0.0	0.0	0.0	0.0	7.8	10.1	0.0	0.0	0.0	0.0
Dy	0.0	0.0	0.0	0.0	5.9	7.2	0.0	0.0	0.0	0.0
Ho	0.0	0.0	0.0	0.0	1.1	1.4	0.0	0.0	0.0	0.0
Er	0.0	0.0	0.0	0.0	3.0	3.7	0.0	0.0	0.0	0.0
Yb	0.0	1.8	0.0	0.0	2.4	2.8	0.0	0.0	0.0	0.0
Lu	0.0	0.3	0.0	0.0	0.4	0.4	0.0	0.0	0.0	0.0
SrI	0.702849	0.702929	0.000000	0.000000	0.702839	0.000000	0.000000	0.000000	0.702884	0.000000
NdI	0.000000	0.000000	0.000000	0.000000	0.512909	0.512894	0.512854	0.000000	0.000000	0.000000
Pb 8/4	0.000	0.000	0.000	0.000	40.072	0.000	40.065	0.000	0.000	0.000
Pb 7/4	0.000	0.000	0.000	0.000	15.783	0.000	15.789	0.000	0.000	0.000
Pb 6/4	0.000	0.000	0.000	0.000	20.764	0.000	20.741	0.000	0.000	0.000

Table C2 Whole rock analyses

	186	184	215	217	220	218	190	222	223	224
	SWLS 1340	SWLS 1360	SWLS 1380	SWLS 1400	SWLS 1415	SWLS 1420	SWLS 1845	SWLS 1900	SWLS 1940	SWLS 1958
SiO2	44.64	44.78	44.64	45.22	42.55	46.78	45.11	42.82	46.88	44.10
TiO2	2.54	2.47	3.57	3.20	3.72	3.41	2.77	2.61	3.08	2.39
Al2O3	12.87	12.73	12.92	17.08	15.61	17.57	14.20	11.86	15.98	12.65
Fe2O3	12.39	12.31	14.68	11.88	13.27	12.53	12.24	12.67	12.35	11.94
MnO	0.18	0.19	0.21	0.17	0.21	0.18	0.18	0.22	0.18	0.18
MgO	9.82	10.68	10.32	5.19	5.47	4.83	8.75	9.97	3.69	10.16
CaO	10.89	10.67	11.49	10.39	10.69	10.69	11.43	12.66	8.21	11.53
Na2O	2.12	1.92	2.52	2.91	2.41	3.03	2.43	1.80	3.64	1.85
K2O	0.78	0.73	0.95	1.11	1.18	1.18	0.93	0.66	1.66	0.70
P2O5	0.43	0.42	0.46	0.51	0.62	0.58	0.46	0.37	0.82	0.39
L.o.I.	2.34	2.50	1.47	2.62	0.00	1.98	1.52	4.46	1.81	2.41
Cr	553.00	605.00	310.00	73.00	101.00	69.00	402.00	623.00	3.00	598.00
Co	60.00	56.00	59.00	45.00	50.00	42.00	50.00	62.00	37.00	54.00
Ni	214.00	229.00	189.00	49.00	73.00	47.00	190.00	250.00	5.00	215.00
Cu	88.00	88.00	58.00	97.00	73.00	48.00	75.00	47.00	22.00	77.00
Zn	93.00	109.00	95.00	97.00	102.00	105.00	91.00	92.00	122.00	89.00
Rb	14.00	14.00	15.00	21.00	27.00	20.00	19.00	10.00	29.00	13.00
Sr	429.0	403.0	534.0	642.0	689.0	639.0	524.0	467.0	675.0	419.0
Y	23.0	22.0	22.0	24.0	29.0	25.0	23.0	20.0	37.0	22.0
Zr	187.0	190.0	194.0	242.0	268.0	240.0	199.0	153.0	346.0	173.0
Nb	43.0	45.0	48.0	61.0	71.0	63.0	54.0	39.0	96.0	41.0
Ba	224.0	211.0	247.0	293.0	503.0	318.0	271.0	224.0	463.0	205.0
U	0.0	0.0	0.0	0.0	0.0	0.0	0.0	0.0	0.0	0.0
Th	0.0	0.0	0.0	0.0	0.0	0.0	0.0	0.0	0.0	0.0
Ta	0.0	0.0	0.0	0.0	0.0	0.0	0.0	0.0	0.0	0.0
V	35.0	33.0	36.0	39.0	0.0	44.0	34.0	46.0	60.0	31.0
Sc	38.0	38.0	41.0	26.0	0.0	30.0	36.0	30.0	17.0	36.0
Hf	0.0	0.0	0.0	0.0	0.0	0.0	0.0	0.0	0.0	0.0
La	0.0	31.5	33.8	0.0	0.0	43.6	37.5	0.0	0.0	0.0
Ce	0.0	68.3	72.2	0.0	0.0	93.0	79.6	0.0	0.0	0.0
Pr	0.0	8.2	8.7	0.0	0.0	10.3	11.6	0.0	0.0	0.0
Nd	0.0	32.2	33.9	0.0	0.0	42.4	36.3	0.0	0.0	0.0
Sm	0.0	7.0	7.3	0.0	0.0	8.8	7.5	0.0	0.0	0.0
Eu	0.0	2.3	2.4	0.0	0.0	2.9	2.4	0.0	0.0	0.0
Gd	0.0	6.7	7.0	0.0	0.0	8.5	7.2	0.0	0.0	0.0
Dy	0.0	5.0	5.1	0.0	0.0	6.2	5.2	0.0	0.0	0.0
Ho	0.0	0.9	1.0	0.0	0.0	1.2	1.0	0.0	0.0	0.0
Er	0.0	2.5	2.6	0.0	0.0	3.2	2.7	0.0	0.0	0.0
Yb	0.0	1.9	1.9	0.0	0.0	2.4	1.9	0.0	0.0	0.0
Lu	0.0	0.3	0.3	0.0	0.0	0.4	0.3	0.0	0.0	0.0
SrI	0.000000	0.702844	0.702828	0.702831	0.000000	0.702849	0.702868	0.000000	0.000000	0.000000
NdI	0.000000	0.000000	0.512824	0.512879	0.000000	0.000000	0.512873	0.000000	0.000000	0.000000
Pb 8/4	0.000	0.000	40.093	0.000	0.000	40.070	40.058	0.000	0.000	0.000
Pb 7/4	0.000	0.000	15.795	0.000	0.000	15.793	15.796	0.000	0.000	0.000
Pb 6/4	0.000	0.000	20.839	0.000	0.000	20.745	20.586	0.000	0.000	0.000

	237	238	194
	SWLS 1983	SWLS 1988	SWLS 2050
SiO2	46.10	46.21	45.81
TiO2	2.59	2.31	3.57
Al2O3	14.06	12.18	16.86
Fe2O3	12.58	12.56	12.29
MnO	0.17	0.18	0.18
MgO	8.14	11.92	3.85
CaO	10.53	10.36	9.89
Na2O	2.61	2.11	3.30
K2O	0.81	0.82	1.34
P2O5	0.40	0.38	0.68
L.o.I.	2.56	1.77	1.08
Cr	385.00	763.00	585.00
Co	60.00	60.00	59.00
Ni	175.00	271.00	237.00
Cu	65.00	54.00	51.00
Zn	103.00	93.00	107.00
Rb	16.00	11.00	17.00
Sr	418.0	343.0	693.0
Y	22.0	22.0	20.0
Zr	176.0	184.0	224.0
Nb	42.0	42.0	63.0
Ba	211.0	201.0	347.0
U	0.0	0.8	0.0
Th	0.0	2.9	0.0
Ta	0.0	2.4	0.0
V	32.0	46.0	46.0
Sc	35.0	25.0	35.0
Hf	0.0	4.4	0.0
La	25.6	26.6	0.0
Ce	54.6	57.4	0.0
Pr	7.2	0.0	0.0
Nd	26.5	27.9	0.0
Sm	5.8	6.1	0.0
Eu	1.9	2.0	0.0
Gd	5.6	0.0	0.0
Dy	4.5	0.0	0.0
Ho	0.8	0.0	0.0
Er	2.2	0.0	0.0
Yb	1.8	1.8	0.0
Lu	0.3	0.2	0.0
SrI	0.702834	0.702891	0.000000
NdI	0.512963	0.512943	0.000000
Pb 8/4	39.822	39.840	0.000
Pb 7/4	15.744	15.749	0.000
Pb 6/4	20.488	20.518	0.000

Table C2 Whole rock analyses

	193	207	216
	SW(LS) 2150	SW(LS) 2150	SW(LS) 2150
SiO2	45.44	44.62	45.60
TiO2	2.59	2.37	3.23
Al2O3	13.54	11.59	15.59
Fe2O3	12.69	12.92	13.57
MnO	0.17	0.19	0.19
MgO	9.22	12.73	6.36
CaO	10.98	11.21	9.91
Na2O	2.49	1.89	3.72
K2O	0.35	0.70	0.52
P2O5	0.40	0.36	0.49
L.o.I.	0.93	0.81	0.60
Cr	229.00	784.00	136.00
Co	48.00	60.00	52.00
Ni	92.00	276.00	82.00
Cu	51.00	58.00	69.00
Zn	121.00	92.00	108.00
Rb	27.00	12.00	1.00
Sr	575.0	389.0	583.0
Y	31.0	20.0	26.0
Zr	330.0	168.0	228.0
Nb	82.0	40.0	54.0
Ba	376.0	214.0	268.0
U	0.0	0.0	0.0
Th	0.0	0.0	0.0
Ta	0.0	0.0	0.0
V	74.0	31.0	38.0
Sc	8.0	41.0	34.0
Hf	0.0	0.0	0.0
La	0.0	0.0	0.0
Ce	0.0	0.0	0.0
Pr	0.0	0.0	0.0
Nd	0.0	0.0	0.0
Sm	0.0	0.0	0.0
Eu	0.0	0.0	0.0
Gd	0.0	0.0	0.0
Dy	0.0	0.0	0.0
Ho	0.0	0.0	0.0
Er	0.0	0.0	0.0
Yb	0.0	0.0	0.0
Lu	0.0	0.0	0.0
SrI	0.000000	0.000000	0.702847
NdI	0.000000	0.000000	0.512885
Pb 8/4	0.000	0.000	39.881
Pb 7/4	0.000	0.000	15.717
Pb 6/4	0.000	0.000	20.654

	173	113	114	115	117	120	122	121	123	119
	SWMS 2180	SWMS 2250	SWMS 2275	SWMS 2298	SWMS 2370	SWMS 2421	SWMS 2428	SWMS 2470	SWMS 2543	SWMS 2581
SiO2	45.07	45.47	50.86	51.30	47.11	45.19	47.00	49.68	45.29	46.96
TiO2	1.97	2.44	1.86	1.86	3.14	3.08	3.17	2.61	3.45	2.99
Al2O3	9.44	11.47	17.32	16.86	16.55	15.23	16.45	17.05	16.08	16.92
Fe2O3	12.40	12.77	11.42	11.75	13.13	13.13	12.98	12.84	13.46	12.46
MnO	0.17	0.16	0.19	0.25	0.19	0.19	0.20	0.17	0.21	0.20
MgO	13.26	13.09	2.56	2.27	4.95	6.95	4.40	2.78	4.64	4.53
CaO	11.75	11.36	6.21	6.03	8.83	9.64	8.42	6.80	8.87	8.25
Na2O	2.03	2.48	5.69	4.78	3.41	3.04	3.65	4.38	3.42	4.16
K2O	0.68	0.77	2.20	2.22	1.30	0.96	1.50	1.86	1.34	1.63
P2O5	0.33	0.37	0.85	0.91	0.68	0.50	0.74	0.96	0.69	0.80
L.o.I.	1.24	0.53	0.98	1.64	1.19	1.41	1.08	0.95	0.90	1.47
Cr	952.00	801.00	0.00	0.00	78.00	190.00	47.00	0.00	11.00	14.00
Co	73.00	75.00	41.00	35.00	44.00	54.00	42.00	54.00	47.00	43.00
Ni	392.00	328.00	2.00	9.00	49.00	94.00	36.00	5.00	28.00	23.00
Cu	88.00	40.00	14.00	17.00	52.00	65.00	49.00	27.00	46.00	40.00
Zn	97.00	90.00	142.00	137.00	104.00	100.00	111.00	122.00	125.00	108.00
Rb	14.00	13.00	46.00	43.00	22.00	18.00	28.00	36.00	25.00	30.00
Sr	410.0	395.0	800.0	718.0	675.0	540.0	647.0	684.0	804.0	653.0
Y	20.0	19.0	36.0	46.0	34.0	25.0	37.0	33.0	36.0	32.0
Zr	155.0	177.0	449.0	435.0	282.0	214.0	324.0	379.0	293.0	318.0
Nb	42.0	42.0	125.0	112.0	76.0	52.0	86.0	102.0	83.0	88.0
Ba	430.0	201.0	552.0	572.0	377.0	247.0	421.0	534.0	369.0	430.0
U	0.8	0.0	0.0	0.0	0.0	0.0	0.0	0.0	0.0	0.0
Th	2.9	0.0	0.0	0.0	0.0	0.0	0.0	0.0	0.0	0.0
Ta	2.3	0.0	0.0	0.0	0.0	0.0	0.0	0.0	0.0	0.0
V	35.0	28.0	59.0	68.0	51.0	39.0	57.0	56.0	44.0	46.0
Sc	46.0	46.0	12.0	9.0	27.0	35.0	23.0	14.0	22.0	18.0
Hf	3.9	0.0	0.0	0.0	0.0	0.0	0.0	0.0	0.0	0.0
La	28.0	29.4	0.0	0.0	0.0	32.5	0.0	0.0	54.8	60.8
Ce	57.1	63.6	0.0	0.0	0.0	70.2	0.0	0.0	114.0	122.8
Pr	0.0	7.6	0.0	0.0	0.0	8.9	0.0	0.0	13.5	14.0
Nd	32.0	30.3	0.0	0.0	0.0	32.7	0.0	0.0	50.1	49.5
Sm	6.0	6.7	0.0	0.0	0.0	6.9	0.0	0.0	10.2	9.3
Eu	2.0	2.1	0.0	0.0	0.0	2.3	0.0	0.0	3.3	2.8
Gd	0.0	6.4	0.0	0.0	0.0	6.5	0.0	0.0	8.8	8.1
Dy	0.0	4.8	0.0	0.0	0.0	5.0	0.0	0.0	7.1	6.1
Ho	0.0	0.9	0.0	0.0	0.0	0.9	0.0	0.0	1.4	1.1
Er	0.0	2.4	0.0	0.0	0.0	2.5	0.0	0.0	3.7	3.2
Yb	1.6	1.8	0.0	0.0	0.0	2.0	0.0	0.0	2.8	2.5
Lu	0.2	0.3	0.0	0.0	0.0	0.3	0.0	0.0	0.4	0.4
SrI	0.702929	0.702903	0.702876	0.000000	0.702890	0.702821	0.000000	0.702873	0.702905	0.702869
NdI	0.512909	0.512898	0.512895	0.000000	0.000000	0.512889	0.000000	0.512854	0.512900	0.512878
Pb 8/4	0.000	0.000	39.940	0.000	40.085	0.000	0.000	0.000	0.000	40.104
Pb 7/4	0.000	0.000	15.757	0.000	15.786	0.000	0.000	0.000	0.000	15.780
Pb 6/4	0.000	0.000	20.620	0.000	20.831	0.000	0.000	0.000	0.000	20.824

Table C2 Whole rock analyses

	13	118	11	16	17	18	14	107	104	22
	SWMS 2603	SWMS 2613	SWMS 2623	SWMS 2697	SWMS 2756	SWMS 2783	SWMS 2930	SWMS 2950	SWMS 2977	SWMS 3000
SiO2	43.42	45.56	50.48	51.22	49.85	48.59	49.86	48.10	49.27	44.24
TiO2	3.09	2.94	1.57	2.21	2.42	2.54	2.87	2.78	3.09	3.49
Al2O3	13.11	14.34	16.83	16.28	16.64	16.67	17.03	16.95	18.19	16.95
Fe2O3	14.30	13.34	11.46	11.22	12.34	12.89	14.38	12.40	13.27	12.78
MnO	0.16	0.18	0.28	0.20	0.21	0.25	0.23	0.24	0.17	0.19
MgO	8.81	7.19	2.40	5.23	5.34	3.52	4.10	3.47	2.81	4.81
CaO	10.80	11.40	5.54	8.08	8.13	7.26	6.89	7.83	6.73	10.16
Na2O	2.65	2.45	5.03	4.46	4.19	4.39	5.04	4.12	3.69	2.12
K2O	0.93	0.92	2.49	2.34	1.87	1.95	2.16	1.94	1.81	0.98
P2O5	0.44	0.48	0.84	0.44	0.80	0.98	1.05	1.24	0.86	0.57
L.o.I.	1.44	1.54	0.87	2.06	0.00	0.81	0.67	0.25	2.75	3.60
Cr	699.00	368.00	0.00	296.00	453.00	0.00	20.00	0.00	0.00	34.00
Co	61.00	56.00	29.00	54.00	50.00	36.00	43.00	33.00	34.00	46.00
Ni	298.00	175.00	6.00	145.00	191.00	9.00	28.00	8.00	16.00	36.00
Cu	72.00	67.00	18.00	68.00	57.00	30.00	33.00	28.00	36.00	44.00
Zn	98.00	102.00	130.00	89.00	111.00	129.00	126.00	125.00	115.00	106.00
Rb	12.00	15.00	49.00	12.00	43.00	38.00	44.00	32.00	30.00	9.00
Sr	443.0	522.0	794.0	499.0	601.0	738.0	1047.0	884.0	848.0	877.0
Y	22.0	32.0	36.0	23.0	28.0	37.0	38.0	43.0	68.0	28.0
Zr	190.0	204.0	475.0	187.0	373.0	383.0	462.0	377.0	345.0	234.0
Nb	47.0	49.0	126.0	46.0	97.0	105.0	122.0	105.0	98.0	59.0
Ba	225.0	297.0	559.0	260.0	449.0	482.0	611.0	546.0	524.0	333.0
U	0.9	1.4	0.0	0.0	0.0	0.0	0.0	0.0	0.0	0.0
Th	3.2	3.5	0.0	0.0	0.0	0.0	0.0	0.0	0.0	0.0
Ta	2.6	2.9	0.0	0.0	0.0	0.0	0.0	0.0	0.0	0.0
V	33.0	44.0	64.0	35.0	0.0	60.0	62.0	67.0	61.0	0.0
Sc	39.0	34.0	7.0	37.0	0.0	16.0	12.0	15.0	27.0	0.0
Hf	4.6	4.9	0.0	0.0	0.0	0.0	0.0	0.0	0.0	0.0
La	29.3	42.7	0.0	0.0	0.0	0.0	80.6	0.0	0.0	0.0
Ce	62.5	90.4	0.0	0.0	0.0	0.0	168.7	0.0	0.0	0.0
Pr	71.9	0.0	0.0	0.0	0.0	0.0	17.1	0.0	0.0	0.0
Nd	28.1	47.8	0.0	0.0	0.0	0.0	64.5	0.0	0.0	0.0
Sm	5.9	9.1	0.0	0.0	0.0	0.0	11.6	0.0	0.0	0.0
Eu	1.9	3.0	0.0	0.0	0.0	0.0	3.7	0.0	0.0	0.0
Gd	5.5	0.0	0.0	0.0	0.0	0.0	9.7	0.0	0.0	0.0
Dy	4.2	0.0	0.0	0.0	0.0	0.0	7.1	0.0	0.0	0.0
Ho	0.7	0.0	0.0	0.0	0.0	0.0	1.3	0.0	0.0	0.0
Er	2.1	0.0	0.0	0.0	0.0	0.0	3.7	0.0	0.0	0.0
Yb	1.6	2.4	0.0	0.0	0.0	0.0	2.9	0.0	0.0	0.0
Lu	0.2	0.3	0.0	0.0	0.0	0.0	0.4	0.0	0.0	0.0
SrI	0.702892	0.000000	0.702935	0.000000	0.702909	0.702825	0.702934	0.000000	0.000000	0.000000
NdI	0.512895	0.000000	0.512870	0.000000	0.512865	0.512896	0.512870	0.000000	0.000000	0.000000
Pb 8/4	40.057	0.000	0.000	0.000	0.000	0.000	40.016	0.000	0.000	0.000
Pb 7/4	15.768	0.000	0.000	0.000	0.000	0.000	15.775	0.000	0.000	0.000
Pb 6/4	20.764	0.000	0.000	0.000	0.000	0.000	20.736	0.000	0.000	0.000

	106	131	175	176	195
	SWMS 3091	SWMS 3400	SWMS 3400	SWMS 3400	SWMS 3400
SiO2	54.06	48.95	53.10	53.99	49.92
TiO2	1.98	2.70	0.96	1.93	1.91
Al2O3	14.53	17.28	17.16	17.27	16.68
Fe2O3	12.14	12.64	8.40	9.06	12.51
MnO	0.21	0.17	0.17	0.14	0.24
MgO	3.11	3.08	2.02	2.05	2.55
CaO	6.61	6.81	3.38	3.16	6.29
Na2O	4.00	4.22	6.68	5.29	5.13
K2O	1.69	1.76	3.19	2.89	2.14
P2O5	1.02	0.90	0.60	0.49	1.10
L.o.I.	0.65	1.46	0.54	0.00	0.00
Cr	1.00	0.00	0.00	23.00	0.00
Co	54.00	44.00	25.00	28.00	35.00
Ni	10.00	10.00	10.00	28.00	7.00
Cu	34.00	18.00	8.00	22.00	19.00
Zn	134.00	109.00	122.00	90.00	140.00
Rb	42.00	30.00	82.00	75.00	53.00
Sr	753.0	748.0	773.0	1079.0	696.0
Y	37.0	76.0	34.0	34.0	40.0
Zr	409.0	367.0	674.0	584.0	456.0
Nb	112.0	100.0	175.0	163.0	118.0
Ba	492.0	963.0	575.0	1752.0	583.0
U	0.0	0.0	5.4	0.0	0.0
Th	0.0	0.0	21.0	0.0	0.0
Ta	0.0	0.0	10.5	0.0	0.0
V	69.0	122.0	65.0	79.0	0.0
Sc	12.0	16.0	4.0	10.0	0.0
Hf	0.0	0.0	14.1	0.0	0.0
La	80.5	0.0	88.8	0.0	0.0
Ce	168.9	0.0	162.1	0.0	0.0
Pr	17.9	0.0	16.3	0.0	0.0
Nd	67.1	0.0	50.7	0.0	0.0
Sm	12.0	0.0	8.2	0.0	0.0
Eu	3.5	0.0	2.3	0.0	0.0
Gd	10.0	0.0	6.5	0.0	0.0
Dy	7.3	0.0	5.1	0.0	0.0
Ho	1.3	0.0	0.9	0.0	0.0
Er	3.9	0.0	2.9	0.0	0.0
Yb	2.9	0.0	2.6	0.0	0.0
Lu	0.4	0.0	0.4	0.0	0.0
SrI	0.702917	0.702896	0.703010	0.704571	0.000000
NdI	0.512854	0.000000	0.512872	0.000000	0.000000
Pb 8/4	40.051	0.000	40.154	0.000	0.000
Pb 7/4	15.779	0.000	15.804	0.000	0.000
Pb 6/4	20.721	0.000	20.801	0.000	0.000

Table C2 Whole rock analyses

	20	199	200
	SW(MS) 3100	SW(MS) 3100	SW(MS) 3100
SiO2	45.18	45.73	44.46
TiO2	2.65	3.61	3.43
Al2O3	12.04	16.08	15.36
Fe2O3	13.79	13.26	13.93
MnO	0.19	0.20	0.19
MgO	10.71	5.25	6.42
CaO	11.21	9.34	10.28
Na2O	2.01	3.69	2.94
K2O	0.71	1.35	1.12
P2O5	0.36	0.69	0.50
L.o.I.	3.07	0.49	1.12
Cr	606.00	26.00	93.00
Co	62.00	41.00	54.00
Ni	201.00	38.00	80.00
Cu	53.00	42.00	65.00
Zn	97.00	113.00	112.00
Rb	9.00	26.00	21.00
Sr	387.0	655.0	573.0
Y	30.0	30.0	25.0
Zr	163.0	280.0	209.0
Nb	37.0	76.0	54.0
Ba	225.0	389.0	271.0
U	0.0	1.6	0.0
Th	0.0	5.3	0.0
Ta	0.0	4.3	0.0
V	38.0	0.0	36.0
Sc	46.0	0.0	31.0
Hf	0.0	6.3	0.0
La	0.0	46.3	0.0
Ce	0.0	93.5	0.0
Pr	0.0	0.0	0.0
Nd	0.0	46.8	0.0
Sm	0.0	9.4	0.0
Eu	0.0	3.1	0.0
Gd	0.0	0.0	0.0
Dy	0.0	0.0	0.0
Ho	0.0	0.0	0.0
Er	0.0	0.0	0.0
Yb	0.0	2.5	0.0
Lu	0.0	0.4	0.0
SrI	0.000000	0.000000	0.000000
NdI	0.000000	0.000000	0.000000
Pb 8/4	0.000	0.000	0.000
Pb 7/4	0.000	0.000	0.000
Pb 6/4	0.000	0.000	0.000

	139	140	141	74	75	76	62	63
	SWDS 3100	SWDS 3100	SWDS 3100	SWDS 3175	SWDS 3195	SWDS 3215	SWDS 3305	SWDS 3350
SiO2	44.32	44.31	46.20	45.12	44.33	45.99	54.29	55.18
TiO2	3.16	3.19	3.15	3.29	3.08	3.32	0.80	0.80
Al2O3	13.31	13.88	17.40	15.23	14.64	16.69	17.56	17.68
Fe2O3	14.67	15.21	12.54	13.04	13.11	13.15	10.11	10.41
MnO	0.17	0.16	0.15	0.19	0.20	0.20	0.28	0.26
MgO	8.97	7.08	4.88	6.50	7.80	5.20	1.58	1.41
CaO	11.09	10.03	11.27	9.81	10.24	9.17	3.98	4.11
Na2O	2.73	1.65	3.30	2.98	2.54	3.54	5.91	5.87
K2O	0.95	0.82	1.01	0.88	1.10	1.39	2.78	2.88
P2O5	0.46	0.39	0.50	0.58	0.58	0.66	0.39	0.36
L.o.I.	0.17	3.30	0.47	1.66	2.17	1.56	2.12	2.30
Cr	437.00	404.00	128.00	151.00	237.00	12.00	0.00	0.00
Co	69.00	61.00	49.00	46.00	46.00	49.00	21.00	24.00
Ni	241.00	190.00	73.00	84.00	103.00	38.00	5.00	4.00
Cu	83.00	33.00	63.00	67.00	63.00	21.00	13.00	0.00
Zn	110.00	145.00	107.00	112.00	101.00	109.00	135.00	140.00
Rb	18.00	12.00	17.00	21.00	18.00	25.00	69.00	63.00
Sr	541.0	451.0	656.0	581.0	562.0	734.0	672.0	731.0
Y	25.0	178.0	30.0	30.0	28.0	27.0	37.0	38.0
Zr	193.0	204.0	205.0	264.0	245.0	275.0	640.0	640.0
Nb	51.0	52.0	54.0	66.0	68.0	71.0	162.0	169.0
Ba	276.0	437.0	274.0	327.0	307.0	362.0	702.0	827.0
U	3.7	1.1	0.0	1.8	0.0	0.0	0.0	3.0
Th	1.1	3.6	6.0	4.5	0.0	0.0	0.0	13.1
Ta	2.9	2.9	16.0	3.7	0.0	0.0	0.0	8.4
V	38.0	0.0	39.0	39.0	39.0	0.0	63.0	66.0
Sc	41.0	8.0	34.0	30.0	32.0	0.0	3.0	7.0
Hf	5.1	5.0	0.0	5.9	0.0	0.0	0.0	12.5
La	32.7	37.8	0.0	41.6	41.3	0.0	89.5	95.8
Ce	67.5	82.1	0.0	83.4	87.3	0.0	172.7	173.0
Pr	0.0	11.6	0.0	0.0	10.6	0.0	18.4	0.0
Nd	34.8	48.0	0.0	41.6	38.3	0.0	58.5	65.2
Sm	7.6	13.3	0.0	8.9	7.6	0.0	9.8	11.3
Eu	2.4	4.7	0.0	2.8	2.4	0.0	2.9	3.4
Gd	0.0	18.0	0.0	0.0	6.9	0.0	7.8	0.0
Dy	0.0	17.6	0.0	0.0	5.2	0.0	6.4	0.0
Ho	0.0	4.0	0.0	0.0	0.9	0.0	1.2	0.0
Er	0.0	12.7	0.0	0.0	2.7	0.0	3.6	0.0
Yb	1.8	12.7	0.0	2.2	2.1	0.0	3.2	3.4
Lu	0.3	2.0	0.0	0.3	0.3	0.0	0.5	0.5
SrI	0.702865	0.702831	0.702828	0.702902	0.702894	0.703003	0.702969	0.703083
NdI	0.512885	0.512921	0.000000	0.512871	0.512898	0.000000	0.000000	0.512879
Pb 8/4	39.850	0.000	0.000	40.113	40.104	0.000	0.000	40.059
Pb 7/4	15.739	0.000	0.000	15.786	15.789	0.000	0.000	15.796
Pb 6/4	20.491	0.000	0.000	20.809	20.844	0.000	0.000	20.818

Table C2 Whole rock analyses

	83	85	86	87	92	93
	SWLF 3450	SWLF 3450	SWLF 3450	SWLF 3450	SWLF 3450	SWLF 3450
SiO2	54.00	46.94	47.67	43.35	58.02	57.02
TiO2	1.14	2.76	2.89	2.98	0.24	0.25
Al2O3	18.32	16.12	16.03	14.28	18.87	18.72
Fe2O3	10.66	12.74	12.99	12.70	7.46	7.77
MnO	0.19	0.22	0.18	0.19	0.28	0.25
MgO	0.88	4.14	5.73	7.76	0.30	0.41
CaO	2.97	8.35	9.29	9.98	2.16	2.66
Na2O	5.80	3.72	4.03	2.36	7.86	7.63
K2O	2.67	1.50	1.43	1.06	3.61	3.90
P2O5	0.96	0.82	0.69	0.56	0.15	0.15
L.o.I.	2.14	0.79	0.13	2.19	1.83	1.31
Cr	0.00	73.00	158.00	152.00	0.00	0.00
Co	58.00	46.00	56.00	67.00	33.00	28.00
Ni	8.00	49.00	75.00	84.00	4.00	5.00
Cu	18.00	52.00	24.00	55.00	10.00	12.00
Zn	118.00	128.00	116.00	340.00	159.00	153.00
Rb	66.00	31.00	27.00	27.00	109.00	112.00
Sr	848.0	681.0	643.0	649.0	460.0	490.0
Y	42.0	35.0	31.0	32.0	42.0	38.0
Zr	612.0	329.0	300.0	298.0	849.0	841.0
Nb	144.0	88.0	81.0	79.0	170.0	163.0
Ba	724.0	407.0	367.0	442.0	665.0	679.0
U	0.0	0.0	0.0	1.9	0.0	0.0
Th	0.0	0.0	0.0	5.8	0.0	0.0
Ta	0.0	0.0	0.0	4.2	0.0	0.0
V	78.0	51.0	45.0	48.0	60.0	65.0
Sc	6.0	22.0	29.0	25.0	2.0	2.0
Hf	0.0	0.0	0.0	6.7	0.0	0.0
La	0.0	0.0	50.2	52.3	0.0	108.0
Ce	0.0	0.0	104.3	98.9	0.0	192.0
Pr	0.0	0.0	72.3	0.0	0.0	18.2
Nd	0.0	0.0	43.7	49.2	0.0	54.0
Sm	0.0	0.0	8.5	9.6	0.0	8.0
Eu	0.0	0.0	2.6	3.0	0.0	2.0
Gd	0.0	0.0	7.5	0.0	0.0	6.0
Dy	0.0	0.0	5.7	0.0	0.0	5.8
Ho	0.0	0.0	1.0	0.0	0.0	1.2
Er	0.0	0.0	2.9	0.0	0.0	3.8
Yb	0.0	0.0	2.3	2.5	0.0	3.7
Lu	0.0	0.0	0.3	0.4	0.0	0.6
SrI	0.703517	0.702837	0.702933	0.000000	0.703131	0.702965
NdI	0.512880	0.512854	0.000000	0.512901	0.512857	0.512901
Pb 8/4	0.000	40.055	40.134	0.000	0.000	40.116
Pb 7/4	0.000	15.767	15.806	0.000	0.000	15.790
Pb 6/4	0.000	20.846	20.823	0.000	0.000	20.858

	99	103	116	129	149	150	151	152	153	156
	SWLI 3600	SWLI 3600	SWLI 3600	SWLI 3600	SWLI 3600	SWLI 3600	SWLI 3600	SWLI 3600	SWLI 3600	SWLI 3600
SiO2	60.55	59.74	60.85	57.08	59.78	58.11	59.30	52.99	58.75	62.15
TiO2	0.37	0.07	0.31	0.51	0.07	0.03	0.08	0.75	0.04	0.20
Al2O3	18.03	19.37	17.73	18.07	19.25	18.78	19.22	13.56	19.09	17.83
Fe2O3	7.15	4.33	7.08	9.12	4.35	3.63	4.39	7.73	4.26	4.61
MnO	0.13	0.17	0.11	0.23	0.17	0.18	0.22	0.22	0.19	0.20
MgO	0.23	0.02	0.32	0.51	0.00	0.00	0.08	0.91	0.16	0.11
CaO	1.64	0.90	1.53	3.14	0.88	0.48	0.78	2.99	0.89	0.85
Na2O	6.21	9.09	6.32	7.50	9.08	8.81	7.26	4.85	8.71	6.40
K2O	4.18	4.98	4.11	3.54	4.95	4.75	4.99	2.33	5.13	5.48
P2O5	0.13	0.05	0.11	0.23	0.05	0.06	0.07	0.28	0.05	0.09
L.o.I.	1.32	1.63	1.59	0.90	1.50	3.12	2.53	1.01	1.50	0.79
Cr	0.00	0.00	0.00	0.00	0.00	0.00	0.00	0.00	0.00	0.00
Co	17.00	22.00	17.00	29.00	9.00	10.00	10.00	36.00	11.00	14.00
Ni	9.00	5.00	5.00	2.00	0.00	4.00	5.00	6.00	5.00	5.00
Cu	5.00	3.00	5.00	13.00	0.00	5.00	6.00	10.00	5.00	7.00
Zn	181.00	140.00	142.00	129.00	178.00	201.00	190.00	137.00	207.00	136.00
Rb	138.00	94.00	94.00	87.00	170.00	172.00	159.00	60.00	197.00	166.00
Sr	276.0	150.0	277.0	527.0	36.0	14.0	77.0	598.0	20.0	79.0
Y	185.0	54.0	53.0	39.0	40.0	47.0	36.0	48.0	51.0	40.0
Zr	901.0	916.0	893.0	767.0	1197.0	1436.0	1127.0	622.0	1478.0	1173.0
Nb	214.0	222.0	203.0	180.0	157.0	167.0	153.0	159.0	198.0	213.0
Ba	1095.0	967.0	903.0	740.0	311.0	61.0	408.0	752.0	6.0	323.0
U	0.0	0.0	0.0	0.0	8.8	0.0	0.0	0.0	0.0	0.0
Th	0.0	0.0	0.0	0.0	33.0	0.0	0.0	0.0	0.0	0.0
Ta	0.0	0.0	0.0	0.0	11.3	0.0	0.0	0.0	0.0	0.0
V	137.0	0.0	96.0	64.0	57.0	70.0	66.0	68.0	77.0	0.0
Sc	2.0	0.0	2.0	3.0	0.0	3.0	2.0	6.0	0.0	0.0
Hf	0.0	0.0	0.0	0.0	19.5	0.0	0.0	0.0	0.0	0.0
La	0.0	115.5	0.0	0.0	134.2	0.0	0.0	89.6	0.0	0.0
Ce	0.0	224.8	0.0	0.0	208.1	0.0	0.0	185.1	0.0	0.0
Pr	0.0	23.4	0.0	0.0	18.2	0.0	0.0	17.6	0.0	0.0
Nd	0.0	73.5	0.0	0.0	46.0	0.0	0.0	66.7	0.0	0.0
Sm	0.0	12.8	0.0	0.0	6.2	0.0	0.0	12.0	0.0	0.0
Eu	0.0	2.9	0.0	0.0	1.0	0.0	0.0	3.7	0.0	0.0
Gd	0.0	10.5	0.0	0.0	4.8	0.0	0.0	10.0	0.0	0.0
Dy	0.0	9.3	0.0	0.0	5.1	0.0	0.0	8.2	0.0	0.0
Ho	0.0	1.8	0.0	0.0	1.1	0.0	0.0	1.5	0.0	0.0
Er	0.0	5.5	0.0	0.0	3.7	0.0	0.0	4.7	0.0	0.0
Yb	0.0	5.2	0.0	0.0	4.1	0.0	0.0	4.1	0.0	0.0
Lu	0.0	0.8	0.0	0.0	0.6	0.0	0.0	0.6	0.0	0.0
SrI	0.000000	0.702891	0.703161	0.702908	0.702906	0.704898	0.705142	0.702899	0.706510	0.705266
NdI	0.000000	0.512907	0.000000	0.512885	0.512874	0.512859	0.512839	0.512843	0.000000	0.000000
Pb 8/4	0.000	0.000	0.000	40.057	40.167	0.000	0.000	0.000	0.000	0.000
Pb 7/4	0.000	0.000	0.000	15.790	15.813	0.000	0.000	0.000	0.000	0.000
Pb 6/4	0.000	0.000	0.000	20.788	20.891	0.000	0.000	0.000	0.000	0.000

Table C2 Whole rock analyses

	157	164	167	172	227	231
	SWLI 3600	SWLI 3600	SWLI 3600	SWLI 3600	SWLI 3600	SWLI 3600
SiO2	58.79	59.09	61.66	60.00	61.04	60.74
TiO2	0.07	0.26	0.09	0.07	0.17	0.10
Al2O3	19.12	17.63	17.83	17.96	17.79	17.60
Fe2O3	4.27	6.35	4.99	4.57	5.95	5.12
MnO	0.19	0.21	0.18	0.21	0.20	0.18
MgO	0.00	0.50	0.00	0.05	0.00	0.03
CaO	0.87	1.95	1.19	0.60	1.62	1.09
Na2O	8.96	6.87	7.67	8.13	7.33	7.44
K2O	4.89	4.63	5.10	5.05	4.80	5.10
P2O5	0.07	0.07	0.07	0.06	0.08	0.06
L.o.I.	2.71	1.31	0.67	2.47	0.83	1.37
Cr	0.00	0.00	0.00	0.00	0.00	0.00
Co	11.00	20.00	9.00	13.00	12.00	14.00
Ni	3.00	5.00	6.00	6.00	5.00	4.00
Cu	4.00	6.00	7.00	6.00	7.00	5.00
Zn	176.00	154.00	184.00	234.00	154.00	196.00
Rb	166.00	93.00	150.00	167.00	123.00	150.00
Sr	35.0	124.0	21.0	28.0	111.0	37.0
Y	39.0	65.0	56.0	67.0	46.0	57.0
Zr	1160.0	947.0	1258.0	1453.0	1037.0	1305.0
Nb	151.0	273.0	244.0	233.0	242.0	247.0
Ba	314.0	1275.0	305.0	170.0	1237.0	341.0
U	0.0	0.0	0.0	0.0	0.0	0.0
Th	0.0	0.0	0.0	0.0	0.0	0.0
Ta	0.0	0.0	0.0	0.0	0.0	0.0
V	65.0	88.0	86.0	98.0	87.0	0.0
Sc	2.0	4.0	0.0	0.0	0.0	0.0
Hf	0.0	0.0	0.0	0.0	0.0	0.0
La	0.0	0.0	0.0	0.0	0.0	0.0
Ce	0.0	0.0	0.0	0.0	0.0	0.0
Pr	0.0	0.0	0.0	0.0	0.0	0.0
Nd	0.0	0.0	0.0	0.0	0.0	0.0
Sm	0.0	0.0	0.0	0.0	0.0	0.0
Eu	0.0	0.0	0.0	0.0	0.0	0.0
Gd	0.0	0.0	0.0	0.0	0.0	0.0
Dy	0.0	0.0	0.0	0.0	0.0	0.0
Ho	0.0	0.0	0.0	0.0	0.0	0.0
Er	0.0	0.0	0.0	0.0	0.0	0.0
Yb	0.0	0.0	0.0	0.0	0.0	0.0
Lu	0.0	0.0	0.0	0.0	0.0	0.0
SrI	0.703036	0.000000	0.703616	0.704599	0.703085	0.704592
NdI	0.000000	0.000000	0.000000	0.000000	0.000000	0.000000
Pb 8/4	0.000	0.000	0.000	0.000	0.000	0.000
Pb 7/4	0.000	0.000	0.000	0.000	0.000	0.000
Pb 6/4	0.000	0.000	0.000	0.000	0.000	0.000

Appendix D: Isotope systematics:

D1; Sr-Nd isotope systematics;

The isotopic composition of radiogenic elements is governed by the variation over time of the parent to daughter ratio. Radioactive decay is described by the equation ;

$$N = N_0 \bar{e}^{\lambda t} \quad (D1)$$

in which N is the number of parent atoms remaining of a radioactive element with an original number of atoms (N_0) at time t=0. y is the decay constant for a particular element. *All decay constants used in calculations in this work are the recommended values of Faure(1986).* In the case of $^{87}Sr/^{86}Sr$ D1 then becomes:

$$\frac{^{87}Sr_P}{^{86}Sr_P} = \frac{^{87}Sr_0}{^{86}Sr_0} * \frac{^{87}Rb}{^{86}Sr} * (e^{\lambda t} - 1) \quad (D2)$$

where y is the decay constant and t is the time since isotopic homogenisation (denoted by subscript 0). Subscripted P is the value at time of eruption. Subsequent to eruption the $^{87}Sr/^{86}Sr$ ratio will increase due to decay of ^{87}Rb to ^{87}Sr. Thus to correct the present day $^{87}Sr/^{86}Sr$ to the initial Sr isotopic ratio at eruption it is also necessary for the following increment to be subtracted (multiplied against observed $^{87}Sr/^{86}Sr$);

$$\frac{^{87}Rb}{^{86}Sr} * (e^{\lambda t} - 1) \quad (D3)$$

Here t is the eruption age. All Sr isotope ages have

been corrected using this method. A similar relationship exists for $^{143}Nd/^{144}Nd$ and $^{147}Sm/^{144}Nd$, but age correction is not necessary because of the large half-life of ^{147}Sm and low parent daughter ratios (differences in the sixth place only).

Owing to the widespread use of the Sr-Nd isotope diagram (Fig.7.4) in the literature it is described here in some detail. The diagram is of value as it is informative in illustrating fractionation of the parent daughter ratios over Earth history. It was found on completion of the first combined determinations for Sr and Nd isotopic ratios that a broad array existed between isotopically depleted volcanics with low $^{87}Sr/^{86}Sr$ and high $^{143}Nd/^{144}Nd$ and relatively enriched types with high $^{87}Sr/^{86}Sr$ and low $^{143}Nd/^{144}Nd$. Because this array included the predicted bulk Earth value it was postulated that this array could be produced by an earlier fractionation of the parent daughter ratios, possibly during crust formation (O'Nions et al.1979). If an equal initial concentration of parent and daughter occurs the following relative element concentrations occur due a fractionation event and the different incompatibilities of Rb from Sr and Sm from Nd.

Rb = Sr		Rb > Sr	Rb < Sr
	--->	+	
Sm = Nd	Melting	Sm < Nd	Sm > Nd
Primitive mantle	event	evolved liquid(crust)	residue

If the melt and residue are separated for sufficiently long periods the different parent daughter ratios will confer different isotopic ratios on the two components. The residue that is now erupted as MORB has a low $^{87}Sr/^{86}Sr$ and high $^{143}Nd/^{144}Nd$ as a consequence of the decrease in Rb/Sr and increase in Sm/Nd. A continuum exists to relatively enriched material which has had a higher time integrated Rb/Sr and Nd/Sm ratio. It is important to remember that recent fractionation events may alter the parent daughter ratios without sufficient time for isotopic differences to develop. Similar variants on this scenario have also been proposed. These explain the Sr-Nd "mantle array" as due to mixing of depleted and primitive reservoirs (Wasserburg and De Paolo(1979)), or mixing of enriched and depleted reservoirs (Anderson(1982)). More recent compilations of Sr, Nd isotopic data such as White and Hofmann(1982) have shown substantial deviations from this array, hence more complicated scenarios must be envisaged to account for the complete variation.

D2; U-Th-Pb isotope systematics;

The equation describing the decay of ^{238}U to ^{206}Pb (via a variety of intermediate decay products) in a system for time t is;

$$\frac{^{206}Pb}{^{204}Pb} = \frac{^{206}Pb}{^{204}Pb} + \frac{^{238}U}{^{204}Pb} * (e^{\lambda t} - 1) \qquad (D4)$$

If the Pb has undergone two stages of evolution with different $^{238}U/^{204}Pb$ (denoted by subscripts 1 and 2). Pb ratios this equation becomes;

$$\frac{^{206}Pb}{^{204}Pb} = \frac{^{206}Pb}{^{204}Pb} + \frac{^{238}U_1}{^{204}Pb_1} * (e^{\lambda T} - e^{\lambda t_1}) + \frac{^{238}U_2}{^{204}Pb_2} * (e^{\lambda t_1} - e^{\lambda t_2}) \qquad (D5)$$

Here T is the **age** of the Earth. The relevant single stage Pb evolution equations for the other isotopes of Pb are :

$$\frac{^{207}Pb}{^{204}Pb} = \frac{^{207}Pb}{^{204}Pb} + \frac{^{238}U}{^{204}Pb} * \frac{1}{137.8} (e^{\lambda t} - 1) \qquad (D6)$$

and

$$\frac{^{208}Pb}{^{204}Pb} = \frac{^{208}Pb}{^{204}Pb} + \frac{^{238}U}{^{204}Pb} * \frac{^{232}Th}{^{204}Pb} (e^{\lambda t} - 1) \quad (D7)$$

Complementary two stage Pb evolution equations are similar to D5. The decay of U and Th in natural rocks has produced the distribution of Pb isotopes apparent in Fig.7.7. The possible reasons for such a distribution of Pb isotopes are discussed in section 8.4.

Appendix E:
Theoretical basis of least squares modelling:

E1; A brief introduction to least squares modelling;

The least squares approach is employed in numerous instances in geological science where it is necessary to solve a mass balance problem of the form :

$$S_i = C_{i1} \cdot x_1 + C_{i2} \cdot x_2 + ... C_{ij} \cdot x_j$$

In relation to the problem discussed in Chapter 6 in which a daughter composition is derived from a parent composition by fractionation of certain mineral phases C_{ij} represents the amount of the i th component in the j th phase, S_i represents the amount of the i th component in the sample and x_j represents the amount of the jth phase. A set of linear equations of this form relating the proportion of a particular oxide (S_i) and its abundance in the phases (C_{ij}) is used in the least squares analysis. The system will be overdetermined when considering the full range of major elements and a lesser number of phases. This will produce a discrepancy or residual which is given by the amount by which each oxide fails to match the actual value observed. If the residuals are included within the equations, the system becomes underdetermined and the solutions can be obtained by linear programming techniques. In this method the sum of the squares of the residuals is minimised to give the optimum fit for the data. The sum of the squares of the residuals is an indication of the degree to which the model is fulfilled. An arbitrary value is used - Wright and Doherty(1971) considered 0.1 acceptable. With respect to modelling the fractional crystallisation process, the following questions must be considered;

(1) By what degree of crystallisation is a possible daughter magma related to a parent.

(2) What is the proportion of mineral phases that crystallised to produce this combination?

These questions are answered by adding phases that are thought to relate the parent to the daughter through crystal fractionation processes to the evolved composition in order to obtain the parental composition. The proportions of the fractionating phases and the degree of fractional crystallisation is varied in the model to yield a best estimate of these parameters and produce a good fit between observed and calculated parental composition by minimising the sums of the squares of the residuals. Whether the two rocks are likely to be related is determined by both geological relationships and whether the sum of the square of the residuals is minimised sufficiently. The program LSQPM PASCAL used in the least squared mixing model is a more sophisticated version of that originally applied to petrologic processes by Bryan et al.(1969). A weighted approach is used, with oxides weighted according to their relative error and their distance from the

regression line. This has the effect of downgrading the importance of oxides of low abundance, or those that are inconsistent with the majority of the data. A discussion of the advantages of weighted least squares mixing is given in Reid et al.(1973).

Appendix F :
Theoretical basis of trace element partitioning:

F1; Partition coefficients and definition of element classes;

Trace elements are of great value in modelling processes such as crystal fractionation and partial melting because of their different partitioning between crystal phases and liquids. A rigorous chemical definition does not exist for trace elements. Common usage of the term applies to element concentration below 1%. Below such concentrations elements obey Henry's law:

$$a(i)=kh.x(i) \qquad (F1)$$

where a(i) is the activity of an element i whose concentration in a solution is the mole fraction x(i).

The distribution of an element between two phases, which in the case of interest are a solid and a liquid is given by:

$$Kd = \frac{|i| \text{ in phase A}}{|i| \text{ in phase B}} \qquad (F2)$$

|i| denotes concentration of element i.

Kd is known as the distribution or partition coefficient.

Thus the distribution coefficient is governed by the element concentration in the two phases. For modelling purposes the igneous geochemist is interested in the way in which an element is partioned between a particular mineral and the magmatic liquid which contains it. Thus the general case becomes:

$$Kd = \frac{|i| \text{ solid}}{|i| \text{ liquid}} \qquad (F3)$$

Here Kd is sometimes known as the Nernst partition coefficient. The critical value of D is 1. Elements with D << 1 are known as the **Incompatible** elements. These are preferentially partitioned into the liquid during melting or crystallisation processes. This is a consequence of the incompatible elements' radii and charge characteristics. These parameters differ significantly from the principal constituent elements of rock forming minerals, hence they are not compatible in the structure of these mineral phases. If the behaviour of such an element in a silicate liquid cooled from a high temperature is considered, it will not enter the main crystal lattices until the last stages of crystallisation or alternatively it will form separate phases. Examples of such elements are the Large Ion Lithophile (LIL) elements such as K, Rb, Ba, Th and Sr , the High Field Strength Elements (HFSE) such as Zr, Nb, Ta, Hf and Ti. The Rare Earth Elements (REE) are an important group of largely incompatible elements. The REE are of great value because

they can be used in petrogenetic modelling. Their widespread use occurs because their physio-chemical differences confer small coherent variations in the way in which they partition themselves between liquid and solid. Their ionic radii decrease systematically between La (1.032 A (VI)) and Lu (0.861 A (VI)) which causes a decrease in their incompatibilty from La to Lu. The REE and other incompatible elements are of the most value in petrogenetic modelling because for small degrees of melting they show the largest range in abundance.

F2; Representation of trace element variations;

In addition to the use of ratio-ratio plots, a valuable method of displaying variations of incompatible trace elements is to use a chondrite normalised diagram. This is variously known as a CoryellMasuda diagram or spidergram, depending on the individuals' prejudices! The trace element values are plotted relative to a reference value to enable comparison of elements of widely differing abundances (although a log scale is still required). Elemental abundances are normalised to primordial material represented by chondritic meteorites to enable consideration of trace element variations relative to this material. The volatile elements Rb, K and P do not have chondritic values because these are thought to have been degassed from the earth. Elements are arranged on this diagram according increasing incompatibility from right to left. The degree of incompatibility was established by studies of MORB genesis (Sun et al.(1979). Such diagrams may also be used to indicate trace element variations relative to other materials such as a primitive basalt for example.

Table F1; List of chondrite normalising values from Thompson(1982):

```
Rb ; 0.35.
Ba ; 6.9.
Th ; 0.042.
K  ; 120.
Nb ; 0.35.
Ta ; 0.02
La ; 0.328
Ce ; 0.865
Sr ; 11.8.
Nd ; 0.63.
P  ; 46.
Sm ; 0.203
Zr ; 6.84.
Ti ; 620.
Y  ; 2.
Yb ; 0.22.
```

Compatible elements have D > 1. They are preferentially partitioned into certain phases. For example Ni is compatible within the olivine structure and Cr is compatible in olivine, clinopyroxene and spinel.

F3; Simple melting model equations;

The principles behind the creation of various partial melting and crystallisation models are described below. The problem is approached by considering the simplest solution followed by increasing the complexity of the models towards the complexity of natural systems. All models used involve equilibrium fusion in which the evolving liquid is in equilibrium with the residue until melting is complete, when the two are separated. Because the melt is removed in one increment rather than continuously (many increments) this process is also known as batch melting. Non-equilibrium (Rayleigh) melting is not considered because in this process the melt is removed from the residue instantaneously in small increments. It is noted that natural melting will be somewhere between the two extremes, but that equilibrium melting is more realistic. Rayleigh melting produces a greater magnitude of trace element fractionation, hence smaller degrees of partial melting will be inferred by the use of this equation. It should be noted that these equations only provide an approximate gauge of element fractionation during partial melting because the physical factors considered by Ribe(1988) are not included. The case of partial melting is considered because we are most interested in this situation for elucidation of source region characteristics. The equations can be applied in the reverse case for fractional crystallisation. The simplest situation that can be envisaged is :

(1) Monomineralllc rock, equlllbrlum fuslon

In this case the distribution coefficient (D) governs the enrichment of an incompatible element in the melt fraction (F) according to;

$$\frac{C_l}{C_o} = \frac{1}{D + F(1 - D)} \qquad (F4)$$

C_l / C_0 is the "enrichment factor" produced if C_0 (the concentration of an element in the original solid) is set to 1 and C_l is the element concentration in the evolved liquid. This expression was derived by Shaw(1970). The consequences of this relation are that;

(i) Elements with Kd < 1 (incompatible elements) are selectively partitioned into the melt on fusion.

(ii) C_l / C_0 varies most rapidly at small degrees of fusion.

The situation of a monominerallic rock is of limited application in nature. The modelling can therefore be extended to;

(2) Polymineralllc rock, equlllbrlum fuslon

In this case the variation in distribution coefficients for various phases needs to be taken into account. This is achieved by using a bulk distribution coefficient given by:

$$D(bulk) = x_a \cdot D_a + x_b \cdot D_b + x_c \cdot D_c + ... + x_j \cdot D_j$$

where x is the proportion of the phase a,b,c, ... j. The resulting value of Do(bulk) is then substituted into equation A5. In this instance the phases are assumed to melt in the proportions in which they wee present in the original rock. Owing to variations of temperatures of initial fusion between different minerals the idea of modal melting is not tenable for advanced models, thus a further correction factor is required.

(3) Polymineralllc rock, non-modal equlllbrlum fuslon

In this case the basic equation F4 is modified by a factor P which is dependent on the proportion of various phases. P is given by:

$$P = x_a \cdot D_a + x_b \cdot D_b + x_c \cdot D_c \ .... \ x_j \cdot D_j$$

Here x is the proportion in which a phase (a, b, c, .. j) enters the melt. F4 becomes:

$$\frac{C_l}{C_0} = \frac{1}{D + F(1 - P)} \qquad (F5)$$